PHASE RELATIONSHIPS IN PERALUMINOUS GRANITES: A FIELD, EXPERIMENTAL AND THEORETICAL STUDY

by

John
EWAN J. REID

B.Sc.(Syd. Univ.), M.Sc.(A.N.U.)

Submitted in partial fulfilment of the
requirements for the degree of
Doctor of Philosophy

UNIVERSITY OF TASMANIA
HOBART
1987

This thesis contains no material which has been accepted for the award of any other degree or diploma in any University and, to the best of my knowledge and belief, contains no copy or paraphrase of material previously published or written by another person, except where due reference is made in the text of this thesis.

E. J.
July, 1987.

TABLE OF CONTENTS

List of Figures

List of Tables

List of Plates

PREFACE

It has been my privilege to have been a post-graduate student at two universities, because I have had the opportunity to consider particular petrological problems from different perspectives. At each institution, compelling evidence was presented to support a model process by which granitic magmas were thought to differentiate. However, these processes: restite-unmixing and fractional crystallization cannot both apply to the petrogenesis of the same suite of granites as they are mutually exclusive of each other.

In this work, an attempt has been made to reconcile this dilemma by considering the physico-chemical nature of granitic magmas and specifically the phase relationships within them. By this approach, a more general model of granite magmatic differentiation is obtained, which has some features resembling those of each of the model magmatic processes previously proposed.

ABSTRACT

Knowledge of phase relationships in granitic magmas is of major importance in the understanding of granite petrogenesis. It has implications for models of the nature, provenance, evolutionary processes in and metallogenetic potential of magmas. Peraluminous compositions were chosen because there is substantial information about their subsolidus equilibria on which to base a magmatic study.

A review of the efficacy of five commonly proposed magmatic differentiation processes reveals that each has only limited application in the light of the physicochemical properties of granite magmas.

Granitic rocks from the Furneaux Islands in the northern portion of the Blue Tier Batholith (NBTB) of eastern Tasmania were studied. Six major suites were identified, using chemical, geological and mineralogical criteria. They include hornblende-bearing I-type granodiorites (the Wybalenna Suite), cordierite- and garnet-bearing S-type adamellites and granites (the Musselroe and Boobyalla Suites) and andalusite- and cordierite-bearing A-type alkali feldspar granites (the Babel Island Suite).

Geological, mineralogical and petrographic evidence indicates these to be high-level granites. Porphyries are common. Their textures indicate that most melts were phase multi-saturated. Parageneses constructed on the basis of petrography, indicate probable magmatic assemblages for each suite and implicate the existence of magmatic reactions consonant with the appearance and disappearance of phases.

Compositional data of phases in porphyries are consistent with the operation of magmatic processes which lead to progressive changes in the compositions of the crystalline phases. However, these have been variously modified by subsolidus reactions, especially those in coarser-grained rocks.

In addition to the first order whole-rock chemical characteristics of each suite, there are second-order features which correlate with sample type. Phenocryst-poor whole rocks and matrix-separates form trends which are distinguishable from those of the phenocryst-rich rocks from the same suite. This difference is attributed to differences between the compositional trend for melts and that for the bulk-phenocryst assemblages within the magmas.

Estimates of intensive variables operative during the petrogenesis of NBTB granites were obtained by applying four barometers and seven thermometers to the compositions of matrix separates and minerals. The

cores of phenocryst phases such as the feldspars and garnet, retain chemical features of earlier, high-PT equilibria whereas their rims and the other mafic phases record the chemical features of later, low-P subsolidus equilibria. From these, partial PT paths were constructed for five suites. Source conditions for Boobyalla Suite magmas are estimated to have been ~0.6 GPa P_{Σ}, P_W/P_{Σ} = ~0.4 and ~850°C. Solidus pressures were ~0.15a±0.1 GPa P_W. fO_2-conditions estimated using a new oxygen fugacimeter for (biotite+vapour)-bearing assemblages are close to the QFM-buffer at equilibrium biotite/garnet temperatures of ~550°C.

An experimental study of Fe^*Mg_{-1} exchange equilibria amongst magmatic peraluminous phases was made in a simple-system analogue to that of the natural peraluminous granites: the KFMASHO chemical system, using a pelitic starting composition. Watersaturated experiments were conducted from 800 to 1000°C and at pressures from 0.5 to 1.5 GPa. Addition of TiO_2 to this system influences Al-Fe*-Mg-equilibria. However its major effect is to substantially increase the fO_2 within the charges. Data of this study, together with that of Ellis (1986) for the simpler, FMASHO chemical system, were used to construct Fe^*Mg_{-1} exchange thermometers for biotite+garnet, garnet+melt, cordierite+melt and orthopyroxene+melt assemblages. The biotite/garnet thermometers of Holdaway & Lee (1977), Thompson (1976b) and this work predict similar temperatures. Low-temperature granitic liquids are predicted to be more magnesian than equilibrium garnet, on the basis of the garnet/melt thermometer.

PT and $P_{\Sigma}P_WT$ grids of magmatic equilibria in the KFMASH analogue simple-system were constructed using the methods of Schreinemakers. A $P_{\Sigma}P_WT$ loop through the 3D grid for this system, yields a paragenesis which resembles that for the Boobyalla Suite granitic rocks. Isobaric liquidus surfaces have been constructed for assemblages saturated in alkali feldspars, quartz and vapour.

Major-element phase-relationship modelling of the Boobyalla Suite trend for porphyritic whole-rocks was undertaken, assuming to to have been a magma trend in which the melt compositions are given by the Babel Island whole-rock trend. The results indicate all the magmas to be crystal-rich and that magmatic differentiation occurred by a combination of restite unmixing and peritectoid fractionation. The model requires a side-wall accretionary mechanism. Differentiation by these means has implications for granite classification, the nature of granite magmas, magmatic processes, provenance and metallogensis.

ACKNOWLEDGEMENTS

The support and encouragement of many people, especially those listed below were essential in producing this thesis.

The conceptual content of this work owes much to:

My supervisor, Professor **David H. Green**, for his encouragement and guidance and for the provision of facilities both inside and outside the Department;

David Ellis, for his enthusiasm and encouragement in my seeking to apply phase equilibrium concepts to granite petrogenesis and for our numerous discussions on the subject;

Ron Berry, for his willingness to discuss a diverse range of conceptual problems and for the pragmatism of his advice;

Bruce Chappell, for the many stimulating discussions about granite petrogenesis;

Rick Varne, for equally stimulating discussions on the same subject;

Don Stewart-Richardson, for the insights realized from our discussions of granite petrogenesis undertaken at a mathematical level;

Ron Berry, Rick Varne, David Ellis, Bruce Chappell, Doone Wyborn, Peter Ruxton and Professors Alan White and Wayne Burnham for spending time in the Furneaux Islands, discussing the geology and petrogenesis of granitic rocks; and Alan Thompson, Vic Wall, Shen-Su Sun and Neville Higgins, for excellent petrological discussions.

The following people were essential to the production of the thesis:

June Pongratz, for her extraordinary perseverence and stoicism in typing and retyping the text, help in construction of the bibliography and for draughting most of the diagrams of Chapter 12;

David Obendorf, for help in draughting Figures 7.1, 7.2, 7.6 and 7.8 and for actually hand-copying Appendix H, preparatory to its being typed;

Penny Green, for her superlative organizational abilities put to the construction of the bibliography, cross-checking many parts of the thesis and for single-handedly copying the three large maps and the text of the thesis;

Wayne Taylor, for helping me recognise my frequent abuses of thermodynamics;

Graeme Wheller, for the kind use of his analytical data-base program which tamed large quantities of microprobe analytical output;

Keith Harris, for his advice and help in applying experimental petrological techniques and for help in the preparation of certain starting minerals;

Phil Robinson, for his advice in XRFS and AAS analytical procedures;

Bruce Chappell, for undertaking some difficult tasks in XRFS analysis and for kindly providing calculating and graphing facilities at A.N.U.;

Shen-Su Sun, for undertaking SmNd analyses of three Furneaux granitic rocks and a garnet separate;
Bruce Brown, for deriving the equations describing microprobe analytical precision, used in Chapter 8;
My brother, **Jason**, for help in fieldwork and for his superlative draughting of Map 4;
David, Simon and **Ruth Obendorf** for instruction and help in printing the plates;
Richard Hale, for the artistic stippling on Fig. 11.5;
Michael Muldoon, for spending hours on the lettering machine;
Barbara Jones, for help in constructing the bibliography;
Peter Cornish, for undertaking many workshop requests;
Simon Stephens, for his ability to make near-perfect polished 50x80 mm^2 thin sections;
Prof. David Green, Maree O'Sullivan, David Obendorf, Wayne Taylor and John Adam for constructive critical reading of parts of the thesis.

Fieldwork in the Furneaux Islands was facilitated by the following people:
Peter Frost, who risked much whilst ferrying rocks, myself and others on many occasions around the islands in his boat;
Jamie Mason and **George Ross** for transportation between Babel and Flinders Islands;
John Bowman, Phil Matthews, Soren and Joyce Fuglsang and **Glen Webb** for providing field accommodation;
Don Napier and **Colleen Patterson**, for providing logistical advice; and **Philippa** and **Peter Frost** and family and **Joan** and **Max Mason** for their kind hospitality.

Hospitality in Hobart was extended by Richard Wedekind and Sharon Adrichem, Margaret and Malcolm Wallace, Nick and Kate Odling and especially by John Adam.

Bruce Chappell extended his considerable hospitality whilst I was in Canberra.

Extensive encouragement and inspiration have been given to me by my parents, my siblings and by Kath Dickinson and Robyn Wallace.

Finally, this thesis could not have been produced without the love and support of **David Obendorf, Maree O'Sullivan** and their children: **Simon** and **Ruth**.

Chapter 1
INTRODUCTION

1.1 INTRODUCTION AND AIM OF THESIS

Knowledge of magmatic phase relationships is of major importance in determining the petrogenesis of granites. Only with this knowledge may fundamental petrogenetic problems such as the nature of granitic magmas, of rock/magma relationships, of magma differentiation processes, and of granite provenance, be answered. Each of these problems is dependent upon knowing the magmatic phases and their inter-relationships in PTX-time space.

However, phase relationships in granitic magmas are poorly known. There are a number of reasons for this discrepancy. Firstly, granitic magmas cannot be observed directly, although some felsic volcanic rocks can be shown to have been the extrusive equivalents of adjacent granites (Wyborn et al., 1981; Wyborn & Chappell, 1986; Pitcher, 1987). Secondly, the textures of coarsely crystalline granites are largely the product of subsolidus reactions which have obliterated almost all of the pre-existing magmatic textural features (Luth, 1976; Pitcher, 1987). Accordingly, there is usually little in the way of petrogenetic information with which to determine the proportion and composition of the liquid and solid portions of the original magma. Thirdly, granitic magmas unlike basaltic magmas, can be crystal-rich, because granitic melts can have viscosities which are 6 ± 3 orders of magnitude greater than those of basaltic melts (Shaw, 1963a, 1965, 1972) inhibiting crystal/liquid separation in convecting magma chambers (Marsh & Maxey, 1985). High viscosities for granitic melts are a consequence of their siliceous compositions and polymerized melt structure and of their low magmatic temperatures (estimated eruption temperatures of felsic volcanic magmas are usually ~850±100^{o}C (Ewart et al., 1975; Ewart, 1985; Clemens & Wall, 1979, 1981, 1984; Wyborn et al., 1981; Wyborn & Chappell, 1986; Hildreth, 1979, 1981; Mahood, 1981).

Another reason why granitic phase relationships are poorly known is that magmatic temperatures can be low enough to ensure that phenocrystic plagioclase and garnet are in chemical disequilibrium with the rest of the magma, due to their inherently slow rates of diffusion (Johannes, 1980; Loomis, 1983a; Grove et al., 1984; Ellis, 1986). Phase relationships in granitic magmas can therefore be more complex than those in basaltic magmas, because there can be a significant proportion of disequilibrium phases present.

A fifth reason concerns the equilibrium phase relationships of felsic magmas. On petrographic, experimental and theoretical grounds, low-temperature felsic melts are frequently indicated to be saturated in eight or more other phases. Phase relationships involving such liquids will therefore be more complex than those in basaltic magmas which involve less-saturated, higher temperature melts. Most felsic extrusive rocks contain many phenocryst phases (Wyborn et al., 1981; Clemens & Wall, 1979, 1981; Hildreth, 1979, 1981; Mahood, 1981), as do the low-temperature experimental run-products of partial melting of both analogue and natural granitic bulk-compositions (Whitney, 1975; Siefert, 1976; Huang & Wyllie, 1981; Wyllie & Huang, 1981; Naney, 1982; Clemens & Wall, 1979). Theoretical studies of multicomponent chemical equilibria for granitic bulk-compositions support these data. They predict that the complexity of phase relationships increases as the water-saturated solidus is approached (Grant, 1973, 1985; Abbott & Clarke, 1979; Thompson, 1982; Ellis, 1986). In contrast, the phase equilibria of mafic magmatic systems are simpler. Although mafic melts may be saturated in four or five phases at their source (Jaques & Green, 1980), their subsequent evolution usually involves less than three solid phases at any stage (op. cit.).

The aim of this thesis is therefore to provide information about phase-relationships relevant to the petrogenesis of a subset of granites: the strongly peraluminous (crustally derived) granites. This group was chosen because phase equilibria in their chemical system are relatively well known under subsolidus conditions (Grant, 1973; Thompson & Tracy, 1979; Siefert, 1976; Thompson, 1976a,b; Hensen & Green, 1972; Holdaway & Lee, 1977; Ellis et al., 1980). These equilibria provide the basis for extrapolation into magmatic systems. Models of simple-system peraluminous magmatic equilibria obtained by this method have already been proposed by Abbott & Clarke (1979), Thompson (1982) and Grant (1985).

Three approaches to the determination of phase relationships in the magmas of these granites have been made. Firstly, a field study was undertaken of a portion of the composite Blue Tier Batholith (BTB) of eastern Tasmania, which contains a variety of granites. This approach provided information about the constitution of both the subsolidus and magmatic precursors of particular granites as well as the physical, chemical, phase-assemblage and intensive variable changes which occurred during the magmatic stages of petrogenesis.

The second approach taken was to investigate $Fe^{*}Mg_{-1}$ exchange equilibria amongst ferromagnesian phases in the KFMASHO chemical system, using experimental petrological techniques. The simple system chosen is an analogue system of the natural peraluminous granites. This approach

provided thermochemical information especially about biotite- and garnet-bearing magmatic assemblages. In conjunction with previous experimental studies in simpler chemical systems by Ferry & Spear (1978) and Ellis (1986), it enabled the construction of biotite/garnet and various mineral/melt Fe^*Mg_{-1} exchange thermometers which are applicable to the study of both the magmatic and subsolidus petrogenetic stages of peraluminous granites.

The third approach to obtaining petrogenetic information about phase relationships, was to make a theoretical analysis of the phase equilibria in another analogue system of the peraluminous granites: the hypothetical peraluminous KFMASH simple system within the $P_\Sigma P_W T$ ranges. The $P_\Sigma P_W T$ ranges chosen $\{0 < P_\Sigma(GPa) < 1.2\}$, $\{0.25 < P_W/P_\Sigma < 1\}$ and $\{600 < T(^oC) < 1000\}$ encompass those thought to be relevant to the magmatic petrogenetic stages of most crustally derived granites.

Phase relationship information obtained by these three means were then applied in models of the petrogenesis of particular suites of BTB granites.

1.2 THESIS FORMAT

The remaining part of this chapter is a review of magmatic differentiation processes. In it, the dependence of each process upon knowledge of magmatic phase relationships is described. In the next chapter, granite classification systems are reviewed and the BTB granites studied, are described. The field geology, petrography and rock- and mineral-chemistry are then presented in Chapters 3 to 7. Phase-relationships and -chemistry in the experimental analogue system are described and Fe^*Mg_{-1} exchange thermometers are derived and presented in Chapter 8. In Chapter 9, a variety of barometers and thermometers (including those derived in Chapter 8) are applied to natural mineral data (Chapters 6 and 7) to obtain P, T and fO_2 estimates of equilibrium assemblages. The chemical compositions of bulk rocks and porphyry matrix separates are used in Chapter 10 to assess the nature of magmatic felsic phase relationships. This approach provides qualitative information about the nature of granitic magmas. The theoretical KFMASH study is presented in Chapter 11 and finally the petrogenetic modelling of specific granite suites, incorporating all the relevant information from the preceding chapters, is undertaken in Chapter 12.

1.3 GRANITIC MAGMAS AND THEIR EVOLUTION: A REVIEW

1.3.1 Introduction

Tuttle & Bowen (1958) were the first to show that granitic melts could be obtained by melting quartzofeldspathic protolith compositions under lithospheric PT-conditions. Subsequent experimental investigations have demonstrated that compositions which are broadly granitic can be obtained by partially melting protoliths as diverse as pelite (T.H. Green, 1976a), psammopelite (Mehnert & Busch, 1982), greywacke (Winkler, 1979), tonalite (Huang & Wyllie, 1986), granite (Clemens & Wall, 1979; Clemens et al., 1986) and basalt (Spulber & Rutherford, 1983).

In nature, the link between granite and protolith is vividly displayed in some regional metamorphic terrains, such as the Cooma Complex of southeastern Australia (Joplin, 1942; White et al., 1974; Flood & Vernon, 1978; Reid, 1980), the St Malo Complex of Brittany (Martin, 1979; Weber et al., 1985) and the Manaslu Granitic Complex of Nepal (Le Fort, 1981) and the Trois Seigneurs Massif in the Pyrenees (Wickham, 1987). In these, there is a continuous gradation between granite and protolith, with migmatites and high-grade gneisses occupying intermediate positions. Such granites are interpreted as being the product of partial melting of the surrounding country rocks (op. cit.). Similar metamorphic gradations spanning much smaller distances to those above, occur adjacent to high-temperature intrusive rocks (Reid, 1980; Torres-Roldan, 1983; Evans & Speer, 1984; Powers & Bohlen, 1985). In these rocks, the heat source is known and the dehydration-melting reactions which operated have been identified by comparison of the assemblages of the gneisses and migmatites with the adjacent granites (op. cit.). On mineralogical, chemical and isotopic grounds, many gneissic terrains are interpreted to be the refractory chemically depleted residua left after granite magmas have been extracted (Grant, 1968; Sighinolfi & Gorgoni, 1978; Nesbitt, 1980; Pride & Muecke, 1980; Ross, 1985). These gneisses are regarded as the counterparts of particular high-level granite intrusions and as evidence for the process of partial melting having taken place (op. cit.).

Identification of the protoliths of granitic suites is an important aim of petrogenetic studies. However, subsequent to partial melting, other petrogenetic processes, both magmatic and subsolidus, will progressively modify the chemical, mineralogical and even the isotopic features of earlier assemblages and therefore obscure the nexus of granite and protolith, making the latter difficult to identify. Such overprinting can be used to petrological advantage if particular modifications are known to be specific to particular processes which have operated.

This deductive approach is valid when the mechanisms by which the processes operate are physically and chemically reasonable. Differentiation processes are frequently proposed however, without sufficient knowledge of the magmas upon which they are supposed to have operated. When these magmas are more fully characterised and their chemical and rheological properties assessed, it becomes obvious that the chemical and physical requirements of some commonly invoked processes are either unlikely or impossible. Other processes must therefore be considered in their place.

1.3.2 Differentiation Processes in Granite Magmas

The applicability, efficacy and limitations of the magmatic differentiation processes which are commonly considered to have generated the compositional variations within granitic suites, are now discussed.

Progressive Partial Melting

Progressive partial melting of a single source has been invoked to account for variation in granites from initial low-temperature magmatic compositions to later, more refractory ones (Bailey, 1977; Emmermann et al., 1975; Reid, 1980; Oates & Price, 1983; Collins et al., 1982; Whalen et al, in press; Clemens et al., 1986). Apart from the obvious time constraints for this process to have occurred, other constraints are:

(a) the initial radiogenic-isotopic ratios of the granite derived from the first melting episode must be the same as the age-corrected ratios of the granites of subsequent melting episodes; and

(b) phase equilibria must be consistent with the initial granite magmas having been at lower temperatures than those of the final ones.

Progressive partial melting may to be important in the generation of the class of granites known as A-type granites, described below (Collins et al., 1982; Whalen et al., in press). It can be invalidated if either of the above constraints are not met.

Thermogravitational Diffusion

The underlying principle of this process is the Soret effect, where a chemical concentration gradient is generated by diffusion in a liquid if it is held in a temperature gradient (Schott, 1983). This effect is the response to minimising the free energy of the system and is enhanced by the process of convection (op. cit.). The coupled effect is termed thermogravitational diffusion (TGD). It has been invoked to explain the generation of thermally and compositionally-zoned, phyric-poor magmas, both basaltic (Walker & DeLong, 1982) and rhyolitic (Hildreth, 1979, 1981; Mahood, 1981; Mahood & Hildreth, 1983). It is argued that the extreme trace- and minor-element concentrations found in many high-silica rhyolites cannot be produced by processes other than TGD (op. cit.). Similar element

concentrations in some felsic granites have prompted this process to be invoked for their petrogenesis (Ludington, 1981).

Criticism of the petrogenetic status of TGD comes from a consideration of the time factors required to generate compositional gradients and the nature of the gradients which are produced. In order to generate the compositional gradients observed in typical sized felsic magma chambers (i.e. hundreds of cubic kilometres), times are required which greatly exceed those with which the heat of the intrusion is transferrd to the surrounding country rock (Baker & McBirney, 1985). A continuing supply of thermal energy is therefore mandatory. Furthermore, the compositional gradients generated by the TGD are similar to those which segregate during liquid-liquid immiscibility and are different from those generated by crystal-liquid fractionation (Walker & DeLong, 1983). Si, Na and K diffuse to the hot side whereas Fe, Mg, Ca, Ti and Mn diffuse to the cold side. This movement is the exact reverse of what is required to explain magmatic differentiation (Baker & McBirney, 1985). Extreme chemical concentrations in liquids can in fact be modelled by crystal-liquid fractionation processes (op. cit.; Ewart, 1981; Whalen, 1983; Oates & Price, 1983; Miller & Mittlefehldt, 1984). Compositional gradients in liquids can also be generated rapidly by crystal-liquid processes (McBirney et al., 1985; Nilson et al., 1985; Baker & McBirney, 1985). TGD is therefore considered to be of limited relevance to granite petrogenesis.

Hybridization

The term "hybridization" is used here to denote any process which invokes the mixing of a granite magma with material from a different source, in order to generate a compositional spectrum in a granitic rock suite. It therefore includes both magma-mixing and country-rock assimilation.

Spectacular examples of mingled felsic and mafic volcanic rocks (Macdonald & Katsura, 1965; Yoder, 1973; Gerlach & Grove, 1982) and dyke rocks (Wiebe, 1973; Vogel & Walker, 1975; Vogel & Wilbrand, 1978; Whalen & Currie, 1984) have long been recorded. Similar associations in plutonic rocks on larger scales are also known but are uncommon (Whalen, 1985). However, the occurrence of ovoid, porphyritic mafic inclusions in felsic granite is extremely widespread (Berger & Pitcher, 1972; Didier, 1963, 1973, 1987; Chappell & White, 1974; Compston & Chappell, 1979; Wells and Woolridge, 1931; Vernon, 1983; this work). Geological, microstructural and chemical evidence is consistent with the plutonic occurrences of these rock associations being analogues of extrusive or high-level intrusive rocks, i.e. that magma-mingling or synplutonism has occurred resulting in chilling of one magma by the other. The inclusions in plutonic rocks have a

consistent igneous microstructure (Vernon, 1983). They may be aligned in trains or aggregates (Pitcher & Berger, 1972; Reid, 1980; Reid et al., 1983; Hill et al., 1985; Furman & Spera, 1985; this work) which are interpreted to have been disrupted synplutonic dykes. Dykes continuous with inclusion trains (Reid et al., 1983) and which are themselves back-intruded by granite also occur (Pitcher & Berger, 1972; Hill et al., 1985). The matrixes of the inclusions are usually finer grained at the margins than at the cores (Wells & Woolridge, 1931; Vernon, 1983; Whalen, 1985) consistent with their magmas having been chilled against that of the host granite. Rock chemical compositions intermediate in composition between those of the endmembers also occur (Reid et al., 1983; Whalen, 1985; this work) but are uncommon, relative to the abundances of the endmembers.

Synplutonism of magmas during granite petrogenesis is therefore considered to be a common phenomenon. Its influence on the composition of the host granitic magma is a much more important question and one which is difficult to answer. Furman & Spera (1985) have modelled the rheology of basalt-granite magma synplutonism. They consider that the relative volumes and temperatures and the viscosities of the two magmas are critical factors in determining the spatial scale of the resultant compositional heterogeneity. Their model predicts that **prima facie** map-scale evidence of synplutonism **should** be rare and that for granodioritic magmas at ~800^{o}C which are 50% crystalline and have a viscosity of ~10^{7} poise, then an intruded basaltic magma should become completely dispersed throughout the granite, on scales smaller than that of submetric sized inclusions. Dispersal to microscopic scales should be possible in systems in which the host granite temperature, viscosity and crystallinity are ~900^{o}C, ~10^{5} poise and 10% respectively (op. cit.). Under the latter conditions, chemical modification of the granite magma by magma mixing will be proportional only to the amount of mafic magma injected. In the former case, however, only a minor proportion of the injected mafic magma will mix intimately with the granite magma; most will be present in the form of ovoid inclusions which should remain closed chemical systems relative to their enclosing host granite.

Variations in oxygen, initial strontium or in neodymium isotopic ratios between granite samples are frequently cited as evidence for hybridization processes having occurred in granite magmas. This is because $^{18}O/^{16}O$, $^{87}Sr/^{86}Sr$ and $^{143}Nd/^{144}Nd$ ratios may change only slightly during the temperature ranges or time spans possible during closed-system evolution of granitic magma chambers (Taylor, 1980; De Paolo, 1981a,b). Increases in ε_{Sr} values for the peraluminous granites of the South Mountain Batholith were found by Clarke & Halliday (1981) to occur near the contact

with meta-sedimentary country rock, relative to ε_{Sr} values farther into the intrusion. Such increases have been attributed to the effects of localized country-rock assimilation by the granite magma.

Both Clarke & Halliday (op. cit.) and Frost & O'Nions (1985) identified the complementary hybridization process which occurred in country-rock metasedimentary xenoliths within granites of the South Mountain and Etive Batholiths of Nova Scotia and Scotland, respectively. They showed that ε_{Sr} values of the country-rock metasedimentary xenoliths were substantially lower than values for the country rock itself. The latter authors also showed that in contrast to the behaviour of ε_{Sr}, ε_{Nd} values for country rocks and country-rock xenoliths were indistinguishable. These data provide sound evidence for the process of isotopic and chemical hybridization of granitic magmas. However, the role of the process of country-rock assimilation in the modification of the composition of an entire granitic pluton has yet to be established. Taylor & Silver (1978), De Paolo (1981a,b), Halliday et al. (1980) and De Paolo & Farmer (1984) advocate country-rock assimilation by mantle-derived magma as the major petrogenetic process responsible for compositional variations between the granites of entire batholiths and even whole granite provinces. They argue for large-scale assimilation on the grounds that the extent of variation of isotopic parameters such as $\delta^{18}O$, ε_{Sr} and ε_{Nd} amongst the samples of a single intrusive body is greater than can be ascribed to closed-system magma evolution and that the strong covariance between these parameters is in the direction predicted by this mixing process.

An alternative hypothesis proposed for the generation of isotopic variations amongst granites of batholiths or terranes, is that isotopic variation existed between the protoliths of the various granites, i.e. that much of the isotopic variation is inherited and is a feature diagnostic of the source region of each particular suite (Kistler & Peterman, 1973; Cortecci et al., 1979; Michard-Vitrac, 1980; Compston & Chappell, 1979; McCulloch & Chappell, 1982; Cocker, 1982; Higgins et al., 1985; Chappell, 1984). Source-inherited isotopic features become more plausible and late-stage assimilation-acquired features less plausible, when it is recognized that enormous chemical and isotopic variations exist amongst potential granite protoliths in the continental lithosphere (Allegre & Othman, 1980) and that there is growing evidence for diversity in the isotopic and chemical characteristics even of the upper mantle (McCulloch et al., 1983; Menzies & Murthy, 1980a, b).

Except for the outer rim of granite close to the country-rock contact, variation in ε_{Sr} within the granites of the South Mountain Batholith of Nova Scotia is considered by Clarke & Halliday (1985) not to

require assimilation, but to have arisen by protracted evolution (11 m.y.) of magma derived from a single source. However, ε_{Sr} variations in some individual plutons do exceed that which can be ascribed to closed system radiogenic decay during the time of evolution of a magma chamber. Those in the Murrumbidgee Batholith of S.E. Australia (Roddick & Compston, 1976, 1977), the Tuolumne Meadows Pluton of the Sierra Nevada Batholith (Kistler et al., 1986) and in the San Jacinto Composite Pluton of the Peninsula Ranges Batholith (Hill et al., 1985) are examples. Rather than ascribe these variations to the process of crustal assimilation during ascent and evolution of the magmas, the respective authors consider that isotopic heterogeneity was a magmatic trait inherited from an isotopically heterogeneous source region, i.e. that there is heterogeneity in lower crustal rocks on a scale less than that of the volume of a single pluton.

It is apparent from the range of scales argued both for the effective operation of the hybridization process of country-rock assimilation and its major alternative (the extent of granite protolith heterogeneity), that an independent assessment of the importance of either of these hypotheses is required.

Combined assimilation-fractionation models have been presented by Allegre & Minster (1978), Taylor (1980) and De Paolo (1981a). They are based on the argument of Bowen (1928) that the two constituent processes should be thermodynamically related: the heat required for assimilation being derived from the heat of crystallization of the granitic melt. The models assume that perfect mixing and crystal settling occur within the granitic magma body and that there is constant access of the magma to the country rocks at a level close to that of final granite emplacement. Unless the granite magma is hot (>900C) then the rheological constraints of high viscosity will prevent all of these model requirements from being met (Furman & Spera, 1985; Sparks et al., 1984; McBirney et al., 1985; Nilson et al., 1985; Baker & McBirney, 1985).

Assimilation is identified as being a viable petrogenetic process, responsible for changing the compositions of high-temperature magmas, such as those of komatiites (Huppert & Sparks, in press) and gabbros (Foland et al., 1985). Hybridization processes are therefore considered to have had the **potential** to be of significance in the petrogenesis of a granite, if its magmatic temperature exceeds ~900^{o}C. Based upon somewhat meagre thermometric data (Clemens & Wall, 1981, 1984; Oates & Price, 1983; Wyborn et al., 1981; this work), this temperature limit probably excludes most of the strongly peraluminous or S-type granites of the Lachlan Fold Belt from having been affected by hybridization processes . Metaluminous plutonic rocks such as the St Marys porphyrite (Higgins et al., 1985), those of the

Boggy Plains Suite (Wyborn, 1983; Wyborn et al., in press), some of the small class of A-type granites (Clemens et al., 1986) and the Barrington Tops granodiorite (Eggins & Hensen, 1987) formed from magmas which were hot enough to allow hybridization processes to have been potential petrogenetic processes. The status of the potential for hybridization processes to have occurred in the petrogenesis of the remaining Lachlan Fold Belt granites (some 50% of all the granites, that is, the bulk of the I-type or weakly peraluminous to metaluminous granites (cf. Chapter 2)) is not known because their magma temperatures have not been estimated.

Restite Unmixing

The restite model of granite petrogenesis proposes that chemical variations within a group of related granites reflect a differentiation process involving the progressive separation of the two physical states: liquid and bulk-solid (the latter being termed "restite") which constituted the granitic magma (White & Chappell, 1977; Chappell et al., in press). Restite unmixing is considered to have been the dominant petrogenetic process in the generation of most of the granites and felsic volcanics of the Lachlan Fold Belt (op. cit., Griffin et al., 1978; Hine et al., 1978; Wyborn et al., 1981; Price, 1983) and in the New England Fold Belt (Chappell, 1978; Flood et al., 1977), the Pressanone Pluton, northern Italy (Visona, 1983), the Hepburn and Wentzel batholiths of northern Canada (Pattison et al., 1982) and the Northern Idaho Batholith, U.S.A. (Hyndman, 1984).

White & Chappell (1977) and Chappell et al. (in press) cite evidence for the process from a variety of sources. Their geological evidence consists of:

(i) the occurrence only in the peraluminous granites, of gneissic peraluminous inclusions which are chemically different from exposed country rock, found throughout the pluton (unlike country rock inclusions, which are usually restricted to pluton margins) and which are most abundant in the most mafic granites. This type of inclusion is considered to be a meso-scale remnant of restite-rich (melt-poor) material;

(ii) the presence of porphyritic, relatively mafic, ovoid inclusions with fine to medium grained matrixes, which occur sparsely throughout peraluminous granites but which are the dominant inclusion type in weakly peraluminous to metaluminous granites. These inclusions are considered to represent restite-enriched related magmas;

(iii) contact aureoles which are the same width beside felsic granite as those beside mafic granite, indicating that mafic granite magma was not noticeably hotter than felsic granite magma. This feature is

consistent with the model interpretation of granites having represented low-temperature magmas which differed only in the relative proportions of suspended restite; and

(iv) the presence in granites of small clots of mafic phase crystals, especialy biotite, which are interpreted as being small fragments of disrupted restitic material.

Petrological evidence cited is:

(i) the occurrence of cores in phases such as plagioclase and zircon and other accessory phases such as apatite and monazite, all of which are petrographically early, with zircon cores having pre-magmatic Pb-U ages similar to model whole-rock Sm-Nd ages (McCulloch & Chappell, 1982) and monazites having Pb-U ages which predate granite emplacement by ~20 m.y. (Williams et al., 1985). Such crystals are regarded as having been suspended crystalline restite;

(ii) the occurrence within felsic volcanic equivalents of nearby granites of both felsic and mafic phase phenocrysts which can have complex inclusion trains considered to have formed during solid-state (porphyroblastic) growth, rather than having formed by crystallization from a melt (Wyborn et al., 1981; Wyborn & Chappell, 1986); and

(iii) the occurrence in the same volcanic rocks, of plagioclase phenocrysts with compositions indistinguishable from those of the cores of plagioclase crystals from related plutonic rocks.

Experimental petrological evidence in support of the process is the very low solubilities in felsic igneous melts of the major mafic phases (Piwinskii & Wyllie, 1968; Huang & Wyllie, 1986) and accessory phases such as sphene (Hellman & Green, 1979), apatite (Watson & Green, 1981), zircon (Watson, 1979, 1980; Watson & Harrison, 1982) and monazite (Montel, 1985).

Chemical evidence for restite unmixing is considered to be straight-line trends on covariance diagrams for any two elements (White & Chappell, 1977; Chappell, 1984; Chappell et al., in press). Such distributions contrast with the curved or scattered covariant trends featured for data from granites thought to have evolved largely by fractional crystallization, e.g. the Tuolumne Meadows Pluton of the Sierra Nevada batholith (Bateman & Chappell, 1979) and the Boggy Plains Pluton of the Kosciusko Batholith (Wyborn, 1983; Wyborn et al., in press).

Thermobarometric evidence for restite unmixing includes low to moderate temperatures (~800^{o}C) at moderate pressures (0.5-0.6 GPa) deduced from the compositions of phenocryst assemblages from felsic volcanic rocks

of the Lachlan Fold Belt using various thermobarometers (Wyborn et al., 1981; Wyborn & Chappell, 1986). These PT conditions are considered to be those under which the volcanic and related plutonic magmas were generated (op. cit.). Such conditions implicate high heat flows of ~40°C per km, for southeast Australian continental crust during Siluro-Devonian times.

The rheological evidence in support of restite unmixing are the extremely high viscosities which have been experimentally determined for felsic melts at low to moderate temperatures (Shaw, 1963a, 1965, 1972) and even higher viscosities, calculated for felsic melt-solid suspensions by McKenzie (1985), which indicate that such magmas should retain their crystalline load over geologically long time periods (op. cit.; Marsh & Maxey, 1985; Baker & McBirney, 1985).

Restite unmixing appears to provide a simple mechanical means of generating an extensive chemical variation amongst granitic rocks, at temperatures well below those which are required for the generation of similar variations by fractional crystallization processes.

A major implication of the model is that the protolith composition can be estimated because it is constrained to lie on the unmixing line which joins the two fixed compositions for melt and restite (White & Chappell, 1977; Chappell et al., in press). If the positions of the latter two compositions can be estimated, then the protolith composition may be located because the source is considered to have contained ~30 **wt%** proportion of the anhydrous melt composition (op. cit.). This protolith composition constraint is based upon the value of ~35 **vol%** for the proportion of melt in crystal/melt mixtures for which a dramatic drop in sustainable shear stress occurs (Arzi, 1978; van der Molen & Paterson, 1979). Separation of melt is expected to occur when this degree of partial melting is exceeded. Source compositions have been estimated for various Lachlan Fold Belt granite suites by Reid (1980) and Price (1983) using this method.

In detail however, the restite model is internally inconsistent. It assumes fixed compositions for the melt and bulk-solid endmembers throughout the magmatic evolution, yet it considers that most of the phases present in the magma will remain in mutual equilibrium as the magma moves through PT space (White & Chappell, 1977, p.18). The chemical consequence of the latter will be to **change** the compositions of the model endmembers, which is contrary to the initial assumption. To have fixed melt and bulk-solid compositions requires that the compositions of all phases remain the same, throughout magmatic evolution, i.e. for there to be no equilibrium amongst magmatic phases, subsequent to the magma leaving the source region. Equilibrium amongst many of the magmatic phases is considered to be

inevitable, from a consideration of the rates of diffusion in minerals and melts (Jambon & Semet, 1978; Brady & Yund, 1983; Freer, 1981; Lasaga, 1979, 1983; Ellis, 1986; this work). The complexity of the theoretical equilibria proposed even for simple granite analogue systems, indicates that many reactions should occur within granite magmas, during their evolution (Abbott & Clarke, 1979; Thompson, 1982; Grant, 1985; Ellis & Thompson, 1984; Ellis, 1986; Chapter 11). Chemical compositional changes of both the melt and the bulk suspended-solid constituents are therefore expected during magmatic evolution.

Chappell et al. (in press) use the term "primary restite" to describe the residual solid-phase assemblage in a granitic magma which is unmodified from that which existed in the magma at source region. They denote part of the remaining solid-phase assemblage as "secondary restite", referring specifically to the hydrous mafic phases: amphibole and biotite, which were derived from pre-existing phases such as clinopyroxene and orthopyroxene, garnet or cordierite, etc. by low-pressure net transfer reactions during magmatic evolution.

However, these hydrous phases

(a) would have been in chemical equilibrium or near-equilibrium with other magmatic phases at PT conditions removed from those in the source region, and

(b) largely or completely replaced pre-existing mafic minerals and hence were absent from the source region or had different chemical compositions to those present in the source region.

They therefore had no physical or chemical connection with the source region, and should not be described as a type of "restite".

With the recognition of equilibrium and disequilibrium phases in magmas, it is useful to designate two types of magmatic solid-phase assemblage: restite and non-restite. In this work, the term **restite** is used to describe the assemblage of magmatic solid phases, each of which maintain the chemical and isotopic composition they had in the source region, despite the magmas' translation in PTX time-space. Restite then consists of relict phases with disequilibrium compositions.

By contrast, **non-restite** refers to the assemblage of magmatic solid phases, each of which change their compositions so as to maintain chemical and isotopic equilibrium with the melt phase as the magma is translated in PTX time-space. Non-restite also includes those magmatic phases which have been generated subsequent to the magma having left the source region.

This division, though not absolute, enables most solid magmatic phases to be petrogenetically classified.

Fractional Crystallization

Fractional crystallization is the magmatic differentiation process which is most commonly invoked in the petrogenesis of granites. It consists of the continuous removal of crystals from a crystallizing liquid. The process involves only reactions of the form:

liquid → Solid A + Solid B + Solid C + ...

This process may therefore also be termed eutectoid fractionation referring to the type of chemical reaction upon which it relies (eutectoid crystallization). For it to occur, the magma must therefore be either:

(i) a pure liquid , or

(ii) a suspension in which the solid phases have interdiffusion rates insufficient to enable them to attain volume equilibrium with the melt.

Given a **mechanism** of separating crystals from melt, then extensive changes in composition are possible for both the residual liquids and their complement: the solid-rich cumulates. Crystal-liquid separation mechanisms include:

(i) gravitational crystal fractionation (Sparks et al., 1984; Marsh & Maxey, 1985);

(ii) side-wall crystallization (McBirney, 1980);

(iii) convective or liquid fractionation (Rice, 1981; Sparks et al., 1984; McBirney et al., 1985; Nilson et al., 1985; Baker & McBirney, 1985); and

(iv) the Bagnold boundary effect (Bagnold, 1954; Barriere, 1976; Thompson & McBirney, 1985).

Crystal fractionation, specifically crystal-settling, has been the traditional mechanism by which fractional crystallization of granitic magmas is considered to have been achieved (Carmichael et al., 1974). In many petrogenetic models however, it is implied rather than stated, as is the assumption that the initial granitic magma was wholly liquid. Hildreth (1979) has shown that crystal-settling cannot operate in felsic magmas, because of the prohibitively high viscosities of rhyolitic liquids under the P-T-X_w conditions relevant to natural felsic magmas. Rice (1981) argues that because silicate liquids are strongly non-newtonian (i.e. they have a finite yield strength), then the difficulty of engendering fractional crystallization by the mechanism of crystal fractionation is compounded. He presents geological evidence for this mechanism being untenable in facilitating the differentiation of even basaltic magmas. Sparks et al. (1984) come to similar conclusions using rheological modelling techniques. They contend that convection is the hallmark of all chambered magmas, even those of rhyolite, the viscosities of which range from 10^5-10^9 poise (Shaw, 1963a, 1965; Ewart et al., 1975). As such,

crystal-settling is severely inhibited (op. cit.). Marsh & Maxey (1985) have rheologically modelled the crystal fractionation mechanism in convective regimes. Their results support the above studies. They consider the mechanism to be ineffective for systems in which the melt viscosity exceeds 10^4 poise.

Fractionation **could** occur however, if both crystallization and the resulting crystals were restricted to the cooler chamber walls, rather than occurring throughout the magma, as is implied by the mechanism of crystal-settling. This alternative mechanism, is termed side-wall crystallization.

Unlike crystal-settling, it is not dependent upon the viscosity of the magma, nor should it be dependent on the proportion of suspended solids in the magma. Fractional crystallization of liquid magmas via the mechanism of side-wall crystallization should lead to chemical zonation from a mafic margin to a felsic core (McBirney, 1980). It has been proposed for the petrogenesis of strongly zoned plutons such as the West Farrington Pluton of North Carolina (Ragland & Butler, 1972), the Mt Givens and Tuolumne Meadows Plutons of the Sierra Nevada Batholith, California (Bateman & Nokleberg, 1978 and Bateman & Chappell, 1979, respectively), the Captains Bay Pluton in the Aleutian Islands (Perfit et al., 1980) and the Boggy Plains Pluton in the Kosciusko Batholith (Wyborn, 1983; Wyborn et al., in press).

The chemical zoning generated by side-wall crystallization should become less pronounced as the volume fraction of suspended crystals in a magma is increased, whether these be of restite or melt-crystallized origin. Thus the subtle concentric zoning in the peraluminous granites of the Clear Range Pluton, in the Murrumbidgee Batholith (Reid, 1980) could have been generated by side-wall crystallization of a crystal-rich magma.

Mathematical and analogue modelling of side-wall crystallization of **liquid** magmas (McBirney, 1980; Sparks et al., 1984; McBirney et al., 1985; Nilson et al., 1985) has lead to the characterization of another crystal-liquid separation mechanism proposed initially by Rice (1981), termed here: convective liquid fractionation. In this mechanism, an evolved liquid which forms subsequent to side-wall crystallization is continuously drawn off in a buoyant boundary layer, to pool (in the case of felsic liquids) at the top of the magma chamber (op. cit.). Sparks et al.(1984) and Baker & McBirney (1985) consider that the extreme extent of magmatic differentiation indicated for high-silica igneous rocks, may be efficiently generated by the process of fractional crystallization utilizing this mechanism. Contrary to the contention of Hildreth (1979, 1981) therefore, the extreme viscosities of rhyolitic magma should not be seen as barriers to magmatic differentiation by the process of fractional crystallization.

Liquid-rich felsic magmas in which the dominant differentiation process was fractional crystallization (facilitated by the mechanism of convective liquid fractionation), were probably those of the Bishop Tuff, the Coso and Twin Peaks Volcanic Fields, the rhyolites of the Western Chihuahua Province, and the Sierra La Primavera Tuffs of southeastern North America (op. cit.; Miller & Mittlefehldt, 1984; Bagby et al., 1981; however, see Hildreth, 1979, 1981; Bacon et al., 1981; Crecraft et al., 1981; Mahood, 1981; Mahood & Hildreth, 1983), the Osuzuyama Volcanic Complex of Japan (Nakada, 1983), and the Tertiary silicic volcanics of central northeastern Victoria (however see Oates & Price, 1983). Plutonic rocks similarly derived are probably the Ackley City Batholith of southeast Newfoundland (Whalen, 1983), the Pattison Pluton of Alaska (Lynch & Pride, 1984), the felsic granites of the St Francis Mountains, Missouri (Bickford et al., 1981; Cullers et al., 1981), and the Redskin Granite of the Pikes Peak Batholith, Colorado (however, see Ludington, 1981).

Many felsic igneous magmas however, can be shown to have been crystal-rich (Wyborn et al., 1981; Wyborn & Chappell, 1986; Chappell et al., in press) rather than having been liquid-rich, like those which generated the above rocks. For these magmas, the extent of segregation of an evolved liquid during wall-rock crystallization might be compromised by further crystallization close to the pluton wall (Nilson et al., 1985). However another boundary effect, that of dispersive shear pressure, termed the Bagnold effect, operates in convecting suspensions and draws suspended solids away from a fixed boundary (op. cit.; Bagnold, 1954). This crystal-liquid separation mechanism has been mathematically modelled by Thompson & McBirney (1985) and by Marsh & Maxey (1985) and appears to be viable in convecting magma chambers. The mechanism is expected to facilitate that of convective liquid fractionation, thereby enabling evolved liquids to be derived and pooled, during the evolution of crystal-containing magmas (op. cit.). However, the process may be self-limiting, because during side-wall crystallization, crystal concentrations in the main magma could build to levels sufficient to disrupt the rising buoyant boundary layer and cause it to remix with the main magma. Many factors can influence fluid dynamics in crystal-containing chambered magmas and an understanding of their rheology is far from complete (op. cit.).

In summary, three mechanisms of crystal-liquid separation are probably able to operate in granitic magmas. They are side-wall crystallization, convective-liquid fractionation and the Bagnold boundary effect. The first of these mechanisms is a pre-requisite of the second and is the most important. The third may augment the second, which leads to the generation of evolved, zoned magmas near the roofs of magma chambers.

With the establishment of mechanisms for separating crystals from liquid, then the process of fractional or eutectoid crystallization as defined earlier, will have operated, providing that the magma was either:

(i) a pure liquid, or

(ii) a suspension in which the solid phases were only in a state of surface equilibrium with the melt.

However, the former criterion is frequently not met because granitic magmas can often be shown to have contained substantial proportions of suspended crystals. The latter condition will rarely be met because many solid magmatic phases such as biotite, cordierite and the pyroxenes have diffusion rates sufficient for them to approach a state of volume equilibrium with the melt. Fractional crystallization is therefore considered to have restricted application to the petrogenesis of many granites, especially crustally derived granites.

1.3.3 Conclusion

In this review, the differentiation processes commonly proposed for the evolution of granite magmas have each been shown to have restricted application. Although they may theoretically account for a given set of (usually geochemical) granite data, they are often incompatible with the deduced petrological or rheological properties of the magmas. The approach taken in this study is therefore to estimate the chemical, physical and phase features of the granite magmas and to then propose differentiation processes which are compatible with the data.

Chapter 2

CLASSIFICATION OF FURNEAUX ISLANDS GRANITES

2.1 INTRODUCTION

Classification systems exist which categorize granitic rocks on the basis of sets of geological, mineralogical, chemical, isotopic or tectonic environmental features. All classifications are descriptive of the rocks, but some such as those of Chappell & White (1984) and Pearce et al. (1984) are also genetic, because they designate the provenance of the granites on the basis of their features.

The identification of suites of granitic rocks is the first stage in any classification process (Chappell & White, 1984; Chappell et al., in press). Suites are groups of rocks which have common or smoothly varying sets of features. Chemical compositional features are the most useful because they are quantified and because so many are available. Granitic rocks of the Blue Tier and Scottsdale Batholiths have now been divided into 14 suites on the basis of their chemical, mineralogical and (where available) isotopic features (McClenaghan, in press; Reid, in press). Seven suites have been identified amongst the Furneaux Granites. Two suites are known only from these islands whereas the others are represented within the batholith to the north and south. The Gardens Suite occurs extensively in the mainland Tasmanian portion of the Blue Tier Batholith. It is presently represented in the Furneaux Islands by only one sample and will not be described in detail.

2.2 MINERALOGICAL CLASSIFICATION

The classification which is most frequently used to categorize granites is that based upon the modal mineral proportions of the three major felsic phases: quartz, alkali feldspar and plagioclase (Streckeisen, 1973, 1976; Chappell & White, 1984). Space enclosed by this set of endmembers can be regarded as the mineralogical analogue of the chemical space enclosed by the CIPW normative endmembers: orthoclase + albite, anorthite + albite, and quartz, which constitute a ternary projection of the rhyolite tetrahedron. The analogy is only approximate however, because the normative mineral albite is not evenly distributed between the two feldspars and because of the lack of correspondence of normative and real granitic mineralogies (the former being exclusively anhydrous whereas the latter includes hydrous phases such as biotite and amphibole). For any given sample, these differences lead to smaller proportions of modal alkali feldspar and larger proportions of quartz, relative to their CIPW normative counterparts.

The analogy is petrogenetically advantageous however, because they enable qualitative information about magmatic phase relationships to be deduced from rock compositions (see Chapter 10). Phase equilibria in the rhyolite tetrahedron have been studied under certain $P\text{-}T\text{-}X_{W=1}$ conditions (James & Hamilton, 1969; Winkler et al., 1975). Compositions with the lowest water-saturated solidi lie within the CIPW normative orthoclase-albite-quartz plane of the rhyolite tetrahedron which corresponds to positions along the alkali feldspar-quartz line of the modal mineral diagram. Compositions which plot closer to the anorthite and plagioclase apices of the respective normative and modal mineral diagrams, have higher water-saturated solidus temperatures.

Disadvantages of the modal mineralogical classification are that

(i) it ignores the effects on magmatic equilibria of all non-quartzofeldspathic phases (which may constitute up to 90% of the rock in the case of the Streckeisen (1976) classification);

(ii) plagioclase with compositions more sodic than An_5 which are to be designated as alkali feldspar (Streckeisen, 1973), must be distinguishd from more anorthitic plagioclase, even when the two occur in the same crystal; and

(iii) modal analysis cannot be obtained for phyric-poor rocks with fine grained matrixes such as many of the granitic porphyries from the Furneaux Islands.

The final two disadvantages may be overcome if the proportions of the appropriate magmatic minerals are calculated from each bulk composition. The calculations require that the compositions of biotite and amphibole be calculated and that the felsic solid solutions be correctly assigned. Such sets of model phase compositions of hydrous phase assemblages are termed **mesonorms** and were first defined and used by T.F.W. Barth. Sophisticated mesonormative calculations for granitic mineralogies have been devised by Chappell (1966). Ninety-six mesonormative quartz-alkali feldspar-plagioclase proportions have been calculated from the compositions of whole rocks and porphyry matrix separates of granitic rocks from the BTB. They are depicted in Fig. 2.1. The method used is described in Appendix B. The assumptions used to determine these mesonorms are that:

(i) sub-assemblages of {quartz, alkali feldspar, plagioclase, biotite, aluminosilicate, ilmenite, apatite and clinopyroxene} adequately approximate the mineralogy observed in the samples;

(ii) biotite compositions may be approximated by the equation:

$$Bi = 3hy + or - 3qz$$

where (hy), (or) and (qz) are the molar proportions of the CIPW normative endmembers hypersthene, orthoclase and quartz;

Figure 2.1

MESONORMATIVE (Qz–Af–Pl)–COMPOSITIONS

OF FURNEAUX GRANITIC ROCKS

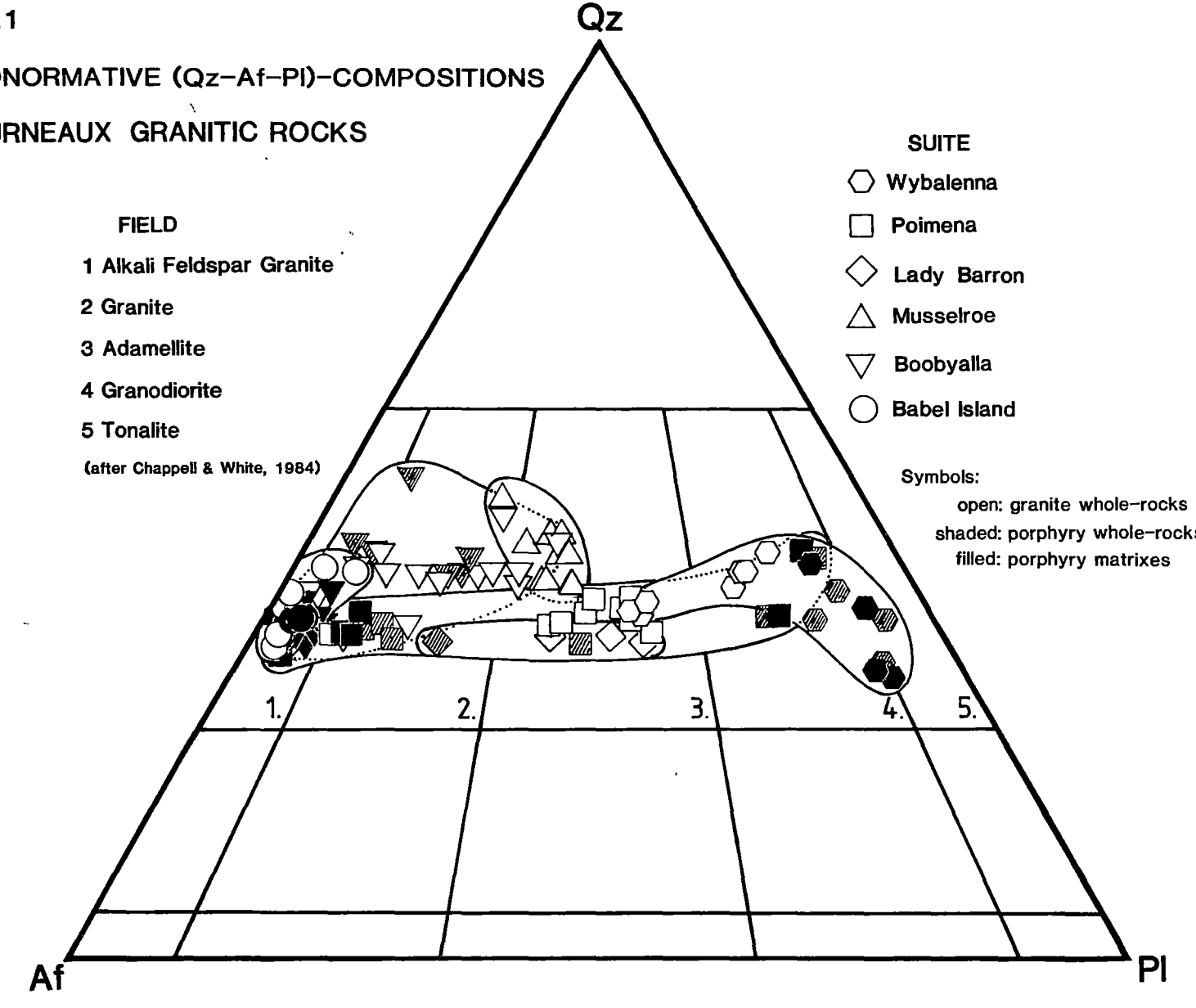

(iii) plagioclase is a binary anorthite-albite solid solution in which the proportion of anorthite $\geq$ 25 mol%; and

(iv) alkali feldspar may consist of both potassium-rich feldspar ($or_{75}ab_{25}$) (similar to the composition of perthitic alkali feldspar phenocrysts from the porphyry #62595), and (where it exists) sodium-rich feldspar with a composition of an_5ab_{95}.

The proportions of the three felsic mesonormative phases are not significantly altered either by simplifying the biotite composition from its natural titanium- and tschermak-containing composition or by assuming that clinopyroxene occurs in the rocks instead of hornblende. The effects of mis-assignment of the correct potassium-rich feldspar composition in the alkali feldspar will be offset by complementary changes in the proportion of the component of sodium-rich feldspar and lead to a similar overall proportion of alkali feldspar relative to the other mesonormative phases. Assuming a compositional discontinuity in plagioclase between An_{25} and An_5 is reasonable in the light of the composition profiles determined for phenocrysts (Fig. 7.10).

On the above basis, northeastern Tasmanian granitic compositions span five fields of Fig. 2.1. Alkali feldspar granites and granites (in the strict sense: s.s.), which are quite rare elsewhere in the Lachlan Fold Belt are common in northeastern Tasmania. Babel Island Suite rocks are exclusively and Boobyalla Suite rocks almost exclusively, of these types. Some suites have extensive ranges, for example, compositions of the Poimena Suite range from those of granite (s.s.) to those of granodiorite. It is this suite that is the most prospective for tin mineralization in northeastern Tasmania with tin being most abundant in the granitic (s.s.) members of the suite (Chapters 5 and 6). The Wybalenna Suite samples are generally poorest in alkali feldspar. However alkali feldspar megacrystic varieties do occur and plot as adamellites on the felsic phase diagram (Fig. 2.1).

Matrix-separate compositions usually plot on the (alkali feldspars+quartz)-rich side of those of their corresponding whole rocks. For the Boobyalla and Poimena Suites, matrix compositions are located at the plagioclase-poor ends of suite trends. These relative positions are consistent with the matrixes representing the least-refractory portion of the rock samples.

In summary, granitic rocks of northeastern Tasmania range from alkali feldspar granite through granite (s.s.), adamellite and granodiorite to tonalite. Some suites have restricted distributions (such as those of the

Babel Island and Musselroe Suites) whereas others (especially the Poimena Suite) have extensive mesonormative mineral distributions.

2.3 MAJOR ELEMENT CHEMICAL CLASSIFICATIONS

Chemical classifications may be applied to all felsic igneous rocks regardless of their grainsize. That of Shand (1927) uses molar ratios of major element concentrations to distinguish broad categories of felsic rocks. These are:

(i) peraluminous rocks - where $mol[Al_2O_3/(Na_2O+K_2O+CaO)] > 1.0$
i.e. where Al_2O_3 is present in excess of the CIPW normative feldspars, i.e. CIPW corundum normative compositions;

(ii) metaluminous rocks - where $Na_2O+K_2O < [Al_2O_3/(Na_2O+K_2O+CaO)] < 1.0$
i.e. CIPW diopside normative compositions; and

(iii) peralkaline rocks - where $(Na_2O+K_2O)/Al_2O_3 > 1.0$
i.e. CIPW acmite or sodium disilicate normative compositions.

Using this classification BTB granitic rocks are all subalkaline. Five Wybalenna Suite compositions are metaluminous, as is the sole Gardens Suite sample #62576. The requisite metaluminous phases in these rocks are hornblende and actinolite (the latter at least, is after clinopyroxene) while the biotite in these rocks is characteristically tschermak-poor (cf. Chapter 7).

The remaining samples of the Wybalenna Suite are peraluminous, as are all samples from the other five suites. The requisite peraluminous phases for these compositions variously include biotite, garnet, cordierite and also the matrix assemblage, which is considered to have been derived from the peraluminous melt phase. Values for the molar $Al_2O_3/(Na_2O+K_2O+CaO)$ ratio for each suite are listed in Table 2.1. Their overlap is considerable.

Table 2.1

Ranges of al-values for whole rocks from six suites of the BTB

Suite	Range in mol $Al_2O_3/(Na_2O+K_2O+CaO)$
Wybalenna	0.965 - 1.089
Poimena	1.037 - 1.155
Lady Barron	1.133 - 1.207
Musselroe	1.100 - 1.306
Boobyalla	1.046 - 1.260
Babel Island	1.055 - 1.235

Figure 2.2

A'F'M DIAGRAM for MAJOR ELEMENT CHEMICAL CLASSIFICATION OF FURNEAUX GRANITES

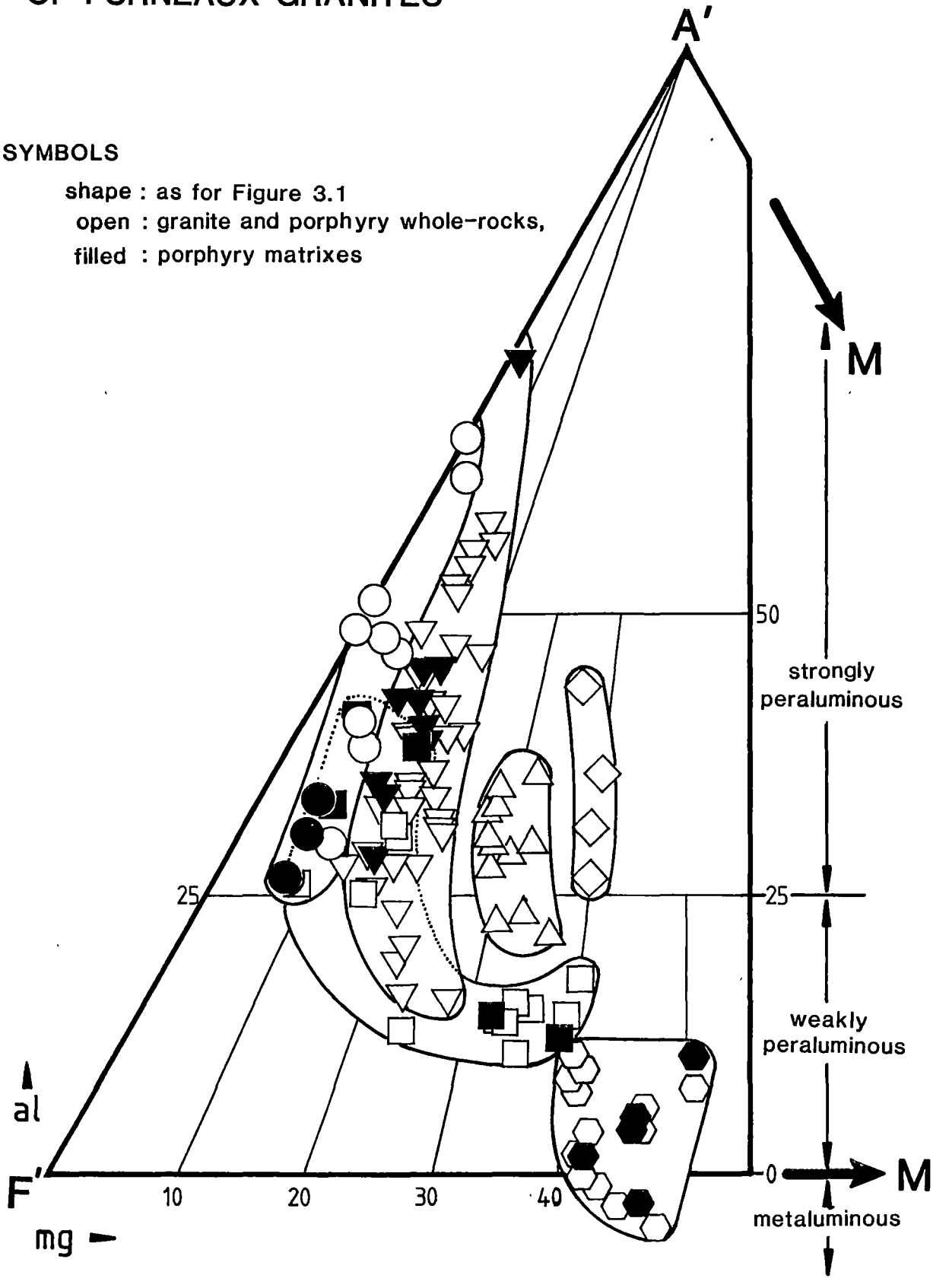

The Shand (1927) classification alone, therefore, distinguishes very few of the BTB granites from each other.

Distinctions may be made however, using the molar A'F'M diagram of Barker (1961) modified for natural rock compositions by A.B. Thompson (pers. comm., 1982), in which

$A' = Al_2O_3 + Fe_2O_3 - (K_2O + Na_2O + CaO)$

$F' = FeO + MnO$

$M = MgO.$

The percentage ratio: 100*A'/(A'+F'+M), symbolized (al), is a useful index of peraluminous-ness because it describes excess Al_2O_3 and Fe_2O_3 in terms of most of the major components of the rock (all except SiO_2 and TiO_2). It is therefore descriptive of rock mineralogy. An (al) value of 0 corresponds to the composition of stoichiometric Si-rich biotite, a value of 25 to that of garnet, ~50 to that of cordierite, and 100 to that of aluminosilicate. The al values of bulk-rock compositions will lie between those of its constituent A'F'M phases. The granitic rocks of northeastern Tasmania have been divided into weakly and strongly peraluminous compositions using total iron as FeO (FeO*) and al-value limits of 25 and 50 (Fig. 2.2).

The data for the six suites depicted on this diagram are adequately distinguished from each other; there is limited overlap of suite compositional fields.

The Wybalenna Suite is magnesian and metaluminous (Shand, 1927) to weakly peraluminous, consistent with its hornblendic and tschermak-poor biotitic mineralogy. The Poimena Suite is weakly to strongly peraluminous, consistent with its mildly aluminous mineralogy and the presence of rare cordierite, garnet and muscovite in the most felsic varieties. The compositions of matrixes from rhyolites and porphyries of this suite indicate that melt was the most important peraluminous phase in the felsic members of this suite. The Musselroe and Lady Barron Suites are more magnesian and strongly peraluminous, consistent with their cordierite-rich mineralogies. The Boobyalla and Babel Island Suites are iron-rich (especially the latter) and range from weakly to very strongly peraluminous character, consistent with many samples of these suites containing an aluminosilicate phase.

The use in this classification of components other than Al_2O_3, CaO and the alkalis is evident in its ability to predict the corderite- and andalusite-containing mineralogies of samples such as the matrixes of porphyries, which have Shand molar $[Al_2O_3/(Na_2O+K_2O+CaO)]$ ratios as low as 1.08.

Figure 2.3: TECTONIC SETTINGS OF GRANITES USING TRACE ELEMENTS.

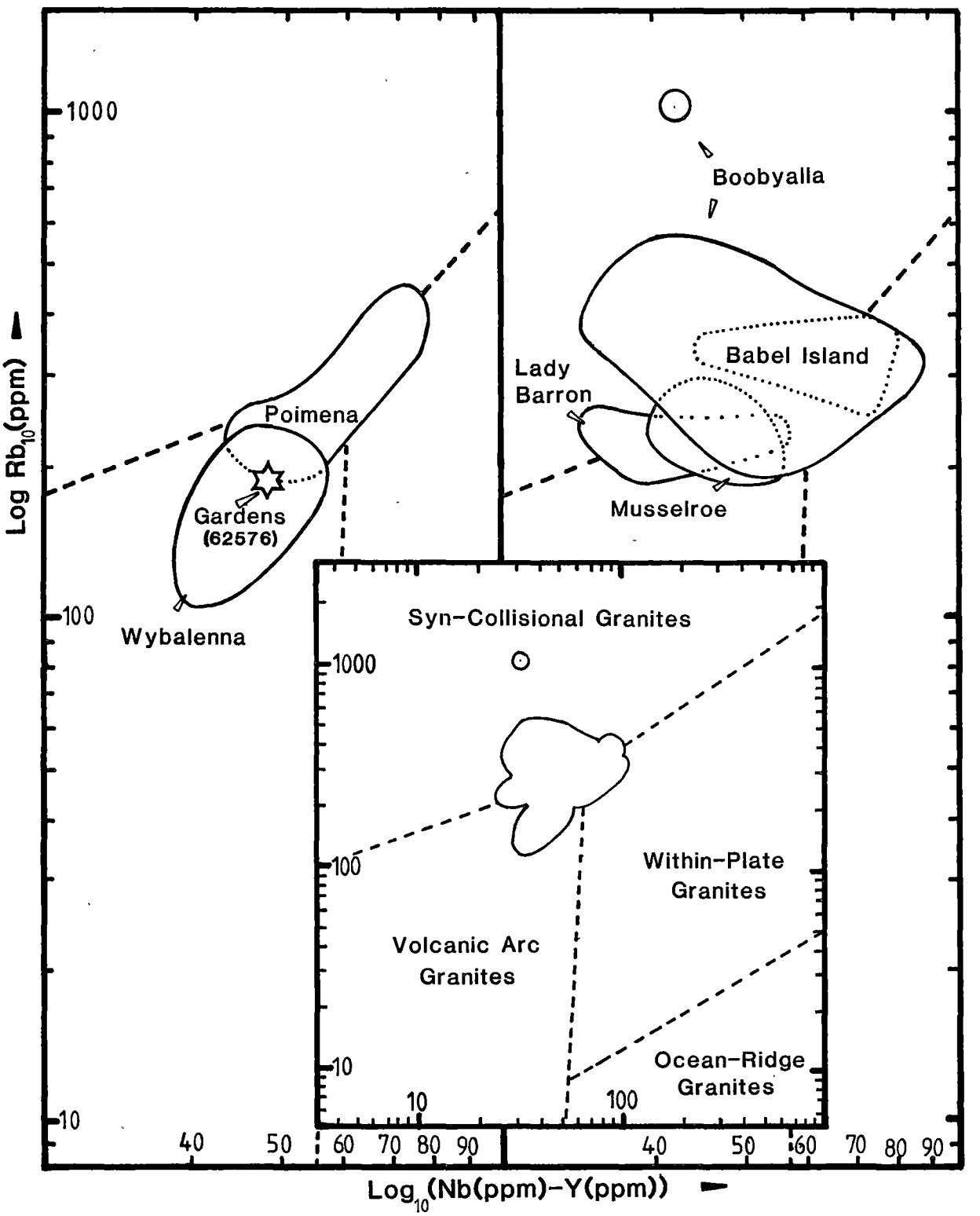

2.4 TRACE ELEMENT CHEMICAL CLASSIFICATION

Pearce et al. (1984) have subdivided granites on the basis of their relative contents of certain trace elements. They discriminate four granite groups, each of which are considered to represent a particular plate-tectonic setting into which the constituent granites intruded. The classification is therefore also genetic because it alludes to the provenance of the granites, be it mantle or lithospheric. The four groups are ocean-ridge, volcanic-arc, within-plate, and collisional granites. Elements used to discriminate these types are Nb, Rb, Ta, Y and Yb. Fig. 2.3 shows Rb versus Y+Nb data for northeast Tasmanian granites. There is little discrimination of the granite suites using this plot, whereas the suites are clearly discriminated on an A'F'M diagram (Fig. 2.2) or on conventional covariance diagrams (cf. Chapter 5). The data, furthermore, are located at the intersection of the fields of three of the four granite types.

The location of the data for the Wybalenna Suite is the least ambiguous and according to Pearce et al (1984), is indicative of the magmas of this suite having been derived in a volcanic arc environment from the partial melting of sub-oceanic lithosphere as a consequence of plate subduction. The classification is of limited use because of its inability to either categorize or distinguish the more peraluminous granites constituting the remaining five suites. It is a model-dependent classification which considers all granites to have been derived during plate-tectonic processes, by either fractional crystallization, crustal assimilation or volatile metasomatic processes operating upon pure liquid magmas (op. cit.). These model magmas were assumed to have been generated by the partial melting of either enriched or depleted mantle protoliths or two representative lithospheric protoliths: a greywacke and a quartz diorite (op. cit.). Many of these assumptions are considered to be invalid, in the light of the evidence of the nature of granite magmas and their magmatic processes, presented in the previous chapter. Furthermore, the chemical and isotopic complexity of the lithosphere precludes the selection of two protoliths for the generation of all lithospherically-derived granites. The trace-element classification of Pearce et al. (1984) adequately categorizes granites with little or no crustal component, such as the Tertiary metaluminous granites of New Britain and New Guinea (Whalen, 1985). It is considered to be of limited use, however, in the classification of strongly peraluminous granites.

2.5 COMBINATION CLASSIFICATION

The I-S-A classification (Chappell & White, 1974; Collins et al., 1982; McCulloch & Chappell, 1982; Compston & Chappell, 1979; Chappell, 1984; Chappell et al., in press) uses a combination of geological, petrographic, chemical and isotopic features, to categorize granites. Three categories are recognized, each of which has features thought to reflect those of their particular protolith (op. cit.). The protoliths of I-type granites are considered to have resided in the lower lithosphere where they were derived by accretionary processes from the mantle. S-type protoliths are considered to have been supracrustal, whereas the protoliths of the uncommon A-type granites are proposed to have been residua of the previous extraction of a granite magma. The genetic nature of this classification follows from the axiom that granites image their sources (Chappell, 1984).

Criteria for distinguishing I-type granites include the presence of calcic or metaluminous phases such as hornblende, low-Al biotite, pyroxene, sphene and allanite. Relative to S-types, I-types have high degrees of inter-element chemical covariance, large ranges in element concentrations, high ratios of CaO/FeO* (total iron as FeO), Fe_2O_3/FeO and Al_2O_3/K_2O, molar $Al_2O_3/(Na_2O+K_2O+CaO)$ ratios usually below 1.1, high Sr (>150 ppm), low $\delta^{18}O$ (<10.2%), low ε_{Sr} ($\leq$112: i.e. $(^{87}Sr/^{86}Sr)_{init.} \leq 0.712$) and a wide range in ε_{Nd} from +4.4 to -9.0 (op. cit.). These features are consistent with the derivation of I-type granites by partial melting of chemically primitive, mafic mantle-derived material of various ages, producing magmas which had high CaO activities and low Al_2O_3 activities.

Corresponding S-type features include the presence of peraluminous phases such as Al-rich biotite, garnet, cordierite and aluminosilicates, Ca-poor accessory monazite or xenotime, scattered covariance trends with small element concentration ranges, moderate to high silica contents, low CaO/FeO*, Fe_2O_3/FeO and Na_2O/K_2O ratios, molar $Al_2O_3/(Na_2O+K_2O+CaO)$ ratios above 1.0, Sr usually below ~150 ppm, $\delta^{18}O$ above 9.2% , ε_{Sr} >70 (Sr_i >0.708), and a restricted range in ε_{Nd} from -6 to -9.8 (op. cit.). These features are consistent with the magmas of S-type granites having had high activities of Al_2O_3 and low activities of CaO relative to those of I-type magmas. S-type protoliths should have compositional characteristics resembling the geochemically-evolved compositions, such as those of the crustal metasediments (Nance & Taylor, 1977; Reid, 1980, this work; Bhatia & Taylor, 1981; Kitto, 1982).

Features of A-type granite suites include very silicic compositions, very small ranges of chemical component concentrations, accessory fluorine-bearing phases, very low CaO/FeO* ratios, moderate, rather than extreme

Figure 2.4

ASPECTS OF THE
I/S/A CLASSIFICATION OF GRANITES

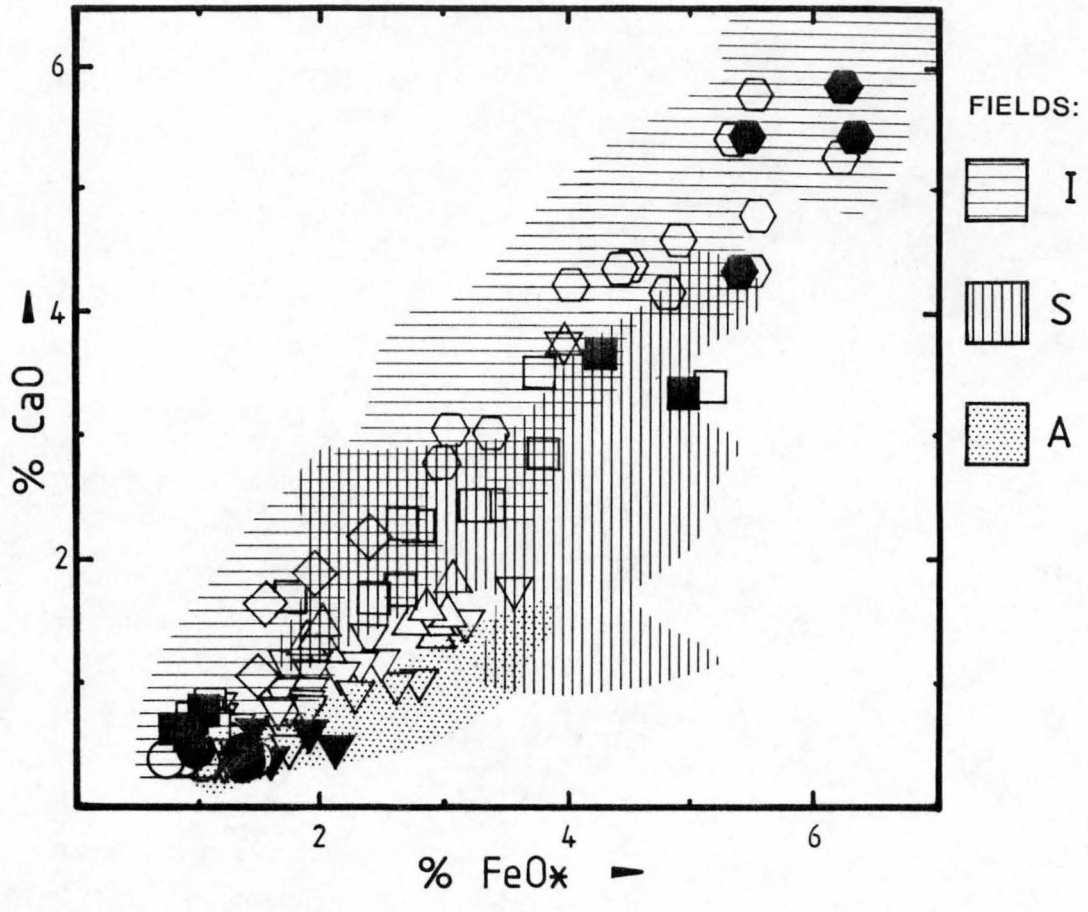

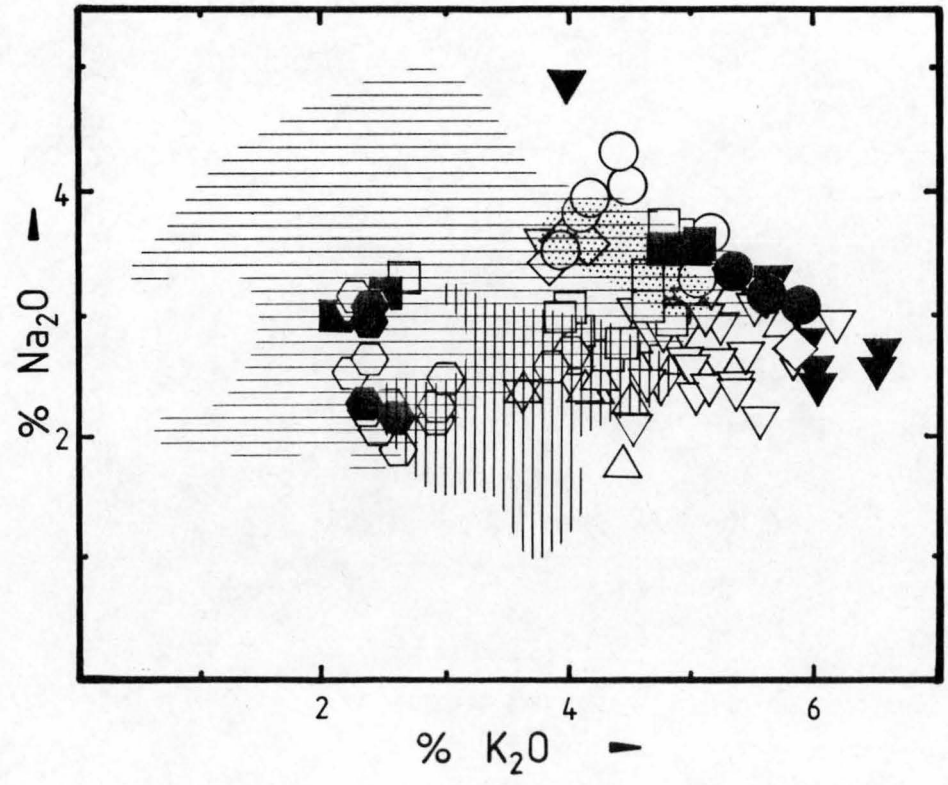

molar $Al_2O_3/(Na_2O+K_2O+CaO)$ ratios (between 0.98 and 1.1) and high to very high concentrations of high-valence transition elements such as Ga, Sc, Y, REE's, Zr, Hf, Nb and Ta, relative to the concentrations of these elements in adjacent I- and S-type granites. Sm/Nd and Rb/Sr isotopic parameters for A-type granites from the LFB fall int the range indicated for the I-type granites (B.W. Chappell, pers. comm.). A-type granite protoliths are considered to have been the halogen-enriched residua left after the previous extraction of a granitic magma (op. cit.; Clemens et al., 1986). The A-type granites are therefore regarded by these authors, as being the products of two-stage progressive partial melting.

The distinguishing criteria for I-S-A classification have been applied to the NBTB granites, although it is recognised that these granites only just occur within the spatial limit of $\geq 148^{\circ}E$, set by Chappell & White (1984) for the strict applicability of the classification.

Some major-element chemical data used in the I-S-A categorization of granites are shown in covariance diagrams in Fig. 2.4. Reference areas are in mainland S.E. Australia. Reference characteristics shown for A-type granites are from Collins et al. (1982). Those for I- and S-type granites are from Chappell & White (1984).

Relative to ELFB granites, those of the Wybalenna, Poimena and Gardens Suites are I-type whereas the Musselroe Suite are S-type, and the Babel Island Suite: A-type. The remaining two suites are difficult to classify; the Boobyalla Suite granites are much more felsic and potassic than ELFB S-type granites and form a continuum with the A-type granites of the Babel Island Suite. The Lady Barron Suite has many I-type features despite its peraluminous chemical character (cf. Figs 2.2), and its cordierite-rich magmatic mineralogy (cf. Chapter 4). It could be regarded as either a "calcic S-type" or an "aluminous I-type" suite.

According to Chappell & White (1984) and Collins et al. (1982) therefore, the Musselroe and possibly the Boobyalla and Lady Barron Suites as well, were derived from metasedimentary protoliths in the crustal lithosphere, whereas the Wybalenna, Poimena and Gardens Suites were derived from accreted mantle-derived sources in the subcrustal continental lithosphere. Granites of the Babel Island Suite and some Boobyalla Suite granites as well, would be accorded a more complex petrogenesis, with their protoliths having undergone a previous partial melting and granite magma extraction process.

Advantages of the I-S-A classification are that a wide variety of rock features are used to designate the granite type. Few features are exclusively characteristic of one granite type, yet taken altogether, a

diagnosis can usually be made. Most granites can therefore be succinctly categorized as being of either I-, S- or A-type.

A disadvantage of this classification is the lack of widespread application of much of the discriminatory criteria. They apply strictly to those granites which are proximal to those from which the classification was empirically derived, i.e. to granites occurring east of longitude 148°E within the Lachlan Fold Belt (Chappell & White, 1984). Although similar I- and S-type granites occur side-by-side in other tectonic terrains, they will not have exactly the same ranges of features as those in the eastern Lachlan Fold Belt (ELFB) above, because their protoliths are unlikely to have been identical to those of these granites (op. cit.). For instance, although the granites of the New England Fold Belt (NEFB) of eastern Australia exhibit an I/S dichotomy, the distinction is much less clear-cut than that in the ELFB (Hensel et al., 1985). Chemical studies suggest that there was a significant volcanogenic sedimentary component in the protoliths of the NEFB S-type granites and isotopic studies imply that both S- and I-type protoliths were relatively young (op. cit.). It is for these reasons, for example, that only a marginal distinction between the I- and S-type granites of the NEFB may be made on the basis of neodymium or strontium isotopic parameters,

Another disadvantage is that classification of granites becomes progressively more difficult as they become more felsic. Felsic I-type granites are devoid of hornblende, distinctly peraluminous and have Sr concentrations below 100 ppm and so resemble S-type granites. Ambiguity arises because the range of each quantified parameter used to distinguish one granite type overlaps with those of the other granite types, as shown in Fig. 2.4.

A more important criticism is that ultimately it is a genetic classification. When a granite is classified in terms of its features, and is designated a granite type, both its protolith and the petrogenetic processes by which it was generated, are also designated. The granites of a particular suite are assumed to have been derived from a single protolith by closed-system petrogenetic processes, such that their resulting features reflect those of this protolith. Though many granites may have been derived by such petrogeneses, others have not. For instance, granites which

(a) had more than one source, such as those derived by magma-mixing (cf. Chapter 1), or
(b) have been hydrothermally altered subsequent to emplacement, or
(c) transcend a single category, yet can be shown to have come from a common source (cf. Chapter 12),

cannot be meaningfully classified.

In this thesis, suites will usually be referred to by name and described in terms of their features. Only after an independent assessment of probable petrogenetic processes, are protoliths suggested for the Boobyalla and Babel Island Suite granites (Chapter 12).

Chapter 3

GEOLOGY OF THE FURNEAUX ISLANDS GRANITES

3.1 INTRODUCTION

In this chapter, the regional geology is described and compared with that of other parts of the Lachlan Fold Belt. The granites of N.E. Tasmania are then briefly described. Previous geological, radioisotopic, petrogenetic and metallogenetic studies of the Blue Tier Batholith (BTB) granites are then reviewed. The geology of each of the granite suites presently known from the Furneaux Islands is then described. Finally, various types of mineral accumulations found within the granites are described and descriptions and petrogenetic assessments of them made.

3.2 REGIONAL GEOLOGY

3.2.1 Terranes of the Southern Lachlan Fold Belt

The Palaeozoic granites of the Furneaux Island Group cover an estimated pre-Mesozoic area of 1350 km^2. They constitute the northern part of the Blue Tier Batholith of eastern Tasmania. This is the largest of a series of batholiths which form part of a narrow (~200 km wide) linear granite-flysch terrane, termed the Bassian Terrane by White (1986). It extends for at least 550 km down the central part of the Palaeozoic Lachlan Fold Belt (LFB) of Gondwana (Fig. 2.1).

In Tasmania, the Bassian Terrane is bounded to the west by the Tamar Lineament. This lineament has features consistent with it being a boundary between two terranes. Magneto-telluric studies by Hermanto & Parkinson (1986) indicate it to be a narrow (~5 km wide) high-conductivity anomaly to depths of at least 3 km. The lineament also juxtaposes the shallow-water shelf deposits of western Tasmania with deep-water quartz-rich flysch: the Mathinna Beds, of N.E. Tasmania (Baillie, 1985). The western Tasmanian or Taswegian Terrane (White, 1986)is somewhat enigmatic. It has no known correlate elsewhere in the LFB. Baillie (1985) considers its basement to be part of the Precambrian Kanmantoo Fold Belt of South and Central Australia.

Regional aeromagnetic patterns are interpreted to indicate that the granites of the Bassian Terrane extend on to the continental shelf eastwards from the Tasmanian coastline. The Bassian Terrane may extend further south onto other Gondwanan fragments such as New Zealand (the Nelson Province: Burrett & Findlay, 1984) and Antarctica (Baillie, 1985). Burrett & Findlay (1984) however consider the latter, on palaeontological grounds, to be a different Palaeozoic terrane to that of eastern Tasmania.

In the Bass Strait, the Bassian Terrane is flanked and partially covered by Mesozoic to Cainozoic sedimentary basins: the Bass Basin to the west and the Gippsland Basin to the east (Etheridge et al., 1985). North of the Furneaux Group, the Palaeozoic granites are exposed in the Kent, Hogan and Curtis Island groups. They have a collective area of only ~20 km^2.

Bassian Terrane granites crop out on the northern side of the strait in the Wilsons Promontory Batholith. This batholith covers an area of ~600 km^2. The northern part of this batholith is covered by a zone of Gippsland Basin sediments. Palaeozoic rocks of the Melbourne Terrane (White, 1986) extend northwards from beneath this Mesozoic cover for a further 250 km before they in turn are covered by Cainozoic sediments of the Murray basin (op. cit.).

The Bassian and Melbourne Terranes may be part of a larger single terrane because there are many similarities between the various petrological, tectonic and stratigraphic units within them. For example, the opaque mineralogies and the emplacement ages of the Bassian and Melbourne Trough granites are similar: they are reduced or ilmenite series granites (Ishihara, 1977; Whalen, 1980) of Middle Devonian age (White, 1986; B.W. Chappell, pers. comm.). In contrast, the terranes which bound the Melbourne Terrane to the east, the west and also to the north, contain abundant oxidized (magnetite-series: Ishihara, 1977; Whalen, 1980) granites of Lower Devonian age (White, 1986). Further eastwards again is the high-grade metamorphic Wagga Terrane containing still older (Ordovician) granites (Prof. A.J.R.White, pers. comm.).

SmNd source model ages for all BTB granites except the uncommon alkali feldspar granites, are ~1.5 b.y.; the latter cluster at ~1 b.y. (depleted mantle reference, Sun et al., 1986). The relative consistency of these model ages, despite their range in petrographic, chemical and Sr-isotopic features from those of S- to I-type, contrasts with the model ages of the granites of the Wagga, Canberra and Bega Terranes further east which have their source model ages ranging from 0.4 to 2 b.y. (McCulloch & Chappell, 1982). Zircons from the granites in the latter terranes indicate a similar age variation for their inherited components (Williams et al., 1985).

The Bassian-Melbourne terrane may therefore be a strip of the LFB which has age-constrained lower-crustal components and which is sandwiched between portions of the LFB with more complex lower crustal components of contrastingly diverse age. The large-scale tectonic significance of the geometry of these LFB terranes is presently unknown.

3.2.2 Tasmanian Granites of the Bassian Terrane

The Bassian Terrane granites of Tasmania occur in two batholiths, or spatial groupings of granitic rocks. These are the Scottsdale and Blue Tier Batholiths. The Scottsdale Batholith is known only within N.E. Tasmania. It occurs close to the western boundary of the terrane and covers an estimated pre-Mesozoic area of ~1800 km^2. It consists only of I-type granites. The three known suites are all characteristically rich in Na_2O compared with those of the Blue Tier or other batholiths (McClenaghan, in press; B.W. Chappell, pers. comm.).

The Blue Tier Batholith is separated from the Scottsdale Batholith to the west, by a screen of Mathinna Beds flysch. The screen is narrowest in the north where the batholiths come to within 6 km of each other.

The Blue Tier is a large composite batholith containing granites with A-, S- and I-type features. Eleven suites are presently recognised (McClenaghan, in press; Reid, in press). Within Tasmania, it covers an estimated pre-Mesozoic area of ~4000 km^2, although extensive submarine exposures should considerably augment this figure. Granite exposures at Bicheno, the Freycinet Peninsula, Schouten and Maria Islands, and the Tasman Peninsula may also be part of this batholith.

Turner et al. (1983) consider that the 600 km^2 area of strongly peraluminous (S-type) granites to the north and west of Eddystone Point, N.E. Tasmania, constitutes a separate batholith which is juxtaposed with BTB granites to the south by a faulted country-rock screen. They have termed this the Eddystone Batholith. However, the spatial separation of these two granite regions is considered to be insufficient to warrant the designation of another batholith. Neither is a division warranted on the grounds of the spatial distribution of granite types or suites, because the major granite suite, the I-type Poimena Suite, is recognised throughout the batholith.

In this study, the granites which extend from Ansons Bay northwards through the Furneaux Islands, are collectively termed the northern portion of the Blue Tier Batholith (or NBTB) granites; the granites of the Furneaux Islands are termed the Furneaux Granites.

3.3 PREVIOUS STUDIES OF BLUE TIER BATHOLITH (BTB) GRANITES

Important geological studies of these granites were undertaken by Groves (1970, 1972), Gee & Groves (1971), Cocker (1977), Williams (1979), McClenaghan & Williams (1982), Kitto (1982), McClenaghan et al. (1982), Baillie (1986), Higgins et al. (1986), Turner et al. (1986), McClenaghan (in press) and Reid (in press). Only the first, fourth and last of these references however describe the geology of Furneaux granites.

McDougall & Leggo (1965) pioneered KAr and RbSr studies on these granites. Their work yielded a whole-rock plus mineral RbSr isochron for the Scamander Tier Pluton and KAr biotite ages (which are lower limits to emplacement ages) for numerous plutons of the Blue Tier and Scottsdale Batholiths.

The detailed radioisotopic studies of Cocker (1977, 1982) yield whole-rock RbSr isochrons for 12 plutons as well as an errorchron for the Mathinna Beds country rock. Numerous KAr biotite ages were also obtained.

The SmNd studies of Sun et al. (1986) have shown that S- and I-type granites in the batholith have indistinguishable source-rock model ages (see previous section). The A-type granites however, have distinctly younger source-rock model ages.

Radioisotopic studies of Furneaux granites are confined to three KAr biotite ages obtained by Brooks (1971) and preliminary ε_{Nd} determinations of three whole-rocks and one garnet-separate by S-S. Sun (pers. comm.). The KAr ages range from Lower Devonian (379 ± 3 m.y. for biotite from the Clarke Island Pluton of the Musselroe Suite) to uppermost Devonian (361 ± 3 and 354 ± 3 m.y.) for biotites of the Chappell Islands and Modder River Plutons (Wybalenna and Poimena Suites, respectively) from western Cape Barren Island. The former age is consistent with the emplacement ages deduced for other BTB granites. The latter may date a period of deformation which generated strong planar fabrics and even mylonites in this Wybalenna Suite granite. The similar Poimena Suite age may reflect isotopic resetting because this sample though not noticeably foliated, was taken from within 2 km of the foliated Wybalenna Suite sample.

The preliminary SmNd data for the whole-rocks are consistent with those of other BTB granites. ε_{Nd} values for the S-type Boobyalla Suite granites are distinctly lower (-5.6 at 370 m.y.) than are those obtained from an A-type porphyry from the Babel Island Pluton (-3.4 at 370 m.y., cf. Appendix T).

Petrogenetic studies of BTB granites were undertaken by McCarthy & Groves (1979), Cocker (1982), Kitto (1982) and Higgins et al. (1985). The first study chemically modelled the entire spectrum of BTB granites as having been derived from a common mantle-derived source by prolonged fractional crystallization. The radioisotopic study of Cocker (1982) however, showed that the range of emplacement ages is too small to account for the large range of strontium isotope initial ratios by such a petrogenesis. Instead, a variety of protoliths with different isotopic characteristics, is indicated (op. cit.).

The studies of Kitto (1982) and Higgins et al. (1985) chemically modelled subsets of the spectrum of BTB whole-rock data, in accordance with

Figure 3.1

Furneaux Granitic Units and their Intrusive Relationships

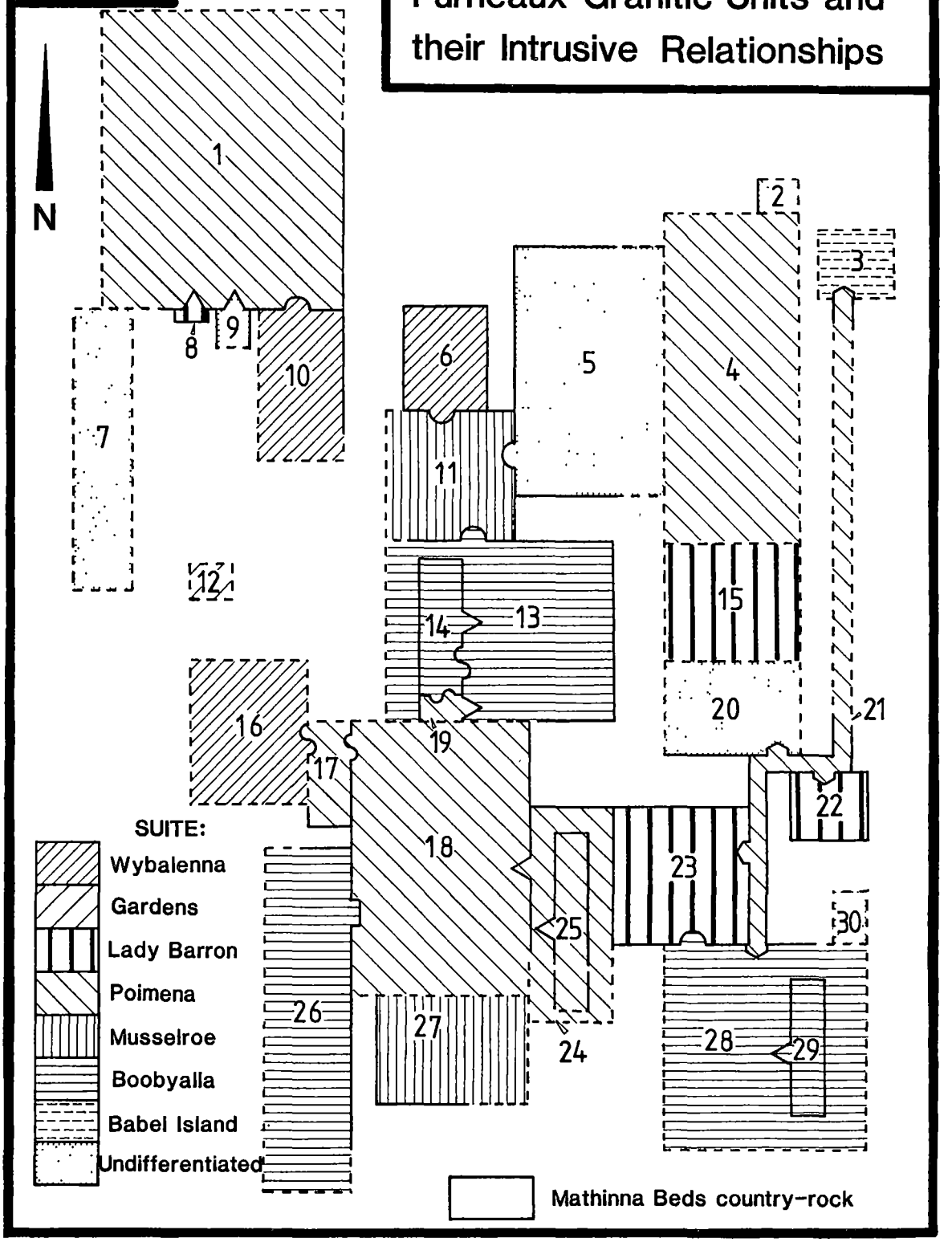

BASIS OF DESIGNATING INTRUSIVE RELATIONSHIP :

- Dyking or angular inclusions
- Chilled Margins
- Phenocryst Allignment
- Synplutonism
- Shape of contact
- Unknown

UNIT BOUNDARY:

- known
- unknown

Figure 3.1

The numbered units are indicated as being either granite (g) or porphyry (p).

UNIT	
1	Lughrata (g)
2	Red Bluff (p)
3	Babel Island (g)
4	The Patriarchs (g)
5	Sitting Goose (g)
6	Pats River (g)
7	Prime Seal Island (g)
8	Castle Rock Point (p)
9	Emita (p)
10	Wybalenna (g)
11	Martins Rise (g)
12	Little Chalky Island (g)
13	Strzelecki (g)
14	Loccota (p)
15	Lady Barron (g)
16	Chappell Islands (g)
17	The Corner (g)
18	Modder River (g)
19	Holts Point (g)
20	Franklin Sound (g)
21	Long Toms Nose (p)
22	Puncheon Point (g)
23	Dover River (g)
24	Rooks River (g)
25	Battery Hills (p)
26	Rum Island (g)
27	Clarke Island (g)
28	Cape Barren (g)
29	Hogans Hill (p)
30	Thirsty Lagoons (p)

the protolith constraints indicated by Cocker (1982). Whole-rock trends for each subset were chemically modelled as liquids undergoing Rayleigh (eutectoid-type) fractionation (Kitto, 1982; Higgins et al., 1985). Country-rock contamination is considered by each to have had a subordinate role in modifying the whole-rock chemical compositions (op. cit.).

Metallogenic studies of the tin deposits associated with the BTB granites were undertaken by Groves (1972), Groves & McCarthy (1978) and Higgins et al. (1985). These works stress the role of fractional crystallization in generating tin-enriched magmatic precursors to ore deposits. Higgins et al. (1985) stress the importance of high-temperature metasomatism of granite in the generation of ore deposits.

3.4 GEOLOGY OF THE FURNEAUX GRANITES

The total area of the Furneaux Island Group is ~1830 km^2. Twenty-two of the islands exceed 1 km^2 in area. Granitic rocks constitute ~75% of the Palaeozoic exposure with turbiditic quartz-rich distal flysch (metamorphosed to greenschist facies grade) making up the rest (Groves, 1970). Uncommon cross-cutting doleritic mafic dykes of possible Mesozoic age occur and Cainozoic units (minor quartz tholeiitic to nephelinitic volcanics, marine and eolian calcarenites, limestones and alluvium) extensively cover older lithologies (Kershaw & Sutherland, 1972).

General discriminatory features of the seven granitic suites which have so far been identified in the Furneaux Group, have been described in Chapter 2. In this section, the geological characteristics of the granites of each suite are described. The spatial distribution of these suites is indicated on Map 2 and Fig. 3.1 illustrates the spatial intrusive relationships amongst the 30 intrusive bodies that have been recognised to date.

3.4.1 Wybalenna Suite

This mafic hornblende-bearing I-type suite crops out over a wide, largely submarine area on the western side of the batholith. On land, it forms topographic depressions (e.g. the catchment of the Pats River, on the Pats River pluton), in contrast to the highs formed by the more felsic suites.

Rocks of this suite have a ubiquitous tectonic foliation (aligned biotite, hornblende and strained, smeared, subgrained quartz crystals) which parallels the main tectonic foliation in the adjacent country-rock flysch near Cape Sir John on Cape Barren Island. These features support a forceful mode of emplacement, for example by diapirism (Schwerdtner, 1978; Dutch, 1979). Supporting this proposal is the dearth of both stoped blocks

PLATE 1

This plate consists of photographs of metric-scale geological features of Furneaux Island rocks:

Fig. A Marked contact between Loccota Porphyry and underlying Strzelecki Granite on the escarpment west of Lovetts Hill (at GR ER895458) (pack for scale) At this point, the ring dyke bends over to form a sill (cf. section on Map 3).

Fig. B Tourmaline patches on pavement of Babel Island alkali feldspar granite (GR FR147768).

Fig. C Distorted biotite-rich zone at the contact between two porphyries, Babel Island (GR FR147761).

Fig. D Complex biotite schlieren within granitic dyke of The Corner Pluton, Cape Barren Island (GR ER852298). Truncation of bands indicates a facing direction younging to the top (right).

Fig. E Accumulations of garnet phenocrysts (near hammer) and alkali feldspar megacrysts (foreground) thought to be generated during relative motion between crystal-rich magma and stoped blocks of solidified roof-rock (felsic equigranular granite on left of field). GR ER877237

Figs F & G Zoned porphyry dyke, The Corner Pluton (GR ER859303). From the edge to the centre of the portion shown in Fig. F are:

a) aphyric leucocratic aplite
b) phenocryst-poor porphyry with weakly developed biotite schlieren
c) porphyry containing small (~15 mm long) feldspar megacrysts
d) porphyry containing larger megacrysts (~40 mm long)

The centre of a triangular intersection occurring where the dyke changes direction (Fig. G) contains a fifth zone: a cumulate mass of alkali feldspar megacrysts.

Fig. H Contact metamorphosed Mathinna Beds country-rock flysch ~600 m from the Strzelecki Pluton (GR ER998434). Spotting in the left-hand unit is due to growth of cordierite (now pseudomorphed). Foliation surface (S_1?) is parallel to the compositional surface (S_0).

PLATE 1

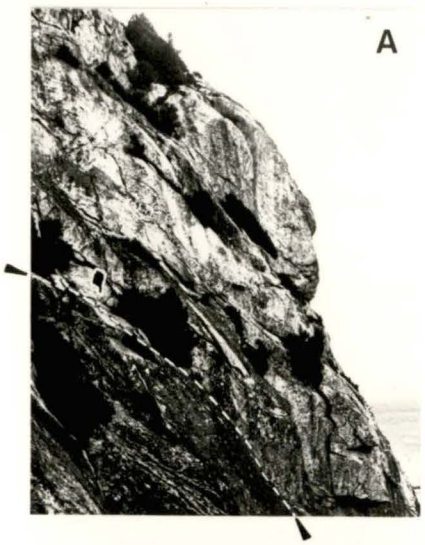

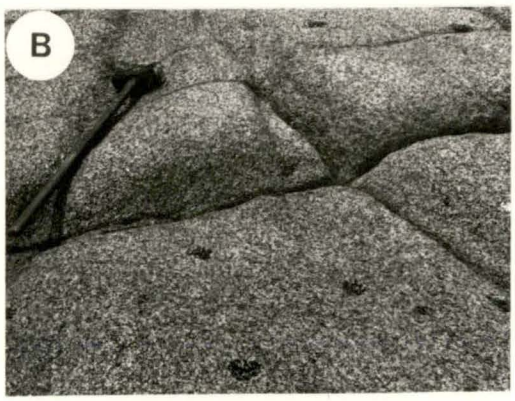

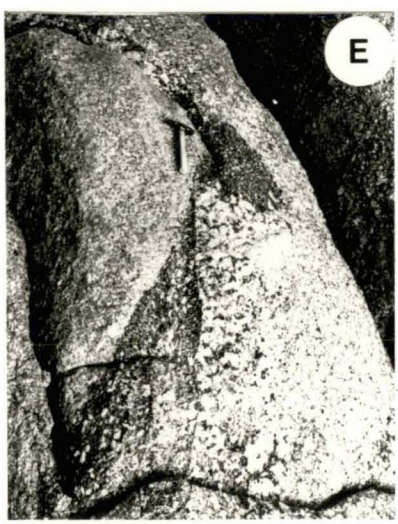

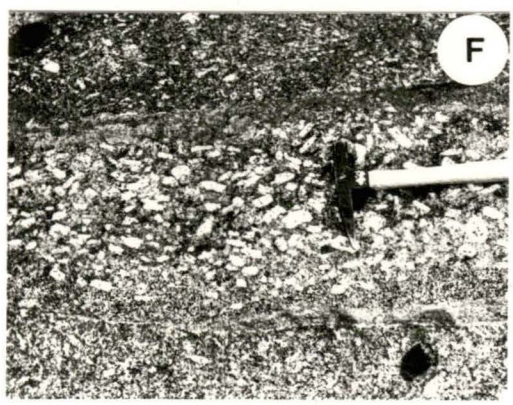

(except for sample #62636 in host sample #62635 at GR ER749692) and non-ductile multiple intrusion features which are characteristic of the brittle regime of high-level and/or cooler magmatic emplacement (Pitcher, 1978, 1979, 1981).

Spheroidal phyric porphyry inclusions are very common. They are not considered to be restite, i.e. the refractory remnants of the magma-generating partial-melting event (White & Chappell, 1977), but to be the result of pillowing and rapid freezing of synplutonically intruded, relatively mafic magmas. This is because:

a) phase and whole-rock compositions are very similar to those of sinuous tongues of porphyry (Plate 2, Fig. E) which are best interpreted to be parts of disrupted synplutonic dykes (Hill et al., 1985). They in turn may contain enclaves of phyric-rich finely-matrixed granite (Plate 2, Fig. G), again suggestive of synplutonism;

b) large inclusions have matrix grainsizes which increase inwards, consonant with heat-loss from the edge (i.e. chilling) (Vernon, 1983, 1984; Whalen & Currie, 1984; Whalen, 1984;.

c) microtextures are igneous rather than the annealed textures of granulitic partial-melt remnants (Vernon, 1983, 1984; Vernon et al., 1983).

Inclusions can be considerably more mafic than the host granite, with their fine-grained matrixes attaining andesitic compositions (e.g. matrix separate analyses of porphyries #62589, 62593 and 62610; Appendix E).

3.4.2 Gardens Suite

This metaluminous hornblende-bearing suite, well represented in the Blue Tier Batholith, is presently known only from Little Chalky Island on the western side of the Furneaux Batholith (#62576, ex-Tasmanian Department of Mines; #77-889, Jennings, 1980). The suite may be more extensive as the islands west of Flinders Island are poorly sampled. Geological features of this suite are not known.

3.4.3 Poimena Suite

This mildly peraluminous suite of biotite adamellites to granodiorites (Fig. 2.1), is the most extensive suite in the Blue Tier Batholith. It occurs throughout the Furneaux Group. Intrusive relationships indicate that many plutons of this suite have been emplaced relatively early in the intrusive sequence. However, the Long Toms Nose Porphyry was intruded as a dyke swarm late in this sequence (Fig. 3.1).

Although porphyry inclusions of the same suite occur, some porphyry inclusions are derived from Wybalenna Suite magmas (e.g. GR ER844292). Another example of hybridisation in this suite is the occurrence of

PLATE 2

This plate consists of photographs of pegmatitic and synplutonic features of Furneaux porphyries.

Fig. A Triangular section of andalusite-bearing pegmatite (#68547) surrounded by porphyry consisting of leucocratic aphyric aplite (#62616) and melanocratic layers of cumulate biotite segregations (#62615). GR ER886449.

Fig. B Section of sill consisting of layered porphyry with overlying pegmatite (GR ER939420).

Fig. C Accumulation of spheroids of phenocryst-poor porphyry with interstices of equigranular granite. Each spheroid has an alkali feldspar megacryst at its core (GR ER966418).

Fig. D Part of ~80 m wide synplutonic zone consisting of large ($\leq$2 m diam.) spheroids of fine-grained mafic Poimena Suite granite (e.g.#62581) within coarse-grained megacrystic granite of the same suite (e.g. #62582). This zone may mark the contact between the Modder River and The Corner Plutons (GR ER857300).

Fig. E Tongue of mafic (andesitic) porphyry (#62593) synplutonically intruding Wybalenna Suite granite at Settlement Point (GR ER733690).

Fig. F Hybrid zone generated during the synplutonic intrusion of the Holts Point Porphyry (Poimena Suite) into Loccota Porphyry (Boobyalla Suite). Dark spheroids of the former unit occur in a matrix of the latter. The pentagonal inclusion near the hammer is leucocratic equigranular-textured Boobyalla Suite granite, containing miarolytic cavities.

Fig. G Tongue of Wybalenna Suite granite within the mafic porphyry shown in Fig. E, demonstrating synplutonism for these two units.

Fih. H Globules of meta-basalt within the fine-grained felsic quartz-phyric porphyry of the Long Toms Nose dyke swarm (#67530, Vansittart Island, GR FR101390).

PLATE 2

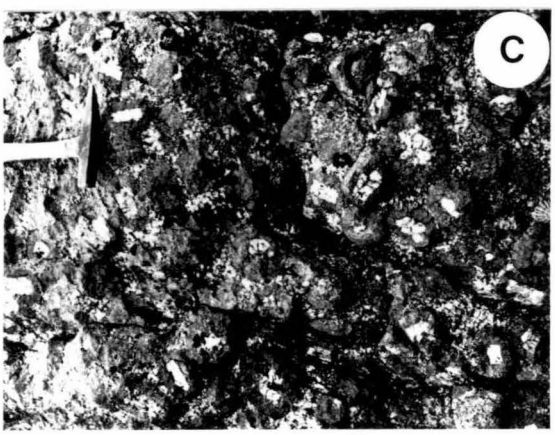

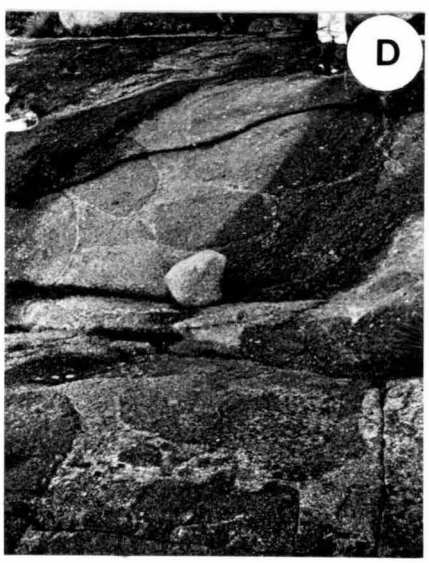

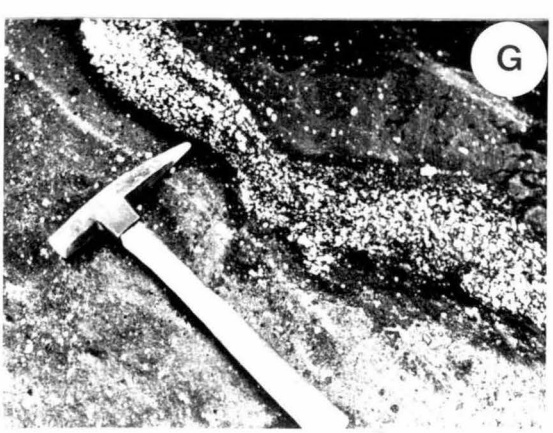

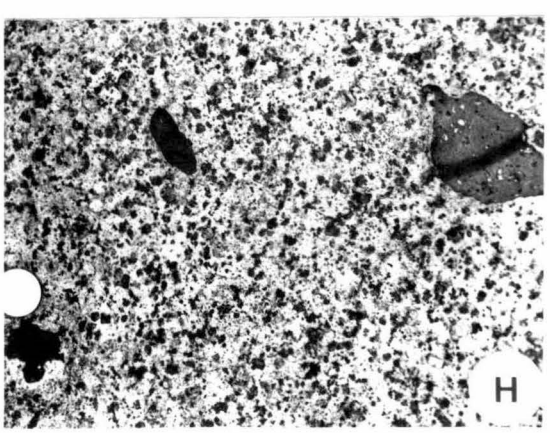

chlorite-rich blobs with basaltic chemistry (Analysis #62538, Appendix E) within a dyke of Long Toms Nose Porphyry on Vansittart Island (Plate 2, Fig. H).

A more extensive area in which magma-mixing in this suite occurred involves two varieties of granites (Plate 2, Fig. D). At this location, closely packed metre-sized inclusions of fine-grained porphyritic granite (analysis #62581; Appendix E) occur within a more felsic alkali feldspar megacrystic granite (analysis #62582).

Prominent mineral banding (both biotite and megacrystic alkali-feldspar) is a characteristic feature of this suite and will be described below. Localised boron metasomatism is indicated by the occurrence of abundant tourmaline patches which occur in coarsely crystalline granite proximal to porphyry intrusions (e.g. GR ER845292) within the Modder River Pluton. Pegmatites are present (e.g. GR ER859302 and ER917339) indicating magma saturation in a water-rich vapour phase. Development of miarolytic cavities in the felsic phyric-poor Battery Hills Porphyry (Cocker, 1977), is consistent with final emplacement depths for Poimena Suite magmas of less than ~0.1 GPa (Prof. C.W. Burnham, pers. comm.).

A more passive style of emplacement is indicated for Poimena Suite plutons compared with those of the Wybalenna Suite. The former lack the pervasive tectonic foliation of the latter, and have regions where extensive stoping and multiple intrusion has occurred (in the Rooks River Granite, Cocker, 1977). Such features are typical of emplacement into the brittle (non-ductile) regime of high crustal levels (Pitcher, 1979, 1981). These contrasting geological features could have arisen from

(a) initial emplacement of Wybalenna Suite plutons to moderate depths followed by uplift, erosion and emplacement of Poimena Suite plutons; or

(b) initial emplacement of Wybalenna Suite plutons at high temperature followed by those of the Poimena Suite at significantly lower temperature, without the need for a period of uplift and erosion.

3.4.4 Lady Barron Suite

This strongly peraluminous suite (Fig. 2.2) of two-mica adamellites (Fig. 2.1) crops out largely on the eastern side of the island group. Its intrusive relationships are poorly known. Outcrop is typically poor and topography low. Pegmatites, porphyry intrusions and inclusions are all uncommon and stoped blocks associated with intrusion are unknown. These features if not merely reflective of insufficient outcrop exposure, suggest that magmatic evolution had reached neither the stage of large-scale vapour-saturation nor emplacement to high crustal levels as is suggested for the plutons of other suites. Minor pegmatites and locally migmatised

flysch occur in the veneer of country rock which forms a roof zone over the northern 2 km^2 of the Puncheon Point Pluton (GR FR125378) between Puncheon Point and Vansittart Island. The Dover River pluton has been assigned to this suite solely on the basis of petrography.

3.4.5 The Musselroe Suite

This moderately peraluminous suite (Fig. 2.2) of adamellites (Fig. 2.1) is represented in the Martins Rise and Clarke Island Plutons. It occurs also on mainland Tasmania (the Musselroe and Ansons Bay Plutons) to the south. The granites of the Strathbogie Batholith in the Melbourne Terrane of central Victoria are close correlates of this suite (cf. Chapter 5). Geochemical sampling of this suite in the Furneaux Islands, is limited. The granites contain variable quantities of megacrystic alkali feldspar and traces of garnet can usually be seen.

Mafic mineral segregations associated with synplutonic intrusions are known on mainland Tasmania (GR FQ105583).

3.4.6 The Boobyalla Suite

This moderately to strongly peraluminous suite (Fig. 2.2) of garnet-bearing granites to adamellites (Fig. 2.1) is widespread in the northern part of the batholith. In addition, many granites of the Wilsons Promontory Batholith at the northern end of the Bassian Terrane are, on petrological and chemical grounds, close correlates of this suite (cf. Chapter 5). In the Furneaux Islands, the plutons of this suite were emplaced late in the intrusive sequence (Fig. 3.1). Pegmatites, miarolytic cavities and same-suite porphyry intrusions and inclusions are all common. Sills are often segregated with pegmatitic tops overlying phenocryst-poor porphyry (Plate 2, Figs A and B) which may grade down to phenocryst-rich basal varieties (Plate 2, Fig. A). The top part of this stratigraphy may be repeated to yield laminated stacks of phenocryst-poor porphyry and pegmatite analogous to the "line-rock" sills associated with the Cornish tin granites (Badham, 1980) as shown on Fig. B of Plate 2.

These features may be the result of multiple intrusion. Alternatively, they might have been generated by double diffusive convection, where the density of a single magma body is controlled not only by a temperature gradient but also by a gradient in another intensive variable, such as water activity (Huppert & Turner, 1981; Sparks et al., 1984; Marsh & Maxey, 1985). During such convection, a large number of stacked cells can develop within the enclosed volume of magma (op. cit.). Exsolving of a water-rich fluid from the silicate-rich liquid will follow the attainment of vapour-saturation which might lead to the development of the discontinuous linear structures, each one after a flat stacked cell in original convecting magma.

Many angular granitic inclusions (up to 200 m in length) have been recognised in shoreline exposures of both the Rum Island and Strzelecki Plutons (Plate 1, Figs E and G; Map 3). They are composed of equigranular felsic granite which contains numerous miarolytic cavities, indicative of high-level emplacement. They are interpreted as being stoped blocks of a particularly felsic variety of Boobyalla Suite granite. They are probably remnants of felsic roof-rocks which have subsequently been reintruded and broken up by its related phenocryst-rich magma. These features suggest that both of the Rum Island and Strzelecki plutons were compositionally zoned in the vertical direction. This is supported by observations made across the outcrop of the Strzelecki pluton within the Strzelecki National Park. These show that the granite along the shoreline is rich in large alkali feldspar megacrysts and is relatively mafic. In contrast, granite near the summits of the Strzelecki Peaks (777 m) and Mt Razorback (610 m) are more felsic and consist of low to moderate concentrations of alkali feldspar, quartz and plagioclase phenocrysts in a finer grained granitic groundmass. In addition to the vertical zonation, a horizontal compositional zonation may exist. Granites near the inferred margins of plutons (e.g. #62584 from the Rum Island Pluton and #67548 from the Strzelecki Pluton) are more mafic than those near pluton centres (e.g. #62625 from the Strzelecki Pluton).

Large-scale same-suite intrusions are associated with Boobyalla Suite plutons, such as the ring-dyke and sill complex of the Loccota Porphyry (Plate 1, Fig. A; Fig. 3.1) and the Hogans Hill Porphyry of the Cape Barren Pluton, respectively. These are features typical of the large-scale intrusive mechanism of cauldron subsidence which occurs during high-level emplacement. Spectacular features ascribed to this intrusive mechanism have been described from the Andean Cordillera (Pitcher, 1974, 1978, 1979, 1987) High levels of emplacement for the Boobyalla Suite plutons are therefore indicated.

An extensive area of synplutonism occurs within the Strzelecki Pluton at Holts Point (Plate 2, Fig. F), where a mafic Poimena Suite porphyry, the Holts Point Porphyry (#62612), intrudes both the Loccota Porphyry and the host Strzelecki Granite. Megalithic flysch C.R. inclusions are also present. A complete continuum from massive Holts Point Porphyry through pillowed mixtures to an intermediate relatively uniform hybrid (#62614) occurs. Other examples of extensive hybridization have been documented by Whalen (1985), Vernon (1983, 1984) and Vernon et al. (1983).

3.4.7 Babel Island Suite

This suite consists of the Mt William granite (Groves, 1972) on mainland Tasmania and the Babel Island granite in the Furneaux Islands.

They are medium to coarsely crystalline equigranular alkali feldspar granites. The geomorphology of Babel Island suggests it to be a large-scale sheet-like body dipping gently to the west, away from the low lying Cat and Storehouse Islands further east. It therefore resembles the morphology of the Mt William granite which has a sheet-like form (op. cit.; Kitto, 1982).

Pegmatites and synplutonic porphyry intrusions and inclusions are widespread. Sills are frequently laminated (e.g. GR FR147760) as they are within Boobyalla Suite intrusions. Garnet-rich mineral segregations do occur, but are rare (e.g. GR FR137758).

Large areas ($10^3 m^2$) of granite containing abundant patches of tourmaline occur on pavements along the Babel Island shoreline (Plate 1, Fig. B). They are only found within about 3 m of porphyry sills and dykes or that of their projected positions. They testify to vapour-phase transmission of boron (boron metasomatism) into the surrounding host rock from the porphyry magma.

3.5 MINERAL ACCUMULATIONS AND THEIR ORIGINS

Poimena Suite granites, and especially its dykes, often contain areas in which there are abundant biotite-rich bands. In dykes they form linked cuspate biotite schlieren, which are sections of superposed shallow to deep bowl-shaped surfaces. They are extensively developed near the footwall and poorly developed at or absent from the hangingwall (Plate 1, Fig.D).

Schlieren have a fine grained biotite-rich sharp-edged boundary at the base. This grades diffusely upwards, coarsening to a more homogeneous and representative granitic mineralogy. This facing direction (diffuse towards the dyke centre and sharp towards the dyke edge) is maintained even when complex superposition of schlieren occurs or when the original dyke is distinguishable from the host granite only in terms of subtle mineralogical contrasts. Isolated paired or single, often distorted biotite schlieren (e.g. Plate 1, Fig. C) frequently delineate remnants of deformed dismembered synplutonic dykes. Similar banding has been described by Barriere (1976) in the hornblende/biotite granite unit of the P'loumanach Complex of Brittany. He interprets superposed schlieren as being due to the fluid dynamic effects of changing convection cells within a dyke which is in an overall state of accreting solid-enriched magma onto its walls (op. cit.).

Impressive concentrations of alkali-feldspar megacrysts often occur along the centre line of porphyry dykes. Megacrysts are uncommon adjacent to intrusion margins.

Many features of these banded structures can be understood as the manifestation of two simultaneously operating fluid dynamic processes:

(a) the Bagnold Effect (op. cit.; Bagnold, 1954; Komar, 1976; Thompson & McBirney, 1985; Marsh & Maxey, 1985) which will propel suspended crystals away from a dyke wall according to crystal size, crystal concentration and dyke narrowness (op. cit.) and

(b) Gravitational crystal fractionation which sediments crystals according to the crystal/magma density contrast, grainsize and magma velocity (Marsh & Maxey, 1985).

The simultaneous operation of these two processes appears to qualitatively account for:

(a) the decrease in the mean grainsize across schlieren in the direction from the dyke centre to dyke margin;

(b) the occurrence of weak but symmetrically disposed biotite schlieren at the margins of dykes which are vertical (Plate 1, Fig. F) in contrast to the assymetric development of schlieren (extensive at the base and diminutive or absent at the top in dipping dykes or in sills (Plate 2, Figs A and B);

(c) the common development of schlieren in narrow (<1 m wide) dykes and the paucity of schlieren development in large (~100 m wide) dykes; and

(d) the prevalence of the biggest schlieren in intrusions containing pegmatites (e.g. Plate 2, Fig. A) which indicate magmatic vapour saturation and therefore minimal melt viscosities for any particular magmatic temperature (Shaw, 1963a, 1965, 1972; Burnham, 1975, 1979; Scarfe, 1986).

Narrow intrusions may be so intensely zoned as to appear to be composite. Sharp boundaries delineate five distinct zones tonguing one into the next, in a dyke within the Modder River Pluton (GR ER845295). In order, these are:

a) an ~30 mm wide aplite selvage at the edges, then

b) a microgranitic zone with weak biotite schlieren development, then

c) an alkali feldspar phenocryst-rich zone containing well sorted crystals about 15 mm long, then

d) a similar zone populated by well-sorted megacrysts ~40 mm long, and finally

e) a localized cumulate core zone consisting of packed alkali feldspar megacrysts.

All but the last zone are shown in Fig. F of Plate 1. The temporal sequence of bulk compositions from aplite to crystal-rich magma is the

reverse of that predicted by pure fractional crystallization of an initial melt. The latter would predict the most refractory composition at the dyke margin and the least refractory composition at the core, rather than the reverse. An explanation involving the relative movement of the solid and liquid phases in a suspension, as has been described above, is in qualitative accordance with the features exhibited. It is also possible however, that the magma which was tapped by the dyke was itself a layered series of suspensions.

Chemical (rather than rheological) processes are not thought to have been dominant in generating these mineral bands, although sequential crystallization of melt in dykes might be expected to generate marginal rocks which are richer in biotite compared with those at the dyke core because biotite nucleates more rapidly than do framework silicates during undercooling. However such a process should generate symmetric rather than assymetric zoned intrusions. Crystallization is expected merely to augment the development of schlieren generated largely by rheological processes (Barriere, 1976).

Another more localized form of mineral banding is exhibited at the contact of the Clarke Island Pluton of the Musselroe Suite, with the Mathinna Beds flysch. It is marked by a ~2 m wide zone of orbicular structures consisting of subangular hornfelsed flysch inclusions and magmatic alkali feldspar megacrysts, each with ~15 mm wide leucocratic rind of radiating alkali feldspar and quartz dendrites (analysis #62588R). These occur within a medium-grained granitic matrix (analysis #62588). Radiating crystal textures similar to those in these orbicular rinds have been produced experimentally in felsic haplogran(odior)itic magmatic systems by Fenn (1977) and Swanson (1977). They require high degrees of undercooling ($> \sim 150^{\circ}C$) and indicate high growth rates ($\sim 10^{-5}$ mm s^{-1}). However the geological location of this mixed rock at the pluton/country rock contact, together with the alkali feldspar-rich non-minimum melt composition of these rinds suggest that vapour derived either from the magma or from country rock dehydration could have been important in generating the features of this mixed rock. Similar phenomena have been ascribed to local fluidisation and gas-coring effects in the Donegal Batholith (Pitcher & Berger, 1972). A vapour-saturated magmatic environment in rind development also accords with the proposal of Vernon (1985) that structures such as these form from locally superheated magmas.

Spectacular knots and trains of large ($\leq$15 mm diam.) garnet crystals and alkali feldspar megacrysts ($\leq$100 mm diam.) (Plate 1, Fig. E) occur as cylindrical streamlines to megalithic inclusions or as isolated accumulations within many phyric-rich Boobyalla Suite granites (e.g. GR

ER966418). They are interpreted as resulting from the combined processes of filter pressing and the Bagnold Effect (described for the Poimena Suite, above) which operated as the large blocks of equigranular granite stoped off during high-level intrusion, sank through crystal-rich magma below.

Examination of these crystal accumulations shows that the mean size of their alkali feldpsar megacrysts is smaller than that in the surrounding granite. This indicates that growth of alkali feldspar crystals has occurred subsequent to stoping. Accordingly, the magma at the time of stoping was somewhat less phenocryst-rich than is indicated by the present proportion of phenocrysts to groundmass phases within Boobyalla Suite porphyritic granites. In the host granite, megacrysts often contain rings (surfaces) of inclusions (quartz, plagioclase, biotite or garnet) which probably indicate an acceleration in the growth rate of alkali feldspar. Such rate changes may result from purely physical causes, e.g. an increase in the degree of under-cooling (Swanson, 1977; Fenn, 1977) or from a change to a more alkali feldspar-rich equilibrium magmatic assemblage associated with progressive magmatic evolution.

Garnets within the mineral accumulations are usually larger than isolated garnets within the host magma which if they occur at all, are present only as remnant cores sheathed in biotite. Garnets were clearly in a reaction relationship with the magma subsequent to (and possibly during) the stoping stage of emplacement. There is no evidence for garnet (or biotite) formation by any localized inclusion-melt reaction during stoping, as suggested by Kitto (1982) and Higgins et al. (1985) because:

(a) the edges of stoped megaliths have the same (very low) colour index as do their cores; and

(b) growth rates of garnet and alkali feldspar are not likely to be high enough to yield the large crystals observed during the time passage of a sinking block.

Microgranitic patches and selvages occur adjacent to the megalithic inclusions. They are interpreted as being the chilled liquid-enriched counterparts to the crystal-enriched streamlines (GR ER896439). Accumulations of ~90 mm diameter spheroids occur at one location near a megalithic inclusion (GR ER908429). Each spheroid consists of a single alkali feldspar megacryst within a microgranitic rind (Plate 2, Fig. C) with equigranular granite interstitial to them. This feature might have resulted from the coating of megacrysts concentrated during stoping, by silicate melt expelled during filter-pressing.

Chapter 4
PETROGRAPHY AND PARAGENESIS

4.1 INTRODUCTION

In this chapter, rock and mineral textures are described with the aims of:

a) supporting the view that most Furneaux granitic magmas were suspensions of crystals in melt,

b) deducing the phases which were present in the magmas of each granitic suite, and

c) demonstrating that (re)crystallization and subsolidus reactions have variably modified the pre-existing magmatic features.

Phase parageneses are then constructed which show that solid/melt reactions occurred during the magmatic stages of petrogenesis.

4.2 TEXTURAL VARIATION AMONGST ROCKS

Most of the textural variation amongst these granitic rocks may be conveniently described in terms of a **grainsize range**, reflecting variation from aphyric to porphyritic textures and a **matrix grainsize**, reflecting variation from cryptocrystalline to coarsely crystalline textures.

These two aspects of rock texture are not independent. Rocks with a coarse matrix grainsize will usually have a smaller range in grainsize, few phases occurring as phenocrysts and phenocryst identification will be more ambiguous.

Some rocks exhibit a third textural aspect: **mineral alignment**. This feature may be non-penetrative and localized, where it may be ascribed to fluid dynamic flow during its magmatic stages of petrogenesis (cf. Chapter 3). This type of alignment is especially marked in porphyry intrusions (Plate 1, Fig F; Plate 2, Fig. A). In other rocks, alignment is penetrative as for example in the Chappell Islands granite at Cape Sir John. In this case, the alignment was generated during post-magmatic stages of petrogenesis. Foliation development may be locally intense, with development of mylonites (GR FR836252, sample #67534). Penetrative alignment development, unlike the non-penetrative kind, progressively obliterates all other textures. Pursuit of the magmatic features of granites is therefore best undertaken in rocks where penetrative foliation development is minimal.

These textural aspects lead directly to the following petrogenetic conclusions:

(a) In rocks with a large grainsize range, a small matrix grainsize and no discernible mineral alignment, then the matrix is an analogue of the former melt phase.

(b) In rocks with a small grainsize range, large matrix grainsize and no discernible mineral alignment, the identification of phenocrysts, xenocrysts and the crystallised melt phase is difficult or entirely subjective. Slow cooling and/or rapid crystal growth maximize the likelihood that the final coarsely crystalline rock must be interpreted as having been an indeterminate mix of phenocrysts and xenocrysts in a melt phase.

(c) In rocks where a significant non-penetrative mineral foliation is present and/or where mineral segregations occur, the operation of select mechanisms associated with magma emplacement are indicated. These are (i) physical mechanisms of crystal/melt separation partially modified by (ii) chemical crystallization of the melt. as discussed in the previous chapter.

(d) In rocks with a significant penetrative mineral alignment, solid-state deformation - often having continued down-temperature from inception during forceful magmatic emplacement - has lead to extensive or complete replacement of the pre-existing magmatic phases and their textures.

Rocks in group (a) will therefore provide the most information about the earlier (for instance: magmatic) stages of petrogenesis. However, certain matrix-poor mineral segregations in group (c) rocks provide critical information about mafic magmatic phases. Estimates of the nature of the magmas of the rocks of groups (b) and (d) may then be augmented with information obtained from mineralogically and chemically related rocks from groups (a) and (c).

4.3 MAGMATIC PHASES AND THEIR TEXTURES

A petrographic description of all identified phases is given in Table 4.1. Porphyry matrixes are the analogue of the critical magmatic phase: melt. The mean matrix grainsizes of porphyries vary continuously from the arbitrarily chosen upper limit of 1 mm, down to the cryptocrystalline scale. In the latter matrixes (e.g. #67533), melt flow-lines and spherulitic devitrification textures are widespread. Even tiny opaque-phase crystals (~0.05 mm long) are clearly recognised as phyric phases. At the other end of the porphyry matrix grainsize scale (e.g. #62595), most accessory minerals (ilmenite, apatite, zircon, monazite and xenotime) can no longer be distinguished clearly as phyric phases. Much of the biotite present may even be disguised microphenocrysts, in the light of the small

Table 4.1

Petrography of Furneaux Granitic Rocks

Abbreviations: (linear dimensions in mm)

ac	actinolite	ad	andalusite
af	alkali feldspar	al	allanite
anh	anhedral	ap	apatite
as	arsenopyrite	bi	biotite
bl	blue	bn	brown
cd	cordierite	cl	chlorite
cm	cummingtonite	col	colourless
cp	clinopyroxene	cuboct	cuboctahedra
cy	chalcopyrite	d	diameter
esp	especially	euh	euhedral
ext	extinction	FI	fluid inclusions
fl	fluorite	ga	garnet
gn	green	gr	granite(s)
gu	grunerite	hm	hematite
i	inclusions	il	ilmenite
interstit	interstitial	l	length
lq	liquid	LTNP	Long Toms Nose Porphyry
mn	monazite	min segrs	mineral segregations
mod	moderately	mo	molybdenite
ms	muscovite	mot	mottled
myrm	myrmekite	mt	magnetite
op	orthopyroxene	octah	octahedra
pegm	pegmatite(s)	oscill	oscillatory
pleo	pleochroism	pl	plagioclase
poik	poikiloblast(s/ic)	po	pyrrhotite
por	porphyry	pseud(s)	pseudomorph(s)
qz	quartz	repl	replacing
ru	rutile	sauss	sausseuritized
si	sillimanite	sn	sphene
sp	spinel	tm	tourmaline
tz	topaz	u	uraninite
v	very	var	various
vp	vapour	w	width
xn	xenotime	xtl(s)	crystal(s)
yl	yellow	zr	zircon
<	less than	>	greater than
~	approximately		

TABLE 4.1 PETROGRAPHY OF FURNEAUX GRANITIC ROCKS.

SUITE / PHASE	WYBALENNA	GARDENS	POIMENA	LADY BARRON	MUSSELROE	BOOBYALLA	BABEL ISLAND
QUARTZ	a) anh xtl aggregates <15 l strained, subgrained with undulose ext b) ~0.5 m (bi+qz+pl+hb) hb sheathed pseud (after op?) i: pl, ru (a), bi, ap, af	Weakly strained anh to subh xtls <8 d i: bi, ap, pl	a) Anh xtls <8 d b) interstices to other phases c) embayed euh (-qz)<6 d in LTNP i: bi, pl, af, ap	Anh xtls <9 d mod. sub-grained, undulose ext. i: bi, mu, zr, ap, pl, af, mt	Anh xtls <7 d, ribbon subgrained, undulose ext i. bi, cd, ap, zr, ga	a) anh-subh xtls (qz) <10 d, some with rutilited cores, clear mantles b) anh-euh <200 l in pegmatites c) botryoidal sheaves <100 w intergrown with ms i: Fl (lq, vp) bi, ru, ga, ap, zr, af	a) anh xtls <10 d coarsely subgrained, intergrown with pl, af, to b) graphic intergrowths with pl, af in mgr c) anh-euh xtls <50 d in pegm i: bi, zr, ap, mu, cd
PLAGIOCLASE	a) In gr: mot. An53 cores <8 d, 1 or 2 narrow (~0.05w sauss shells (after An-rich spikes?). Normal + oscill. zoned mantles i: zr, ap, hb, bi, qz murm at af boundary b) In por: frequent corroded shell remnants of calcic pl in uniform cores with strong oscill. zoning in mantles.	Weakly mot. cores, An77, <5 d, occasionally oscill. zoned i: il Normal + oscill. zoning in narrow mantles.	Weakly mot. to clear cores <10 l of An55 then wide mantle of normal + oscill. zoning i: qz, bi, ap, il, zr myrm. at af boundary	Mot. An25 cores <8 d mantles with normal + oscill. zoning. i: ap, bn, bi (at rims), ad myrm at af boundary	Subh An40 cores <15 l, wide normally zoned mantles i: ap, zr, bi, il, cd	Subh patchy An44 cores <12 l, wide mantles with normal to normal+oscill. zoning to An3 i: ap, zr, bi, qz, af	Broadly normally zoned anhed. from An30 <8 d intergrown with af, qz i: af, qz, ad
ALKALI FELDSPAR	a) Perthite anh xtls inter-stit. to other phases b) Perthitic euh. prismatic megacrysts <60 d c) dendritic poik. in mgr. i: other phases myrm at pl boundary.	Perthitic anh xtls interstit. to other phases.	a) perthitic anh xtls inter-stit. to other phases b) Coarsely perthitic euh. prismatic megacrysts <80 d i: qz, bi, pl, zr, ap, often in shells of i. tracing growth rate spurts	a) Perthitic anh xtls inter-stit. to other phases b) Perthitic euh. prismatic megacrysts <50 d i. bi, qz, pl, ap, cd	a) perthitic euh prismatic megacrysts <100 d b) smaller (<3 d) perthitic anh xtls with similar qz+pl i: ms(repl), bi, qz, pl, ap, zr, cd	a) perthitic euh prismatic megacrysts <120 d b) smaller (<3 d) perthitic anh xtls with similar qz+pl i: bi, qz, pl, ap, zr, ga, cd c) yellow subh <200 l in pegm.	a) microcline anh xtls <10 d intergrown with qz, pl, graphically in mgrs, pegm i: pl, qz, bi, ga
BIOTITE	a) subh. flakes <5 d with kakhi pleo. where hb-richest to bn pleo. where hb-absent b) bn pleo flakes repl. hb topoaxially i: zr, ap, mt, il, al c) small (<0.5 d) bn flakes with qz+hb+pl pseuds (after op?)	Bn subh. flakes <3 d proximal to or repl. hb. Colour becomes reddish when partly repl. by cl along (001) i: il, zr, ap	a) bn subh. flakes <7 d. b) small (<0.5 d) bn flakes with qz, il as mafic min. pseuds (after op?). c) small (<0.1 d) red-brown i in v. rare ga d) pale brown flakes <0.5 l in v. rare schistose (bi+sp+si) i. i: il, ap, zr, sn	a) red brown subh. flakes <4 d grading to fine grained (<0.2 d) loose clusters in qz, all interstit. to large pl, qz, cd grains. i: ap, zr, il, sn b) pale green intergrowths with ms+cl after cd. c) fine grained (<0.5 d) intergrowths with qz, il after op?	a) red-bn subh flakes <8 d grading to b) red-bn (<1 d) flakes intergrown with qz, il in pseuds after ga and other mafic phases (<10 d) c) reddish subh i in ga i: il, zr, ap, mn, xn d) pale bn networks with qz after mafic i in ga e) pale gn intergr with ms±cl after cd f) gn flakes after ga	a) red-bn subh flakes <9 d, grading to b) red-bn (<1 d) flakes intergrown with qz, il in pseuds after ga and other mafic phases (<10 d) c) reddish subh i in ga i: il, zr, ap, mn, xn d) pale bn networks with qz after ah-cm i in ga e) pale gn intergr with ms±cl after cd f) gn flakes after ga g) red-bn flakes <100 d in pegm	a) small (~1 d) red-bn flakes as matrix phase usually partly to wholly altered to cl+ms+Ti oxides b) <3 d pale gn flakes intergrown with ms±cl as pseuds after cd c) rare corroded flakes <5 d usually partly repl by (cl+ms+Ti oxides)

Table 4.1 cont.

SUITE / PHASE	WYBALENNA	GARDENS	POIMENA	LADY BARRON	MUSSELROE	BOOBYALLA	BABEL ISLAND
MUSCOVITE			rare flakes <1 d oriented parallel to bi flakes at interface of bi and af.	a) flakes <3 d in intergrowths with gn, bi+cl after cd. b) <0.7 d flakes in sauss. pl cores c) sheaved of flakes <1 d after or mantling ad.	a) flakes <3 d as intergrowths with gn bi±cl after cd b) skeletal networks repl late-stage af c) tiny flakes (<0.5 d) in pl cores	a) flakes <3 d as intergrowths with gn bi±cl after cd b) sheaves of flakes <1 d after or mantling ad c) skeletal poik <10 l repl late-stage af or mgr matrix phases d) tiny flakes (<0 5 d) in pl cores e) large blades <100 l intergrown with qz in botryoidal textured habit in pegm	a) sheaves of flakes <2 d after or mantling ad b) coronas of small (<0.05 d) flakes around altered bi flakes c) flakes <2 d with dendritic fringes as alteration [product of af
HORNBLENDE	bn cored, bl-gn rimmed euh-subh prisms <6 d grading inwards both towards ac after cp? and cm after op. Sheathed and partly repl. by bi i: pl, op, mt, il, bi	brown to blue-green zoned euh-subh prisms <4 l, or as rims to ac. Rings of pl. i occur at graded boundary between brown and green hb i: ac, bi (repl), pl, zr, hm					
ACTINOLITE	pale green-yellow fibrous patches <1 5 d in hb both grading in pleo. and with sinuous discontinuity with hb after cp? Abuts rare corroded op xtls then grades to hb	bladed masses <3 d rimmed by and grading into and partly distontinuously abutting peripheral hb.					
CUMMINGTONITE GRUNERITE	<0.3 w discontinuous coronas of cm around op remnants, mantled in turn by actinolitic hb					very rare prisms of gn <0.4 l in subrounded i <1 d in ga possibly after op	
ORTHOPYROXENE	a) rare corroded subh xtls <1.5 l, mantled by ac grading into hb, sheathed in bi b) ac cores to hb after op (or cp?)	ac cores to hb after op (or cp?)	some (bi+qz) intergrowths possibly pseuds after op		some (bn bi+qz+il) intergrowths possibly pseuds after op both as phens or as i in ga	a) some (bn bi+qz+il) intergrowths possibly pseuds after op, both as phens or as i in ga b) as possible precursor to ah-cm i in ga	

Table 4.1 cont.

SUITE / PHASE	WYBALENNA	GARDENS	POIMENA	LADY BARRON	MUSSELROE	BOOBYALLA	BABEL ISLAND
GARNET			a) v. rare corroded grains <8 d, within (yl bi+qz) schistose matrix i: reddish bi b) v. rare qz enveloped grains <0.3 d in por matrixes		Large (<10 d) euh to anh xtl remnants often within bn bi and/or qz i: red-bn bi, gn bi (repl) il, zr, ap, cd, si, sp, Fl (rare, at edges)	a) large (<12 d) euh to anh remnants often within bn bi or qz or (ex) cd. i: red-bn bi, gn bi (repl), il, zr, ap, ah, cm b) small <2 d subh xtls in bi prograde after bi within 50 cm of edge of granitic megalithic i c) v. rare grains <0.4 d in por matrices	Rare <3 d subh xtls surrounded by qz envelope within af
CORDIERITE			V. rare corroded grains <8 d, within (yl bi+qz) schistose matrix i: reddish bi b) v. rare qz enveloped grains <0.3 d in por matrixes	a) <10 l intergrowths of (pale gn bi+ms±cl) after cd i: ap, zr b) small (<0.5 d) rhombic intergrowths of (pale gn bi+ms±cl) after subh prisms of cd	a) euh prisms <0.5 l as incl in ga b) large <10 d subh prisms / anh xtl interstices to other phases in mafic min. segr. (var. replaced) c) remnants <2 d in pinite or (gn bi+ms±cl) pseuds after cd phens <12 d in host granite d) small (~0.5 d) subh xtls with felsic phases and bn bi interstit. to qz, pl, af phens e) dendritic poik <12 d in por matrices	a) large to small <12 l rhombs of pinite to (gn bi+ms±cl) pseuds after cd in gr, por b) small (<0.2 d) (gn bi+ms ±cl) pseuds after cd in por matrices c) dendritic poik <12 d in por matrices and in mafic min segrs where ga occurs as remnants d) large <10 l rhombs in mafic min segrs (var. repl). e) large (<70 x 30) clear purple euh prisms in pegm	a) med to small (<7 d) pinite to (gn bi+ms±cl) pseuds after euh cd b) dendritic poik <20 d in por matrices
TOURMALINE			a) skeletal poik <30 l repl af proximal to pegm with straw col. cores then sharp boundary with orange-gn rims and occasional blue fringes (TS). Rim-tm co-existing with bi b) poik tm <200 d patches in por and host gr. may be the only AFM-type phase, locally		Anh crack infilling within corroded ga, with pl pleo.	a) khaki schorl. after ga b) sharply zoned ochre/ khaki schorl in pegm or granites, may be the only AFM-type phase, locally c) poik tm (<200 d) ("suns") in por and host gr. may be the only AFM-type phase, locally	a) orange pleo poik. (<200 d) patches in host gr local to por intrusions, may be the only AFM-type phase, locally b) sprays of euh coexisting with cd in pegm.
SILLIMANITE			Tiny (<0.2 w) fibrolitic needles in v. rare (sp+yl bi) i in gr		Euhed prisms (<0.4 l) as subparallel oriented in in ga		

Table 4.1 cont.

PHASE \ SUITE	WYBALENNA	GARDENS	POIMENA	LADY BARRON	MUSSELROE	BOOBYALLA	BABEL ISLAND
ANDALUSITE				a) uncommon pink to col. pleo. corroded remnants (<2 d) of stubby phens <5 l), mantled in ms b) small (<0.2 d euhed prisms in mantle pl		a) corroded remnants to subh stubby prisms (<6 l) often with pink pleo cores, var. repl. by ms b) primsatic subh needles <8 x 1 with pink pleo cores in pegm.	a) common non-pleo subh to anh remnants <4 d in gr and mgr b) small (<0.2 l) rhombic i in pl
SPINEL			v. rare schistose intergr {sp(<0.2 L)+bi(<0.5 l)+ si(<0.2 w)} i ingr		small (<0.1 d) octah i within cd i, in ga cores	tiny ~0.02 d octah in (gn bi+ms±cl) speuds after cd within 50 cm of edges of megalithic gr i	
MAGNETITE	cuboct <0.1 d in hb or bi pseuds after oip, cp or hb	cuboct <0.1 d in hb or bi repl hb		v. rare cuboct <0.5 d in qz			
URANINITE?						tiny (~0.005 d) rhombic i within xn i, within red-bn bi i in ga from a mafic min segr (only U peaks in micro-probe energy spectrum)	
ILMENITE	a) subhed to anh xtls <0.3 l in bn bi, hb b) thin (<0.05 w) plates parallel to 001) in bn bi c) tiny (<0.1 l) onented i in bn cores to hb phens i: ap, zr	a) stubby subh xtls <0.25 l assoc. with mafic phases b) thin (0.05 w) plates parallel to (001) in bn bi i: po	a) stubby subh xtls <0.4l assoc. with mafic phases b) thin (<0 05 w) plates parallel to (001) in bn bi	as <0 3 l platey xtls in bn bi var. altered to sn	a) large <0.7 l subh plates with (qz+bn bi+ap+zr+mn+ xn) pseuds after mafic phase b) thin (<0.05 w) plates parallel to 001 in bn bi i: zr, ap, mn, xn	a) large <1 l subh plates with (qz+bn bi+ap+zr+mn+ xn) pseuds after mafic phases b) thin (~0.05 w) plates parallel 001 in bn bi i: zr, ap, mn, xn	very rare i in bn bi: usually altered to sn
SPHENE	rare euh xtls <0.5 l	rare euh xtls <0.5 l	a) intergrown with cl+il as pseuds after bn bi esp. those within af megacrysts b) Al-rich var. as clusters of subh xtls <0.5 l in cl after il in bn bi within LTN por	as subh xtls <0.5 l i after il in bn bi			
ALLANITE	rare khaki euh prisms <0.7 l		growth-zoned khaki euh prisms <0.7 l i: ap				

Table 4.1 cont.

SUITE / PHASE	WYBALENNA	GARDENS	POIMENA	LADY BARRON	MUSSELROE	BOOBYALLA	BABEL ISLAND
APATITE	tiny (<0.1 w) needles within bi	tiny (<0.1 w) needles within bi, qz, pl	a) large (<0.5l) stubby euhed prisms assoc with bi, to b) small (<0.03 w) needles, often arranged in rings within bi	a) large (<0.4 d) stubby euh prisms assoc with bn bi, to b) small (~0 01 w) needles within bn bi c) small (~0.02 w) stubby euh prisms within il	a) large stubby (<0.6 l) euh prisms assoc with bn bi, to b) tiny (~0.01 w) needles within bn bi, pl, af	large (<0.4 d) stubby euh prisms assoc with bn bi, to b) tiny (~0.01 w) needles within bi i: zr	rare stubby euh prisms <0.2 d, in clusters of ~5 in qz
XENOTIME					squat (~0.1 d) euh prisms in (qz+bn bi+il) pseuds after ga	squat (<0.3 l) euh prisms in (qz+bn bi+il) pseuds after ga i: ur	
MONAZITE					squat (~0.1 d) euh prisms in (qz+bn bi+il) pseuds after ga	squat (<0.3 l) euh prisms in (qz+bn bi+il) pseuds after ga	
ZIRCON	subh prisms <0.15 l in bi sometimes cored	rare uncored euh prisms <0.1 l in bh	large (<0.4 l) euh prisms in bi, usually zoned	zoned euh prisms <0.15 l esp. assoc with bi	unzoned euh prisms <0.15 within (bn bi+qz+il) pseuds after ga	unzoned euh prisms <0.5 l within (bn bi+qz+il) pseuds after ga	small <0.1 l unzoned euh to subh prisms assoc with bi
FLUORITE						rare poik <1 d within (bn bi+qz+il) pseuds after mafic phases	purple euh prisms <6 d with po and ms in miarolytic cavities in phyric-poor por
TOPAZ					v. rare euh prism ~1 l with cd, bn bi, interstit to qz Endented by bi i: Fl (multiphase), bi, zr		anh <4 d xtls with qz, (trace) mo, in vein cutting Babel Is gr
PYRRHOTITE		small (~0.03 d) xtls within il	large (<2 d) anh grains repl bi in LTNP		a) elongate (<10 l) anh xtls interstit to ga in mafic min segrs b) stubby anh xtls <0.3 d with il in (bn bi+qz+il) mafic min pseuds	stubby anh xtls <0.3 d with il in (bn bi+qz+il) mafic min pseuds b) xtl aggreg <8 with bn bi (gn bi+ms±cl) pseuds after cd in granitic mega-lithic i	squat anh xtls <5 d with fl in miarolytic cavities in phyric-poor por
CHALCOPYRITE					small (<0.2 w) patches or ribbons in po	small (<0.1 w) patches or ribbons in po in gr & mgr	veins and xtl aggreg in qz veining in shear zone, Babel Island

Table 4.1 cont.

SUITE / PHASE	WYBALENNA	GARDENS	POIMENA	LADY BARRON	MUSSELROE	BOOBYALLA	BABEL ISLAND
ARSENOPYRITE						isolated wedge-shaped euh xtls <8 d in altered phyric por	
MOLYBDENITE							flakes <10 d in (qz+tz) vein rock (silexite) intruding Babel Is gr
CHLORITE	large (<5 l) flakes pseud bi i: ap, zr, il, ru	large (<5 l) flakes pseud bi i: ap, zr, il, ru	large (<5 l) flakes pseud bi i: ap, zr, il, ru	a) large (<5 l) flakes pseud bi b) small (<1 l) flakes in (gn bi+ms+cl) pseuds after cd	a) large (<5 l) flakes pseud bn bi b) small (<1 l) flakes in (gn bi+ms+cl) pseuds after cd	a) large (<4 l) flakes pseud bn bi b) small (<1 l) flakes in (gn bi+ms+cl) pseuds after cd	a) <4 l flakes pseud bn bi b) small (<1 l) flakes in (gn bi+ms+cl) pseuds after cd
RUTILE?			tiny (<0.01 w) needles hexagonally distributed in cl after bi	tiny (<0.01 w) needles hexagonally distributed in cl after bi		tiny (<0.01 w) needles with cores of phen qz	
HEMATITE		rare anh xtls <0.2 d in hb-ac				rare anh xtls <0 2 d in (bn bi+qz+il) pseuds after mafic phases	

Table 4.2

Magmatic Phases of Furneaux Porphyries

Sample Number	Mean matrix grainsize (mm)	Suite	Phases
62589	0.2	Wybalenna	qz pl
62590	0.65	"	qz pl hb
62593	0.25	"	qz pl bi hb
62602	0.25	"	qz pl hb cp?
62610	0.1	"	pl hb cp?
62594	0.25	Poimena	qz pl bi il
62596	0.70	"	qz pl af bi cd il al ap
62597	0.60	"	qz pl af bi cd il ap
62598	0.35	"	qz pl af bi cd il ap
62601	0.15	"	qz pl bi
67532	<0.01	"	qz pl af bi sn al ap
62612	0.45	"	qz pl $(af)_x$ op $(ga)_x$
67533	<0.01	"	qz pl af bi mt?
67537	0.25	"	-
67545	0.15	Lady Barron	qz bi cd
62546	0.2	Lady Barron	qz cd tm
62595	0.8	Boobyalla	qz pl af bi ga cd
62605	0.4	"	qz pl bi cd
62606	0.4	"	qz pl af bi ga cd ap
62616	0.3	"	qz? bi?
62617	0.4	"	bi?
62618	0.4	"	qz pl af bi ad il ap
62619	0.3	"	qz pl af bi ca ga ed ad il ap zr
62620	0.6	"	qz pl af bi ga cd ad il ap zr
62624	0.4	"	
62626	0.3	"	qz pl af bi ap
62627	0.5	"	qz pl af bi ga ap
62575	0.35	Babel Island	qz pl af bi cd ad vp
62579	0.25	"	cd bi?
67244	0.3	"	qz pl af bi cd ad
67530	<0.05	Poimena/basalt	qz pl $(af)_c$ bi,hb
67531	<0.05	"	qz pl $(af)_c$ bi,hb
62614	0.65	Boobyalla/Poimena	qz pl $(af)_c$ bi ga cd

x - xenocrysts introduced during high-level synplutonism
c - corroded crystals

PLATE 3

This plate consists of photographs of slabs of porphyry which have been stained with trisodium hexanitritocobaltate III. The scale bars are 10 mm long.

Fig. A Loccota Porphyry (Boobyalla Suite) containing phenocrysts of alkali feldspar (pale grey, e.g. central megacryst), plagioclase (~white), quartz (dark grey due to transparency), biotite (small black rhombs) and garnet (rounded biotite pseudomorphs, e.g. towards lower right-hand corner). Matrix is speckled material between phenocrysts. Sample #62620.

Fig. B Basal portion of sill of Loccota Porphyry rich in mafic phenocrysts (#62619). Phenocrysts are of plagioclase (white, with coronas of evergrowth plagioclase), biotite (black elongate, angular crystals) and biotite pseudomorphs after garnet (dark grey patches).

Fig. C Porphyry from Wybalenna Granite (#62593), containing plagioclase (white) and quartz (dark grey) phenocrysts and biotite-containing pseudomorphs probably after orthopyroxene (some of the dark patches).

Fig. D Poimena Suite porphyry (#62594) containing plagioclase (light grey), quartz (dark grey) and biotite (small black grains) phenocrysts. This sample also contains biotite + quartz pseudomorphs which are probably after orthopyroxene.

Fig. E Phenocryst-poor porphyry from Babel Island (#62579) containing patches rich in green Ti-absent biotite after cordierite.

Fig. F Rhombic sections of cordierite phenocryst pseudomorphs (now muscovite-green biotite-quartz assemblages) in a Boobyalla Suite porphyry (#62606).

Fig. G Hybrid Long Toms Nose Porphyry (#67530) (Poimena Suite/basalt) showing globular plagioclases mantling or completely replacing alkali feldspar (mottled white areas), rhombic plagioclase phenocrysts (white) and β-quartz phenocrysts (dark grey/black). Globular chloritic patches after basalt (cf. Fig. H, Plate 2) are difficult to discern on stained surfaces (e.g. patch on top edge near left-hand corner).

Fig. H Hybrid Boobyalla/Poimena Suite porphyry at Holts Point (#62614) showing rapikivi-textured feldspar phenocryst (top right-hand corner and at centre on bottom of photograph), plagioclase phenocryst with core (lower left-hand corner), quartz phenocrysts (~centre) and biotite phenocrysts (small black areas).

PLATE 3

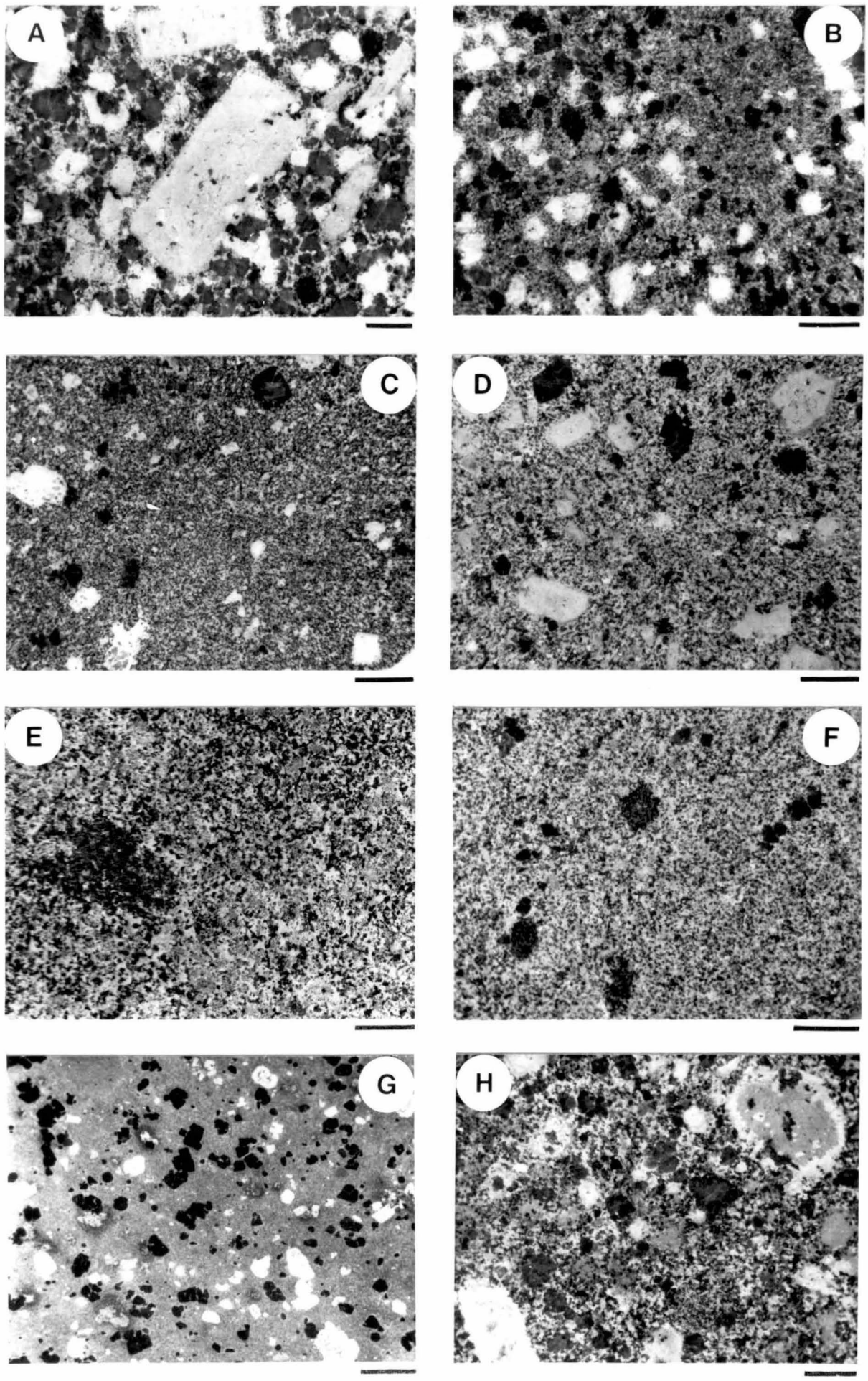

size (~2 mm wide flakes) of the biotites sedimented from felsic magmas of the same suite elsewhere in the batholith (#62615).

Within the identification limits set by the matrix grainsize, the phyric phases or their pseudomorphs within porphyries are interpreted as having been phenocrystic or xenocrystic phases or their pseudomorphs. Table 4.2 lists these, for each of the porphyries that were sampled and analysed. Petrographic descriptions of these magmatic phases and their pseudomorphs are now given.

Alkali feldspar

In porphyries, alkali feldspar varies dramatically in form. Some porphyries with relatively mafic matrix compositions, contain localized interstitial intergrowths of alkali feldspar with other matrix phases (Plate 3, Fig. C). In these samples alkali feldspar was a late-crystallizing, near-solidus phase. In porphyries with more felsic matrixes however, megacrysts up to ~80 mm in diameter occur (Plate 3, Figs A and H).

In some Boobyalla and Musselroe Suite granites, megacrysts may have diameters of 130 mm. They often contain shells of inclusions (commonly biotite or quartz but sometimes garnet (cf. Cocker, 1977)) which could be due to an acceleration in the feldspar growth-rate (Tracy, 1982). The inclusions delineate a core-crystal which is comparable in size to

i) megacrysts in related porphyries, and

ii) megacrysts in filter-pressed accumulations proximal to megalithic inclusions (Plate 1, Figs E and G), where subsequent crystal growth was restricted because of the limited interstitial melt volume.

Accordingly, accelerated late-stage magmatic growth of alkali-feldspar in granites is considered to have occurred at the site of high-level emplacement, onto core crystals formed at earlier petrogenetic stages.

Core-crystals may contain inclusions of earlier phases such as quartz, garnet, highly titaniferous biotite and narrow-rimmed plagioclase crystals, indicating that core-alkali feldspar was also an earlier magmatic phase (Plate 3, Fig. A). These inclusion relationships also indicate that melts were saturated in three felsic phases for an extensive part of their history.

Subsolidus effects which variably mask the magmatic features described for this phase are (i) solid-state growth, (ii) perthitic exsolution and (iii) partial replacement by muscovite or tourmaline (e.g. Plate 5, Fig. G). It is only their extraordinary size which allows recognition of their phyric status even in coarsely crystalline granites.

Allanite

Euhedral allanite phenocrysts up to 0.2 mm in diameter occur in the Poimena Suite porphyries of the Long Toms Nose dyke swarm (e.g. #67533). They have a rhythmic brown and khaki coloured optic zonation.

Andalusite

This late-stage magmatic phase is widespread in the Boobyalla and Babel Island Suites. It occurs as phenocrysts also in the Dover River Granite (#68527) assigned to the Lady Barron Suite. The phase occurs in granites, porphyries and in pegmatites. Rose to colourless core to rim optical zoning occurs only in phenocrysts within Boobyalla Suite rocks (Plate 6, Figs A and B). Its zoning is considered to be largely a feature of growth rather than of diffusion, because diffusion-rates in the aluminosilicates are very low (Loomis, 1983a). The ferric endmember ($FeAlSiO_5$) (Grambling & Williams, 1985) which is responsible for the colour, occurs in amounts up to 3.4 m%. The colour gradient is considered to reflect a temperature and/or fO_2 gradient during growth during late magmatic to subsolidus conditions (see Chapter 9).

Muscovite coronas (Plate 6, Figs A and B) or replacements, are expressions of subsolidus reaction of this magmatic phase.

Apatite

Apatite morphologies range from small (~0.02 mm diameter) needles within biotite to large (~0.2 mm) squat or interstitial grains in aplites (e.g. #62624) or in garnet pseudomorphs (#68529). These are thought to be early and late magmatic occurrences, respectively.

Biotite

In porphyries, biotite occurs in a variety of forms because it is the major pseudomorphing phase of all other mafic magmatic phases.

Petrographic relationships indicate that in the Boobyalla and Musselroe Suites, biotite had an extensive magmatic history. Large phenocrysts and inclusions within early phases have a deep foxy reddish colour (Plate 6, Figs C and D) which correlates with their high TiO_2 contents. Garnet and probably orthopyroxene and cordierite as well are pseudomorphed by (brown biotite + quartz ± minor phases) assemblages under magmatic or near-magmatic conditions (Plate 3, Figs A, B and H; Plate 4, Figs C, D and E). In mafic mineral segregations, growth-zones in brown late-stage magmatic biotite which pseudomorphs garnet, are delineated by strings of tiny xenotime crystals (Plate 4, Fig. H).

Under subsolidus conditions, pale green coloured (titanium absent) biotite partly pseudomorphs garnet, orthopyroxene and cordierite (Plate 4, Figs B and G.

PLATE 4

This is one of two plates (Plates 4 & 5) of photomicrographs. The scale bars are 500μm long. All but the last photomicrograph of this plate are taken with uncrossed nicol prisms.

Fig. A Fresh cordierite mantling a corroded garnet crystal in the shape of a hand (right-hand side of photograph). Biotite is also present (e.g. near upper edge). The cordierite grain has been fractured and the fracture infilled by quartz. Sample #67539.

Fig. B Martins Rise Granite (#62638) containing garnet (left-hand side) and pseudomorphs after cordierite (right-hand side). Pseudomorphs consist of patches of intergrown muscovite, magnesian, titanium-absent green biotite and sometimes chlorite.

Fig. C Shows mineralogy of the mafic mineral segregation #68525. Wormy remnants of a resorbed garnet phenocryst (lower right-hand corner) occur within quartz. Large ilmenite grains are frequently mantled by a single biotite crystal (e.g. lower left-hand corner). Intergrowths of biotite and quartz (upper left-hand corner) may be pseudomorphs after orthopyroxene.

Fig. D Possible orthopyroxene pseudomorph consisting of oriented biotites within quartz (centre), ilmenites (upper left-hand corner) and accessory phases. Mafic mineral segregation #68525, Boobyalla Suite.

Fig. E Biotite/quartz pseudomorph after mafic phase (garnet?) containing accessory xenotime, monazite, apatite and zircon (#68529).

Fig. F Orthopyroxene from the Crooked Lake Orthogneiss, Vestfold Hills, eastern Antarctica showing an embayment filled with a biotite/quartz intergrowth similar in morphology to that of Fig. D above. Biotite in the replacement assemblage occurs as plates parallel to the cleavage in the host orthopyroxene.

Fig. G Mass of grunerite crystals pseudomorphing an orthopyroxene inclusion within a garnet from the Cape Barren Granite (#68524).

Fig. H Wormy textured twinned biotite phenocryst (crossed nicols), showing the pseudomorphing assemblage within the extint portion of the host-grain. The pseudomorphing assemblage consists of transparent, low-birefringent phases.

PLATE 4

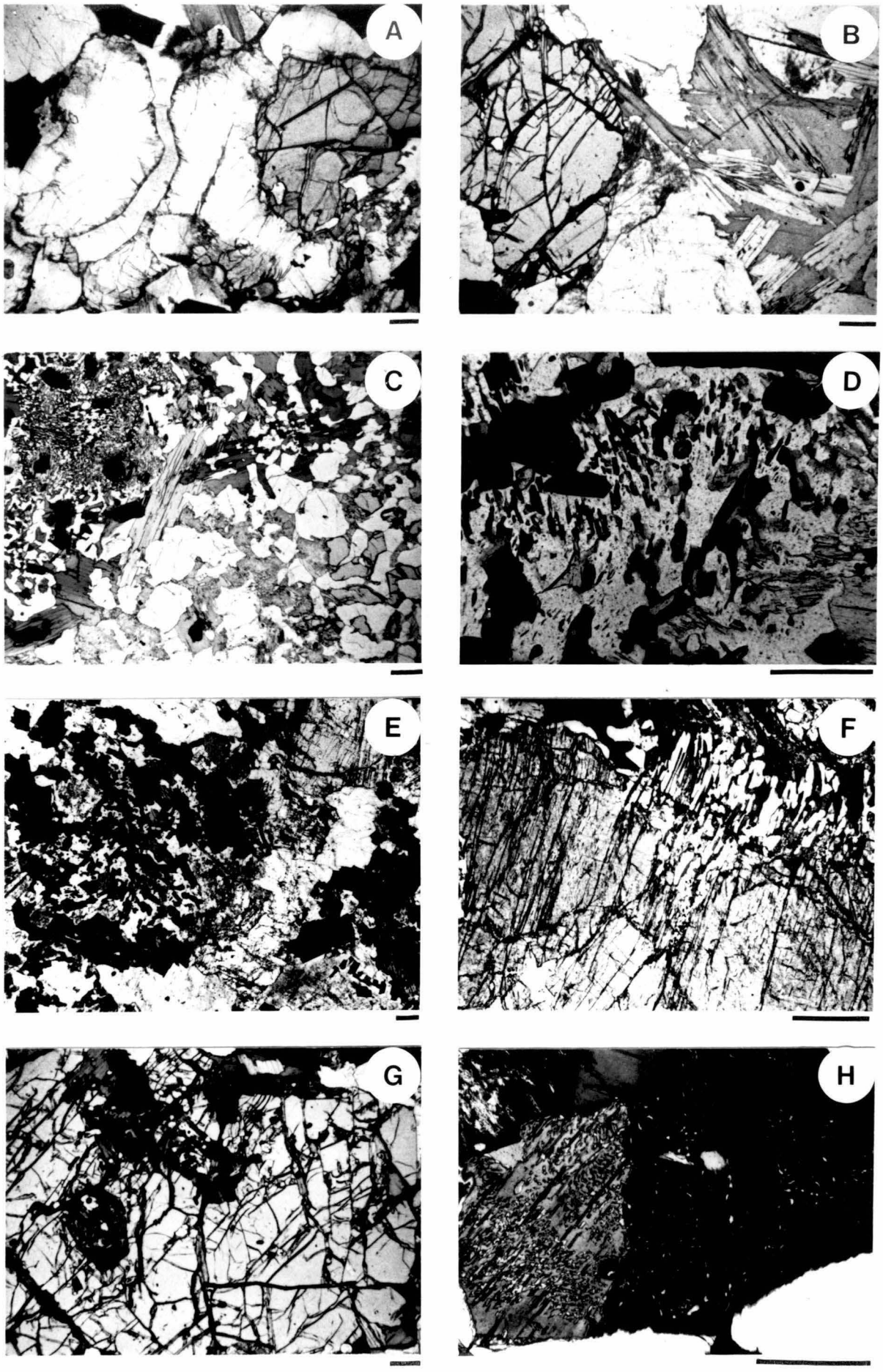

In the metaluminous porphyries of the Wybalenna Suite, biotite is a late magmatic phase. It mantles and replaces amphibole (Plate 5, Figs D and F) and occurs in clots which are interpreted as being pseudomorphs after orthopyroxene (Plate 3, Figs C & D). Biotite also appears to be a late-stage pseudomorphing phase in the Lady Barron Suite granites.

Incipient chlorite replacement across the (hkO) surface of biotite, with simultaneous growth of a titanium phase (ilmenite, sphene or a Ti-oxide) is a variably developed ubiquitous product of subsolidus reaction in all rocks.

Cordierite

A long magmatic history is indicated for this phase in the moderately peraluminous suites. It is the dominant mafic phase of the Lady Barron Suite granites. In these, it texturally predates magmatic biotite.

In mafic mineral segregations of the Musselroe Suite, inclusions of early cordierite within garnet are widespread (e.g. #67539, Plate 7). Large rhombic phenocrysts were also present in these rocks. They have usually been pseudomorphed by muscovite, green biotite, chlorite and quartz (Plate 4, Fig. B). Late-stage iron-rich cordierite interstitial to other phases occurs in the same segregations, especially in the vicinity of resorbed garnet (Plate 4, Fig. A). Latest-stage magmatic cordierite is indicated in the widespread occurrence of this phase, or its pseudomorphs, in pegmatites and felsic phenocryst-poor porphyries (Plate 3, Figs E and F).

Cummingtonite

Cummingtonite mantles around resorbed phenocrystic orthopyroxene occur in one Wybalenna Suite sample (#62628, Plate 5, Fig. B). Cummingtonite in turn is mantled and replaced by brown biotite. Because the biotite is probaby a late magmatic phase in this suite, then the cummingtonite which preceded it is also likely to have been a late magmatic phase.

Fluorite

Fluorite occurs as a rare late-stage phase in the Boobyalla Suite where it occurs with tourmaline in mafic mineral segregations (Plate 5, Fig. H) where it is interstitial to garnet remnants. It is more common in the Babel Island Suite where it frequently occurs as green to purple crystals up to 8 mm diameter with pyrrhotite and (fluor?) muscovite in miarolytic cavities.

Garnet

Garnet is one of the earliest magmatic phases in the Musselroe, Boobyalla and Babel Island Suite granites. It is rarely found in phenocryst-poor rocks because of its tendency to react with the melt near

or at the site of high-level intrusion. It is found in abundance however in mafic mineral segregations (Plate 1, Figs E and G) where the melt-to-garnet ratio could be sufficiently low such that garnet was an excess phase.

The best preserved segregation from the Ansons Bay South pluton (#67539) contains rare garnets with an abundance of cordierite ± sillimanite ± gahnitic spinel ± ilmenite inclusions. The inclusions within one such garnet delineate arcs of shallow curvature (Plate 6, Figs A and B; Plate 7). These inclusions are not considered to have been occluded during liquidus growth of garnet because

a) the inclusion trains sweep through the centre of the crystal and are not sub-parallel to its (resorbed) surface as might be expected,

b) reconstruction of a garnet assuming the inclusions to have been trapped during liquidus growth implicates an improbably large garnet $\geq$25 mm in diameter. Garnets are usually less than 12 mm in diameter (Table 4.1).

The inclusion trails are therefore considered to trace an S-surface occluded during solid-state garnet growth. This and other garnet cores containing similar inclusions, are therefore regarded as being xenocrysts, either from the source-region of partial melting (that is, restite garnet) or possibly from a higher level via country-rock contamination during intrusion.

The typical magmatic pseudomorph after garnet contains brown biotite, quartz, ilmenite, apatite, zircon, xenotime and monazite (Plate 4, Fig. E). The last two phases form from melt-reaction with the yttrogarnet component ($Y_3Al_2Al_3O_{12}$, Deer et al., 1982), which constitutes about 0.3% of the garnet (c.f. Chapter 6).

Subsolidus replacement of garnet consists of green (titanium-absent) biotite and minor muscovite (e.g. #68529).

Hornblende

This phase is present in rocks of the Wybalenna and Gardens Suites and in basalt-hybridized Poimena Suite porphyries (#67530-31). It has a restricted magmatic paragenetic range. Phenocrysts occur in Wybalenna Suite poprhyries either as small prisms with green-brown cores and blue-green rims or as green mantles to actinolitic patches which are interpreted as subsolidus replacement of clinopyroxene. Khaki-coloured (magmatic) hornblende mantles and presumably replaces orthopyroxene in one granite (#62628, Plate 5, Fig. B). The same paragenesis is deduced to have occurred in other metaluminous granites (e.g. Reid, 1980). This interpretation of granite textures accords with the order of appearance of mafic phases in

PLATE 5

Fig. A Plagioclase phenocryst from Poimena Suite porphyry #62594 (cf. compositional profile in Fig. 7.10). Only minor compositional changes attend the oscillatory zoning visible in this section. The rims are more anorthic than the core (crossed nicols).

Fig. B Three orthopyroxene crystals in the Pats River Granite #62628 (Wybalenna Suite) occur as high-relief grains partially replaced by pale-coloured low-relief cummingtonite which is in turn, replaced by darker-coloured hornblende. Biotite (dark phase) completes the sequence by replacing hornblende (uncrossed nicols).

Fig. C Phenocryst of plagioclase from Laby Barron granite (#62640) which has an optically and compositionallly distinctive core (cf Fig. 7.10). In this suite, the cores of plagioclases are distinctly more calcic than the rims.

Fig. D Hornblende prism from Wybalenna Granite #62635 partially replaced by khaki biotite which replaces the host phase in directions parallel to its cleavage (uncrossed nicols).

Fig. E Plagioclase phenocryst from the Loccota Porphyry (#62619) (cf. Fig. B, Plate 3) showing its core-mantle structure. The cores of these phenocrysts have an ~An_{43} composition (cf. Fig. 7.10).

Fig. F Actinolite pseudomorph probably after clinopyroxene from the Wybalenna Suite porphyry #62610. Actinolite is pale-coloured, hornblende darker and biotite is the darkest phase (uncrossed nicols).

Fig. G Elongate crystals of optically and compositionally zoned tourmaline from with 2 m of the contact between the Clarke Island granite and the Mathinna Beds flysch (#68588) (uncrossed nicols).

Fig. H Fluorite is shown in high (negative) relief occurring as a matrix to small biotite, muscovite, ilmenite and apatite grains in an assemblage interstitial to large garnet crystals within the Boobyalla Suite mafic mineral segregation #68529. The assemblage in this photomicrograph is flanked by tourmaline (mid-grey) which was replacing adjacent garnets (not shown) (uncrossed nicols).

PLATE 5

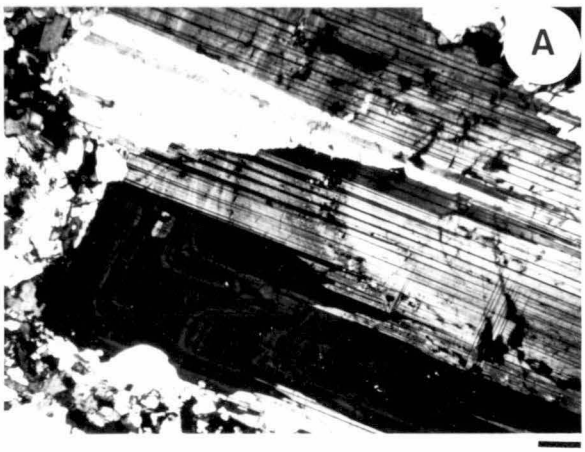

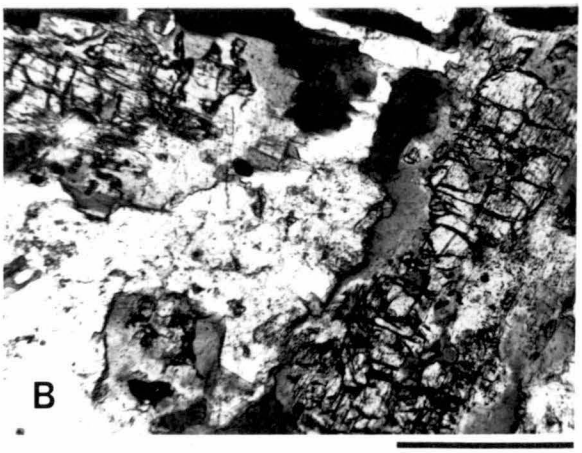

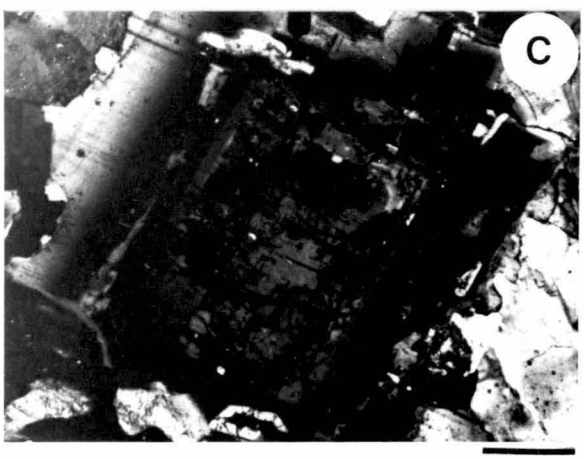

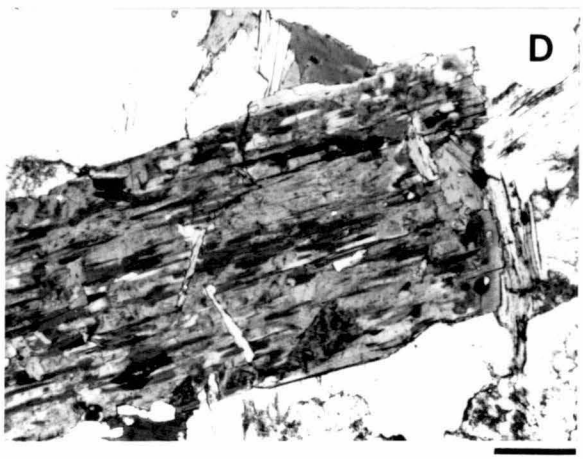

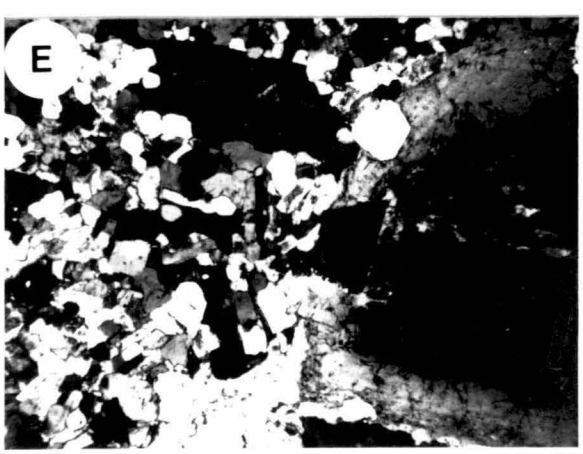

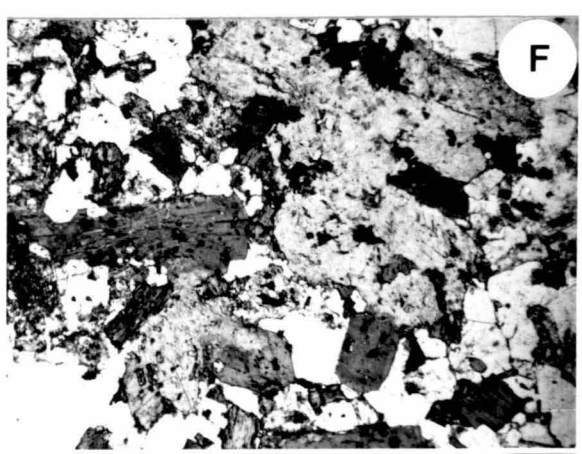

0.5 GPa liquidus experiments undertaken on a metaluminous tonalitic bulk-composition by Crawford and Harris (in prep.).

Hornblende in turn, is in part replaced by khaki-coloured biotite. This replacement probably occurred at near-solidus to subsolidus conditions because similar biotite and green amphibole constitute the mafic phases of the matrixes of these porphyries.

Ilmenite

A long magmatic history, largely associated with biotite equilibria, is indicated for this phase in the Boobyalla, Musselroe and Babel Island Suites. It occurs as inclusions in early formed plagioclase and garnet cores (Plate 7) and is an abundant phase in magmatic pseudomorphs after mafic silicate phases (Plate 4, Figs C, D and E). In contrast to this habit, late-stage exsolution of ilmenite from early titaniferous biotite is very common. Ilmenite phenocrysts frequently grow to occlude the accessory phases (such as apatite, zircon, xenotime and pyrrhotite) which occur in the pseudomorphs after garnet.

The replacement of ilmenite by sphene in the Poimena and Lady Barron Suites may be a consequence of the increased Ca-activity associated with subsolidus saussuritization of the calcic cores of plagioclase crystals, because this sphene has an unusual aluminous composition (Appendix H) and a fine-grained dendritic morphology.

Orthopyroxene

This phase occurs as phenocryst remnants in a Wybalenna Suite granite (Plate 5, Fig. B). It is partly replaced by cummingtonite as described above. Small clots of biotite in Wybalenna Suite porphyries may be pseudomorphous after orthopyroxene.

In the mafic Poimena Suite porphyry #62612, large (10 mm diameter) clots of fine-grained magnesian chlorite and quartz are likely to have been pseudomorphous after orthopyroxene.

In the strongly peraluminous suites, the most direct evidence of the presence of orthopyroxene is the occurrence of an inclusion pseudomorph in garnet, which consists of a nest of grunerite crystals (Plate 4, Fig. G; #68524).

Less substantial evidence of the former presence of orthopyroxene comes from certain quartz/biotite textures occurring in mafic mineral segregations (Plate 4, Fig. D). These bear a close resemblance to the bladed biotite in quartz which has replaced orthopyroxene parallel to cleavage, in the Crooked Lake orthogneiss, of eastern Antarctica (Collerson et al., 1983) (Plate 4, Fig. F).

Though orthopyroxene has never been observed in Bassian Terrane S-type granitic rocks, it occurs widely in the Violet Town Volcanics, the

PLATE 6

Figs A & B (uncrossed and crossed nicols respectively) Needle-like phenocryst of andalusite from the Boobyalla Suite pegmatite #68547 (cf. Fig. A, Plate 2) containing an irregular-shaped iron-containing core (dark grey regions in Fig. A) and an iron-poor to -absent mantle and rim. The crystal is mantled and partially replaced by muscovite (Fig. B). Scale bar is 250 μm long.

Figs C & D (uncrossed and crossed nicols respectively) This large corroded garnet crystal is from the Musselroe Suite mafic mineral segregation #67539. It contains a variety of inclusions (Fig. B). Two areas within it outlined by dashed lines, were studied in more detail (cf. Plate 7, Fig. 7.8, Appendix I). The scale bar is 1 mm long.

PLATE 6

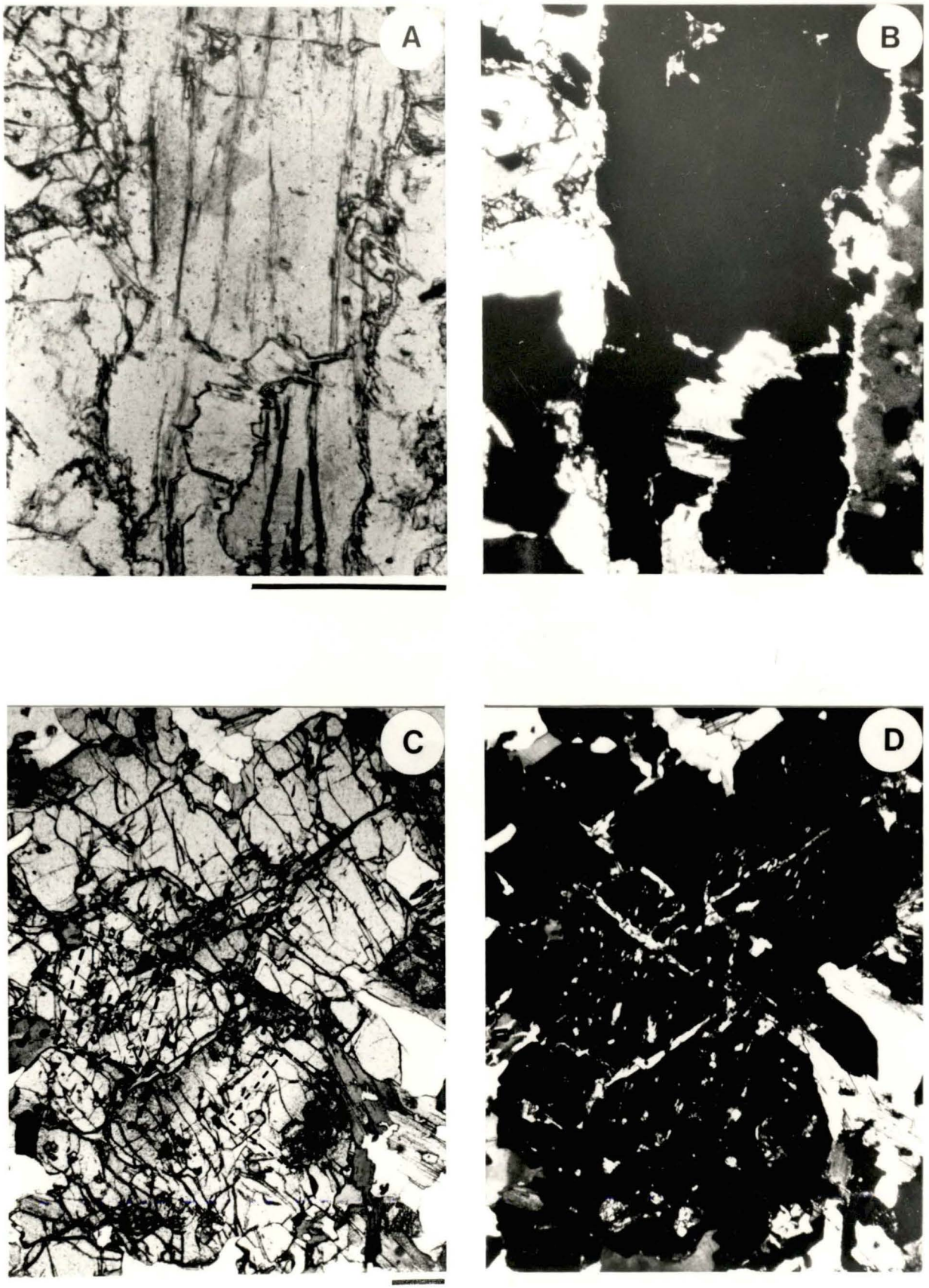

extrusive equivalents of the Strathbogie Granite, in the Melbourne Terrane of central Victoria (Clemens and Wall, 1981, 1984).

Plagioclase

Textures suggest that in all but the Babel Island Suite, plagioclase has had a long magmatic history. Plagioclase cores were amongst the earliest of magmatic phases, as is suggested by their general lack of inclusions other than early magmatic phases such as zircon or ilmenite.

Plagioclase phenocrysts typically have subhedral calcic mottled cores, separated from more sodic normal and oscillatory-zoned rims by a steep optical and compositional gradient (Plate 3, Fig. B; Plate 5, Figs A, C and E). Mottled core textures are interpreted as resulting from incipient phenocryst melting brought about either by a slight temperature increase over equilibrium conditions or by a change in the phase assemblage, as has been shown by the experimental studies of Tsuchiyama and Takahashi (1983) and Tsuchiyama (1985). This explanation is supported by the experimental studies of Johannes (1978, 1980, 1984) which show that by increasing the number of felsic phases in which the melt is saturated then the (pseudo-) equilibrium plagioclase T-X loop becomes both increasingly flattened and depressed to lower temperatures.

Further support for this explanation for the generation of mottled core textures comes from consideration of some example of this morphology in the plagioclase crystals from the hybrid Boobyalla/Poimena Suite #62614. This textural feature may be linked with other petrographic features of the rock and ascribed to thermal and chemical disequilibria resulting from the mixing of magmas of two different suites. Small ragged patches of calcic plagioclase occur within the cores of plagioclase phenocrysts in certain Wybalenna Suite porphyries (e.g. #62610) and larger core-remnants occur in some plagioclase crystals from the above-mentioned hybrid (#62614). They are considered to be remnants of early plagioclase crystals, variably resorbed during a heating event more extensive than that which would have produced mottled textures. This explanation accords with both theoretical and experimental studies which indicates that diffusion in plagioclase at temperatures below ~900^{o}C is extremely slow, so that modal melting is the only possible response to extensive overheating (op. cit.; Tsuchiyama and Takahashi, 1983; Tsuchiyama, 1985).

Plagioclase rims about alkali feldspar phenocrysts (Rapikivi textures: Sederholm, 1891) are common in hybrid porphyries (e.g. #62612, 62614, 67530, 67531, see Plate 3, Figs G and H). They are considered to be a response to magma-mixing, where the hybrid melt produced was simultaneously supersaturated in plagioclase and undersaturated in alkali feldspar (Hibbard, 1981). The replacement process can be traced to

completion to yield plagioclases with euhedral calcic rims and mottled cores (e.g. #67530, Plate 3, Fig. G). The alternative explanation of Hibbard (1981) for this texture, by hopper-textured dendrite crystallization followed by infilling, without the involvement of alkali feldspar, is therefore not supported.

Plagioclase crystals in Babel Island Suite rocks are sodic and are only weakly zoned. Their rims grade into those of alkali feldspar phenocrysts or quartz and single feldspar graphic intergrowths. These features indicate that late-stage hypersolvus crystallization of feldspar occurred in magmas of this suite.

In summary then, the generalized plagioclase paragenesis is considered to be the following:

i) generation of uniform core crystals,
ii) development of mottled or remnant resorption textures by either a thermal pulse such as that attending magma-mixing and/or the change in equilibrium caused by the appearance of another felsic phase,
iii) development of a normal plus oscillatory zoned mantle,
iv) growth of hypersolvus feldspar in magmas which are sufficiently poor in Ca.

Quartz

Amongst the granitic suites, contrasting magmatic histories are indicated for this phase. In rocks of the Boobyalla Suite, for instance, quartz inclusions occur within paragenetically early phases such as in the cores of plagioclase (Plate 3, Fig. A) and garnet crystals. In contrast to this occurrence however, quartz is absent or merely a minor phyric phase in the porphyries of the Wybalenna Suite. Quartz saturation of the melts of these rocks is indicated to be a late magmatic event.

In porphyries with the finest matrix grainsize (i.e. in the Long Toms Nose Porphyry dyke swarm, e.g. #67530 to #67533), quartz occurs as embayed euhedra with striking beta-quartz hexagonal bipyramidal morphologies (Plate 3, Fig. G). In contrast to these, quartz phenocrysts from porphyries with coarser grained matrixes (e.g. #62595, 62618, 62619), have spheroidal anhedral crystal forms (Plate 3, Figs A, B, C, D, F and H). Quartz resorption is therefore thought to reflect the role of magmatic reactions induced by in situ re-equilibration in the low pressure regime at the site of high-level intrusion. This explanation accords with the trend to increasingly siliceous minimum melt compositions, with decreasing pressure (Tuttle and Bowen, 1958). It is also consistent with decompressional melting, which is predicted from the geometry in $P_T P_W T$ space of univariant reactions in the KFMASHO chemical system, as described in Chapter 11.

Sillimanite

The cores of Musselroe Suite garnets contain uncommon prisms or needles of sillimanite. These can be locally abundant, as is shown in Plate 7 and Fig. 7.8. This phase contains a minor ferrisillimanite ($FeAlSiO_5$) component (c.f. Chapter 7, Fig. 7.1). Sillimanite is not known from rocks of any other suite. However the 1 cm diameter aggregates of andalusite crystals in the Boobyalla Suite sample #62583 may be pseudomorphs after phenocrystic sillimanite.

Tourmaline

In the strongly peraluminous suites, zoned tourmaline occurs both in pegmatites (Plate 5, Fig. G), and as large dendritic patches proximal to porphyry intrusions (Plate 1, Fig. B). In the latter occurrence, tourmaline is usually the sole mafic phase, the boron-containing vapour emanating from these porphyries apparently having led to the replacement of any pre-existing biotite or cordierite. The ability of boron to lower solidi is well established (e.g.Pichavant, 1981) and phenocrysts of this phase occur in the Macusani Volcanics of southeastern Peru (Noble et al., 1984; Kontak et al., 1984; Pichavant et al., 1987). Tourmaline is therefore regarded as a latest-stage magmatic to subsolidus phase.

Zircon

Zircons of the Wybalenna, Poimena, Lady Barron, Boobyalla and Musselroe Suites may have discrete cores with those in the Poimena Suite containing up to three zircon generations. The cores of zircons are likely to be source-phase (restitic) remnants of the partial melting event rather than the expression of a higher-level country-rock contaminant, because they have a widespread distribution, rather than being restricted to the granite at the margins of plutons.

Xenotime and Monazite

These phases occur in the strongly peraluminous suites as equant euhedra. They are common in the pseudomorphing assemblages of garnet, as described above.

4.4 SUITE PARAGENESIS

Parageneses for each suite have been constructed from the petrographic data (Fig. 4.1). In these diagrams the estimated phase-ranges for each suite are plotted against an arbitrary time-scale.

Paragenetic diagrams provide an indication of the sequences of coeval assemblages present throughout petrogenetic evolution. In turn, these assemblage sequences indicate the existence of the discontinuous reactions which occurred throughout petrogenesis.

FIGURE 4.1:

MINERAL PARAGENESES FOR FURNEAUX GRANITE SUITES

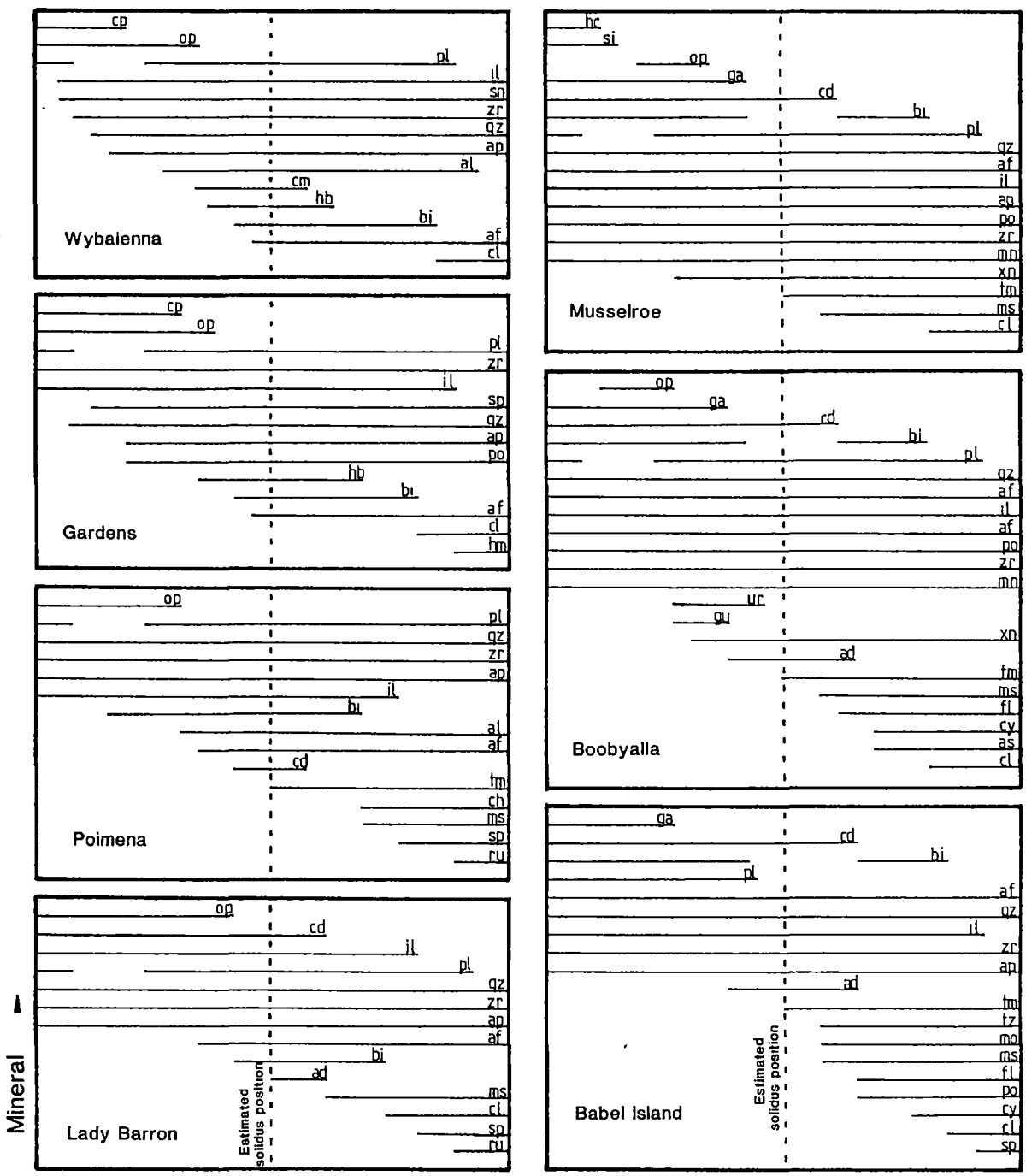

ad: andalusite, af: alkali feldspar, al: allanite, ap: apatite, as: arsenopyrite, bi: biotite , cd: cordierite, cl: chlorite, cm: cummingtonite, cp: clinopyroxene, cy: chalcopyrite, fl: fluorite, ga: garnet, gu: grunerite, hm: haematite, il: ilmenite, mn: monazite, mo: molybdenite, ms: muscovite, op: orthopyroxene, pl: plagioclase, qz: quartz, ru: rutile, sp: sphene, tm: tourmaline, tz: topaz, ur: uraninite, xn: xenotime

More phases are apparent in the late (subsolidus) stages of petrogenesis, than the earlier (magmatic) stages. This is partly due to the scale of equilibrium which becomes progressively more localized as the temperature decreases and kinetic factors assert control in mineral reactions (Loomis, 1983a). More phases may occur therefore in subsolidus assemblages than could occur if large-scale equilibrium were complete.

A second reason is that the ability to determine the existence of phases decreases as one projects back in time towards the earlier magmatic stages.

Chapter 5

WHOLE-ROCK AND PORPHYRY MATRIX CHEMISTRY

5.1 INTRODUCTION

Rock compositions are important in granitic classification because they provide quantitative data with which to compare samples. Rocks may be grouped if they form coherent trends on chemical variation diagrams. Such groups, termed chemical suites, are thought to be petrogenetically related.

Rock compositions are also important in petrogenetic studies of granites. Sample trends on chemical variation diagrams for example, may be compared with compositional paths for model magmas in order to gauge the effects of model magmatic processes (McCarthy & Hasty, 1976; Higgins et al., 1985; White & Chappell, 1977; Chappell et al., 1987).

In this chapter, the distinguishing chemical features of granites, porphyries and porphyry matrix separates from the major suites in the NBTB are described, compared and illustrated. Chemical features of the suites are then compared with those of certain Victorian granites, country-rock flysch, hybrid porphyries and a basalt. Finally, petrogenetic implications of the data are briefly discussed, preparatory to more detailed consideration in later chapters.

5.2 METHODS

Samples of 40 granites, 29 porphyries, 2 aplites, 2 mafic mineral segregations, 3 country-rock metasediments and a metabasaltic dyke were collected from the Furneaux Islands for chemical analysis. A garnet-rich mineral segregation (#67539) was also collected from the N.E. Tasmanian mainland.

Acquisition of most of these samples required the use of an internal-combustion percussion rock-drill. Samples of granites, phenocryst-rich porphyries and the garnet-rich segregations each weighed between 5 and 15 kg. Samples of fine-grained aphyric rocks such as porphyries and aplites were between 1 and 5 kg in weight.

Twenty-five matrixes were separated from phenocryst-poor porphyries by the following procedure. Porphyry blocks were thinly sliced (<1 mm) using a diamond saw and the saw-cuts ground off on a lap using silicon carbide grit. The slices were washed and dried then soaked in methylated spirits for 24 hours to extract the cutting oil. They were then rinsed and ultrasonically cleaned in water and dried. Matrixes and phenocrysts were then cut out by hand using a hardened steel crimping tool.

Matrices and phenocrysts were separated in amounts such that the estimated errors in chemical compositions which can be attributed to sample

size variations were within a factor of 2 of each other (see Appendix C for method).

Whole-rock and matrix-separate samples were analysed for major and selected trace elements by X-ray Fluorescence Spectroscopy (XRFS). MgO was redetermined by atomic absorption spectroscopy (AAS), where the proportions indicated by XRFS were less than 1%. A more accurate determination of Mg was required because this element is frequently present only in trace amounts. Trace elements determined using XRFS are Ba, Rb, Sr, Zr, Nb, Y, Sc, V, Mn, Ga and Sn. Analytical procedures are described in Appendix D. The chemical compositions obtained are presented in Appendix E.

Compositional data for granite whole-rocks, porphyry whole-rocks and matrix separates are presented in Fig. 5.1. In Fig. 5.2, data of certain mafic prophyry inclusions, hybrid porphyries, hybrid porphyry matrix separates, Mathinna Beds country-rock, a metabasaltic dyke and an aplite are presented.

Data depicted include those of 23 granites, 14 whole-rock porphyries and 5 metasediments from Cocker (1977: 7 granites and 12 porphyries), Higgins et al. (1985: 2 granites), Dr N.C. Higgins, B.M.R. (unpublished data: 6 granites), Kitto (1982: 12 granites, 2 porphyries and 5 metasediments) and Dr B.W. Chappell, A.N.U. (unpublished data: 11 granites). Data for the seven analyses of Cocker (1977) were averaged with those obtained by Higgins et al. (1985) using the same respective sample powders.

FeO* (total iron as FeO) is most often used as the reference component in the diagrams because it distinguishes chemical suites more effectively than do other components. This is due largely to:

(a) the proportionally large range of FeO* contents indicated for each suite;
(b) the high precision with which Fe can be determined by XRFS; and
(c) the small sampling error of the mineral biotite, in which most of the iron is present, due to the relatively small grainsize and widespread distribution of this phase.

5.3 CHEMICAL CHARACTERISTICS OF THE SUITES

Data of six chemical suites are depicted on sixteen sets of covariance diagrams (eight sets each for major and trace element data) in Fig. 5.1. For clarity, the data of each suite are plotted separately. Data of up to three sample types: granite whole-rocks, porphyry whole-rocks and matrix separates, are shown on each diagram. Linear regressions have not been drawn because they tend to obscure features such as curvature which are indicated for many of the trends.

Figure 5.1 **Covariance Diagrams for Six Granitic Suites from the Blue Tier Batholith.**

Data presented are for the following suites:
Babel Island (BI), Boobyalla (BO), Musselroe (MU), Lady Barron (LB), Poimena (PO) and Wybalenna (WY).
Data are shown for three sample types: granite whole rocks (open squares), porphyry whole rocks (crosses), and porphyry matrix separates (filled squares). Sixteen sets of covariance diagrams are presented: the first eight are of major element data, the second eight are of trace element data. FeO* = total iron as FeO.
al = mol. % A′/(A′+F′+M) where
A′ = Al_2O_3 - (K_2O+Na_2O+CaO)
F′ = FeO*+MnO
M = MgO.

FeO*

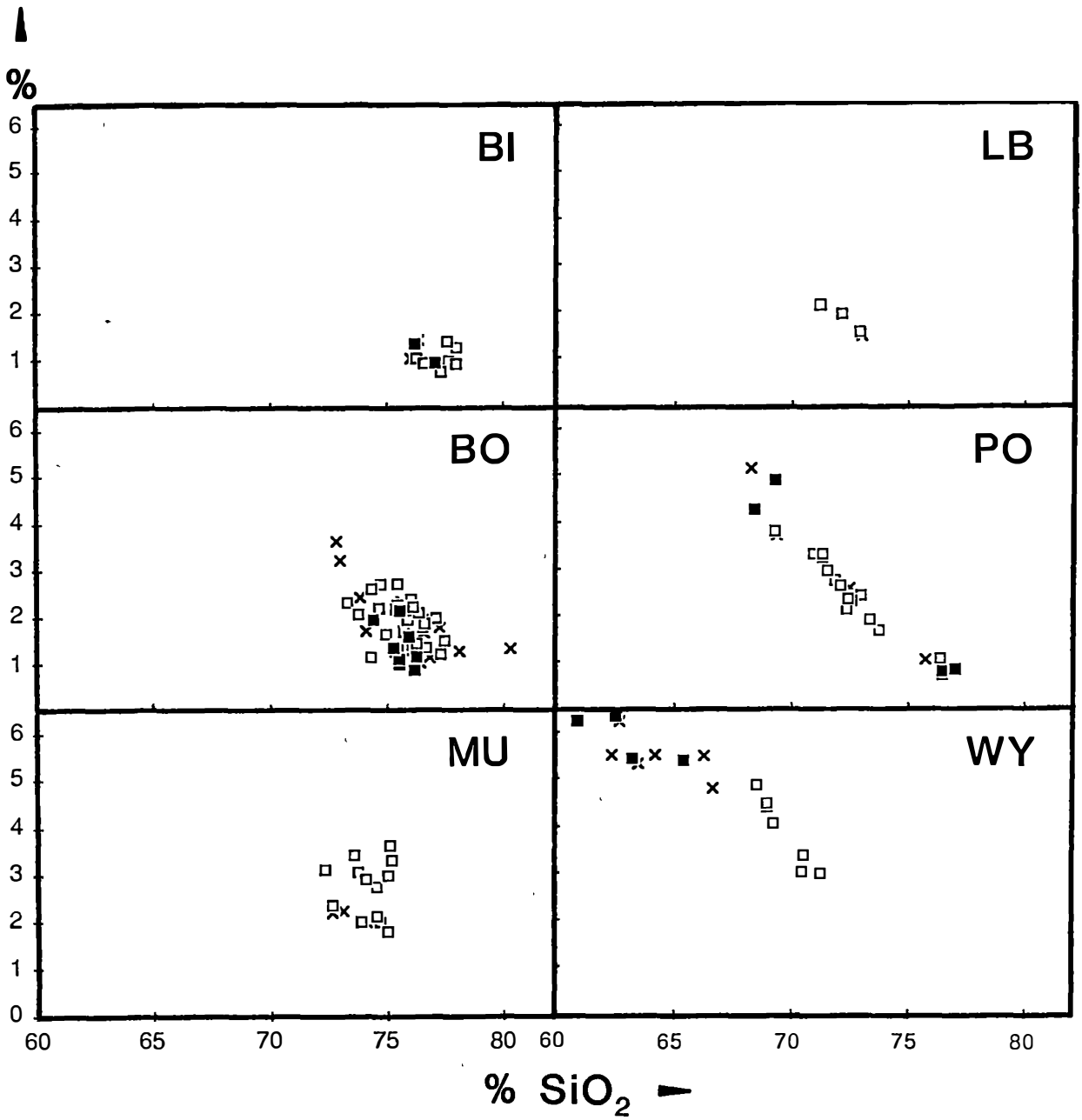

Al_2O_3

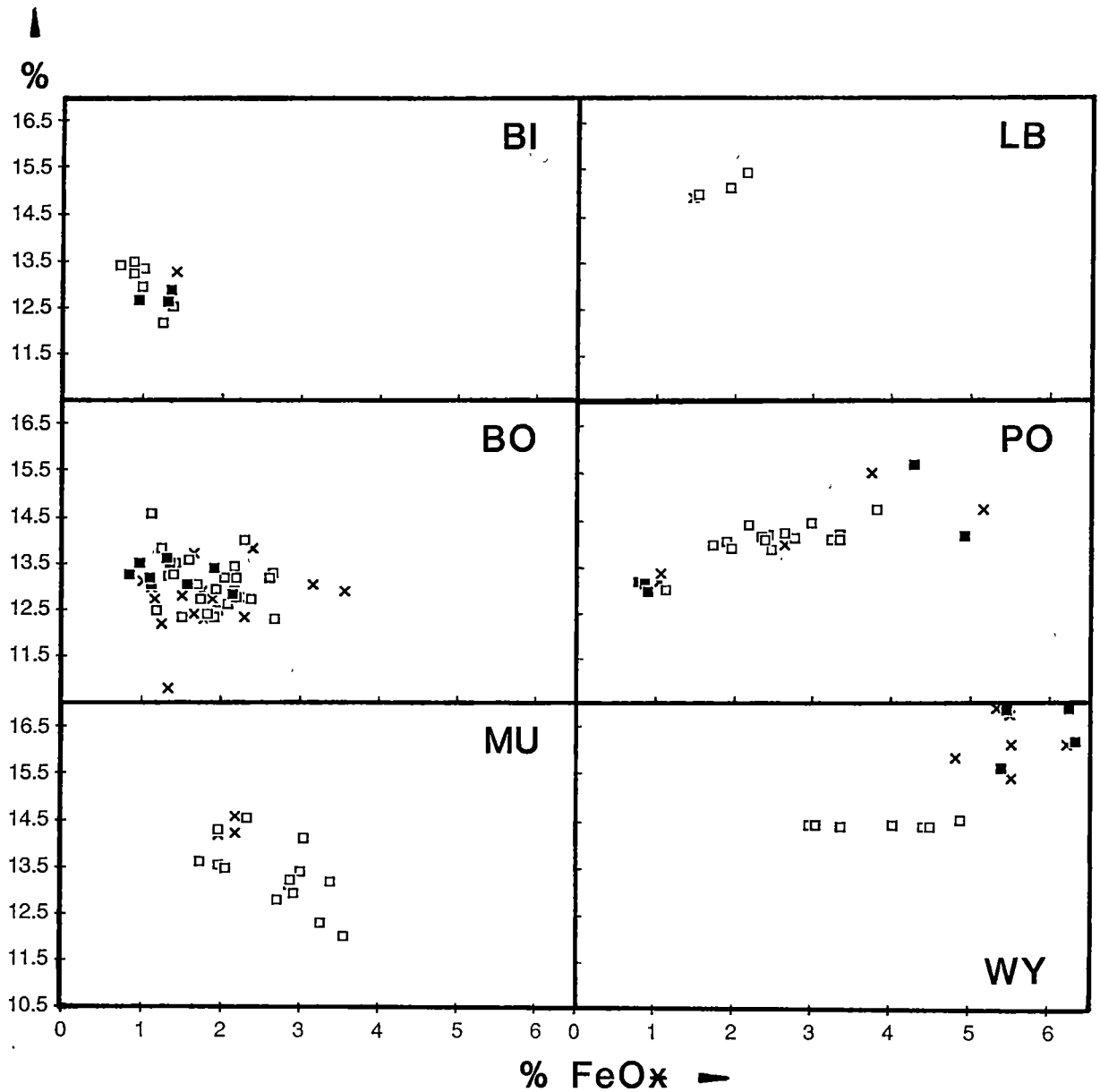

TiO_2

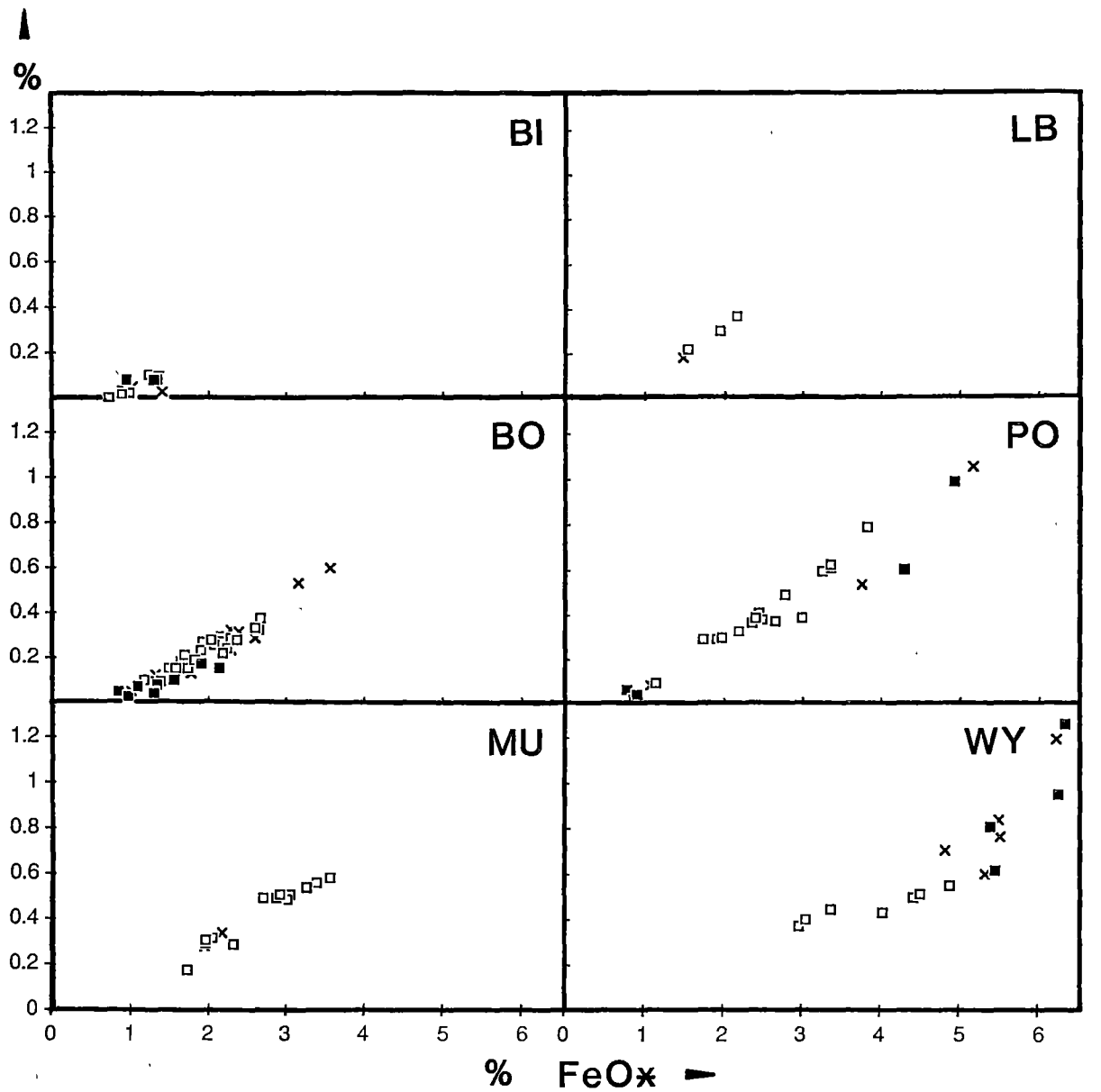

al

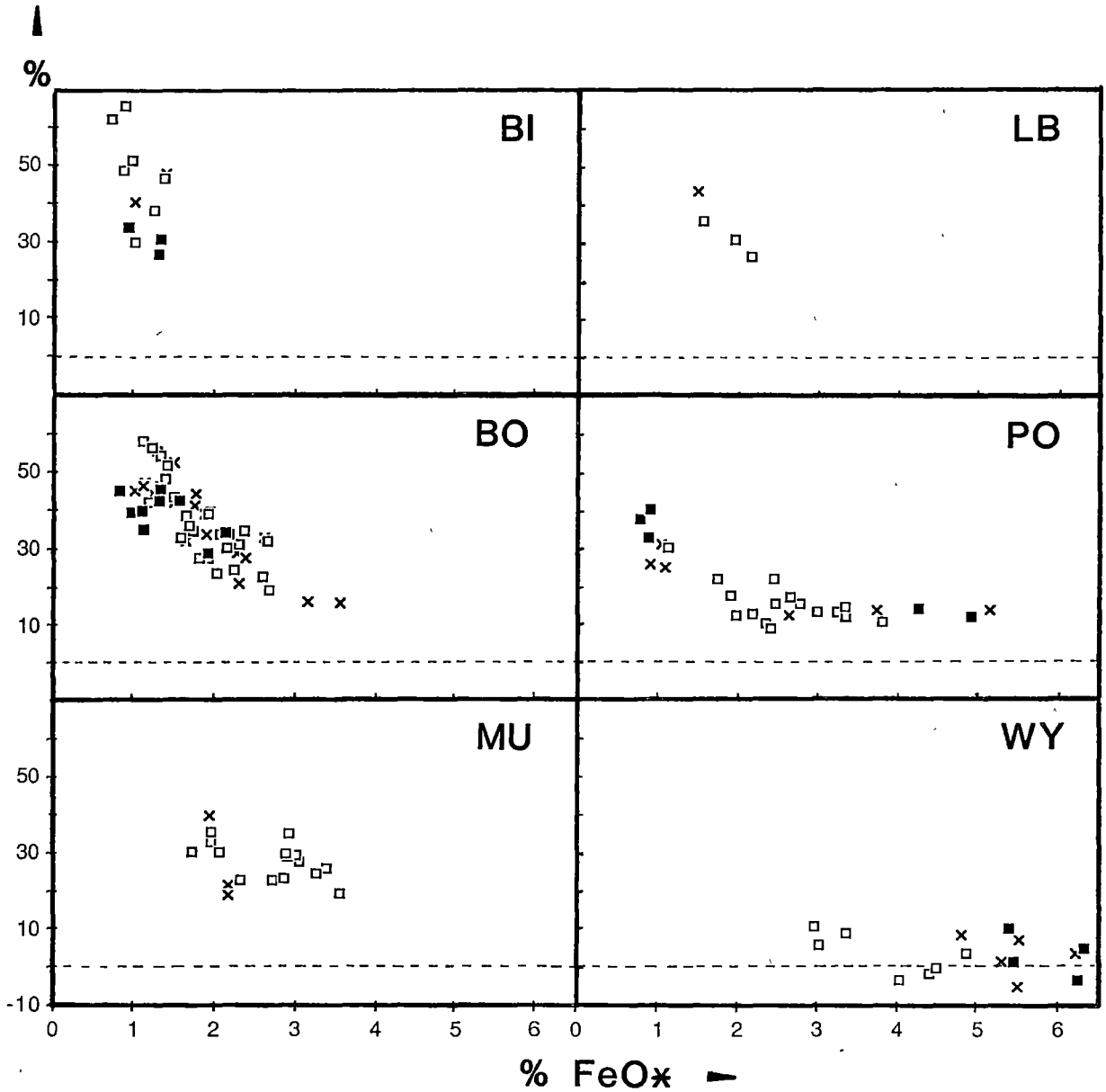

CaO

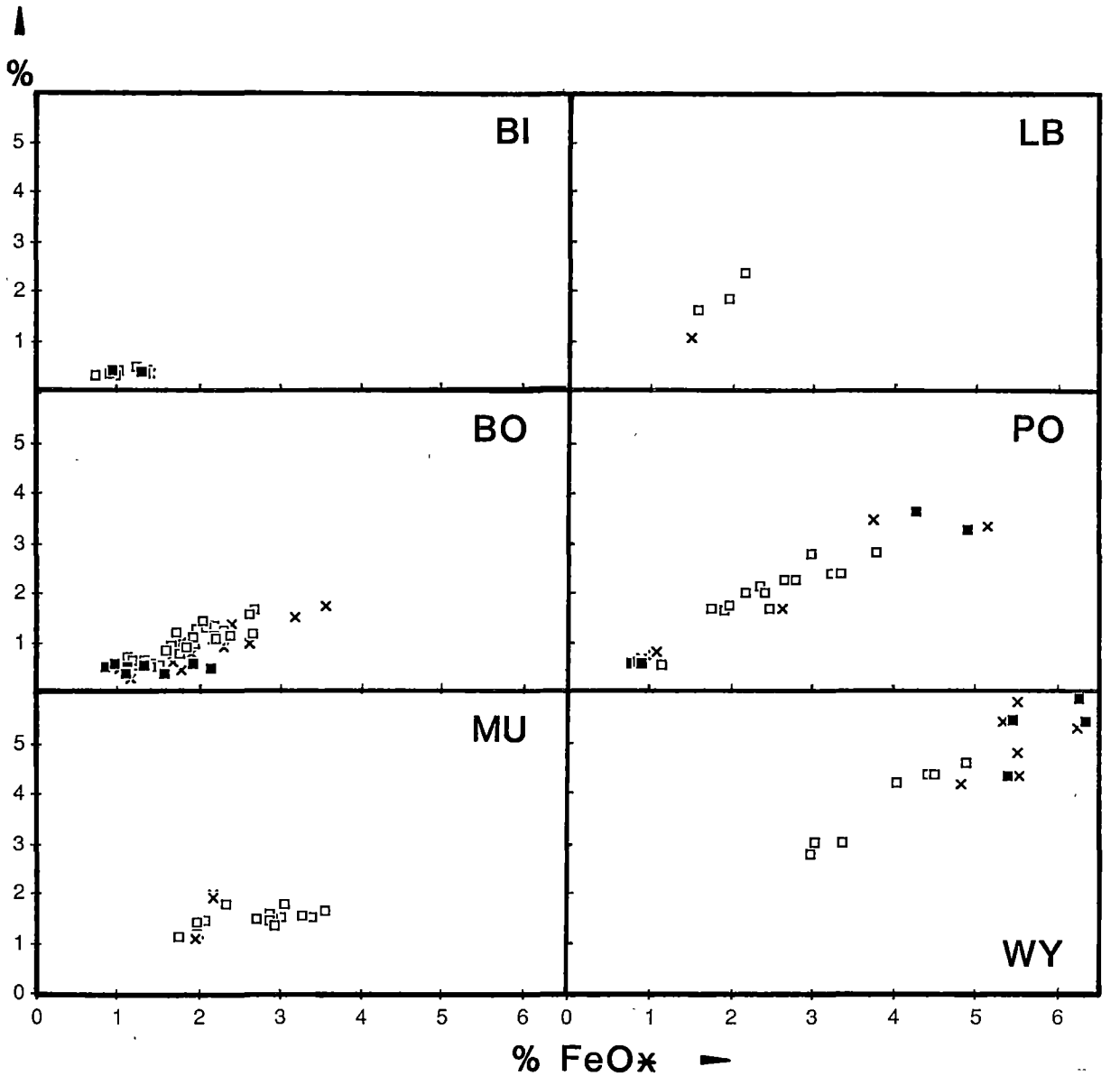

MgO

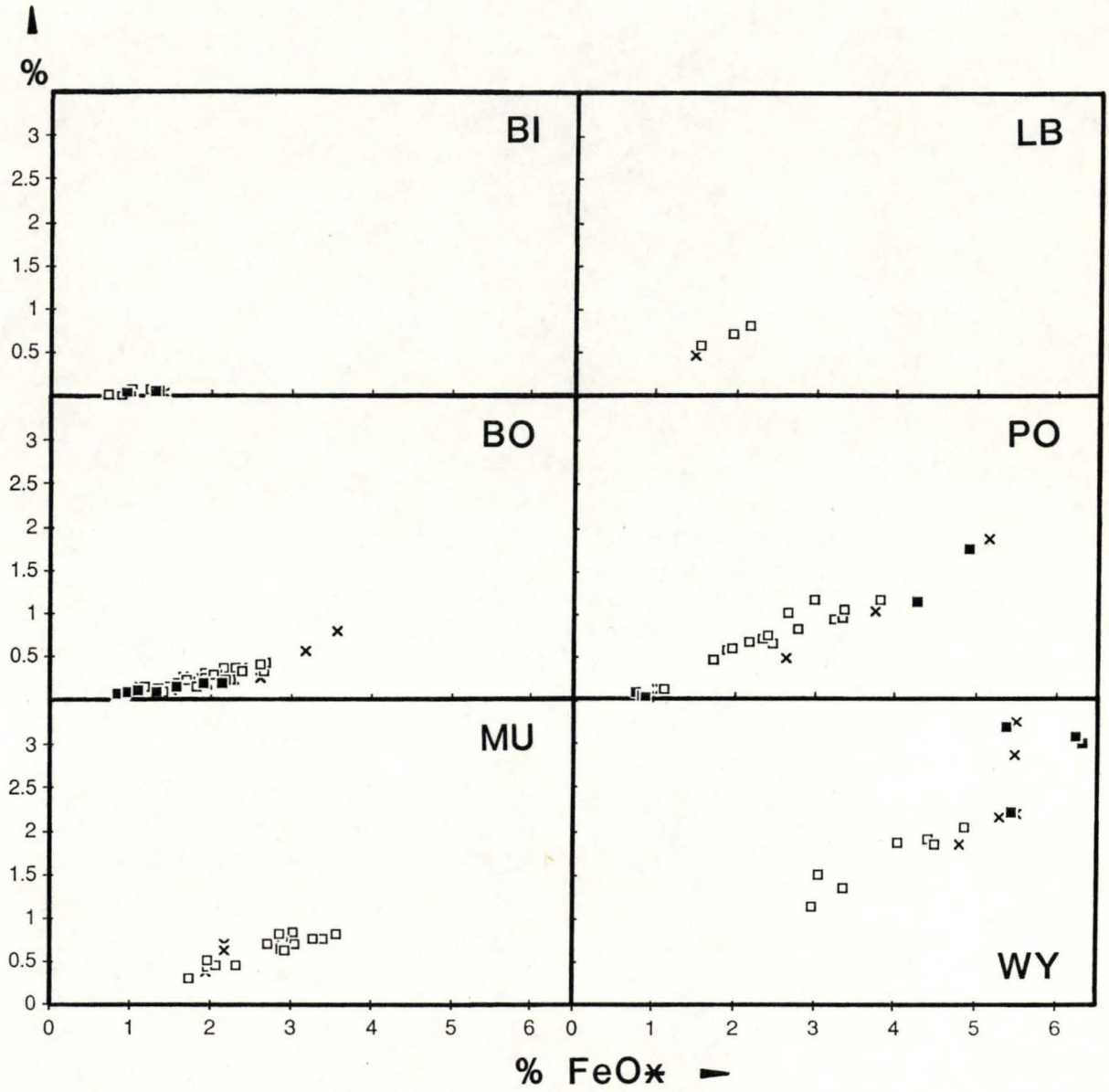

Na_2O

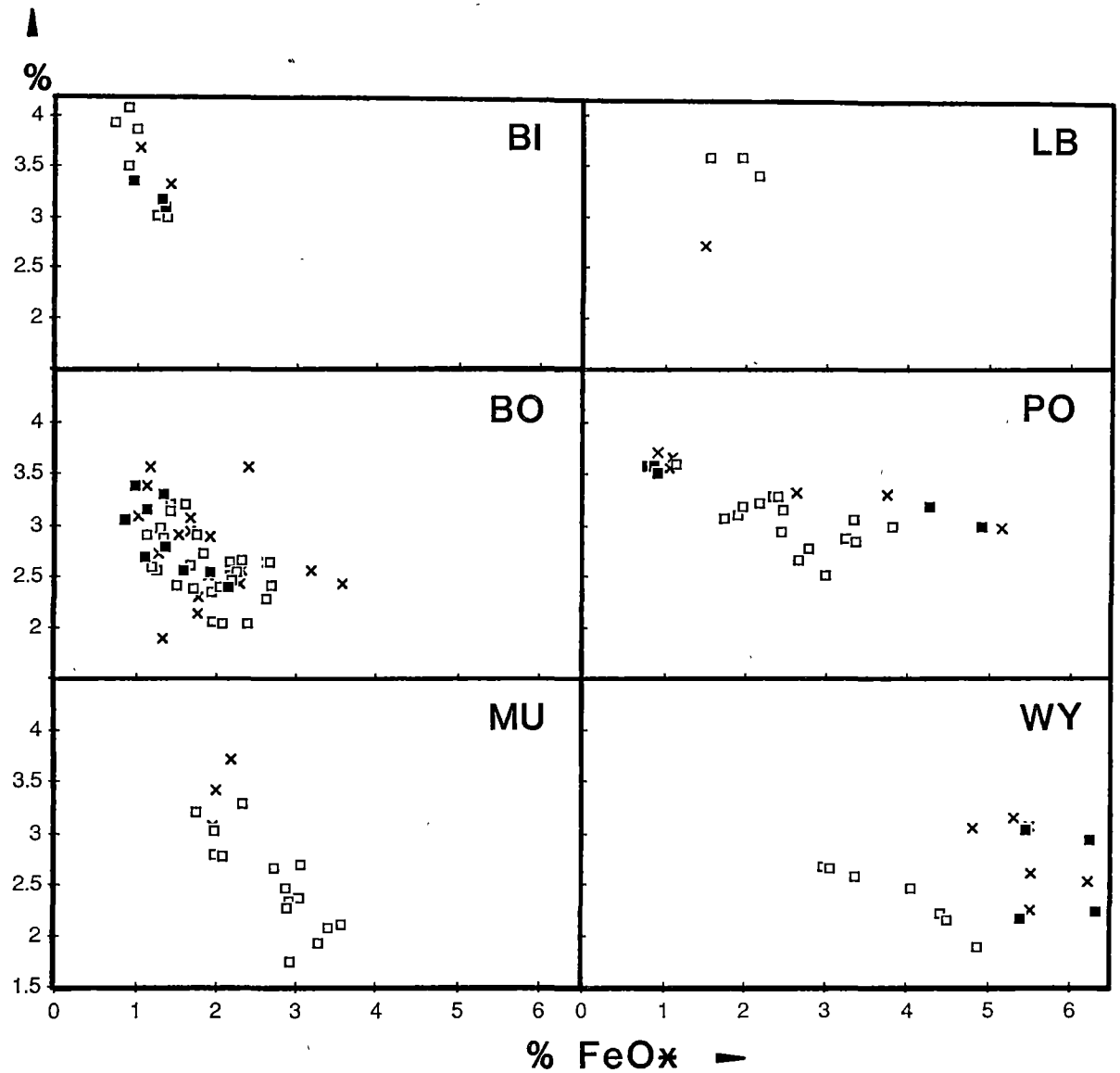

K_2O

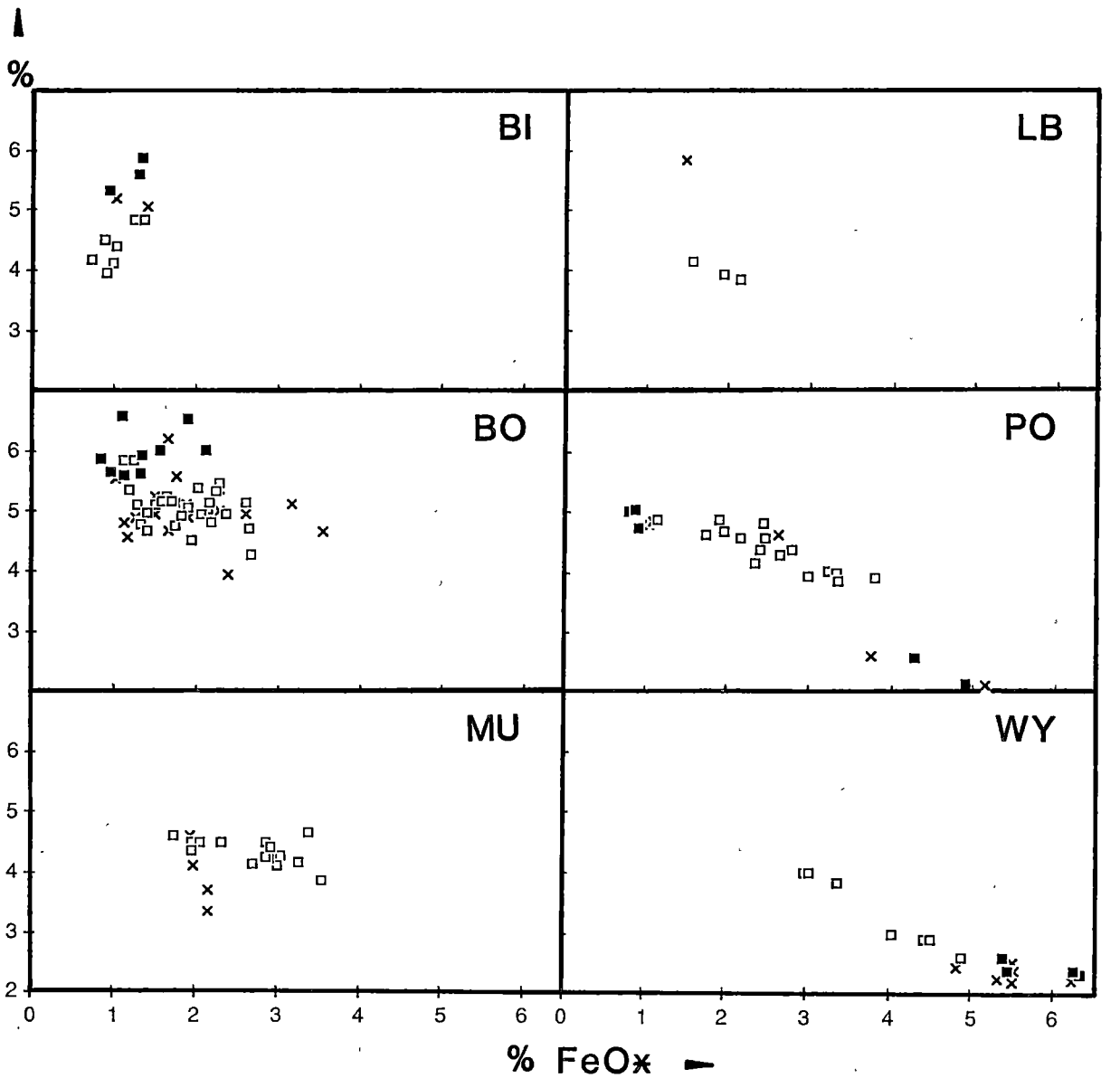

Ba

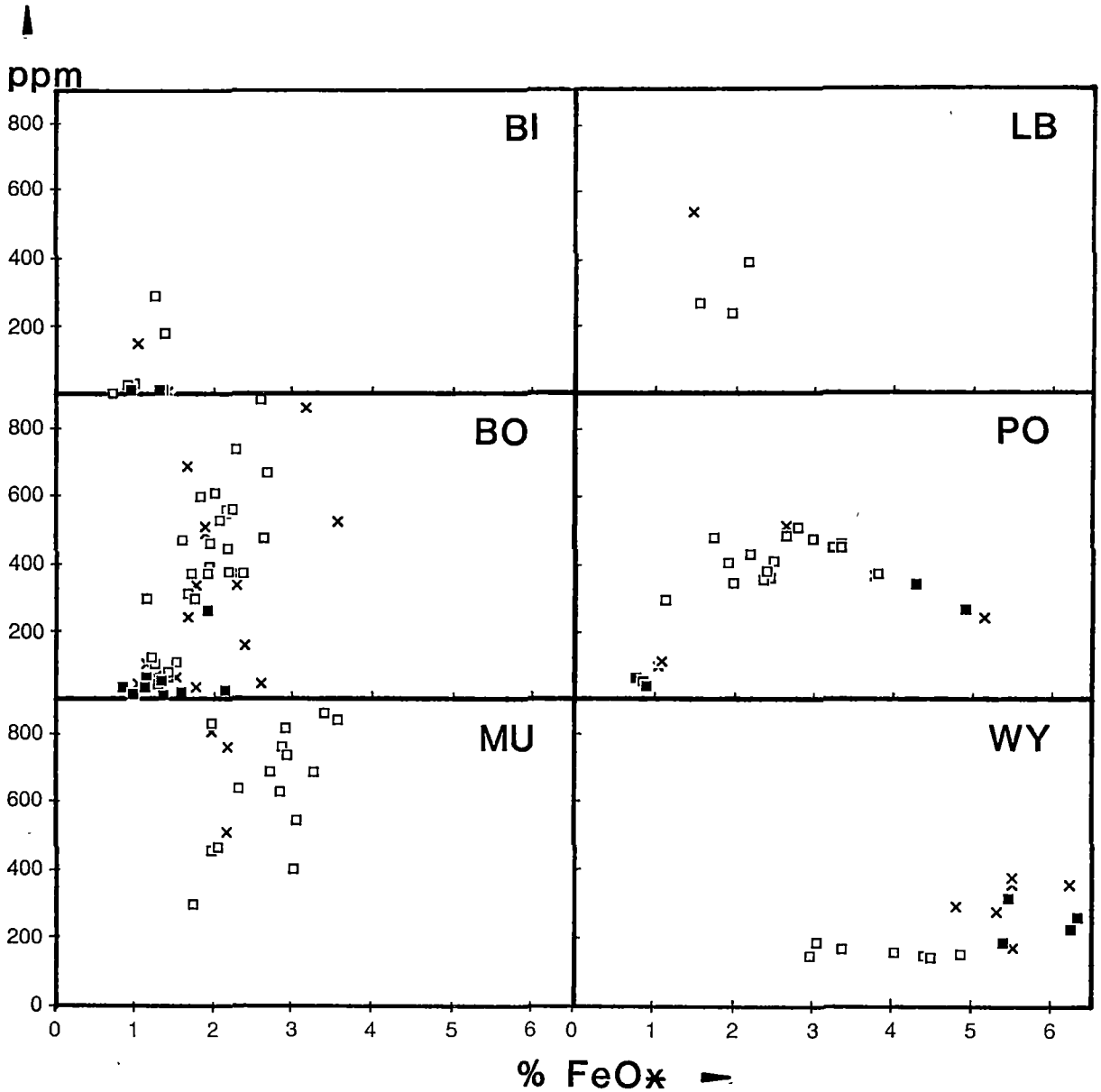

Rb

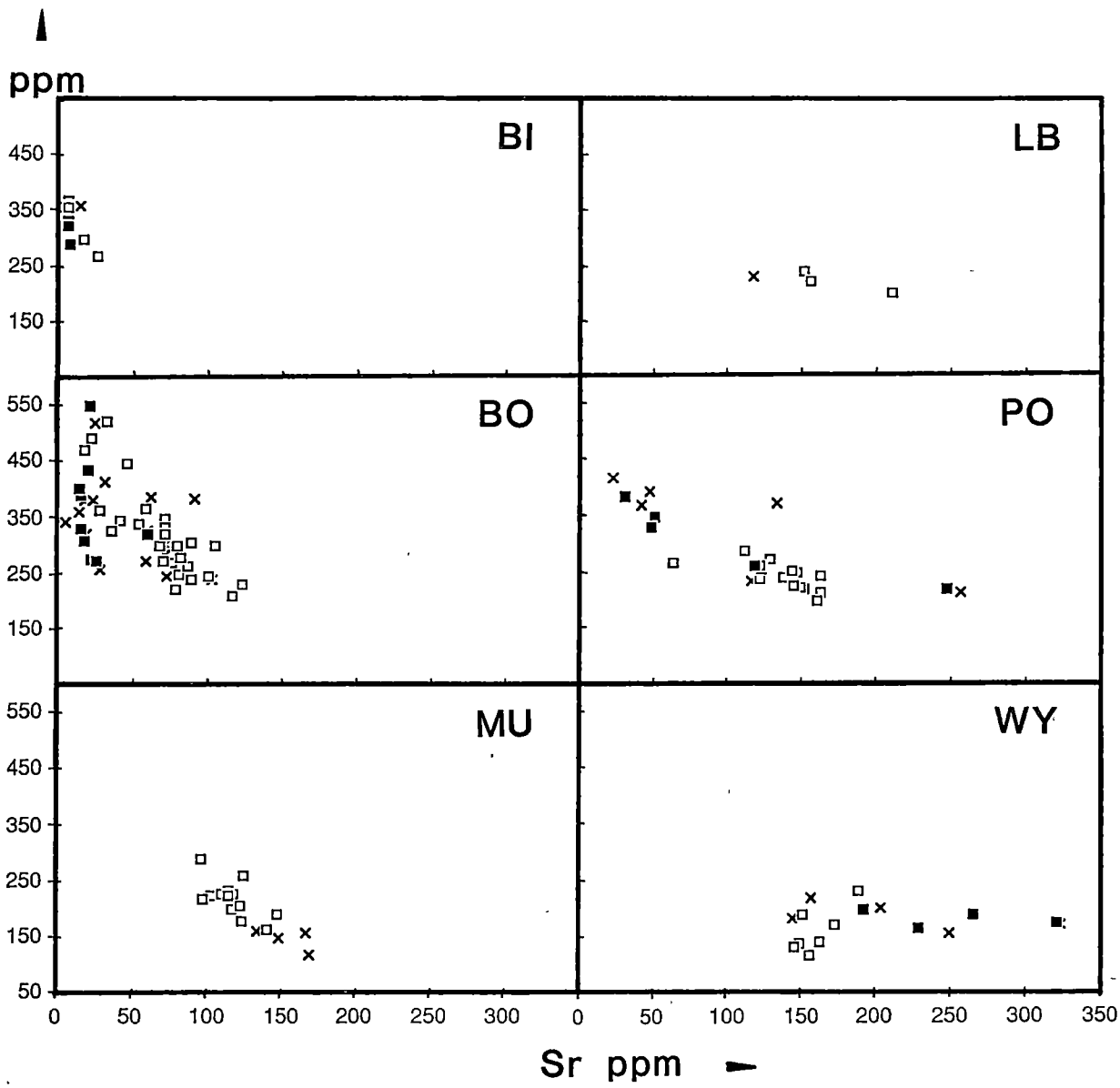
ppm
BI
LB
BO
PO
MU
WY
450
350
250
150
550
450
350
250
150
550
450
350
250
150
50
0 50 100 150 200 250 300
0 50 100 150 200 250 300 350
Sr ppm

Nb

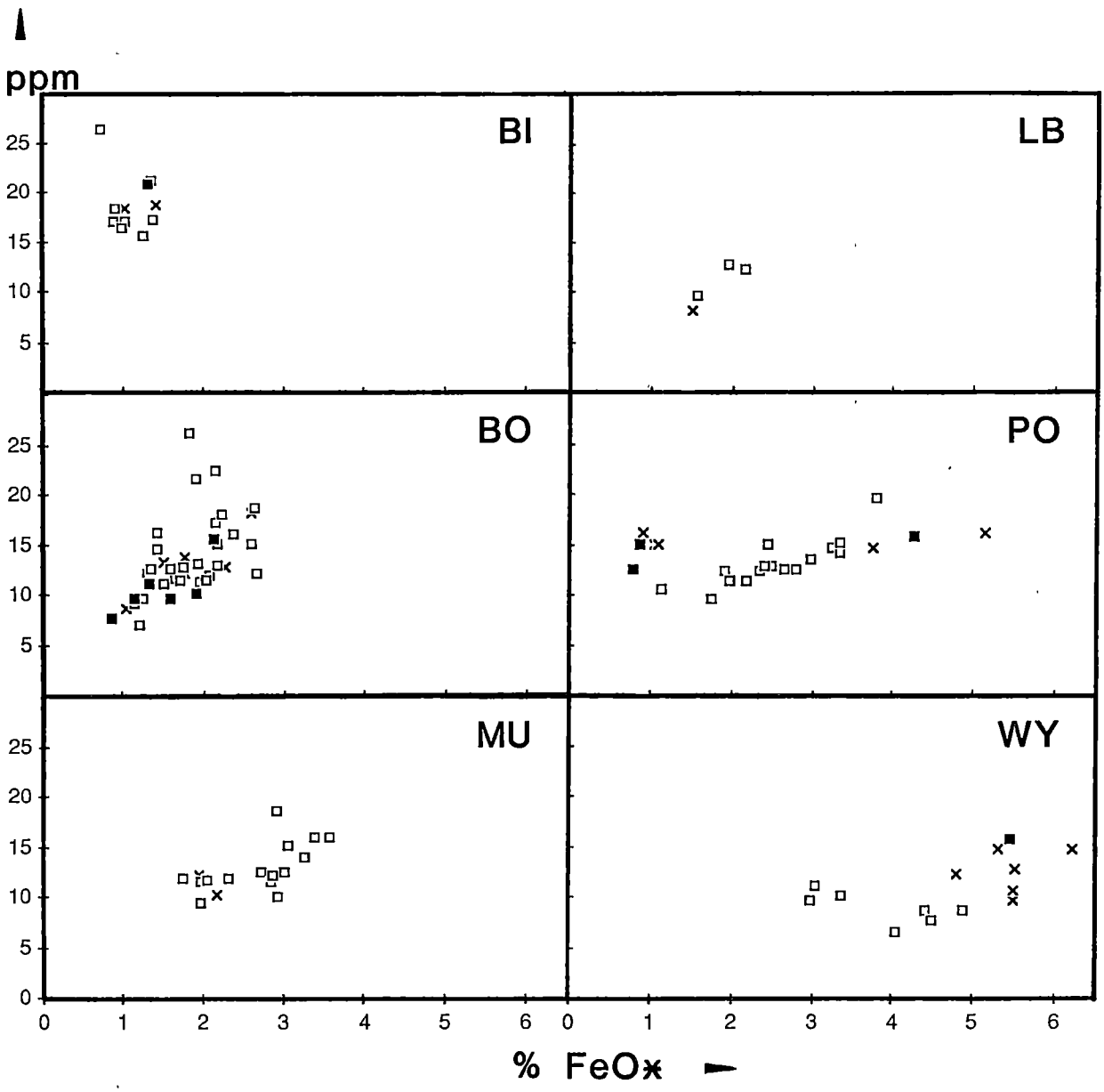

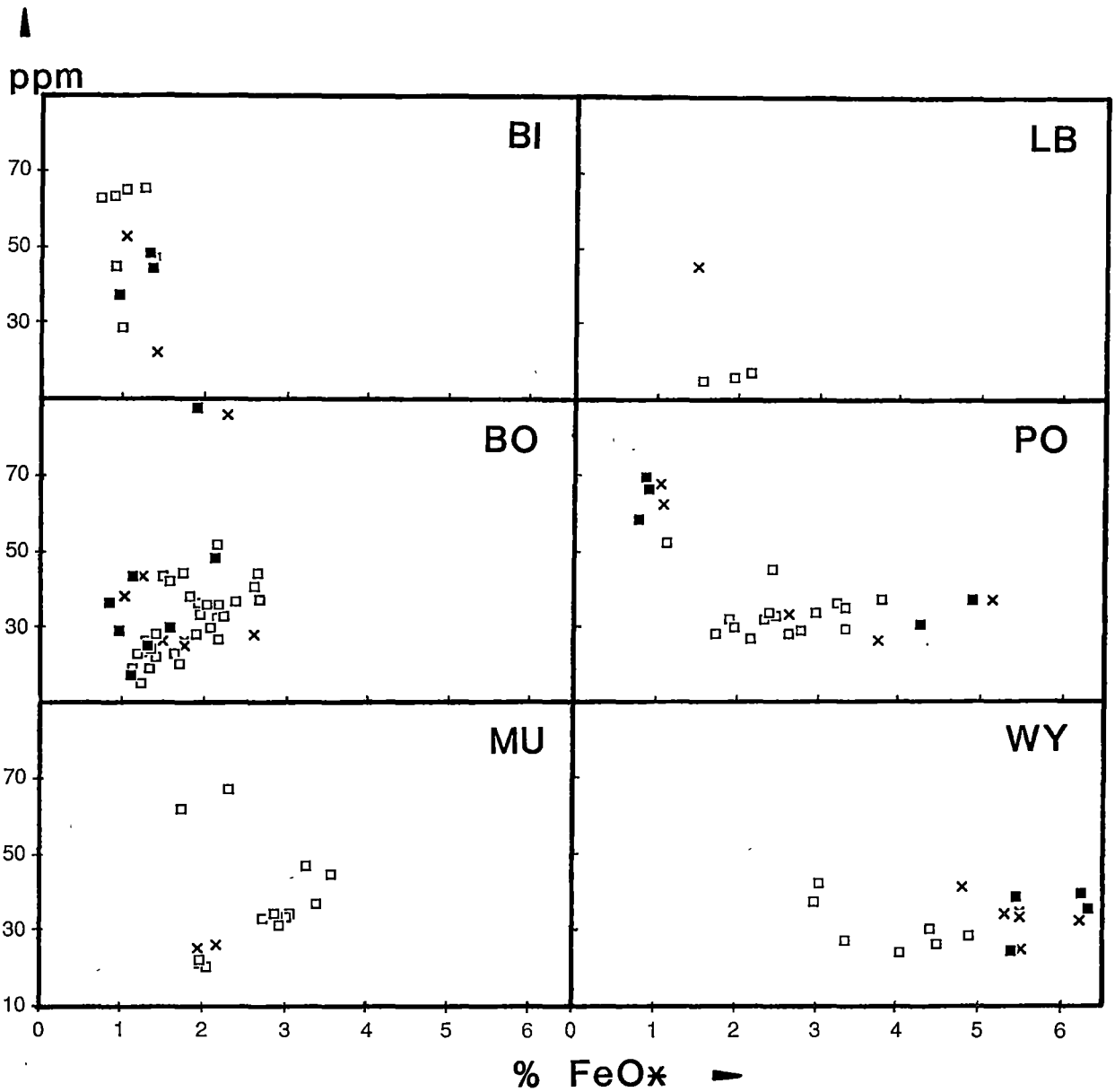
Y
ppm
BI
LB
BO
PO
MU
WY
70
50
30
10
0
1
2
3
4
5
6
% FeO*

Sc

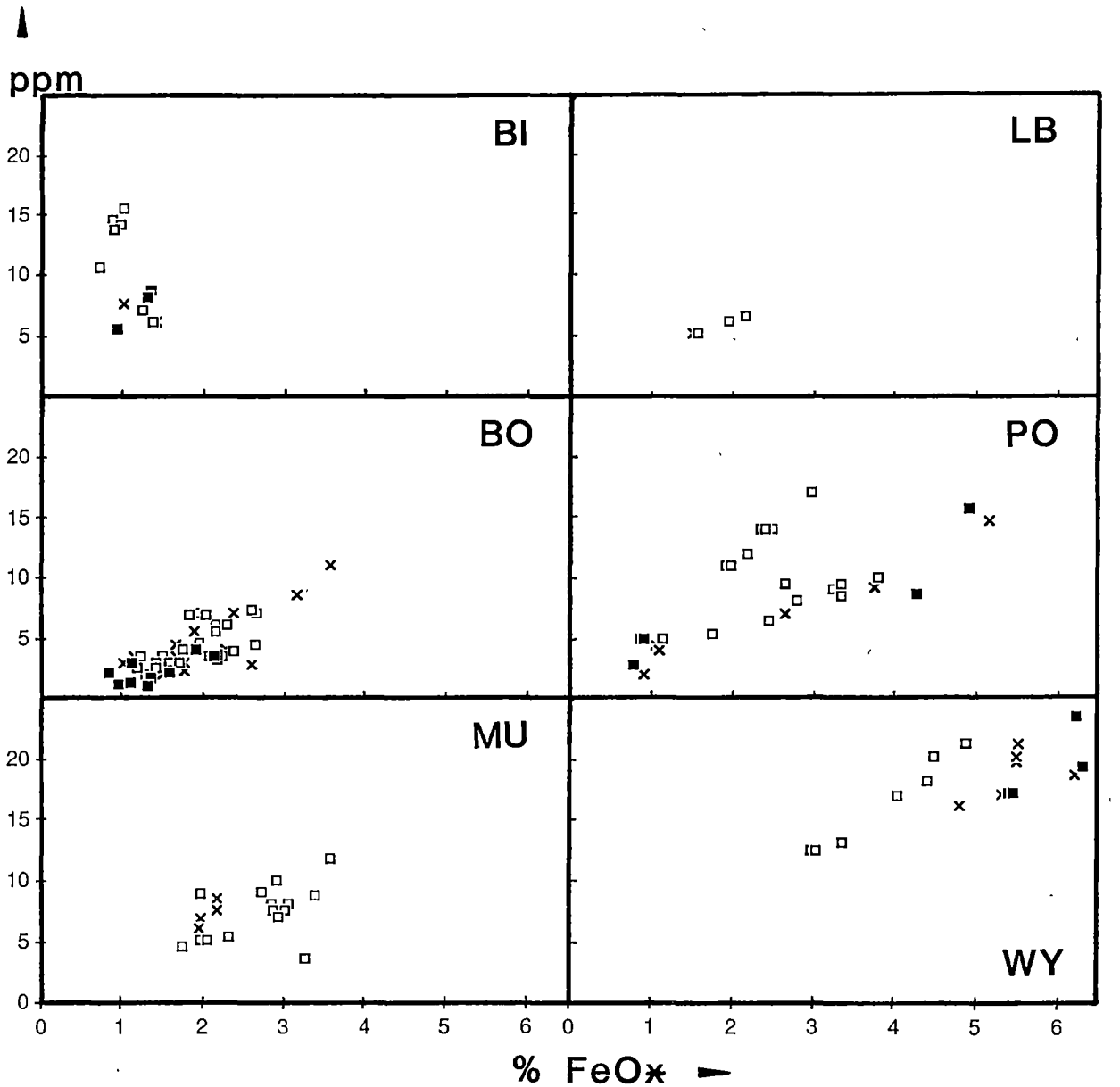

V

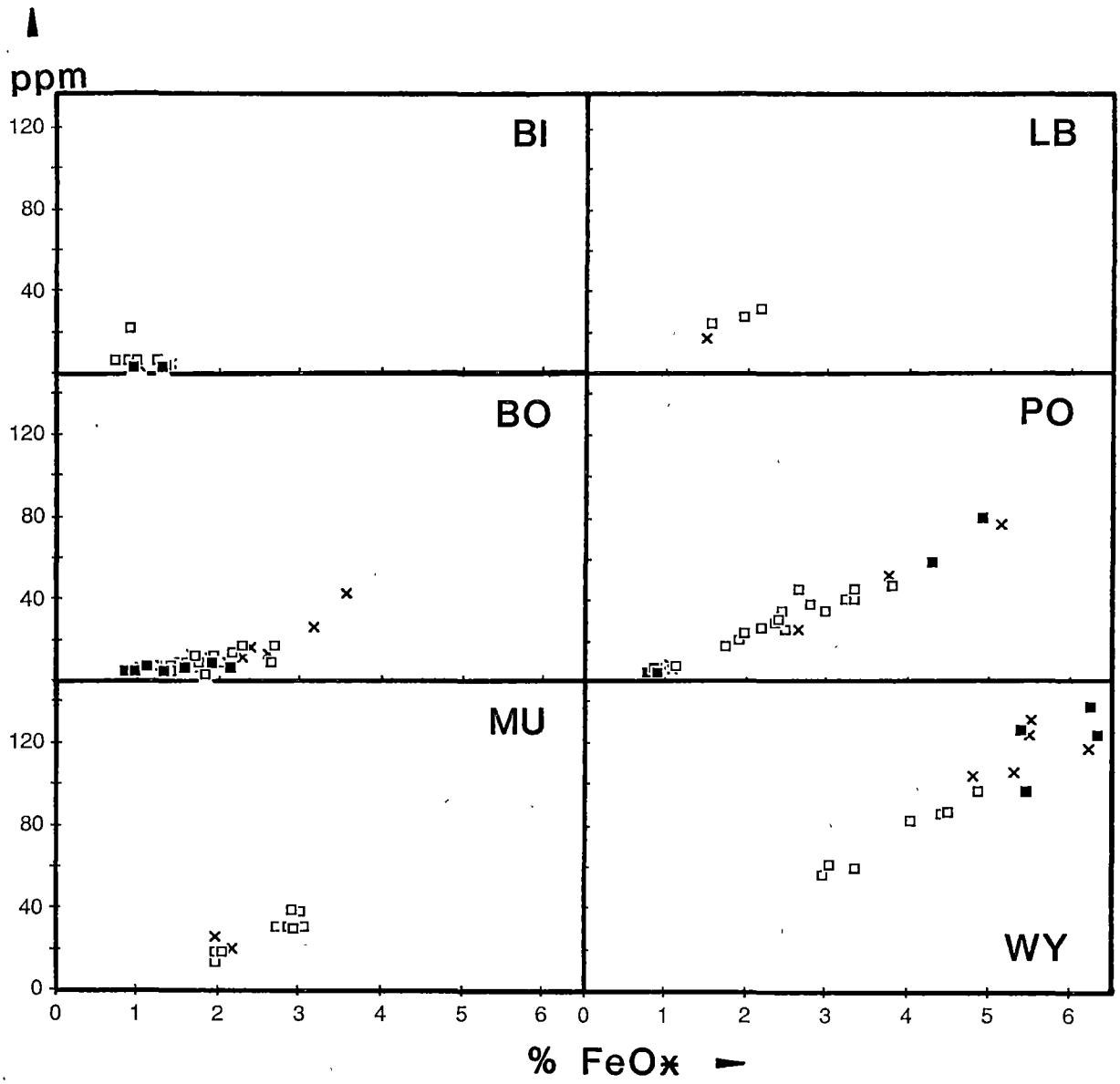

Ga

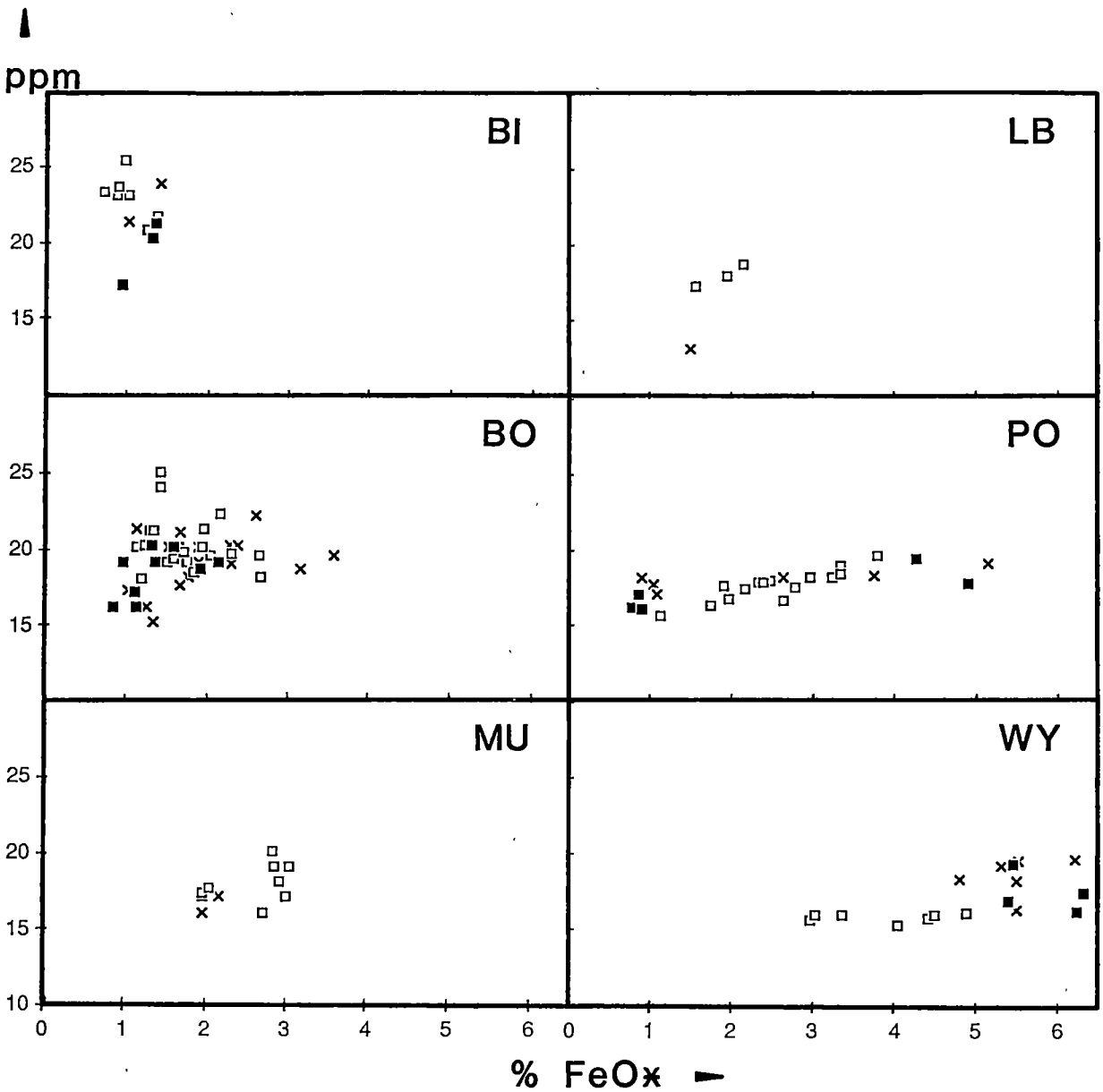

Sn

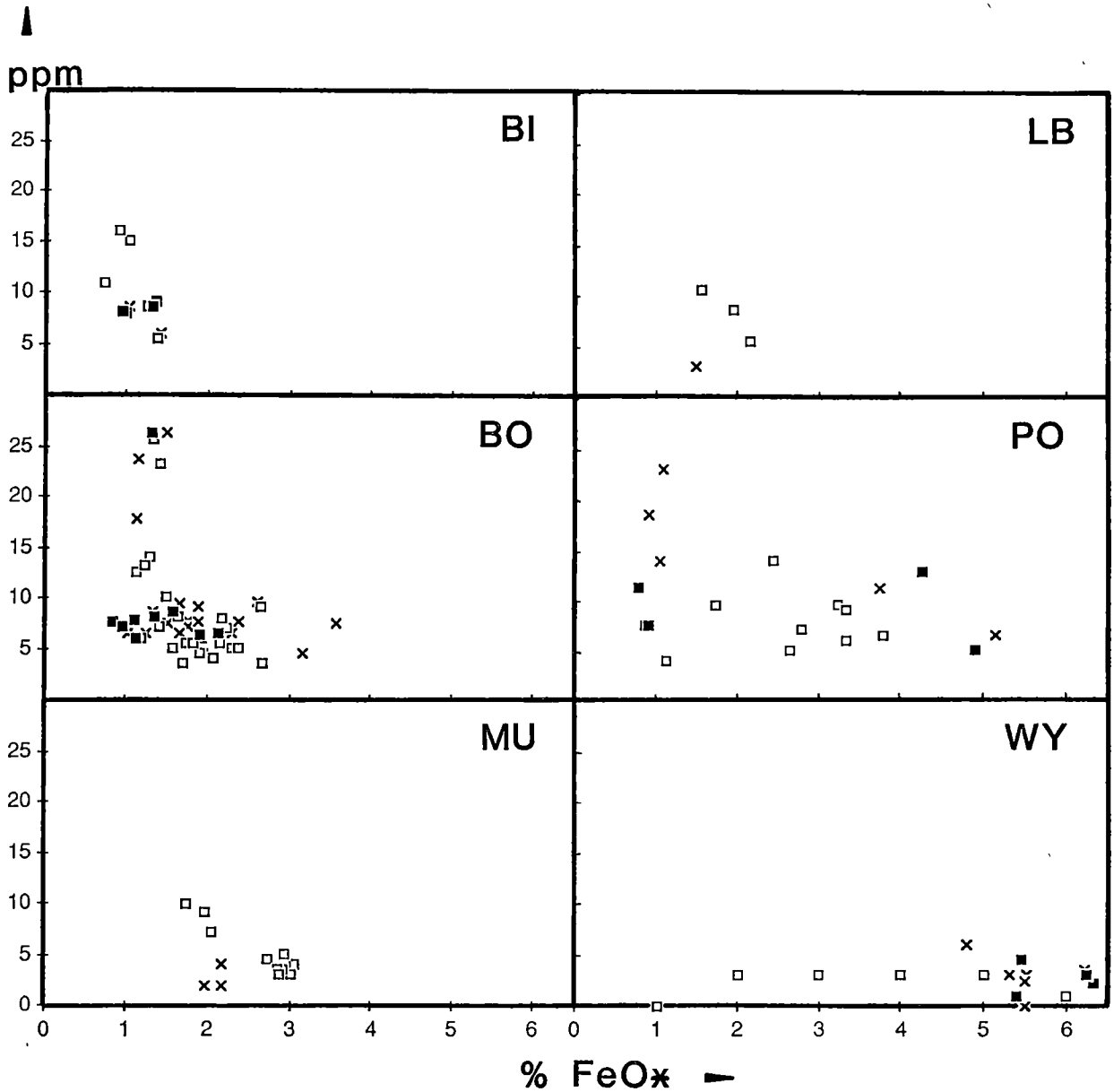

When taken together, the collective data for all three sample types yields suite trends which can usually be distinguished from each other, when the data for each suite are superimposed on the one diagram. Some trends overlap (e.g. on the FeO* versus SiO_2 diagram). However, when all 16 composite diagrams are considered, each chemical suite is seen to have unique features. Suite trends are graphical presentations of the first-order chemical differences between sample groups (Chappell et al., in press).

Wybalenna Suite compositions are more cafemic than those of the other suites. They have the lowest peraluminous (al) indices [molecular excess Al_2O_3 as a percentage of excess Al_2O_3+FeO*+MnO+MgO], consistent with their hornblende-bearing mineralogies. Alkalis behave incompatibly, increasing strongly with decreasing FeO*. As with other mafic I-type granites, Sr, Sc and V contents are high whereas Rb, Ba, Ga and Sn contents are low (Chappell & White, 1984).

Poimena Suite compositions form impressive large-range linear trends which are typical of I-type granitic suites (White & Chappell, 1977). They are often curved (e.g. (al) versus FeO*, Rb versus Sr, and Ba versus FeO*). TiO_2 contents are high. Alkalis increase moderately with decreasing FeO*. The peraluminous (al) index remains low for much of the trend but curves upwards at its felsic end. The Ba versus FeO* trend is strongly curved. Data for the granites and the phenocryst-rich porphyry #67532 plot on the high-Ba side whereas those of the phenocryst-poor porphyries and matrixes plot on the low-Ba side of the trend. The Sn versus FeO* trend is broad. The mean Sn concentration for rocks of this suite is higher than those of the other suites. The biggest known alluvial Sn deposits in the Furneaux Islands were derived by weathering of Poimena Suite granites (Chapter 2).

Data for Lady Barren Suite rocks are scarce, and the association of the phyric-poor porphyry from Castle Rock Point (western Flinders Island) with the granites of the Lady Barren and Puncheon Point Plutons (from southeastern Flinders Island and Cape Barren Island) is tentative at present. The rocks of this suite have very high Al_2O_3 contents but are only moderately peraluminous because they are more calcic than those of the other S-type granites in the batholith. Peraluminous indices increase strongly with decreasing FeO*.

Musselroe Suite rocks are siliceous and have the restricted compositional ranges typical of S-type granites. Covariance diagram trends are usually more scattered than those of the I-type Poimena and Wybalenna suites: another S-type granite characteristic. For a given FeO*, rocks of this suite are rich in TiO_2 and Ba. Al_2O_3 increases markedly with decreasing FeO*, unlike the trends for the I-type suites. The peraluminous

index increases only marginally in the same direction however, because the Na_2O trend parallels that of Al_2O_3.

Boobyalla Suite compositions superficially resemble those of the Musselroe Suite. They are felsic and yield scattered trends on covariance diagrams. They are however, both less cafemic and less titaniferous than are Musselroe Suite compositions. The peraluminous index increases strongly with decreasing FeO*. The Rb versus Sr and Sn versus FeO* trends have substantial curvature; FeO*-poor rocks of this suite have higher Rb and Sn than those of the other suites reaching 1041 and 67 ppm respectively in the aplite #62624 (Fig. 5.2). The ranges and the maximum concentrations of Ba, Y, Nb and Ga (see below) are also greatest for the Boobyalla Suite, although covariance diagram trends for these elements are less regular than those with other elements.

Babel Island Suite compositions are very siliceous and have small to very small ranges in major-element concentrations. They are the least cafemic and least titaniferous but are the most sodic. Although their Al_2O_3 contents are low compared with those of other suites, they are the most peraluminous, because their contents of femic components are extremely low. This feature accords with the peraluminous mineralogy indicated for rocks of this suite (Chapter 4). K_2O decreases with decreasing FeO*, a major-element feature which distinguishes it from all other suites. Babel Island Suite composition have high concentrations of the trace elements Nb, Y, Sc and Ga and low concentrations of Ba, Sr and V. Bulk trends for this suite are distinguished from felsic extensions of Boobyalla Suite bulk trends on each of the K_2O, Y, Nb, Sc and Ga versus FeO* diagrams and the Rb versus Sr diagram.

5.4 ROCK-TYPE CHEMICAL CHARACTERISTICS

Second-order chemical features often occur within each chemical suite. They reflect the sample type and their features can be recognised on covariance diagrams.

Granites

Granite data yield compact trends with short ranges. Granite trends for the Wybalenna and Poimena Suites are less scattered than those of the other suites. However, for all the suites there is a variation in the amount of scatter from one diagram to another. Components plotted with respect to FeO*, which exhibit the least scattered trends are TiO_2, MgO and V; those with the greatest scatter are Na_2O, Ba, Y, Nb and Sn.

Porphyries

Data for porphyry whole-rocks form different trends in different suites. The phenocryst-poor porphyries of the Wybalenna Suite are inclusions from Wybalenna and (in the case of #62602) Poimena Suite granites. They are all relatively mafic. On covariance diagrams, they may form elongate trends which are not always colinear with those of the granites. For example, the porphyries may form cross-cutting or en echelon trends to higher TiO_2, Al_2O_3, Na_2O, Ba and Ga, but to lower SiO_2 and Sc, than the granite trends or their linear extensions (Fig. 5.1).

Poimena Suite porphyries span large ranges both in SiO_2 (68.2% to 76.5%) and in FeO* (0.9% to 5.2%). The felsic samples are from high-level intrusions. One mafic sample (#62594) is an inclusion from Poimena Suite granites. The other (#62612) is of the Holts Point Porphyry, which intrudes Boobyalla Suite granites. They are more peraluminous than the granites or mafic porphyries. They are enriched in Rb and Sr and depleted in Sr relative to the granite compositions. These mafic compositions have higher SiO_2 and lower Al_2O_3 and CaO than do Wybalenna Suite porphyries with similar FeO* contents. Otherwise, they resemble these porphyries in composition.

Compositions of Boobyalla Suite porphyries yield trends which extends beyond those of the granites. Scatter is most pronounced in FeO* covariance diagrams of Ba and the alkalis, and on the Rb versus Sr diagram. This feature is thought to largely reflect variations in proportions of Ba- and Rb-rich megacrystic alkali feldspar and Ba- and Sr-poor matrix in the whole-rocks. This interpretation is supported by petrography; phyric-poor porphyries have less Ba and Rb than do phyric-rich porphyries.

Matrixes

Matrix separate data from Wybalenna and Poimena Suite porphyries are similar to those of the respective bulk rocks from which they were extracted. Like their host rocks, the matrixes from the felsic Poimena Suite porphyries are strongly depleted in Ba and Sr and enriched in Rb, Nb and Y compared with other samples of the same suite.

Boobyalla Suite matrix compositions yield oxide trends which can often be distinguished from those of the suites' granites. For a given FeO* content, matrixes have lower SiO_2, TiO_2, MgO, CaO, Sr, Ba, Nb, Sc, V and Ga contents and higher K_2O, Y and Sn contents than do most of the whole-rocks.

The three sample types from the Babel Island Suite cannot be distinguished from each other on the basis of composition and the collective trends for this suite are superficially similar to those of the

FIGURE 5.2

COVARIANCE DIAGRAMS FOR SOME VICTORIAN GRANITES

MATHINNA BEDS FLYSCH AND OTHER ROCKS

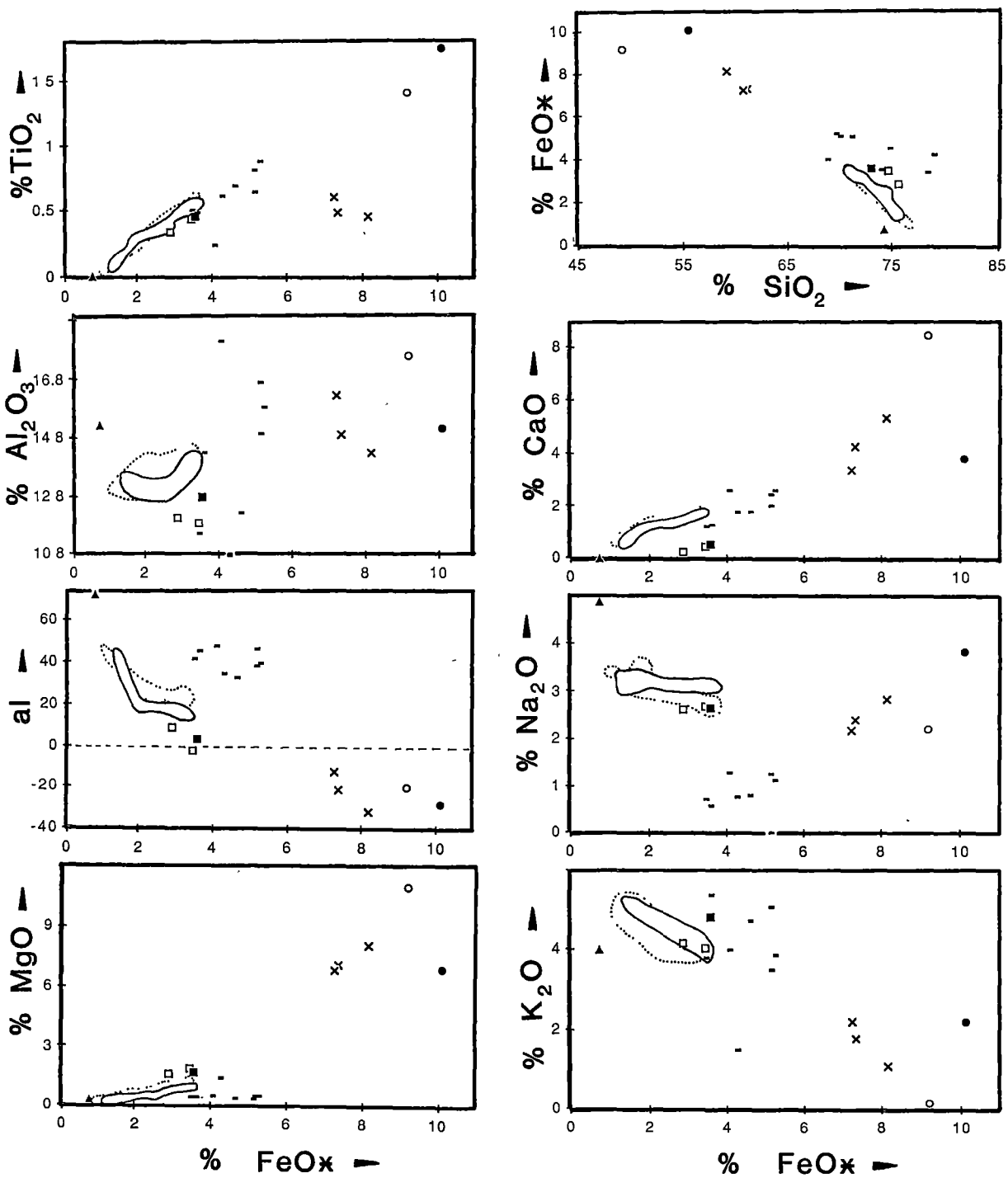

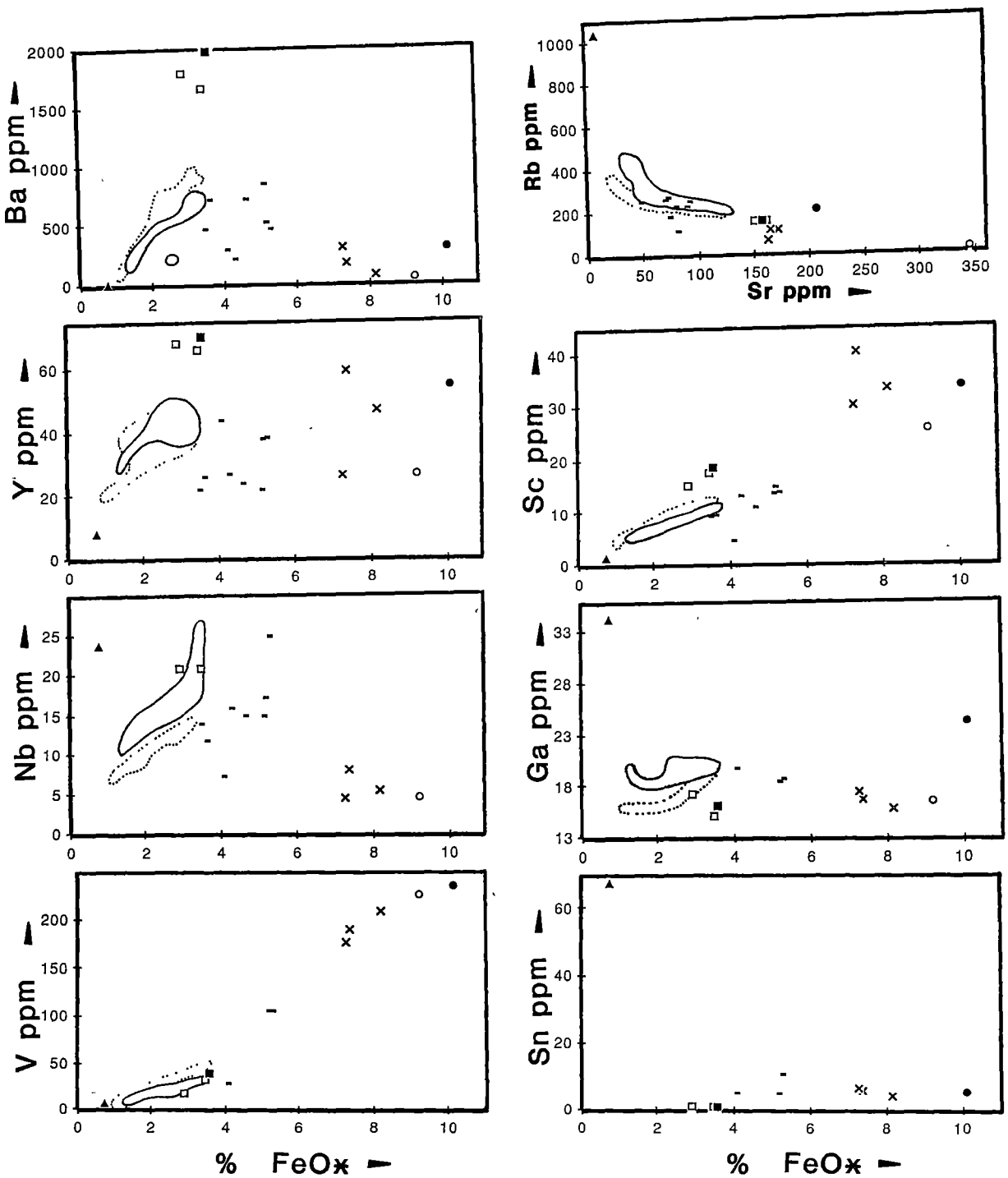

Data presented are for: Wilsons Promontory granites (field marked by continuous line); Strathbogie granites (field marked by dashed line); Mathinna Beds flysch: #67540-67542 and flysch samples in Appendix O (dashes); Boobyalla Suite aplite: #62624 (triangle) ; Poimena Suite/basalt hybrid porphyries: #67530, 67531 (open squares); Poimena Suite/basalt hybrid porphyry matrixes from #67530 (felsic matrix - filled square, mafic matrix - dot); mafic inclusions from the Pats River Granite: 62629, 62630 and 62632 (crosses) and a metabasalt: #67538 (circle).

Boobyalla Suite matrix trends. However in detail the Babel Island Suite compositions are richer in Na_2O, FeO*, Nb, Y, Sc and Ga and poorer in K_2O, Al_2O_3 and MgO than are the matrixes of the Boobyalla Suite.

Other Rock Types

Fig. 5.2 consists of 16 covariance diagrams depicting data of selected porphyries from Wybalenna Suite granites, hybrid Poimena Suite porphyries and matrix separates, country-rock flysch, a basalt from a dyke intruding the Lady Barren Pluton, and a Boobyalla Suite aplite. Also illustrated on each diagram are the outlines of two trends formed by:
(a) data of 15 granites from the Wilsons Promontory Batholith, and
(b) data of 25 granites from the Strathbogie Batholith.
These are Victorian batholiths, occurring respectively 110 km and 250 km to te northwest of Flinders Island. The following features are indicated from a comparison of the data of Figs 5.1 and 5.2:

(a) that the Wilsons Promontory granites are chemically indistinguishable from and therefore belong to the Boobyalla Suite;

(b) the Strathbogie granites belong to the Musselroe Suite;

(c) Wybalenna Suite granite magmas forming the Pats River Pluton, were mixed with phenocryst-poor andesitic magmas to generate the porphyry incusion suite. The andesitic magmas were not directly related to the dacitic magmas which intruded the Cape Sir John and Wybalenna Pluton granite magmas to generate the porphyry inclusions of the same suite whch are compositionally illustrated in Fig. 5.1. The andesitic inclusions are less aluminous, less titaniferous, more metaluminous and richer in Ga (Fig. 5.2) than are the linear expressions of the trends of the dacitic inclusions (Fig. 5.1);

(d) data for the andesitic inclusions from the Pats River Pluton and the metabasaltic dyke intruding the Lady Barron Granite frequently form a single trend, consistent with these rocks being petrogenetically related;

(e) the finely dispersed metabasaltic matrix separated from the hybrid Poimena Suite porphyry (#67530) is richer in SiO_2, TiO_2, FeO*, Na_2O, K_2O, Ba, Rb, Y, Sc and Ga but poorer in Al_2O_3, MgO, CaO, (al) and Sr than the metabasaltic dyke rock #67538. Most of these differences can be attributed to reactive exchange with the felsic liquid in the composite dyke which is richer in components of the first group and poorer in components of the second group, relative to component concentrations in the metabasaltic dyke. The precise origins of the metabasaltic component of the composite dyke however, are unknown;

(f) the whole rocks and felsic matrix separate from the basalt-hybridized Poimena Suite porphyries #67530 and #67531 have lower SiO_2, Al_2O_3,

(al), Na_2O, K_2O, Rb and Sn but higher TiO_2, MgO, CaO, Ba, Sr, V and Sc than do unhybridized dyke rocks and matrixes of the same suite (see Fig. 5.1). These compositional differences are consistent with the reactive exchange described in (e) above. However the Ba, Nb and Mn contents of the composite dyke rocks and the felsic matrix separate are higher than either of the endmember compositions. This feature indicates that processes more complex than two-component mixing were in progress during magma mixing. Such processes include the phase-selective dissolution and replacement of alkali feldspar phenocrysts by plagioclases, described petrographically in Chapter 4. High Ba contents might be derived in this manner. The anomalous Mn and Nb contents may have been generated by selective dissolution of phases such as ilmenite, cordierite or biotite present in the original felsic magma;

(g) many Boobyalla and Babel Island Suite granitic rocks are more peraluminous than the country-rock flysch;

(h) none of the compositions of the granitic suites can be generated from any other, by two-component mixing with country-rock flysch; and

(i) the Boobyalla Suite aplite #67624 has extremely high contents of Al_2O_3, Na_2O, Rb and Ga, and extremely low contents of MgO, K_2O, Ba and Sr, relative to other Boobyalla Suite compositions. These features are thought to reflect the chemical nature of the most evolved melts of the magmas of this suite.

5.5 DISCUSSION

The second-order features illustrated on the diagrams in Fig. 5.1, are considered to have implications for the nature of the magmas of each suite. For all but the Babel Island Suite, differences can be observed between the chemical features of phyric-poor porphyries plus matrix separates on one hand, and phyric-rich porphyries plus granites on the other. Good examples of this dichotomy are indicated by Poimena Suite data on the Ba versus FeO* plot and by Boobyalla Suite compositions on the MgO, CaO, K_2O and Ba plots. This dichotomy is interpreted as indicating that:

(a) the melt phases in the magmas of the Boobyalla, Poimena and Wybalenna Suites at least, had extensive compositional ranges;

(b) the melt and the bulk-solid constituents of these magmas had different compositional trends; and

(c) the granites of these suites were probably derived by solidification from crystal-rich rather than liquid-rich magmas.

There are major implications for granitic classification, magmatic processes and provenance in the existence of separate liquid and bulk-solid compositional trends. For example, the existence of compositional trends for melts precludes magmatic evolution solely by restite-unmixing because during evolution by this process the melt is assumed to have a fixed chemical composition (White & Chappell, 1977; Chappell et al., in press). Some form of chemical fractionation process is therefore implicated during the magmatic evolution of many of the BTB granites.

If an efficient means of separating melt from solid during magma evolution exists, then it is possible for two different chemical suites to be derived from the one protolith: one derived from crystal-poor magmas and the other from crystal-rich magmas.

Babel Island Suite chemical data form a single trend for all rock types which has many similarities to the chemical trend defined by the compositions of the porphyry matrix separates of the Boobyalla Suite. These similarities could reflect a common source for the rocks of these two suites. This notion is persued in Chapter 12.

Chapter 6
MINERAL SEPARATE CHEMISTRY

6.1 INTRODUCTION

Minerals were separated from porphyries and mineral segregations so as to obtain trace-element chemical data to augment the major element data obtained by microprobe chemical analysis (Chapter 7).

The methods by which mineral separates were obtained and analysed are described in this chapter. Mineral compositions are then presented and described. Finally, the significance of mineral and matrix-separate compositions for granite petrogenesis is discussed.

6.2 METHODS

Eighteen phenocryst phases (5 alkali feldspars, 12 plagioclases and 1 biotite) and a pseudomorphing biotite were separated from selected granitic porphyries and porphyritic granites of the Furneaux Islands. Seven additional minerals (1 alkali feldspar, 1 plagioclase, 2 biotites, 2 garnets and 1 cordierite) were extracted from coarsely crystalline mafic mineral segregations.

Most of these minerals were hand-picked from thin slices of whole rocks, in the same manner as porphyry matrices were separated (cf. Chapter 5). Biotite and garnet samples from the two mafic mineral segregations were however augmented by separates from the crushed whole rock.

Extracted phases were washed in water, dried then ground. A Franz magnetic separator and heavy liquids (tetrabromoethane and diiodomethane) were used to extract impurities.

After processing, many of the mineral separates were present in amounts insufficient to make both sintered glass discs and a pressed powder pill (for major and trace element XRF analysis respectively). They were therefore diluted by grinding each with weighed quantities of spectroscopically pure ("Spex") SiO_2 in an agate mortar under acetone. The quantities of quartz dilutant used in each case are listed in Appendix F.

The resulting mineral or mineral+quartz powders were analysed by XRF spectroscopy for major and selected trace elements as described for the whole rock and matrix separate powders in the previous chapter. For the feldspar separates, lead was analysed and magnesium was reanalysed using high-resolution XRF spectroscopy on pressed powder pellets by Dr B.W. Chappell (Australian National University). The conditions used for these analyses are described in Appendix D.

6.3 RESULTS

Cordierite, garnet and feldspar separates are estimated to have <1% of impurities. Garnet contains traces of biotite, apatite, ilmenite and xenotime. Feldspar separates contain traces of biotite. The biotite separates contain zircon, xenotime and apatite in combined amounts of <1%. They also contain quartz amounting to between ~3% and ~10% of the separate. At least some of the quartz contaminant is thought to have come from the agate mortar during the final hand grinding process. Estimates of biotite compositions devoid of quartz and apatite contaminants were made by normalising the XRF compositions to the average SiO_2 and P_2O_5 contents of the same biotites determined by electron microprobe analysis (Appendix H).

The major and trace element compositions of both the mineral separates and the separate plus "Spex" silica mixtures, are listed in Appendix F.

6.3.1 Major Element Compositions

Plagioclases vary from 100 an/(an+ab) = 56 (An_{56}) for the cores of phenocrysts from Wybalenna Suite porphyries, to An_{30} for those from the felsic Boobyalla Suite granite #62622. The cores of alkali feldspar phenocrysts vary from 100 or/(or+ab) = 74 (Or_{74}), for those from the porphyry #62595, to Or_{66} for those from granite #62622 and the porphyry #62627.

The two garnet separates have almandine-rich bulk compositions. The molar proportions of five endmembers are listed in Table 6.1, below.

Table 6.1

Endmember Compositions of Garnet Separate Bulk Compositions

Endmember	Formula	Garnet source: #62634	Garnet source: #67539
Almandine	$Fe_3Al_2Si_3O_{12}$	82.7	78.4
Pyrope	$Mg_3Al_2Si_3O_{12}$	7.3	10.0
Spessartine	$Mn_3Al_2Si_3O_{12}$	5.6	6.9
Grossular	$Ca_3Al_2Si_3O_{12}$	4.2	4.4
Yttrogarnet	$Y_3Al_2Al_3O_{12}$	0.3	0.3
mg		8.1	11.3

Semi-microdeterminations of iron oxidation state for these separates were made by E. Kiss (Australian National University) (Appendix G). They indicate that only minor quantities ($\leq$1%) of andradite endmember are present. Low totals for the garnet separate analyses (Appendix F) are consistent with the presence of substantial amounts of yttrium.

The cordierite separate from segregation #67539 has a magnesium number of 37.7. It contains ~0.3% of both Na_2O and K_2O and only traces of TiO_2 and CaO. Biotites are aluminous and iron-rich. They contain moderate amounts of TiO_2 (~3%). Ferrous/ferric ratios in biotite separates range from 28.1 to 9.1. A low K_2O content for the biotite from segregation #67539 indicates the presence of secondary chlorite.

6.3.2 Trace Element Compositions

Alkali feldspars contain substantial quantities of barium. Their normative percentages of celsian ($BaAl_2Si_2O_8$) vary from 0.9% for the separate from the mafic Boobyalla Suite porphyry #62595, to 0.2% for that from the mafic mineral segregation #62634 of the same suite.

The amounts of barium in the remaining phases decreases in the order: biotite (~300 ppm) > plagioclase (~200 ppm) >> garnet (~30 ppm) > cordierite (12 ppm).

Rubidium is most abundant in the biotites, where it is present in amounts up to 1820 ppm. Its concentrations in the other phases are: alkali feldspar - ~550 ppm, plagioclases - ~50 ppm, and cordierite - 27 ppm. Most of the rubidium in the garnet separates (12 ppm) is estimated to be present in the biotite contaminant.

Plagioclases and alkali feldspars contain ~400 ppm and ~150 ppm of strontium, respectively. The other separates contain negligible amounts of this element.

Alkali feldspars contain the highest concentrations of lead (~60 ppm). Plagioclases and biotites contain about 50% and 25% respectively of this amount. There is negligible lead in the garnet and cordierite separates.

Contents of zirconium are thought to largely reflect the relative proportions of zircon inclusions contained within each separate. These are highest in the biotite separates (Zr $\leq$ 840 ppm).

Biotites contain up to 200 ppm of niobium. This element is unlikely to be present in zircon (Deer, Howie & Zussman, 1962) and is thought to be a true component of the biotite. Similar concentrations of niobium occur in biotites from felsic granites of the Boggy Plains Suite in N.S.W. (Dr D. Wyborn, pers. comm.). This element is present in negligible concentrations in the other phases.

Garnet contains up to 1860 ppm of yttrium. Some of this is present in the xenotime contaminant. Limits to the quantity in xenotime may be made by assuming that all the phosphorus of the analyses is due to the presence of the xenotime endmember: YPO_4, that is, neglecting the roles of the HREE in xenotime, and those of other phosphates such as monazite and apatite, which are also present. Maximum proportions of one-third of the yttrium content can be removed in this manner. The rest at least is believed to occur in solid solution as yttrogarnet (Deer et al., 1982). The garnet separates are therefore estimated to contain ~0.3% of this endmember (cf. Table 6.1). This is supported by the usual presence of slight excesses in Al over the quantities required to generate the four major endmembers from microprobe analyses of garnet (Appendix H).

Biotite separates contain up to 272 ppm of yttrium. This is probably present largely in contaminating xenotime because biotite and xenotime are part of the pseudomorphing assemblage of phenocrystic garnet (cf. Chapter 4).

Only minor concentrations of yttrium occur in the other phases.

Scandium is present in amounts up to 174 ppm in the garnet separates. It is also abundant in the biotites (up to 102 ppm in the biotite from sample #62634). However, the amount of scandium which is present in solid solution in garnet and in biotite compared with that present in contaminating phases such as xenotime, is not known.

Up to 235 ppm of vanadium occurs in biotite. Garnet contains about a third as much vanadium as biotite. The other phases contain negligible vanadium.

Manganese is a major chemical component of garnet and a minor component of both cordierite and biotite. A significant proportion of the manganese present in the feldspars (plagioclases ~80 ppm, alkali feldspars ~30 ppm) is probably present in contaminating biotite.

The highest gallium concentrations occur in biotite ($\leq$95 ppm). They decrease in the order: biotite (~75 ppm) > cordierite (52 ppm) > plagioclase (~30 ppm) > alkali feldspar (~18 ppm) > garnet (~12 ppm). Molar rations of Ga/Al decrease in the same order: biotite (~8 x 10^{-4}) > cordierite (3 x 10^{-4}) > plagioclase (~2.3 x 10^{-4}) > alkali feldspar (~1.8 x 10^{-4}) > garnet (~10^{-4}).

Biotite contains the highest concentrations of tin: up to 60 ppm for biotites from the Boobyalla Suite porphyry #62619. Most feldspars contain ~3 ppm although some separates, such as the plagioclases of the mafic porphyry inclusions within Poimena Suite granites (#62594 and #62602), have anomalously high tin contents (13.5 and 20.0 ppm, respectively). Tin was not detected in either the cordierite or the garnet separates.

6.4 APPLICATION: APPARENT PARTITION COEFFICIENTS

6.4.1 Introduction

Partition coefficients describe the distribution of chemical components between pairs of phases. They have been formulated from the geochemical data for mineral separates (Appendix F) described above and that of porphyry matrix separates described in the previous chapter. The latter are first-order estimates of the compositions of the granitic melt phase. Mineral/matrix coefficients are therefore limits to the mineral/melt partition coefficients (or Berthelot-Nernst distribution coefficients) which are pre-requisites for many petrogenetic models of granites (McCarthy & Hasty, 1976; McCarthy & Groves, 1979; Rapela & Shaw, 1979; Cullers et al., 1981).

6.4.2 Description

Apparent mineral/matrix partition coefficients (APC's) derived from the chemical data of this and the preceding chapter, are listed in Table 6.2. They are quoted to a maximum of two significant figures.

APC's for alkali feldspar/matrix pairs (Table 6.2) are within ±30% of published partition coefficient (PC) values for sanidine/glass pairs from

(a) high-silica rhyolites of the Yellowstone volcanic field (Leeman & Phelps, 1981) for Na, K, Ba and Fe*, and

(b) rhyolites and rhyodacites from the Twin Peaks Complex, Utah (Crecraft et al., 1981; Nash & Crecraft, 1985) for Ca, Na, K, Ba, Rb, Sr, Pb and Fe*.

Sanidine/glass PC's for a Binna Burra rhyolite (calculated from data for sample #Q71 of Ewart et al., 1977) are approximately 0%, 40%, 60% and 100% higher but 20% and 100% lower than the corresponding alkali feldspar/matrix APC's in Table 6.2, for the elements K, Na, Sr, Ba, Ca and Rb, respectively. Sanidine/dacitic glass PC's for Ba, Rb and Sr obtained experimentally at 720-780°C and 0.8 GPa P_W by Long (1978) are all about 50% of their corresponding APC values (Table 6.2).

APC's for the plagioclase/matrix pair from sample #62595 are within 30% of published PC values for plagioclase/glass pairs from:

(a) the Miocene rhyolites and rhyodacites of Sardinia (Vernieres et al., 1977) for Ca, Na, K, Ba and Sr, and

(b) the Twin Peaks rhyolites and rhyodacites (Crecraft et al., 1981; Nash & Crecraft, 1985) for Ca, Na, Ba, Rb, Sr, Sc, Pb and Mn. By contrast, the corresponding Sr and Ba APC's from sample #62619 are respectively ~250% and ~370% higher than the corresponding PC's for the Twin Peaks felsic volcanics (op. cit.), though values for the other APC's are comparable.

Table 6.2

Apparent Partition Coefficients Between Mineral and Matrix Separates

Num. Phase	Denom. Phase	Granitic Suite	Sample#	Si	Ti	Al	Fe*	Mn	Mg	Ca	Na	K	Ba	Rb	Sr	Pb	Nb	Sc	V	Ga	Sn
alk	matrix	Boobyalla	62595	0.90		1.4	0.09	0.062	0.19	0.57	1.0	1.7	13	1.3	2.8	1.9	~0	~0	0.7	1.0	1.5
fs			62627	0.87		1.4	0.23	0.29	0.18	0.92	1.0	2.0	18	1.4	4.9	2.4	~0	~0	0.6	0.95	0.4
		Poimena	62596	0.87		1.4	0.26	0.18	0.43	0.47	0.69	2.3	18	1.5	5.7	1.4	~0	0.4	0.6	0.97	0.23
plag	matrix	Boobyalla	62595	0.80		1.9	0.12	0.37	0.18	12.0	2.3	0.16	1.1	0.19	7.0	0.67	~0	0.2	0.3	1.9	0.5
			62619*	0.81		1.9	0.12	0.46	0.28	16.0	2.6	0.13	5.9	0.14	18.0	0.92	0.06	0.7	0.7	1.6	0.20
		Poimena	62594	0.89	0.02	1.7	0.055	0.13	0.062	2.2	2.2	0.22	0.55	0.03	3.8	2.2		~0	0.23	1.6	2.7
			62612	0.86		1.6	0.073	0.13	0.04	2.1	2.1	0.31	0.50	0.18	1.8	4.1	~0	0.3	0.16	1.7	0.3
		Wybalenna	62593	0.89	0.02	1.6	0.057	0.079	0.02	1.8	1.9	0.24	0.45	0.10	1.6	1.5	~0	0.1	0.07	1.4	0
			62602	0.93	0.04	1.6	0.062	0.052	0.05	1.6	2.7	0.26	0.57	0.14	2.0	1.9		~0	0.2	1.5	9
			62610	0.93	0.02	1.6	0.051	0.057	0.022	1.6	1.9	0.30	0.61	0.10	2.1	1.6		0.1	0.07	1.6	0
bio	matrix	Boobyalla	62619ph*	0.45	33.0	1.6	16.9	15.0	19.0		0.08	1.5	16	4.4	0.36	0.58	19.0	20.0	27.0	4.7	7.1

* Matrix is from phyric-poor #62618 taken 0.5 m from phyric-rich #62619 within the same porphyry.

For most elements, plagioclase/matrix APC values change as the porphyry matrix becomes more mafic, that is, from the Boobyalla to the mafic Poimena to the Wybalenna Suite (Table 6.2). APC's that decrease in value in this direction are those for Al, Fe*, Mn, Mg and Ca and to a less extent for Ba, Rb, Sr, V and Ga. APC's that increase as the matrixes become more mafic, are Si, Ti and K.

APC's for the biotite/matrix pair are

(a) within the range indicated for biotite/glass PC's from the Twin Peaks rhyolites and rhyodacites (Crecraft et al., 1981; Nash & Crecraft, 1985) for the elements Ba, Rb, Sr, Pb, Sc, Mn and Fe*; and

(b) higher than the biotite/glass PC's from the Bishop Tuff rhyodacite (Mahood & Hildreth, 1983) for Rb, Sc, Mn and Ba by ~10%, 30%, 50% and 200%, respectively.

6.4.3 The Nature of Solid/Liquid Elemental Partitioning

The partitioning of a major element between a crystalline solid-solution phase and a melt phase is governed by exchange reaction equilibria. Partitioning is influenced by pressure, temperature and the compositions of the coexisting phases (Broecker & Oversby, 1971). In addition, kinetic factors can be important in chemical equilibria (Johannes, 1980; Kirkpatrick, 1981) so that crystallization or melting rates may also influence major element partitioning.

Trace element partitioning between a melt and a crystalline phase may occur in different ways. Elements may occur in solution within each phase, whereupon partitioning between phases can be described by trace-element exchange-reaction equilibria when dilutions are sufficient for Henrys Law to be obeyed (Broecker & Oversby, 1971; Arth, 1976; O'Nions & Powell, 1977). Partitioning is dependent upon pressure, temperature, phase compositions (op. cit.; Mahood & Hildreth, 1983). It can also be affected by kinetic factors such as crystal growth rates (Dowty, 1977; Lindstrom, 1983).

Trace elements may also occur in minerals in crystal defect sites (Buseck & Veblen, 1978). The role of this mode of occurrence varies both with the mineral and the element concerned (op. cit.). Trace-element solid-liquid partition coefficients are therefore complex functions of pressure, temperature, phase chemistry, mineralogy, cooling or heating rates and the partitioning element concerned.

6.4.4 Discussion

The progressive increase in element APC values for plagioclase+matrix pairs from porphyries of the Wybalenna Suite to those of the mafic Poimena Suite and those of the Boobyalla Suite, could be interpreted as reflecting a progressive decrease in equilibrium magmatic temperature. This effect

has been experimentally demonstrated by Long (1978) who obtained inverse coefficients for each of Ba, Rb and Sr and temperature under isobaric, and near-isochemical conditions.

Alternative explanations for the observed progression of APC's are:

(a) an increase in the activities of Si- and K-containing species in the melt from the Wybalenna to the Boobyalla Suite, leading to decreases in the activities of trace-element species in the melt through melt-structural exclusion. This phenomena shifts trace-element exchange-equilibria by promoting higher solid to liquid concentration ratios (Jensen, 1973; O'Nions & Powell, 1977; Mahood & Hildreth, 1983); and

(b) the occurrence of disequilibrium calcic cores in the plagioclase phenocrysts from the Boobyalla Suite porphyries leading to meaningless APC values.

Alkali feldspar, plagioclase and biotite solid/matrix APC's from Boobyalla Suite porphyries for most elements (Table 6.2) have similar values to corresponding PC's for mineral/glass pairs from the felsic volcanic rocks of the Twin Peaks Complex of Utah (e.g. Nash & Crecraft, 1985). Such similarities might suggest that phenocryst- and matrix-separate compositions are acceptable as magmatic phenocryst- and melt-phase compositions respectively, so that the APC's derived could be used for trace-element petrogenetic modelling of the granites of this suite.

However, the term "apparent" is used because it cannot be assumed that these coefficients represent those which were applicable to the volume equilibrium partitioning of elements under magmatic conditions. There is ample evidence (cf. Chapters 7 and 9) for major-element exchange between the matrix and the mafic phases: biotite, cordierite and garnet, occurring down to low subsolidus temperatures. The trace-element concentrations in these rock constituents are therefore also likely to reflect subsolidus rather than magmatic equilibria.

Thermobarometry based upon major-element chemical data indicates that the cores of plagioclase phenocrysts and alkali feldspar megacrysts can retain chemical information about early magmatic equilibria (Chapter 9). The major- and trace-element concentrations of these minerals should therefore be those of magmatic phases. However, APC's generated using their compositions will not be magmatic coefficients because the matrixes used will have inappropriate subsolidus chemical compositions. Only for phases extracted from unaltered volcanic rocks, should apparent partition coefficients be regarded as magmatic partition coefficients.

6.5 CONCLUSION

Trace-element data of phenocryst- and matrix-separates from porphyries have been assessed in the context of major-element equilibria amongst the same rock constituents. The trace-element contents of coexisting phases in magmatic assemblages cannot be determined for any suite. Trace-element petrogenetic modelling has therefore not been undertaken because of the lack of knowledge of both the magmatic trace-element partition coefficients and their dependencies upon each of the operative intensive variables. Instead, major-element petrogenetic modelling of two granite suites has been undertaken (Chapter 12). Partitioning of these elements between a number of the model magmatic phases is made using thermobarometric exchange-reaction relationships which have been established either under experimental conditions or by the independent calibration of natural assemblages (Chapters 8 and 9).

FIGURE 7.1

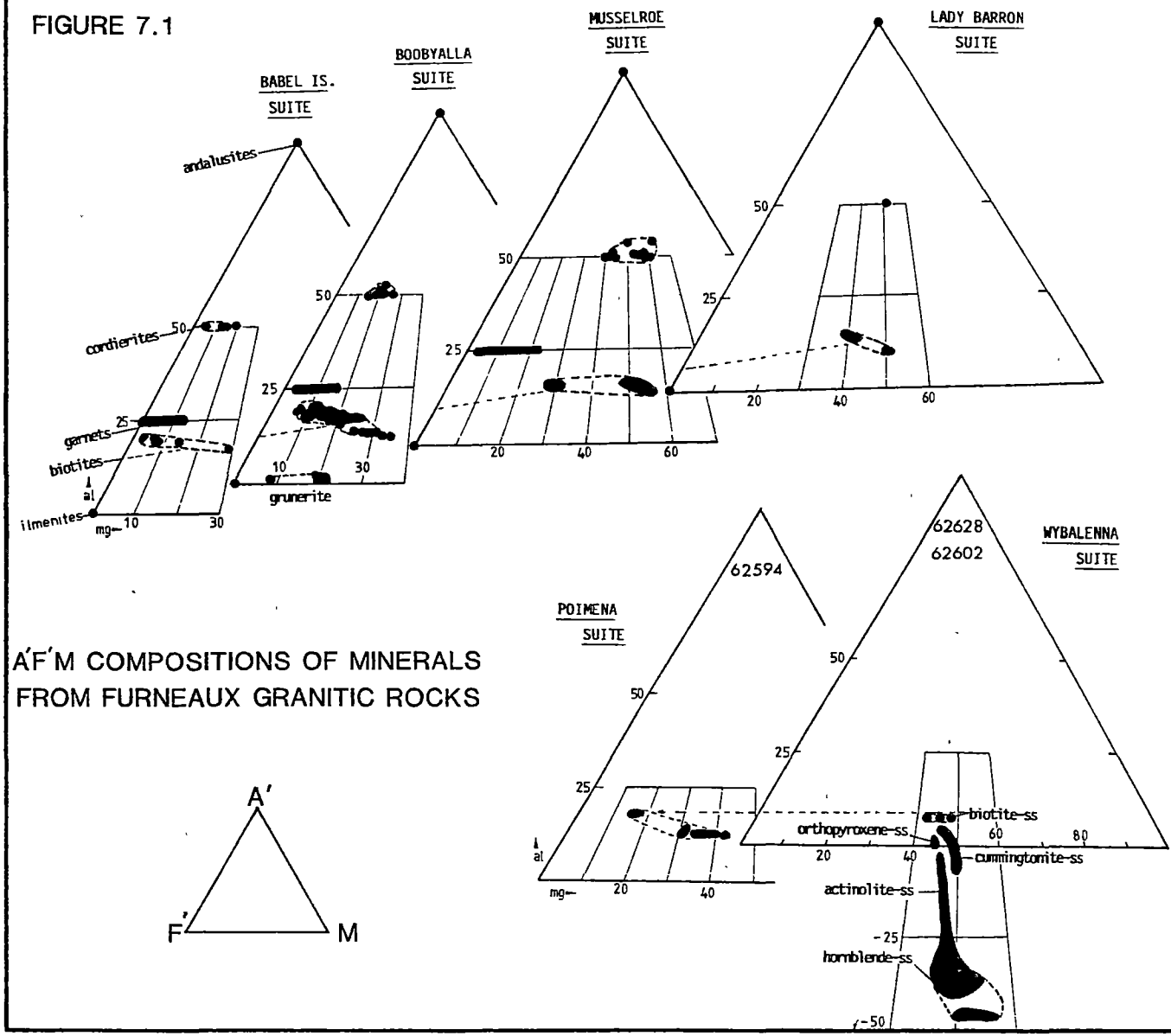

A′F′M COMPOSITIONS OF MINERALS FROM FURNEAUX GRANITIC ROCKS

Chapter 7

THE CHEMICAL COMPOSITIONS AND ZONATION OF MINERALS

7.1 INTRODUCTION

In this chapter, the compositional variations within crystals (or their pseudomorphing assemblages) of most of the major magmatic phases, are described. The petrogenetic significance of these compositional variations is then discussed and some general conclusions are drawn.

The compositions of ferromagnesian phases are expressed in terms of the major element indexes (al) = 100•A′/(A′+F′+M) and mg′ = 100•M/(M+F′) where A′ = mol. Al_2O_3 - (Na_2O+K_2O+CaO)

F′ = mol.FeO*+MnO

and M = mol.MgO

The phase compositions described in this chapter are used to:

(a) obtain estimates of intensive variables in granitic rocks and magmas (Chapter 9); and

(b) estimate the compositions of phases used to model the magmatic evolution of selected suites of Blue Tier Batholith granites (Chapter 12).

7.2 DATA AQUISITION

Eight hundred and eighty-three single and averaged electron microprobe analyses of mineral phases and their pseudomorphing assemblages were obtained from thin section samples of Furneaux and other Blue Tier Batholith granitic rocks. They are listed in Appendix H.

7.3 PHASE COMPOSITIONS

The compositions of the major mineral phases from the six major Furneaux Granitic Suites are depicted graphically on A′F′M diagrams in Fig. 7.1.

Aluminosilicates

Both andalusite and sillimanite occur in granites from the Blue Tier Batholith. Sillimanite is known only from Musselroe and Boobyalla Suite rocks. In these, it occurs rarely as fibrolitic needles. Sillimanite also occurs as prismatic inclusions in garnets from Musselroe Suite mineral segregations (Plate 6, Figs C,D; Plate 7; Table 4.1). Such crystals contain minor amounts of iron, amounting to the solid solution of ~1.7 mol% of the ferrisillimanite ($FeAlSiO_5$) endmember. No Fe-zonation was noted in this inclusion phase.

Andalusite phenocrysts from Lady Barron and Babel Island Suite rocks do not contain detectable iron. However andalusite from the Boobyalla

FIGURE 7.2

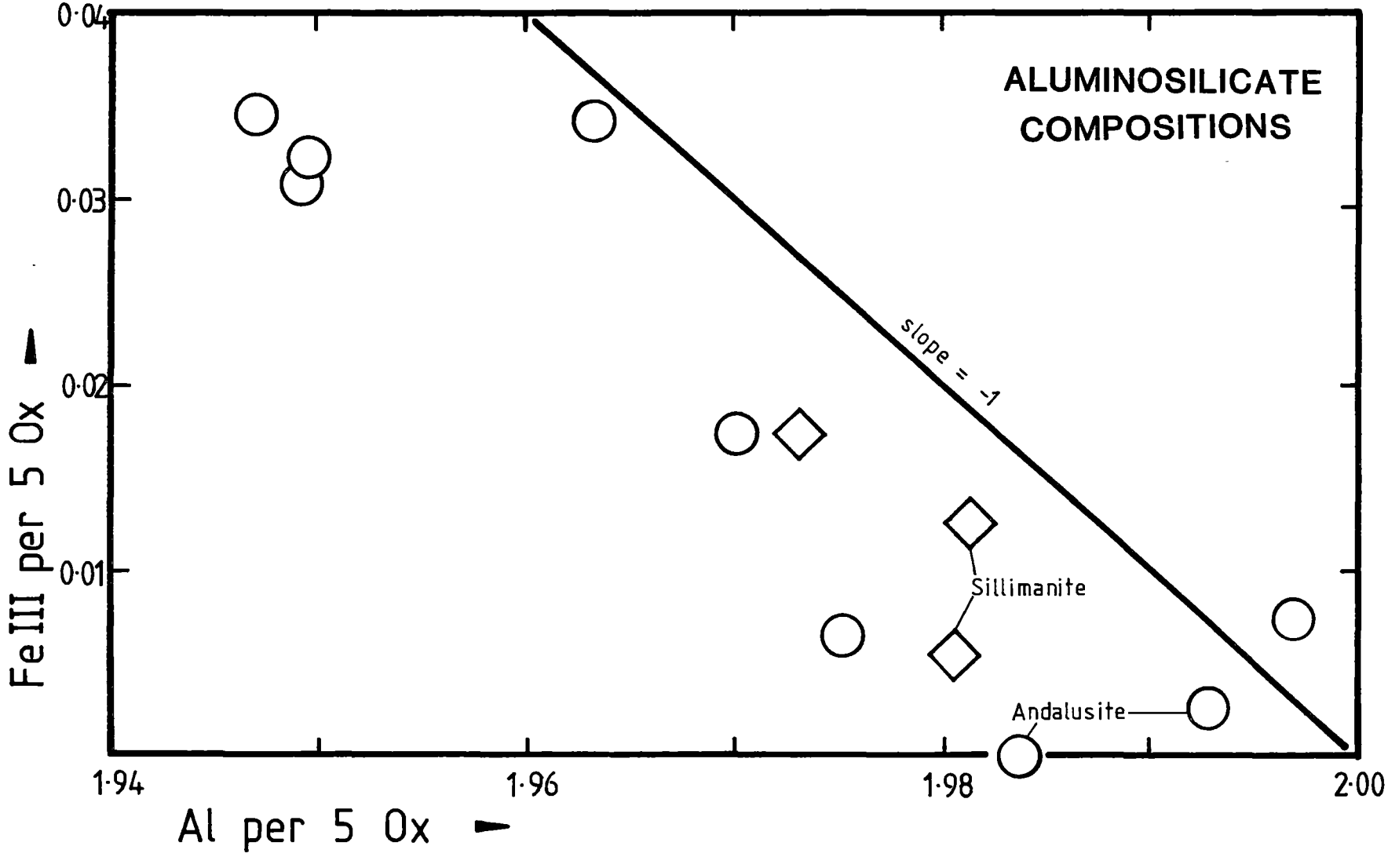
ALUMINOSILICATE
COMPOSITIONS
slope = -1
Sillimanite
Andalusite
0·04
0·03
0·02
0·01
Fe III per 5 Ox
1·94
1·96
1·98
2·00
Al per 5 Ox

Suite often has strongly pleochroic pink cores containing up to 3.4 mol% of $FeAlSiO_5$. Core compositions grade steeply to colourless iron-absent rims. In all suites, phenocrysts of this phase have coronas of muscovite (Plate 6, Figs A,B). Fig. 7.2 shows an approximate inverse relationship between FeIII and Al for the collective aluminosilicate analyses. This trend is consistent with these phases being crystalline solutions of the two dominant endmembers: Al_2SiO_5 and $AlFeSiO_5$. Displacement of the distribution towards the origin from the ideal two-component mixing line could be due either to systematic analytical error (namely a Si/Al bias) or to the presence of a small quantity of the solid-solution component: kanonaite ($MnAlSiO_5$; Vrana et al., 1978). However manganese has never been detected in analyses of this phase (detection limit for MnO: 0.2% (Appendix D)).

Apatite

In Boobyalla Suite rocks, this phase ranges in composition from a pure calcic endmember found in the mafic mineral segregation containing the most magnesian garnet cores (#68529), to compositions which contain ~1.3 m% of both manganoapatite ($Mn_5(PO_4)_3(OH,F)$) and ferroapatite ($Fe_5(PO_4)_3(OH,F)$ for apatites from porphyries such as #62595 and #62619.

Apatites containing up to 3 m% of manganoapatite and 2 m% of ferroapatite occur in the mafic mineral segregation #68550 from the Babel Island Pluton.

Biotite

The extent of the compositional variation in this phase varies with the suite, the textural environment, crystal size, and with the chemical components being considered. Chlorine was detected in many analyses at concentrations of ~0.1%. However, the 2σ absolute error for Cl_2O_{-1} is ±0.2% (Appendix D). Chlorine concentrations reach 0.6±0.2% for matrix biotites from the Babel Island Suite sample #67544. Chlorine was not included in the analyses of Appendix H.

Suite Variation: In each suite there is a spectrum of compositions which plot as a band on the A'F'M diagram, extending from A'-rich variants at the F'-rich end to A'-poorer variants at the M-rich end (Fig. 7.1). Although A'F'M trends for all suites except for the metaluminous Wybalenna and Gardens Suites overlap, the F'-rich limits are diagnostic for the four more strongly peraluminous suites; mg' numbers {100*mol.Mg/[mol(Mg+Mn+Fe*)]} increase in the order Babel Island mg' >3.4, Boobyalla mg' = >9.5, Musselroe mg' = >27.5, Lady Barron mg' = >38. The A'F'M trend for biotites of the Poimena Suite extends to more M-rich, A'-poor limits than that for the Boobyalla Suite, but is otherwise indistinguishable from it. A'F'M

FIGURE 7.3

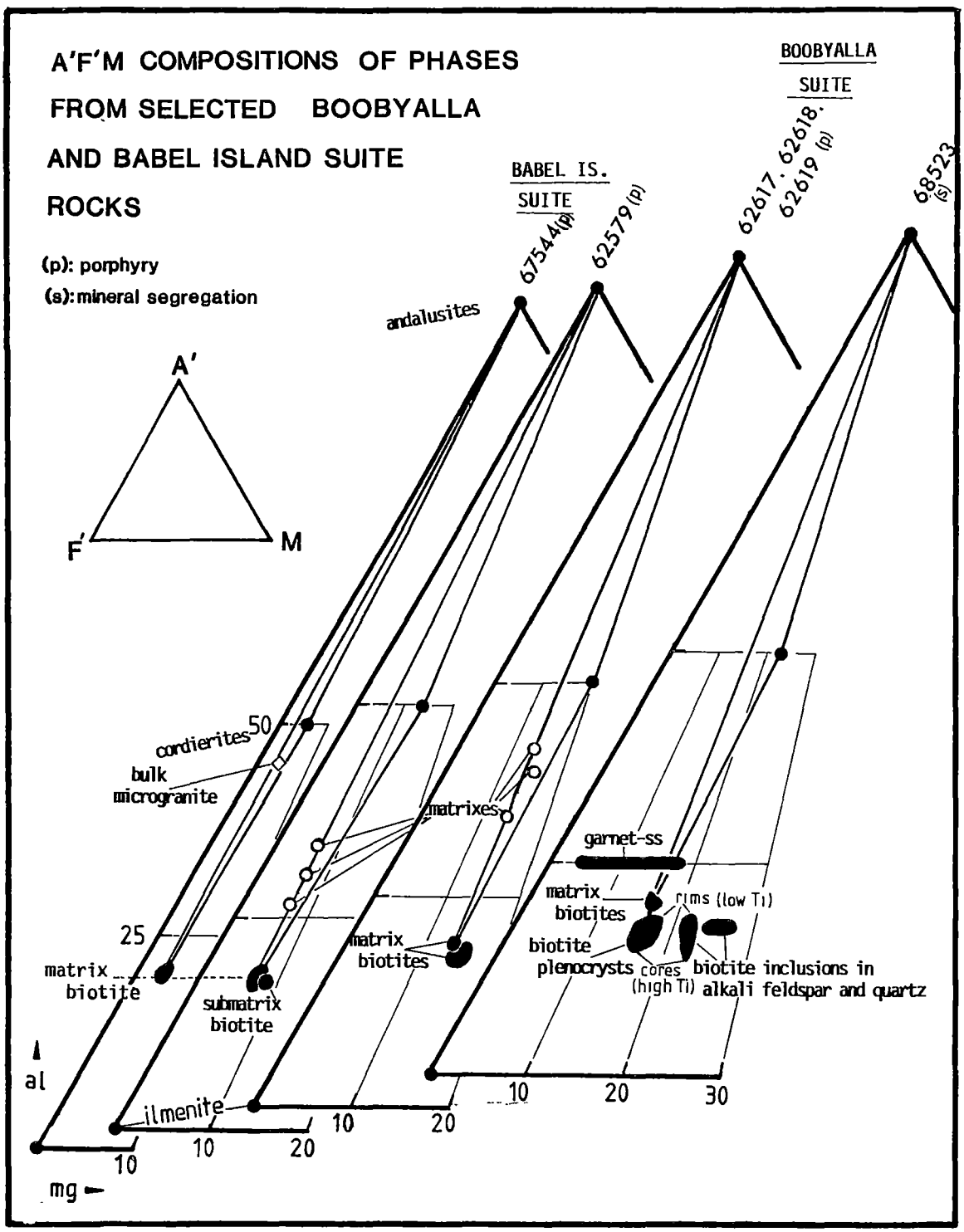
A'F'M COMPOSITIONS OF PHASES FROM SELECTED BOOBYALLA AND BABEL ISLAND SUITE ROCKS
(p): porphyry
(s): mineral segregation
BOOBYALLA SUITE
BABEL IS. SUITE
67544 (p)
62579 (p)
62617, 62618, 62619 (p)
68523 (s)
andalusites
A'
F'
M
cordierites
50
bulk microgranite
matrixes
garnet-ss
matrix biotites
rims (low Ti)
biotite phenocrysts
cores (high Ti)
biotite inclusions in alkali feldspar and quartz
25
matrix biotite
submatrix biotite
matrix biotites
al
ilmenite
10
20
30
mg

FIGURE 7.4

Ti versus Al6 COMPOSITIONS OF BIOTITES

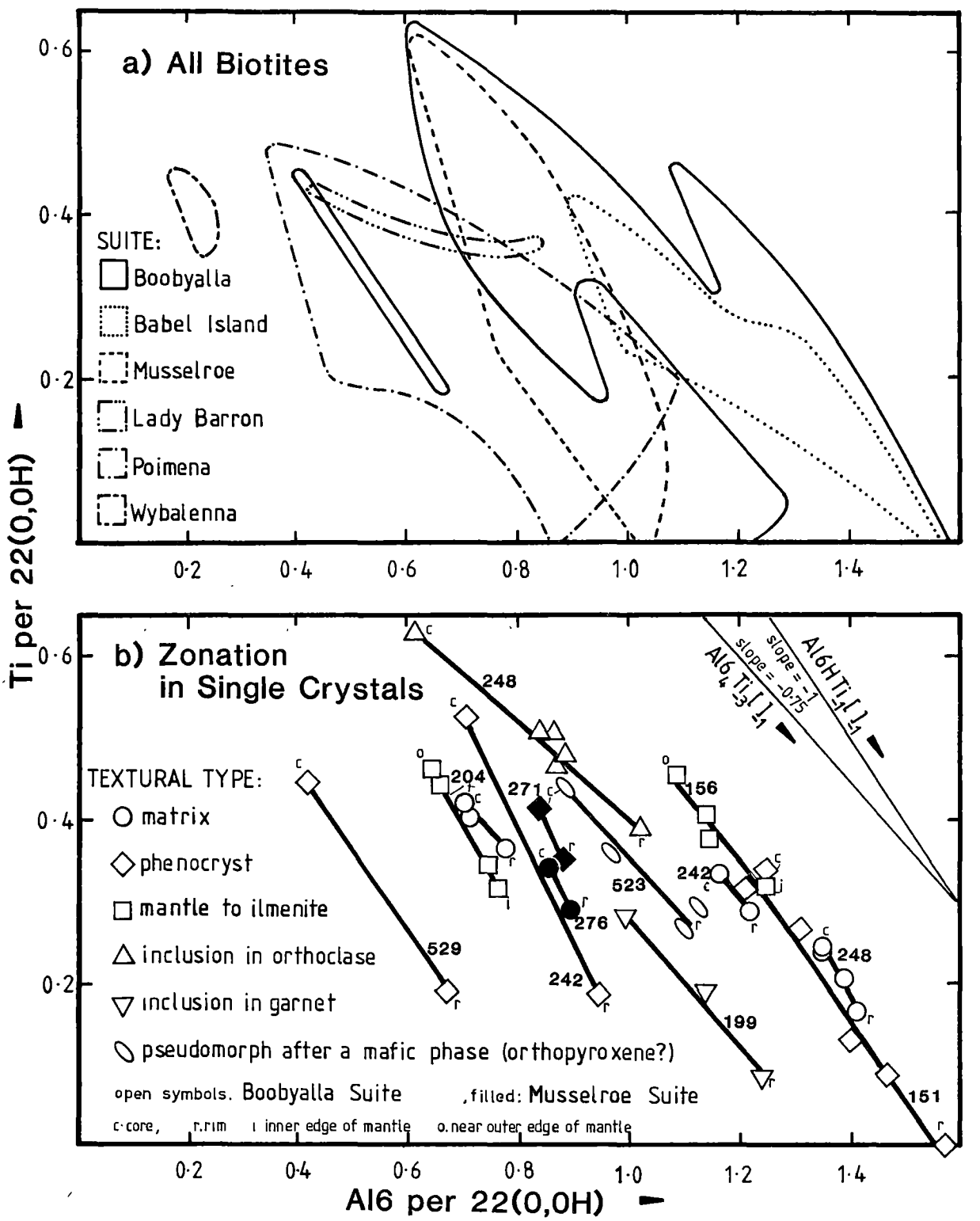

trends for biotites of the Wybalenna and Gardens Suites are **en echelon** to lower al and higher mg′ values from those of the peraluminous suites.

Textural Environment: Porphyritic rocks have a considerably greater spread of biotite compositions than do the coarsely crystalline rocks where all biotite compositions are remarkably similar. In porphyries, matrix, phenocrystic, pseudomorphing and inclusion biotites may be distinguished compositionally as well as texturally from each other. In any suite, porphyry matrix biotites are the richest in FeO*, MnO, Al_2O_3 and in Cl. They are generally lowest in K_2O, Na_2O and in TiO_2. Phenocrystic biotites are marginally richer in MgO, TiO_2, K_2O and Na_2O and poorer in MnO, Al_2O_3 and in Cl compared with matrix biotites. Inclusion biotites are the most refractory. They are richest in MgO, TiO_2 and in Na_2O and poorest in Al_2O_3, MnO and in Cl. Some chemical distinctions between these three textural classes of biotite are shown for two suites in Figs 7.3.

Pseudomorphing biotites may range from titanium-absent compositions (e.g. those after cordierite (Plate 4, Fig. B) and garnet (Appendix H)) to titanium-rich compositions which are indistinguishable from the compositions of biotite phenocrysts, in the case of the brown biotites in mafic mineral pseudomorphs and garnet coronas (Plate 4, Figs C, D and F).

Crystal Size: Small crystals (plates $\lesssim 0.5$ mm in diameter) exhibit only minor chemical zonation. Larger crystals exhibit peripheral zonation in TiO_2 and Al_2O_3 as described above. When adjacent to large ilmenite euhedra, large biotite crystals are zoned in FeO* and MgO as well.

The most spectacular chemical variations in biotite single crystals, are in Ti and Al6 occuring near the edges of the larger crystals. Similar zoning has been noted by Schreurs (1985) in high-grade pelites from S.W. Finland. The feature is independent of the suite considered, as shown in Fig. 7.4. The 13 single-crystal mol. Ti versus Al6 trends shown, have slopes which average -1.02 ± 0.28 (1σ) and is consistent with a substitution involving these two elements. Exchange solely within the octahedral site would implicate the $Al6_4Ti_{-3}[\ ]_{-1}$ vector, with a diagram slope of -0.75, which is within the limits estimated for the slope, given above. However, a slope of -1 is possible, if exchange in the hydroxyl and octahedral sites are combined in the coupled substitution: $Al6_4HTi_{-1}[\ ]_{-1}$. In this exchange, the gradient in H should parallel that of Al6. If the latter substitution is validated, then crystal cores have a substantial proportion of an oxy-Ti-biotite component in crystalline solution.

Another possible coupled exchange involves iron: $Al6FeIIITi_{-1}[\ ]_{-1}$. It could attend late-stage subsolidus oxidation. The existence of this substitution could be sought using either for by Mossbauer spectroscopy or microanalytical analysis of the iron oxidation state of the core versus the

FIGURE 7.5

Ti versus mg COMPOSITIONS OF BIOTITES

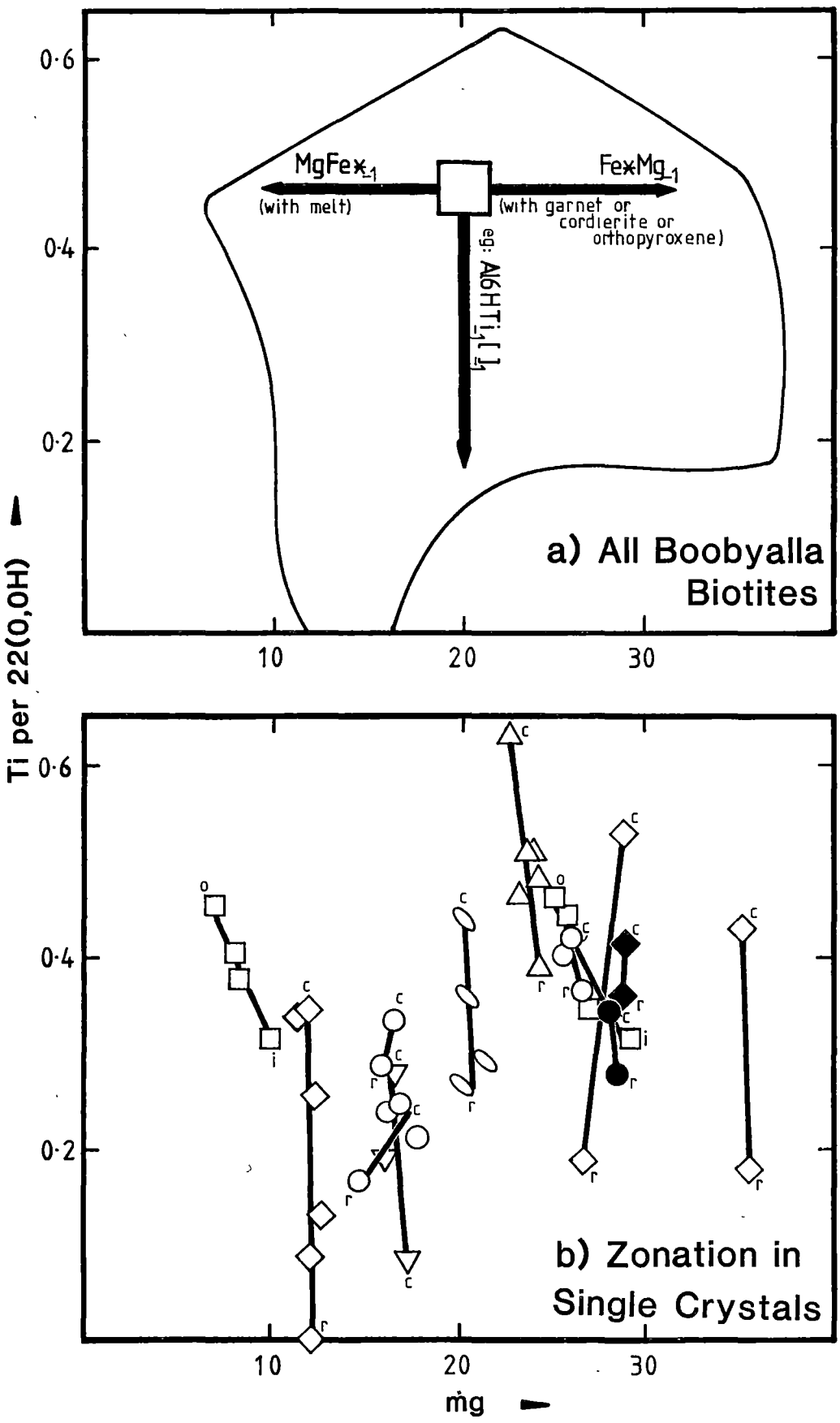

rim compositions of phenocrystic biotite. Confirmation of the existence of the $Al6HTi_{-1}[\ ]_{-1}$ substitution requires quantitative measurement of hydrogen, e.g. by isotope dilution mass spectrometry, of core- and rim-biotite samples.

Fe^*Mg_{-1} zonation in biotite single crystals is often negligible as indicated in Fig. 7.5. However, Fe^*Mg_{-1} zonation does occur in those biotites which form coronas about large ilmenite grains. In these, the low TiO_2-biotite adjacent to euhedral ilmenite is richer in both MgO and Al_2O_3 than are the high-TiO_2 compositions within the outer edge.

Amongst all the crystals of a particular suite, a large scattered Ti versus mg′ distribution is exhibited (e.g. data for 126 Boobyalla Suite biotites shown in Fig. 7.5).

Cordierite

Few fresh cordierites have been analysed because of their rarity, even in granites such as those of the Lady Barron Suite in which cordierite was the major mafic magmatic phase. Cordierite was found to be best preserved in mafic mineral segregations (e.g. in #62634 and #67539). It is possible however, to estimate the Fe-rich limit of the FeMg compositions of cordierites which have been pseudomorphed by sheet-silicate phases. Analyses of cordierite-pseudomorphing chlorite, green TiO_2-absent biotite, and Na-rich muscovite or their mixtures, yield slim compositional trianglar trends extending across the A′F′M diagram (Figs 7.6). The intersection of these trends with the al = 50 line yield an estimate of the mg′ value of the pre-existing cordierite.

By this means, cordierite compositional trends have been constructed for each of the relevant suites (Fig. 7.1). The F′-rich limits of these trends are: Babel Island mg′ $\geq$6, Boobyalla mg′ $\geq$15, Musselroe mg′ $\geq$40, and Lady Barron mg′ ~ 52. This is the same order of suites as that indicated for the limiting iron-rich biotites that were described above.

Compositional variation in cordierite single crystals is slight but is somewhat greater than that in biotites. FeMg variation occurs in some cordierite inclusions in Musselroe Suite garnets (Fig. 7.8, Plate 7).

Alkalis occur in cordierite to the extent of ~0.25 atoms per 18 oxygens. They have mol.(Na/K) ratios > 2.2. There is no discernible relationship between alkalis, aluminium and silicon to suggest an edenitic type of substitution $[Si\ Al_{-1}(Na,K)_{-1}]$ as described by Schreyer (1986). Alkali metal ions are therefore best interpreted as being indiscriminant occupants of the c-axis channels in the cordierite structure.

Cummingtonite

This phase occurs as topotaxial replacements of orthopyroxene in granites of the Wybalenna Suite (Plate 5, Fig. B). Compositional zonation

FIGURE 7.6

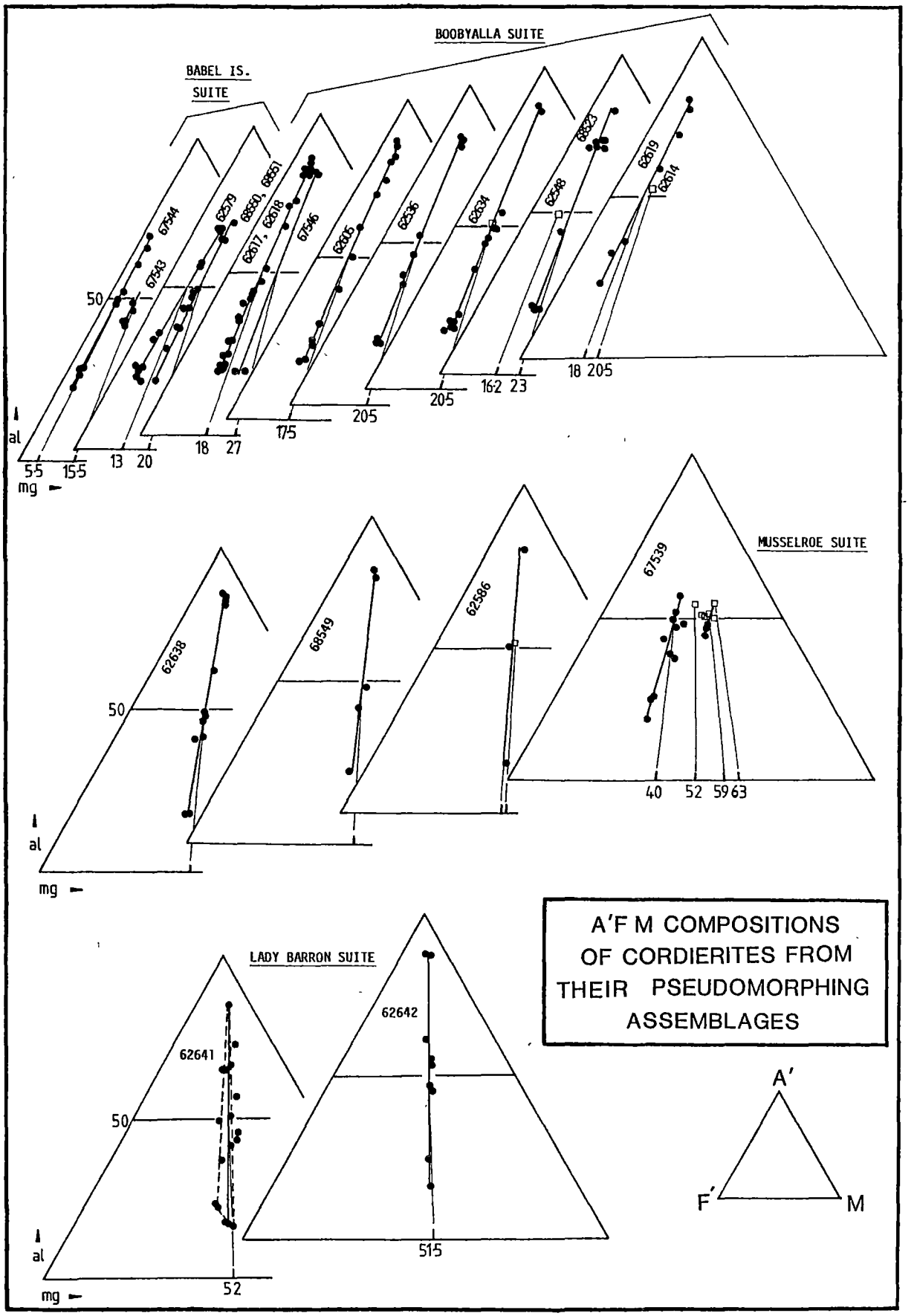
BOOBYALLA SUITE
BABEL IS. SUITE
67544
67543
62579
68550, 68551
62617, 62618
67546
62605
62536
62634
62548
68823
62619
62614
50
al
mg
5·5
15·5
13
20
18
27
17·5
20·5
20·5
16·2
23
18
20·5
MUSSELROE SUITE
62538
68549
62586
67539
50
al
mg
40
52
59
63
LADY BARRON SUITE
62641
62642
50
al
mg
52
51·5
A'F M COMPOSITIONS OF CORDIERITES FROM THEIR PSEUDOMORPHING ASSEMBLAGES
A'
F'
M

FIGURE 7.7 Fe–Mg–Mn–Ca COMPOSITIONS OF GARNETS

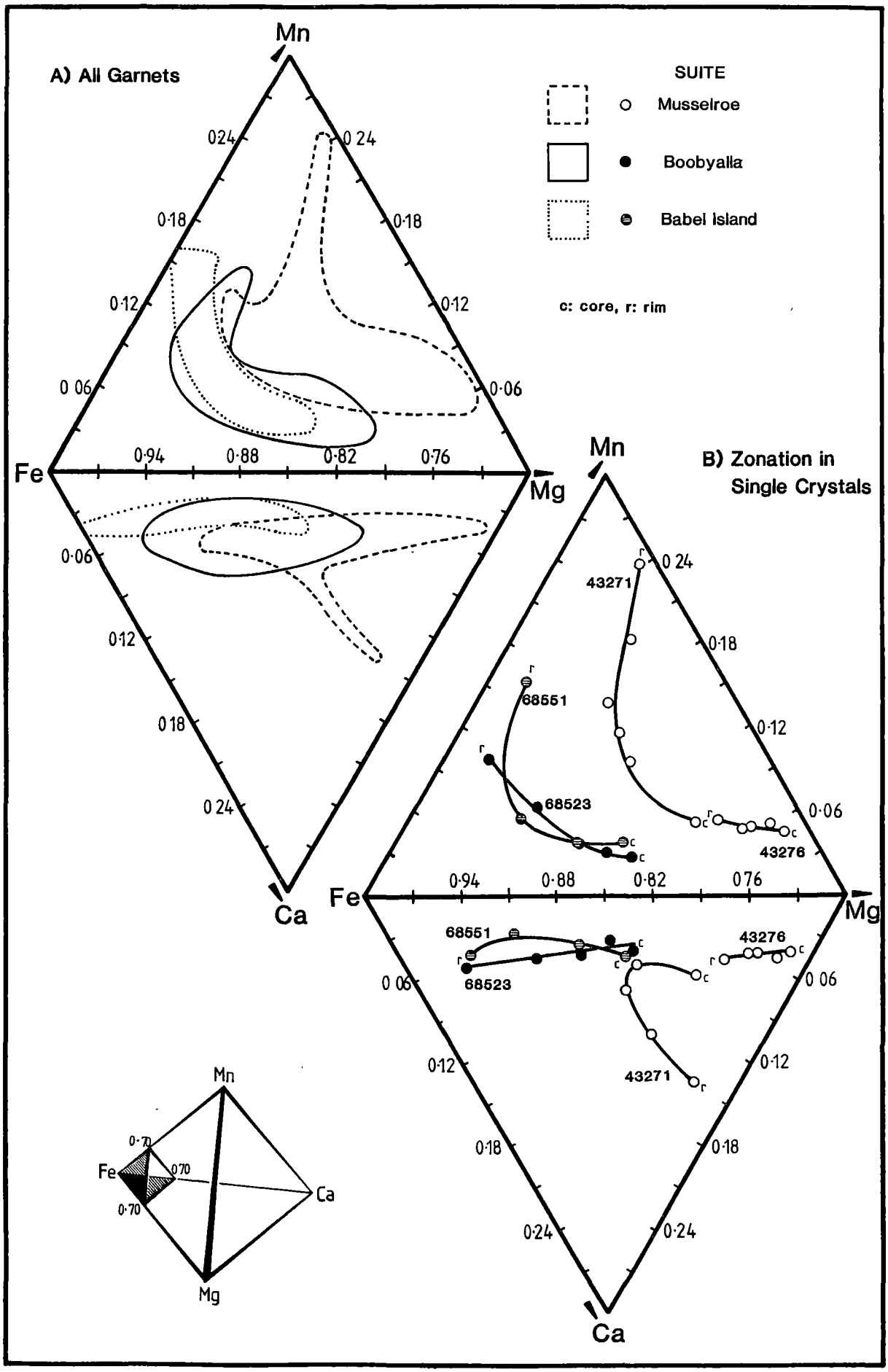

PLATE 7

This plate shows enlargements of the two areas of the garnet shown on the preceeding plate. In the area of Fig. A, needles and prisms of sillimanite are the most common inclusion type. Large inclusions of cordierite also occur (centre) and these may contain inclusions of sillimanite, gahnitic spinel, ilmenite and quartz (cf. Fig. 7.8). The two large crystal forms on the upper edge of Fig. B are pinitized cordierites. The hexagonal crystal in the lower right-hand corner of the photomicrograph is a titanium-absent biotite (cf. biotite #2A1 in Appendix H) and is probably a pseudomorphing rather than an included phase. The square across it is the area-scan raster-pattern from the microprobe electron-beam. The scale bars are 500 μm long.

FIGURE 7.8

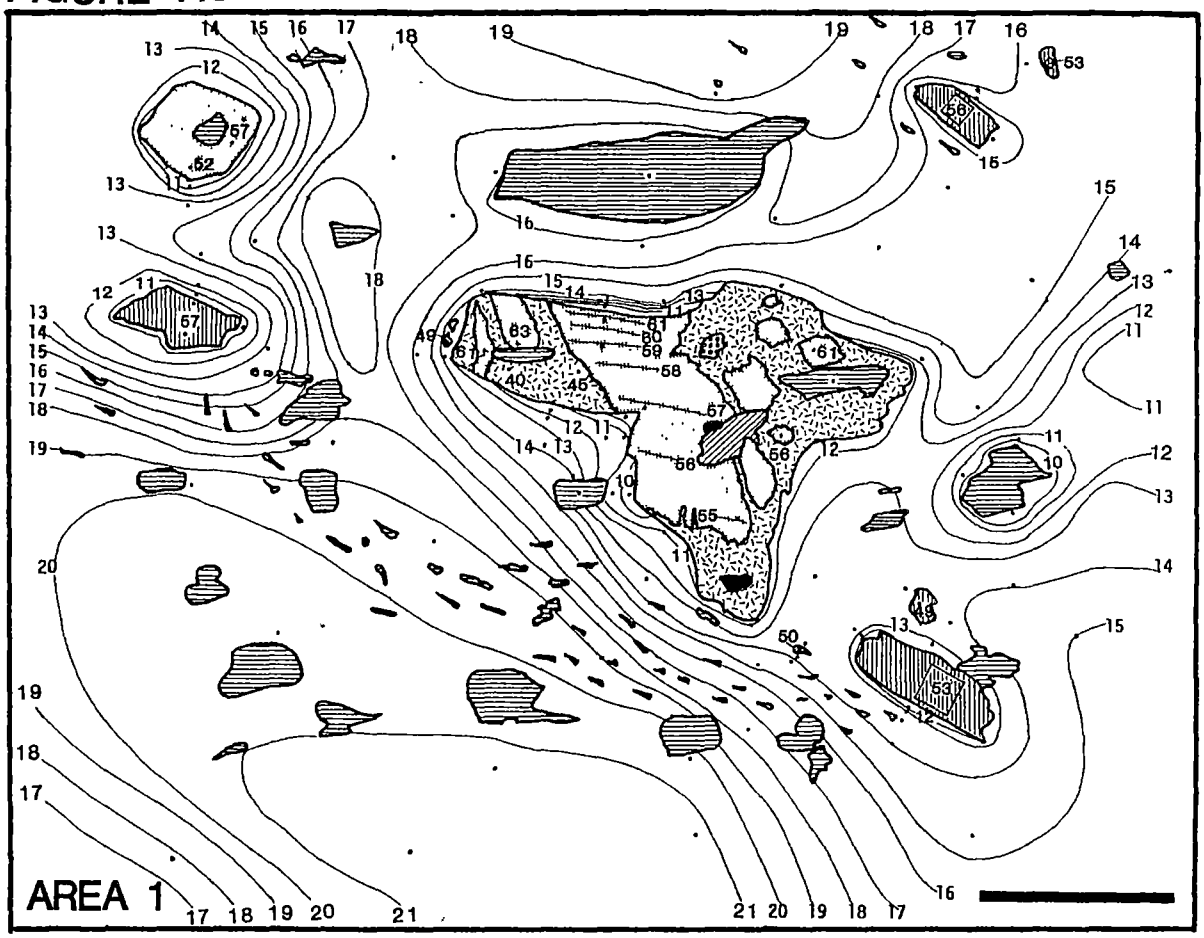

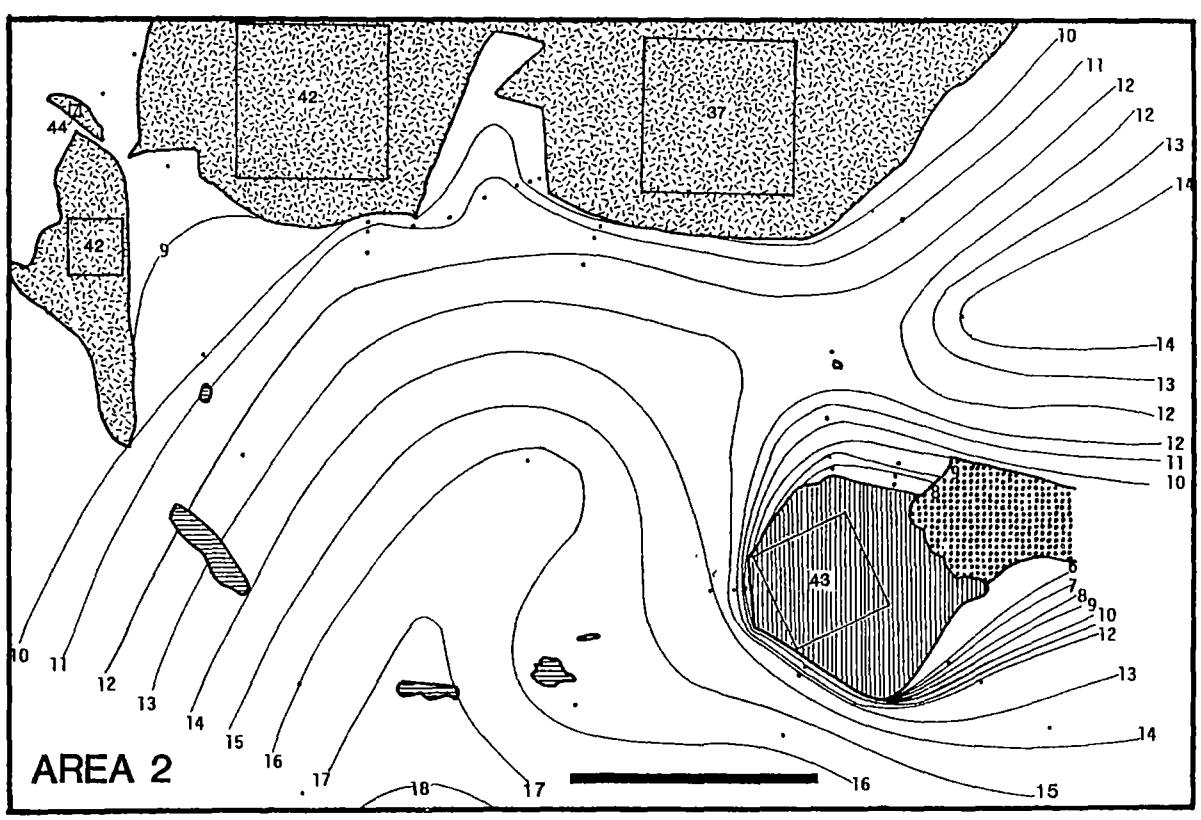

garnet cordierite biotite sillimanite quartz hercynite ilmenite pinite(ex-cord)

Figure 7.8 Maps of mg-isopleths of two areas within an inclusion-containing garnet. This garnet is from the Musselroe Suite sample #67539. It is shown in Plates 6 and 7. Scale bars are 500μm long.

PLATE 7

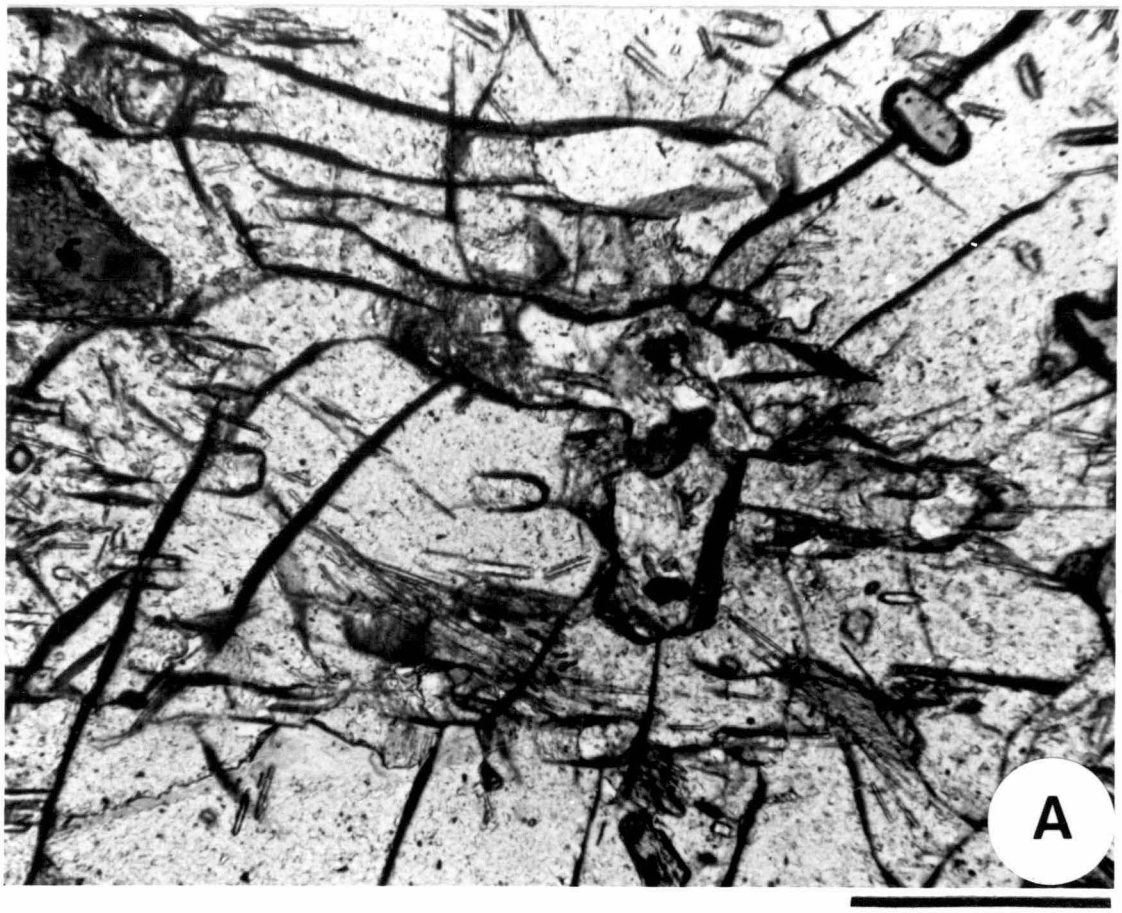

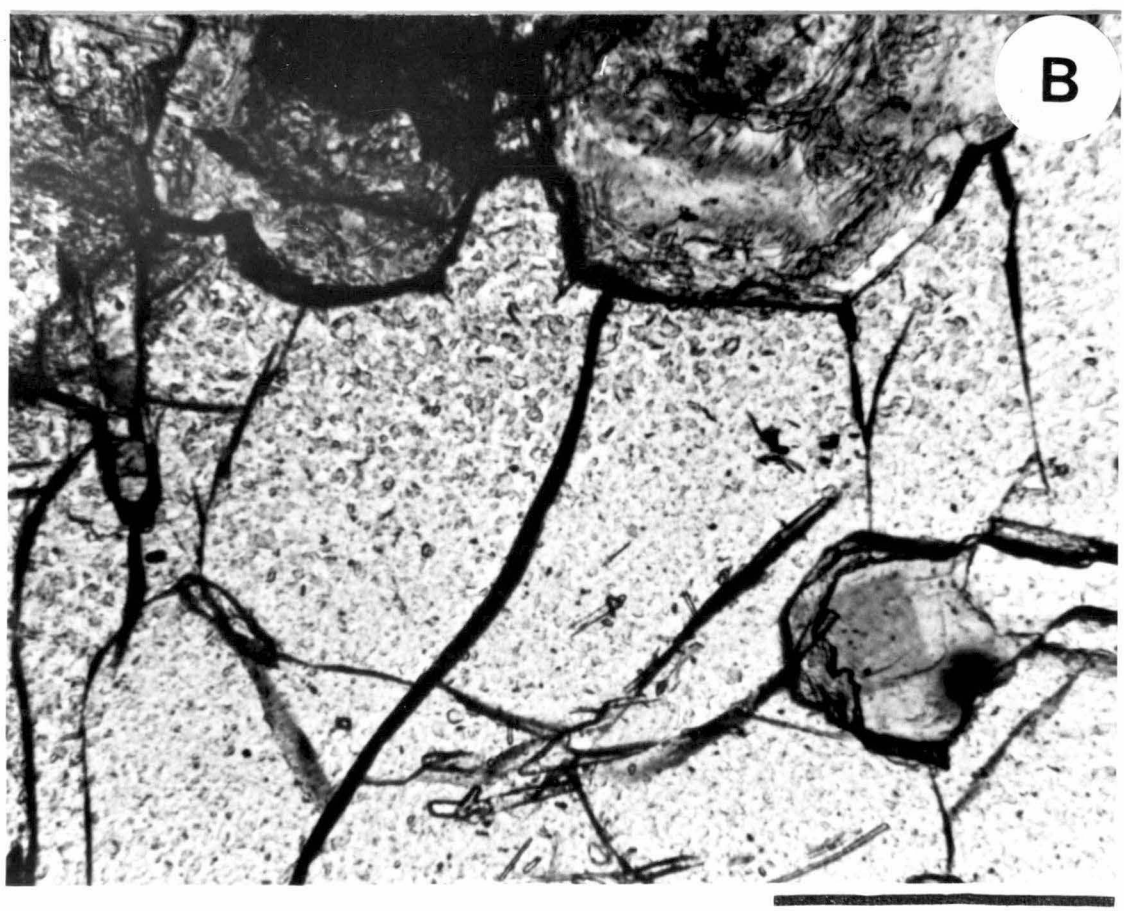

(Fig. 7.1) extends from (al) values of ~5 where the phase is adjacent to biotite (which has (al) values of 7.5) down to (al) values of -7.5 where it is adjacent to hornblende-actinolite-ss (which has (al) values of ~-40). The latter compositional limit for cummingtonite is more magnesian than the former, consistent with coexisting hornblende-actinolite-ss being more magnesian than coexisting biotite.

Garnet

Garnet occurs as a minor phase in the Boobyalla and Musselroe Suites. It is a trace phase in the Babel Island and Poimena Suites. Garnet from the last suite has not been analysed. Compositions consist of solid solutions of at least five known endmembers, the proportions of which decrease in the order: almandine >> pyrope $\gtrless$ spessartine > grossular > yttrogarnet (cf. Table 6.1). Semi-microdetermination of the oxidation state of iron in two garnet separates indicated very low proportions of FeIII/FeII (Appendix I). The component of andradite in solid solution therefore appears to be very minor. The FeIII deduced stoichiometrically from the garnet compositions in Appendix G may therefore be in part due to miscalibration of the microprobe analyser (e.g. the under-estimation of Fe by $\leq$1%). Molecular {FeII,Mg,Mn} and {Fe,Mg,Ca} ternary projections of the quaternary solid solutions have been constructed, ignoring the contribution of the minor yttrogarnet and andradite components. These projections collectively discriminate two populations of garnets. Babel Island and Boobyalla Suite garnets are indistinguishable whereas Musselroe Suite garnets are poorer in almandine. The two garnet A'F'M trends partially overlap each other (Fig. 7.1), but have distinctive magnesian (core) compositional limits. These are: Musselroe mg' <20.2, Babel Island and Boobyalla mg' <16.1.

Crystal chemical zonation trends show that the major overall exchange is $MgMn_{-1}$ from pyrope-rich cores to spessartine-rich rims. Musselroe Suite garnets are also slightly richer in yttrogarnet endmember, than are garnets of the Boobyalla Suite (cf. Table 6.1).

Chemical zonation maps of portions of an inclusion-rich Musselroe Suite garnet (Plate 7) have been constructed from data in Appendix H (Fig. 7.8). Zonation in (mg) occurs with mg gradients having a broad inverse relationship to mg value. This relationship delineates plateaux of high mg-value distal from inclusions and regions of steep gradients adjacent to biotite, cordierite and some sillimanite inclusions.

Grunerite

The mosiac of grunerite prisms included within garnet from sample #68524 (Plate 4, Fig. G) have mg'-values ranging from 8 to 21 (Fig. 7.1). No zonation pattern is discernible.

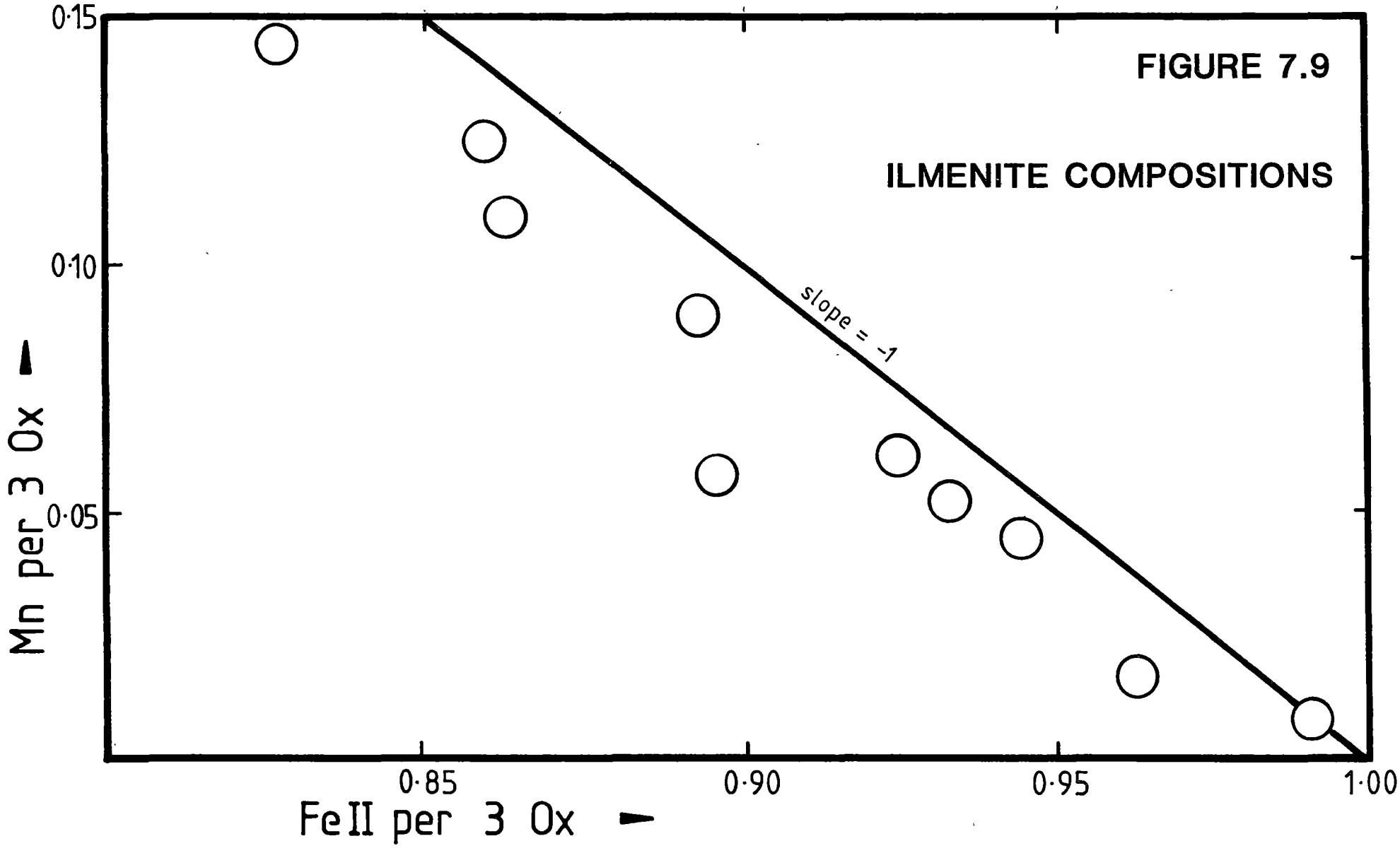
FIGURE 7.9
ILMENITE COMPOSITIONS
slope = -1
0·15
0·10
0·05
Mn per 3 Ox
0·85
0·90
0·95
1·00
FeII per 3 Ox

Hornblende-Actinolite

This extensive solid-solution series occurs in the metaluminous suites. Green euhedral hornblende grades both into mosaic patches of actinolite presumably after clinopyroxene (Plate 5, Fig. F) and into cummingtonite, which itself mantles orthopyroxene (Plate 5, Fig. B). Euhedral green hornblende phenocrysts may have brown titaniferous cores containing clouds of opaque inclusions. Cores have the most A'-poor and M-rich A'F'M compositions in the solid-solution spectrum (Fig. 7.1).

Hornblende is progressively pseudomorphed by khaki-coloured, low (Al6) biotite (Plate 5, Fig. D).

Ilmenite

Ilmenites contain only minor stoichiometrically inferred FeIII and Mg has not been detected. They may contain however, up to 15 mol% of the $MnTiO_3$ endmember. The latter component is most abundant in the ilmenites within brown biotite pseudomorphs after garnet. It is least abundant in ilmenite inclusions within garnet. These data together with analytical data of the mafic phases occurring in mafic mineral separates (Appendices F and H) show that equilibrium partitioning of [Mn/(Mn+FeII+Mg)] between phases increases in the order: biotite < cordierite < ilmenite < garnet < apatite. The order indicated for the first four phases was previously described by Thompson (1976a).

The slope of the molar Mn versus FeII trend in Fig. 7.9 is close to the ideal value of -1 for two-component mixing. Departure of the trend towards the origin may be due either to a minor undetected giekelite ($MgTiO_3$) component present in solid solution or to a systematic analytical bias.

Muscovite

Textural environment is important in muscovite compositional variation. Muscovite which pseudomorphs alkali-feldspar is devoid of ferromagnesian chemical components. Muscovite occurring as coronas about andalusite phenocrysts have concentrations of FeO*, MgO and Na_2O which increase from low levels adjacent to andalusite to compositions at the periphery which contain up to 7.5 mol% of trioctahedral mica and 3 mol% of paragonite in solid solution (Appendix H). The muscovite in cordierite pseudomorphs typically contains ~7.5 mol% of both of these endmembers in solid solution.

Orthopyroxene

Only slight core to rim chemical zonation occurs in the phenocrysts of this phase which occurs in the Wybalenna Granite sample #62628 (Plate 5, Fig. B). Cores contain ~1 mol% of clinopyroxene endmember, whereas rims

FIGURE 7.10

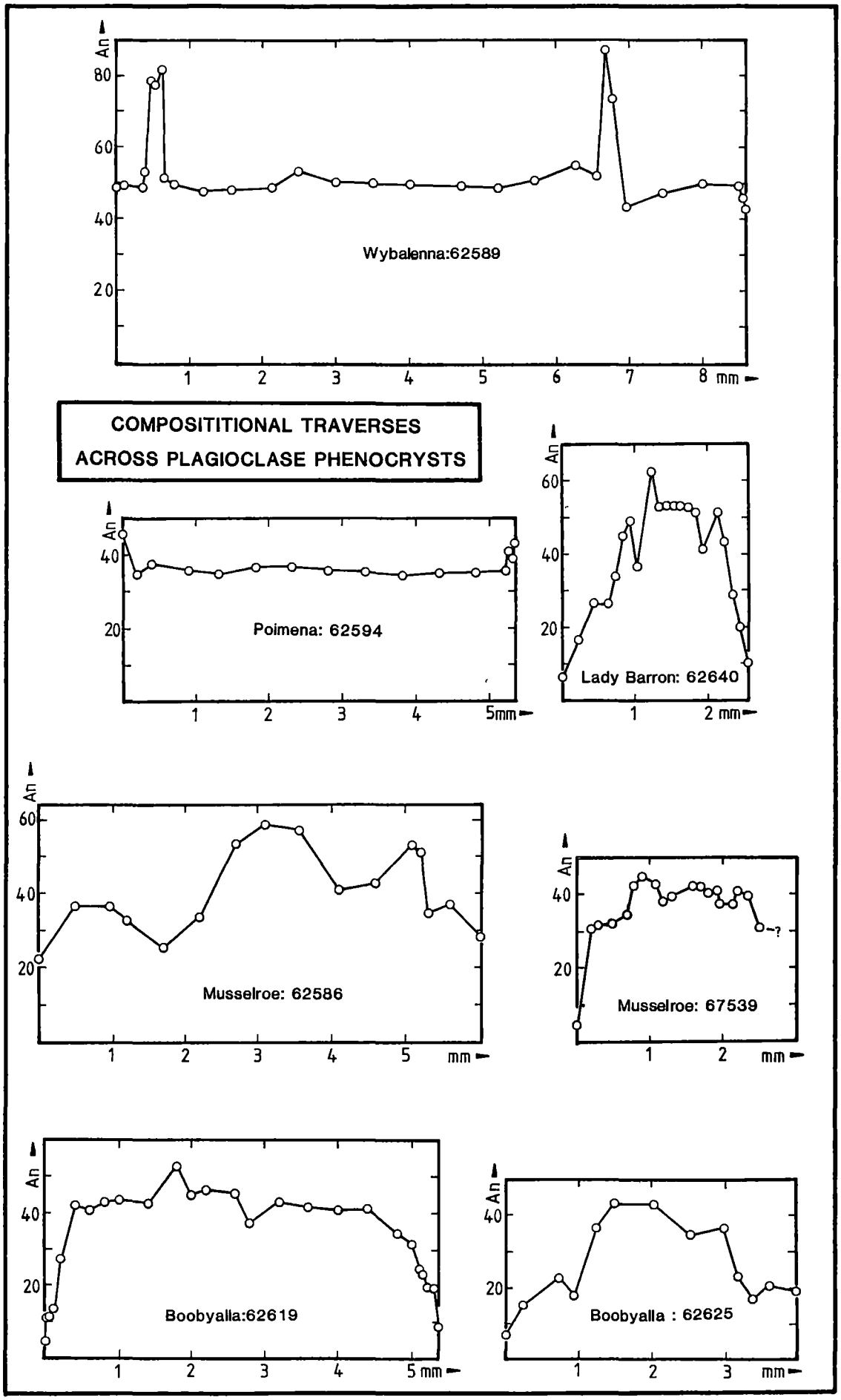

An: 100 mol.Ca/(mol.(Ca-Na-K))

contain ~2 mol%. The tschermakite [(FeIIMg)Al_2SiO_6] content is less than 2%.

Plagioclase

Fig. 7.10 shows compositional profiles for plagioclase phenocrysts from rocks of five granitic suites. Other plagioclase compositions are given in Appendices F and H. The anorthite contents of the cores of plagioclase phenocrysts are similar for the Wybalenna, Lady Barron and Gardens Suites (~An_{50-60}) where An = mol.% Ca/(Ca+Na). Boobyalla Suite cores are ~An_{40-45} whereas those of the Poimena Suite are ~An_{35-61}. Musselroe Suite core compositions are usually ~An_{42} (cf. #67539) but can attain compositions up to An_{58} (cf. #62586). The cores of Babel Island Suite plagioclases rarely exceed An_{25}. The suite order for the lower limit to the An content of plagioclase cores is therefore similar to that for the lower limits of biotite and cordierite mg'-values, as has been described above.

Morphological features of phenocrysts from porphyries include high core-volume fractions which tend to increase with the FeO* content of the porphyry matrix. They also have simple mantle compositional profiles which grade to albite-rich rims if the matrix composition is felsic (e.g. #62619) or rims of similar or even more calcic composition (e.g. #62594) if the porphyry matrix is relatively mafic. The phenocrysts from #62589 and #62594 contain hundreds of tiny biotite inclusions distributed throughout their cores whereas the cores of plagioclases in #62619 and in most other porphyries are inclusion-poor.

Wybalenna Suite plagioclases from porphyry inclusions may have spectacular spikes on their profile plateaux which represent intersections with calcic "shells" within the core. Similar features occur in plagioclases from the metaluminous Gardens Suite.

By contrast, phenocrysts in granites have lower core to mantle volume fractions. They also have complex "humped" mantle profiles which always culminate in sodic rim compositions. Inclusions are uncommon.

Tourmaline

Partial analyses of this minor phase were obtained using the microprobe (Appendix H). Analyses neglect B_2O_3, F_2 and H_2O which probably amount collectively to some 13 wt%. Analyses of spectacularly zoned, elongated crystals from the Musselroe Suite, mixed-rock sample #62588 from Clarke Island (Plate 5, Fig. G) show the mean compositions of the rim zone to be richer in TiO_2, MgO, CaO and alkalis and poorer in SiO_2, Al_2O_3 and FeO* compared with the paler coloured core region. A sharp compositional discontinuity separates the two zones. Each zone grades outwards to

slightly more FeO*- and Na_2O-rich compositions, i.e. towards the F′ apex of the A′F′M diagram.

7.4 DISCUSSION: THE PETROGENETIC SIGNIFICANCE OF COMPOSITIONAL VARIATIONS OF MINERAL GRAINS

A lack of substantial Fe^*Mg_{-1} zonation in most biotite crystals (Fig. 7.5) is interpreted to indicate that Fe^*Mg_{-1} exchange has a low activation energy and is likely to continue down to low subsolidus temperatures. High Mg diffusion coefficient values for biotite (Spear, 1981) support this conclusion. Subsolidus Fe^*Mg_{-1} exchange between biotite and other mafic phases will therefore change magmatic compositions. Only biotite inclusions within felsic phenocryst phases can be regarded as retaining most of the characteristics of former magmatic compositions. Strong $TiAl6_{-1}$ zonation towards the rims of biotites indicates that the diffusion rate of this exchange is lower than that for $FeIIMg_{-1}$ exchange.

If the $TiAl6_{-1}$ exchange in biotite is coupled either to FeII-FeIII or to O-OH, then it should prove to be of considerable potential in the determination of the intensive variables: fH_2O and/or fO_2 in petrological systems.

Biotite inclusions within garnets may retain their original high-TiO_2 contents, but will lose their original (mg) signature due to exchange with the host garnet (cf. Fig. 7.8). Biotite will also undergo Fe^*Mg_{-1} exchange with all the other FeMg phases, as the temperature decreases.

Estimates of the **direction** of the compositional change of biotite due to exchange with each of the mafic phases: garnet, cordierite, orthopyroxene and melt, may be made using the formulations of the Fe^*Mg_{-1} exchange thermometers listed in Table 8.3. By combining these formulations algebraically, one may obtain thermometric expressions for the Fe^*Mg_{-1} exchange reaction equilibria between biotite and each of the other four phases. Each expression has the form of equation 8.18 in which temperature is described as a function of pressure and the $\ln K_D^{Fe^*Mg}$ between the two phases concerned. Hypothetical $K_D^{Fe^*Mg}$ -crossover temperatures may then be obtained for each biotite-bearing two-phase assemblage at a given pressure, for the case when the magnesium number of both phases is equal (i.e. when $\ln K_D^{Fe^*Mg} = 0$).

For Furneaux granite assemblages, equilibrium solidus pressures are estimated to be ~0.15 GPa (Chapter 9). The corresponding $K_D^{Fe^*Mg}$-crossover temperatures for biotite-bearing two-phase assemblages at this pressure are listed in Table 7.1.

FIGURE 7.11

DIRECTIONS OF COMPOSITITIONAL CHANGE IN FERROMAGNESIAN PHASES WITH DECREASING TEMPERATURE

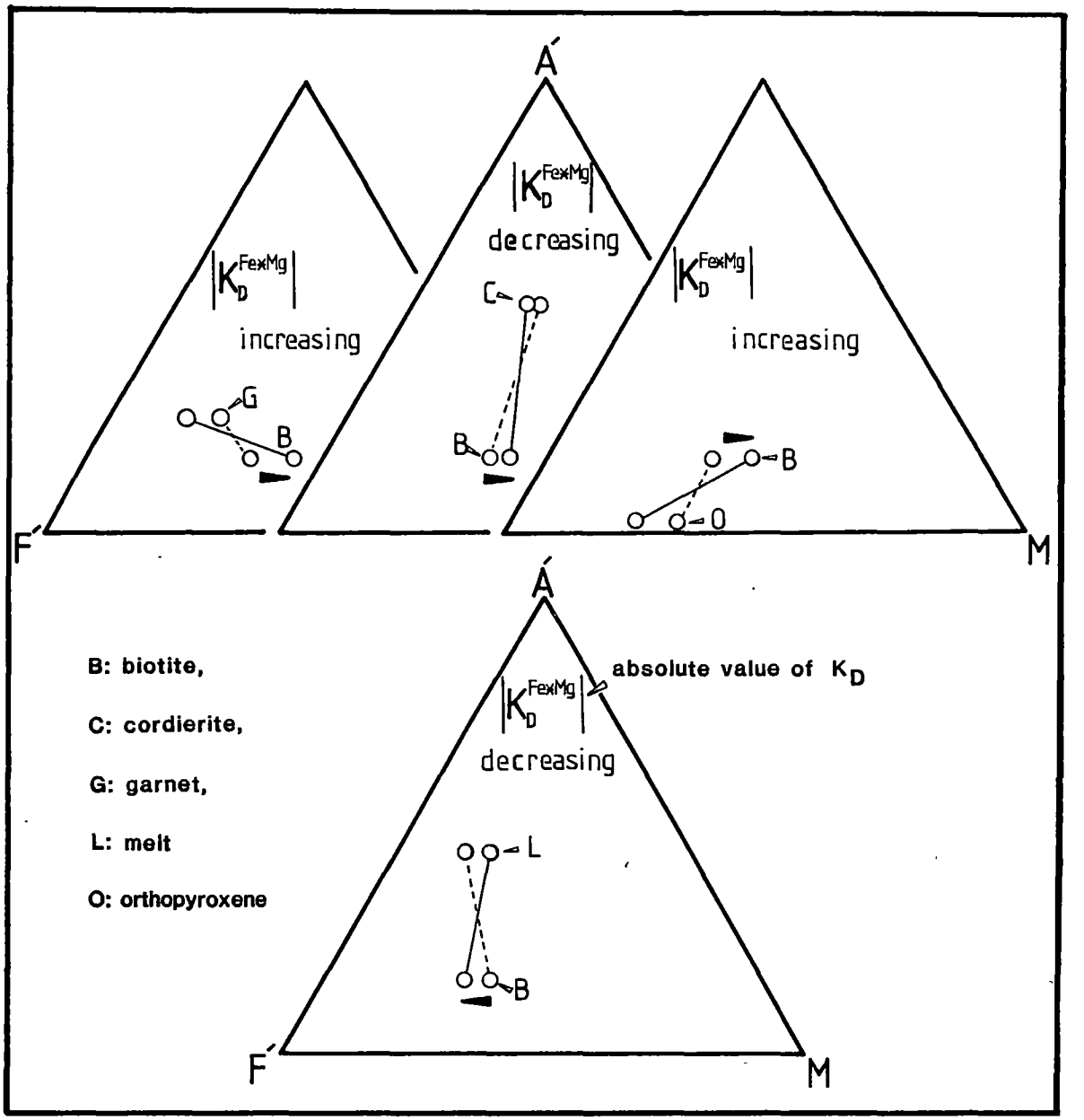

Tie-lines: high temperature (dashed), low temperature (continuous). Solid arrow marks direction of compositional change in biotite, with decreasing temperature.

Table 7.1

Hypothetical K_D^{Fe*Mg}-Crossover Temperatures for Biotite-Bearing Two-Phase Assemblages at 0.15 GPa P_W

Phase in Addition to Biotite	K_D^{Fe*Mg}-Crossover Temperature (°C)
Garnet	1120
Orthopyroxene	902
Melt	204
Cordierite	-564

K_D^{Fe*Mg} values for each two-phase assemblage will approach unity as the hypothetical crossover temperature is approached. Below the estimated emplacement temperature of ~850°C for the Babel Island, Boobyalla and Musselroe Suite magmas (Chapter 9), the phase compositions will change in accordance with these exchange equilibria, given that the relative (mg) values for the five phases concerned, increase in the order:

garnet $\gtrless$ melt < orthopyroxene < biotite < cordierite,

over typical (ultra)metamorphic temperatures (Thompson, 1976a; Chapters 8 and 11). This is schematically depicted on A'F'M diagrams in Fig. 7.11. With decreasing temperature, tie-lines between co-existing equilibrium phases will rotate in the directions shown. $Fe*Mg_{-1}$ exchange with each of the three solid phases will generate more magnesian biotite with decreasing temperature. Exchange with melt (or glass) will change biotite to more iron-rich compositions. Accordingly, the compositions of the magmatic biotites which were present in melt-dominated assemblages (such as those of the phenocryst-poor porphyries #62605 and #62606), will have been more magnesian than those now present in these rocks. In contrast to these, the magmatic biotites which were present in solid-phase enriched assemblages (such as those of the mafic mineral segregations #68523 and #68529) will have been more iron-rich than those presently in the rocks. $Fe*Mg_{-1}$ exchange, coupled with exchanges such as $Al6HTi_{-1}[\ ]_{-1}$ is therefore considered to have broadened any pre-existing magmatic trend in biotite compositions, contributing to the dispersions of compositional data depicted in Figs 7.1 and 7.5.

Limited $Fe*Mg_{-1}$ zonation in cordierite single crystals indicates a diffusion rate for this exchange in this phase to be higher than that in biotite but lower than that in garnet. The compositions of cordierite inclusions in other mafic phases must therefore be regarded merely as

magnesian limits to their pre-existing magmatic compositions. This phase evolved towards more Fe*- and Mn-rich compositions in each cordierite-bearing magma.

Phase equilibrium data indicate that [cummingtonite (mg ~50)-quartz-orthopyroxene (mg ~50)] assemblages are stable at ~775°C in the FMASH chemical system at 0.25 GPa P_W (Fonarev & Korolkov, 1980). Cummingtonite mantles to orthopyroxene crystals may therefore have been a supersolidus magmatic phase, that is, to have formed by the reaction of orthopyroxene with melt.

Chemical zonation in garnet could be due either to positive (growth) or negative (resorptional) net-transfer reactions or to simple polyvariant exchange reactions, under either magmatic or subsolidus conditions (Loomis, 1982, 1983a; Lasaga, 1983). Zoning to iron-rich rim compositions perpendicular to crystal faces in rare euhedral garnets included within felsic phases because euhedral crystals are rare and only two examples are known (in #67543 and #43252) Zonation in these crystals is strongly suggestive but is not proof of growth zonation because exchange reactions could also have been responsible. Garnets usually occur as anhedral remnants and zoning is parallel to resorbed edges, cracks and the interfaces with included crystals (Fig. 7.8). Zoning is not truncated by these features. This indicates that zonation produced by diffusional exchange has post-dated any gradients generated during crystal growth.

The mg-composition maps of Fig. 7.8 show steep gradients in garnet beside many included phases and are indicative of Fe^*Mg_{-1} exchange. Temperatures obtained using exchange thermometers (cf. Chapter 9) indicate that this zonation was produced during subsolidus conditions.

Iron-enrichment of garnet adjacent to some sillimanite prisms indicates that some Fe^*Mg_{-1} exchange has operated by surface processes involving the interface between sillimanite and the host garnet.

The corollary of the assignment of steep mg-gradients to subsolidus processes is the assignment of the high-mg compositional plateaux within garnet as Fe-rich limits to the garnet compositions at peak magmatic conditions. Subsequent magmatic compositions should be represented by more Fe*- and Mn-rich compositions at the edges of crystals which are now largely resorbed.

Grunerite, muscovite and actinolite are considered to have been subsolidus rather than supersolidus phases, in view of their known stability limits at low pressures (Forbes, 1977; Robinson, 1982; Chatterjee & Johannes, 1974; Gilbert & Popp, 1982), recognising that the stability of each of these phases is lowered in the presence of quartz (Chatterjee & Johannes, 1974; Wones & Gilbert, 1982). Their subsolidus status is also

indicated from their frequent fine-grained mosaic-like replacement textures.

Ilmenite and tourmaline are both considered to have been magmatic phases although they also grew over a wide range of subsolidus conditions (cf. Chapter 4). The occurrence of Fe*- and Ti-poor biotite adjacent to euhedral ilmenite is interpreted as indicating growth of ilmenite at the expense of biotite at temperatures below or at rates above those at which Fe^*Mg_{-1} could homogenise biotite compositions in these components (assuming that FeIII/FeII zonation is negligible). Much of the modal ilmenite in coarsely crystalline granites is therefore considered to have been generated during the subsolidus reaction of high-Ti magmatic biotite.

Plagioclase data are interpreted in the light of experimental and theoretical studies (Lofgren, 1972, 1980; Klusman, 1972; Lasaga, 1983; Loomis, 1983a,b; 1982; Kirkpatrick, 1982) which indicate that at temperatures below ~900^{o}C, plagioclase compositions are strongly influenced by kinetic factors such as the activation energy for atomic attachment to the crystal face and melt-phase binary diffusion rates in addition to the ambient intensive variables. The relative time-rates of diffusion, crystallization, nucleation and thermal change are therefore all important in the determination of plagioclase compositions (op. cit.).

Cores may have grown either during high-grade metamorphism prior to partial melting or in the presence of a melt phase during magmatic evolution. Plagioclase cores could therefore be either restitic or an early phenocrystic phase generated in the magma subsequent to the magma leaving the source region.

Calcic shells are considered to have formed by growth at higher than ambient temperatures and chemically register the existence of a thermal pulse during petrogenesis. Such a pulse might have been associated with magma mixing during its magmatic evolution. In Fig. 7.10a however, plateau plagioclase compositions are similar on each side of the pulse which suggests that there was no major difference in magma bulk-composition before and after the pulse, i.e. that there was no substantial magma mixing during the transient heat event.

Simple zonation of mantles to more sodic compositions occur in the plagioclase phenocrysts from Boobyalla Suite porphyries (cf. Fig. 7.10f). The compositions indicated by this profile could have been produced by crystallization from a melt which became progressively more sodic and/or cooler. Sodium enrichment of the melt is indicated from the porphyry matrix separate compositions for this suite (Chapter 5, Appendix F). Boobyalla Suite plagioclases are therefore considered to have approached a

state of surface rather than of volume equilibrium with the rest of the phases in the magmas.

In contrast to these, the plagioclases from porphyries with relatively mafic matrixes such as in samples #62589 and #62594, have very small mantles. These plagioclases are therefore interpreted as having approached a state of volume equilbrium with their enclosing melt phase.

The humped mantle profiles in granite plagioclases (profiles c, d and g of Fig. 7.10) may have arisen from the capture of melt-gradients proximal to normally zoned phenocrysts during slow cooling of near-solidus interstitial melt.

In addition to the compositions of the phyric phases, the bulk composition of porphyry matrix assemblages also vary because their constituent assemblages can vary especially in directions away from phenocryst phases. Visible zonation of porphyry matrixes may occur within ~1 mm of phyric phases or mafic synplutonic inclusions (e.g. that proximal to plagioclase in #62619, Plate 3, Fig. B; or that beside metabasaltic inclusions in #67530, Plate 3, Fig. G).

7.5 CONCLUSIONS

The extent of the subsolidus modification of magmatic equilibria is roughly proportional to the matrix grainsize because porphyries (the products of accelerated cooling of granitic magmas), have compositional ranges for most phases which are substantially greater than the compositional ranges of the same phases present in coarsely crystalline (i.e. slower cooled) rocks. Porphyries therefore retain considerably more petrogenetic information than do coarsely crystalline granites.

Data from porphyries are consistent with chemical fractionation processes having operated during magma evolution, leading to progressive compositional changes in all phase solutions. In the Boobyalla Suite magmas, for example, melts became more felsic and (al)-rich (cf. Chapter 5), while plagioclases accreted mantles of progressively more sodic composition. Biotite became less titaniferous and more Al-, Fe*-, Mn- and Cl-rich, whereas cordierite and garnet became more Fe*- and Mn-rich. Ilmenite and apatite each became more Mn-rich, and andalusite became less FeIII-rich.

Possible restitic solid-solution phases, preserved throughout magma evolution and subsolidus reaction are abundant in many Boobyalla and Musselroe Suite rocks. They include the cores of plagioclase and garnet. Sillimanite, magnesian cordierite, titaniferous biotite, ilmenite and gahnitic hercynite (a phase which also occurs as inclusions within garnet, cf. Fig. 7.8) may also have been restite phases in early Musselroe Suite

magmas, because they occur as inclusions within garnet cores. In the Poimena and Wybalenna Suite magmas however, plagioclase appears to have been in equilibrium with low-pressure melts and was therefore not a restite phase.

Chapter 8

Al-Fe-Mg PARTITIONING BETWEEN BIOTITE, GARNET AND MELT: AN EXPERIMENTAL STUDY IN THE KFMASHO CHEMICAL SYSTEM

8.1 INTRODUCTION

A knowledge of major-element partitioning amongst magmatic phases is essential for igneous thermobarometry. It is critical also to an understanding of igneous phase equilibria.

In felsic igneous systems, this knowledge is restricted largely to partitioning of the alkalis and calcium between feldspars and melt (e.g. Tuttle & Bowen, 1958; James & Hamilton, 1969; Johannes, 1978, 1980, 1984), as discussed in Chapter 10. Partitioning of Fe and Mg between mafic phases and melt in these systems is also poorly known. As a consequence, the thermobarometry of and mafic phase equilibria in felsic igneous systems is poorly known.

To supplement these data, an experimental study of the partial melting of peraluminous KFMASHO and KFMASHTO simple-system compositions has been undertaken. These compositions are analogues of those of pelites. Upon melting, they yielded silica-rich glasses with compositions which are analogues of natural granites. They therefore support the finding of Green (1976a) that pelite can be a granite protolith.

In this chapter, the experimental materials and methods are described. Compositions of the generated phases are then given. The dependence of $Fe^{*}Mg_{-1}$ exchange between biotite and garnet and between garnet and melt, upon pressure, temperature and phase composition are then determined. The effect on $K_D^{Fe^{*}Mg}$ values of changes in fO_2, X_{Fe}, X_W, X_K and X_{Ti} are then discussed. Finally, implications of these simple system phase equilibria for granitic phase equilibria, are considered.

8.2 STARTING COMPOSITIONS

Starting compositions consisted of mineral mixes which were prepared from synthetic and natural minerals (Table 8.1). Analar grade chemicals were used to prepare the synthetic phases using the methods indicated in Appendix J. Mixes were prepared by grinding appropriate amounts of these phases together under acetone for 1 hour.

The compositions of Mixes 1 and 2 were chosen to resemble those of natural pelites. Mix 2 supercedes Mix 1, which contains a large proportion of the refractory phase: garnet.

Table 8.1

Compositions of Experimental Mixes

	Mix			
	1	2	3	4
Phases (wt.%)				
Quartz	13.10	22.65	18.52	
Sanidine	30.82	12.43	9.73	
Sillimanite	4.64	17.05	16.15	
Cordierite	7.25	2.19	8.80	
Phlogopite	6.96			
Biotite An_{26}		40.31	31.57	
Almandine	37.23	5.37	4.21	
Fayalite				
Ilmenite			11.02	66.77
Magnetite				33.23
Oxides (wt.%)				
SiO_2	55.00	55.00	52.51	
TiO_2			4.95	35.16
Al_2O_3	19.57	19.08	18.22	
Fe_2O_3				22.92
FeO*	16.12	15.52	14.82	41.92
MgO	3.02	2.90	2.77	
K_2O	6.00	6.00	5.73	
H_2O	0.30	1.49	1.00	
Molecular Indices (mol.%)				
mg	25.0	25.0	25.0	
al	30.0	30.0	30.0	

where mg = % mol.MgO/(MgO+FeO*)

and al = % mol.$(Al_2O_3-K_2O)/[Al_2O_3+FeO^*+MgO-K_2O]$

Mix 3 has, on an anhydrous basis, the composition of Mix 2 plus 4.95 wt% TiO_2. The compositions of Mixes 1, 2 and 3 plot in the same position on the A'FM diagram.

The composition of Mix 4, the fO_2-sensor mix, was chosen on the basis of the results of the experimental study of Spencer & Lindsley (1981). The study predicts that the ulvospinel-magnetite and ilmenite-hematite solid solutions present in Mix 4 should be present in roughly equal quantities at ~800°C, with fO_2 close to the CCO or NNO oxygen buffers (that is, close to the fO_2 conditions estimated for the furnace assembly).

8.3 RUN PROCEDURES

$Ag_{75}Pd_{25}$ capsules were used in conjunction with salt or talc-pyrex pressure media in order to reduce iron loss to negligible amounts (Ellis, 1984). To about 12 mg of a starting mix, sufficient water was added (15 to 25 % of the charge) to ensure a water-saturation under run conditions. Only in run T1573 was the quantity of water reduced, in order to generate a water-undersaturated chemical environment. In two of the three fO_2-sensor runs, ~0.4 mg quantities of Mix 4 were sealed inside tiny $Ag_{75}Pd_{25}$ tubes constructed from small-bore (1.8 mm ID) capsule tubing. These were then sealed into the capsules with the charge. In the fO_2-sensor run #T1485, Mix 4 alone was run.

High pressure experiments were undertaken using piston cylinder apparatus at the Geology Department, University of Tasmania. Experimental techniques are similar to those described by Green & Ringwood (1967) except that a zero friction correction was adopted for the NaCl pressure medium (Johannes et al., 1971). Temperature was recorded using a $Pt/Pt_{90}Rh_{10}$ thermocouple. The recorded temperature was controlled to within ±5°C of the set point. The precision of the measurement when allowance is made for temperature gradients within the capsule, is ±10°C. Pressure precision is estimated to be ±0.05 GPa.

The run times chosen varied in proportion to the temperature. Runs at 1000°C were of ~1 day duration, 950°C runs ~2 days, 900°C runs ~1 week, 850°C ~2 weeks and T1542 at 800°C was run for 1 month.

The visible expulsion of water upon capsule-piercing for all silicate-containing runs other than the water-undersaturated run: T1573, is consistent with their having been water-saturated. Run products consisted of glass containing a variety of crystalline phases and vapour bubbles. When melting was extensive, physical separation of crystals from melt occurred. Large fragments containing representative assemblages, were mounted in epoxy resin for chemical analysis by electron microprobe. Other fragments were lightly crushed and examined optically.

8.4 ANALYTICAL METHODS

Polished epoxy-resin mounted fragments were analysed by microprobe. Large area scans were obtained to minimize losses of potassium by volatilization. Glasses totalled ~80%, depending upon the starting water content. They were recalculated to 100%, on an anhydrous basis. Biotites totalled ~96% and cordierite (in T1491) ~98%, due presumably to their structural water. These phases were arbitrarily totalled to 96% and 98% respectively. Oxide phase totals were <100% due to the presence of extra oxygen associated with FeIII. These were retotalled to 100% upon calculation of FeIII contents, on the basis of stoichiometry. Garnet compositions totalled ~100%.

Limiting ferromagnesian rim-compositions of zoned garnets were determined by scanning narrow windows along the garnet/glass interface at high scanning electron microscope (SEM) magnification. Minor compositional contributions from the glass (e.g. <1% K_2O) were removed using the averaged glass composition. Rim-garnet compositions were then obtained by regressing a set of core to recalculated rim compositions against magnesium number (mg), using the rim composition mg-value as a limit.

For the oxide phases, a similar method was applied because analysed compositions of their tiny crystals free of contamination from the enclosing melt, were often unobtainable. Compositions indicating the least amount of melt contaminant were regressed with the averaged melt composition, against SiO_2. The oxide phase composition was then obtained assuming it to have been free of SiO_2.

Estimates of the precision of averaged compositions were obtained assuming that for a component (y):

$$\sigma_y^2 = \frac{\Sigma(y^2) - (\Sigma y)^2/n}{n-1} \qquad (8.1)$$

for n = number of determinations

For compositions obtained by regression, precision was estimated by the equation derived by Dr B.M. Brown (Department of Mathematics, University of Tasmania):

$$\sigma^2_{y_{x=L}} = \left(\frac{(n-1)\ (\sigma_y^2 - m^2\ \sigma_x^2)}{n-2}\right) \cdot \left(\frac{1}{n} + \frac{(L - \bar{x})^2 (n-1)}{\sigma_x^2}\right) \qquad (8.2)$$

FIGURE 8.1

MAGMATIC ASSEMBLAGES
FROM KFMASHO-SYSTEM EXPERIMENTAL RUNS

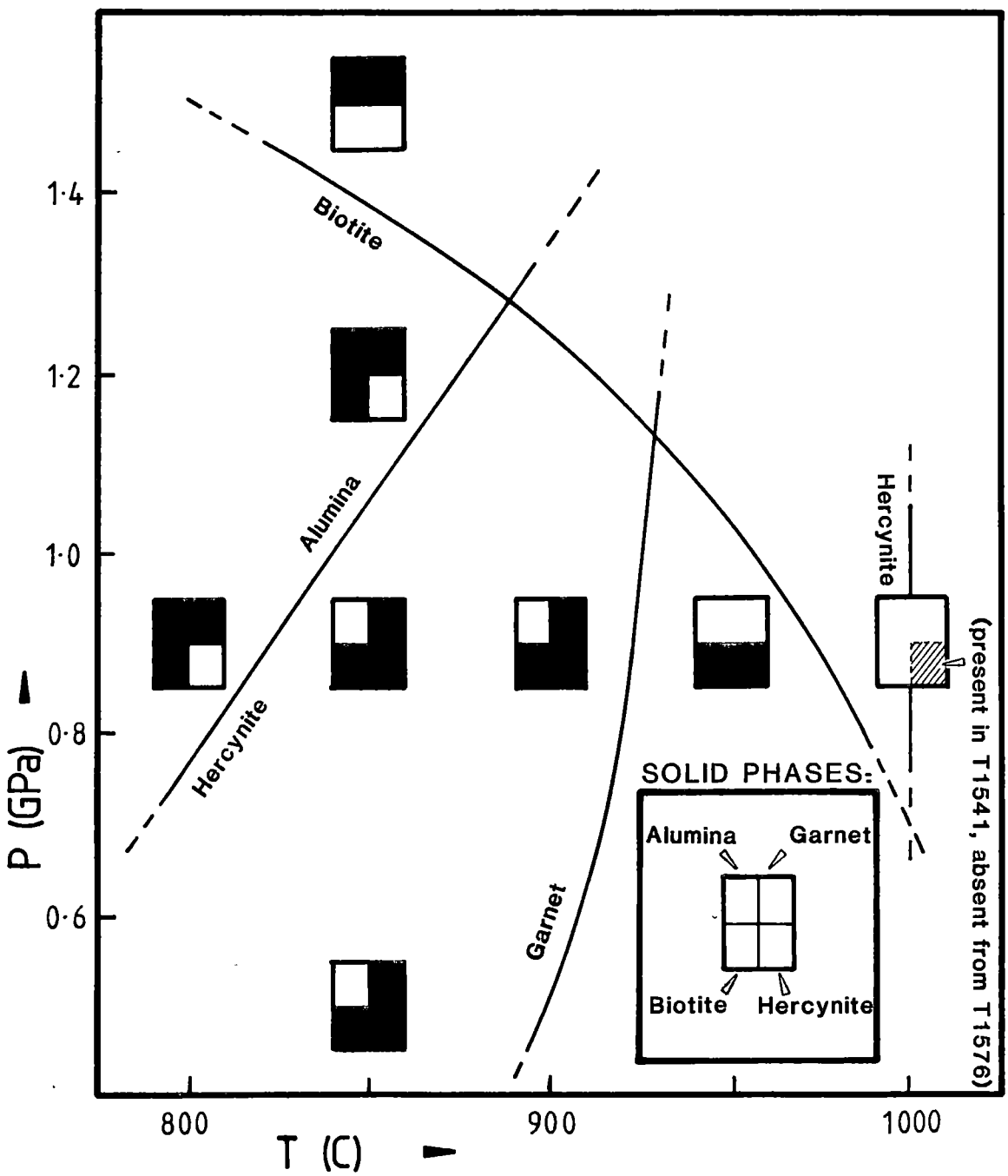

for (x) the independent variable,

(y) the dependent variable, and

(L) the limiting value chosen for the independent variable.

σ_x^2 and σ_y^2 are described by equation 8.1. and

$$m = \frac{[\Sigma(xy) - (\Sigma x \Sigma y/n)]}{[\Sigma(x^2) - (\Sigma x/n)^2]} .$$

For the cordierite from T1491 and for those garnet compositions obtained by regression however, the precision of FeO* and MgO is only approximate, because for these oxides, the variable (mg), against which they were regressed, is not independent.

The compositions and their 2σ error estimates of all product phases are given in Appendix K. They are depicted diagrammatically in Fig. 8.2.

8.5 RESULTS

8.5.1 Petrography

A P_WT phase diagram showing the distribution of run products is shown in Fig. 8.1. Run product glasses were free of quench crystals, except for the 1000°C runs. In these, a cryptocrystalline birefringent phase (biotite?) occurs throughout the charge, giving the glass an opalescent appearance.

All melts were undersaturated in quartz, sanidine and aluminosilicate. However an aluminium oxide phase (β- Al_2O_3?) occurs as needles in run products at high presures ($\geq$ 1.2 GPa) and at low temperature (800°C). It is not known if this phase is in stable equilibrium with the melt or is metastable. It has been previously reported from pelite melting experiments by Green (1976a).

Cordierite was present only in the low-pressure titanium-bearing run (T1491). It occurs as rhombs about 20 μm on edge.

Biotite is widely distributed. It is absent only from the runs at highest pressure (1.5 GPa) and highest temperature (1000°C). It occurred as thin pale green flakes, up to 0.25 μm across in titanium-absent runs and pale brown flakes in runs containing TiO_2.

Garnet is absent from the low-pressure titanium-bearing run: T1491 and from water-saturated runs above 900°C. However it was stabilized at 950°C by undersaturating the charge in water (run T1573). It occurs as rounded pink grains ~5 μm in diameter. Garnet in runs at pressures above 0.9 GPa had well-developed crystal faces and were larger than the garnets originally present in the starting mix, indicating growth of garnet during the runs.

FIGURE 8.2

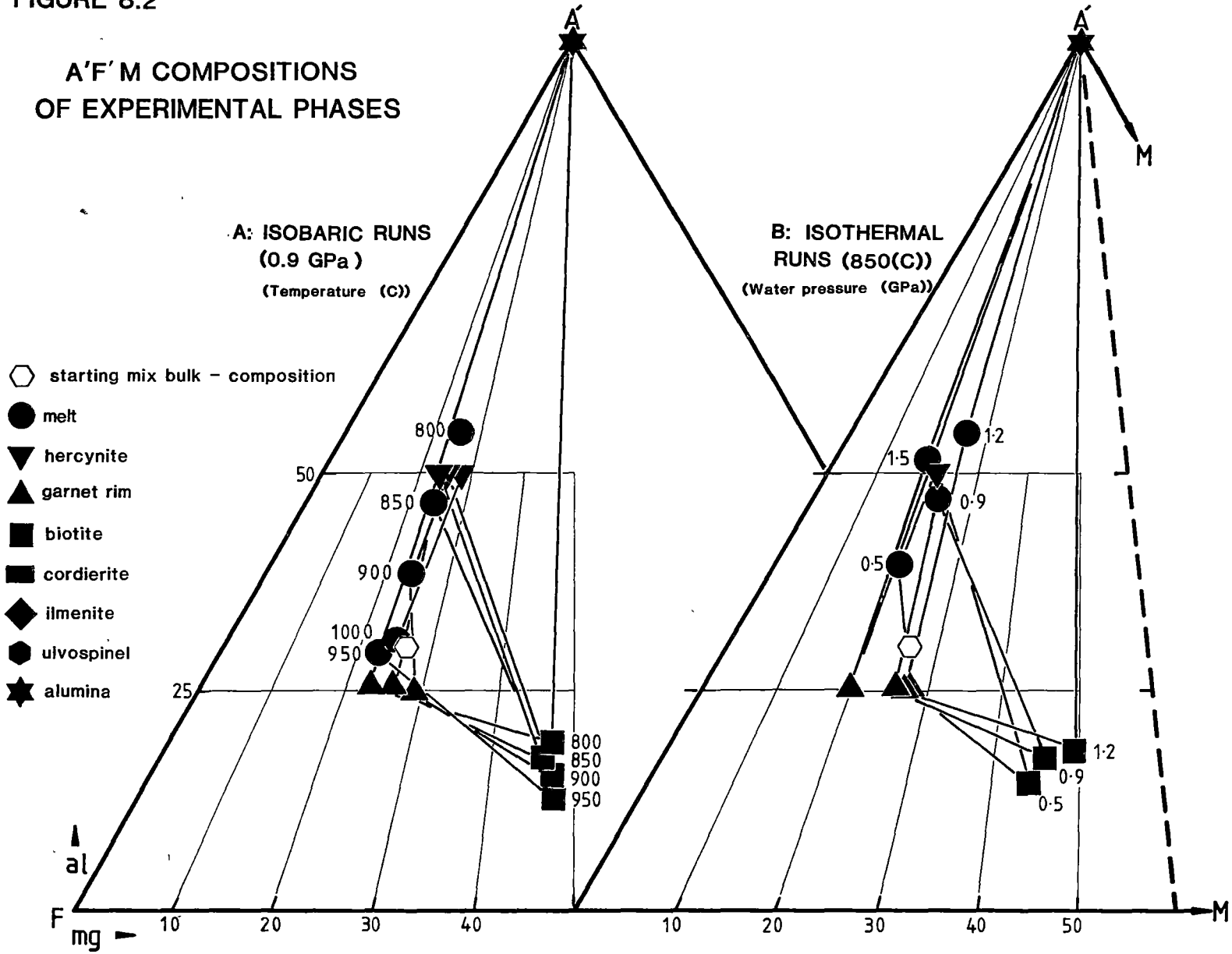
A'F'M COMPOSITIONS
OF EXPERIMENTAL PHASES
A: ISOBARIC RUNS
(0.9 GPa)
(Temperature (C))
B: ISOTHERMAL
RUNS (850(C))
(Water pressure (GPa))
starting mix bulk - composition
melt
hercynite
garnet rim
biotite
cordierite
ilmenite
ulvospinel
alumina
A'
M
800
850
900
1000
950
50
25
1·2
1·5
0·9
0·5
al
F
mg
10
20
30
40
50

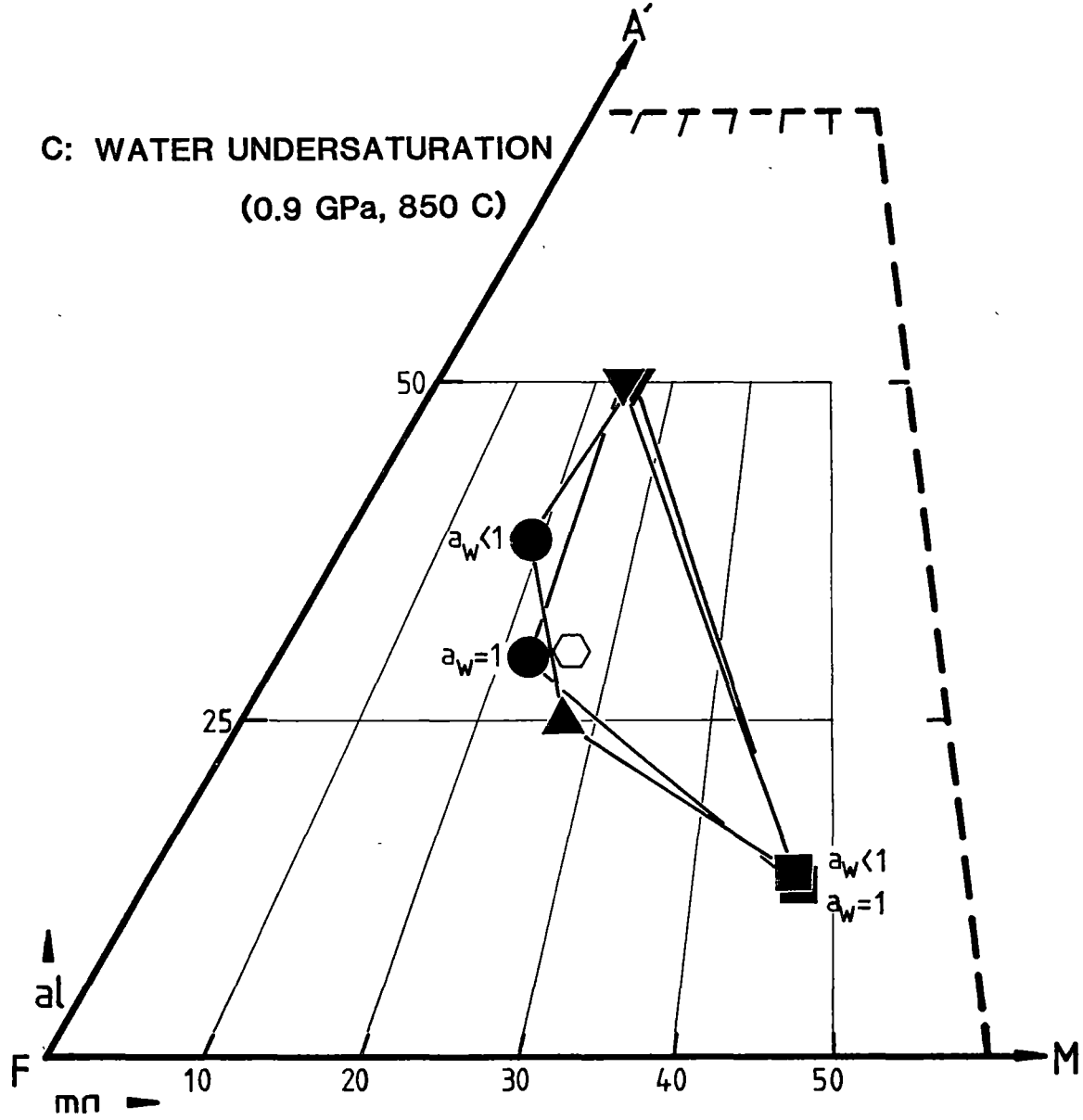
C: WATER UNDERSATURATION
(0.9 GPa, 850 C)
A´
50
25
a_w<1
a_w=1
a_w<1
a_w=1
al
F
mn
10
20
30
40
50
M

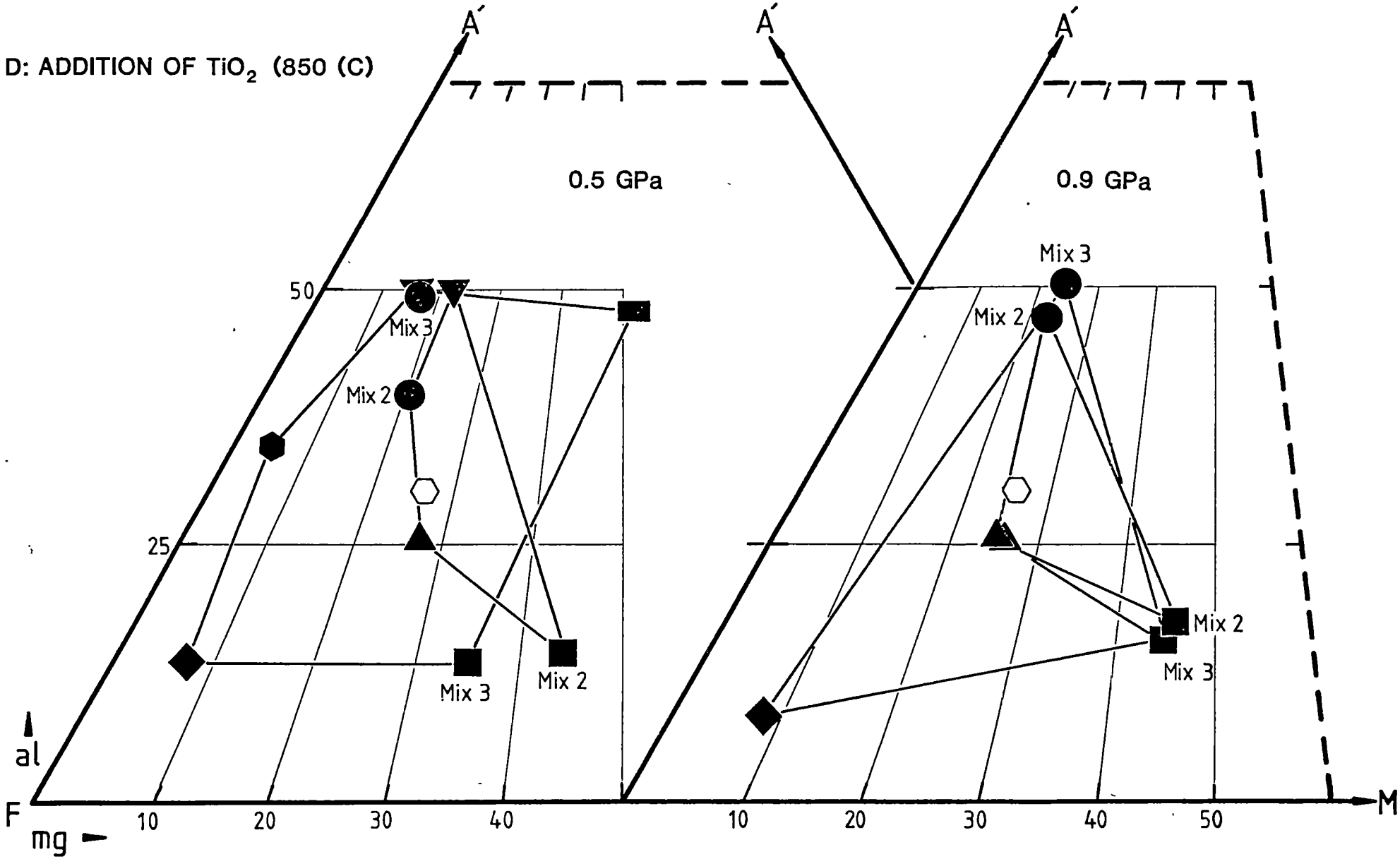
D: ADDITION OF TiO2 (850 (C)
A´
A´
A´
0.5 GPa
0.9 GPa
50
25
Mix 3
Mix 2
Mix 3
Mix 2
Mix 3
Mix 2
Mix 2
Mix 3
al
F
mg
10
20
30
40
10
20
30
40
50
M

Hercynite is absent only from those runs containing alumina and from one of the 1000°C runs (T1576). It is the liquidus phase at 0.9 GPa (run T1541). It occurs as small facetted green cube-octahedra <5 μm across.

In both titanium-bearing runs, the biotite is light brown in colour. Ilmenite occurs as small plates <6 μm long. In run T1491, ulvospinel is present as octahedra up to 10 μm across.

8.5.2 Phase Compositions in the Water-Saturated KFMASHO Chemical System

Biotite flakes are always chemically unzoned. They have consistent compositions throughout the charge. At 800°C and 0.9 GPa, biotite has an (al) value of 19.0 (Fig. 8.2). With increasing temperature however, it becomes less peraluminous, with (al) values dropping to 12.7 by 950°C.

With increasing pressure, biotite becomes more magnesian. This is thought to reflect the increasing abundance of garnet and the corresponding decreased modal abundance of biotite with increasing pressure.

Garnet has almandine-rich cores in all runs except those in T1573, at 950°C, where garnet was found to be unzoned. In runs at lower temperatures, strong zoning is apparent. In the highest pressure run (T1558) complex zoning to iron-rich rim compositions occurs whereas zoning to magnesian rim compositions is observed in all other garnet-bearing runs. Almandine-rich cores to garnets occur in all runs except those in T1573.

Hercynite A'FM compositions have FeII/FeIII ratios which decrease from 10.5 at 900°C and 0.9 GPa with both decreasing pressure and increasing temperature, reaching 6.3 at 850°C and 0.5 GPa and 5.1 at 1000°C and 0.9 GPa.

Alumina contains <1% of Fe_2O_3.

Glasses show considerable chemical variation. At low temperatures and high pressures, they are more peraluminous and siliceous than at other conditions. Glasses can even be more peraluminous than the mineral: cordierite (Fig. 8.2). With increasing temperature, melt compositions become both less peraluminous and less siliceous, approaching the bulk composition of the starting mix, as the liquidus is approached.

Traces of titanium in biotites and chromium in hercynites occur presumably due to selective scavenging of these impurities present originally in the Analar-grade oxides used to prepare the starting minerals.

8.6 DISCUSSION

8.6.1 Diffusion of Iron

High-temperature near-liquidus runs have compositions which are very similar to that of the starting mix (Appendix K, Fig. 8.2), indicating that Fe loss has been negligible. Crystal-liquid separation precludes bulk compositional estimates being made of the sub-liquidus runs by the method of large-area scanning of the run product using the electron microprobe. However there is no obvious indication from phase compositions (such as zoning to magnesium-rich run compositions) that iron-loss has occurred. Nor could iron be detected in the $Ag_{75}Pd_{25}$ capsule of T1573, run at 950°C for 1 week. These results support those of Ellis (1984) and indicate that the use of this capsule material in conjunction with salt or talc/pyrex pressure media, is effective in minimizing the problem of iron-loss at low to moderate run temperatures and low pressures.

8.6.2 Scale of Equilibrium

Run T1573 (950°C, 0.9 GPa, $a_w^m < 1$ and t = 189 hrs) produced garnet crystals which were chemically homogeneous. In all other runs, garnet was zoned and relict iron-rich cores were often present. Zonation was to magnesian rims except in run T1558 which contained garnets with iron-rich rims on magnesian mantles often with iron-rich cores. The only other known to be chemically zoned mineral is the cordierite from the titanium-zontaining run:: T1491. Its chemical gradients are much smaller than those in garnet. It has magnesian cores and iron-rich rims.

Diffusion in glasses is usually faster than that in crystalline phases and diffusion in melts is faster still (Freer, 1981; Jambon & Semet, 1978). Accordingly, the relative magnitudes of the FeMg chemical gradients observed in the four silicate phases: garnet (Ga), cordierite (Cd) and the unzoned) biotite (Bi) and melt (Me) are consistent with $FeMg_{-1}$ interdiffusion rates, as described by the interdiffusion coefficients: D_{FeMg}, which increase in the order:

$$D^{Ga}_{FeMg} < D^{Cd}_{FeMg} << D^{Bi}_{FeMg} < D^{Me}_{FeMg} \qquad (8.3)$$

The relative rates of $FeMg_{-1}$ interdiffusion in garnet and biotite described by this inequality are supported by published self-diffusion data for Mg in biotite compiled by Freer (1981, table 2, equation 4) and for Mg in pyrope determined experimentally by Cygan & Lasaga (1985). These data indicate that self-diffusion rates for Mg are $>7 \times 10^9$ times faster in biotite than in garnet at 900°C and $>4 \times 10^{14}$ times faster at 800°C. These rate ratios are **lower** limits because the self-diffusion coefficient for Mg in biotite is that determined at low temperatures ($22 < T(^oC) < 122$, Freer,

1981) and is likely to be greater than the quoted value at the temperatures of 800°C to 900°C considered here because diffusion rates often have a temperature dependency due to the operation of different diffusion mechanisms at different temperatures (op. cit.; Lasaga, 1983).

However, net-transfer reactions also occurred in the experimental runs, because the phases and their proportions changed over the duration of the runs. Chemical gradients in phases will in fact be dependent upon both exchange and net-transfer reaction rates. For example, positive net-transfer reactions for garnet (i.e. garnet growth) will broaden $FeMg_{-1}$ gradients in this phase, thereby increasing the time required for the attainment of wholesale equilibrium in the charge, but facilitating the determination of garnet-rim compositions. In contrast, negative net-transfer reactions for this phase (i.e. resorption of garnet seeds) will steepen these gradients, hastening the time required for attainment of wholesale equilibrium but making rim compositions more difficult to determine.

In the systems studied, net-transfer reaction rates are faster than the rates of $FeMg_{-1}$ exchange between garnet and other phases, because large variations in the modal proportions of product phases occurs over the P and T ranges applied, yet chemical zonation in garnet is still observed. Accordingly, the rate-determining step for the achievement of wholsale equilibrium within garnet-bearing charges is the $FeMg_{-1}$ interdiffusion rate in garnet.

The relationship between self-diffusion coefficients and interdiffusion coefficients in ionic solutions is imprecisely known (see discussion by Anderson, 1981, p.253). However, it may be approximated, for the case of FeMg interdiffusion, by the equation (Brady, 1975):

$$D_{FeMg} \approx \left(\frac{D_{Fe} \cdot D_{Mg}}{X^{\Phi}_{Fe} D_{Fe} + X^{\Phi}_{Mg} D_{Mg}} \right) \cdot \frac{d \ln a^{\Phi}_{Fe}}{d \ln^{\Phi}_{Fe}} \qquad (8.4)$$

for self-diffusion coefficients D_{Fe} and D_{Mg} and mole fractions and activities of the Fe and Mg endmembers in phase Φ, of X^{Φ}_{Fe}, X^{Φ}_{Mg} and a^{Φ}_{Fe} respectively. For Fe-Mg garnet (Ga), this equation reduces to

$$D^{Ga}_{FeMg} \approx D^{Ga}_{Mg} \qquad (8.5)$$

if it is assumed that activity/composition relationships in this solid solution are ideal (Newton & Haselton, 1981) and that Fe self-diffusion coefficients are similar to those of Mg (Cygan & Lasaga, 1985). A relationship similar to that of (8.5) is expected to hold for $FeMg_{-1}$

interdiffusion in biotite. By these arguments then, FeMg interdiffusion is therefore expected to be 12 ± 3 orders of magnitude faster in biotite than in garnet under run conditions (800-900°C), assuming that only exchange reactions operate to change phase compositions.

Homogenization times for zoned garnets can be calculated from the diffusion data of Cygan & Lasaga (1985, equation 12), assuming that

(a) the self-diffusion coefficient for Mg in pyrope is approximately equal to the $FeMg_{-1}$ interdiffusion coefficient in garnet, and

(b) the phases in the charge react only by $FeMg_{-1}$ exchange.

Then at 800°C, homogenization of a spherical garnet 10 μm in diameter is estimated to take ~9 years. This time is reduced to ~1 month for a crystal which is 1 μm in diameter. These calculations show that wholesale equilibrium within charges can only be achieved for realistic run times at temperatures down to 800°C if the garnet crystals are $\leq$ 1 μm in diameter.

By virtue of the extreme difference in $FeMg_{-1}$ interdiffusion rates of garnet and the other phases, there were in effect, two constituent sub-assemblages in charges containing zoned garnet. These are:

(a) a disequilibrium sub-assemblage consisting of garnet cores, and

(b) a **localized** equilibrium sub-assemblage (in the sense of Loomis, 1983a) consisting of garnet rims, biotite, hercynite and melt.

With time, phase compositions in sub-assemblage (b) will change progressively, as the reservoir of iron in garnet is slowly dissipated, causing the activities of chemical components in the sub-assemblages to change slowly at constant P and T. At any time, there will be virtual equilibrium amongst the constituent phases of this sub-assemblage because $FeMg_{-1}$ interdiffusion within each phase at physical scale being considered is rapid.

Consequences of slow $FeMg_{-1}$ interdiffusion in garnet are therefore:

(a) the occurrence in charges containing zoned garnet of a sub-assemblage from which equilibrium $FeMg_{-1}$ exchange reaction parameters may be obtained, but

(b) uncertainty in the bulk compositions of the localized equilibrium assemblage and

(c) uncertainty in the equilibrium assemblage for the bulk composition of the entire charge.

8.6.3 Oxygen Fugacimetry

The {magnetite-ilmenite} fO_2-sensor mix (Mix 5) was run at 850°C and 0.7 GPa (T1485), 950°C and 0.9 GPa (T1573) and at 1000°C and 0.9 GPa (T1576). Ulvospinel and ilmenite solid solutions were generated both in these runs and in the Mix 4 run: T1491, at 850°C and 0.5 GPa. The phase compositions from these four runs (Appendix K), have been recast into

Table 8.2

Cation Proportions and Endmember Designations of Ulvospinel + Ilmenite Pairs

	Mix 4		Mix 4		Mix 4		Mix 3	
Run	T1485		T1573		T1576		T1491	
T (°C)	850		950		1000		850	
P (Gpa)	0.7		0.9		0.9		0.5	
Phase	Il-ss	Us-ss	Il-ss	Us-ss	Il-ss	Us-ss	Il-ss	Us-ss
Ti	1.9033	0.7415	1.8834	0.7424	1.8601	0.7172	1.7240	0.3070
Al		0.0199		0.00169	0.0259	0.1204	0.0841	0.4630
FeIII	0.1938	0.4984	0.2357	0.4986	0.2544	0.4453	0.4690	0.9246
FeII	1.9029	1.7396	1.8799	1.7420	1.7934	1.6809	1.6004	1.2429
Mg					0.0662	0.0362	0.1225	0.0625
gk					2.8		4.0	
il	95.1		93.9		89.0		80.0	
hm	4.9		6.1		6.8		11.7	
us		74.0		74.2		71.7		30.6
mt		24.9		24.9		22.3	46.2	
sp-hc		1.0		0.8		6.0	2.1	23.1
ru		0.1			0.7		2.2	0.1
il/ (il+hm)	95.1		93.9		92.9		87.2	
us/ (us+mt)		74.8		74.9		76.3		39.8
$\log_{10} fO_2$	-14±0.75		-12.4±0.75		-11.4±0.75		-11.4±0.75	
T°C(est.)	895±60		965±60		1020±60		910±60	

for: gk - giekelite ($MgTiO_3$), il - ilmenite ($FeTiO_3$), hm - hematite, us - ulvospinel, mt - magnetite, sp-hc - spinel-hercynite, ru - rutile.

FIGURE 8.3

OXYGEN FUGACIMETRY OF EXPERIMENTAL RUNS

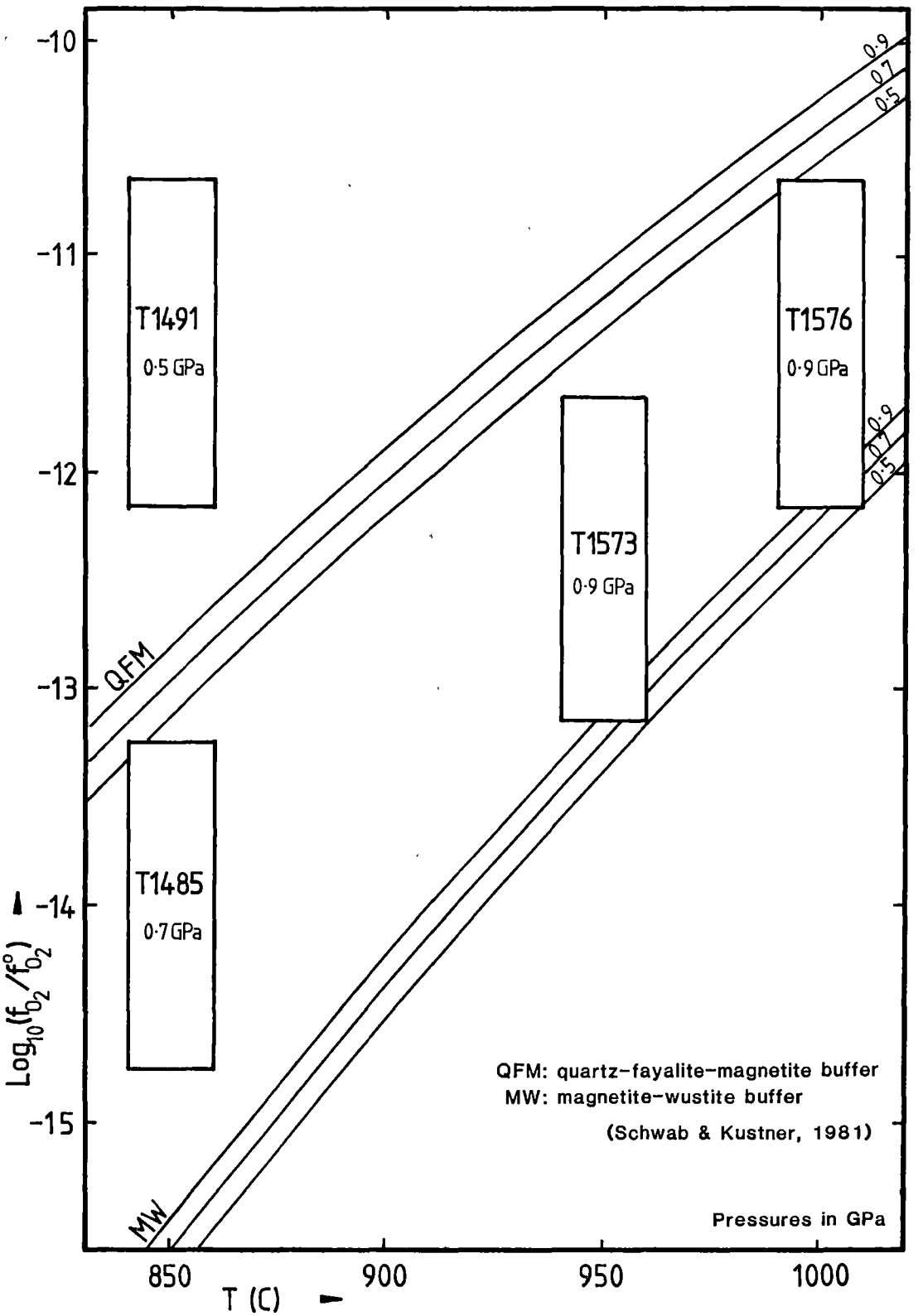

cation and endmember proportions. They are listed in table 8.2 below, together with temperatures and oxygen fugacities estimated using the ulvospinel-ilmenite solution model of Spenser & Lindsley (1981).

Model temperatures are all higher, but within error of their respective run temperatures. The greatest disparity betwen model and run temperature is for run T1491. This feature may be due to the effects of extensive amounts of other oxide endmembers in each solid solution from this run.

Oxygen fugacities are depicted on a $\log_{10} fO_2$ versus temperature graph, in Fig. 8.3. Fields for each of the four assemblages are constrained by the experimental temperature precision of $\pm 20^{\circ}C$ and oxygen fugacity error estimates of ± 0.75 $\log_{10} fO_2$ units (Spenser & Lindsley (1981).

Reference curves are for the quartz-fayalite-magnetite (QFM) and the magnetite-wustite (MW) oxygen buffers (Schwab & Kustner, 1981). Curves for three pressures (0.5, 0.7 and 0.9 GPa) are given for each buffer.

KFMASHO system oxygen fugacities form a trend between the QFM and MW buffers. This trend defines the "assembly buffer" of the high pressure experimental apparatus. Relative to the fO_2 on this trend at $850^{\circ}C$, the assemblage in the KFMASHTO system run T1491 is ~3 $\log_{10} fO_2$ units more oxidized.

8.6.4 The Role of TiO_2

Phase compositions in KFMASHTO system runs are considerably different from those in the corresponding runs for the simpler KFMASHO system. Ti therefore exerts considerable influence on the chemical equilibria. Titan-biotites, as with their natural counterparts (Chapter 7) are less peraluminous than their Ti-absent counterparts (Fig. 8.2). Melts, on the other hand, are more peraluminous than their Ti-absent counterparts, especially at lower pressure.

The most important effect of TiO_2 addition is to substantially increase the ambient fO_2 within the charge. This is indicated by:

(a) the high Fe_2O_3 content of hercynites ;
(b) Fe_2O_3 solid solution in ilmenite in excess of that indicated for assembly-buffered ilmenites (Fig. 8.2) (see below);
(c) the occurrence of the FeIII phase: ulvospinel in the 0.5 GPa run; and
(d) the presence of Ti in garnet, which enters garnet only if FeIII is also present through the double substitution: $FeIIITiAl_{-1}Si_{-1}$ (Huggins et al., 1977).

An increase in fO_2 within the charge is consistent with titanium entering biotite by the double substitution: $Ti(\ )Al_{-1}H_{-1}$, as is suggested for the natural biotites in the previous chapter. Hydrogen liberated during

titanoxybiotite formation will gradually diffuse out of the capsule to leave an oxidized charge. The high proportion of failures of runs containing Mix 3 is consistent with their capsules having burst from the internal pressure of hydrogen resulting from this titanium substitution mechanism in biotite.

8.6.5 The Role of H_2O

From a comparison of the data from runs T1502 and T1573 (Appendix K), it is seen that glass compositions become more peraluminous with water-undersaturation (Fig. 8.2). As a result, garnet becomes a stable liquidus phase in addition to biotite and hercynite. The liquid also becomes more iron-rich relative to biotite, that is, the biotite/glass K_D^{Fe*Mg} increases with water-undersaturation.

8.7 APPLICATION: DERIVATION OF $Fe*Mg_{-1}$ EXCHANGE THERMOMETERS

8.7.1 Introduction

Biotite/garnet and garnet/melt $Fe*Mg_{-1}$ exchange thermometers have been derived by the methods described below, using mineral and glass compositional data from Appendix K. A thermometric expression based upon biotite/glass compositional data was not derived because the range in K_D^{Fe*Mg} values for this assemnlage (0.32 to 0.38) is too small.

Garnet/glass, orthopyroxene/glass and cordierite/glass $Fe*Mg_{-1}$ exchange thermometers have also been derived by similar methods, using the experimentally derived compositional data for FMASHO-system phases obtained by Ellis (1986) and this work.

Regular variations in binary distribution coefficients with temperature occur in coexisting mineral/melt pairs enabling empirical thermometric expressions to be derived which describe the corresponding two-phase exchange equilibria (Roeder & Emslie, 1970; Ghiorso et al., 1983; Ellis, 1986). These expressions are not built upon a formal thermodynamic basis as are the expressions of similar form derived for mineral/mineral exchange equilibria (for instance, the biotite/garnet $FeMg_{-1}$ exchange thermometer of Ferry & Spear, 1978) because activity/composition relationships in melts are only poorly understood. This is because the cation sites within the polymeric structures of silicate liquids are less distinctive than those within minerals (e.g. Fraser, 1977, Chapter 5). The structures of melts have only recently been studied (e.g. Burnham, 1975, 1979; Oxtoby & Hamilton, 1978; Okuno & Marumo, 1982; Mysen & Virgo, 1985; Spiering & Seifert, 1985; Burnham & Nekvasil, 1986; Nekvasil & Burnham, 1987) and the thermodynamic characteristics of melts have yet to be obtained. Reaction coefficient activity ratios in mineral/melt equilibria must therefore be approximated by distribution coefficient mole-fraction

ratios. A consequence of this approximation is that application of mineral/melt thermometers should be restricted to assemblages in which the constituent phases have compositions which are not drastically removed from those used to derive the particular thermometer.

8.7.2 Biotite/Garnet

Introduction

The reaction describing Fe^*Mg_{-1} exchange equilibrium between biotite and garnet is:

$$1/3\ KMg_3AlSi_3O_{10}(OH)_2 + 1/3\ Fe_3Al_2Si_3O_{12} = 1/3\ KFe_3AlSi_3O_{10}(OH)_2 + 1/3\ Mg_3Al_2Si_3O_{12} \quad (8.6)$$

which has an equilibrium constant:

$$K = \left(\frac{a^{Bi}_{ann} \cdot a^{Ga}_{pyr}}{a^{Bi}_{phl} \cdot a^{Ga}_{alm}} \right)^{1/3} \quad (8.7)$$

in which Bi = biotite, Ga = garnet, ann = annite ($KFe_3AlSi_3O_{10}(OH)_2$), phl = phlogopite ($KMg_3AlSi_3O_{10}(OH)_2$), pyr = pyrope ($Mg_3Al_2Si_3O_{12}$) and alm = almandine ($Fe_3Al_2Si_3O_{12}$).

Activity Models

The activities of components in solid solutions depend upon the extent of atomic disorder on each crystallographic site (Wood & Fraser, 1977, Chapter 3). For example, if there is total disorder amongst the various ionic species which mix on each type of site and if mixing is ideal then, in the case of biotite:

$$a^{Bi}_{phl} = X_K \cdot X_{Mg(M1)} \cdot X^2_{Mg(M2)} \cdot X^4_{Al+Si} \cdot X^2_{OH} \quad (8.8)$$

for $X_K = K^+/(K^+ + H_3O^o + [\ ]^o)$ in the dodecahedral site,

$X_{Mg(M1)} = Mg^{2+}/(Mg^{2+} + Fe^{2+} + Fe^{3+} + Al^{3+} + [\ ]^o)$ in the M1 octahedral site,

$X_{Mg(M2)} = Mg^{2+}/(Mg^{2+} + Fe^{2+} + Fe^{3+} + Al^{3+} + Ti^{4+} + [\ ]^o)$ in the M2 octahedral site

$X_{Al+Si} = (Al^{3+} + Si^{4+})/(Al^{3+} + Fe^{3+} + Si^{4+})$ in the tetrahedral site,

and $X_{OH} = OH^-/(OH^- + O^{2-})$ in the hydroxyl site.

This activity model accords with:

(a) the presence of two octahedral sites per formula unit in most trioctahedral micas: a larger M1 site and two smaller M2 sites between which site occupancies (ions and vacancies) may variously partition (see the compilation of octahedral site occupanices of Bailey, 1984, table 5), and

(b) the lack of ordering of Al and Si ions amongst the four tetrahedral sites in Fe*Mg biotites (Bailey, 1984, p.40).

Activity coefficients (γ) are required in order to specify component activities which depart from ideality. If mixing on each site in biotite is non-ideal (i.e., the solid solution has free energy in excess of that of the sum of the molar proportions of the endmember components), then activity coefficients must be used in order to describe the activities of endmember components. Equation 8.8. then becomes:

$$a^{Bi}_{phl} = X_K \cdot X_{Mg(M1)} \cdot X^2_{Mg(M2)} \cdot X^4_{Al4+Si} \cdot X^2_{OH} \cdot \gamma_K \cdot \gamma_{Mg(M2)} \cdot \gamma^2_{Mg(M2)} \cdot \gamma^4_{Al4+Si} \cdot \gamma^2_{OH} \quad (8.9)$$

However in this work, simpler models for the activities of phlogopite and annite in biotite are used, namely::

$$a^{Bi}_{phl} = X_K \cdot X^3_{Mg} \cdot \gamma^3_{Mg} \quad \text{and} \quad a^{Bi}_{ann} = X_K \cdot X_{Fe*} \cdot \gamma^3_{Fe*} \quad (8.10)$$

where X_{Mg} = Mg/3 and X_{Fe*} = Fe*/3 in the octahedral site.
These simplifications have been made because of

(a) the lack of knowledge of the partitioning of octahedral occupancies between the M1 and M2 sites in biotite (apart from assigning the trace quantities of Ti to M2 (Ohta et al., 1982), justifying their merging into one octahedral site;

(b) the relatively small proportion of FeIII/ΣFe expected to occur in biotite under the low fO_2 conditions prevailing in the KFMASHO system charges (see below), together with the inability to distinguish di- from trivalent iron using the Microprobe Analyzer, thereby justifying the designation of the analyzed iron as Fe* (i.e. total iron as FeII);

(c) the inability of the microprobe to detect hydrogen so that X_{OH} and X_{H3O} cannot be determined;

(d) the recognition that vacancies (the proportions of which are indeterminable by charge-balancing techniques without knowledge of FeIII and H contents) are valid occupants of sites, as far as site order/disorder is concerned, so that X_K, X_{Mg} and X_{Fe*} are specified relative to the total number of the relevant sites in the 11-oxygen formula unit: i.e. 1, 2 and 3, respectively, rather than to the total number of occupied sites determined in each case;

(e) the lack of knowledge of γ_K, assuming therefore that K mixes ideally on the dodecahedral site;

(f) the absence of tetrahedrally co-ordinated FeIII in peraluminous biotites (Bailey, 1984), thereby designating full occupancy of the

tetrahedral sites to Al and Si ions and hence unit value to the quantity: $(X^4_{Al4+Si}\gamma^4_{Al4+Si})$.

For garnet, by similar arguments,

$$\left.\begin{aligned} a^{Ga}_{pyr} &= X^3_{Mg}\gamma^3_{Mg} \quad \text{and} \quad a^{Ga}_{alm} = X^3_{Fe*}\gamma^3_{Fe*} \\ \text{for} \quad X_{Mg} &= Mg/3 \text{ and } X_{Fe*} = Fe*/3 \end{aligned}\right\} \qquad (8.11)$$

where Mg and Fe represent the number of atoms per 12 oxygens in the formula unit.

Substituting equations 8.10 and 8.11 into equation 8.7 yields the expression for the equilibrium constant:

$$K = \left(\frac{X_{Fe*}}{X_{Mg}}\right)_{Bi} \bullet \left(\frac{X_{Mg}}{X_{Fe*}}\right)_{Ga} \bullet \left(\frac{\gamma_{Fe*}}{\gamma_{Mg}}\right) \bullet \left(\frac{\gamma_{Mg}}{\gamma_{Fe*}}\right).$$

i.e.

$$\ln K = \ln\left[\frac{X^{Bi}_{Fe*} \bullet X^{Ga}_{Mg}}{X^{Bi}_{Mg} \bullet X^{Ga}_{Fe*}}\right] + \ln\left[\frac{\gamma^{Bi}_{Fe*} \bullet \gamma^{Ga}_{Mg}}{\gamma^{Bi}_{Mg} \bullet \gamma^{Ga}_{Fe*}}\right] \qquad (8.12)$$

or $\ln K = \ln K_D + \ln K_\gamma$.

Activity Coefficient Models

The activity coefficients for Fe* and Mg in garnet, using the binary regular solution model are:

$$\gamma^{Ga}_{Fe*} = \exp\left[\frac{X^2_{Mg} W^G_{Fe*Mg}}{RT}\right] \quad \text{and} \quad \gamma^{Ga}_{Mg} = \exp\left[\frac{X^2_{Fe*} W^G_{Fe*Mg}}{RT}\right]$$

where W^G_{Fe*Mg}, the Fe*Mg Margules or interaction parameter, is a function of the excess free energy of mixing for the solid solution (Wood & Fraser, 1977, Chapter 3). Newton & Haselton (1981) assumed that in garnet, W^G_{Fe*Mg} was zero by analogy with the near-zero estimate for W^G_{Fe*Mg} in olivine by Sack (1980). With this assumption of ideality, the activity coefficient ratio:

$$\gamma^{Ga}_{Mg}/\gamma^{Ga}_{Fe*} = 1 . \qquad (8.13)$$

The biotites from KFMASHO system runs (Appendix K) consist largely of three endmembers: $(KMg_3AlSi_3O_{10}(OH)_2)$, annite $(KFe_3AlSi_3O_{10}(OH)_2)$ and the hypothetical aluminous endmember: tschermakite $(KAl_3Al_4O_{10}(OH)_2)$. These endmembers are related to each other by the exchange vector: $Al^{[4]}Al^{[6]}Si^{[4]}_{-1}(MgFe*)^{[6]}_{-1}$ (where superscripts refer to the coordination

number of the respective ions). Minor components in solid solution are the FeIII-containing, K-absent and Ti-containing endmembers which have been ignored in the following treatment. Activity coefficients for Fe* and Mg in these biotites may then be modelled using a strictly regular symmetric ternary solid-solution model (Wood & Fraser, 1976, Chapter 3), for which

$$\gamma^{Bi}_{Fe*} = \exp\left[\frac{1}{RT}\left(X^2_{Mg}W^G_{Fe*Mg}+X^2_{Al6}W^G_{Fe*Al6}+X_{Mg}X_{Al6}(W^G_{Fe*Mg}+W^G_{Fe*Al6}-W^G_{MgAl6})\right)\right]$$

and (8.14)

$$\gamma^{Bi}_{Mg} = \exp\left[\frac{1}{RT}\left(X^2_{Fe*}W^G_{Fe*Mg}+X^2_{Al6}W^G_{MgAl6}+X_{Fe*}X_{Al}(W^G_{MgFe*}+W^G_{MgAl6}-W^G_{Fe*Al6})\right)\right]$$

If iron and magnesium are assumed to mix ideally over the octahedral sites (i.e. $W^G_{Fe*Mg} = 0$ as it does on the cubic sites in garnet), equations 8.14 yield:

$$(\gamma^{Bi}_{Fe*}/\gamma^{Bi}_{Mg}) = \exp\left[\frac{X_{Al6}(X_{Al6}+X_{Fe*}+X_{Mg})}{RT} \bullet \Delta W^G_{Al6}\right] \qquad (8.15)$$

for $\Delta W^G_{Al6} = (W^G_{Fe*Al6} - W^G_{MgAl6})$

W^G terms each consist of three component terms for the excess enthalpy, entropy and volume of mixing at standard temperature and pressure (W^H, W^S and W^V, respectively (op. cit., equation 3.36)). Equation 8.15 may therefore be expanded to give:

$$(\gamma^{Bi}_{Fe*}/\gamma^{Bi}_{Mg}) = \exp\left[\frac{X_{Al6}(X_{Al6}+X_{Fe*}+X_{Mg})}{RT}(\Delta W^H_{Al6}+(P-0.0001)\Delta W^V_{Al6}-T\Delta W^S_{Al6})\right] \qquad (8.16)$$

where $\Delta W^H_{Al6} = (W^H_{Fe*Al6}-W^H_{MgAl6})$, $\Delta W^V_{Al6} = (W^V_{Fe*Al6}-W^V_{MgAl6})$ and $\Delta^S_{Al6} = (W^S_{Fe*Al6}-W^S_{MgAl6})$.

Formulations

By the Second Law equation, the free energy of a reaction: ΔG_R is

$$\left.\begin{aligned}\Delta G_R &= \Delta H_R + (P-0.001)\Delta V_R - T\Delta S_R\\ &= -RT\ \ln K\\ &= 0 \text{ at equilibrium}\end{aligned}\right\} \qquad (8.17)$$

where ΔH_R, ΔV_R and ΔS_R are the enthalpy, molar volume and entropy of the reaction, P is pressure (GPa), T is temperature and R is the gas constant. Substituting equations 8.12, 8.13 and 8.16 into equation 8.17 and re-arranging yields the general thermometric expression:

FIGURE 8.4

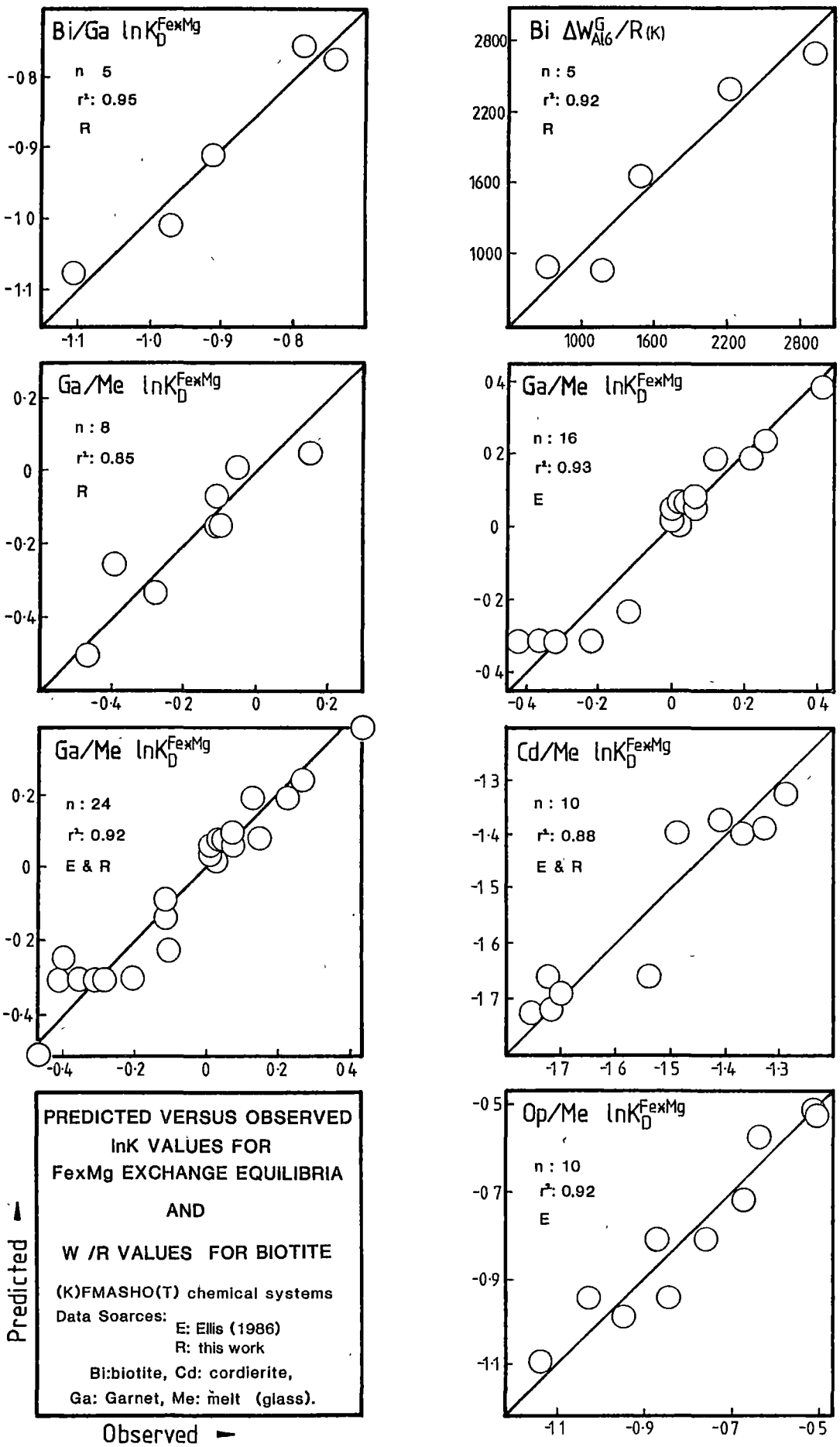
Bi/Ga lnK$_D^{FexMg}$
n 5
r^2: 0.95
R
Bi $\Delta W_{Al6}^G/R_{(K)}$
n : 5
r^2: 0.92
R
Ga/Me lnK$_D^{FexMg}$
n : 8
r^2: 0.85
R
Ga/Me lnK$_D^{FexMg}$
n : 16
r^2: 0.93
E
Ga/Me lnK$_D^{FexMg}$
n : 24
r^2: 0.92
E & R
Cd/Me lnK$_D^{FexMg}$
n : 10
r^2: 0.88
E & R
Op/Me lnK$_D^{FexMg}$
n : 10
r^2: 0.92
E
PREDICTED VERSUS OBSERVED
lnK VALUES FOR
FexMg EXCHANGE EQUILIBRIA
AND
W /R VALUES FOR BIOTITE
(K)FMASHO(T) chemical systems
Data Soarces:
E: Ellis (1986)
R: this work
Bi:biotite, Cd: cordierite,
Ga: Garnet, Me: melt (glass).
Predicted
Observed

$$T(K) = \left\{ \frac{\mathbf{H} + (P-0.0001)\cdot\mathbf{V}}{\mathbf{S} - \ln K_D^{Fe*Mg}} \right\} \qquad (8.18)$$

for $\mathbf{H} = 1/R\bullet(\Delta H_R + \Delta W^H_{Al6}\bullet X^{Bi}_{Al6})$, $\mathbf{V} = 1/R\bullet(\Delta V_R + \Delta W^V_{Al6}\bullet X^{Bi}_{Al6})$ and
$\mathbf{S} = 1/R\bullet(\Delta S_R + \Delta W^S_{Al6}\bullet X^{Bi}_{Al6})$.

Unknowns in this equation are the ideal terms: ΔS_R, ΔH_R, ΔV_R and the excess terms: ΔW^S_{Al6}, ΔW^H_{Al6} and ΔW^V_{Al6}.

Two solutions to equation 8.18 have been obtained below. In each, the statistical technique of the multiple regression of PTX data, was used to obtain estimates of the unknown quantities. In the first solution, no attempt was made to distinguish ideal from excess terms in the functions **H**, **V** and **S**. The procedure consisted of multiply regressing ln K_D values for biotite/garnet pairs from runs T1470, T1486, T1489, T1492 and T1542 (Appendix K), against the appropriate values of the predicted variables: 1/T and (P-0.0001)/T, according to the re-arranged version of equation 8.18:

$$\ln K_D = A\bullet(1/T) + B\bullet((P-0.0001)/T) + C \qquad (8.19)$$

where A = **-H**, B = **-V** and C = **S**.

Regression was undertaken with an IBM microcomputer using the package of interactive statistical programs called "Microstat" (a product of Ecosoft Inc., Indianapolis, U.S.A.), at the Australian National University Computer Centre. The value of r^2 for the regression is 0.95, indicating a good correlation between the observed and predicted values of ln K_D (see Fig. 8.4). Parameters obtained are:

$$\left.\begin{aligned} A = -\mathbf{H} &= 3720 \pm 840 \text{ K mol}^{-1} \\ B = -\mathbf{V} &= 380 \pm 100 \text{ K GPa}^{-1}\text{mol}^{-1}, \text{ and} \\ C = \mathbf{S} &= 2.71 \text{ mol}^{-1}. \end{aligned}\right\} \qquad (8.20)$$

Precision is to the 1σ level of confidence.

These parameters are listed in Table 8.3. They are compared with similar parameters for this exchange reaction deduced from other studies, in Chapter 9 (Table 9.2).

The thermometric expression obtained by substituting equations *20 into 8.18 and re-arranging, is:

$$T(K) = \frac{3720 + 380\ P(GPa)}{2.71 - \ln K_D^{Fe*Mg}} \qquad (8.21)$$

for the distribution coefficient $K_D^{Fe*Mg} = \left(\frac{X^{Bi}_{Fe*}\bullet X^{Ga}_{Mg}}{X^{Bi}_{Mg}\bullet X^{Ga}_{Fe*}} \right)$

Table 8.3

Fe^*Mg_{-1} EXCHANGE REACTION THERMOMETERS

Eqn No.	Phases	Appropriate Chemical Systems	Number of Points	r^2	**H** (K mol^{-1})	**S** (mol^{-1})	**V** (K $GPa^{-1}mol^{-1}$)	Defined P range (GPa)	Defined T range (^oC)	Data Sources
8.21	biotite/garnet	water saturated peraluminous KFMASHO	5	0.95	3720	2.71	380	0.5–1.2	800–900	this work
8.27	biotite/garnet	watersaturated KFMASHO			$2089 + 12800f(X^{Bi}_{Al6})$	$0.782 + 15.0f(X^{Bi}_{Al6})$	$95.6 + 2620f(X^{Bi}_{Al6})$	0.5–1.2	~800	Ferry & Spear (1978) and this work
8.30	garnet/glass	peraluminous (KFMASHO and KFMASHOT)	8	0.85	-4570	-4.47	-310	0.5–1.5	800–950	this work
8.31	garnet/glass	peraluminous FMASHO	16	0.93	-4600	-4.02	.181	0.7–3.0	800–1000	Ellis (1986)
8.33	garnet/glass	peraluminous FMASHO±K±T	24	0.92	$-4580 - 1700f(X^{Gl}_K)$	$-4.0 - 2.4f(X^{Gl}_K)$	$-185 - 340f(X^{Gl}_K)$	0.7–1.5	800–900	Ellis (1986) and this work
8.34	orthopyroxene/ glass	peraluminous FMASHO	10	0.92	-2210	-3.0	-580	0.6–1.2	850–1100	Ellis (1986)
8.35	cordierite/ glass	peraluminous (FMASHO and KFMASHO)	10	0.88	-500	-2.5	-830	0.5–1.1	850–1100	Ellis (1986) and this work

for $\mathbf{H} = \frac{1}{R}(\Delta H_R + \Delta W^H)$, $\mathbf{S} = \frac{1}{R}(\Delta S_R + \Delta W^S)$, $\mathbf{V} = \frac{1}{R}(\Delta V_R + \Delta W^V)$, $f(X^{Bi}_{Al6}) = X^{Bi}_{Al6}/(X^{Bi}_{Al6}+X^{Bi}_{Fe^*}+X^{Bi}_{Mg})$ and $f(X^{Gl}_K) = X^{Gl}_K/(X^{Gl}_K+X^{Gl}_{Fe^*}+X^{Gl}_{Mg})$.

This formulation of the biotite/garnet thermometer is applicable to those water-saturated KFMASHO-system assemblages in which biotite contains substantial Al6.

In the second solution to equation 8.18, values for the thermochemical excess terms ΔW^{H}_{Al6}, ΔW^{S}_{Al6} and ΔW^{V}_{Al6} in **H**, **S** and **V**, respectively, were estimated. This was accomplished by incorporating the thermochemical data of Ferry & Spear (1978) which was experimentally derived for the exchange reaction also in the KFMASHO chemical system but over a temperature range from 600°C to 800°C at 0.2 GPa P_W. However, their compositional data was obtained from assemblages containing tschermak-poor to -absent biotites, i.e. to near binary solid solution biotites with compositions lying along the phlogopite-annite join. By contrast, equation 8.21 was derived using the compositions of biotites containing up to 21 mol.% of the ternary tschermak biotite endmember.

For K_D^{Fe*Mg} values > 0.2 at water pressures of 0.1 GPa, the calibration of Ferry & Spear (1978) predicts temperatures which are higher than those given by equation 8.21 (and by the six other calibrations considered in Section 9.3.3 of the next chapter - see Fig. 9.7). Conversely, for temperatures > 575°C at 0.1 GPa, the calibration of Ferry & Spear (1978) predicts lower K_D values than does equation 8.21. That higher K_D values occur for assemblages in which the biotite contains Al6, may be understood in terms of biotite crystal chemistry. Because of the small size of the Al6 ion, tschermak substitution ($Al4Al6(Fe,Mg)_{-1}Si_{-1}$) will lead to shrinkage of the octahedral layer relative to other layers in the biotite unit cell (Indares & Martignole, 1985). This distortion can be counteracted by increasing the proportion of large Fe* to small Mg ions in the octahedral layer, relative to the proportion which would exist if no Al6 were present (op. cit.). This amounts to an increase in the biotite/garnet K_D^{Fe*Mg} with increasing tschermak substitution of the biotite.

For equilibrium in assemblages in which the biotite is an ideal phlogopite-annite solid-solution, then:

$$\ln K_D = 0.782 - \frac{2089}{T(K)} - \frac{95.6P(GPa)}{T(K)} \qquad (8.22)$$

(Ferry & Spear, 1978)

Equating the coefficients of terms in equations 8.22 and 8.18 for the case where $\Delta W^{G}_{Al6} = 0$, yields:

$$\left.\begin{aligned} \Delta S_R/R &= 0.782 \text{ mol}^{-1} \\ \Delta H_R/R &= 2089 \text{ K mol}^{-1} \\ \Delta V_R/R &= 95.6 \text{ K GPa}^{-1}\text{mol}^{-1}. \end{aligned}\right\} \qquad (8.23)$$

Substituting these equations into equation 8.18 for the case of equilibrium in assemblages containing non-ideal, ternary Al-Fe*-Mg biotites and re-arranging, yields:

$$\frac{[T\bullet(\ln K_D - 0.782) + 2089 + 95.6(P-0.0001)]}{X^{Bi}_{Al6}(X^{Bi}_{Al6}+X^{Bi}_{Fe*}+X^{Bi}_{Mg})} = - \frac{T\bullet\Delta W^S_{Al6}}{R} - \frac{\Delta W^V_{Al6}}{R}(P-0.0001) - \frac{\Delta W^H_{Al6}}{R} \qquad (8.24)$$

This equation has the form:

$$\delta = \epsilon\bullet T + \xi\bullet(P-0.0001) + \nu$$

in which $\delta = \frac{[T\bullet(\ln K_D - 0.782) + 2089 + 95.6(P-0.0001)]}{X^{Bi}_{Al6}(X^{Bi}_{Al6}+X^{Bi}_{Fe*}+X^{Bi}_{Mg})} = - \frac{\Delta W^G_{Al6}}{R}$,

$$\epsilon = \frac{\Delta W^S_{Al6}}{R},\ \xi = \frac{-\Delta W^V_{Al6}}{R} \text{ and } \nu = \frac{-\Delta W^H_{Al6}}{R}.$$

Values of δ were calculated for each of runs T1470, T1486, T1489, T1492 and T1542, using the PTX data of Appendix K. These values were multiply regressed against run temperature and (run pressure-0.0001). The value of r^2 for the regression is 0.93 indicating a good fit (cf. Fig. 8.4). The regression yielded the following values for the excess terms:

$$\epsilon = \frac{\Delta W^S_{Al6}}{R} = 15.0 \pm 4.9\ K^{-1}mol^{-1}$$

$$\xi = \frac{\Delta W^V_{Al6}}{R} = -2620 \pm 690\ K\ GPa^{-1}mol^{-1}, \text{ and} \qquad (8.26)$$

$$\nu = \frac{-\Delta W^H_{Al6}}{R} = -12800\ K\ mol^{-1}.$$

Substituting equations 8.26 and 8.23 into equation 8.18 yields the thermometric expression:

$$T(K) = \frac{2089 + 12800f(X^{Bi}_{Al6}) + P(GPa)\bullet(95.6+2620f(X^{Bi}_{Al6}))}{0.782 + 15.0f(X^{Bi}_{Al6}) - \ln K_D^{Fe*Mg}} \qquad (8.27)$$

for $f(X^{Bi}_{Al6}) = X^{Bi}_{Al6}(X^{Bi}_{Al6}+X^{Bi}_{Fe*}+X^{Bi}_{Mg})$.

This formulation of the biotite/garnet thermometer is a general thermometric expression for KFMASHO-system assemblages which have fO_2 values between those of the QFM and MW oxygen buffers (cf. Fig. 8.3).

8.7.3 Garnet/Melt

Introduction

Fe^*Mg_{-1} exchange between these phases may be described by the reation:

$$1/3\ Mg_3Al_2Si_3O_{12} + 1/x Fe^*_xZ = 1/3\ Fe^*_3Al_2Si_3O_{12} + 1/x\ Mg_xZ \qquad (8.28)$$

Written in this form, only one Fe* and Mg atom are exchanged, even though both the reaction coefficient for the melt (1/x) and the number of Fe* and Mg atoms (x) in the endmember melt components (Fe^*_xZ and Mg_xZ), are not specified. This equilibrium is represented in an approximate manner, by the distribution coefficient, because activities in the melt phase are unknown. Thus:

$$K = \frac{(a^{Ga}_{Fe^*})^{1/3} \cdot (a^{L}_{Mg})^{1/x}}{(a^{Ga}_{Mg})^{1/3} \cdot (a^{L}_{Fe^*})^{1/x}} = K_D^{Fe^*Mg} = \left(\frac{X^{Ga}_{Fe^*} \cdot X^{Gl}_{Mg}}{X^{Ga}_{Mg} \cdot X^{Gl}_{Fe^*}}\right) \qquad (8.29)$$

Formulations

Compositional data of all eight garnet/glass pairs from this study were used in determining formulations of the garnet/melt exchange thermometer. These include data from water-saturated KFMASHO- and KFMASHOT-system assemblages and those from the water-undersaturated KFMASHO-system run T1573. That formulations can be derived from this collective data set, suggests that neither titanium (present only in low concentrations in both phases), nor water exert a substantial influence on the Fe^*Mg_{-1} exchange between garnet and melt.

In the first formulation, the ln $K_D^{Fe^*Mg}$ values were equated with their appropriate values of the predictor variables: 1/T and (P-0.0001)/T, (i.e. written in the form of equation 8.19) and multiply regressed. This yielded estimates of the coefficients A and B and the constant C, of 4570 ± 100, 310 ± 140 and -4.47 respectively (r^2 = 0.85, Fig. 8.4). These regression parameters are empirically derived estimates of the thermodynamic functions **-H**, **-V** and **S**, respectively. The resulting thermometric expression for the garnet/melt Fe^*Mg_{-1} exchange thermometer is:

$$T(K) = \frac{4570 + 310\ P\ (GPa)}{4.47 + \ln K_D^{Fe^*Mg}} \qquad (8.30)$$

where the distribution coefficient is described by equation 8.29.

Multiple regression of the data of 16 garnet/glass pairs from the K-absent FMASHO-system experimental study of Ellis (1986) was also undertaken. These assemblages are from runs with different AFM bulk-chemical compositions and different water contents (op. cit.). The data of one pair (that from run T1431, op. cit.) was rejected because it yielded a disparate K_D value. This exclusion resulted in an increase in the correlation coefficient for the regression from 0.89 to 0.93 (see Fig. 8.4). The resulting thermometric expression is:

$$T(K) = \frac{4600 + 181\ P\ (GPa)}{4.02 + \ln K_D^{Fe*Mg}} \qquad (8.31)$$

It applies only to assemblages in the K-absent FMASHO chemical system.

A comparison of equations 8.30 and 8.31 may be made for the case where garnet and melt have the same magnesium number, i.e. when the distribution coefficient has unit value. Equation 8.31 indicates K-absent liquids become more magnesian than co-existing garnet, at temperatures below ~(871 + 45 P (GPa))^{o}C. In the K-bearing system, however, this compositional crossover (i.e. K_D reversal) occurs at (749 + 69 P (Gpa))^{o}C, i.e. up to ~120^{o} **below** that in the K-absent system. Potassium in the liquid therefore influences the $Fe*Mg_{-1}$ exchange between garnet and melt, causing a decrease in the K_D at any particular P and T.

The influence of potassium can be gauged by multiple regression of the ln K_D values for **both** the K-bearing and the K-absent assemblages, against the five predictor variables: i.e. 1/T and (P-0.0001)/T (as before) plus the three compositional variables, $f(X_K^{Gl})$, $f(X_K^{Gl})/T$ and $f(X_K^{Gl})\bullet(P-0.0001)/T$, where $f(X_K^{Gl})$ is the compositional term relating X_K^{Gl}, X_{Fe*}^{Gl} and X_{Mg}^{Gl}:

$$fX_K^{Gl} = X_K^{Gl}/(X_K^{Gl}+X_{Fe*}^{Gl}+X_{Mg}^{Gl}). \qquad (8.32)$$

This method yields the same results as the method which was used to obtain the X_{Al6}^{Bi} excess terms in the biotite/garnet thermometric expression (equation 8.27), i.e. relating the ln K_D values of two sets of assemblages: one with and one without a K_D^{Fe*Mg}-influencing component present in one of the phases.

The resulting regression has a correlation coefficient (r^2 value) of 0.92 indicating a good fit (Fig. 8.4). It yields the thermometric expression:

$$T(K) = \frac{(4580+1700fX_K^{Gl}) + P\ (GPa)\bullet(185+340fX_K^{Gl})}{4.0 + 2.4fX_K^{Gl} + \ln K_D^{Fe*Mg}} \qquad (8.33)$$

This general version of the garnet/melt thermometer for KFMASHO(T)-system assemblages, is similar in form to that of equation 8.18. For the specific case when $\ln K_D = fX_K^{Gl} = 0$, it reduces to a nearly identical expression for the K_D-reversal temperature to that obtained for K-absent assemblages from equation 8.31. Equation 8.33 indicates that the K_D-reversal temperature increases with pressure and decreases with increasing K_2O in the melt.

Discussion

The effect of melt potassium on the Fe^*Mg_{-1} exchange reaction equilibrium between garnet and melt is consistent with there being a molecular association of potassium and iron in the melt. Such an association was identified by Carmichael & Nicholls (1967). They showed that the FeIII/FeII ratio increases independently of fO_2 with increasing $(X_{K+Na})_{melt}$ and termed the phenomenon the **alkali-ferric iron effect**. They consider that the effect reflects the formation of melt complexes containing $[(K,Na)FeIIIO_2]^\circ$ units (op. cit.). These units are analogues of the framework-forming $[(K,Na)AlO_2]^\circ$ units proposed to occur in quartzofeldspathic melts (e.g. Burnham, 1975, 1979). Some iron in KFMASHO(T)-system glasses is therefore likely to be associated with potassium as $[KFeIIIO_2]^\circ$ in the framework portion of the liquids' structure, therefore being unavailable for exchange with the magnesium in garnet. This could be counteracted by increasing the total iron (Fe*) to magnesium ratio of the melt relative to that of garnet, i.e. by decreasing the garnet/melt $K_D^{Fe^*Mg}$ at any particular P and T, as is observed in K-bearing versus K-absent simple-system assemblages. These data therefore support the existence of a $[KFeIIIO_2]^\circ$ component in the framework portion of the melt phase.

However, recent studies by Spiering & Seifert (1985) of liquids at high P and T using Mossbauer spectroscopy reveal that not only are there different sites in peraluminous silicic liquids for FeIII and FeII, but that there are also two distinctly different octahedrally co-ordinated sites in melts for FeII. These authors propose that the FeII sites are generated by different sets of anionic complexes and that one of these is destabilized by pressure (op. cit.). The nature and specificity of the anionic groups around each FeII site has yet to be established.

Both spectroscopic and chemical data (op. cit.; Carmichael & Nicholls, 1967; Ellis, 1986; this work) therefore indicate that Fe^*Mg_{-1} exchange between ferromagnesian minerals and melts are likely to be dependent upon concentrations of melt components, additional to Fe* and Mg. In the case of garnet/melt equilibria, the thermometric equation 8.33 accords with the experimental results of Green (1976b) and Ellis (1986) and supports the petrological argument of Ellis (op. cit.) that liquids more

magnesian than garnet can be generated during lithospheric partial melting at temperatures below ~900°C, to leave Fe-rich refractory residua.

8.7.4 Orthopyroxene/Melt and Cordierite/Melt

A thermometric expression was formulated for the Fe^*Mg_{-1} exchange reaction between orthopyroxene and glass in the FMASHO chemical system, using the data of Ellis (1986). Data for one pair from run T1257 (op. cit.) was rejected because it yielded a disparate K_D value. The technique used consisted of multiple regression of ln K_D values against the predictor variables: 1/T and (P-0.0001)/T, as was used to derive the biotite/garnet and garnet/melt thermometric expressions of equations 8.21 and 8.30, respectively. The correlation coefficient for the regression was 0.92 indicating a good fit between the observed and predicted ln K_D values (see Fig. 8.4). The resulting expression is:

$$T(K) = \frac{2210 + 580\ P}{3.0 + \ln K_D^{Fe^*Mg}} \qquad (8.34)$$

A thermometric expression for the Fe^*Mg_{-1} eschange reaction between cordierite and melt was formulated using the compositional data of Ellis (1986, excluding the data of runs T1138 and T1302) for FMASHO-system assemblages, and those of run T1490 of this work (Appendix K), which is a KFMASHOT-system assemblage. The value or r^2 for the regression was 0.88, indicating a reasonable fit (see Fig. 8.4). The resulting expression is:

$$T(K) = \frac{500 + 830\ P}{2.5 + \ln K_D^{Fe^*Mg}} \qquad (8.35)$$

Data of a K-bearing assemblage were used with those of K-absent assemblages to derive this expression despite the knowledge that K in the melt can influence Fe^*Mg_{-1} exchange equilibria between minerals and melt. This seems a reasonable option in the specific case of cordierite/melt Fe^*Mg_{-1} eschange equilibria because $K_D^{Fe^*Mg}$ values for this assemblage are so large. Relative changes in the $K_D^{Fe^*Mg}$ values for cordierite/melt assemblages due to the influence of melt potassium, should therefore be considerably less than those for garnet/melt assemblages.

The thermometric expressions derived in this chapter (cf. Table 8.3) can be used to estimate temperatures given mineral and melt equilibrium compositional data. Alternatively, they may be inverted and combined with one another, to obtain mineral or melt compositions for given equilibrium pressures and temperatures (cf. Chapter 12).

Chapter 9

INTENSIVE VARIABLES DURING PETROGENESIS OF FURNEAUX BATHOLITH GRANITES

9.1 INTRODUCTION

9.1.1 Aims

The aims of this section are to estimate values of the intensive variables: pressure, temperature, oxygen fugacity and water fugacity which were operative during granite petrogenesis and using these data, to reconstruct the $P_{\Sigma}P_{W}T$ paths travelled during the petrogenesis of selected granitic suites. Estimates of intensive variables have been made using both previously published and newly constructed thermobarometers (previous chapter).

9.1.2 Location of the Water-Saturated Solidus

Of major importance is the location in PT space, of the low temperature limits of the liquid phase, that is, the granite vapour-saturated solidus. This is a set of linked univariant eutectic reactions which separates the magmatic from the subsolidus stages of petrogenesis. Because of the chemical diversity in natural systems, there will be a spectrum of such solidi. Some of them can be used as reference curves in the study of granite petrogenesis. The water-saturated solidus in the quartz + feldspar portion of the KNASH chemical system (the haplogranite system), is in turn, the simple system reference with which to compare the vapour-saturated solidi of the more complex natural chemical systems. It has been experimentally studied for three decades (e.g. Tuttle & Bowen, 1958; Johannes, 1984).

Addition of anorthite component to the haplogranitic system generates the haplogranodioritic system, in which the water-saturated solidus is raised in temperature for all crustal pressures (e.g. James & Hamilton, 1969; Winkler et al., 1977; Johannes, 1984). The effects on phase equilibria of chemical components outside the compositional range defined by quartz, the feldspars and water, have been documented by many workers. Components which partition most strongly into the vapour-phase such as HCl, CO_2 or CH_4, will increase the phase field of vapour, thereby raising the solidus at a given pressure (e.g. Kilinc & Burnham, 1972; Swanson, 1979). Hydrogen also acts to raise the vapour-saturated solidus by operating in a manner opposite to that of water (Luth & Boettcher, 1986); hydrogen polymerizes hydrous melts by extraction of non-bridging oxygens to form water, thereby decreasing the non-bridging oxygen to tetrahedral cation (NBO/T) ratio (op. cit.). Those components which partition most strongly into the melt, such as F_2O_{-1} (Hards, 1976) and to a lesser extent B_2O_3 (Pichavant, 1981) will increase the phase field of liquid, thereby

depressing the solidus (op. cit.; Manning et al., 1980; Burnham & Nekvasil, 1986; Nekvasil & Burnham, 1987). Excess Al_2O_3 also lowers the solidus (Voigt, 1983, and Joyce, 1985, **in** Burnham & Nekvasil, 1986). Experimental studies on natural granitic compositions indicate water-saturated solidi close to that for the haplogranite system (e.g. Naney, 1982; Clemens & Wall, 1981; Mehnert & Busch, 1982), indicating that the minor components MgO, FeO, MnO, Fe_2O_3 and P_2O_5 collectively exert only a small effect in depressing the water-saturated solidus.

A model vapour-saturated granite solidus has therefore been chosen in order to distinguish the probable magmatic from subsolidus assemblages examined in this section. This solidus is for peraluminous melt compositions, but is considered relevant to both peraluminous and metaluminous granites because

(a) felsic liquids in equilibrium with amphibole and clinopyroxene in CMASH simple systems are peraluminous in composition (Ellis & Thompson, 1986); and

(b) the felsic end-members of many predominantly metaluminous I-type granite suites are peraluminous (Chappell, 1984), indicating the presence of a peraluminous magmatic phase such as melt (Cawthorne & O'Hara, 1976; Ellis & Thompson, 1986) and biotite.

The model peraluminous solidus chosen is equal to the haplogranitic solidus of Johannes (1984) minus $10^{o}C$. It is used as a reference throughout this work. Its position in PT space, compares favourably with that determined by or deduced from experimental studies for peraluminous granitic compositions (e.g. Mehnert & Busch, 1982; Clemens & Wall, 1981).

9.2 BAROMETRY

Reactions which make good barometers have shallow slopes on PT diagrams, that is they have low dP/dT slopes and, therefore, through the Clausius-Clapyron equation, low values of $\Delta S_R/\Delta V_R$. The best of these are net-transfer reactions which involve material transfer from one assemblage of phases into another (J.B. Thompson, 1982). Four such reactions have been used to estimate pressure in Furneaux Batholith granitic rocks. They are:

(a) andalusite --> sillimanite,

(b) anorthite --> grossular + aluminosilicate + quartz,

(c) aluminosilicate + Fe-biotite + quartz --> Fe-cordierite + alkali feldspar + water vapour, and

(d) sillimanite + biotite + quartz --> cordierite + garnet + alkali feldspar + vapour.

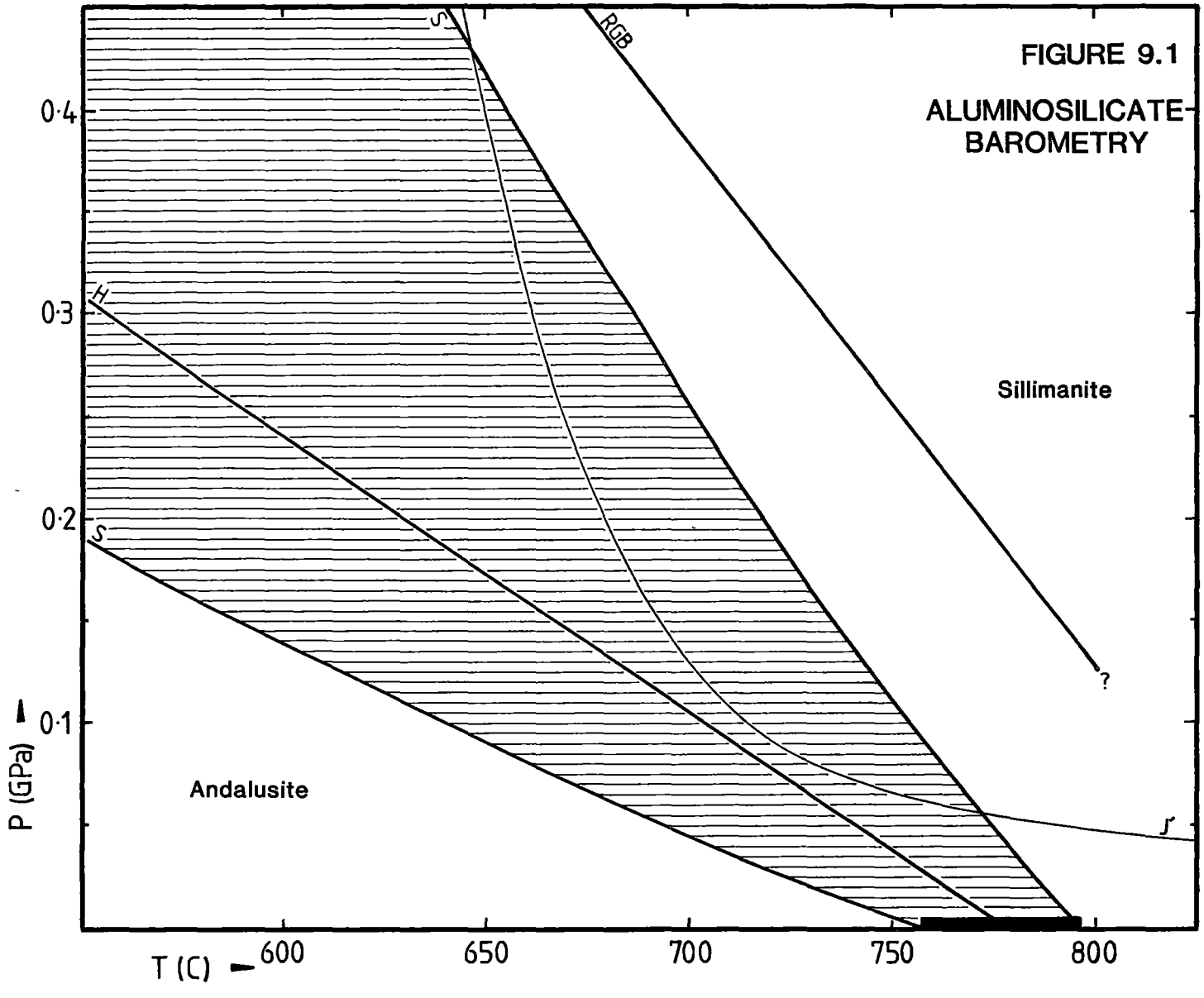
FIGURE 9.1
ALUMINOSILICATE-BAROMETRY
S
RGB
H
S
Sillimanite
Andalusite
?
J'
P (GPa)
0·4
0·3
0·2
0·1
T (C)
600
650
700
750
800

Estimated PT positions for the co-existence of sillimanite and andalusite:
1. shaded field bounded by curves marked "S" (Salje, 1986)
2. curve RGB (Richardson et al., 1969)
3. curve H (Holdaway, 1971)
4. filled bar at 0.0001 GPa (Wiell, 1966 **in** Holdaway, 1971)

Curve J′ is the reference water-saturated solidus for granitic systems and corresponds to that of Johannes (1984) minus 10 °C (see text for explanation). Curves J′ and H are used as references in the succeeding PT diagrams of this thesis.

In the case of the reaction andalusite to sillimanite, a small value of $\Delta S_R/\Delta S_R$ is also partly attributable to an anomalously small value of ΔS_R (Richardson et al., 1969; Salje, 1986), rather than to a large value of ΔV_R.

Each barometer, its application and results, will be described in turn. Unfortunately, none of these barometers is applicable to Wybalenna and Poimena Suite (i.e. the I-type) granites, whereas they are all applicable to the Musselroe, Boobyalla and Babel Island (S-type) Suite granites.

9.2.1 Andalusite --> sillimanite

The widespread occurrence of andalusite rather than sillimanite in the Furneaux granites (Chapters 3 and 4) indicates that the andalusite/sillimanite phase transition should be of considerable use in constraining petrogenetic PT conditions, especially as petrographic evidence exists indicating that andalusite was a magmatic phase in Babel Island and Boobyalla Suite magmas (Chapter 4). The PT conditions for magmatic andalusite are restricted to those above the water-saturated solidus and below the andalusite-sillimanite boundary.

However, the position of this aluminosilicate phase boundary is very poorly known. The two major experimental studies undertaken of aluminosilicate phase equilibria in the (AS) chemical system (Richardson et al., 1969; Holdaway, 1971), yielded andalusite/sillimanite boundaries which were 200-300°C apart. Such a range could still be within the realm of equilibrium rather than disequilibrium behaviour, because of the anomalously low free energy for the reaction. Richardson et al., (1969, fig. 4, p.269) showed that a Gibbs free energy change for the reaction of only 0.4 kJ mol^{-1} could shift the boundary through 160°C at a given pressure. For comparison, the same change in $\delta(\Delta G_R)$ for the breakdown of phlogopite to orthopyroxene, kalsilite and vapour, is 8°C (op. cit.).

In his review of aluminosilicate equilibria, Essene (1982) assessed the position of the aluminosilicate triple point to be probably within 0.05 GPa and 50°C of that at 501°C and 0.376 GPa deduced by Holdaway (1971). He considered that the position of the andalusite/sillimanite boundary is known only to within 50-100°C (op. cit.).

Based upon thermochemical calculations which use new determinations of low-temperature heat capacities of natural aluminosilicates, Robie & Hemingway (1984) show that the reaction is likely to have considerable curvature (concave upwards to higher pressure). They estimate the triple point to be at 0.4 ± 0.05 GPa at 517 ± 25°C, that is, at slightly higher P and T than that of Holdaway (1971).

Spectroscopically-based determinations of the heat capacities (C_p) of four high-purity natural sillimanites have been recently made by Salje (1986). His samples included fibrolitic, bulky prismatic and gem-quality varieties of the mineral. He found consistent relative differences of up to 4% in the heat capacities amongst these textural varieties. These variations cannot be attributed to differences in the degree of Al/Si disorder or to the degree of $Al_2OSi_{-1}[\ ]_{-1}$ exchange towards the mineral mullite (Cameron, 1977) or $FeIIIAl_{-1}$ exchange towards ferrisillimanite (Grew, 1980), between samples.

The differences in ΔG_R for the andalusite to sillimanite reaction resulting from variations in H^o_{sill} and S^o_{sill} associated with the observed differences in C_p of the different sillimanites, are of sufficient magnitude to cause shifts in the phase boundary of up to 280° at pressures of 0.32 GPa (op. cit., fig. 3, p.1369). The aluminosilicate triple point in which gem-quality sillimanite is a participating phase is estimated to be at ~440°C and 0.32 GPa, whereas that with fibrolitic sillimanite is at ~660°C and 0.59 GPa. The latter is close to the triple point of Richardson et al. (1969) who used fibrolitic sillimanite in their experiments. With C_p data of bulky prismatic sillimanite, intermediate triple point estimates are obtained, which are close to the triple point of Holdaway (1971). He also used the bulky prismatic variety of sillimanite in his experiments.

Salje (1986) attributes the enhanced specific heat of the fibrolitic material to the higher defect densities in this textural variety compared with the defect density of gem-quality sillimanite. Evidence consists of

(a) defect densities in sillimanite as high as 5% per unit cell (Lefebvre & Paquet, 1983, **in** Salje, 1986) and

(b) a consistent ~2% increase in 14 heat capacity measurements over a 50°C temperature range due only to the effects of fine-grinding of a sample of bulky prismatic sillimanite.

Salje (1986) therefore considers it possible that all the experimental studies in this sytem may have yielded valid phase equilibrium data, but which are relevant only to the specific type of sillimanite used. He questions the validity of using a particular set of experimentally derived data to calibrate the PT conditions of natural assemblages and therefore the aluminosilicates in crustal thermobarometry.

Chemical substitutions cause additional complexities. The stability field of andalusite solid-solution is strongly expanded to higher pressures and temperatures by both the $Mn^{III}Al_{-1}$ and $Fe^{III}Al_{-1}$ substitutions, resulting in the generation of extensive multiphase P-T-X fields (Abs-Wurmbach et al., 1983; Grambling & Williams, 1985). Andalusite in the Boobyalla Suite contains up to 3.4 mol % of ferri-andalusite: $FeAlSiO_5$ (Chapter 7, Plate

6). It is therefore likely to have been stable to PT conditions higher than those of the Fe-absent crystal rims.

Figure 9.1. shows the position of the reference granite solidus in P_WT space, relative to estimated positions of the andalusite/sillimanite boundary. A region of overlap is indicated where magmatic andalusite could exist. Using the range in the andalusite/sillimanite boundary calculated by Salje (1986, fig.3, p.1369), a PT field from ~0.05 GPa at 775°C to ~0.43 GPa at 650°C within 35°C of the water-saturated solidus is indicated in which magmatic andalusite could exist. This field will be expanded with increasing $FeIIIAl_{-1}$ in the andalusite and increasing FeIII, HF, B_2O_3 etc. in the melt.

The chemical and phase equilibrium evidence for the existence of magmatic andalusite described here therefore supports the arguments based upon textural evidence, both in the Furneaux Granites (Chapter 4) and elsewhere (e.g. Clarke et al., 1976; Lorenzoni et al., 1979). Phenocrysts of andalusite and even tourmaline occur in the Macusani ash-flow tuffs of S.E. Peru (Noble et al., 1984; Kontak et al., 1984; Pichavant et al., 1987).

The andalusite/sillimanite transition is therefore considered to provide only a lower limiting pressure estimate (of 0.05 GPa at ~775°C) to the stability of the (andalusite, melt) assemblage in the Boobyalla and Babel Island Suite magmas.

Prismatic sillimanite occurs in the Musselroe Suite as inclusions within garnet phenocrysts. It is therefore considered to be an early, even pre-magmatic petrogenetic phase (see Chapter 4). Only rare fibrolitic sillimanite is known to occur in the Boobyalla Suite (Chapter 4). However, 1 cm diameter masses of tiny andalusite crystals in the Boobyalla Suite granite sample #62583 are thought to be a pseudomorph after phenocrystic sillimanite (Chapter 4). The widespread abundance of phenocrystic iron-containing andalusite, together with the rarity of sillimanite in Furneaux Batholith porphyries is interpreted to indicate that the liquids of this suite became saturated in aluminosilicate only at conditions close to those at the vapour-saturated solidus (Fig. 9.1). Colourless iron-free andalusite occurring in the groundmass of porphyry matrixes or rimming pink, iron-containing phenocrysts (e.g. Plate 6) could be subsolidus occurrences of this phase.

More precise PT estimates of andalusite stability require:

(a) better knowledge of the position of the andalusite-sillimanite boundary in the pure AS chemical system, and

(b) the determination of H_f^o and S_f^o for endmember ferri-andalusite ($FeAlSiO_5$), or knowing two occurrences of andalusite solid solution

which have different mole fractions of ferri-andalusite endmember but are contained within the same relevant $X_{FeAlSiO5}$-buffering assemblage at known PT conditions (as demonstrated by Grambling & Williams, 1985). Activity modelling of $FeAlSiO_5$ may also be important in thermodynamic calculations involving andalusite (op. cit.).

9.2.2 Aluminosilicate-garnet-plagioclase-quartz

The reaction relating these phases, termed for brevity the AGPQ-reaction, describes the transfer of CaO between the grossular component of garnet and the anorthite component of plagioclase. The reaction is:

$$2(Ca_3Al_2Si_3O_{12})_{gar} + 2Al_2SiO_5 + SiO_2 \text{ --> } 3(CaAl_2Si_2O_8)_{plag}.$$

Its use in thermobarometry was pioneered by Kretz (1964) and Ghent (1976). Advantages of the use of this assemblage in barometry are:

(a) that it involves relatively simple solid-solutions in the phases garnet, plagioclase and aluminosilicate;

(b) that it does not involve the thermodynamically complex phases: vapour or liquid;

(c) that binary diffusion rates in both solid solutions are very low (e.g. Lasaga, 1983; Loomis, 1982, 1983a; Grove et al., 1984) so that magmatic compositions may remain unchanged through the waning stages of metamorphism; and

(d) that the grossular contents of the garnets of the Furneaux and Eddystone Batholiths at ~3.5%, are within the ranges of those of the garnets used in calibrating each version of the barometer used in this study (Ghent, 1976; Ghent et al., 1979; Newton & Haselton, 1981).

Specific disadvantages are:

(a) the appropriate assemblage is restricted to the Musselroe Suite, with Boobyalla Suite magmas possibly also having contained the assemblage;

(b) extensive zonation of garnet and plagioclase restricts application of the AGPQ reaction to using only the core compositions of these phases;

(c) relatively large uncertainties for the standard entropies and enthalpies of formation of the aluminosilicates needed to change ΔG_R for the experimentally determined endmember reaction involving kyanite (Hays, 1967; Hariya & Kennedy, 1968; Goldsmith, 1980) to the metastable counterpart involving sillimanite; and

(d) uncertainty in activity-composition relationships, for the two major solid-solutions: plagioclase and garnet.

With due consideration of these disadvantages, three versions of this thermobarometer (derived explicitly in Appendix L) have been applied to estimate PT conditions of the magmas thought to have contained the requisite assemblages.

FIGURE 9.2 AGPQ BAROMETRY

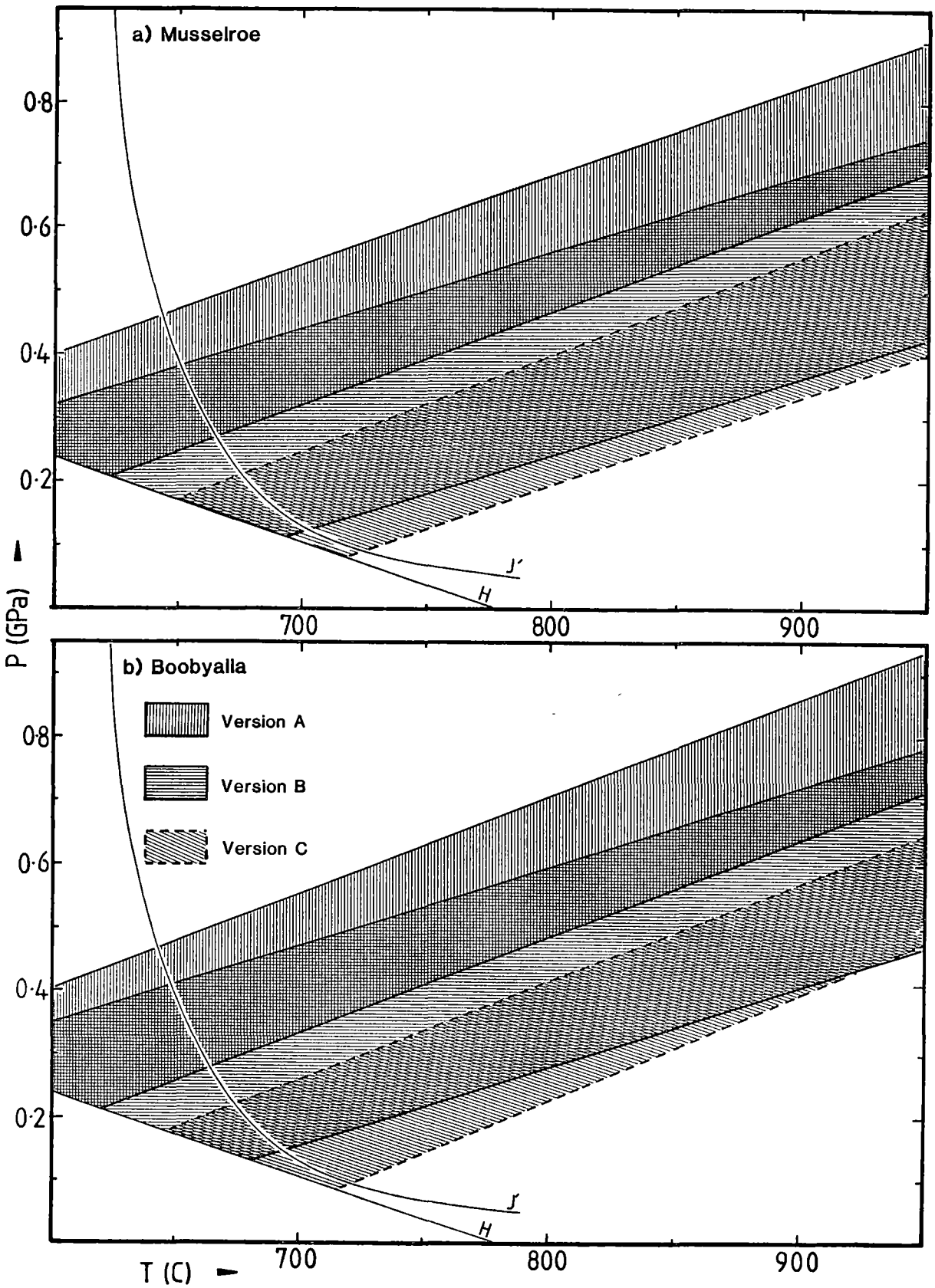

The first version, based upon that of Ghent (1976) and Ghent et al. (1979), uses

(a) the experimental data of Hayes (1967) and Hariya & Kennedy (1968) for the kyanite endmember reaction;

(b) the kyanitic/sillimanite boundary of Holdaway (1971); and

(c) an empirical value of +0.4 for the logarithm of the activity coefficient function: $\log_{10} \{(\gamma_{pl}^{an})^3/(\gamma_{ga}^{gr})\}$, a value back-calculated from the experimentally derived equation, and applied to selected samples the equilibrium conditions of which were considered to lie on the kyanite/sillimanite boundary (Ghent et al., 1979).

Estimated errors in predicted pressures given by this version are ±0.16 GPa (op. cit.).

The second version uses

(a) the sillimanite endmember reaction of Froese in Ganguly & Saxena (1984) which is based upon the experimental data of Goldsmith (1980);

(b) the activity model for anorthite in plagioclase of Newton & Haselton (1981),

(c) the ternary (Ca,Fe,Mg) activity model for grossular in garnet of Newton & Hazelton (1981), assuming ideality for $FeMn_{-1}$; and

(d) a ternary (CaFeMg) model for the partial molar volume of grossular in garnet based upon the experimental studies of CaFe and CaMg binary garnet solid solutions of Cressy et al. (1978) and Cressy (1981), again assuming ideality for $FeMn_{-1}$.

Estimated errors in predicted pressures given by this version are probably similar to that of the related version of the barometer described by Newton & Haselton (1981), i.e. ~±0.11 GPa.

The third version of this barometer differs from the second only in the expression for the activity of anorthite in plagioclase. That used is from Carpenter & Ferry (1984) who present ranges in activity coefficients of anorthite in plagioclase over a temperature range from 500° to 1500°C. Their coefficients are based upon a consideration of the free energy charge which attends the $C\bar{1}/I\bar{1}$ (Al/Si order/disorder) transition in plagioclase at high temperatures. They are considerably higher at any given temperature than the activity coefficients of Newton & Haselton (1981). Carpenter & Ferry (1984) ascribe this to non-equilibrium Al/Si disorder in the plagioclases of the hydrothermal exchange experiments of Orville (1972), the compositional data of which form one basis of the activity model of Newton & Haselton (1981).

The estimated error in the pressures predicted from the third version of the AGPQ barometer is unknown.

Each version of the barometer has been applied using the mean core compositions of phases in the assemblages of the two appropriate suites. These data are listed in Table 9.1.

Table 9.1.
Compositional Data Used For AGPQ Barometry

Suite	Garnet X_{Fe}	Garnet X_{Mg}	Garnet X_{Mn}	Garnet X_{Ca}	Plagioclase X_{Ca}	Plagioclase $(X_{Na}+X_{K})$	Sillimanite $X_{Al2SiO5}$
Musselroe*	0.706	0.194	0.068	0.032	0.41	0.59	1
Boobyalla**	0.778	0.157	0.029	0.036	0.43	0.57	1 (assumed)

* Sample #67539 ** Sample #68529

The results of these applications are shown in Fig. 9.2. The PT-fields delineated using all three versions span a pressure range in excess of 0.5 GPa. Version B yields the highest pressures and the estimates using version A overlap those of the other two versions. Version C yields pressure estimates which are considerably lower than those of the other two versions. They are poorly constrained however because the estimated pressure range is that attributed only to the range given for the activity of anorthite in plagioclase; error in other parameters will increase the estimated pressure range for this version. For this reason, the most valid equilibrium pressure range for the AGPQ barometer is probably that which is common to the ranges predicted by the A and B versions.

Pressure ranges estimated using Boobyalla Suite data are ~0.035 GPa higher than those estimated using Musselroe Suite data. The former however, are only lower limits to the equilibrium pressure because the existence of sillimanite in this early assemblage has yet to be established.

The PT field common to versions A and B for both suites includes the region around 0.6 GPa and 850°C. This PT region is also identified from the application of other thermobarometers (see below).

9.2.3 Aluminosilicate, biotite, quartz, alkali feldspar, cordierite, vapour

The univariant Fe-endmember dehydration reaction relating these phases: aluminosilicate + Fe-Al biotite + quartz --> Fe-cordierite + orthoclase + water vapour is referred to henceforth as the ABCKQV reaction. It has been located experimentally by Holdaway & Lee (1977) in the KFASHO chemical system. They realised that because of its shallow PT slope ($+0.001$ GPa K^{-1}), it had the potential for being a low-pressure barometer.

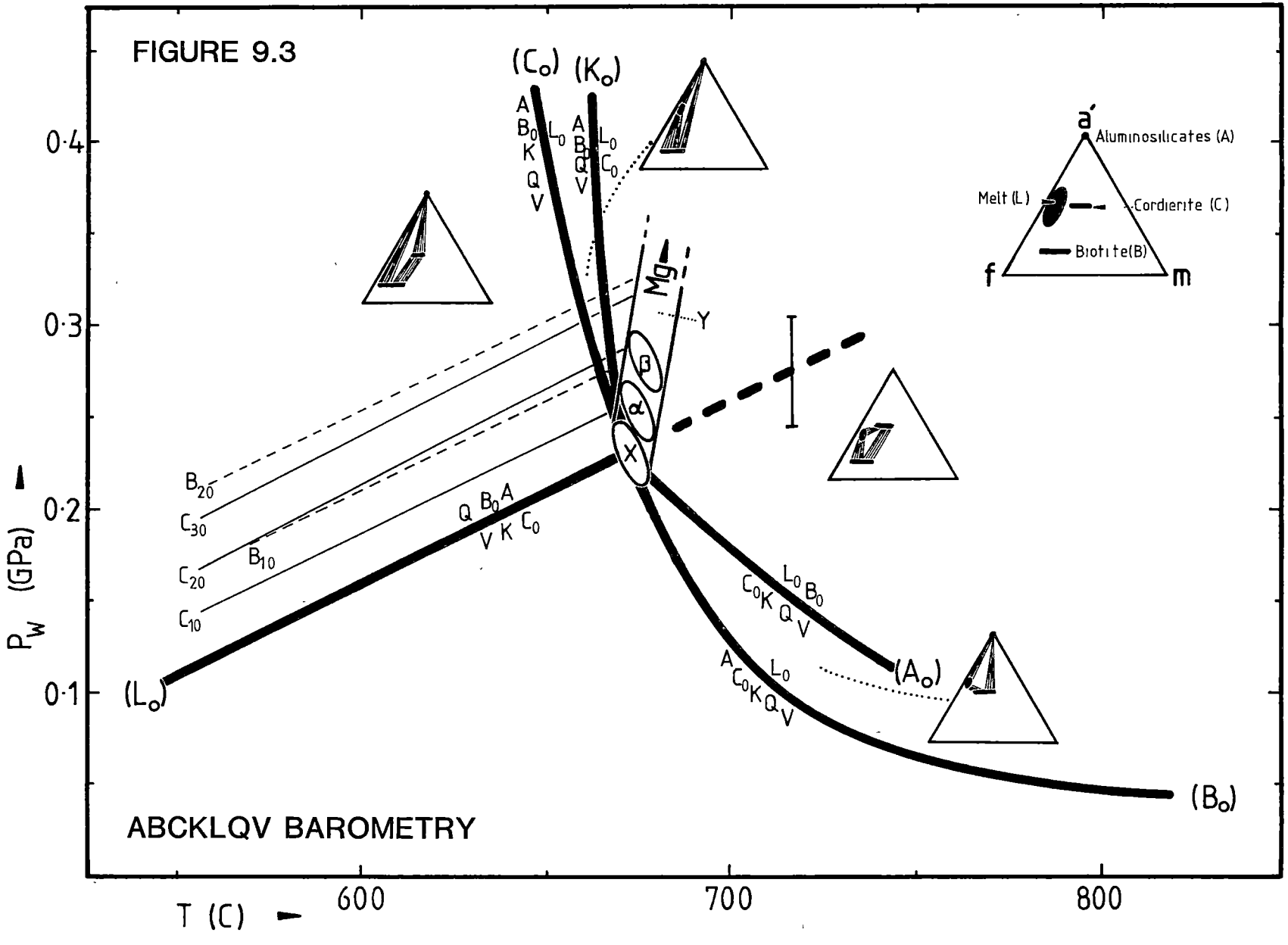
FIGURE 9.3
(C$_o$) (K$_o$)
A B$_o$ L$_o$ K Q V
A B$_o$ L$_o$ Q V C$_o$
a'
Aluminosilicates (A)
Melt (L)
Cordierite (C)
Biotite(B)
f
m
Mg
Y
β
α
X
B$_{20}$
C$_{30}$
C$_{20}$
B$_{10}$
C$_{10}$
Q B$_o$ A V K C$_o$
(L$_o$)
L$_o$ B$_o$ C$_o$ K Q V
(A$_o$)
A C$_o$ K Q V L$_o$
(B$_o$)
ABCKLQV BAROMETRY
P$_w$ (GPa)
0·4
0·3
0·2
0·1
T (C)
600
700
800

Advantages of the use of this assemblage for determining pressure are:

(a) the low value of dP/dT for the reaction;

(b) the common occurrence of the assemblage {aluminosilicate + biotite + cordierite + alkali feldspar + quartz} in Boobyalla, Babel Island and rarely, Musselroe Suite rocks; and

(c) the natural phase compositions used consist largely of Fe-endmember reaction constituents, so dilution is minimal.

Disadvantages are that

(a) binary diffusion coefficients for biotite, cordierite and alkali feldspar are high relative to those of other phases such as garnet or plagioclase (Lasaga, 1983; Freer, 1981), so that these phases of the assemblage are prone to being chemically reset;

(b) vapour compositions, the content of HF, FeIII and H in biotite and that of CO_2 in cordierite are unknown;

(c) a model for the extent of hydration of cordierite, is known only for the magnesium endmember (Bhattyachara & Sen, 1985); and

(d) activity models for cordierite and (especially) biotite are unknown or incomplete.

The ABCKQV reaction is univariant in the KFASH chemical system. It is important in the generation of the KFMASH system petrogenetic grid, derived in Chapter 11. It is one of a bundle of reactions emanating from an invariant point located on the KFASH water-saturated solidus (Figs 11.1, 11.2). The reaction is important in the barometry of peraluminous granitic rocks because not only can it be used to designate pressure, but by the method described below, the PT positions of other related univariant reactions can also be estimated and used to constrain pressures and temperatures, even in complex natural systems.

The position in PT space of the ABCKQV reaction of Holdaway & Lee (1977) is shown on Fig. 9.3. Calculations using the method of Thompson (1976b) (Appendix M), indicate that the position of the analogous reaction in a more complex chemical system containing Na_2O, Fe_2O_3 and TiO_2 (in amounts sufficient to yield mineral compositions comparable with those in the peraluminous granitic rocks of the BTB), is within the PT field subscribed by the ± 0.03 GPa experimental error quoted for the simple system reaction (Holdaway & Lee, 1977). This is so because the shift of the reaction to higher pressure upon addition of Na_2O (which alone would expand the phase field of the assemblage to higher pressures by stabilizing alkali feldspar on the low pressure side of the reaction) is compensated by the effects of the addition of TiO_2 and Fe_2O_3 to biotite and Fe_2O_3 to andalusite (which alone, would expand the phase field of the assemblage in

the opposite direction, i.e. to lower pressures by stabilizing these two phases which occur on the high-pressure side of the reaction. The position of the KFASHO-system reaction is therefore an estimate of the position of the analogous reaction in the more complex, natural, KNFASHTO-chemical system. In Fig. 9.3, this reaction is symbolized (L), indicating that its equilibrium assemblage is liquid-absent. It will be a divariant band in the KFASHO system which will widen to lower pressures with increasing fO_2. Buffered at low fO_2 and in the presence of Na-feldspar and ilmenite, reaction (L) will be one of a bundle of related reactions emanating from a univariant PT region, located at the intersection of reaction (L) with the water-saturated reference solidus (region X on Fig. 9.3). This solidus is considered to be appropriate because it is thought to involve phases with CaO- and MgO-absent compositions (see Chapter 11) like those being considered here. Neglecting the effects of minor components such as MnO, B_2O_3 and HF, this bundle will therefore be a natural system analogue of the bundle of invariant lines about the KFASH system invariant point, symbolized (9) in Figs 11.1 and 11.2. Addition of MgO to both the simple and complex systems, will extend all equilibria towards higher pressures. The magnesium-absent univariant region X will then be the low-pressure end of a divariant region Y which extends to higher pressures and temperatures, with increasing MgO content. This occurs because each cordierite stability field will expand, relative to the fields of the other phases as this mineral partitions more Mg relative to Fe* than does biotite. This shift is shown in the case of the ABCKQV reaction in Fig. 9.3. The reactions symbolized (L) and (A) and the low-pressure PT field between them (Fig. 9.3) are of importance in low-pressure barometry.

For the Boobyalla and Babel Island Suites, there is abundant petrologic evidence for biotite having reacted during the latter stages of magmatic petrogenesis and for cordierite to be a late-stage magmatic phase after it (Chapter 4). This feature is consistent with the PT paths having crossed the PT field of reaction (A), where biotite reacts with liquid to produce a cordierite-containing assemblage (Fig. 9.3).

By these arguments, solidus pressures below regions α and β at ~0.25 and 0.27 GPa within the divariant region Y (Fig. 9.3) are suggested for the respective PT paths of Babel Island and Boobyalla Suite rocks. These two regions are indicated using the compositions of matrix biotites (mg ~3.6 and ~7 respectively: Appendix H, samples 67544 and 43156) and those of cordierites reconstructed from the compositions of their pseudomorphing phases (mg $\geq$ 6 and $\geq$ 16 respectively, Fig. 7.6). The ABCKQV barometer therefore yields upper-pressure estimates for the solidus assemblages of the magmas of these two suites.

FIGURE 9.4 ABCGKQV BAROMETRY

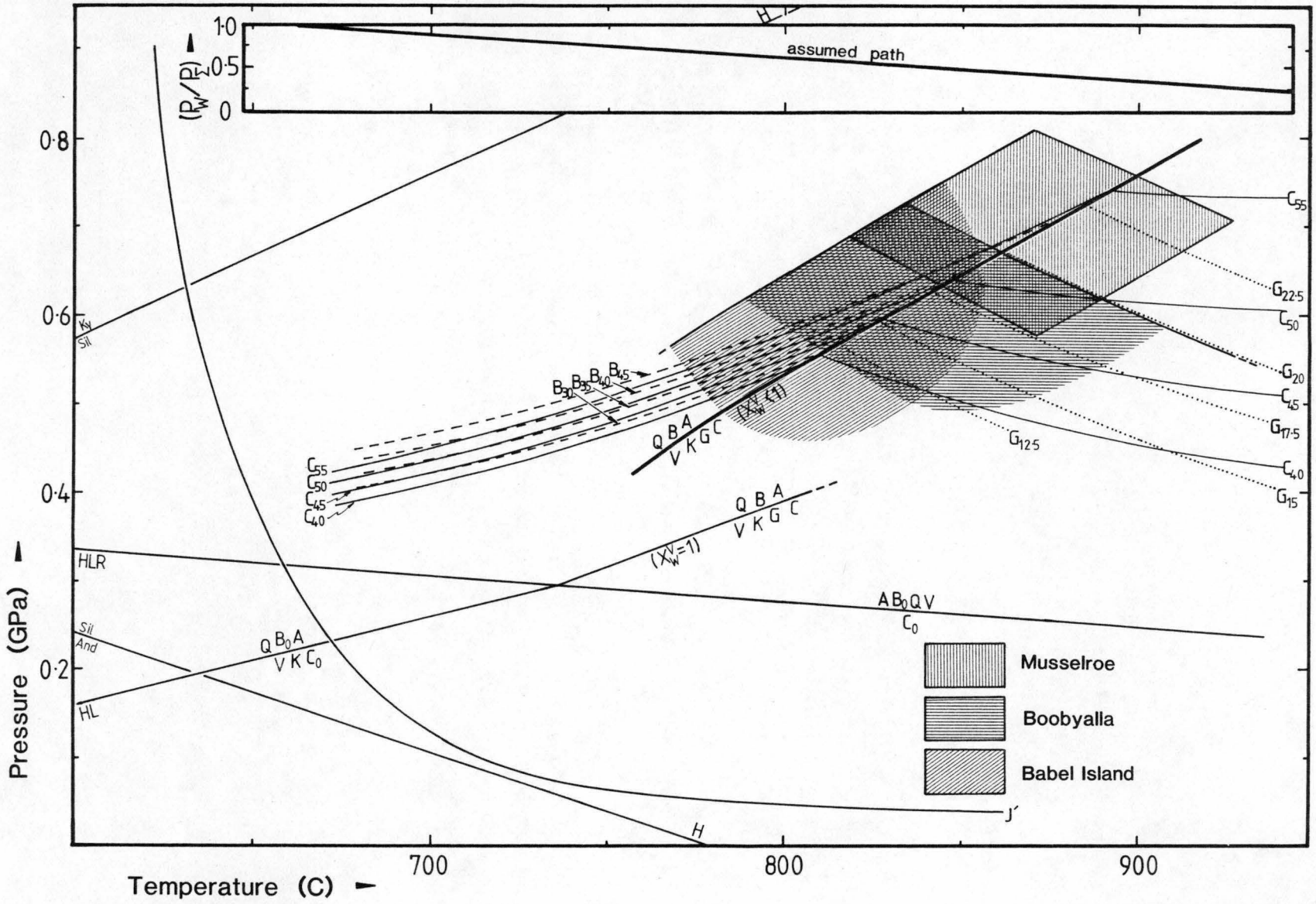

The presence of fluorine phases in rocks of the Babel Island Suite (Chapter 4) also makes the above a maximum pressure estimate because fluorine, by preferentially partitioning into biotite and liquid, will shift all equilibria to lower pressures.

9.2.4 Sillimanite, biotite, cordierite, garnet, alkali feldspar, quartz, and vapour

The reaction relating the phases of this, the ABCGKQV assemblage, was first proposed and investigated by Holdaway & Lee (1977). In the KFMASH chemical system, it is a univariant reaction and occurs at the intersection of the Fe-Mg divariant field of the ABCKQV reaction described in the previous section, with that of a similar divariant field for the degenerate FMASH reaction relating the phases {sillimanite, cordierite, garnet and vapour}, i.e. the ACGQV reaction (op. cit.). The Fe-endmember limit to the last reaction is the terminal reaction of Fe-cordierite: Fe-cordierite --> almandine + sillimanite + quartz + water vapour. It has been studied experimentally by Richardson (1968), Wiessbrod (1973) and Holdaway & Lee (1977). The grids for the ABCKQV and ACGQV reactions of Fig. 9.4 were each constructed using the pressure-transposing technique described in Appendix M.

Based on the Fe-endmember reactions of Holdaway & Lee (1977), PT space is contoured in mg-isopleths for biotite garnet and cordierite (Fig. 9.4), using the method described in Appendix M, assuming that:

(a) the reaction involves a titantium-absent biotite of constant tschermak [$Al_2(FeMg)_{-1}Si_{-1}$] composition equal to that for which molar volume data is known (Holdaway & Lee, 1977) (such biotite is similar in composition to Al-rich, Ti-poor biotites in the Musselroe, Boobyalla and Babel Island Suites);

(b) the reaction involves an alkali feldspar of constant composition equal to that of the average Boobyalla and Poimena Suite alkali feldspar separate composition of $Or_{72}(AbAn)_{28}$ (Appendix F);

(c) the mole fraction of water in equilibrium with (Fe-Mg) cordierite is equal to that given as a function of P,T,G_W^T and f_W for Mg-cordierite by Bhattyachara & Sen (1985);

(d) that garnet core compositions are remnant magmatic compositions which can be used as references with which to reconstruct the equilibrium Fe-Mg compositions of the former coexisting cordierite and biotite, using the Fe-Mg exchange equilibria of Holdaway & Lee (1977) (the latter phases invariably have compositions reflective of low-temperature re-equilibration (see next section)); and

(e) the activity of almandine in garnet is described by the pseudo-ternary solution model of Newton & Haselton (1981) whereas the activities of

Fe-biotite and Fe-cordierite are simple functions of the mole fractions of the Fe and Mg endmembers in the respective solid solutions.

As was recognized by Holdaway & Lee (1977), the entire length of the ABCGKQV reaction is metastable with respect to melt in the fully hydrated KFMASH chemical system; only with water-undersaturation will the assemblage be revealed. Therefore the degree of water-undersaturation of the assemblage as a function of pressure and temperature must also be modelled. The grids of each of the constituent divariant reactions have been calculated assuming that $X_W^{vap} = P_W/P_\Sigma$ varies from 0.9 at 700°C through 0.5 at 840°C to 0.25 at 940°C, independent of pressure. This variation of X_W^{vap} with temperature parallels that found by Bohlen et al. (1983) from melting experiments in the quartz-sanidine-water-carbon dioxide system. In this study, isobaric variation of X_w^{vap} with temperature occurred above 0.7 GPa at 700°C ($X_w^{vap} = 1$) to above 0.3 GPa at ~940°C ($X_w^{vap} = 0.25$) (op. cit.). The choice of this X_w^{vap} function is considered reasonable because KASH-system melts are analogues of granitic melts (normative quartz and orthoclase constitute some 60-70% of the compositions considered to have been the anhydrous components of Boobyalla and Babel Island Suite melts and normative quartz, orthoclase and albite constitute 90-95%, cf. Chapter 10). The reaction will terminate at ~900°C where biotite melts incongruently in the presence of quartz at $X_w^{vap} \simeq 0.35$ (Bohlen et al., 1983; Burnham, 1979).

The grids shown in Fig. 9.4 have been constructed using the data obtained from the magnesian cores of garnets from the Musselroe Suite samples #67539 and #43276 and the Boobyalla Suite sample #68529. The compositions of each mafic mineral are depicted using mg-isopleths. Those for biotite and garnet terminate at the ABCGKQV reaction whereas those for cordierite cross from one grid to the other with an angular discontinuity at the seven-phase reaction.

In natural peraluminous granitic compositions, minor chemical components such as CaO, TiO_2, MnO and Fe_2O_3 will broaden the reaction line somewhat into a polyvariant band.

Intersection of water-undersaturated melting curves with the reaction will mark the start of **vapour**-undersaturated melting for the reaction:

sillimanite + biotite + quartz --> cordierite + garnet + alkali feldspar + melt.

These reactions will trace $P_\Sigma T$ trajectories which have steeper but indeterminant $(\partial P_\Sigma/\partial T)_{P\Sigma}$ slopes than that of the vapour-bearing seven-phase reaction. The latter reaction may then be considered to trace the locus of $P_\Sigma P_W T$ conditions marking the start of vapour-absent partial melting in this assemblage.

Results for the Musselroe Suite assemblages indicate PT conditions of ~0.65 GPa at ~860°C for sample #67539 which has a core composition of mg = 20 ± 1.5 (Fig. 7.8). The garnet in this sample contains inclusions of sillimanite, cordierite, biotite and quartz (alkali feldspar is assumed to have also been present). The results for this sample are a more reliable estimate of early Musselroe Suite petrogenetic conditions than the results for sample #43276 of ~0.72 GPa at ~890°C (garnet core composition of mg 22.5) because the garnet in this sample contains inclusions only of biotite and quartz.

The compositions of the garnet cores from the Boobyalla Suite sample #68529 are mg $\leq$ 17.2 and yields pressures of 0.60 GPa at 850°C. Garnet cores contain inclusions only of biotite and quartz. Pseudomorphs interpreted to have been after cordierite occur in the same rocks (Chapter 4) and an andalusite aggregate possibly after sillimanite is known from sample #62583 of this suite. Alkali feldspar is thought to have been present in view of the results of two-feldspar thermobarometry described in the next section. If sillimanite was not present at the time of garnet core formation, that is, $a^{assemblage}_{Al2SiO5} < 1$, then the resulting six-phase assemblage will exist at pressures **below** the ABCGKQV reaction line, at any given temperature (cf. Appendix M). The pressure (±0.1 GPa) estimated assuming all seven phases to have been present is therefore an upper limit and the temperature (±50°C) , a lower limit to the equilibrium conditions of the six-phase Boobyalla Suite assemblage.

For the Babel Island Suite sample #68550, garnet core compositions reach mg = 13.5, corresponding to ABCGKQV pressures of ~0.55 GPa at ~810°C. Equilibrium PT conditions for this suite are poorly constrained because the assemblage is not known to have contained sillimanite and because only a small number of garnets have been analysed from rocks of this suite so that more magnesian core compositions are likely to be found. They lie to the high-temperature side of the ABCGKQV line (±50°C).

9.2.5 Summary

Four geobarometers have been used in order to estimate the pressures at which granitic assemblages have equilibrated. They are applicable only to the more peraluminous granites because they all involve mineral phases more peraluminous than biotite.

Estimates of initial magmatic PT conditions are those given by both the AGPQ and ABCGKQV barometers. For the Musselroe and Boobyalla Suites, these conditions are similar at ~0.6 GPa and ~850°C.

The estimated solidus pressure for the Boobyalla and Babel Island Suite granite magmas is 0.15 ± 0.10 GPa. This value is consistent with

the results of both aluminosilicate and ABCKQV (and related) thermobarometry.

9.3 THERMOMETRY

9.3.1 Introduction

Reactions which make good thermometers have equilibria which are dependent largely on temperature rather than pressure or compositional variables. On PT diagrams they therefore have high dP/dT values, a reflection of the high values of the $\Delta S_R/\Delta V_R$ terms in the Second Law expressions of their equilibria. As a group, exchange reactions make good thermometers because their small molar volume terms yield high values of $\Delta S_R/\Delta V_R$ values (J.B. Thompson, 1982). Seven exchange reactions have been used to estimate temperatures in Furneaux and Eddystone Batholith granitic rocks. The first three are mineral/mineral equilibria:

(a) [KNa(Ca)] alkali feldspar + [Ca(K)] plagioclase
<==> [K(Ca)] alkali feldspar + [CaNa(K)] plagioclase

(b) almandine + Mg-biotite <==> pyrope + Fe-biotite

(c) almandine + Mg-cordierite <==> pyrope + Fe-cordierite

The last four are mineral/melt equilibria:

(d) $(ZrO_2)_{melt} + (SiO_2)_{melt} <==> (ZrSiO_4)_{zircon}$

(e) Na-hornblende + K-melt <==> K-hornblende + Na-melt

(f) almandine + Mg-melt <==> pyrope + Fe-melt

(g) Fe-cordierite + Mg-melt <==> cordierite + Fe-melt.

As in the preceeding section, each equilibrium will be described, assessed and applied in turn.

9.3.2 Alkali Feldspar + Plagioclase

The two-feldspar thermobarometer is based upon the temperature and pressure dependence of Na, K and Ca exchange between coexisting feldspars. Though used as a thermometer, the pressure dependence is larger than that of many other exchange reactions, because of the effect of the inbuilt pressure-dependent net-transfer reaction:

alkali feldspar + plagioclase <==> feldspar_{ss}

describing the stability of the critical feldspar composition.

The development of the thermobarometer was pioneered by Barth (1951). Brown & Parsons (1981) reviewed attempts to formulate the thermobarometer, prompted by the gross inconsistencies in the various sets of results to given compositional data. They rejected the formulation of Stormer (1975), arguing that he invalidly assumed that feldspars could be treated as binary solutions by ignoring (Or) in plagioclase and (An) in alkali feldspar. They also rejected the formulation of Powell & Powell (1977), arguing that to ignore the role of (An) in alkali feldspar as they had done, is to

FIGURE 9.5 TWO FELDSPAR THERMOMETRY

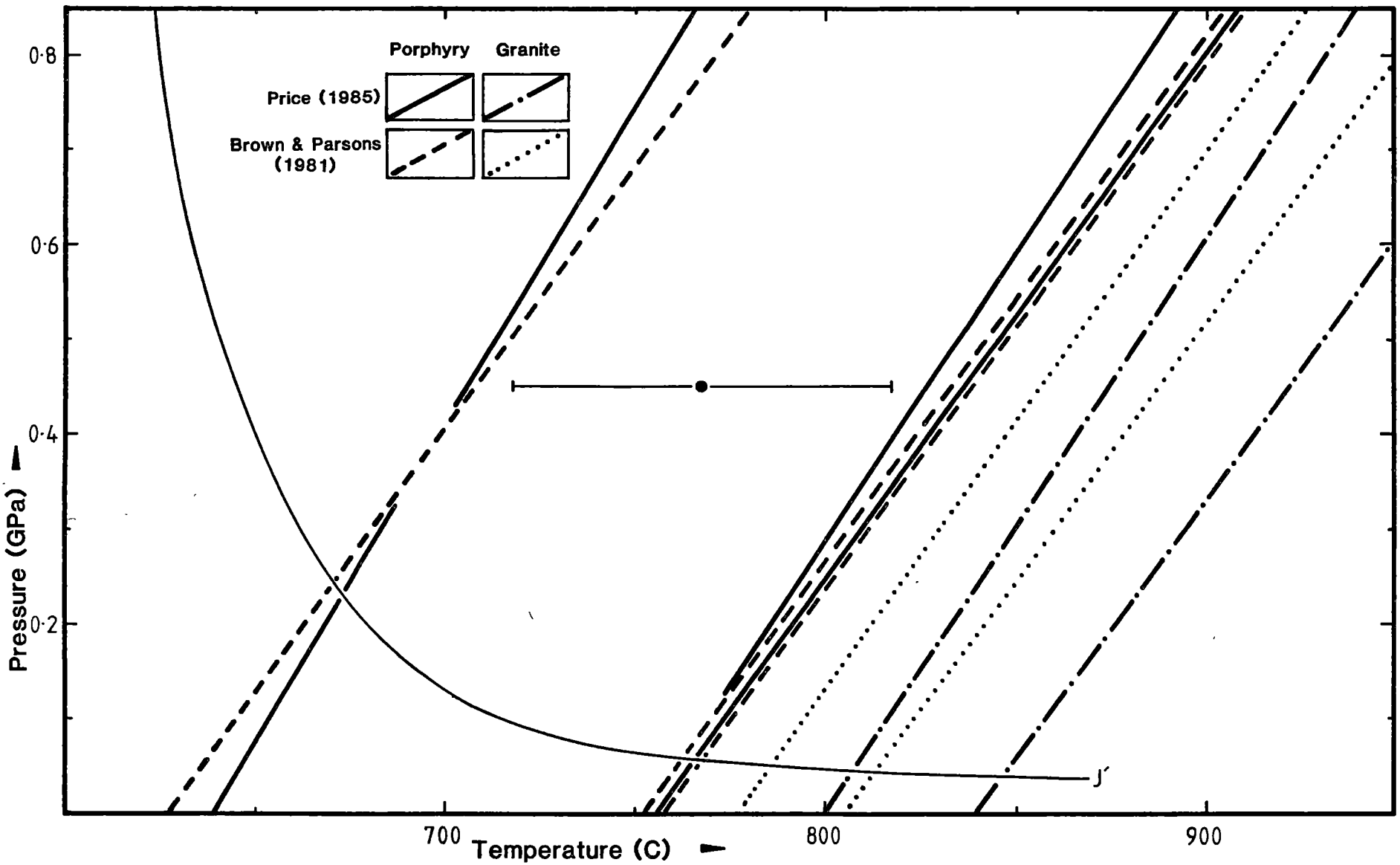

assume that $CaAlK_{-1}Si_{-1}$ exchange has no effect on a_{Ab} in either feldspar and that this assumption is unlikely to be true.

Brown & Parsons (1981) presented a graphical PTX_{Ab}-solution at 0.1 GPa, formulated using ternary asymmetric Margules parameters. They assumed that higher pressure equilbria may be obtained by adding 180°C per GPa to the temperature at 0.1 GPa pressure (op. cit.).

More recent formulations include those of Haselton et al. (1983), Ghiorso (1984) and Price (1985). The first yields very high temperatures due to its use of a binary albite-anorthite model for deriving a_{Ab}^{plag}, rather than a ternary model as is used in the later two formulations. The second formulation best fits coexisting ternary feldspar experimental data (Ghiorso, 1984). It equates a_{An} and a_{Or} between the feldspars in addition to a_{Ab}. However, the computer software required for its solution was not available so it was not applied in this study. The last formulation considers the effects of Ba, Rb and Sr on the ideal contribution to the activities of albite in each feldspar (Price, 1985).

In Fig. 9.5, two-feldspar PT estimates are depicted for five sets of feldspars from two granitic suites using both the Brown & Parsons (1981) and Price (1985) formulations. All compositions used are of hand-picked phenocryst core separates of coexisting feldspars (cf. Chapter 6, Appendix F).

The Brown & Parsons and Price formulations yield similar results, differing by <30°C and <0.2 GPa pressure (usually by much less). This variation is less than the quoted error of ±50°C (±~0.27 GPa) quoted for each of the two formulations.

Feldspars separated from the Poimena Suite Rooks River porphyry (sample #62596) yields temperatures ~125°C lower than those for Boobyalla Suite pairs. The PT paths cross the reference water-saturated solidus at ~670°C and 0.22 GPa (Fig. 9.5). The plagioclase from this sample however has been incipiently altered to a microcrystalline secondary assemblage so the inferred PT conditions may not represent equilibrium conditions.

In contrast to this, PT paths for the Boobyalla Suite porphyry feldspar pairs yield much higher PT conditions, consistent with petrographic, geochemical and thermobarometric evidence (Chapters 4, 6 and the previous section, respectively), indicating that the cores of feldspar phenocrysts are not in equilibrium with the enclosing matrix and are remnant phases with compositions determined by higher temperature equilibria.

The best estimates of the PT conditions of these early equilibria are therefore considered to be those derived using core feldspar pairs from each of the porphyries #62595 and #62614. Although the latter is a hybrid

rock derived by mixing of a minor (~10%) mass-fraction of Poimena Suite liquid with a major (~90%) mass fraction of Boobyalla Suite Crystal-rich magma, this should be of little consequence to the chemistry of the **cores** of feldspar phenocrysts and hence to the deduced PT conditions of their equilibrium. The compositions of both sets of feldspar pairs indicate equilibrium temperatures of 850 ± 50°C at pressures of 0.60 GPa. This compares favourably with those derived in the previous section, using both AGPQ and ABCGKQV barometry.

The compositions of separates taken from the porphyritic granite #62622 and the coarsely crystalline mafic mineral segregation #62634 yield higher apparent temperatures for a given pressure, than do those of the finer grained porphyries (cf. Fig. 9.5). This feature is thought to be due to the effects of low-pressure re-equilibration. Re-equilibration should involve the matrix and result in a greater change in the alkali feldspar composition compared with that of plagioclase, due to the lower interdiffusion rates of the latter compared with the former mineral (e.g. Freer, 1981; Grove et al., 1984). The result of these changes will be to derive high apparent temperatures (Price, 1985). As predicted by this explanation, the highest apparent temperatures are yielded by the separates taken from the coarsest grained rock: #62634.

9.3.3 Biotite-garnet

Introduction

The two-phase assemblage {biotite-garnet} Fe^*Mg_{-1} exchange geothermometer was first formulated by Kretz in 1959. It is based upon the end-member exchange reaction:

almandine + phlogopite <==> pyrope + annite

embodied in the $K_D^{Fe^*Mg_{-1}} = (Mg/Fe)_{ga}.(Fe/Mg)_{bi}$. The assemblage constitutes a good thermometer because:

(a) $K_D^{Fe^*Mg_{-1}}$ values are large relative to those for other mineral pairs, so error in estimated temperature due to compositional imprecision is relatively low;

(b) one phase: garnet, has low rates of binary diffusion so that its compositions may remain unchanged in areas distal to re-equilibrated biotite , enabling temperatures to be calculated if independent estimates of biotite compositions can be made; and

(c) the assemblage is widespread in the Musselroe, Boobyalla and Babel Island Suites of the granites of northeastern Tasmania.

Disadvantages of the thermometer are that:

(a) its formulations ignore the roles of FeIII, H and usually F_2O_{-1} in biotite because few data for these components exist (they cannot for example be determined by energy dispersive microprobe analysis); and

(b) activity models for biotite solid solutions are incomplete, because of the chemical complexity of this phase.

Calibrations

Eight formulations of the thermometer have been considered. In that of Goldman & Albee (1977), the $K_D^{Fe/Mg}$ between biotite and garnet for each of thirteen natural rock samples has been expressed as a function of X_{Mn} and X_{Ca} in garnet and $X_{Fe'}$ X_{Ti} and X_{Al6} in biotite in addition to temperature. Their formulation is:

$$T(K) = \left[\frac{985890}{(1.4X^{Bi}_{Fe*}+0.942X^{Bi}_{Ti}-1.59X^{Bi}_{Al6}-1.22X^{Ga}_{Mn}-2.14X^{Ga}_{Ca}-0.492-\ln K_D^{Fe*Mg}-1)}\right]^{1/2} \quad (9.2)$$

The influence of pressure on the K_D^{Fe*Mg} was not considered. They calibrated these compositional terms with oxygen isotopic temperatures derived from quartz-magnetite assemblages within each sample, assuming the four phases: garnet, biotite, magnetite and quartz, to have been in mutual equilibrium.

The remaining formulations describe the K_D as a function of temperature and pressure, with or without compositional terms as well. Each may be written in a form similar to that of equation 8.18 in which multiple excess terms may be present. In accordance with the nomenclature used in Chapter 8, the K_D for the biotite/garnet reaction is equal to $[(Fe*/Mg)_{bi}.(Mg/Fe*)_{ga}]$. The numerical values for the relevant parameters for these six thermometers are listed in Table 9.2.

The thermometers of Thompson (1976b) and Holdaway & Lee (1977) are based upon the compositions of natural assemblages which have been independently calibrated for temperature. Holdaway & Lee (1977) re-appraised the temperature calibration for one set of source data used by Thompson (1976b), thereby changing the formulation slightly to that of #2 in Table 9.2. This change results in a lowering of estimated temperatures above ~500°C, relative to temperatures predicted by the Thompson (1976b) formulation (#1 in Table 9.2).

Three experimental studies of the exchange reaction have been undertaken. That of Perchuk & Lavrenteva (1983) used natural titaniferous and aluminous biotites and Mn-, FeIII- and Ca-containing garnets. Their use of the electron microprobe enabled them to determine the compositions of the rims of minerals in order to better determine equilibrium K_D values.

Table 9.2
Second Law Formulations of the Biotite/Garnet Thermometer

No.	Data Source	Chemical System	H*	S*	V*	Defined PT range (GPa, °C)	Reference
1	N	Natural	2740	1.56	234	500–700	Thompson (1976b)
2	N	Natural	3095	1.978	124	500–700	Holdaway & Lee (1977)
3	E	Natural	3947	2.868		~0.6, 575–900	Perchuk & Lavrenteva (1983)
4	E	Water-sat. non-per-aluminous KFMASHO	2089	0.782	95.6	550–800	Ferry & Spear (1978)
5	E	Water-sat. peraluminous KFMASHO	3720	2.71	380	0.5–1.2, 800–900	This work (Chapter 8)
6	E	Water-sat. KFMASHO	$2089+12800X_{Al6}^{Bi}$	$0.782+15.0X_{Al6}^{Bi}$	$95.6+2620X_{Al6}^{Bi}$	0.5–1.2, ~800	This work (Chapter 8)
7	E,N	Natural	$2089+800X_{Al6}^{Bi}+3749X_{Ti}^{Bi}-1660X_{Ca}^{Ga}$	$0.782-0.755X_{Ca}^{Ga}$	95.6	550–800	Indares & Martignole (1985)

For biotite and garnet formula units based upon 11 and 12 oxygens respectively.

* for definitions, see Table 8.3.

$X_{Al6}^{Bi} = (\frac{\text{moles Al6}}{3})_{Bi}$, $X_{Ti}^{Bi} = (\frac{\text{moles Ti}}{3})_{Bi}$, $X_{Ca}^{Ga} = (\frac{\text{moles Ca}}{3})_{Ga}$.

However, their formulation (#3 in Table 9.2), is not considered to be widely applicable because

(a) strongly zoned, coarsely ground garnet was used as a starting mineral which in view of the extremely small binary diffusion rates for this phase (e.g. Cygan & Lasaga, 1985), should greatly complicate the interpretation of product mineral rim compositions in complex multi-component systems;

(b) Pt capsules were used which will partition iron from the charge and therefore affect the FeMg equilibria between the minerals in the charge (Ellis, 1984);

(c) run times (not given) were sufficiently short for even the rapidly equilibrating phase, biotite, (Freer, 1981) to become compositionally zoned; and

(d) their mixes contained fluxes consisting of varying proportions of $FeCl_2$, NH_4Cl, Fe and oxalic acid which will generate chemically complex fluids under run conditions. Such fluids will alter the activities of the reaction-dependent components, H_2O and O_2, in the system in an unpredictable way.

Ferry & Spear (1978) undertook experiments in the KFMASHO simple system using very finely ground mixtures of synthetic Fe-Mg garnets and biotites without excess Al_2O_3. They used AgPd capsules which at low temperatures absorb little iron from the charge (Ellis, 1984). Run times were up to 8 weeks (at 600°C). Reversals were made which indicate that equilibrium was closely approached. They used garnet-rich mixtures so that garnets need change their compositions minimally in order to reach equilibrium. This strategy was undertaken in order to circumvent the problems associated with the slow kinetics of diffusion in garnet at low temperatures, as well as to facilitate run-product analysis; only the biotite need be analysed to determine the K_D. This was done using XRD spectroscopy. The Fe and Mg content of biotites was verified using the microprobe.

Direct determination of the Al_2O_3 content of starting or product biotites however was not undertaken and excess Al_2O_3 was assumed to have been insignificant. Verification of the homogeneity of product garnets by direct measurement was also not undertaken. The reaction molar volume term was calculated from the endmember partial molar volume terms of Robie et al. (1978) assuming tschermak-free biotite to have been present.

The formulation derived from the results of their study (#4 of Table 9.2) is taken to describe the P-T-X_{FeMg}-dependence of the exchange reaction involving tschermak-free biotites under water-saturated conditions in the KFMASHO chemical system, up to ~800°C. It is not considered to be

applicable to natural peraluminous rocks however, because the biotite from these will contain both titaniferous and tschermak components, both of which could influence the partitioning of Fe and Mg between the two phases (see below). Its value however, is that it forms the basis of formulations such as #5 and #6 of Table 9.2, by which the dependence of the biotite-garnet K_D^{Fe*Mg} upon other chemical substitutions can be experimentally or theoretically determined (Ferry & Spear, 1978).

Formulations #5 and #6 were derived from the results of the experimental study described in the previous chapter, which investigated Fe-Mg-Al partitioning between biotite, garnet rims and melt from partial melts of a pelitic bulk composition in the peraluminous water-saturated KFMASHO chemical system. The experimental and analytical methods used in this study are described in that chapter. Formulation #5 was derived directly from the experimental data. Formulation #6 was derived by combining that of Ferry & Spear (1978) with the data of this study. The resultant relationship contains excess terms which describe the effects on the K_D of Al6 in biotite. They apply to biotite + garnet assemblages in the peraluminous KFMASHO system where the fO_2 is that between the MW and QFM buffers. Formulation #5 specifically applies to assemblages in which the biotite contains substantial (15-21%) Al6, whereas formulation #6 is applicable to assemblages with biotites of any Al6 content.

The final version of the thermometer (#7 of Table 9.2) is that of Indares & Martignole (1985). It, like #6, is based upon that of Ferry & Spear (1978). Indares & Martignole used the compositional data of 13 natural granulite facies assemblages (for which independent equilibrium temperature estimates were made), to obtain excess enthalpy terms describing the effects on the K_D of Al6 and Ti in biotite. Formulation #6 also incorporates excess terms describing the effects on the K_D of Ca in garnet. It assumes that $FeMn_{-1}$ behaves ideally in garnet (Newton & Hazelton, 1981). This formulation contains compositional terms for most of the components in natural biotite/garnet assemblages and should therefore be applicable to them.

Application

The eight calibrations of the biotite-garnet thermometer have been applied, using compositional pairs from assemblages from NBTB peraluminous granites. Only by using the outermost rim compositions of zoned garnet grains, are consistent apparent temperatures obtained either within or between samples. These only are considered to represent equilibrium temperatures. Apparent temperatures derived using core garnet compositions are usually meaninglessly high. Fig. 9.6 shows temperature intervals (ΔT) between temperatures estimated using each formulation in turn and that

FIGURE 9.6

COMPARISON OF BIOTITE/GARNET
Fe*Mg$_{-1}$ EXCHANGE THERMOMETERS

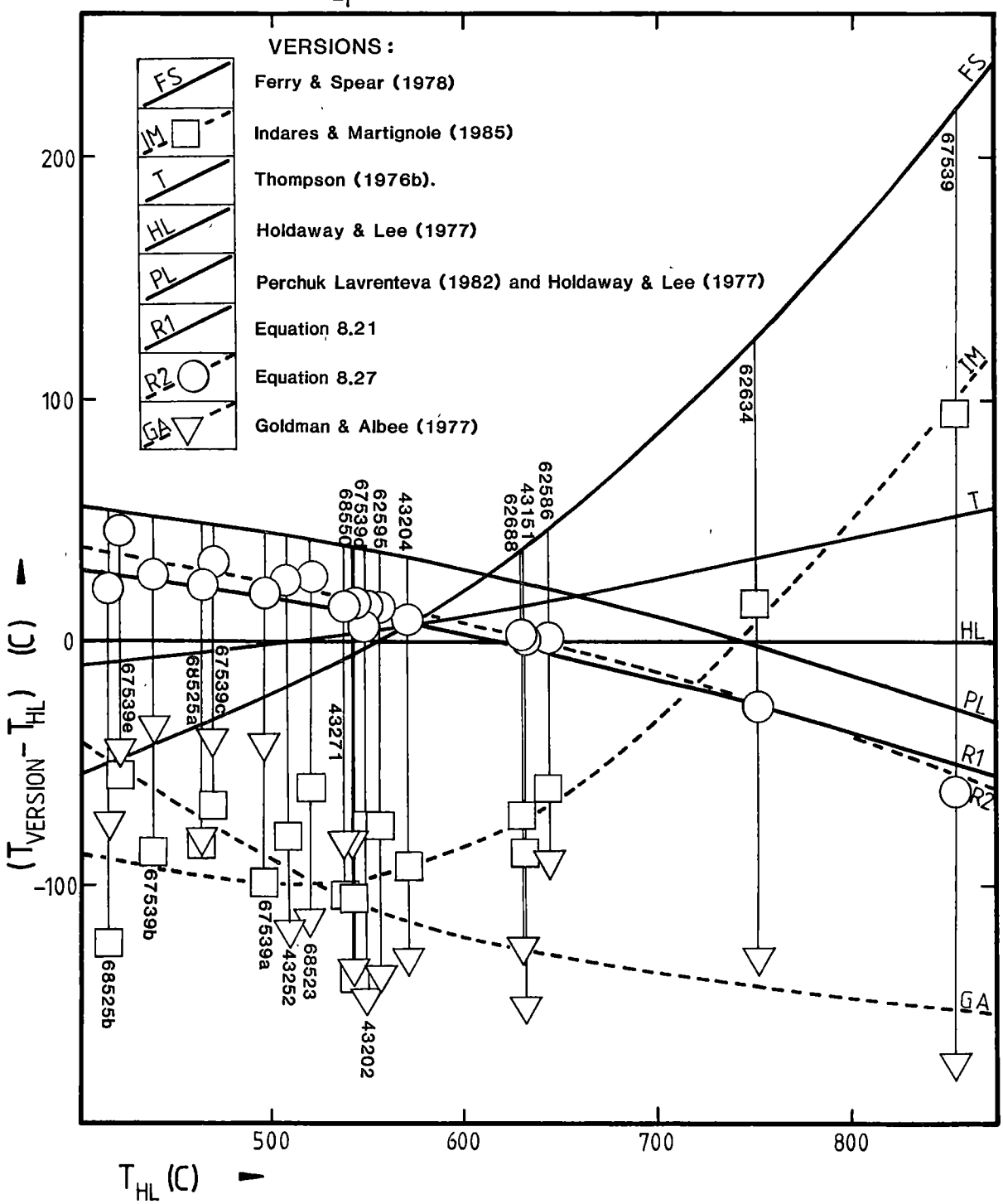

estimated by Holdaway & Lee (1977) (T_{HL}), plotted against T_{HL}, for an assumed pressure of 0.1 GPa. Temperatures from this formulation were used to reference those obtained from the other formulations because the calibration of Holdaway & Lee (1977) is probably the most accurate version of the two derived from the independent temperature calibration of natural garnet/biotite assemblages.

Data of 19 garnet/biotite pairs are illustrated. Seventeen of these pairs are considered to be equilibrium assemblages. Data of two non-equiibrium pairs are included for comparison. They are the sets of bulk-biotite and -garnet separate compositions extracted from mafic mineral segregations (cf Chapter 6). They are disequilibrium mineral pairs because the garnet in both separates is strongly zoned.

The temperature range indicated from all the formulations increases dramatically at high T_{HL} (reaching ~400°C when T_{HL} = 850°C), but everywhere exceeds 100°C. Temperatures estimated using the Goldman & Albee (1977) formulation are the lowest above T_{HL} = 500°C. Essene (1982) considers that this may be the result of isotopic miscalibration of their chemical data because the reference isotopic equilibria used by them are likely to record lower closure temperatures than those of the coexisting biotite/garnet assemblages (op. cit.).

The apparent temperatures obtained using the thermometers of Indares & Martignole (1985) and (especially) Ferry & Spear (1978) are high at high T_{HL}. The differences between the temperatures estimated using each of these versions and that of Holdaway & Lee (1977) (ΔT), are ~100° and 220° respectively, at T_{HL} = 850°C. As well, these versions predict low apparent temperatures at low T_{HL} (ΔT = ~-100° and -55° respectively at T_{HL} = 400°C. Temperatures predicted using the partial formulation of Perchuk & Lavrenteva (1983) in which the Holdaway & Lee (1977) molar volume term for the reaction has been incorporated, are marginally higher than those obtained using the other formulations, at T_{HL} < 600°C. Temperatures obtained using the formulation of Thompson (1976b) exceed T_{HL} above 500°C. The temperature interval: ΔT reaches 50°C at T_{HL} = 850°C.

Temperatures estimated using formulation #5 (equation 8.21 of this work) are within 20°C of T_{HL} over the range {440 < T_{HL}(°C) < 740}. They are higher than T_{HL} at low T_{HL} and lower at higher T_{HL}. They are lower than but within 50° of the temperatures predicted by the formulation of Perchuk & Lavrenteva (1983). Formulation #6 (equation 8.27 of this work) yields temperature estimates which are similar to those estimated by formulation #5. For the 17 equilibrium pairs, temperatures estimated using formulations 1, 2, 5 and 6 of Table 9.2 are usually well within 50°C of each other.

Apparent temperatures obtained using formulation #6 are lowered by 15-20°C when the experimentally derived excess terms of Newton & Haselton (1981) describing the effect of Ca on the partitioning of Fe and Mg in garnet:

$$\left(\frac{\gamma_{Mg}}{\gamma_{Fe^*}}\right) = \exp\left[\frac{X_{Ca}^{Ga}}{R}\left(\frac{1660}{T} - 0.775\right)\right] \qquad (9.3)$$

are incorporated into the formulation. These terms were used by Indares & Martignole in deriving their formulation of the thermometer (#7 of Table 9.2). This modification brings temperature estimates for the 17 equilibrium pairs using the formulations of Holdaway & Lee (1977), Thompson (1976b) and this work, even closer to each other.

The striking difference between the temperatures deduced using the Ferry & Spear (1978) calibration and those of this work (#4, #5 and #6 of Table 9.2 respectively) is attributed to the effect on the $K_D^{Fe^*Mg}$ of Al6 in biotite (cf. Chapter 8). The similarity between the temperatures deduced using formulation #5 and #6 and those via the formulations of Holdaway & Lee (1977) and Thompson (1976b), despite considerable variation in both the Ti content of the biotites and the Mn content of the garnets, suggests that neither Ti in biotite nor Mn in garnet exert a major influence on the $K_D^{Fe^*Mg}$ between biotite and low-Ca garnet. For these reasons, the Al6 excess terms in formulation #5 are preferred to the Al6 term in the formulation #6 of Indares & Martignole (1985). They are also preferred because they were derived from the comparison of the results of two experimental studies in the same chemical system. The Al6 parameter of Indares & Martignole (1985) was deduced using natural phases, in which many chemical components could have influenced the Fe-Mg partitioning between biotite and garnet and for which an isothermal **and** isobaric calibration was assumed.

Pressure has been plotted against Holdaway & Lee (1977) apparent temperatures in Fig. 9.7. The pressure path deduced in the previous section is also shown. Recognising that all temperatures have an estimated error of ±50°C (op. cit.), then it is possible that no equilibrium pair represents part of a magmatic assemblage. Equilibrium temperatures broadly correlate with the inverse of the matrix grainsize of the rock in which the assemblage occurs. Highest equilibrium temperatures (~630°C) are recorded from fine grained rocks (e.g. #43151, #62586, #62588) whereas the lowest temperatures (~420°C) are recorded from coarsely crystalline rocks (e.g. #67539, #68525). This feature is consistent with the coarser rocks having experienced slower rates of cooling than those which are expected to have

generated the fine grained rocks. There is no apparent correlation between the suite of a mineral pair and its equilibrium temperature.

If the biotite compositions of the mineral separate (disequilibrium) pairs are combined with the microprobe-determined rim compositions of their respective zoned garnets, then the apparent temperatures drop dramatically to subsolidus temperatures which are similar to those derived from the compositions of the equilibrium assemblages shown in Figs 9.6 and 9.7. This feature demonstrates that garnet cores are not in equilibrium with the biotite present in the rocks.

Summary

Formulations of the biotite-garnet thermometer derived in this work have been compared with six published thermometers. The results of their application compare favourably with those of the Thompson (1976b) and Holdaway & Lee (1977) thermometers. The Holdaway & Lee (1977) thermometer has been applied to biotite-garnet compositional pairs from northeast Tasmanian granitic rocks. Subsolidus temperatures are indicated for all equilibrium assemblages. Finely crystalline rocks yield higher temperatures (<~630°C) than do the coarsely crystalline rocks (>~420°C) and suites cannot be distinguished on the basis of their garnet-biotite temperatures.

It is concluded that for Fe and Mg, biotite approached a state of volume equilibrium whereas garnet approached a state of surface equilibrium with other phases.

9.3.4 Cordierite-Garnet

This assemblage is a good Fe-Mg exchange thermometer because

(a) K_D^{Fe*Mg} values are very large so errors in estimated temperature due to compositional imprecision are small; and

(b) the cordierite solid solutions usually considered are chemically simpler than either those of biotite or garnet so the influences of chemical components other than Fe and Mg on temperature are probably minimal.

The major disadvantage is the rarity of the occurrence of the cordierite-garnet assemblage, due to the widespread destruction of cordierite during the subsolidus stages of petrogenesis.

Three formulations have been considered. Those of Thompson (1976b) and Holdaway & Lee (1977) have been derived from data of independently calibrated natural assemblages. The latter formulation has been constructed using the data of the former, together with extra data. The formulation of Perchuk & Lavrenteva (1983) is from the same experimental study described in the previous section. Temperatures predicted by these

FIGURE 9.7

GARNET/BIOTITE AND GARNET/CORDIERITE $Fe \times Mg_{-1}$ EXCHANGE THERMOMETRY

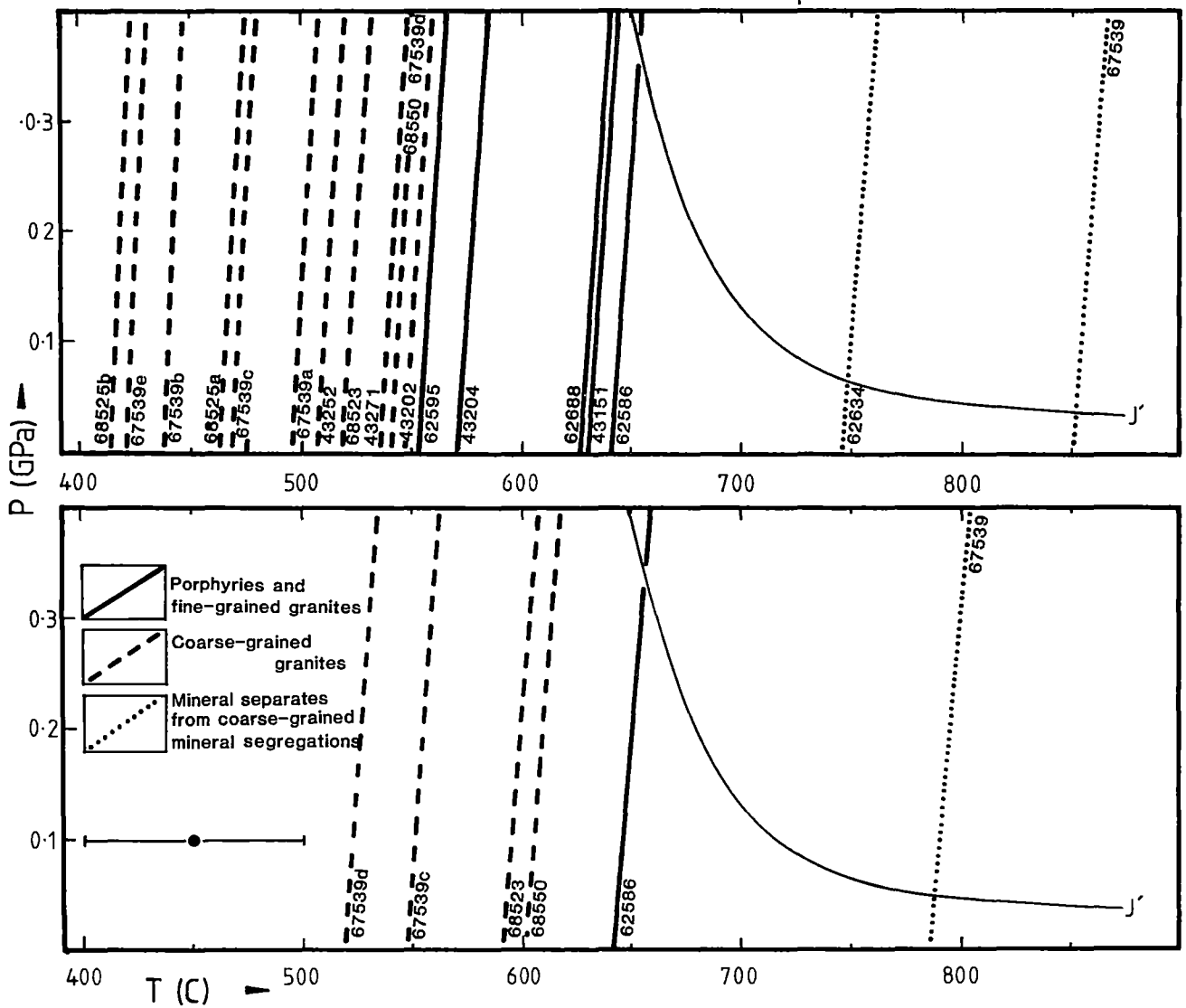

thermometers are within 40°C of each other in the temperature range from 400-700°C (H&L).

Fig. 9.7 depicts pressure plotted against Holdaway & Lee (1977) cordierite-garnet temperatures. Subsolidus equilibrium temperatures at pressures below ~0.15 GPa, are indicated for the five pairs for which garnet **rim** compositions were matched with either cordierite or reconstructed cordierite compositions. Disequilibrium assemblages generate high temperatures due to the (inappropriate) use of garnet compositions other than those of the rims (e.g. samples #62634 and #67539).

Equilibrium cordierite-garnet temperatures range from 650°C down to 525°C. They are highest for assemblages from fine-grained rocks and lowest for those from coarsely crystalline samples, as are the biotite-garnet temperatures (above).

Cordierite-garnet temperatures are up to 80° higher than corresponding biotite-garnet temperatures in (cordierite,biotite,garnet) assemblages. This feature may reflect a higher closure temperature for Fe^*Mg_{-1} exchange between (cordierite,garnet) than between (biotite,garnet) assemblages, consistent with the observation that cordierite exhibits a greater degree of Fe^*Mg_{-1} zonation than does biotite, both in natural and experimental assemblages (Chapters 7 and 8). Accordingly, natural cordierites may not have attained the degree of volume Fe^*Mg_{-1} equilibrium as has biotite.

9.3.5 Zircon-Melt

Introduction

The reaction relating these phases involves the equilibrium exchange of ZrO_2 between the phases: melt and zircon. It has been studied experimentally by Watson (1980) and Watson & Harrison (1983). They found that zircon solubility in siliceous silicate melts was not only temperature dependent but also dependent upon the concentrations in the melt of Na_2O, K_2O and to a lesser extent CaO. For a pressure of about 0.6 GPa, the reaction may be described by the relationship:

$$\ln D_{Zr}^{\text{zircon/melt}} = (12900/T^{\circ}K - 2.95 - 0.85M) \qquad (9.2)$$

for M, the melt phase cation ratio: [(Na + K + 2Ca)/(Al*Si)].

Their experiments were conducted from 750°C to 1020°C. Thermometric precision of this thermometer is governed by the precision of their Zr determinations made using the electron microprobe. Exponential regression of their 2σ errors in Zr plotted against mean Zr for the experimental melts, yields an error function: 2σ Zr = ± [16.16 exp(0.0225(Zr ppm))] ppm,

with $r^2 = 0.79$. Application of this function to the reaction equation gives an estimate of the 2σ error in temperature of $\sim\pm 60^{\circ}C$.

Assumptions made in the application of this thermometer to Furneaux Batholith porphyry matrix separates are that:

(a) the melts were saturated in zircon;

(b) matrix compositions represent those of the anhydrous component of melts;

(c) there is no compositional dependence upon the solubility product, $D_{Zr}^{zircon/melt}$, by components other than SiO_2, Al_2O_3, CaO, Na_2O and K_2O; and

(d) the solubility product has no substantial pressure dependency.

Results and Interpretation

The first two assumptions severely limit the application of this thermometer. The presence of cores in zircon phenocrysts in a porphyry is required to indicate that the pre-existing magma contained a zircon-saturated melt. However, the absence of cores does not preclude zircon-saturation of the melt. The zirconium contents of matrix separates can rarely be assumed to represent former melt concentrations because the mean grainsize of most porphyry matrices exceeds that of zircon phenocrysts: phenocrysts may occur in a matrix but they may not be recognised.

Only for the Poimena Suite rhyolites of the Long Toms Nose dyke swarm are matrix mineral grainsizes small enough to allow phenocrystic zircon to be recognised. It has not been identified in the aphyric sample #67533 (Chapters 3 and 4). At the same time, the melt is thought to have been saturated in zircon because:

(a) Poimena Suite granites contain zircons which are usually cored (Chapter 4); and

(b) the zirconium concentration of the zircon-containing phyric-rich sample (#67532) from the centre of a 5 m wide dyke is much greater than that of sample #67533, taken from the flow-banded aphyric margin of the dyke (Appendix E).

The zirconium content of sample #67533 at 90 ppm implies a magmatic temperature of $780^{\circ}\pm 60^{\circ}C$.

9.3.6 Hornblende-Melt

An expression for the temperature dependence of the Na-K exchange reaction between hornblende and melt was obtained by Helz (1979), from partial melting studies of basalts at 0.5 GPa P_W. It is:

$$T(K) = \frac{4258}{3.25 - \ln K_D} \qquad \text{for } K_D = (X_K/X_{Na})_{Hb}\ (X_{Na}/X_K)_{melt} \qquad (9.3)$$

FIGURE 9.8

HORNBLENDE-MELT THERMOMETRY

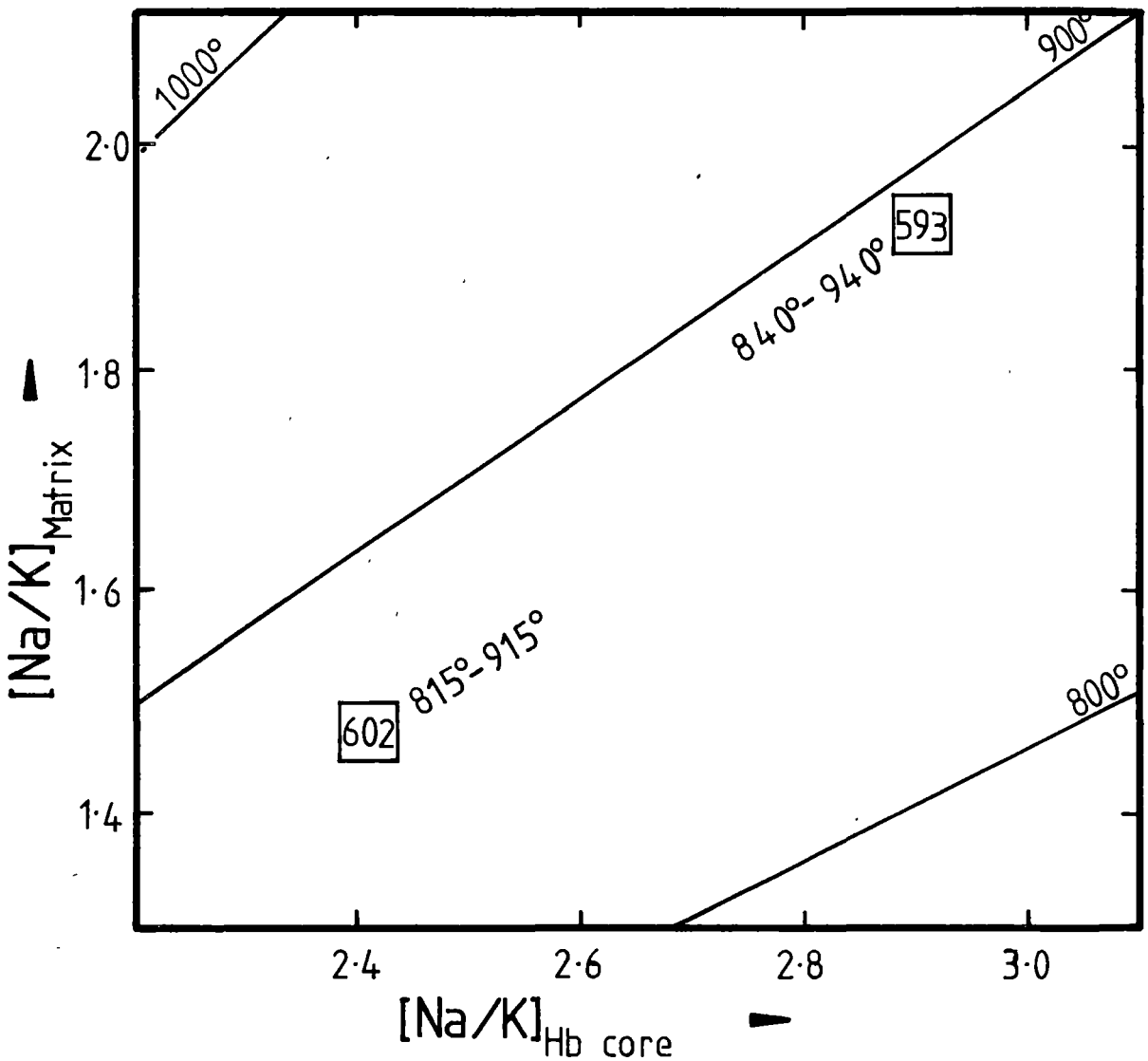

Samples numbers are shown without their "62" prefix.

Temperatures predicted using this equation have a quoted error of ±50° (op. cit.). Application of this thermometer to the hornblende-bearing samples of the Wybalenna Suite requires the following assumptions to be made:

(a) that Na/K ratios in porphyry matrix separates are the same as those of the melts which preceded them;
(b) that the cores of phenocrystic hornblende were in equilibrium with the melt and have retained their equilibrium compositions;
(c) that the assemblage was water-saturated; and
(d) that the thermometer is insensitive to pressure.

In porphyries, phenocrystic hornblende is rare. Only two occurrences are known. The phase is strongly zoned from brown to straw-coloured cores out to blue-green rims. The rim-hornblende is typical of that regarded by Miyashiro (1975) as being of subsolidus rather than of magmatic origin. The two hornblende-matrix temperatures determined are shown in Fig. 9.8. They are 865 ± 50°C for the assemblage in sample #62602 and 890 ± 50°C for that in sample #62593.

9.3.7 Fe^*Mg_{-1} Exchange Equilibria Between Melt and Crystalline Phases

Pressure-dependent thermometers describing the Fe^*Mg_{-1} exchange equilibria between peraluminous melt and each of the crystalline phases: garnet and cordierite, were derived in Chapter 8 from phase compositional data obtained from experimental studies in the FMASHO and KFMASHO chemical systems undertaken by Ellis (1986) and the author. Each equilibria can be described by the general equation 8.5 into which the relevant thermometric parameters listed in Table 8.3 have been substituted.

Apparent temperatures have been derived using these thermometers assuming that:

(a) the Fe*/Mg ratios of porphyry matrix separates were the same as those of the original liquids;
(b) mafic phases were in equilibrium with their host melts;
(c) chemical components, other than those in the experimental runs, do not markedly affect the calibrations; and
(d) equilibrium pressures were 0.1 GPa.

The apparent temperatures indicated for each thermometer are listed in Table 9.3.

Table 9.3
Apparent Temperatures for Mineral-Matrix Pairs
from Furneaux Island Porphyries

Phase in equilibrium with melt	Approximate apparent temperature (P = 0.1 GPa)	Sample numbers	Suites
Cordierite (#7)*	~100°	67544, 62579, 62605, 62617 62618, 62619	Babel Is., Boobyalla
Garnet (rim) (#5)*	427°** (Reid calibration, this work)	62595	Boobyalla

* Formulation used (Table 8.3).
** Assuming that $(Na)_{matrix}$ can be equated with $(K)_{matrix}$ on a molar basis in formulation #5.

These results indicate that in the two suites considered, phenocrystic garnet and cordierite have exchanged Fe* and Mg, with the matrix below the solidus; relative to the matrix, they are too iron-rich to have been magmatic phases or matrix compositions are too magnesian relative to phenocryst compositions to have been equilibrium melt compositions. Melts are therefore considered to have been more iron-rich than the matrix separates and the magmatic ferromagnesian phenocrysts more magnesian, than are the present phyric phases.

9.3.8 Summary

Three mineral-mineral and four mineral-melt exchange thermometers have been used to estimate temperatures at which granitic assemblages have equilibrated. The two-feldspar thermobarometer yields temperatures and pressures for the Boobyalla Suite which are consistent with early petrogenetic conditions for assemblages of this suite being ~0.60 GPa and ~850°C as was deduced for different mineral assemblages in the previous section. The cores of the feldspars, like those of garnet, are therefore regarded as being phases residual from the source regions of the Boobyalla Suite magmas.

The hornblende-melt thermometer indicates magmatic temperatures of ~875°C for Wybalenna Suite I-type porphyries. The zircon-melt thermometer indicates a magmatic temperature of 780±60°C for a Poimena Suite rhyolite.

The garnet-biotite and garnet-cordierite thermometers record subsolidus equilibria with the more rapidly cooled finer-grained rocks yielding higher temperatures (~640°C) than the slower cooled coarsely crystalline rocks (down to ~400°C). Fe^*Mg_{-1} exchange equilibria between

melt and each of garnet and cordierite also yield low subsolidus temperatures. These results show that, though ultimately of magmatic origin, much of the mineralogy of granitic rocks records late-stage subsolidus equilibria.

9.4 OXYGEN FUGACIMETRY

9.4.1 Introduction

Net-transfer reactions which are also redox reactions and which involve oxygen-containing phases, can be used as oxygen fugacimeters. The most widely applicable reactions of this type contain iron in valency states 2 and 3. Magnetite is usually present, such as in the magnetite-ilmenite-solid solution fugacimeter of Spencer & Lindsley (1981), the fugacimeter of Beane (1974) involving the assemblage (magnetite-biotite-alkali feldspar), that of Wones (1981) using (magnetite-biotite-alkali feldspar-vapour), and that of Zen (1985) involving the assemblage (magnetite-muscovite-biotite-garnet-quartz). Of these fugacimeters, that of Wones (1981) is the most widely applicable to granitic rocks because of the widespread occurrence of the requisite assemblage. However, magnetite is often absent from peraluminous granites, ilmenite frequently being the only oxide phase in these rocks (Ishihara, 1977; Whalen, 1980). All granites though, are considered to have at some stage contained the assemblage (biotite-vapour) so a fugacimeter developed using this assemblage should have widespread application.

9.4.2 (Biotite-Vapour) and (Magnetite-Biotite-Alkali Feldspar-Vapour) Oxygen Fugacimeters

A redox reaction may be written involving endmember components within the two phases: biotite and vapour

$$KFeII_3AlSi_3O_{10}(OH)_2 + 3/4\ O_2 \rightarrow KFeIII_3AlSi_3O_{10}O_2H_{-1} + 3/2\ H_2O \qquad (9.4)$$

which relates the Fe-biotite endmembers, annite (Ann) and proton-deficient oxyannite (PDO). Using the ternary FeII-FeIII-Mg biotite solution model and thermodynamic data of Beane (1974), the volume data of Helgeson et al. (1978) and assuming that other endmember constituents mix ideally in the ternary solution, then a biotite-vapour fugacimeter may be formulated (Appendix N). Both this and the magnetite-biotite-alkali feldspar-vapour fugacimeter of Wones (1981) have been applied in this study. Their formulations are respectively:

$$\log_{10} fO_2/fO_2^o = -25.495 \exp(-0.0009695T) - \frac{775P}{T} + 0.8686 \ln(f_W/f_W^o)$$

$$-27.73X_{PHL}\bullet(1.654)X_{ANN} + 0.3077X_{PHL} - X_{PDO})$$
$$-36.8(X^2_{ANN} - X^2_{PDO}) - 0.5791 \ln(\frac{X_{ANN}}{X_{PDO}}) \quad (9.5)$$

$$\text{and } \log_{10} fO_2/fO_2^o = 0.8686 \ln(f_W/f_W^o) - 9638/T - 13.38 - 2.6058 \ln X_{Ann}$$
$$+ \frac{220\ P}{T} - 1.7372 \ln a_{mt} - 0.8686 \ln a_{or} \quad (9.6)$$

for T = temperature in degrees Kelvin,

P = pressure in GPa,

fugacities in GPa,

X_{ANN}, X_{PDO} and X_{PHL} = the cation proportions of FeII, FeIII and Mg respectively, in the octohedral site of biotite,

a_{mt} = activity of Fe_3O_4 in magnetite,

a_{or} = activity of $KAlSi_3O_8$ in alkali feldspar = $\gamma_{or}X_{or}$,

for

$$\gamma_{or} = \exp\ [X^2_{Ab}(3070/T + 0.8450P/T - 1.15) - X_{or}(3231/T + 0.9260P/T - 0.861)]$$

(Brown & Parsons, 1981)

Four biotite separates were analysed for FeIII and FeII by E. Kiss (R.S.E.S., Australian National University, Canberra) (Appendix G). Two were taken from mafic mineral segregations, one from each of the Boobyalla and Babel Island Suites (samples #62634 and #67539, respectively). The other two were extracted from the phyric-rich Boobyalla Suite porphyry #62619. One is a phenocrystic biotite whereas the other is pseudomorphous after garnet.

Evaluation of equation 9.6 was made using compositions of the biotite and alkali feldspar separates. Alkali feldspar of composition $X_{Or} = 0.7$ was chosen. Assumptions made are that magnetite exists and has a composition given by $X^{mt}_{Fe3O4} = 0.9$, $\gamma^{mt}_{Fe3O4} = 1$ (Czermanske & Wones, 1973), $X^{bi}_F = X^{bi}_{Cl} = X^{bi}_O = 0$, $P_W = P_\Sigma$ and the range in P_Σ as a function of temperature is that illustrated in Fig. 9.9 in accordance with the results of the barometry undertaken in Section 9.2.

Temperature estimates were obtained using the Holdaway & Lee (1977) version of the garnet/biotite thermometer (formulation #2 of Table 9.2). For samples #62634 and 67539, the bulk-biotite and garnet-rim compositions were used to obtain the requisite biotite/garnet $K_D^{Fe/Mg}$ values. Although garnet has not been found in this rock, the pseudomorphic biotite present (Plate 3, Fig. B) is thought to have been after this phase (Chapter 5,

FIGURE 9.9

OXYGEN FUGACIMETRY

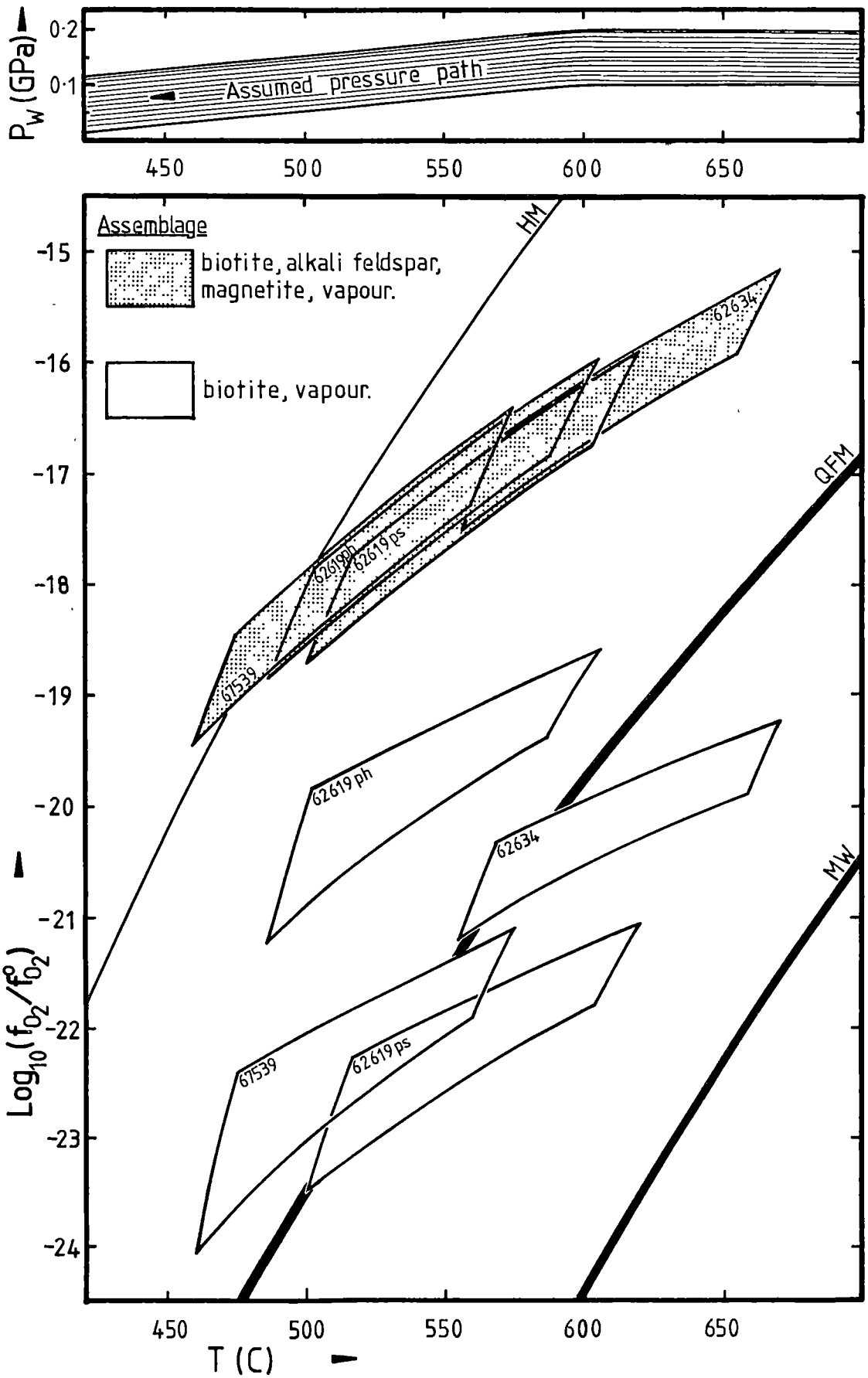

Plate 4, Fig. E). Using the same thermometer, equilibrium temperature estimates were made for these two biotite separates, assuming them to have been in equilibrium with the rims of garnet from the porphyry #62595 ($mg_{garnet\ rim}$ = 2.9). This garnet compositon is similar to many other garnet-rim compositions from this suite. Sample #62595 contains biotites which have magnesium numbers very similar to those of the bulk biotite separates from #62619 (Appendix G).

Evaluation of equation 9.5 was made using the same data and relevant compositional intensive variable assumptions as before.

9.4.4 Results and Discussion

Fig. 9.9 shows $\log_{10}fO_2$,T fields derived for the assemblages containing the four biotites, using both fugacimeters. Those delineated using the magnetite-bearing fugacimeter are up to 4.2 $\log_{10}fO_2$ units higher than those fields defined using the magnetite-absent fugacimeter. The former are hypothetical fields because magnetite is not present in their assemblages. They give upper limits to the fO_2 of the (biotite-alkali feldspar-vapour) equilibria in the rocks.

The fields defined using the magnetite-absent fugacimeter cluster around the band for the QFM buffer, except for one: that involving the biotite #62619ph which returned twice the FeIII/FeII ratio of the other separates. The reason for this discrepancy is unknown. Oxygen fugacities in this fO_2-T region, for these granites are consistent with their more reduced magnetite-absent, ilmenite-bearing assemblages. The biotite-vapour fugacimeter is therefore considered to be a useful formulation to determine the fO_2 of granitic assemblages, especially those which do not contain magnetite.

The major limitation of each of the applied fugacimeters is considered to be their simplistic activity models of endmember components in the complex mineral: biotite. The Wones (1981) fugacimeter considers only the molar proportion of annite in biotite, i.e. some 50 mol% of the Musselroe and Boobyalla Suite biotite separate compositions. The biotite-vapour fugacimeter considers some 65 mol% of these biotites but ignores potential roles of octahedral aluminium and titanium. These two constituents are considered to play an important role in the buffering of both water and oxygen in granitic assemblages because of their inter-relationships through the proposed substitution mechanism: $Al6HTi_{-1}[\ ]_{-1}$ (Chapter 7 and 8).

9.5 WATER FUGACIMETRY

For the granitic assemblages of northeastern Tasmania, f_W is poorly known. Abundant pegmatites in the Boobyalla, Babel Island, Musselroe and Poimena Suites are interpreted to indicate that water was the dominant constituent of the vapour phase during the magmatic and subsolidus stages of the petrogenesis of these granites. An upper limit for P_W is therefore the total pressure (P_Σ) deduced for these granites.

The roles of other potential vapour constituents such as HF, HCl, B_2O_3 and CO_2 cannot be quantitatively assessed at present. Some shifts noted in the position of the quinary cotectic line of the rhyolite tetrahedron for felsic porphyry matrix compositions have been ascribed in the next Chapter, to the effects of $B_2O_3 \pm$ HF in the melt . The shifts could be ascribed to ~4% B_2O_3 or to ~1% of HF in the melt phase which would implicate a vapour containing up to 12% B_2O_3 or up to 0.2% HF using the vapour/haplogranite melt partition coefficients for B_2O_3 and HF of Pichavant (1981) and Hards (1976), respectively. Fluorine was not determined in biotites so the role of fluorine in the petrogenesis of the granites of suites other than those of the fluorite- and topaz-containing Babel Island Suite is unknown. Chlorine is present in many biotites, usually at concentrations of $\leq$0.1%. However concentrations up to ~0.6% occur in matrix biotites of the Babel Island Suite. HCl is partitioned largely into the vapour phase, relative to melt (Burnham, 1967) so this component was a significant constituent of some vapours.

The content of water in the magmas of the northeast Tasmanian granites prior to their being vapour-saturated, can be constrained using experimental petrological data of the stability of the hydrous phase: biotite. Burnham (1979) considers that melts must contain mole fractions of water (X_w^m) in excess of 0.3 in order to stabilize the hydrous phases: hydroxylhornblende and hydroxybiotite. This limit may be decreased if fluorine or titanium are present. These elements form the thermally stable components: fluoamphibole, fluobiotite (Burnham, 1979; Foley et al., 1986), and probably titanoxy-amphibole and -biotite. The resulting dilution of hydroxy-phase components will allow the respective solid solutions to exist in melts in which $X_w^m < 0.3$ (Burnham, 1979). Although they may exist in melts with $X_w^m = 0.3$, the maximum thermal stability of both hydroxy-phases is attained when $X_w^m \sim 0.5$ (Yoder & Kushiro, 1969; Holloway & Burnham, 1972).

Biotite is an early petrogenetic phase in the peraluminous suites of northeastern Tasmania (Chapter 4). In the Boobyalla Suite, it was present throughout magmatic evolution and is considered to have been a phase in the source region. For this suite, estimates of the weight percent, the mole

fraction and the activity of water in the early melt phase of 4.65, 0.45 and 0.46 respectively may be obtained, using the albite-analogue model for solution of water in silicate melts of Burnham (1975, 1979), assuming that:

(a) the composition of the anhydrous portion of the melt was that of the relatively mafic matrix separate from porphyry #62595;

(b) for this composition, water-saturation ($a_w^m = 1$) occurred at a pressure of 0.15 GPa as is deduced in Section 9.2 and a temperature of 825°C; and

(c) the source region of partial melting was at 850°C and 0.6 GPa P_Σ (as deduced in Sections 9.2 and 9.3 above).

The X_w^m value of 0.46 is consistent with the stability of magmatic biotite. The deduced water content in the initial melt of 4.65% is similar to that determined by Clemens & Wall (1981) of 3-5% required to generate the phenocryst phases which occur in volcanics of the Musselroe Suite cropping out in the Strathbogie Batholith of central Victoria.

For the metaluminous Wybalenna Suite, biotite is a late petrogenetic phase which replaces hornblende. The late appearance of biotite is likely to be due to low a_{K2O}^m rather than to low X_w^m, because alkali feldspar (the phase richest in K_2O) is petrogenetically later still and because the X_w^m required to stabilize the earlier hornblende is about the same as that required to stabilize the biotite that pseudomorphs it (Burnham, 1976). X_w^m values for the early melts of **this** suite were probably less than 0.3, however, because hornblende itself is rarely a phenocrystic phase and usually pseudomorphs pyroxenes (Chapters 4 and 7).

9.6 PT PATHS FOR GRANITE SUITES

9.6.1 Introduction

Investigation of phase equilibria in the granitic rocks of northeastern Tasmania has shown that many solid solution phases have compositions reflecting subsolidus equilibrium conditions. Only the cores of garnet and plagioclase phenocrysts and those of alkali feldspar megacrysts retain compositions which are determined by the conditions during the early stages of magma evolution. Whole biotite, cordierite and orthopyroxene and rim garnet and hornblende, as well as porphyry matrixes have compositions which reflect various subsolidus equilibrium conditions. Hornblende phenocryst cores and plagioclase mantles occupy intermediate positions with their compositions probably being determined during late magmatic stages. The composition of the solid solution phases are therefore reflective of many different equilibria with disequilibrium between sub-assemblages being common.

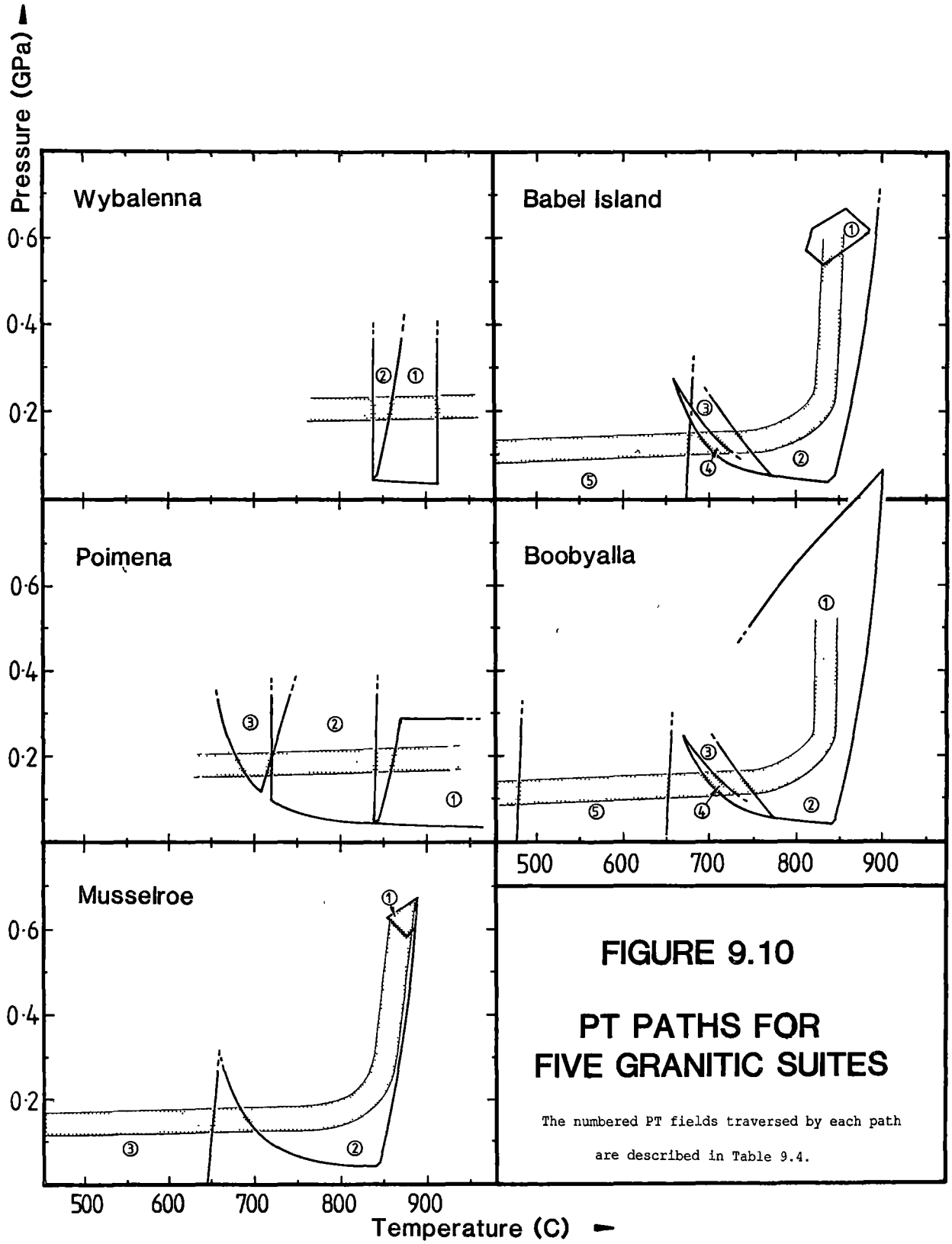

FIGURE 9.10

PT PATHS FOR FIVE GRANITIC SUITES

The numbered PT fields traversed by each path are described in Table 9.4.

By combining intensive variable data derived for different equilibria in any one suite, it is possible to reconstruct portions of the PT paths travelled during petrogenesis. This has been undertaken for five suites of the NBTB. Graphs depicting these PT paths are shown in Fig.9.10. Equilibria used to construct the PT fields of Fig. 9.10 are listed in Table 9.4.

9.6.2 Wybalenna Suite

The PT path for this suite is poorly constrained. Neither source PT conditions nor emplacement pressures are known. Hornblende-melt (Na/K) exchange temperatures for two porphyries (Fig. 9.9) give lower limiting estimates of the emplacement temperature of ~865°C with $X_w^m \geq 0.3$. However, other magmas of this suite such as those which produced the porphyries #62589 and #62610, had $X_w^m < 0.3$ because the only mafic phenocrysts present were clinopyroxene (now pseudomorphed by actinolite). This feature suggests emplacement temperatures may have been higher than those estimated above.

9.6.3 Poimena Suite

For this suite, source region PT conditions are unknown, as are emplacement temperatures. The latter temperatures however exceeded that of the stability of the assemblage (biotite+quartz) (assuming that a_w^m was >0.3) because quartz but not biotite phenocrysts occur in the porphyry #62612. A zircon-melt temperature of 780±60°C was derived using the matrix composition of porphyry #67533. Pressure has not been constrained using phase equilibria of this suite. However the Holts Point Porphyry (#62612) has synplutonically intruded the crystal-rich Boobyalla Suite Loccota Porphyry (Plate 2, Fig. F), for which emplacement pressures of 0.15±0.05 GPa have been deduced (Section 9.2, above). Emplacement pressures for the Poimena Suite are therefore considered to be comparable with those of the Boobyalla Suite.

9.6.4 Musselroe Suite

Estimated source conditions for this suite are 0.62 GPa and 875°C, based upon compositional data of the mafic mineral segregation #67539 from the Ansons Bay Pluton (Section 9.2). Emplacement temperatures of $\leq$~850°C and pressures of >0.04 GPa are likely because biotite is thought to have been present throughout magmatic evolution.

9.6.5 Boobyalla Suite

Source conditions for this suite are estimated to have been ~0.60 GPa and ~850°C, using data from the mafic mineral segregations: samples #67523 and #67529. Emplacement temperatures of <850°C are likely because (quartz+biotite) assemblages are ubiquitous and because estimates of a_w^m exceed the limit of 0.3 below which biotite is unstable. Solidus pressures

Table 9.4

Equilibria Constraining PT Paths During Petrogenesis of NE Tasmanian Granites

Suite	PT-field Number	Equilibrium Symbol	Samples
Wybalenna	1	a,b,h	62602 (no phenocrystic biotite)
	2	a,b,h	62593 (phenocrystic biotite)
Poimena	1	a,d,h	62612 (no phenocrystic biotite)
	2	a,c	67533
	3	a,e	62596
Musselroe	1	f,g,h	67539
	2	a,h	62538, 67539
	3	i,j	43271, 62586, 62588, 67539
Boobyalla	1	e	62595, 62614
		f,g	68523, 68529
	2	a,h	62595, 62605, 62606, 62616-62619, 62624, 62627
	3	a,k	62613, 62614, 62616-62618, 67547, 67548 68523, 68548 (all with andalusite phenocrysts)
	4	l	43156 (melt corroded, low-mg biotite phenocrysts)
	5	i,j	43151, 62595, 43204, 43202, 43252, 68525, 68523
Babel Is.	1	g,h	68550 (with phenocrystic biotite)
	2	a,h	62575, 62579 (with phenocrystic biotite)
	3	a,k	62543, 62544
	4	l	62544 (with melt-corroded low-mg biotite phenocrysts)
	5	i	68550

Constraining Equilibria:

a Peraluminous granite water-saturated solidus (Johannes, 1984 -10°C).
b Hornblende-melt (Na-K) exchange thermometry (Fig. 9.9).
c Zircon-melt thermometry.
d Upper pressure limit of the synplutonically intruded Holts Point Porphyry deduced from the occurrence of corroded biotite phenocrysts of composition mg = 13.5 in the Boobyalla Suite sample #62618, implying $P_W \leq 0.29$ GPa by ABCKLQV barometry (Fig. 8.4).
e Two-feldspar NaKCa exchange thermometry (Fig. 9.5).
f AGPQ barometry (Fig. 9.2).
g ABCGKQV thermobarometry (Fig. 9.4).
h Estimated upper limit to stability of assemblage (quartz+aluminous, titaniferous biotite) (Bohlen et al., 1983 +20°C).
i Biotite-garnet Fe^*Mg_{-1} exchange thermometry (Fig. 9.7).
j Cordierite-garnet Fe-Mg exchange barometry (Fig. 9.7).
k Andalusite-sillimanite melt barometry (Fig. 9.1): limit after Salje (1986).
l ABCKLQV barometry (Fig. 9.3).

are 0.15±0.05 GPa, estimated on the basis of ABCKQV barometry and the stability field of the assemblage (andalusite+melt).

9.6.6 Babel Island Suite

Source conditions are poorly constrained for this suite. Pressures are limited to those between 0.86 and 0.42 GPa and temperatures to between 775°C and 900°C using compositional data from phases present in the mafic mineral segregation #68550. As for the preceding two suites, emplacement temperatures are considered to have been <850°C, limited by the ubiquity of the (quartz+biotite) assemblage. The solidus pressure is considered to have been within the range estimated for the Boobyalla Suite (above), using the same criteria.

Cooling paths for Musselroe, Boobyalla and Babel Island Suite magmas are shown in Fig. 9.10 as having two stages:

(a) near-isothermal decompression followed by

(b) near-isobaric cooling.

The latter stage is similar to the PT path tracing the phase boundary of vapour-containing low-pressure magmas undergoing second boiling, as indicated by the albite-water analogue model of granitic melts of Burnham (1979).

PT paths such as those derived in this section (Fig. 9.10) are essential in the petrogenetic modelling of granitic suites. Such modelling is undertaken for the Boobyalla and Babel Island Suites, in Chapter 12.

Chapter 10
FELSIC PHASE RELATIONSHIPS

10.1 INTRODUCTION

In this chapter, experimentally-determined phase relationships in felsic simple-system magmatic systems are briefly reviewed and their relevance to the petrogenesis of granites discussed. The CIPW normative compositions of northeast Tasmanian granites, porphyries and porphyry matrix separates are then described. The differences between the trends of these three rock types is then used (in the context of the simple-system relationships described previously) to estimate the physical nature of the former magmas of the coarsely crystalline granites. By this method, information may be obtained about the nature of the magmas of rocks which have lost almost all magmatic textural features.

The general physical nature of the granite magmas deduced in this chapter is used in Chapter 12, where detailed petrogenetic models are constructed of the former magmas of the Boobyalla and Babel Island Suite granites.

10.2 MAGMATIC RELATIONSHIPS IN GRANITIC SIMPLE SYSTEMS

The haplogranite system is the fundamental simple-system analogue of granite systems. It is a quaternary system, involving the normative components: albite, orthoclase, quartz and water, symbolized (ab), (or), (qz), (w). Magmatic equilibria below 1.0 GPa in this system, have been experimentally studied by Tuttle & Bowen (1958), Luth et al. (1964) and Steiner et al. (1975, **in** Luth, 1976). Their data are depicted on a pseudoternary (qz, ab, or) diagram projected from (W) (Fig. 10.1A). Shown on this diagram is the path of quartz-alkali feldspar minima (below the alkali feldspar singular point at ~0.36 GPa P_W and ~660^oC (Luth, 1976) and quartz-potassic feldspar-sodic feldspar eutectics (at pressures above those of the singular point), over a pressure range of from 0.05 to 1 GPa P_W.

This is the trace of the two univariant eutectic reactions which meet at the singular point and which together constitute the solidus at pressures below 1.0 GPa $P_W = P_\Sigma$, in this system. The P_W-T position of this solidus was recently redetermined experimentally by Johannes (1984). It is his solidus minus 10^oC, which has been used as a reference solidus for granites, as described in the introduction of the previous chapter.

Also shown on Fig. 10.1A are the high (or) portions of the (quartz+alkali feldspar) cotectics for pressures of 0.05, 0.1 and 0.3 GPa and the (quartz+potassic feldspar) cotectic for P_W = 0.5 GPa. These lines depict the TX loci of liquids in equilibrium with quartz and potassic

alkali feldspar. They are also the TX paths travelled from right to left, by cooling liquids which are fractionating these two phases. Studies of vapour-undersaturated equilibria yield conflicting results. Data of Luth (1969) and Steiner et al. (1975, **in** Luth, 1976) indicate that vapour-undersaturated melts in equilibrium with quartz and alkali feldspar at a given pressure are more potassic and slightly more silicic than their vapour-saturated counterparts. However the application of the quasi-crystalline albite-analogue melt model to the haplogranitite system by Burnham & Nekvasil (1986) and Nekvasil & Burnham (1987) predicts the opposite, that is, with increasing vapour-under/saturation, haplogranitic melts become increasingly more sodic and less silicic.

Equilibria in the haplogranite system though simple, are relevant to the petrogenesis of many Blue Tier Batholith granites because

(a) the equilibria are reasonably well known (Luth, 1976; Burnham & Nekvasil, 1986; Nekvasil & Burnham, 1987) and therefore provide an adequate reference set with which to compare the compositions of natural rocks; and

(b) most of the rock compositions concerned contain >90% normative (ab+or+qz), except for those of the mafic I-type granites, which contain $\geq$70% of these components.

Addition of other components will affect equilibrium boundaries in the haplogranite system or its subsystems. For instance, both the (or-qz) and (ab-qz) system eutectics are lowered in temperature and shifted to higher (qz) mass fractions when normative corundum is added to each system (Voigt, 1983 and Joyce, 1985, in Burnham & Nekvasil, 1986). This feature is shown in Fig. 10.1C for $P_W = P_\Sigma = 0.2$ GPa. The amount of normative corundum required to effect these shifts is that required to saturate the eutectic melt in sillimanite: a mere 3.4% (op. cit.). Although only the two quartz-containing subsystems have been studied, it is likely that the entire quartz feldspar cotectic line in the quinary (ab-or-qz-co) system (for (co): normative corundum), is shifted towards the (qz) apex in the pseudoternary (ab-or-qz) projection, as depicted in Fig. 10.1C.

Addition of either F_2O_{-1} or B_2O_3 to the haplogranite system at $P_W = P_\Sigma = 0.1$ GPa, causes the quartz-feldspar cotectic line to shift away from the (qz) apex (e.g. Manning, 1981; Pichavant, 1981). Furthermore, minimum positions are shifted towards the (ab) apex, an effect most marked with F_2O_{-1}; systems containing 1% F have cotectics displaced a similar amount to those of systems containing ~4.5% B_2O_3 (op. cit.). The depression of the solidus temperatures with the addition of each of these components however, are comparable (op. cit.). These changes to haplogranitic phase boundaries are shown in Fig. 10.1D.

LIQUIDUS PHASE RELATIONSHIPS FOR VAPOUR-SATURATED QUARTZO FELDSPATHIC COMPOSITIONS

FIGURE 10.1

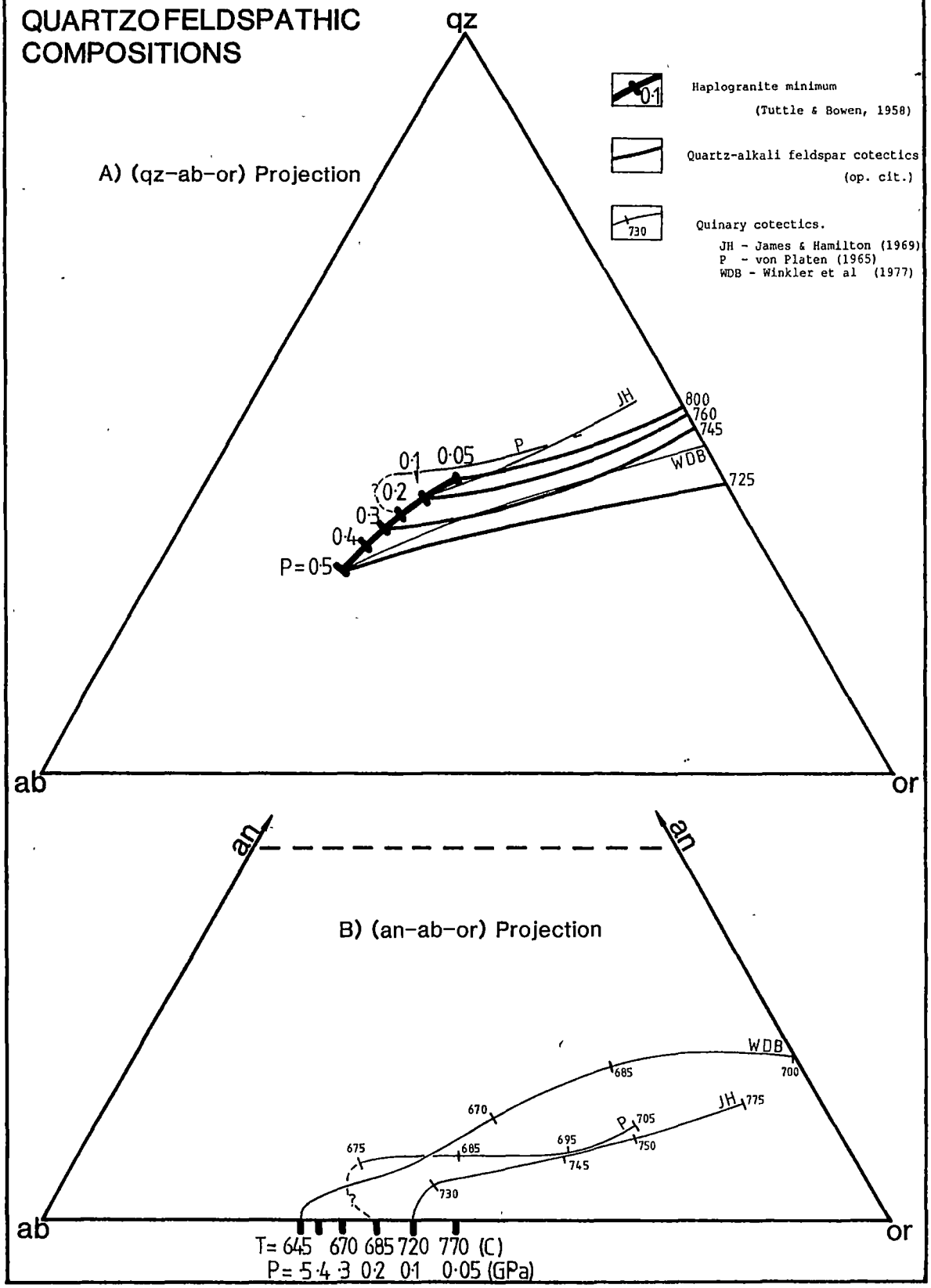

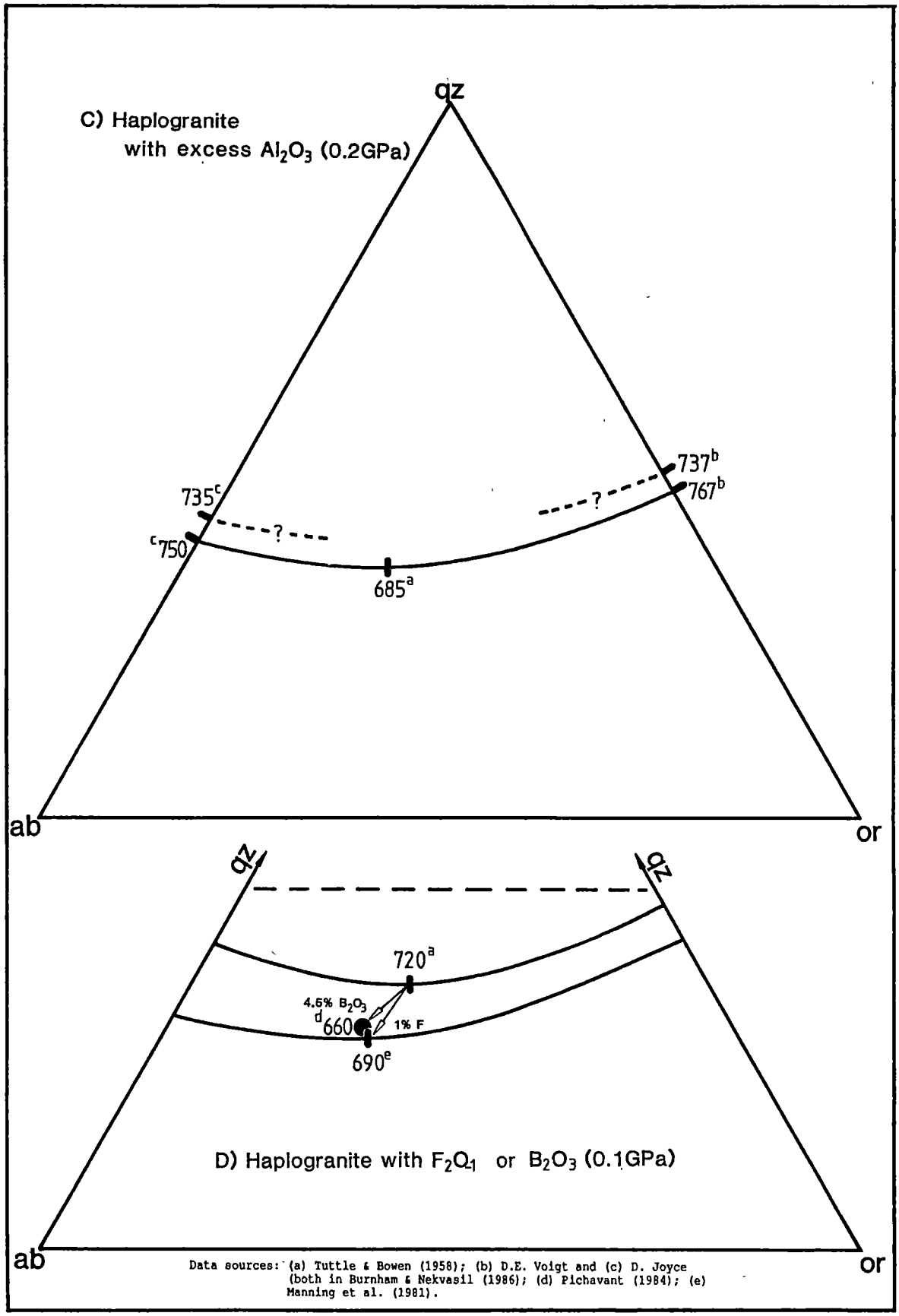

Data sources: (a) Tuttle & Bowen (1958); (b) D.E. Voigt and (c) D. Joyce (both in Burnham & Nekvasil (1986); (d) Pichavant (1984); (e) Manning et al. (1981).

Addition of anorthite to the haplogranite system generates the quinary (ab-an-or-qz-w) or haplogranodiorite system. Phase relationships in this system have been experimentally studied by von Platen (1965), James & Hamilton (1969), Whitney (1975) and Winkler et al. (1977). They are most commonly depicted within the (ab-an-or-qz) or rhyolite tetrahedron, projected from (w), for the case when $P_W = P_\Sigma$ (e.g. Presnall & Bateman, 1973; Carmichael et al., 1974, p.228). The rhyolite tetrahedron contains, for a given pressure, temperature-contoured cotectic surfaces, separating the phase volumes of quartz, plagioclase and alkali feldspar. These surfaces meet to define a quinary cotectic line along which the five phases: liquid, two feldspars, quartz and vapour, coexist. This line terminates at a point on the an-absent face of the tetrahedron, on the vapour-saturated haplogranite solidus at pressures above the alkali feldspar singular point at 0.36 GPa, but at points above the (qz-ab-or) plane containing the haplogranite solidus, at pressures below 0.36 GPa. The projection of the 0.1 GPa cotectic line of James & Hamilton (1969), the 0.2 GPa P_W line of von Platen (1965) and the 0.5 GPa P_W line of Winkler et al. (1977), are depicted on the (qz-ab-or) and (an-ab-or) pseudoternary projections in Figs 10.1A and B respectively.

Phase relationships in the haplogranodiorite system should be of greater relevance to the study of natural granites than those of the haplogranite system because a greater proportion of the anhydrous compositions of rocks can be described by the (ab-an-or-qz) normative assemblage. On this basis for instance, Presnall & Bateman (1973) proposed that mafic to felsic granite sequences in the Sierra Nevada Batholith were formed by fractional crystallization of the liquid component of a magma generated by partial fusion of a model lower crustal source composition. Relative to schematic phase boundaries within the rhyolite tetrahedron estimated for equilibria at 0.5 GPa P_W, the trend of the normative (ab-an-or-qz) compositions of the rocks extends in a crescent, from within the plagioclase phase field at moderate values of an/(an+ab+or+qz) to the vicinity of the plagioclase-quartz cotectic surface and down this surface to the vicinity of the quinary cotectic line at low an/(an+ab+or+qz) values. They consider this trend to indicate that the liquid of the magma producing each mafic to felsic sequence, was initially only plagioclase-phyric, then evolved to become plagioclase+quartz-phyric and finally plagioclase+ quartz+ alkali feldspar-phyric.

Data trends within the rhyolite tetrahedron however, must be interpreted with caution. Although the analysis by Presnall & Bateman (1973) was restricted to rocks with $\leq$20% of **non**-quartz-feldspathic normative components, it has already been shown (Fig. 10.1C,D) that other

components which could have been present, can shift phase boundaries. Like water, most of both the fluorine and the boron in a magmatic assemblage will be lost from the system below the solidus, leaving little evidence of their former presence other than their influence on the magmatic phase relationships.

Marked inconsistencies between the positions of the 0.1 and 0.2 GPa $P_W = P_\Sigma$ quinary cotectic lines within the rhyolite tetrahedron (Fig. 10.1B) indicate that little information is available to fix the positions of the cotectic surface at these or at other pressures (Luth, 1976). Furthermore, vapour-undersaturated phase relationships in the haplogranodiorite system are poorly known. However, the studies of Whitney (1972, 1975) indicate that the position of the cotectic surfaces within the rhyolite tetrahedron is dependent upon the partial pressure of water, in addition to total pressure.

The most important criticism of the use of the haplogranodiorite system as an analogue for granites, is the possibility that none of the boundaries yet mapped within the rhyolite tetrahedron are representive of equilibrium phase relationships (Johannes, 1978, 1980, 1984); plagioclase appears to melt nearly stoichiometrically at temperatures below $\sim$800°C, even under water-saturated experimental conditions, with equilibrium requiring run times of $\geq 10^5$ years for temperatures $\leq$730°C (op. cit.). These data imply very low rates of binary diffusion in plagioclase, consistent with the low rates given for this phase by Freer (1981).

The consequences of the metastable melting of plagioclase is that the phase boundaries identified by von Platen (1965), James & Hamilton (1969) and Winkler et al. (1977) are all likely to be too calcic. Run times of James & Hamilton (1969) were $\leq$26 days for temperatures within the range 745° to 855°C whereas those of Winkler et al. were only 7 days for runs within the temperature range 700° to 730°C.

Although the phase equilibria in the rhyolite tetrahedron are poorly known, phase boundaries estimated to extend from the 0.1 GPa P_W quinary cotectic line of James and Hamilton (1969) have been used in projections of the tetrahedron, as references with which to compare distributions of normative data of the Furneaux granitic rocks. The use of these boundaries is justified because:

(a) they can be used as high (an) estimates of equilibrium 0.1 GPa P_W phase boundaries;

(b) solidus (and probably emplacement) pressures for many of the Furneaux suites are considered to have been about 0.1 GPa (see Chapter 9); and

(c) anorthite is a substantial proportion of the normative composition of at least the adamellitic to tonalitic compositions (see Fig. 1.1); and

FIGURE 10.2 CIPW NORMATIVE COMPOSITIONS OF FURNEAUX GRANITIC ROCKS

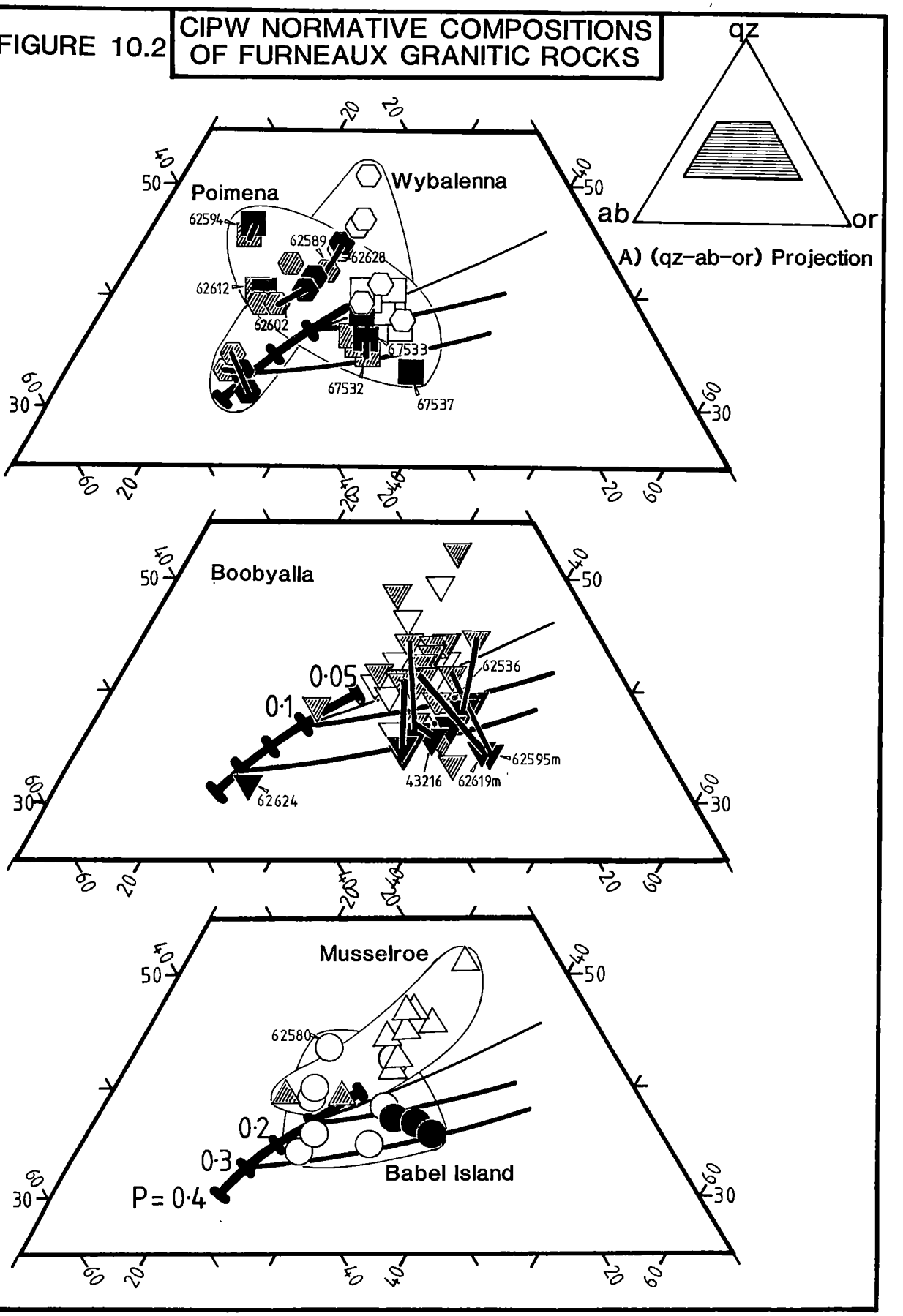

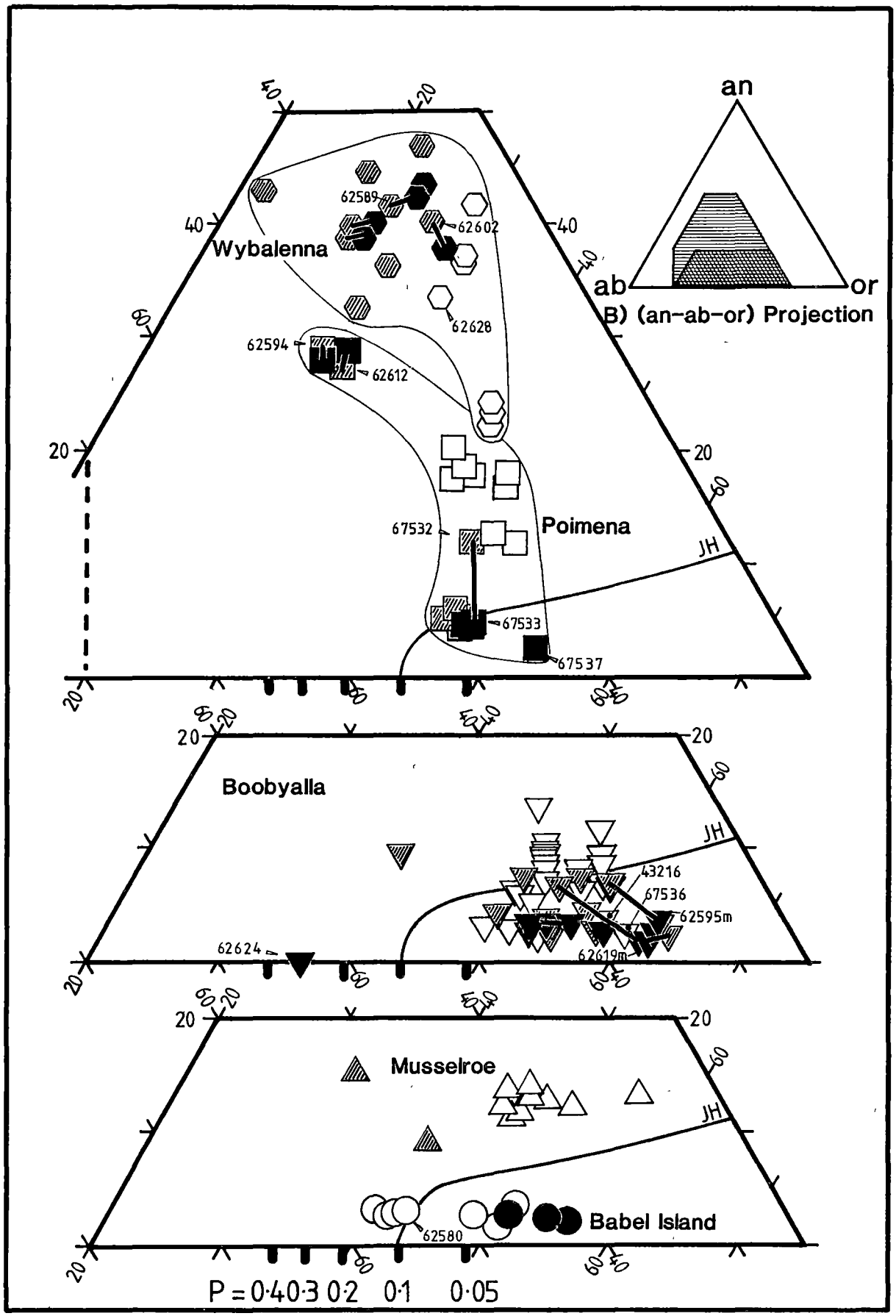

Symbols: open - granites, shaded - porphyries, filled - porphyry matrixes. Cotectic lines as in Fig. 10.1, pressure in GPa.

(d) the boundaries are used only in a qualitative way, to locate and propose the nature of the magmatic assemblages that the samples represented, as undertaken by Presnall & Bateman (1973) for the granites of the Sierra Nevada Batholith. No attempt is made to designate pressures or temperatures using the phase boundaries.

10.3 NORMATIVE COMPOSITIONS OF FURNEAUX BATHOLITH GRANITIC ROCKS

The normative compositions of 55 granites, 37 porphyries and 25 porphyry matrix separates from five granite suites have been studied (cf. Appendix E). Eighty-eight samples (37 granites, 26 porphyries and the matrixes) are from the Furneaux granites (this work), and 29 samples (18 granites and 11 porphyries) are from the Furneaux and NBTB granites (data from Cocker, 1977; Higgins et al., 1985; and courtesy of Dr M. McClenaghan, Tasmania Department of Mines, and Dr B.,W. Chappell, Australian National University). Where Fe_2O_3 has not been determined, such as in the data obtained in this study, analyses were recalculated assuming an Fe_2O_3/FeO weight ratio of 0.25.

The resulting normative data have been plotted on (qz-ab-an) and (an-ab-an) projections of the rhyolitic tetrahedron (Fig. 10.2). The trends within the tetrahedron are located relative to the estimated positions of the 0.1 GPa P_W phase boundaries of James & Hamilton (1969). The locations are listed in Table 10.1.

Features thought to indicate the physical nature of the former magmas of each rock type are now described.

10.3.1 Matrixes

Matrix points are located near low-pressure phase boundaries except for some for the Wybalenna Suite which form an extension into the plagioclase phase field from the (plagioclase+quartz) cotectic surface at high proportions of (an). Porphyry matrix separates have the haplogranodiorite-system compositions expected of melts which were in equilibrium with the set of felsic phyric phases present in each porphyry. In each suite, there is a trend of matrix points which parallels part of the broad curved path of whole-rock data which Presnall & Bateman (1973) consider traces the trend of low-pressure fractional crystallization of magmas of Sierra Nevada Batholith granites.

10.3.2 Porphyries

For coexisting (porphyry whole-rock+matrix) pairs, whole-rock points do not plot in the same position as matrix points. Tie-lines joining the two positions extend from the matrix point through the whole-rock point in a direction towards the normative composition of the porphyries' bulk phyric assemblage. For the Wybalenna Suite and for the mafic porphyries of

the Poimena Suite, tie-lines extended through whole-rock points intersect either the tetrahedron's (an-ab-qz) face or its (ab-or-qz) face, near the (ab) apex. This is consistent with their plagioclase-rich, alkali feldspar-absent phyric assemblages (Chapter 4). For the Boobyalla Suite and felsic rocks of the Poimena Suite however, tie-line extensions intersect all except the (qz-ab-or) face (i.e. the base) of the tetrahedron. Boobyalla Suite and felsic Poimena Suite porphyry whole-rocks are generally richer in (an) and (qz) than are the (or)-rich matrixes, consistent with the presence of quartz and calcic and plagioclase phenocrysts in these rocks (Chapter 4).

10.3.3 Granites

Data trends for granites are usually located **within** phase fields, rather than being proximal to low-pressure phase boundaries like most of the matrix trends. An exception is the Wybalenna Suite granite trend which forms a linear trend lying close to the estimated position of the (plagioclase+quartz) cotectic surface.

Normative positions for Poimena Suite and felsic Wybalenna Suite granites have anorthite proportions which are considerably greater than those of the quinary cotectic reference line, even though these rocks contain alkali feldspar megacrysts. These same granites are generally richer in (or) than are porphyries or even the porphyry matrixes of each respective suite.

10.4 INTERPRETATION

10.4.1 Matrixes

Relative to the estimated equilibrium phase boundaries in the rhyolite tetrahedron, matrix trends appear to be first-order estimates of liquid trends. Matrix points are located close to the positions estimated for low-pressure phase boundaries which are appropriate for the variety of felsic phases present in the phyric phase assemblage of each porphyry.

Matrixes which were extracted from porphyries containing three felsic phases, have matrix points which are displaced from the 0.1 GPa $P_W = P_\Sigma$quinary cotectic line of James & Hamilton (1969) into the alkali feldspar phase field of the tetrahedron. This feature probably reflects the overly calcic compositions of the (metastable) melts used to define the reference cotectic line, as described above.

The main matrix trend for the Boobyalla Suite extends from the haplogranite system cotectic line at ~1.5 kbar to that at ~3.5 kbar for the aplite #62624. This apparent low to high pressure trend probably reflects the effects of increasing concentrations of boron (and possibly fluorine) in the evolving melt, as evidenced by the occurrance of tourmaline patches

throughout or adjacent to this and many other felsic dyke rocks of this suite.

The Poimena Suite aplite #67537 also contains tourmaline which may explain the high apparent pressure indicated from its composition.

The reason for the displacement of the matrix points of two Boobyalla Suite porphyries (#62595 and #62619) towards the (or) apex from those forming the main matrix trend, is unknown. Possible explanations are that:

(a) the magma of #62595 may have been water-undersaturated and the melt therefore more potasic than that of the melts of other porphyries (Luth, 1969, 1976);

(b) the matrix of sample #62695 may contain some of the phenocrystic alkali feldspar or biotite present in the porphyry, because the mean matrix grainsize at 0.8 mm is larger than that of other sepearated matrixes, making physical separation of this matrix from its phyric assemblage less likely; and

(c) sample #62619 was taken from the base of a sill occurring within ~1 m of a large pegmatite. The matrix may therefore have been altered subsequent to intrusion, by exchange with high B_2O_3 (Pichevant, 1981) or K^+/H^+ (Rose & Burt, 1979) hydrothermal fluids.

10.4.2 Porphyries

The direction of tie-lines between porphyry whole-rock and matrix pairs reflects the mineralogies of the magmatic phyric assemblages as described above.

10.4.3 Granites

Four mafic granites of the Wybalenna Suite are rich in (an) contain calcic-cored plagioclase pohenocrysts but do not contain phenocrystic alkali feldspar (Chapter 4). The normative composition of the most felsic sample (#62628) of this group, is close to that of the matrix of the related porphyry #62589. This sample could therefore have been derived from the **in situ** crystallization of a pure melt. However the other samples of the group are richer in both (qz) and (or) than are the matrixes of the related porphyries #62589 and #62602, two samples which are thought to lie in a low-pressure plagioclase+quartz cotectic region. These petrographic and normative compositional features are consistent with their magmatic assemblages having contained plagioclase and quartz phenocrysts in melts which were richer in (or) than the matrixes of porphyries of this suite, but which were still undersaturated in alkali feldspar.

Felsic granites of this suite however, contain megacrystic alkali feldspar, though in minor amounts. These granites also contain calcic cored plagioclase and are richer in (or) than the porphyry matrixes of the suite. These features are consistent with their magmatic assemblages

having contained plagioclase, quartz and alkali feldspar phenocrysts in multi-saturated melts. Such melts must have been located in the quinary cotectic region of the rhyolitic tetrahedron and must have had (an) proportions considerably lower than those of the bulk rock compositions. These estimated low (an) positions, compared with the high (an) positions for the granite whole-rock compositions indicate that the magmatic assemblages for these samples were rich in crystals. Petrographic and phase equilibrium data are therefore inconsistent with the whole-rock trend for this suite being that of a liquid line of descent. The data are consistent however, with most magmatic assemblages of this suite having contained substantial proportions of suspended crystalline phases.

For the Poimena Suite, the granite trend is located mostly within the phase-field of (ab)-rich plagioclase, rather than lying close to a cotectic boundary. The Poimena Suite granites contain calcic-cored plagioclase phenocrysts and megacrystic alkali feldspar indicating that their magmas contained low-(an) multi-saturated melts. Bulk compositions of many of these granites are richer in (an) than is considered possible for a low-pressure alkali feldspar-saturated melt, consistent with the petrographic data, indicating that the magmatic assemblages of these granites (like those of the felsic granites of the Wybalenna Suite) contained substantial proportions of suspended crystals.

Further evidence for these granites having been crystal-rich magmatic assemblages, comes from consideration of two samples taken from a Poimena Suite dyke. Sample #67532 with 44 vol.% of phenocrysts (Appendix Q) contains all three phyric phases. It was taken from the dyke core. Its normative composition lies in the granite trend for this suite. It has considerably more (an) than does the matrix, as indicated from the composition of the aphyric sample #67533b, from the dyke edge. By analogy with sample #67532 therefore, the magmas of the Poimena Suite granites are likely to have been crystal-rich assemblages, .

The most mafic Poimena Suite granites are the most anorthitic and the poorest in alkali feldspar megacrysts. Initial melts in the magmas for this suite may therefore have been under-saturated in alkali feldspar, like the melts of the mafic porphyries #62594 and #62612 of this suite.

The normative compositions of the Boobyalla Suite granites have low proportions of (an) and extend through all three phase fields of the tetrahedron. Many of these granites are more anorthitic than the compositions of the phyric-rich porphyries and like them, contain calcic-cored plagioclases. These cores have a consistent composition of ~ mol. an/(an+ab) = 0.43 (Appendix H, Fig. 7.9) and have compositions reflecting high pressure equilibria (Chapter 9). They are therefore interpreted as

being suspended restitic, solid-phase constituents of the low-pressure granitic magmas of this suite. Most of the granites are richer in (an) than are the porphyry matrix separates (the melt analogues) from this suite. Therefore these granite magmas were crystal-containing suspensions.

In contrast to these, some Boobyalla Suite granites (e.g. samples #43216 and #67536) have compositions falling close to the main matrix trend. These granites have an equigranular, rather than a porphyritic texture. They are likely to have been derived from crystal-poor magmas.

All Boobyalla Suite granite compositions are sufficiently (an)-poor to have been assemblages in which the liquids were saturated in all three felsic phases. There is no indication from their normative data, that alkali feldspar undersaturated liquids participated in their generation.

All Babel Island Suite granites have compositions with very low proportions of (an). Some samples (e.g. #62580) have high proportions of (qz), relative to the low-pressure haplogranite cotectic lines. This may indicate that they were derived from quartz-phyric magmas. It could also be due to a phase boundary shift caused by high contents of normative corundum in the melt, as is experimentally indicated in simple systems (Fig. 10.1C). These plagioclase-poor alkali feldspar granites could therefore have been derived from crystal-poor rather than crystal-rich magmas.

Musselroe Suite granites have compositions which plot well within the quartz phase-field. They are therefore likely to have been derived from quartz-phyric magmas. The granites also contain megacrystic alkali feldspar and calcic cored plagioclase. They were therefore derived from crystal containing magmas.

10.5 CONCLUSIONS

A qualitative graphical comparison is made between the normative compositions of granites, porphyries and matrix separates from five Blue Tier Batholith granite suites. Experimentally-derived simple-system phase boundaries have been used to reference these data. These boundaries however, are considered to indicate compositions which are more calcic than are the true equilibrium boundaries. Conclusions are that:

(a) haplogranodiorite system compositions for matrixes are reasonable estimates of those of felsic melts;

(b) porphyries have normative compositional features consistent with textural and petrographic interpretations (Chapters 3 and 4) indicating them to have been liquid-rich to crystal-rich magmas;

(c) most granites have normative and petrographic features consistent with them having been crystal-rich rather than liquid-rich magmas;

(d) some granites have normative and petrographic features indicating the reverse: viz. that they were derived from liquid-rich rather than crystal-rich magmas;

(e) the only normative granite trend which could trace a **liquid** line of descent is that for the Babel Island Suite; and

(f) normative granite trends for the Wybalenna, Poimena, Musselroe and Boobyalla Suites largely trace the trends of crystal-rich multi-phase magmas.

Chapter 11

MAGMATIC EQUILIBRIA IN THE KFMASH SIMPLE SYSTEM: A SYNTHESIS

11.1 INTRODUCTION

The KFMASH (K_2O-FeO-MgO-Al_2O_3-SiO_2-H_2O) system is a useful analogue of strongly peraluminous granites such as the Boobyalla, Babel Island and Musselroe Suites of the Blue Tier Batholith, because:

(a) the six components in this simple system collectively constitute ~95% of these granites; and

(b) all of the major phases, other than plagioclase, thought to have been present in the magmatic precursors to these granites, also occur in the KFMASH or simpler systems.

Liquidus phase equilibria in natural peraluminous magmas should therefore resemble those in the peraluminous KFMASH system. However, melting reactions will be displaced to lower temperatures relative to their simple-system counterparts because components such as Na_2O and Fe_2O_3 will partition strongly into the melt, thereby expanding the PT field of this phase to lower temperatures. Natural system reactions will also involve additional phases such as plagioclase, ilmenite, apatite, zircon, monazite and xenotime.

In this chapter, a PT grid of KFMASH and simpler system univariant reactions is derived. This grid is then extended to three dimensions using P_W (that is, P_{H2O}) as the third intensive variable. This is achieved using a P_{total}-P_{H2O}-T ($P_\Sigma P_W T$) relationship for KFMASH-system melts which was derived from the results of the experimental $P_\Sigma P_W T$ study of KASH-system melts of Bohlen et al. (1983), as described below.

The Boobyalla Suite phase sequence determined petrographically in Chapter 4 is then compared with a sequence derived from the intersection of a $P_\Sigma P_W T$ path through the 3D KFMASH-system grid derived in this chapter. This comparison leads to a better understanding of phase equilibria in the natural peraluminous granite magmas.

11.2 PHASES AND PHASE COMPOSITIONS

The phases chosen are: andalusite, biotite, cordierite, garnet, hercynite, melt, olivine, orthopyroxene, osumilite, potassium feldspar, quartz, sillimanite and vapour. They are all known to be present in felsic magmas and most are also known in granitic rocks.

For KFMASH equilibria involving most of these phases, the relative K_D values for both the $FeMg_{-1}$ and the tschermak ($Al_2Si_{-1}(Fe,Mg)_{-1}$) exchange vectors must be established for the relevant solutions. The following relative values for each of these exchanges have been assigned:

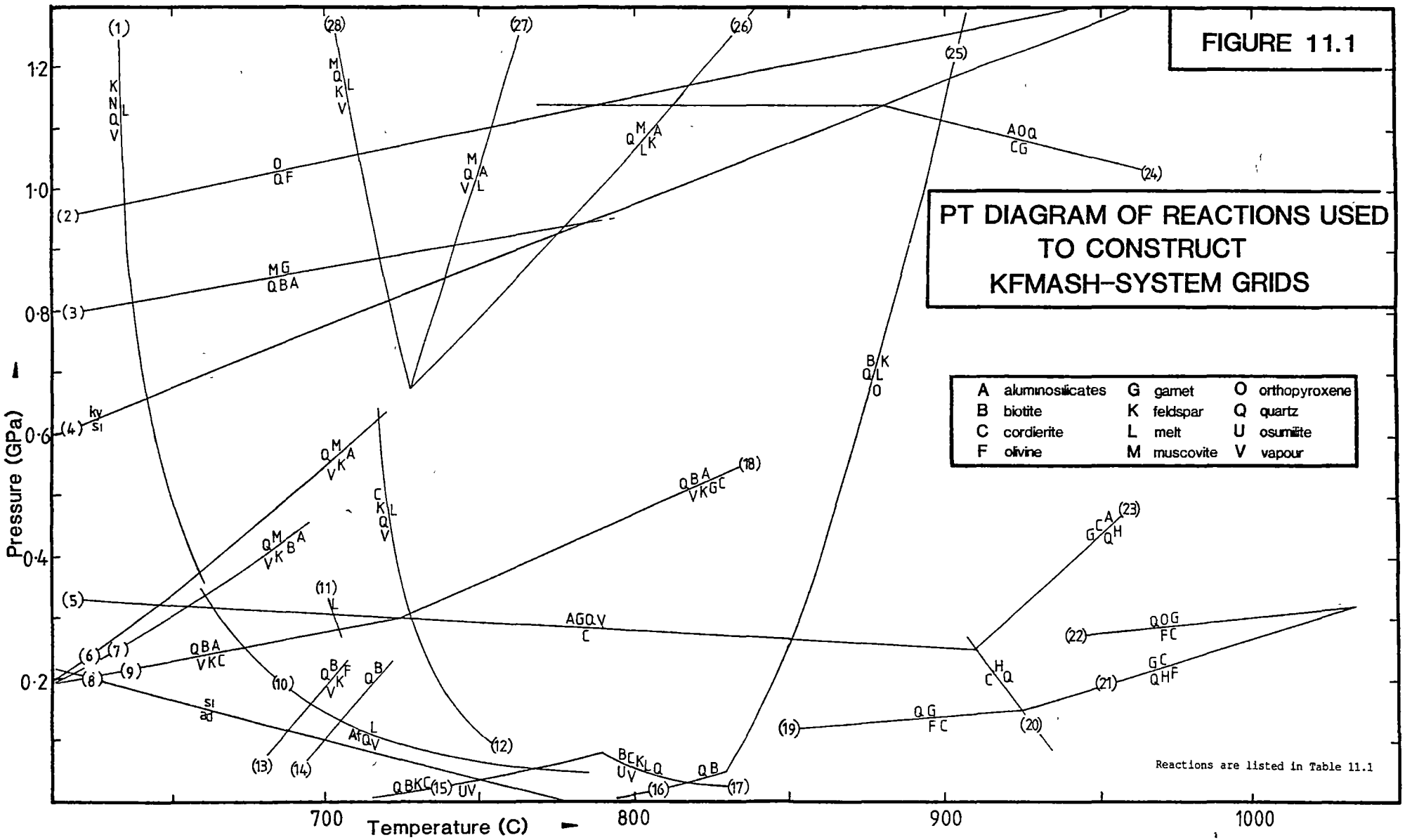
FIGURE 11.1
PT DIAGRAM OF REACTIONS USED TO CONSTRUCT KFMASH-SYSTEM GRIDS
A aluminosilicates
B biotite
C cordierite
F olivine
G garnet
K feldspar
L melt
M muscovite
O orthopyroxene
Q quartz
U osumilite
V vapour
Reactions are listed in Table 11.1
Pressure (GPa)
Temperature (C)
1·2
1·0
0·8
0·6
0·4
0·2
700
800
900
1000

(a) $mg = \frac{100 \text{ mol. Mg}}{\text{mol.(Mg+Fe*)}}$: melt $\gtrless$ hercynite $\lessgtr$ garnet < olivine $\lessgtr$ melt < orthopyroxene < biotite < cordierite < osumilite $\lessgtr$ muscovite; and

(b) $al = \left(\frac{200 \text{ mol. Al}}{2 \text{ mol. Al+Fe*+Mg}}\right)$: olivine < orthopyroxene < biotite < melt $\lessgtr$ garnet < osumilite $\lessgtr$ hercynite = cordierite $\lessgtr$ melt < muscovite < aluminosilicates.

These ranges are represented schematically on an A'FM diagram in Fig. 11.3 Melt is the phase with the greatest compositional variation, both in (mg) and (al), relative to the other phases. The melt field will of course extend further at higher temperatures when the variance is ≥ 3.

Evidence for these compositional relationships comes from various theoretical studies (e.g. Thompson, 1976a,b, 1982; Abbott & Clarke, 1979; Lonker, 1981; Ellis et al., 1980; Grant, 1968, 1973, 1985) and from experimental studies (e.g. Hensen, 1970; Hensen & Green, 1972, 1973; Ellis & Thompson, 1986; Ellis, 1986; Chapter 8).

11.3 BASIS FOR PETROGENETIC GRIDS

Twenty-eight univariant reactions from published papers and from unpublished theses, have been used as the basis of the grid. They are described in Table 11.1 and illustrated in Fig. 11.1. Most have been determined directly by experiment (those designated study-type E of Table 11.1). Some have been deduced from the intersections of experimentally determined divariant assemblage fields (study-type D of Table 11.1). Others have been estimated on the basis of theoretical phase equilibria (study-type T of Table 11.1). Most of the reactions are for assemblages from chemical systems which are subsets of the KFMASH system. The KNASH haplogranite minimum is also included for reference purposes.

11.4 PT GRID

11.4.1 Construction

The PT grid was constructed using the thermodynamically-based geometric methods of Schreinemakers (1915-1929), as described by Korzhinskii (1959) and Zen (1966). The simplest systems were constructed first. Univariant reactions in more complex systems were derived from these, by employing the following principles:

(a) addition of another chemical component to the system of a particular univariant assemblage, creates a divariant assemblage which will extend in PT space, in a direction favouring the assemblage which most strongly partitions the new component; and

(b) when this is undertaken for two univariant reactions emanating from the same invariant point, then intersection of the two resultant sets of divariant fields will generate a univariant reaction line in the

Table 11.1
Reactions used to construct KFMASH grids

Run #	Reactants	Products	Type Study	Chemical System	Reference	Remarks
1	KNQV	L	E	KNASH	Johannes, 1984	Eutectic melting
2	O	FQ	E	FS	Bohlen et al., 1983	Stability limit of Al-absent orthoferrosilite
3	GM	ABQ	T	KFASH	Thompson, 1982	Stability limit of {GM} assuming that $(SiFeAl_{-2})_B = (Al_2Fe_{-1}Si_{-1})_M$
4	Ky	Sil	E	AS	Holdaway, 1971	Aluminosilicate stability
5	C	AGQV	E	FASH	Weissbrod, 1973 Holdaway & Lee, 1977	Stability limit of sekaninaite (Fe-cordierite)
6	MQ	AKV	E	KASH	Chatterjee & Johannes, 1974	Stability limit of pure M in the presence of Q
7	MQ	ABKV	T	KFASH	Thompson, 1982	Stability limit of {MQ} where M contains $(FeSiAl_{-2})$
8	And	Sil	E	AS	Holdaway, 1971	Aluminosilicate stability
9	ABQ	CKV	E	KFASH	Holdaway & Lee, 1977	
10	AfQV	L	E	KNASH	Tuttle & Bowen, 1958	Eutectic melting
11	ACKQV	L	E	KFASH	Holdaway & Lee, 1977	Observed beginning of melting in KFASH system
12	CKQV	L	E	KFASH	Seifert, 1976	Stability of Mg cordierite in presence of K-feldspar quartz and vapour
13	BQ	FKV	E	KFASH	Eugster & Wones, 1962	Stability limit of {BQ} for B = stoichiometric annite
14	BQ	CFKV	T	KFASH	Richardson, 1968	Estimated stability of {BQ} where B is aluminous annite, assuming the peraluminous product phase is cordierite
15	BCKV	U	E	KMASH	Olesch & Seifert, 1981	Stability limit of magnesian U under vapour-saturated conditions
16	BQ	KOV	E	KMASH	Luth, 1967; Wones & Dodge, 1977	Stability of {BQ} where B is stoichiometric phlogopite
17	UV	BCKLQ	E	KMASH	Olesch & Seifert, 1981	Stability limit of magnesian U under vapour-saturated conditions
18	ABQ	CGKV	D	KFMASH	Holdaway & Lee, 1977	
19	GQ	FC	T	FAS	Hensen, 1970	Slope recalculated using:
20	C	HQ	T	FAS	Hensen, 1970	Terminal reaction of sekaninaite (Fe-cordierite) at high teperature
21	CG	FHQ	D	FMAS	Hensen & Green, 1973	
22	GOQ	CF	D	FMAS	Hensen, 1973	
23	AG	CHQ	D	FMAS	after Hensen & Green, 1972	Phases re-arranged from that of Hensen & Green (1972) for case where $mg_H < mg_G$
24	CG	AOQ	E	FMAS	Hensen & Green, 1972	Limiting stability of {CG}, recognising C is a hydrous phase
25	BQ	KLO	E	KMASH	Bohlen et al., 1983	Limiting stability of {BQ} where B is stoichiometric phlogopite
26	MQ	AKL	E	KASH	Huang & Wyllie, 1974	Limiting stablity of pure M in presence of Q
27	MQV	AL	E	KASH	Huang & Wyllie, 1974	Limiting stability of pure M in presence of Q and V
28	KMQV	L	E	KASH	Huang & Wyllie, 1974	Eutectic melting

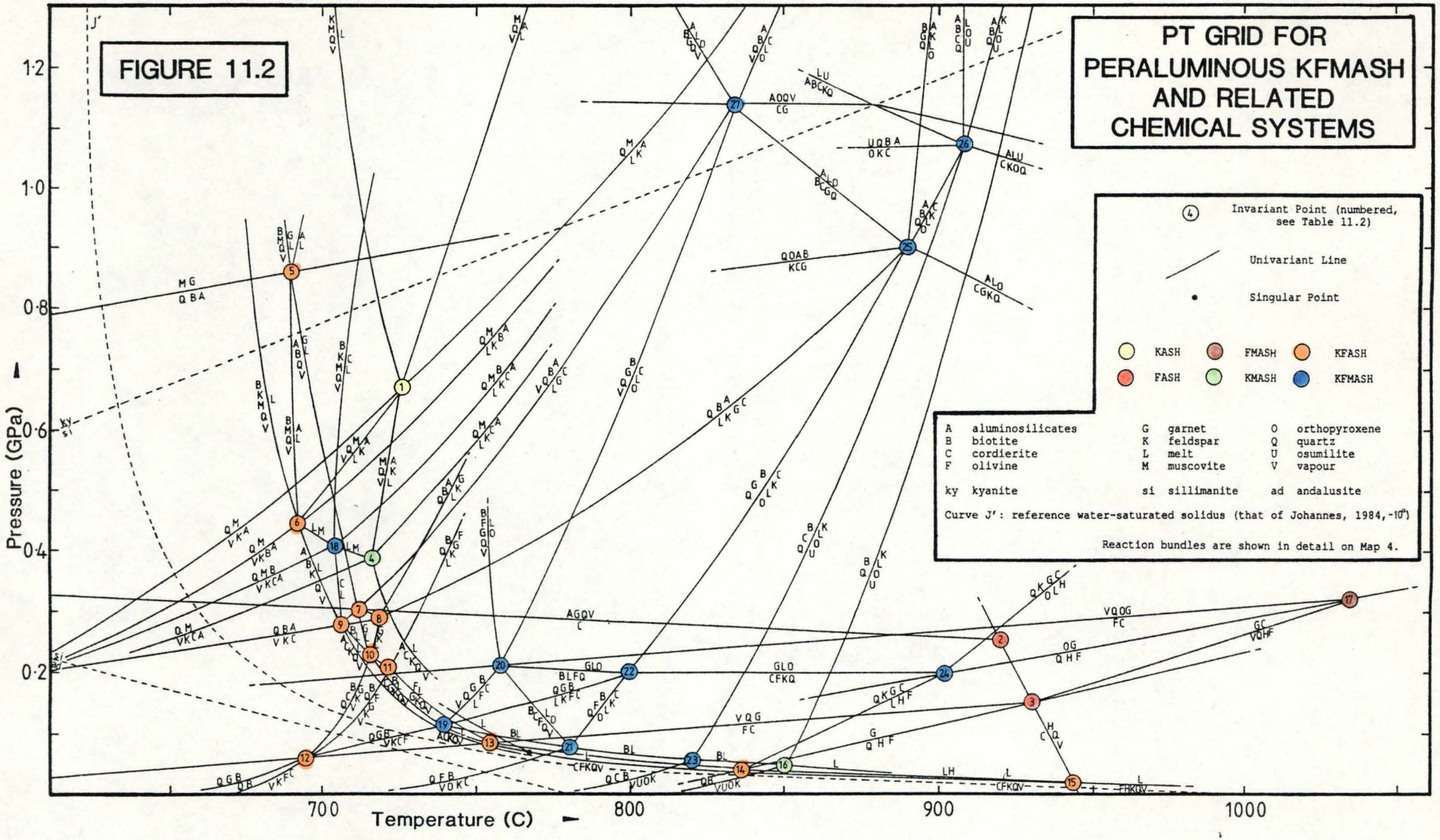
FIGURE 11.2
PT GRID FOR PERALUMINOUS KFMASH AND RELATED CHEMICAL SYSTEMS
Pressure (GPa)
Temperature (C)
1·2
1·0
0·8
0·6
0·4
0·2
700
800
900
1000
Invariant Point (numbered, see Table 11.2)
Univariant Line
Singular Point
KASH
FMASH
KFASH
FASH
KMASH
KFMASH
A aluminosilicates
B biotite
C cordierite
F olivine
G garnet
K feldspar
L melt
M muscovite
O orthopyroxene
Q quartz
U osumilite
V vapour
ky kyanite
si sillimanite
ad andalusite
Curve J': reference water-saturated solidus (that of Johannes, 1984, -10°)
Reaction bundles are shown in detail on Map 4.

complex system. This univariant reaction will involve all the phases present at the simple-system invariant point and will terminate at the invariant point of the simple chemical system.

The KFMASH grid is generated from the KFASH and KMASH grids by these means, utilizing the Al-Fe*-Mg partitioning amongst the A'FM phases as described above.

The following phase equilibrium assumptions have also been made:

(a) addition of water to cordierite-bearing assemblages in anhydrous chemical systems should expand the phase-field of cordierite, because it can be a hydrous phase (Newton, 1972; Newton & Wood, 1979; Lonker, 1981);

(b) osumilite is an A'FM phase at temperatures above ~830°C at low pressures, as indicated from the occurrence of phenocrysts of this phase in peraluminous felsic volcanic rocks from various localities in Japan (Miyashiro, 1956; Miyachi & Miyachi, 1978; Kobayashi, 1978) and from Sardinia (De Michele, 1974);

(c) the terminal reaction of MgAl-biotite in the presence of quartz occurs in the endmember KMASH chemical system and involves the generation of osumilite;

(d) biotite containing $Al_2Si_{-1}(Fe,Mg)_{-1}$ has greater thermal stability than that without (Richardson, 1968; Grant, 1985; Miyashiro & Shido, 1985); and

(e) muscovite containing $(Fe,Mg)SiAl_{-2}$ has greater thermal stability than that without (Thompson, 1982; Miyashiro & Shido, 1985).

11.4.2 Results and Applications

The resulting grid (Fig. 11.2) contains 27 invariant points occurring within the pressure range $0 < P(GPa) < 1.2$ and the temperature range $670 < T(C) < 1035$. Reactions are in the AS, KASH, FAS, FASH, FMAS, FMASH, KMASH, KFASH and KFMASH chemical systems. The invariant points are listed in Table 11.2 and the univariant reaction bundles around each invariant are illustrated in detail in Map 4. The PT area mapped, is that in which most felsic peraluminous magmas are derived and subsequently evolve.

The KFMASH-system melts become Mg-poor both at low P and low T (Fig. 11.2), leading to a water-saturated solidus which consists of linked eutectic reactions in the KFASH endmember chemical system. This result accords with many felsic natural granitic compositions such as those from the Babel Island and Boobyalla Suites, which contain Mg merely as a trace element.

Water-saturated solidus assemblages all contain melt, quartz, (potassium) feldspar and vapour. The remaining two phases in each reaction assemblage change along the solidus from:

Table 11.2

Grid Invariants

#	Chemical System	Phases Present	Approx. P_{Σ}(GPa)	Approx. P_{W}(GPa)	Approx. T (C)	Source
1	KASH	AKLMQV	0.67	0.67	726	Huang & Wyllie (1974)
2	FASH	ACGHQV	0.25	0.25	920	after Hensen (1970)
3	FASH	CFGHQV	0.15	0.15	930	"
4	KMASH	ACKLMQV	0.39	0.39	717	this work
5	KFASH	ABGLMQV	0.82	0.82	692	"
6	KFASH	ABKLMQV	0.44	0.44	692	"
7	KFASH	ABCGLQV	0.3	0.3	714	"
8	KFASH	ABCGKLQ	0.29	0.26	719	"
9	KFASH	ABCKLQV	0.28	0.28	706	"
10	KFASH	BCGKLQV	0.23	0.23	717	"
11	KFASH	BFGKLQV	0.21	0.21	721	"
12	KFASH	BCFGKQV	0.06	0.06	694	"
13	KFASH	CFGKLQV	0.09	0.09	754	"
14	KFASH	CFGHKLQ	0.04	<0.04	836	"
15	KFASH	CFHKLQV	0.02	0.02	943	"
16	KMASH	BKLOQUV	0.05	0.05	850	after Wones & Dodge (1977)
17	FMASH	CFGHOQV	0.32	0.32	1035	after Hensen & Green (1973)
18	KFMASH	ABCKLMQV	0.41	0.41	704	this work
19	KFMASH	BCFGKLQV	0.12	0.12	740	"
20	KFMASH	BCFGLOQV	0.21	0.21	758	"
21	KFMASH	BCFKLOQV	0.07	0.07	780	"
22	KFMASH	BCFGKLOQ	0.2	0.13	800	"
23	KFMASH	BCKLOQUV	0.05	0.05	820	"
24	KFMASH	CFGHKLOQ	0.2	0.08	900	"
25	KFMASH	ABCGKLOQ	0.9	0.3	890	"
26	KFMASH	ABCKLOQU	1.07	0.32	908	"
27	KFMASH	ABCGLOQV	1.14	1.14	834	"

(a) two micas above ~0.44 GPa ($\leq$692°C), to

(b) aluminosilicate (sillimanite) plus biotite from ~0.44 to ~0.28 GPa (~692 to 706°C), to

(c) aluminosilicate (sillimanite or andalusite) plus cordierite from ~0.28 to ~0.07 GPa (~706 to ~770°C), to

(d) fayalite plus cordierite from 0.07 to ~0.015 GPa (~770 to ~943°C), to

(e) fayalite plus hercynite below 0.015 GPa (above ~943°C).

A singular point is predicted at ~0.07 GPa and ~770°C, marking the P_WT conditions at which the eutectic liquid path crosses the feldspar-cordierite join. At pressures below this point, two eutectic minima are predicted which are separated by a thermal divide joining the compositional points for feldspar and cordierite. This divide prevents the existence of the assemblage (aluminosilicate+fayalite) which is not known to occur in either natural low-pressure assemblages as discussed by Schairer & Yogi (1952), nor in low-pressure experimental studies, at least in the FAS and FMAS chemical systems (op. cit.; Hensen, 1970; Hensen & Green, 1973).

These five divisions may be used to categorize the solidus conditions of natural peraluminous granites, after consideration has been made of the temperature-depressing effects of additional components such as Na_2O, HF, B_2O_3 etc. For example, the solidus assemblage (c) is similar to that which is considered to have occurred in magmas of the Boobyalla and Babel Island Suites because the most evolved (least magnesian) rocks of these suites have phenocrysts of cordierite and andalusite. Biotite occurs only as corroded phenocrysts, or as a subsolidus matrix phase (Chapter 4). Fayalite-bearing pegmatites occur in the felsic alkali-rich hypersolvus granites of Hinchinbrook Island, North Queensland (Prof. J. Stephenson, pers. comm.). The more felsic varieties of these granites have (al) index values of 25 to 50 which are comparable to those of the Boobyalla and Babel Island Suite granites. This is consistent with their magmas having contained phases which were more peraluminous than fayalite (al = 0) and biotite (al < 20). Contenders for such phases are melt and cordierite. If cordierite was present, then the presence of a fayalite and cordierite-containing solidus assemblage indicates that the Hinchinbrook granite magmas were probably intruded at higher temperatures and to lower total pressures, than were the magmas of the Boobyalla and Babel Island Suites of the NBTB.

The very low-pressure high-temperature osumilite-bearing assemblages predicted by the grid (cf. invariant points #16 and #23) are consistent with natural occurrence of osumilite in vesicular rhyodacites from Japan (Miyashiro, 1956; Miyachi & Miyachi, 1978). In these rocks, phenocrysts of hypersthene, biotite, quartz and andesine and osumilite occur in a

FIGURE 11.3

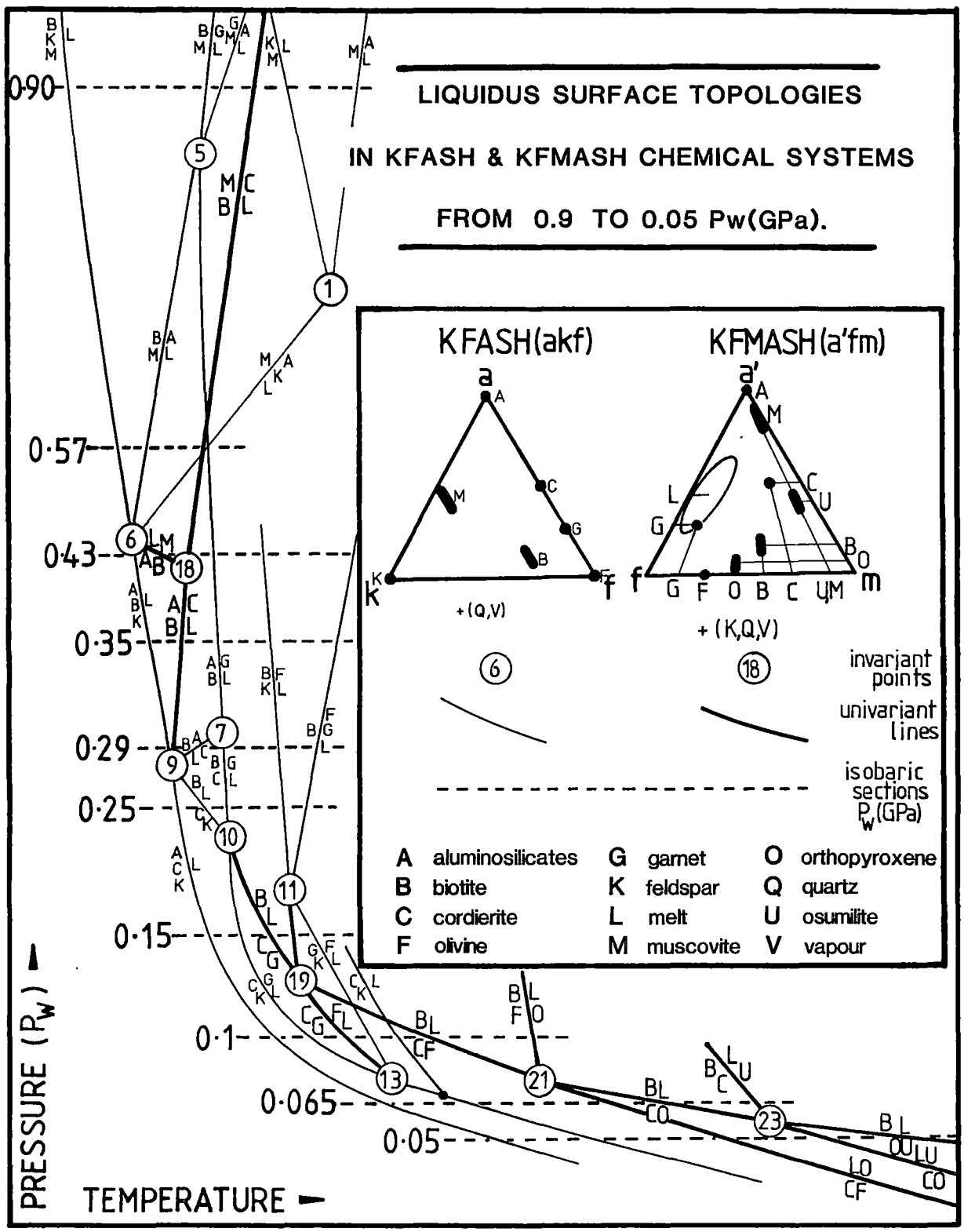
LIQUIDUS SURFACE TOPOLOGIES
IN KFASH & KFMASH CHEMICAL SYSTEMS
FROM 0.9 TO 0.05 Pw(GPa).
KFASH(akf)
KFMASH(a'fm)
+(Q,V)
+(K,Q,V)
invariant points
univariant lines
isobaric sections Pw(GPa)
A aluminosilicates
B biotite
C cordierite
F olivine
G garnet
K feldspar
L melt
M muscovite
O orthopyroxene
Q quartz
U osumilite
V vapour
0·90
0·57
0·43
0·35
0·29
0·25
0·15
0·1
0·065
0·05
PRESSURE (Pw)
TEMPERATURE

P_w(GPa)=

0·90

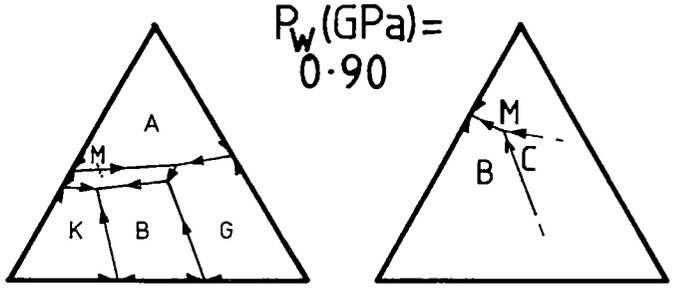

0·25

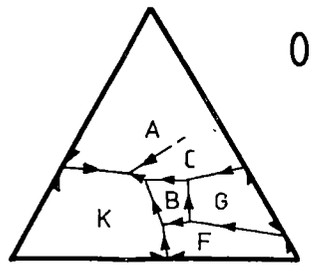

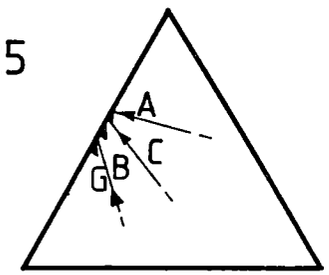

0·57

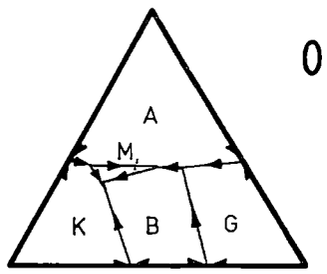

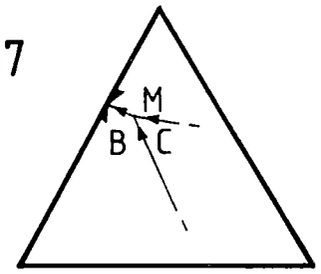

0·15

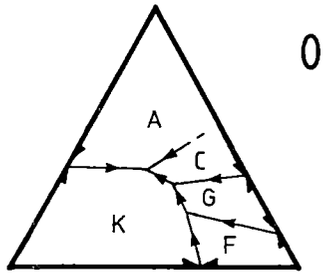

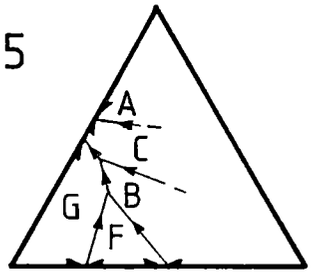

0·43

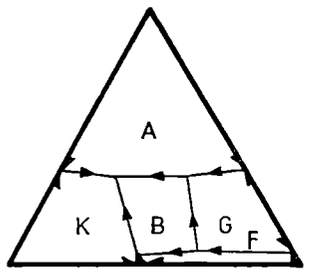

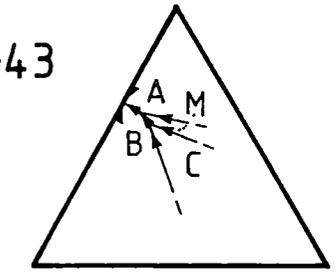

0·1

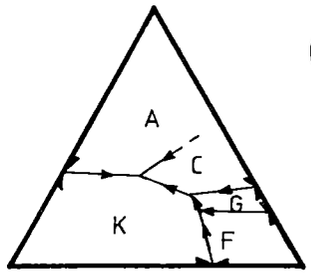

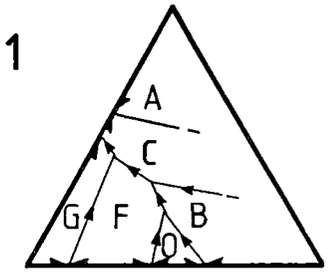

0·35

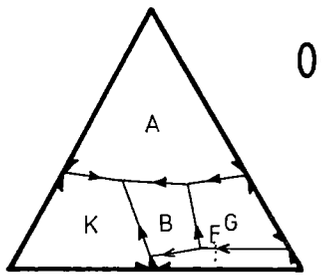

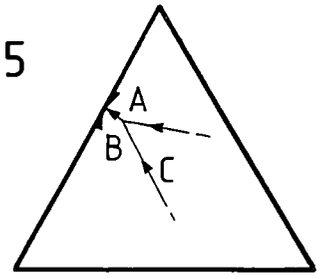

0·065

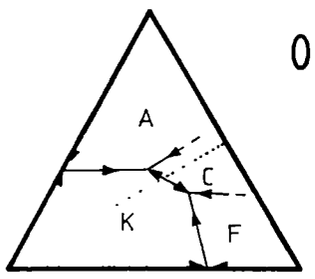

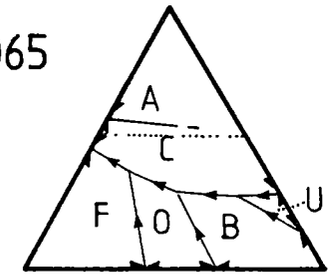

0·29

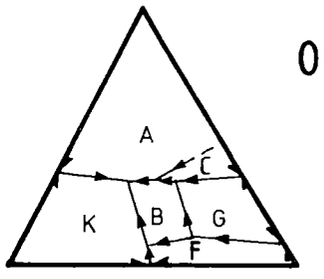

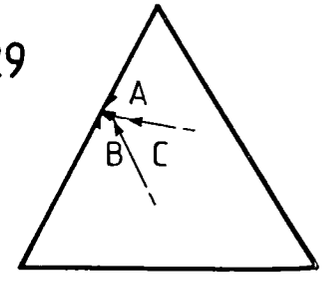

0·05

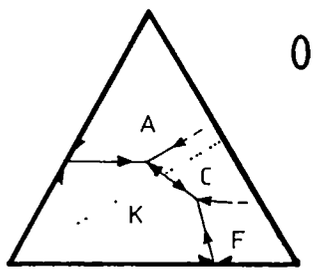

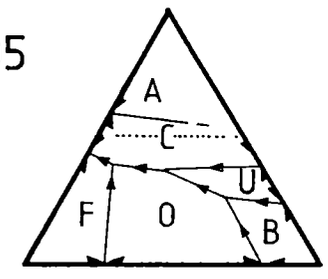

groundmass of tridymite, alkali feldspar, oligoclase, quartz, fayalite, hypersthene, biotite and osumilite (op. cit.).

The grid may also be used to estimate KFASH- and KFMASH-system liquidus topologies in the same manner as those estimated by Abbott & Clarke (1979). Fig. 11.3 shows schematic partial topologies for the near-solidus equilibria in each of these systems (on AKF and A'FM diagrams, respectively). They have been constructed from the (quartz+vapour)-saturated equilibria intersected along each of ten isobaric sections through the grid which range from 0.05 to 0.95 P_W (GPa). Because of dimensional constraints, the KFMASH-system topologies are constructed only from those equilibria also involving potassium feldspar. Topologies involving feldspar-absent equilibria in this system would have to be represented in perspective form. The relevant simplified P_WT equilibria used to generate the liquidus surfaces are also schematically shown. Each intersection of a univariant line in P_WT-space, corresponds to an invariant point (of either distributary, tributary or eutectic type) on a TX surface at the relevant pressure. The divariant P_WT fields between these lines generate cotectic lines on the TX surface. Assumptions used to construct these partial liquidus surfaces are that:

(a) aluminosilicates, fayalite, garnet, and orthopyroxene melt congruently in (water+quartz±feldspar)-saturated systems whereas
(b) muscovite and biotite melt incongruently, and their liquidus fields do not include their compositional points, and
(c) high temperature equilibria for compositions near the A'', A and K apices are not considered so that the leucite field near K and the mullite field near A and A' are ignored.

In both chemical systems, regular progressions of topologies are indicated as P_W is decreased. In the iron-endmember system, the field of liquidus muscovite diminishes rapidly whereas that of biotite shrinks more slowly, with decreasing pressure. The fayalite field expands until, at very low pressures, (fayalite±cordierite) becomes a stable liquidus assemblage.

Addition of MgO stabilizes cordierite to higher pressures and both muscovite and orthopyroxene (which is absent from the iron endmember system in the pressure range considered) to lower pressures. Magnesium also destabilizes liquidus garnet at low pressures and at very low pressures, an osumilite field appears. Endmember KMASH liquids co-crystallize biotite and osumilite at P_W = 0.05 GPa (cf. invariant #15, Map 2).

This set of topologies may be compared with those first presented for the same chemical systems by Abbott & Clarke (1979). Differences between the two sets stem largely from the K_D^{FeMg} relationships chosen to relate the

FIGURE 11.4

P–T–a_w MODEL FOR PERALUMINOUS KFMASH –SYSTEM MELTS

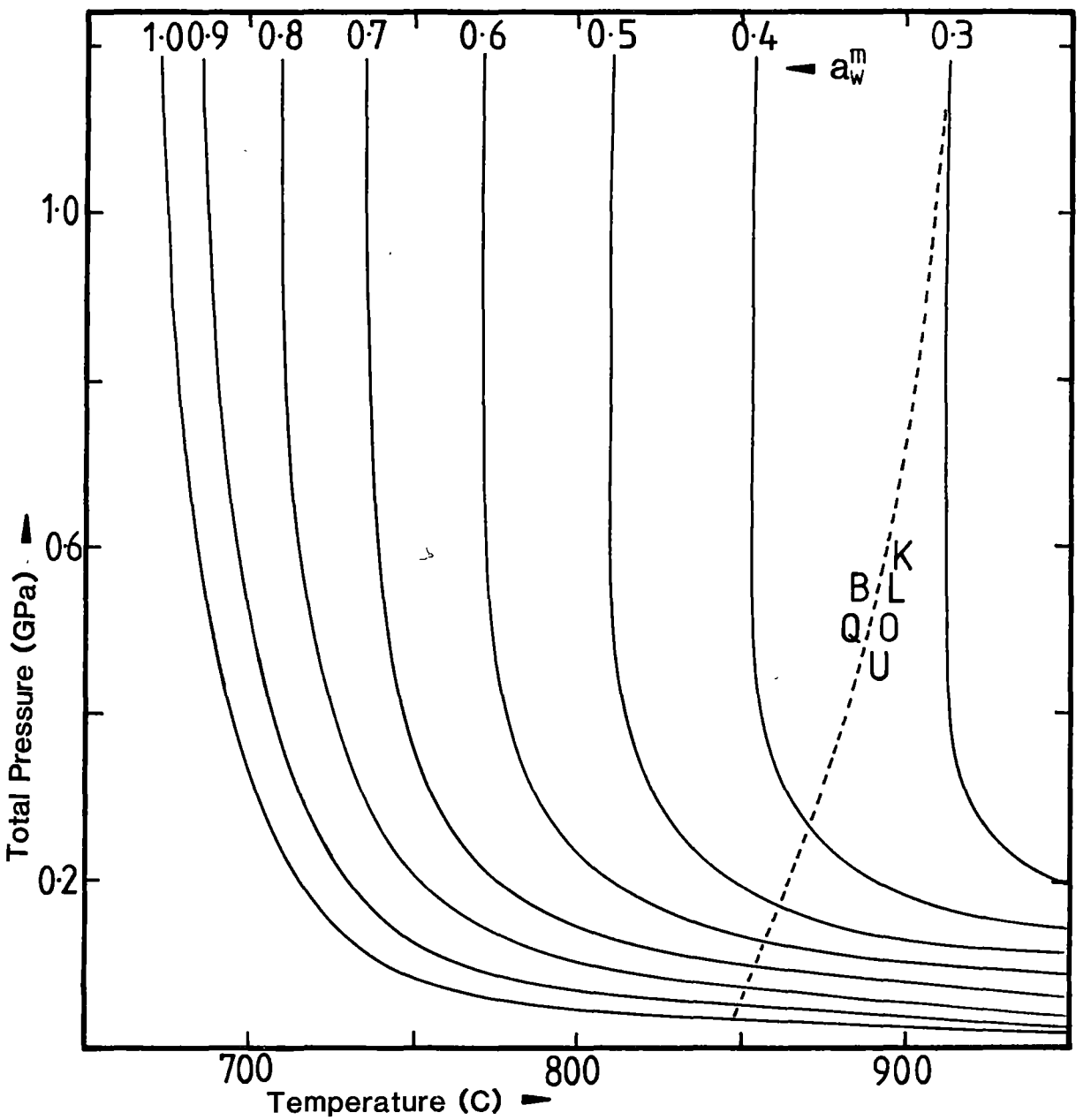

compositions of the various ferromagnesian phases. In particular, the garnet/liquid K_D^{FeMg} is considered to reverse at low temperatures (Green, 1976b; Ellis, 1986; Chapter 8) so that unlike the topologies of Abbott & Clarke (1979), those of Fig. 11.3 are consistent with low-temperature liquids being more magnesian than coexisting garnet.

Theoretically deduced topologies such as those of Fig. 11.3 provide the basis for the direct determination of magmatic phase relationships in granite analogue systems and by inference, those in natural granitic magmas.

11.5 $P_\Sigma P_W T$ GRID

11.5.1 Estimation of P_W for KFMASH System Equilibria

P_W has been roughly estimated over the PT field of interest, using the equilibrium vapour-phase isohydrons: $(X_W)_{PT}$ which were experimentally determined in the quartzofeldspathic KASH+CO_2 system by Bohlen et al. (1983).

A ~50°C temperature interval at constant total pressure separates the water-saturated solidus of the quartz+sanidine system (op. cit.; Shaw, 1963) at high temperatures, from that estimated for the peraluminous KFASH system (Fig. 11.2) at low temperatures. It is attributed to the combined effects on phase equilibria of excess Al_2O_3 and FeO in the melt. Excess Al_2O_3 alone lowers the KASH-system solidus by ~30°C at 0.2 GPa (Voigt, 1983, **in** Burnham & Nekvasil, 1986). The water-saturated solidus in the KFASH system is the location of the $X_w = 1$ isohydron in the KFMASH system, because of the compositional degeneracy described above.

KFMASH-system isohydrons at $P_W < P_\Sigma$ will be complex functions of P_Σ, T and the assemblage-buffered Fe-Mg-Al composition of the melt. Because the water-saturated solidus in the peraluminous quartz-saturated KMASH system is located ~30°C **above** that of the quartz+sanidine system (reaction 12, Table 11.1, Fig. 11.1, Seifert, 1976), then the effect of increasing MgO in the melt is counter to that of adding FeO or Al_2O_3; isohydrons are therefore expected to be raised to higher temperatures by addition of MgO, compared to their positions with KASH system melts. Due to these opposing tendencies, isohydrons near $X_W^V = 0.3$ are probably similarly located in both the KASH and KFMASH chemical systems. Vapour-phase isohydrons for the peraluminous, quartz-saturated KFMASH+CO_2 system, are therefore expected to be similar to those for the quartz+sanidine system at ~$X_W^V = 0.3$ and to extend down to the peraluminous KFASH system water-saturated solidus at $X_W^V = 1.0$.

A relationship between P_W, P_Σ and T may therefore be approximated for peraluminous KFMASH system equilibria, assuming that

FIGURE 11.5

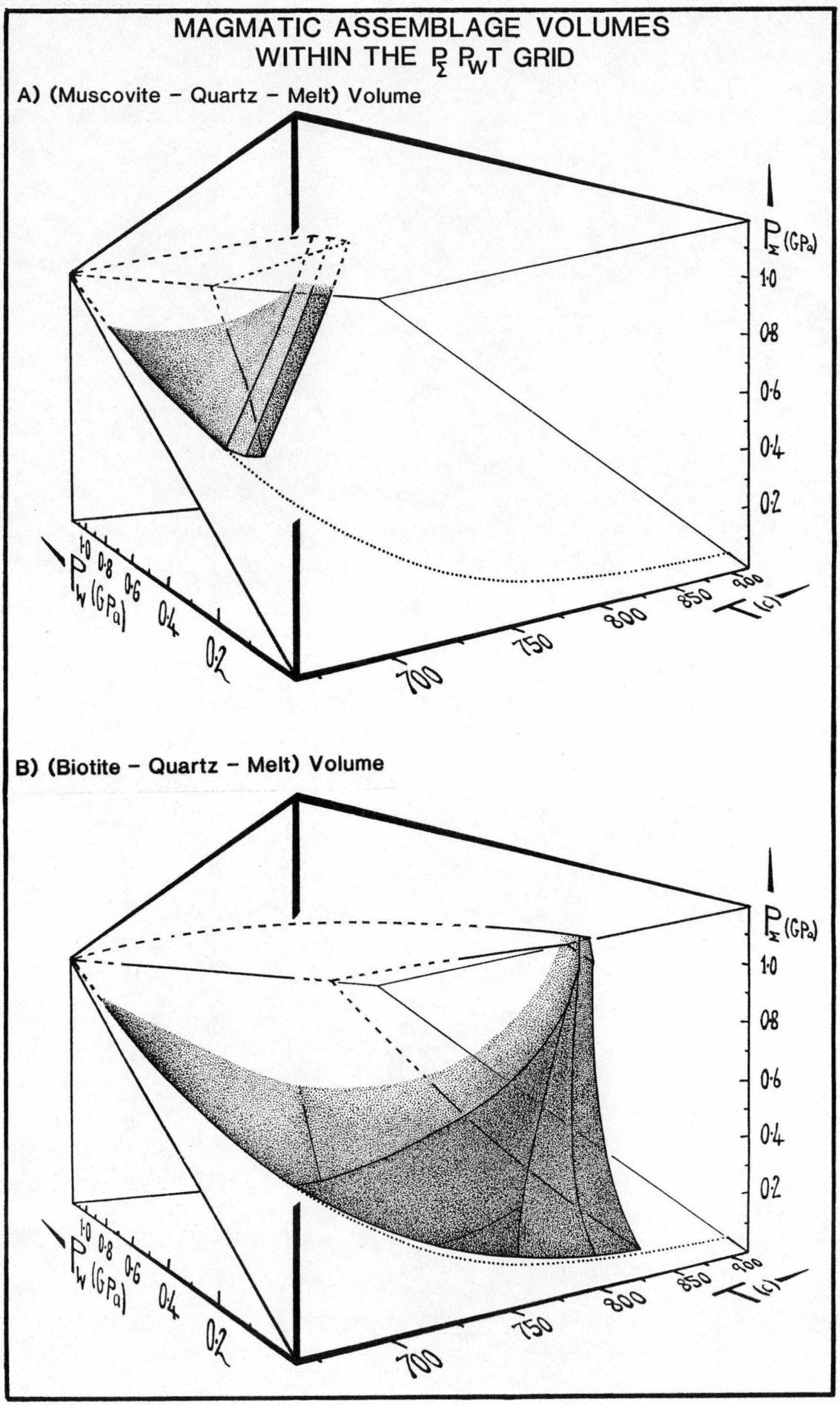
MAGMATIC ASSEMBLAGE VOLUMES
WITHIN THE P_Σ P_WT GRID
A) (Muscovite – Quartz – Melt) Volume
P_Σ (GPa)
1·0
0·8
0·6
0·4
0·2
P_W (GPa)
1·0
0·8
0·6
0·4
0·2
700
750
800
850
900
T (C)
B) (Biotite – Quartz – Melt) Volume
P_Σ (GPa)
1·0
0·8
0·6
0·4
0·2
P_W (GPa)
1·0
0·8
0·6
0·4
0·2
700
750
800
850
900
T (C)

(a) $(P_W/P_\Sigma)_{P,T}$ (as described above) = $(X_W^V)_{\Sigma P,T}$; and

(b) phase equilibria in the KFMASH system (Fig. 11.2 are not significantly changed by the presence of a CO_2-containing vapour so that the X_W^V gradient of Fig. 11.4 can also refer to the P_W/P_Σ gradient in vapour-absent magmas.

The resulting P_W/P_Σ solidus model for KFMASH-system magmatic assemblages, is shown in Fig. 11.4. Using this relationship, each of the seven vapour-absent invariant points in Table 11.2 may be assigned a P_W coordinate where $P_W < P_\Sigma$.

11.5.2 Description and Application of 3D Grid

The peritectic reactions of the PT grid (Fig. 11.2) divide PT space into areas containing different equilibrium assemblages which are of great petrogenetic relevance. However by using P_W as a third intensive variable, a more useful three-dimensional grid may be generated in which these areas become volumes in $P_\Sigma P_W T$ space.

Wyllie (1977) published perspectives of an orthogonal $P_\Sigma P_W T$ grid in which phase equilibria may be plotted. The grid is very useful because it enables the role of the three independent variables, to be visualized (op. cit.). From the origin of this grid, temperature increases and P_W increases in the horizontal plane. P_Σ increases from this plane, in the vertical direction. Within the $P_\Sigma P_W T$ volume, the locus of $P_W = P_\Sigma$ forms a body diagonal plane which divides the grid into two prisms: a lower prism in which $P_W > P_\Sigma$ and an upper prism in which $P_W < P_\Sigma$. Real equilibria are confined to the upper prism, that is, where $P_W \leq P_\Sigma$ (op. cit.).

Most of the invariant points listed in Table 11.2 and depicted in Fig. 11.2 lie on the sloping base of the upper prism of the 3D grid, within the ranges of ($0 < P_\Sigma$ GPa < 1.2), ($P_W \leq P_\Sigma$) and ($670 < T$ (C) $< 920^oC$). However, vapour-absent dehydration-melting curves emanating from these points leave the $P_W = P_\Sigma$ plane and extend into the upper prism where $P_W < P_\Sigma$. The six invariant points for which $P_W < P_\Sigma$, are anchored within the volume of this prism. They are connected to each other or to points on the $P_W = P_\Sigma$ plane, by various vapour-absent univariant reaction lines. The upper prism may then be divided into numerous trivariant subvolumes, each bounded by divariant lines which intersect at the invariant points. Each liquidus phase has a characteristic distribution amongst these subvolumes.

Fig. 11.5 depicts partial quartz-saturated $P_\Sigma P_W T$ liquidus volumes for the micas; these phase volumes are better characterized than those of other phases because the terminal reactions for the micas in both the iron and magnesium endmember systems have been estimated, unlike those of the other phases. Phase volumes for the other phases are partially known and are described qualitatively below. Phase volumes are petrogenetically useful,

because they will resemble the phase volumes present in natural peraluminous granitic systems for which the these systems are analogues. They can therefore be used to estimate the $P_\Sigma P_W T$ conditions appropriate for a given magmatic assemblage.

Liquidus muscovite is confined to a small volume at pressures >~0.4 GPa and temperatures < 790°C at 0.9 GPa and P_W > ~0.8 P_Σ. Bounding invariant points include numbers 6, 18, 4 and 1. In contrast, biotite has a much larger phase volume, which extends to temperatures of ~980°C and to total pressures down to 0.05 GPa. Ratios of P_W/P_Σ may be as low as ~0.3 in the biotite liquidus volume. However, biotite is unstable at the water-saturated solidus, below pressures of 0.3 GPa. Bounding invariant points for its phase volume include numbers 6, 9, 10, 19, 21, 21, 16, 8, 20, 22, 25 and 26.

Cordierite has a huge phase volume, restricted only at high P_Σ and T, and low P_W (where cordierite+feldspar is unstable relative to osumilite) and at high P_Σ and P_W and low T (where cordierite is unstable relative to biotite+muscovite or biotite+aluminosilicate). Cordierite is a water-saturated solidus phase at all pressures below ~0.3 GPa, but not above this pressure.

Garnet has a large stability field at high total pressure, which shrinks with decreasing pressure. The phase volume at high temperatures is restricted to a thin sheet at low P_W/P_Σ. Garnet is unstable along the entire length of the water-saturated solidus.

Hercynite is restricted to very high temperatures and low total pressures. Its field extends to higher pressures only at low P_W/P_Σ ratios where it forms at the expense of garnet. Hercynite is not on the water-saturated solidus in this system, below temperatures of ~943°C.

Fayalitic olivine has a phase volume restricted to low pressures and moderate to high temperatures. It is on the water-saturated solidus at temperatures above ~754°C. Its phase field appears to extend to higher pressures ($\geq$0.3 GPa) at high P_W.

The phase field of orthopyroxene is extensive at high P_Σ and T where it is stable over a wide range in P_W/P_Σ from ($0.3 \leq P_W/P_\Sigma \leq 1$). With decreasing temperature however, its field is restricted to more water-rich conditions, until at ~750°C it is restricted to the water-saturated plane. At no point is orthopyroxene stable on the water-saturated solidus.

Sanidine has a phase field with a shell-like form. It occurs only in a thin PT field near the solidus, where $P_W = P_\Sigma$. This field expands however, at $P_W < P_\Sigma$. At the extreme conditions of high P_Σ and T and low P_W, the field may thin again as the potassic phase osumilite, becomes stable.

11.6 DISCUSSION

11.6.1 Comparison With Other Grids

Reactions and grids of Thompson (1982) have been the basis of the high-P, low-T portion of the grid in Fig. 11.2. KFASH system melts near the low pressure invariant point #9 (Map 2) are thought to be slightly more aluminous than are indicated by Thompson (op. cit.) and hence the reaction topologies about the respective invariant points are slightly different. The topology in this work accords with petrographic features of andalusite-cordierite-alkali feldspar-bearing assemblages in Boobyalla and Babel Island Suite porphyries in which biotite is present merely as a matrix phase or with sparse additional corroded phenocrysts of biotite. These features are interpreted to indicate that the eutectic assemblage at pressures below that of invariant #9 (Map 2) is biotite-absent, rather than being aluminosilicate-absent.

Substantial differences exist between Fig. 11.2 and the grids of Grant (1985). They are in part due to differences in the assumed compositions of liquids in equilibrium with A'FM phases. Ellis (1986) has shown that liquids in equilibrium with the phases of the invariant assemblage #9, will be more aluminous than points along the line joining garnet with corderite, on the A'FM projection. The experimental results of Chapter 8 support these compositional relationships. However, in contrast to this, Grant (1985) considers the projections of such liquids to plot **below** the garnet-cordierite tie-line.

Another significant difference between the grids concerns the existence of aluminous orthoferrosilite on the water-saturated solidus at pressures below that of invariant #9. In contrast to Grant (1985), this phase is not considered to be present in the phases of the low-pressure KFASH-system grid, because of the implications of the results of two separate experimental studies. Bohlen & Boettcher (1981) have shown that FS-system orthopyroxene is not stable below pressures of 1.07 GPa at a temperature of 720^{o}C, corresponding to the orthoferrosilite-bearing invariant point (Als) of Grant (1985, fig. 2, p.413). Pure orthoferrosilite is therefore unable to occur at this ~0.22 GPa invariant point (op. cit.). (see reaction #2, Table 11.1, Fig. 11.1). At a given temperature, orthopyroxene should be stable to lower pressures in the FAS compared with the FS chemical system, because aluminium can partition into orthopyroxene via the tschermak substitution ($Al4Al6Si_{-1}Fe_{-1}$) but cannot substitute into either olivine or quartz. However Harley (1984) showed that the Al-contents of experimental ferromagnesian orthopyroxenes in equilibrium with garnet, decrease with both temperature and the iron content of the orthopyroxene at any given pressure. Extrapolation of his

results suggests that the Al-content of orthoferrsilite in equilibrium with garnet at ~700°C and ≤0.5 GPa pressure (i.e. near the KFMASH system) the water-saturated solidus will be close to zero.

The Al-content of low-temperature orthoferrosilite which is buffered by the presence of cordierite, should be more aluminous than that buffered by the presence of the less aluminous phase: garnet, because cordierite is more aluminous than garnet. However the amount is not likely to be sufficient to depress reaction #2 of Fig. 11.1 over 0.8 GPa, in order for it to intersect with KFASH-system solidus at 0.2 GPa, as is required for the KFASH-system grid of Grant (op. cit.). Orthopyroxene present at these pressures and temperatures is thought to be aluminous, **ferromagnesian** orthopyroxene as indicated from the experimental partial melting study of Hoffer & Grant (1980) (see Fig. 11.2).

Other fayalite- and orthopyroxene-bearing assemblages are expected to occur at high P_Σ and low T within the $P_\Sigma P_W T$ ranges of the grids of this chapter. Reactions relating these assemblages will ultimately be derived from the FS-system reaction:

orthoferrosilite --> fayalite + quartz (reaction 2, Fig. 11.1).

However there are insufficient experimental data in intervening chemical systems to date, to derive these reactions by the methods of Schrienemakers (1915-1925) **in** Korzhinskii (1959) and Zen (1966).

It is possible also that the stability of hercynite within the grids is over-estimated because the hercynites from the furnace-buffered experimental runs of Hensen (1970) and Hensen & Green (1973) are likely to have contained a magnetite component in view of the redox conditions estimated for piston-cylinder apparatus indicated in Fig. 8.4. Pure hercynite may not be stable in the presence of quartz as indicated in the experimental study of Schairer & Yagi (1952). Their runs were buffered down to extremely low oxygen fugacities using the iron-wustite buffer.

Other KFMASH system **phases** may also have quartz-containing liquidus phase fields. In feldspar-absent liquidus assemblages at high P_W and at low T, phases such as staurolite or gedrite might be stable (e.g. Grant, 1968, 1981; Clarke, 1981).

11.6.2 Implications for the Petrogenesis of Peraluminous Granites

A $P_\Sigma P_W T$ path or trajectory through the upper prism of the 3D grid will relate a sequence of intensive variable conditions with a sequence of magmatic assemblages (i.e. a paragenesis), as various phase-fields are entered then exited. By choosing the bulk composition and the $P_\Sigma P_W T$ path, one may qualitatively estimate an analogue system paragenesis which resembles that which has been petrographically deduced from the natural peraluminous granites. Much of the paragenesis deduced for the Boobyalla

FIGURE 11.6

PERSPECTIVE OF A $P_\Sigma P_W T$ PATH THROUGH 3D GRID

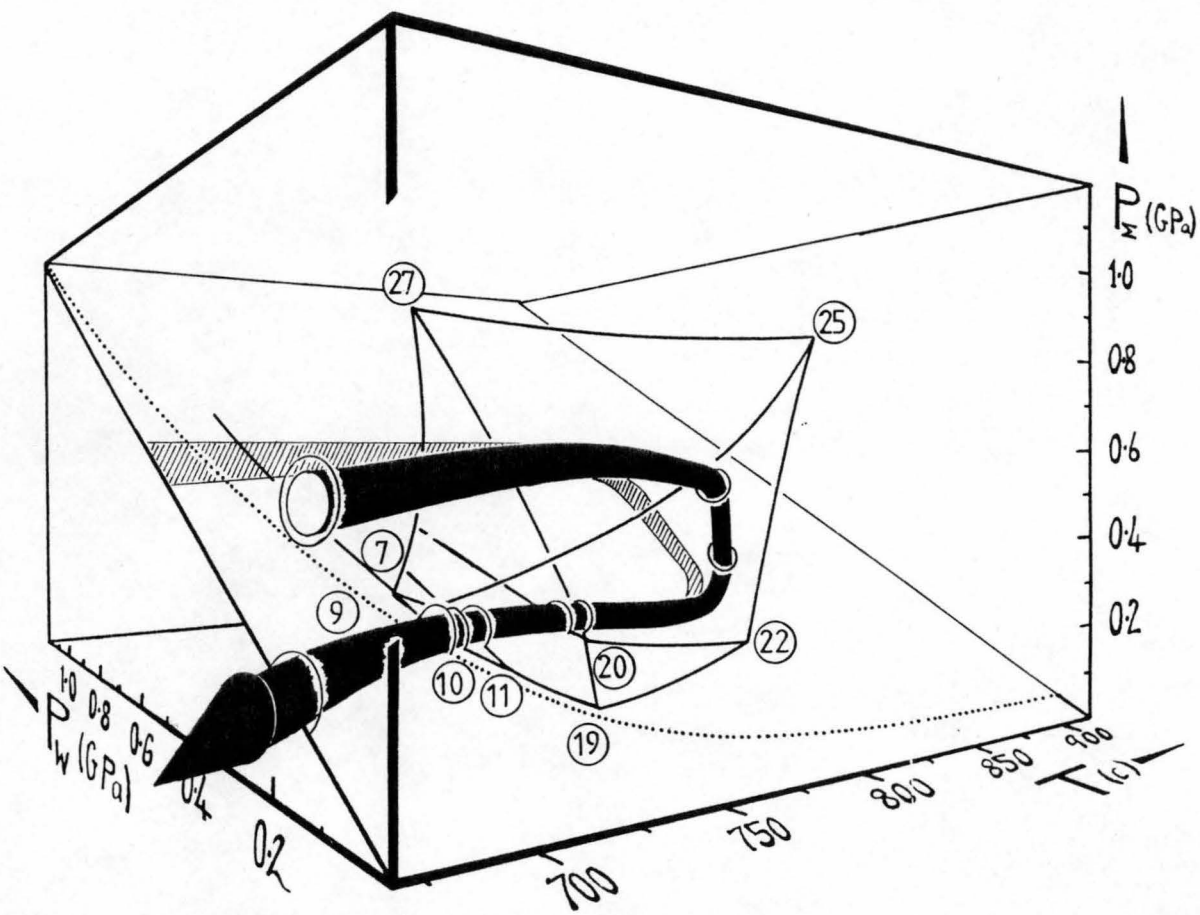

Numbered invariant points are listed in Table 11.2. The shaded band is the projection of the loop onto the water-saturated (P_W=P_Σ) diagonal plane.

FIGURE 11.7

MODEL PARAGENESIS FOR KFMASH COMPOSITIONS TAKING P_Σ P_WT PATH of FIGURE 11.6

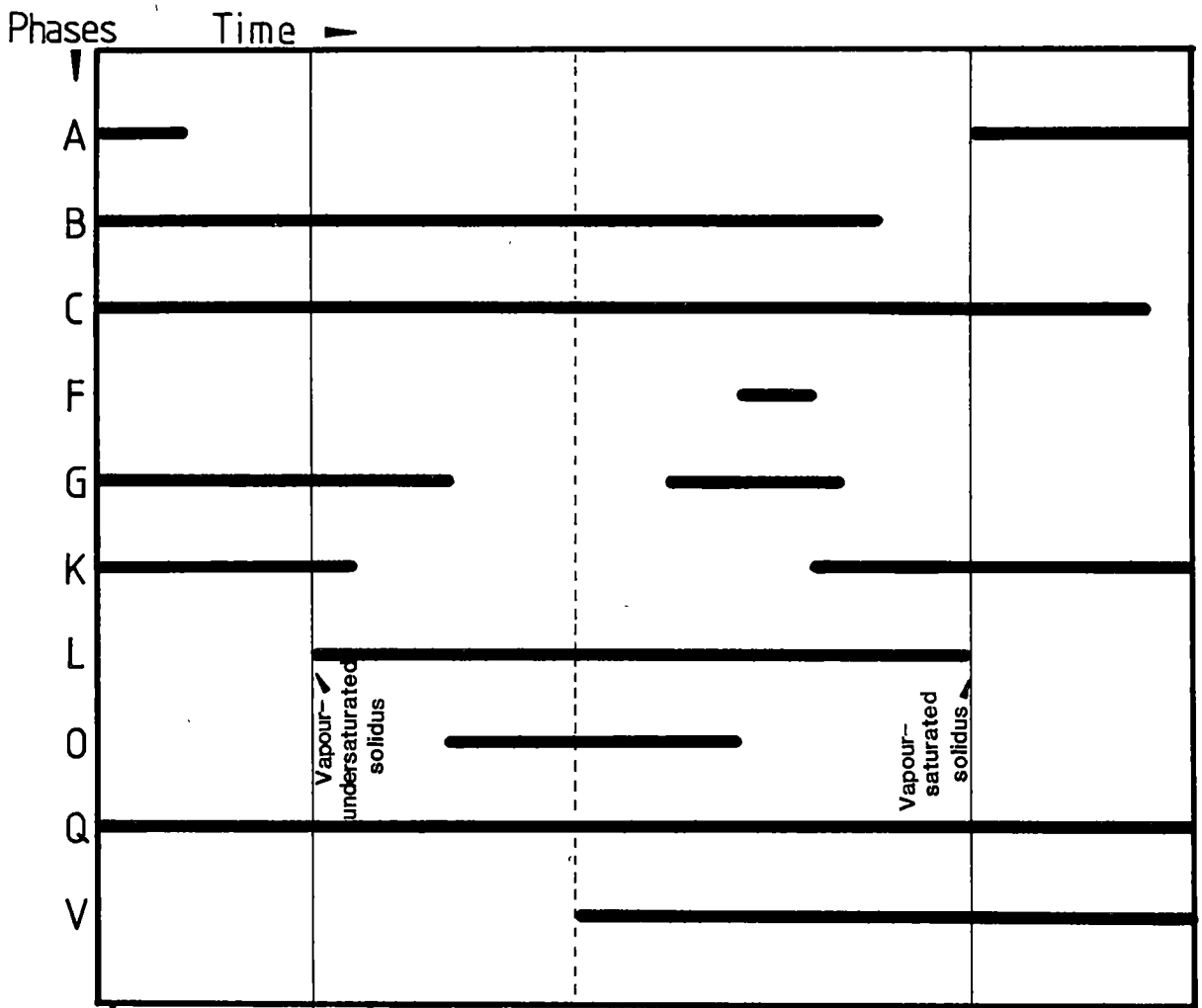

STAGES:	1st.	2nd.	3rd.	4th.
	subsolidus	magmatic	magmatic	subsolidus
T (C)	up to ~850	~850	~850 to ~725	< 725
P_Σ (GPa)	~0·6	~0·6 to ~0·25	~0·25	< 0·25
P_W / P_Σ	down to ~0·4	~0·4 to 1	1	1

Suite (Fig. 4.1) can be reproduced for an analogue granitic bulk composition by intersection of the various phase fields along the trajectory marked in Fig. 11.6. This path passes through the water-undersaturated region with increasing temperature, during the early stages. It then descends to the water-saturated plane whereupon the trajectory turns to lower T, passing across a series of divariant surfaces separated by univariant lines. An estimated parageneses resulting from this path is shown in Fig. 11.7. It results purely from isochemical reaction, without recourse to the involvement of magmatic differentiation processes.

The parageneses of Figs 4.1 and 11.7 have many similarities. One difference is that the natural paragenesis indicates alkali feldspar to have been present over the entire liquidus range, whereas the analogue paragenesis indicates an hiatus for this phase.

A hiatus will result if the phase is not present in an amount sufficient to saturate the melt in that phase. The presence of sufficient inert excess (restitic) alkali feldspar removes the hiatus in the paragenesis of this phase. The hiatus in the distribution of garnet in the analogue system may similarly be removed if initial bulk compositions contain sufficient (restite) garnet.

Another difference is the occurrence of fayalite olivine in the analogue paragenesis; this phase is absent from the natural paragenesis. Olivine is generated at the expense of orthopyroxene, when the $P_{\Sigma}P_{W}T$ path crosses the cordierite-absent univariant reaction which emanates from the KFMASH-system invariant point #20 (cf. Map 2). It will be ultimately destroyed at slightly lower temperatures, when the path crosses the garnet-absent univariant reaction which emanates from the KFASH-system invariant point #11. The small temperature range involved means that magmatic fayalitic olivine is unlikely to be preserved during the latter stages of granite petrogenesis. Thus it may have been present in the natural magmas, but if so, has presumably been destroyed by subsequent magmatic and subsolidus reactions.

The broad similarities between the natural and analogue parageneses indicates that equilibrium magmatic phase-relationships are important in granite petrogenesis. Magma differentiation processes must also be important because only they can generate the regular bulk-compositional trends observed in each peraluminous granite suite (Chapter 5).

A pressure $P_W \geq 0.25$ GPa was required to generate the latter portions of the analogue paragenesis of Fig. 11.7. However similar parageneses could be generated at lower pressures in natural assemblages because of the effects of other chemical components. Na_2O will preferentially partition

into the melt thereby shifting the solidus reactions towards the reference peraluminous granite solidus curve (that of Johannes (1984) -10°C, cf. Fig. 11.2). Each of the liquid-absent KFASH-system reactions (L) emanating from invariant points #9, #10 and #11 (Map 2) are expected to broaden into polyvariant bands. However, in contrast to the behaviour of the eutectic reactions upon increasing the chemical complexity of the system, these bands are expected to maintain their general P_WT positions. Na_2O will preferentially partition into alkali feldspar and therefore tend to expand the low pressure assemblage containing this phase to higher pressures and thereby moving the reactions to lower temperatures. However, this tendency will be compensated by the effects of MgO and TiO_2 which preferentially partition into phases such as biotite and cordierite in the high-pressure assemblages of each of these reactions, thereby tending to move the reactions to higher temperatures. The consequence of maintaining the positions of the liquid-absent reactions but lowering the solidus reactions to lower temperatures, will be to expand the P_WT space bounded by (the multivariant counterparts to) the invariants #9, #7, #8, #11 and #10 (cf. Fig. 11.2). An isobaric cooling path similar to that estimated for the Boobyalla and Babel Island Suites (i.e. 0.15 GPa P_W, Chapter 9) should then generate a paragenesis which is similar to that produced in the analogue system at 0.25 GPa P_W.

Reaction kinetics are of major importance in the application of the above grids. Garnet in particular, persists beyond its equilibrium environment, due to its extremely slow diffusion rates (Loomis, 1983a; Ellis, 1986; Chapter 8). As a consequence, the cores of garnet and even megacrystic alkali feldspar, retain their source compositions to low pressures and temperatures (Chapter 9). Such disequilibrium phases may be termed restite phases.

Other chemical constituents present in natural compositions, can have substantial effects on the phase equilibria of the simple-system grids derived in this chapter. In these Na_2O is the most abundant non-KFMASH component. It partitions strongly into both the melt and sanidine, resulting in the displacement of melt-containing assemblages and equilibria to lower temperatures. CaO, with Na_2O generates the kinetically intransigent phase: plagioclase, which is present in most of the more peraluminous BTB granites.

TiO_2 stabilizes biotite to higher temperatures and lower pressures (both P_W and P_Σ), due to the presence of the titanoxybiotite component: $Ti[\ ]Al_{-1}H_{-1}$, in solid solution (Chapter 8).

MnO promotes the stability of garnet to lower pressures, due to $MnFe_{-1}$ solid solution (Weissbrod, 1973; Green, 1976a).

O_2 and Zn both stabilize hercynite to lower temperatures, due to the effects of magnetite and gahnite solid-solutions, respectively. For example, gahnitic spinel occurred at ~760°C in quartz containing felsic peraluminous magmas of the Macusani region, southeast Peru (Kontak et al., 1984).

Oxygen will also stabilize andalusite (due to the effects of ferriandalusite solid-solution, Grambling & Williams, 1985, cf. Chapter 9) and, with the added solidus-depressing effects of HF and B_2O_3 (Manning et al., 1980; Pichavant, 1981), leads to the occurrence of magmatic andalusite and even magmatic tourmaline (Noble et al., 1984; Kontak et al., 1984).

The combined consequences of these chemical additions will be to blur the edges of the KFMASH-system phase volumes described in this chapter.

Equilibria in the KFMASH system described here provide a template with which to reference more complex chemical systems. For example, equilibria in this analogue system, are used in the next chapter to estimate the peraluminous magmatic mineralogies of the Boobyalla Suite granites.

Chapter 12

PETROGENESIS OF BOOBYALLA AND BABEL ISLAND SUITE GRANITES, NORTHEASTERN TASMANIA

12.1 INTRODUCTION

The Boobyalla and Babel Island Suites have been chosen for petrogenetic investigation because

(a) there are more geochemical, mineralogical and thermobarometric data available for these suites than for those of others;

(b) there is geological, chemical and mineralogical evidence to suggest that these suites are petrogenetically related;

(c) magmatic equilibria in the peraluminous KFMASH chemical system (Chapter 11), can be used as a guide with which to trace the evolution of the magmas of both these suites; and

(d) petrogenetic modelling provides a means of assessing the validity of the magmatic phase relationships in peraluminous granitic magmas (both equilibrium and disequilibrium), which have been proposed in previous chapters.

In this chapter, the nature of the magmatic assemblages of the Boobyalla and Babel Island Suites as deduced from the data of earlier chapters, is described. Next, two alternative major-element models of the Boobyalla Suite granite magmas are presented. One model uses the modified compositional trend of the suites' matrix separates to derive a liquid trend. The other uses the compositional trend of Babel Island Suite granites as the Boobyalla Suite liquid trend. Differentiation processes which could have produced these assemblage sequences are then proposed. Finally, some wider implications of the magmatic modelling of these granites are examined.

12.2 THE NATURE OF THE BOOBYALLA AND BABEL ISLAND SUITE MAGMAS: A SYNTHESIS

Boobyalla and Babel Island Suite granite magmas were suspensions of varying proportions of a variety of crystalline phases in felsic multi-saturated melts (Chapters 3, 4 and 10). Most Boobyalla Suite granite magmas were rich in phenocrysts (Chapter 10). These magmas are considered to have been liquid-poor cumulates generated from magmas with lower, but unknown, crystal/liquid ratios by the mechanism of sidewall accretion (Chapter 1) . In contrast to these, the magmas which generated the Babel Island Suite granites and some Boobyalla Suite granites were poor in phenocrysts (Chapters 3, 4 and 10). These granites therefore appear to

FIGURE 12.1

$P_{\Sigma}P_{W}T$ path for Boobyalla Suite model magmas.

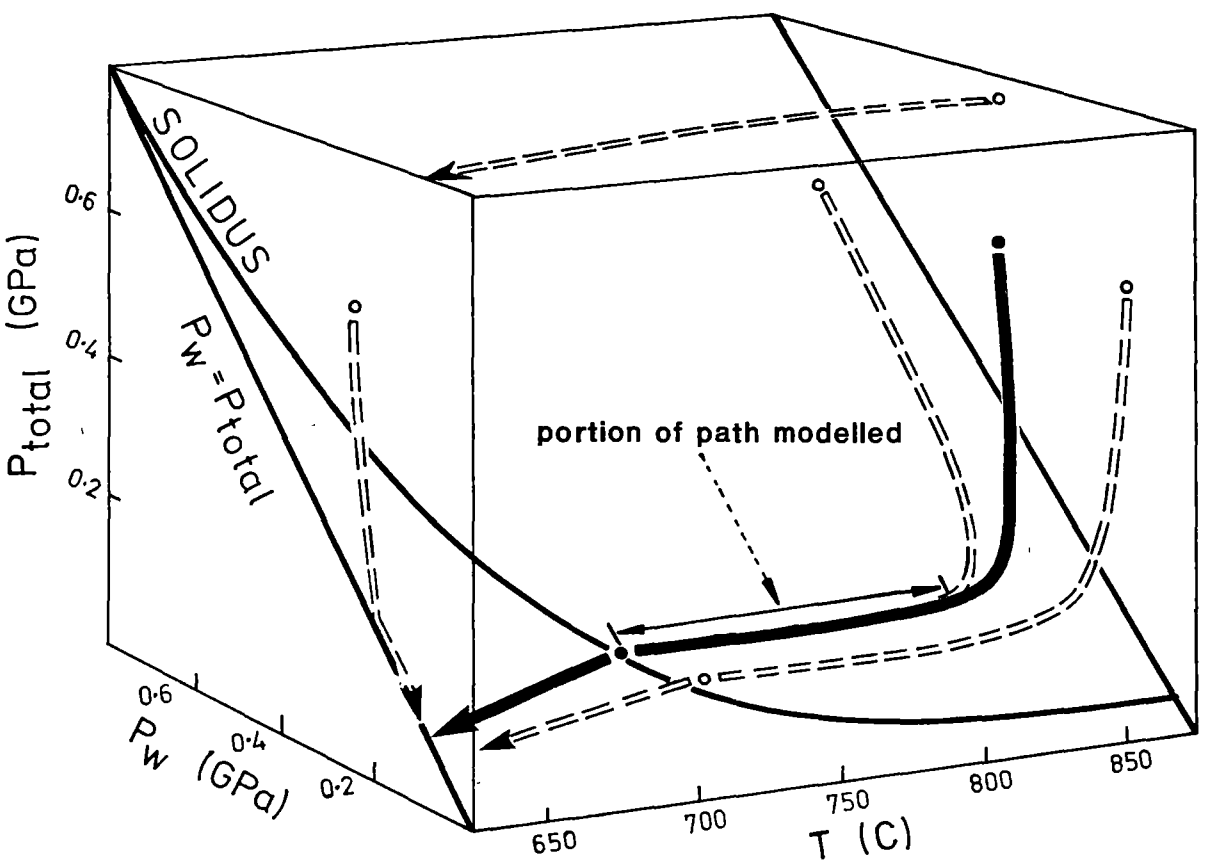

have been derived largely by in situ crystallization of near-liquidus magmas.

Boobyalla and Babel Island Suite rocks have common features, consistent with them having been derived from a common source, despite the fact that they can in detail be chemically distinguished from each other (Chapter 5). Features consistent with a petrogenetic relationship between the two suites are:

(a) a close spatial relationship between granites of the two suites, with those of the Babel Island Suite occurring stratigraphically above those of the Boobyalla Suite (Chapter 3);

(b) the ocurrence of ovoid inclusions of phyric-rich Boobyalla Suite porphyry within the granites of both suites (Chapter 3);

(c) the similarity between most of the mineralogical, chemical, normative and mesonormative characteristics of Babel Island Suite granites, Boobyalla Suite equigranular granites and the porphyry matrixes of both suites (Chapters 1, 4, 5, 6, 7 and 10); and

(d) the similarity in PT paths deduced for each of the suites (Chapter 9).

Magmatic assemblages of the Boobyalla Suite varied continuously from those involving garnet and probably orthopyroxene in the early stages of low-pressure evolution to those involving andalusite in the final stages (Chapters 4, 7 and 9). Most phases can be divided into two categories, on the basis of their relative rates of solid state diffusion (Chapters 1, 7 and 9). Plagioclase, garnet and andalusite are designated a surface equilibrium status, with respect to the melt, whereas biotite, cordierite, orthopyroxene, ilmenite and apatite are designated a volume equilibrium status. Alkali feldspar has an intermediate status (Chapter 9).

The granites of these suites were derived from magmas which evolved approximately isobarically at ~0.15 GPa from ~825^{o}C to ~700^{o}C at $P_W = P_\Sigma$ (Chapters 9 and 11), as depicted in Fig. 12.1.

12.3 MAJOR ELEMENT PHASE-RELATIONSHIP MODELLING

12.3.1 Introduction

Sequences of model magmatic assemblages have been derived from whole-rock compositions of the phenocrystic granites of the Boobyalla Suite. These sequences provide a means of tracing the physical and chemical evolution of the suites' magma, at the site of emplacement. In this section, the method used to derive the sequences, is described.

A model magmatic assemblage can be obtained by statistically fitting a set of estimated major-element phase compositions to a bulk-rock composition, for a given pressure and temperature. This procedure can be represented by the compositional equation:

$$\text{bulk rock} \approx \Sigma(\text{magmatic phases})_{P,T} = (\text{model magma})_{P,T} \qquad (12.1)$$

Over a range of bulk compositions, a set of evaluations of equation 12.1 can be obtained, which by interpolation , can yield a continuous sequence of model assemblages.

12.3.2 Bulk Rock Compositions

Bulk compositions were derived from linear regressions of the compositions of 26 phenocryst-rich granites and porphyries (Appendix R). Modelled mean compositions have ten components: SiO_2, TiO_2, Al_2O_3, FeO*, MnO, MgO, CaO, Na_2O, K_2O and P_2O_5. Water was not included because both the relationship between P_W and P_Σ and the nature of the solute in the vapour phase are insufficiently well known. Bulk compositions range from that containing 1.1% to that containing 2.9% FeO*. This range is slightly greater than that known for the natural rocks. Rock compositional data and their mean trends are depicted on chemical variation diagrams in Figs 12.4 and 12.5.

An isobaric model PT path was chosen. At P_Σ = 0.15 GPa, temperatures vary from 825°C for the most mafic bulk composition, down to 700°C for the most felsic composition.

Linear relationships between temperature and both bulk-rock (magma) and model melt compositions were assumed. These assumptions are necessary because no independent means is known at present, of determining the TX relationships between a melt and the magma in which it exists. Linear TX relationships between the two assumes smooth changes in the compositions of phases and in magmatic phase proportions as a function of temperature. This behaviour is considered likely in multiphase suspensions as complex as those indicated for the Boobyalla Suite magmas.

12.3.3 Phase Compositions

Phases used to model the magmas are alkali feldspar, andalusite, apatite, biotite, cordierite, garnet, ilmenite, melt, orthopyroxene, plagioclase and quartz. Hydrous phases have been recalculated on an anhydrous basis. A compositional model as a function of temperature has been developed for each phase.

Alkali Feldspar

The bulk composition of this phase is deduced to have varied from $(or_{73}ab_{25}an_2)$ to $(or_{64.3}ab_{33.7}an_2)$. A low and constant (an) content accords with the compositions of Boobyalla Suite alkali feldspar separates whereas the range in the or/(or+ab) molar ratio slightly exceeds that indicated from the feldspar separates (Appendix F). The compositions of feldspars from the mafic porphyry #62595 and the felsic porphyritic granite #62622 are especially useful in constraining the compositions of model

alkali feldspars, because these rocks are probably close to the limiting primitive and evolved magmas, respectively.

Within the above limits, the bulk composition of alkali feldspar is assumed to have become increasingly more sodic with decreasing temperature. This non-linear compositional variation is broadly consistent with potassic restite phenocrysts of potassic alkali feldspar having been overgrown by more sodic alkali feldspar which was in equilibrium with more sodic melt compositions.

Andalusite

The compositional model for this phase varies linearly with temperature, from $A_{97}Fa_3$ at 742°C (where Fa is ferriandalusite: $FeAlSiO_5$) down to $A_{99.25}Fa_{0.75}$ at 700°C. The iron-rich compositions are similar to those of the cores of zoned andalusite phenocrysts from this suite (Chapter 7; Plate 6). The bulk-compositional variation is broadly consistent with surface equilibrium crystallization of increasingly aluminous andalusite at growth rates which increase with decreasing temperature.

Apatite

Model apatite has a Ca endmember composition which has been recalculated on a water- and fluorine-free basis.

Biotite

The average composition of high-Ti biotite phenocrysts from the porphyry #43156 and that of high-Ti inclusions in an alkali feldspar megacryst from the porphyry #43248 have been used to derive the biotite compositional trend. Sodium is generally low or absent from biotite compositions (Chapter 7) and has been ignored. The Mn/Fe* molar ratio is assumed to have been constant because its variations with temperature and composition are unknown. The value of 0.004 was chosen because it leads to Mn contents which are broadly compatible with those determined for biotites from this suite.

Given a liquid composition, a relationship between biotite composition and temperature may be formulated by

(i) using the biotite/garnet, garnet/cordierite, and cordierite/liquid Fe^*Mg_{-1} exchange thermometers of Holdaway & Lee (1977) and this work (Chapter 8) respectively;

(ii) using the linear melt composition versus temperature relationships detailed below; and

(iii) assuming that biotite is in volume equilibrium with the melt.

The resulting relationship is:

$$mg_{Bi} = 100/\left[1+\left(\left(\frac{100-mg_{Gl}}{mg_{Gl}}\right).\exp\left[\left(\frac{860+890P}{T}\right) - 2.1\right]\right)\right] \qquad (12.2)*$$

for Bi = biotite, Gl - glass, mg = mol.[100Mg/(Mg+Fe*)], P (GPa) and T (K). This relationship implies that biotite is more magnesian than the equilibrium melt over the PT conditions considered.

Cordierite

A cordierite compositional trend was derived, assuming that compositions had 0.3% Na_2O and 0.2% K_2O, like those of the natural cordierites (Table 6.1 and Appendices F and H). As with biotite, a constant Mn/Fe* molar ratio was assumed. The value of this ratio at 0.007 yields Mn-contents of cordierite which are broadly consistent with those present throughout the natural cordierites (Appendices F and H). It is also consistent with the general equilibrium partitioning relationships between the mafic minerals, which indicate that molar Mn/(Mn+Fe+Mg) should increase in the order: biotite < cordierite < garnet (Thompson, 1976a).

A relationship between cordierite composition, and temperature was established, using the cordierite/liquid Fe^*Mg_{-1} exchange thermometer derived in Chapter 8 (*see footnote, page 12.5), the melt composition versus temperature relationships described below and by assuming that cordierite is in volume equilibrium with the melt.

Garnet

Model garnet is given a constant composition. This is consistent with its composition being largely independent of those of other ferromagnesian phases due to its having lower diffusion rates (Lasaga, 1983). A quaternary composition of $Am_{79.62}Py_{14.05}Gr_{3.33}Sp_{3.00}$ was chosen. It corresponds to that near the magnesian limit of the trend of Boobyalla Suite garnet compositions (Chapter 7). This composition has been chosen, rather than the limiting magnesian core composition, because overgrowth of Fe-rich garnet is considered to have overgrown onto these restitic cores. Evidence for low-pressure garnet growth comes from the occurrence of cummingtonite and (quartz+biotite) pseudomorphs which are probably after

---

* The two equations describing cordierite/melt and orthopyroxene/melt Fe^*Mg_{-1} exchange equilibria used in this chapter are:

(a) $T(K) = \frac{863 + 740\ P}{2.72 + \ln K_D}$, and (b) $T(K) = \frac{2650 + 460\ P}{3.28 + \ln K_D}$ respectively.

These are slightly different from those listed in Table 9.2 and were derived using data from a manuscript of Ellis (1986) which was superceded prior to publishing of this paper. The mg values of biotite, cordierite and orthopyroxene calculated using (a) and (b) above, differ from those listed in Appendix S by less than 5%. The equations of Chapter 9 give slightly more magnesian compositions for the model phenocryst phases than do (a) and (b) above.

orthopyroxene inclusions near the rims of garnet phenocrysts (Plate 4, Figs G, C and D). Pseudomorphs after orthopyroxene are not known to occur in the (high-pressure) cores of garnet.

A low-pressure paragenesis for orthopyroxene in the magmas of this suite is implicated by analogy with the low-pressure occurrence of this phase in the volcanic equivalents of the Strathbogie Batholith (the Violet Town Volcanics) in central Victoria. Garnet phenocrysts in these rocks occur with coronas of hypersthene+cordierite (Clemens & Wall, 1984). This texture is interpreted as being the result of decompression (op. cit.). It is also consistent with theoretical evidence for low-pressure orthopyroxene growth, in the peraluminous KFMASH system above ~800^{o}C, as shown in Fig. 11.3 of the previous chapter. Because orthopyroxene is considered to be a low-pressure phase, then its enclosing host garnet must also be a low-pressure phase.

Garnet grown in surface equilibrium with melts of the compositions chosen below, are more iron-rich (mg ~ 16-5) than the limiting core composition for this phase (mg ~ 17; Chapters 7 and 9), as indicated using the garnet/melt thermometer: formulation #3 of Table 8.3 for which it was assumed that sodium plays an equivalent role in the melt to potassium. The bulk composition of garnet is therefore expected to become more iron-rich during magmatic evolution at the site of emplacement.

However the discontinuous reactions intersected by the PT path as the solidus is approached, all consume garnet (Chapter 11), so the bulk composition of garnet should subsequently increase in (mg) as the iron-rich rim preferentially reacts. These bulk-compositional fluctuations cannot be modelled at the present stage, hence the use of a constant composition for garnet.

Ilmenite

Model ilmenite contains 1% MnO.

Melt

Two alternative model melt trends have been used. **Model A melts** were derived by regressing adjusted compositions of Boobyalla Suite porphyry matrices; adjustment is to more iron-rich compositions. Adjustment is necessary because matrixes are inferred to have exchanged Fe* for Mg with mafic phenocryst phases, during subsolidus stages of petrogenesis (Chapter 9).

Regressed compositions were changed by exchanging Mg for Fe* on a molar basis to yield a model melt trend with compositions which are in Fe*/Mg equilibrium with biotites of mg′ ≈ 26 at the mafic end (at 825^{o}C and 0.15 GPa) and biotites of mg′ ≈ 12 at the felsic end (at 700^{o}C and 0.15

GPa) These limits broadly correspond to those of phenocrystic biotites from Boobyalla Suite rocks (Appendix H).

Without an independent reference for the Fe*/Mg composition of the melt, rock-biotite compositions were chosen as guides for the compositions of magmatic biotites and hence (using equation 12.2) for the melt phase; biotite compositions are expected to have changed **less** than those of the other major ferromagnesian phases: melt (or its subsolidus analogue: matrix) and cordierite. They will have been buffered during magmatic and subsolidus reactions in which cordierite, biotite and melt (or matrix) participate, because cordierite is more magnesian and melt: less magnesian than coexisting biotite (Thompson, 1976a; Ellis, 1986; Chapter 8).

The trend for **Model B melts** was obtained by regression of Babel Island Suite granite and porphyry matrix compositions. No adjustments were made to these compositions.

As described for the bulk compositions above, a linear relationship between model melt composition and temperature has been assumed.

Limiting mafic compositions for each melt trend have been chosen using a rheological criterion: that the model magmas had greater than about 25 vol% liquid. This value corresponds to the volume fraction of space interstitial to packed solid grains of roughly similar size, range and shape (van der Molen & Paterson, 1979; Arzi, 1978). A **weight** proportion lower limit of ~25% is therefore indicated, because the density of the melt will be somewhat less than the density of the bulk solid phases.

Limiting felsic compositions were chosen using phase equilibrium criteria:

(a) that aluminosilicate phases be confined to temperatures below ~750°C;
(b) that biotite be present in all model magmas; and
(c) that the compositions of biotite in equilibrium with the most felsic melts, be similar to those found as phenocrysts in the suites' felsic porphyries (Fig. 7.2, Appendix H).

Orthopyroxene

The trend for this phase was derived, assuming it to have contained 1% CaO present as calcium tschermaks molecule (CaTs: $CaAlSiAlO_6$). A small proportion of this molecular component accords with the quantities of CaO found in low-pressure pyroxenes which are in equilibrium with garnet containing ~5% of grossular (Harley, 1984).

A relationship between the composition of orthopyropxene, the temperature and melt composition was established, using the orthopyroxene/liquid Fe^*Mg_{-1} exchange thermometer derived in Chapter 8 (*see footnote, page 12.5).

Plagioclase

Model compositions for bulk plagioclase varied from $an_{42.68}ab_{54.32}or_3$ in the most mafic, to $an_{30.07}ab_{66.93}or_3$ in the most felsic magma. The most calcic composition is that of the cores of phenocrysts from this suite (see profiles, Chapter 7). The most sodic composition is close to that of the plagioclase phenocryst separate from the felsic phyric granite #62622.

The plagioclase bulk composition is assumed to have become increasingly more sodic with decreasing temperature. This non-linear compositional variation is consistent with calcic restite plagioclase having been overgrown by progressively more sodic rim-plagioclase, as indicated in the compositional profile across the phenocryst in the porphyry #62619 (Fig. 7.10). The bulk-composition versus temperature relationship between the designated limits was arbitrarily assigned. It is asymptotic to the core composition and is described by the relations:

$$\left.\begin{aligned} or/(an+ab+or) &= 0.03, \\ \alpha = an/(an+ab) &= 0.44 \quad \{808 < T(^{\circ}C) < 825\} \\ \text{and } \alpha = an/(an+ab) &= 0.4439-0.0031927 \exp[0.03456(808-T(^{\circ}C)] \\ &\qquad \{700 < T(^{\circ}C) < 808\} \end{aligned}\right\} (12.3)$$

Quartz

Quartz is assumed to be pure SiO_2.

12.3.4 Statistical Fitting Procedure

Statistical solutions to equation 12.1 were obtained using the FORTRAN program PETMIX (the use of which is described by Taylor et al. (1973). Input data consist of the compositions of (p) phases in (c) chemical components, where $p < c$. Output consists of weight fractions of each phase, together with their standard deviations. The degree of the fit is indicated by the sum of the squares of the residuals between the estimated and the target bulk compositions.

Abundant petrographic evidence exists to indicate that the suites' magmas were assemblages of up to eleven major phases, including vapour. Trace phases such as zircon, monazite and xenotime were also present (Chapter 4). By the Phase Rule, they were therefore low-variance assemblages. In the ten component system considered here, nine or ten phases commonly coexist, that is, model assemblages are di- or tri-variant.

Because it is not possible to obtain a meaningful statistical solution when $p = c$, a method was developed whereby the compositions of the two feldspars were merged and their combined composition presented as that of one phase. This was facilitated by assuming that the molar ratio an/(an+ab) in plagioclase was linearly related to the molar ratio

or/(or+ab) in alkali feldspar. Combined feldspar compositions can then be defined using two variables:

α = the molar ratio: an/(an+ab) in plagioclase (above),

and β = the molar range: $\frac{\text{alkali feldspar}}{\text{alkali feldspar + plagioclase}}$.

The weight fractions of the separate feldspars can be calculated from that of the combined feldspar, computed using the PETMIX program, using these same variables.

Obtaining a solution to equation 12.1 requires finding the appropriate values for the compositions of the model magma (bulk rock) and its constituent phases. This is now possible because they have all been modelled as functions of the independent variable: temperature. The procedure used to obtain a solution is to:

(a) assign a magmatic temperature within the range ($700 \leq T(^{o}C) \leq 825$);
(b) determine the target (model magma) composition with which it is linearly related;
(c) find the melt composition;
(d) find the compositions of biotite, cordierite and orthopyroxene which are dependent upon that of the melt using equations 12.2, 8.7 and 8.6, respectively;
(e) determine the molar ratio (α) for the merged feldspar composition;
(f) assign a value for (β), the proportion of alkali feldspar in the merged feldspar and calculate the resulting feldspar composition;
(g) input these compositions, together with those of the appropriate phases with fixed compositions (apatite, ilmenite and quartz) and run the programme PETMIX; and
(h) repeat steps (f) and (g), changing (β) each time, to minimize the sum of the squares of the residuals.

12.4 RESULTS

Two sets of seven solutions have been obtained using the above procedure, one for each of the alternative models. Each set spans the range of phyric whole-rock model magma compositions. They depict the evolution of those magmas which subsequently solidified to form phyric Boobyalla Suite rocks. They therefore represent only part of the magma which was present in the pluton at any one time. The sequences do not represent closed-system evolutionary trajectories from initial to final

FIGURE 12.2 Proportions of phases in Boobyalla Suite model magmas.

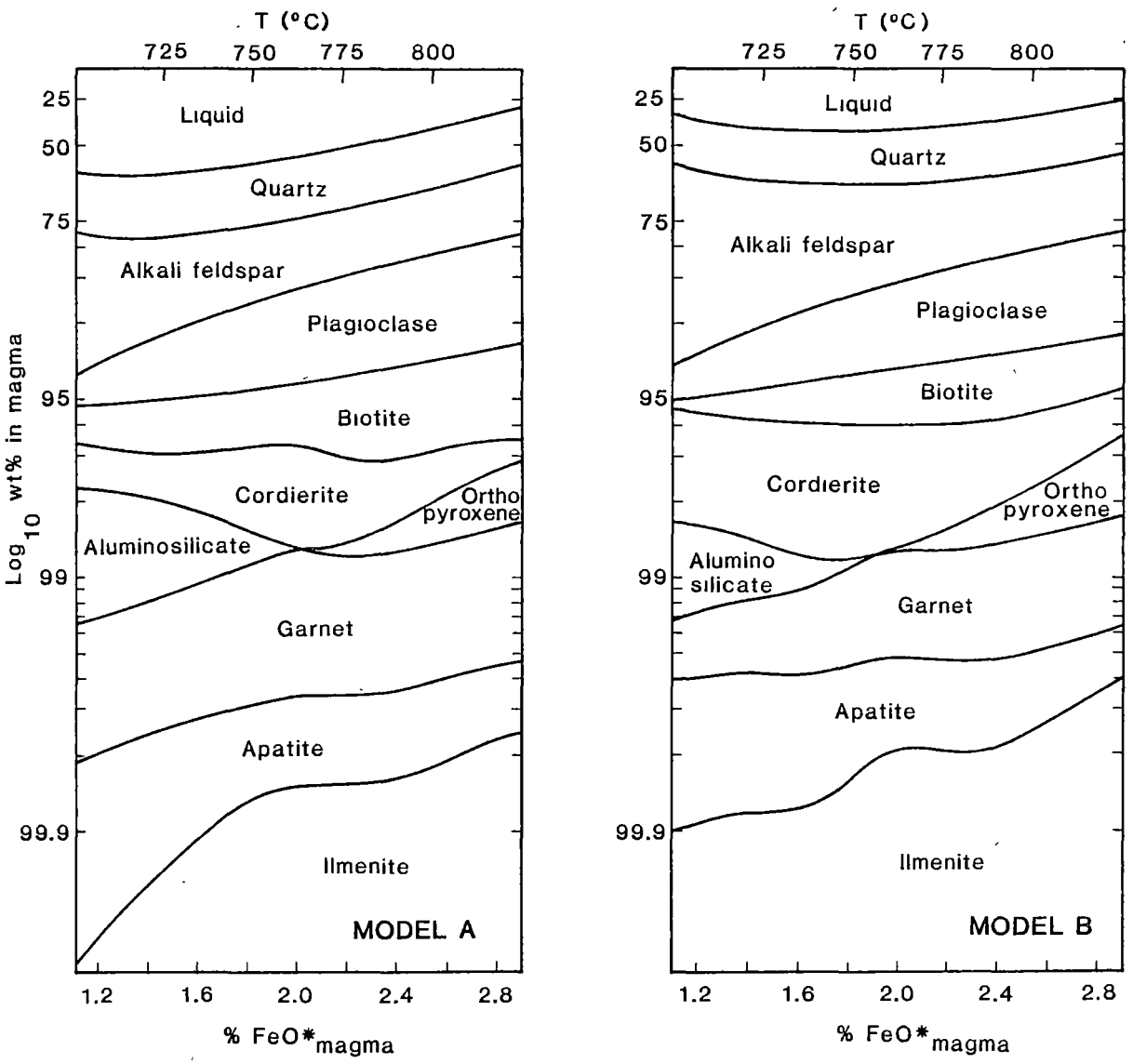

FIGURE 12.3

Distribution of solids to melt in Boobyalla Suite model magmas .

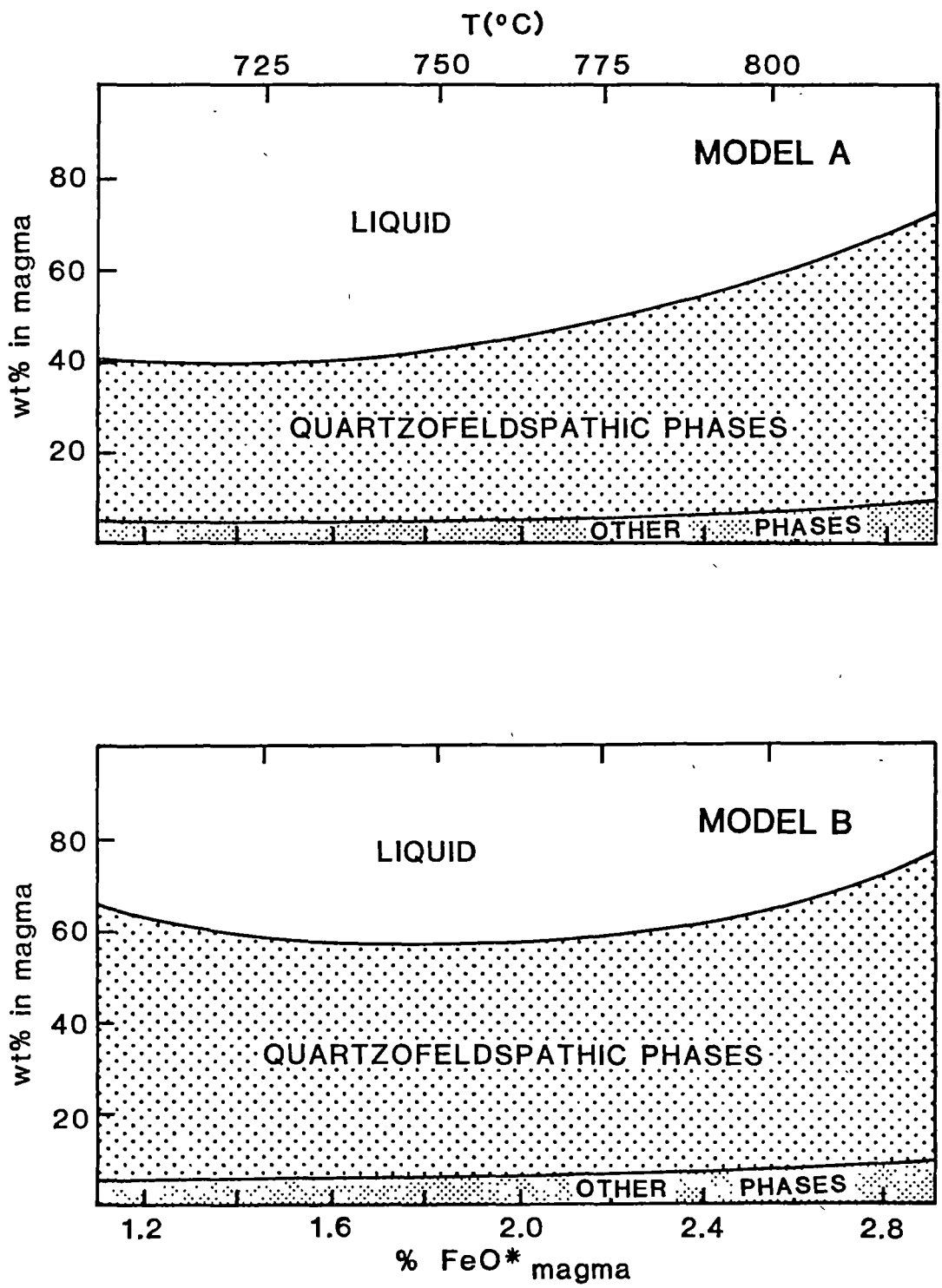

magmas. The data of these solutions are tabulated in Appendix S and presented graphically in Figs 12.2 to 12.6.

The model assemblages obtained have low sums of squares of residuals ($\leq$0.0004), indicating good fit. There is a high degree of consistancy between assemblages within each set, leading to smooth variations in phase proportions within each sequence.

The two sequences have similar general features. They both predict the magmas to have been crystal-rich and indicate evolution to more peraluminous and iron-rich compositions. They have similar assemblage trends.

Differences between the sequences exist. Towards the end, model A magmas become more liquid-rich and poorer in quartzofeldspathic phases than do model B magmas (Fig. 12.2). Consideration of the assemblages in each model (Fig. 12.3) indicates that more residual garnet is present at the end of magmatic evolution in model A, compared with model B. Cordierite is more abundant and aluminosilicate less abundant in the B- than in the A-sequence.

Estimates may be made of the proportion of solid magmatic phases which are restite (that is, are disequilibrium phases from the source region) and that which are non-restite (that is, phases which are in equilibrium with low-pressure melts) (Chapter 1). The restite constituent consists of the cores of quartzofeldspathic phases and the cores of garnet. The non-restite constituent consists of the rest of the solid phases in the magma.

An estimate of the weight fractions of restite phases in these magmas may be made, from a consideration of their nature in the magma at 825^{o}C, subsequent to ascent from the source region, but prior to evolution at the site of emplacement. Near-isothermal decompression of the magma from the source region will result in an increase in P_W relative to P_Σ (cf. Fig. 12.1). By analogy with the equilibrium in the KFMASHO analogue system, this path will result in further melting, with quartz alkali feldspar and garnet being resorbed (Chapter 11). Resorption of alkali feldspar and garnet is predicted because the suite $P_\Sigma P_W T$ path passes out of the magmatic phase volumes of both of these minerals before the water-saturated plane is reached at 825^{o}C and 0.15 GPa in the KFMASH analogue system (cf. Fig. 11.6). Some resorbtion of plagioclase is also likely with continued partial melting. Therefore alkali feldspar, garnet, plagioclase and quartz crystals present in the magma upon emplacement should be residual restitic phases, if exchange-reaction rates were less than net-transfer reaction rates, during magmatic ascent from the source to the emplacement region. This conclusion was also reached by Sykes & Holloway (1987) using

FIGURE 12.4

Proportions of restite and non-restite in Boobyalla Suite model magmas.

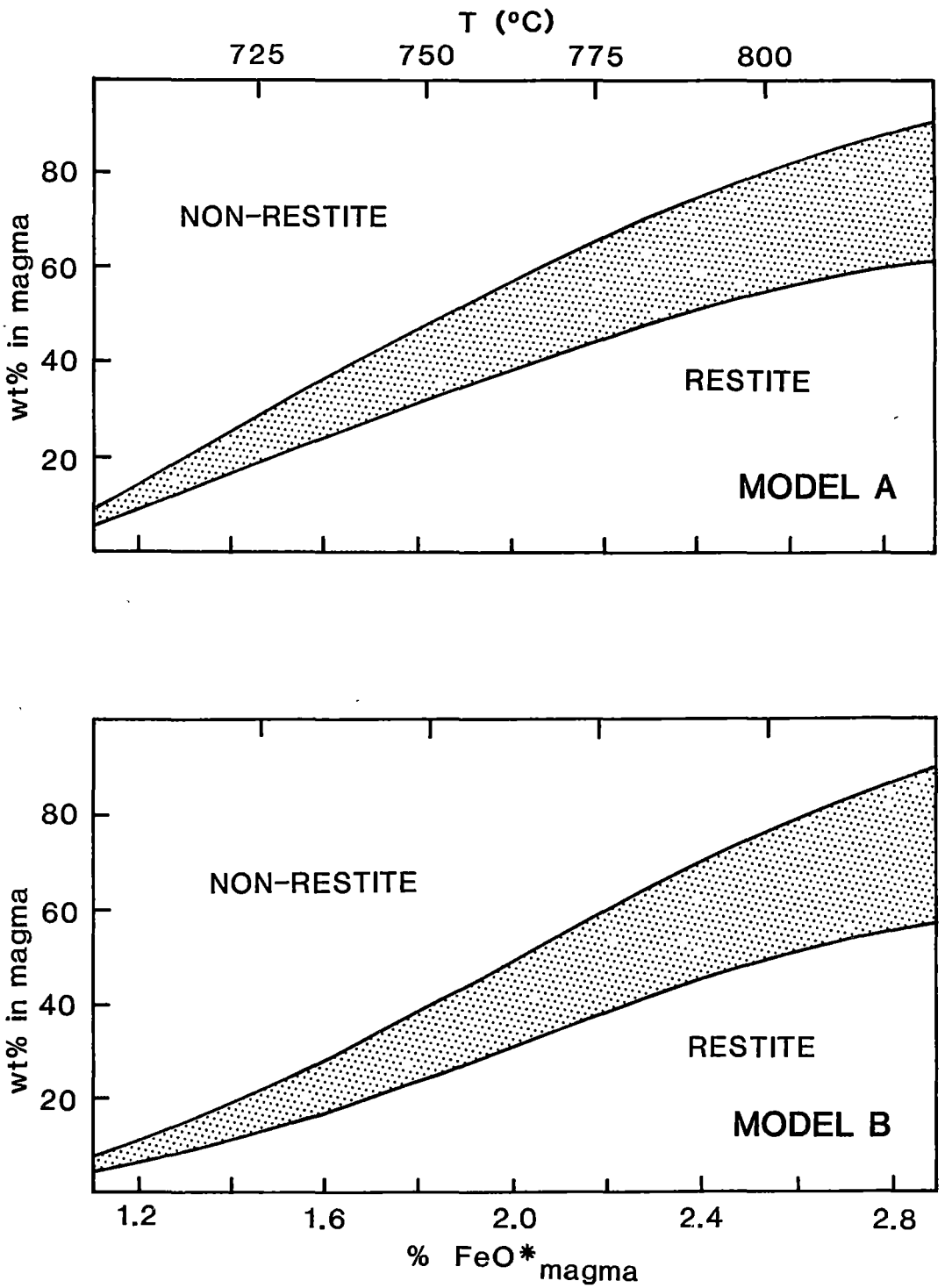

Stippled area: uncertainty of division (see text for details)

thermochemical and rheological arguments. The proportions of both quartz and alkali feldspar in the magma at 825°C, will then be estimates of the restite portions of these phases **throughout** magmatic evolution, providing that:

(a) none of these phases were resorbed at any stage during low-pressure evolution, and

(b) atomic-exchange between core and overgrowth portions of each phase were negligible.

The proportion of non-restite to restite plagioclase at each stage of low-pressure magmatic evolution can be obtained using the proportion at the start (zero: as described above) by assuming:

(a) a proportion at the end of evolution, and

(b) a simple linear growth rate versus inverse temperature relationship for plagioclase.

The proportions of non-restite to restite quartz and alkali feldspar at each stage can then be obtained using the proportion determined for plagioclase, together with the restite proportions of quartz/plagioclase and alkali feldspar/plagioclase described above.

Limiting estimates of the proportion of the total restite assemblage in the solid fractions of the magmas, are depicted for each model in Fig. 12.4. For the **upper limit**, a value of 50% was chosen for the proportion of core-plagioclase at the end of evolution. This value is derived using the shape of the compositional profile of the plagioclase phenocryst, in the porphyry #62619 (Fig. 7.10), assuming the crystal to have had a simple cubic shape, with a core to mantle density ratio of 1. It is an upper limit because:

(a) the plagioclase crystal used to designate the restite to non-restite status of this phase at the end of magmatic evolution, comes from a porphyry which has plagioclase- and biotite-separate bulk-compositions which are respectively too calcic and too magnesian for the host magma to have been a final magma; and

(b) low-pressure growth of garnet was assumed to have been negligible.

A **lower limit** to the proportion of restite in each magma sequence was obtained by not assigning any restitic component to garnet, assuming that alkali feldspar was **always** in equilibrium with the melt phase and by assigning a zero restitic component to the bulk-plagioclase at the end of magmatic evolution.

The resulting proportions of restite and non-restite solid phases in each of the two petrogenetic models, are very similar (Fig. 12.4). The ratio of non-restite to restite for each quartzofeldspathic phase increases

FIGURE 12.5 Comparison of selected major-element chemical data for Boobyalla Suite natural rocks and model magmas.

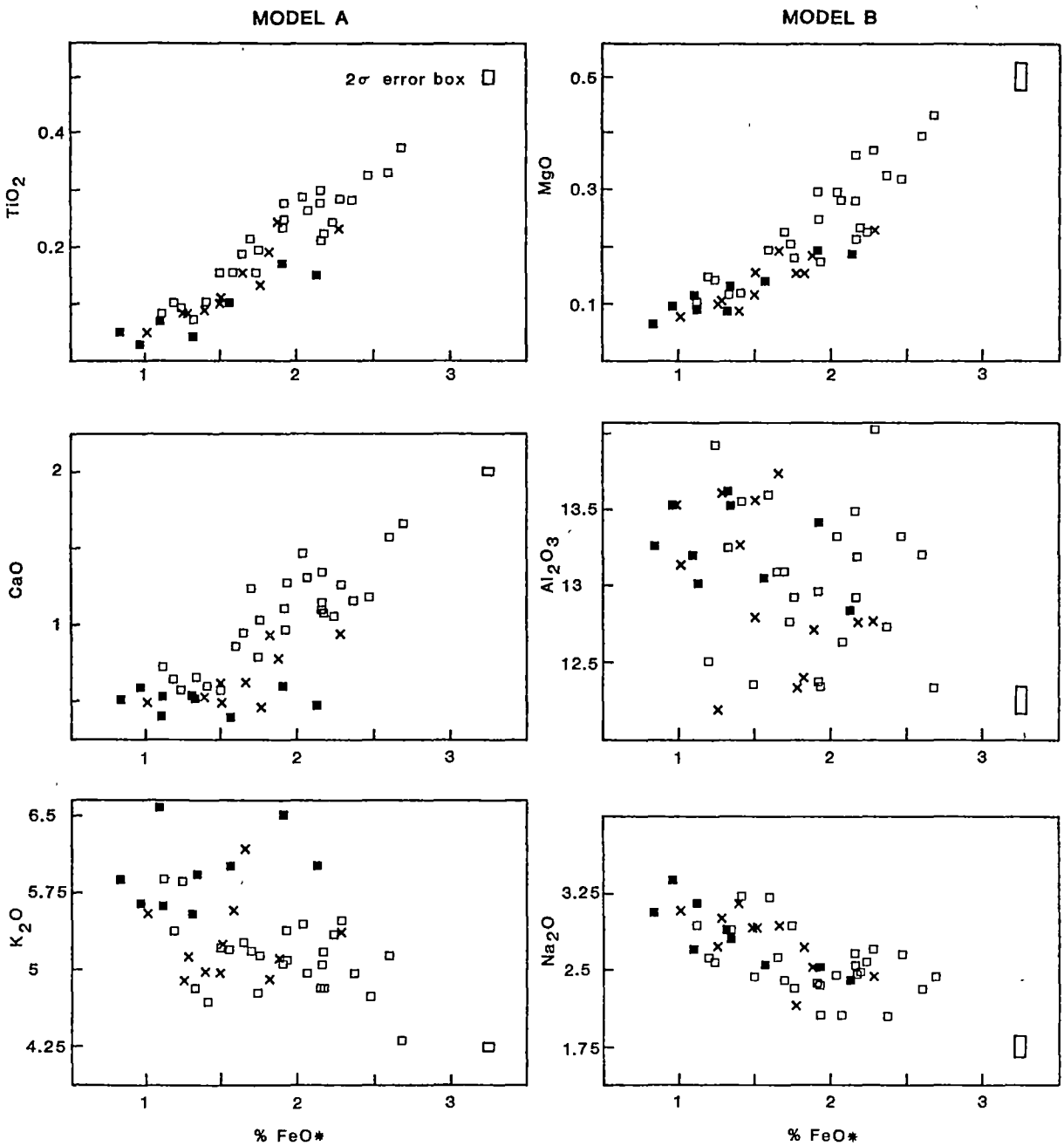

Filled squares: porphyry matrix separates
Open squares: porphyritic granite whole-rocks
Crosses: phenocryst-poor porphyries

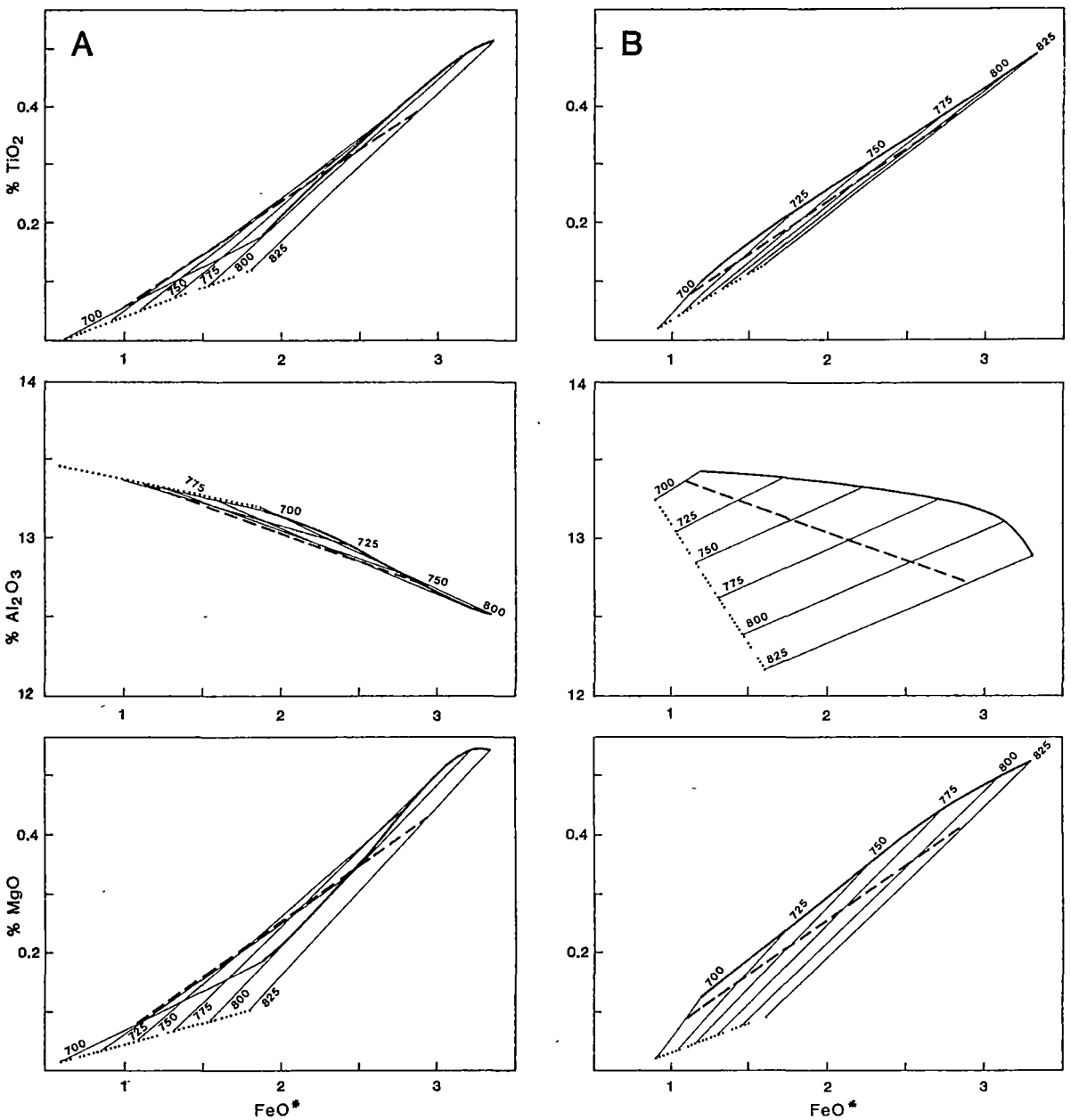
A
B
% TiO2
% Al2O3
% MgO
FeO*
700
725
750
775
800
825
0.2
0.4
12
13
14
1
2
3

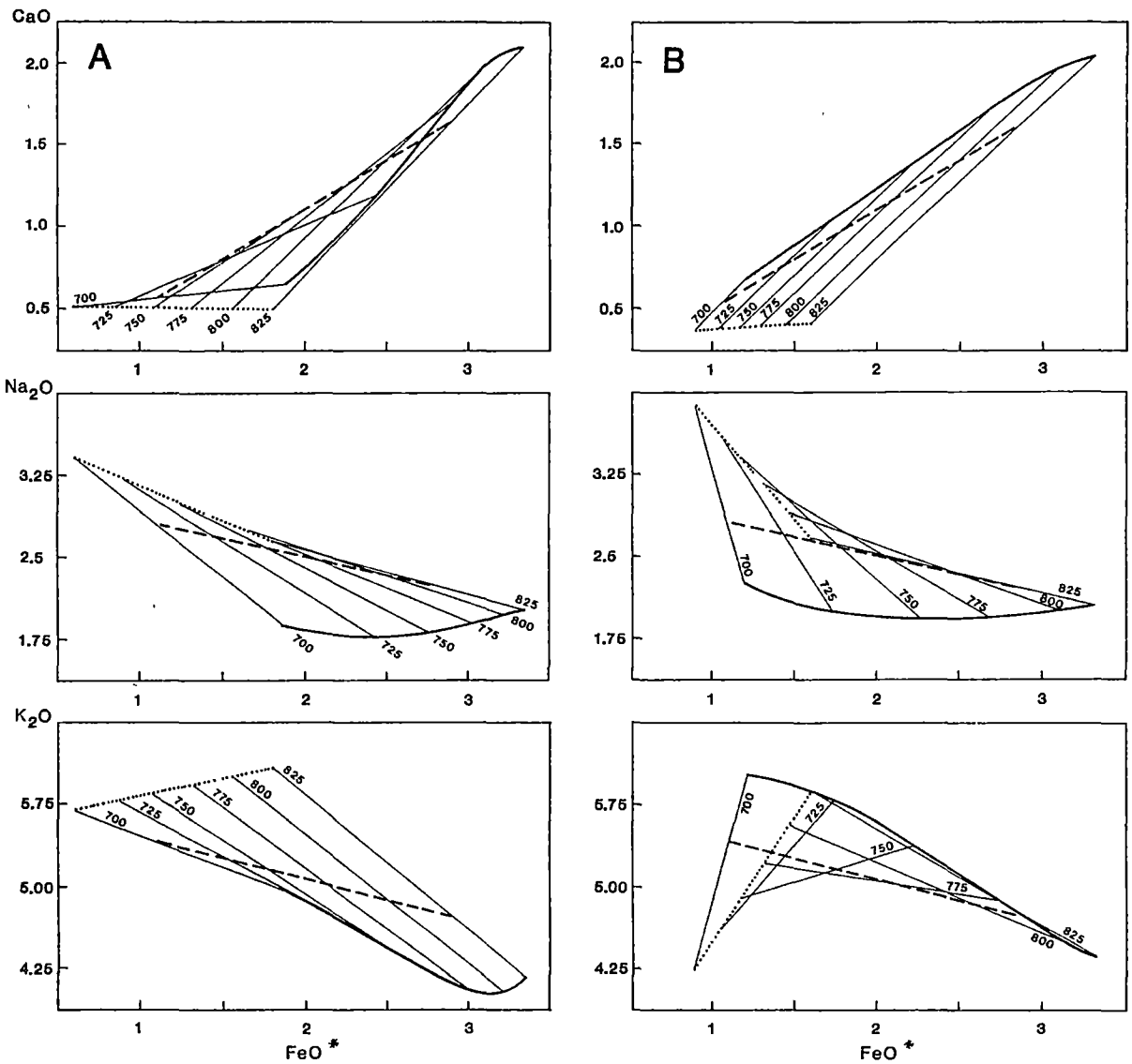

Dotted lines: melt trend
Thick continuous line: bulk-solid assemblage trend
Dashed line: magma trend
Thin lines: isothermal tie lines (temperature: C)

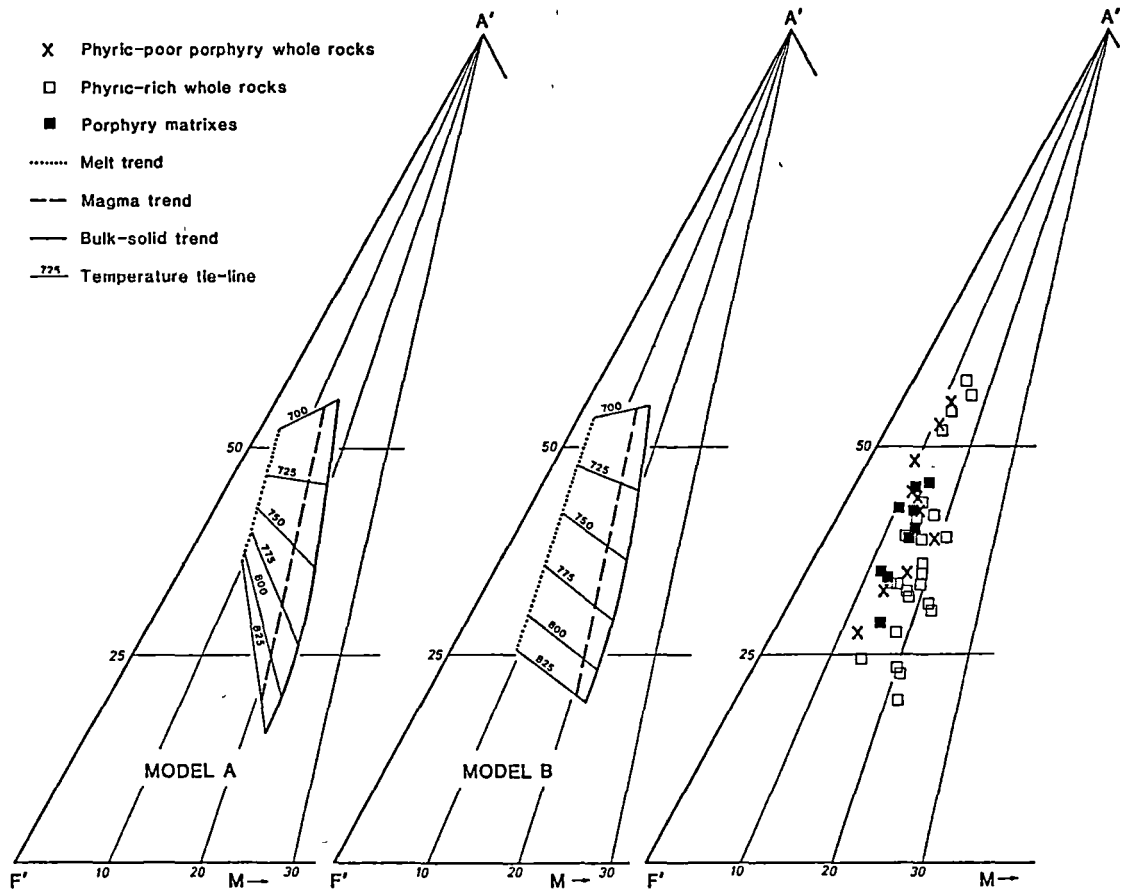

Fig. 12.6 Comparison of A'F'M data for Boobyalla Suite natural rocks and model magmas.

continuously as the temperature decreases. This is consistent with continual growth of each of these three phases, during magma evolution at low pressures. Initially emplaced magmas are indicated to have contained solid fractions with up to ~90% of restite phases. This proportion decreases rapidly as the magmatic temperature and the bulk-magma FeO* content decrease. Eventually restite occurs as only a minor or trace constituent at the end of evolution; the solid assemblages in both models are dominated at this stage by non-restite.

The composition of the bulk solid constituent of each model magma may be calculated from the composition of the individual phases and the computed phase proportions. Accordingly, three **different** compositional trends may be constructed on covariance diagrams. They are respectively, those of the model melt, the bulk-solid and intermediate between these: that of the magma. Isotherms link these trends to form a grid. Such grids trace the physical, chemical and thermal evolution of each sequence of model magmas.

In Figs 12.5 and 12.6, the grids are compared with Boobyalla Suite compositional data of:

(a) the matrix-separates;

(b) the phyric-rich whole-rocks used to derive the magma trend; and

(c) the phyric-poor porphyries and equigranular granites.

On textural grounds, the phyric-poor rocks should have been liquid-rich magmas and their compositions should therefore err in the direction of the liquid-, rather than the solid-trend, in each grid. Phyric-poor whole-rock compositions generally plot between those of the model melts and the magmas on Figs 12.5 and 12.6 in accordance with the assessment on textural grounds.

12.5 DISCUSSION

12.5.1 Choice of Petrogenetic Model

Consideration of the spatial relationships between chemical data and model grids in Fig. 12.6, can go some way towards indicating which model best describes the evolution of the Boobyalla Suite magma. For model A, the melt and bulk-solid trends on TiO_2, Al_2O_3 and MgO versus FeO* diagrams, approach colinearity. Variable separation of solid from liquid along the isotherms, cannot therefore result in significant compositional departures from the mean magma trends, for these element pairs.

The tight linear trends of compositional data for TiO_2 and MgO versus FeO* are consistent with the colinear trend geometries of their respective grids in both of the models. However data for Al_2O_3 are highly variable and are therefore inconsistent with the Al_2O_3 versus FeO* grid of model A.

FIGURE 12.7

RELATIONSHIPS BETWEEN MATRIX , BULK-PHENOCRYST AND WHOLE-ROCK COMPOSITIONS FOR BOOBYALLA SUITE PORPHYRIES

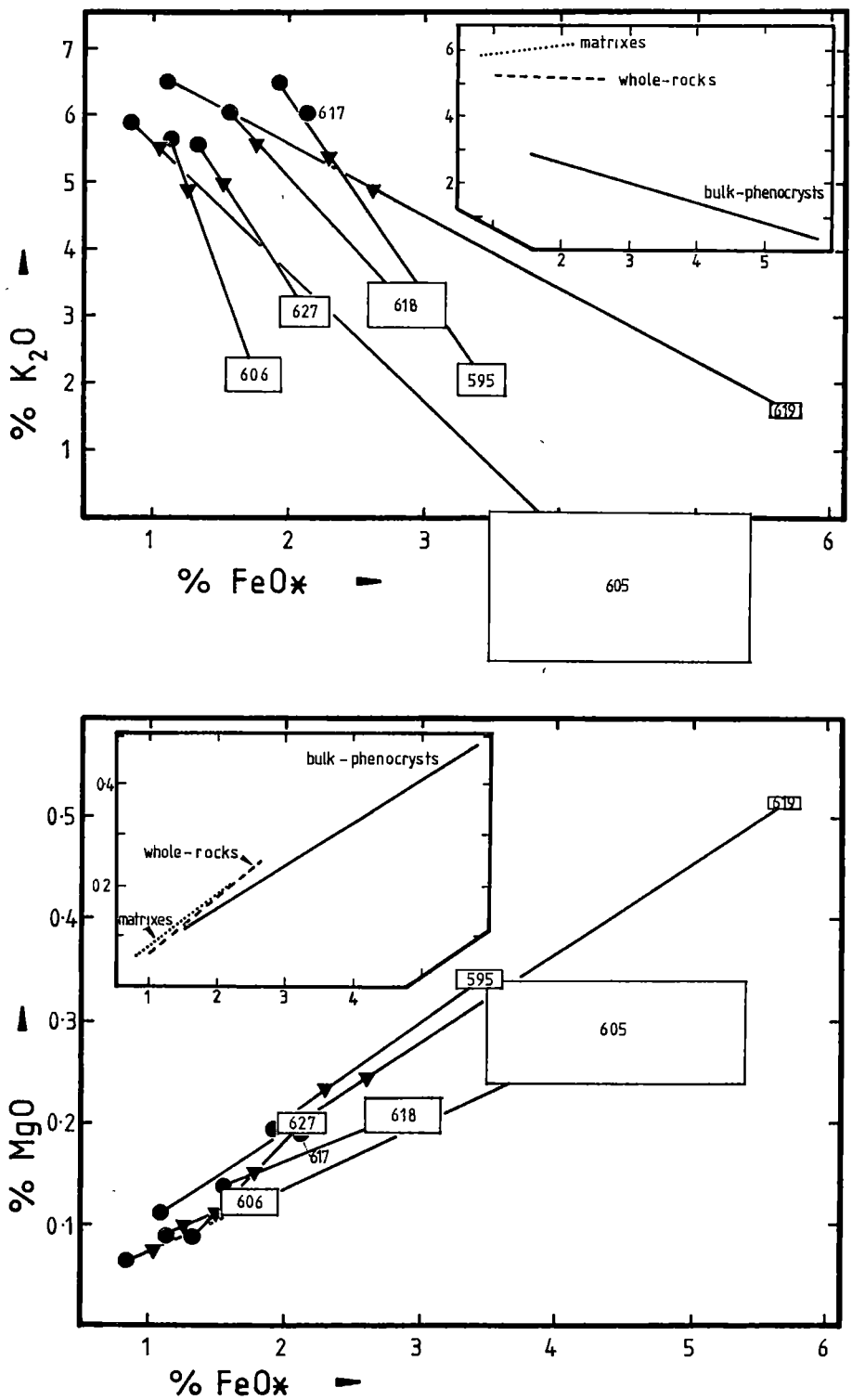

Filled circles: matrix separates; filled triangles: whole rocks; boxes: bulk phenocrysts. Sample numbers are shown without their "62" prefix. Boxes for the 2σ error estimates of the bulk-phenocryst compositions were calculated from XRFS 2σ error estimates (Appendix D) of matrix and whole-rock data (Appendix E) and assuming ±10% error in the modal data (Appendix Q) and ±5% error in the density data (Appendix P).

These data are more consistent with the grid for model B in which the melt and bulk-solid trends are spaced far apart. Variable separation of solid from liquid along model B isotherms will generate bulk compositions which scatter over a large area, just as the data are scattered.

Within the constraints of the computed 2σ compositional precision (Appendix D), model A grids collectively encompass 72% of covariance data (Fig. 12.6), whereas model B grids encompass 81%.

The model B sequence is preferred to that of model A because:

(a) the data regressions used to derive the melt trends of model B have higher correlation coefficients than those used to derive the model A melt trend (Appendix R);

(b) the model B melt trend did not require adjustments to reach compositions consistent with melt/phyric-phase equilibria as was required in order to obtain the model A melt trend; and

(c) its magma-constituent grids better accommodate the whole-rock data.

Differences both in the assemblages (Fig. 12.3) and in corresponding magma-constituent grids (Figs 12.5 and 12.6) predicted by each model, are due to the compositional differences between the two melt trends. The model A melt trend is more potassic, more aluminous and less sodic for a given FeO* content, than is that of model B. Its range of FeO* is also greater than its model B counterpart. These melt trend differences could be due to the porphyry matrixes having contained small proportions of peraluminous phenocrystic phases (as discussed in Chapter 6) and having exchanged Na for K with adjacent feldspar phenocrysts, in addition to the Fe* for Mg exchange with the mafic phenocrysts (Chapter 9).

Diagrams C and F of Fig. 12.6 may be compared with those of Fig. 12.7. The latter depict compositional data for the matrix separates, bulk-phenocrysts and whole-rocks from some Boobyalla Suite porphyries, computed using the compositional density and modal data from Appendices D, E, P and S. There are broad similarities between the granite magma and the porphyry constituent trends for each diagram. Differences between them are ascribed to:

(a) the high and variable extent of solid-phase sorting by the Bagnold boundary effect, associated with the emplacement of the small porphyry intrusions (cf. Chapter 3) in contrast to the lesser extent of sorting envisaged during the larger-scale processes of granite petrogenesis (e.g. Barriere, 1976) described below ; and

(b) the effects of subsolidus chemical exchange such as of Fe* and Mg between porphyry phenocrysts and matrix.

12.5.2 Interpretation

Boobyalla Suite phyric whole rocks have been modelled as low-pressure (0.15 GPa) crystal-rich magmas which spanned a temperature range from 825°C to 700°C. In these magmas, the proportion of restite phases decreases continuously, consistent with the solid component of the magma being continuously augmented by the products of multi-phase magma fractionation. Melt compositions are similar to those of the equigranular alkali feldspar granites which in the field, can overlie the phyric granites. These features are consistent with the phyric granites being derived by solidification of cumulates generated by sidewall accretion during the evolution of the crystal-containing bulk magma. Crystal-poor melt destined to form the Babel Island Suite equigranular granites separated, during sidewall crystallization, as a low-density buoyant boundary layer (Nilson et al., 1985). A range of coexisting magmas from crystal-rich to crystal-poor character are therefore inferred to occur simultaneously in each evolving pluton. Magma chamber evolution is schematically illustrated in Fig. 12.8.

Melt and coexisting solid phases have compositions which indicate that **peritectoid** rather than **eutectoid** reactions occurred within the magma. This accords with a $P_{\Sigma}P_{W}T$ path which, by analogy with the KFMASH system grids of Chapter 11 (Fig. 11.6), starts inside and proceeds through the grid of peritectic reactions below the liquidus, on its way to the vapour-saturated solidus. The low-pressure model magmatic assemblages (Figs 11.8 and 12.2) are similar to those predicted for the vapour-saturated cooling stage in the analogue system, with orthopyroxene-bearing assemblages and then garnet-bearing assemblages giving way to biotite-cordierite and finally to andalusite-biotite-cordierite assemblages (Figs 11.8 and 12.2). The same sequence of mafic phase assemblages is indicated in the natural rocks of this suite (Fig. 4.1).

12.5.3 Potential Tests of the Petrogenetic Model

In this section, rheological, experimental, petrological and isotopic tests of this model are suggested.

Analogue studies of aqueous suspensions might determine whether features proposed for evolving aphyric magmas such as the occurrence of a buoyant boundary layer and crystallization largely from the walls (McBirney et al., 1985) are feasible also for evolving crystal-containing magmas. Such studies would augment theoretical work already undertaken, which predicts that the concentration of suspended crystals should decrease towards the chamber walls due to the Bagnold boundary effect, thereby facilitating magma evolution by convective liquid fractionation (Baker & McBirney, 1985).

FIGURE 12.8

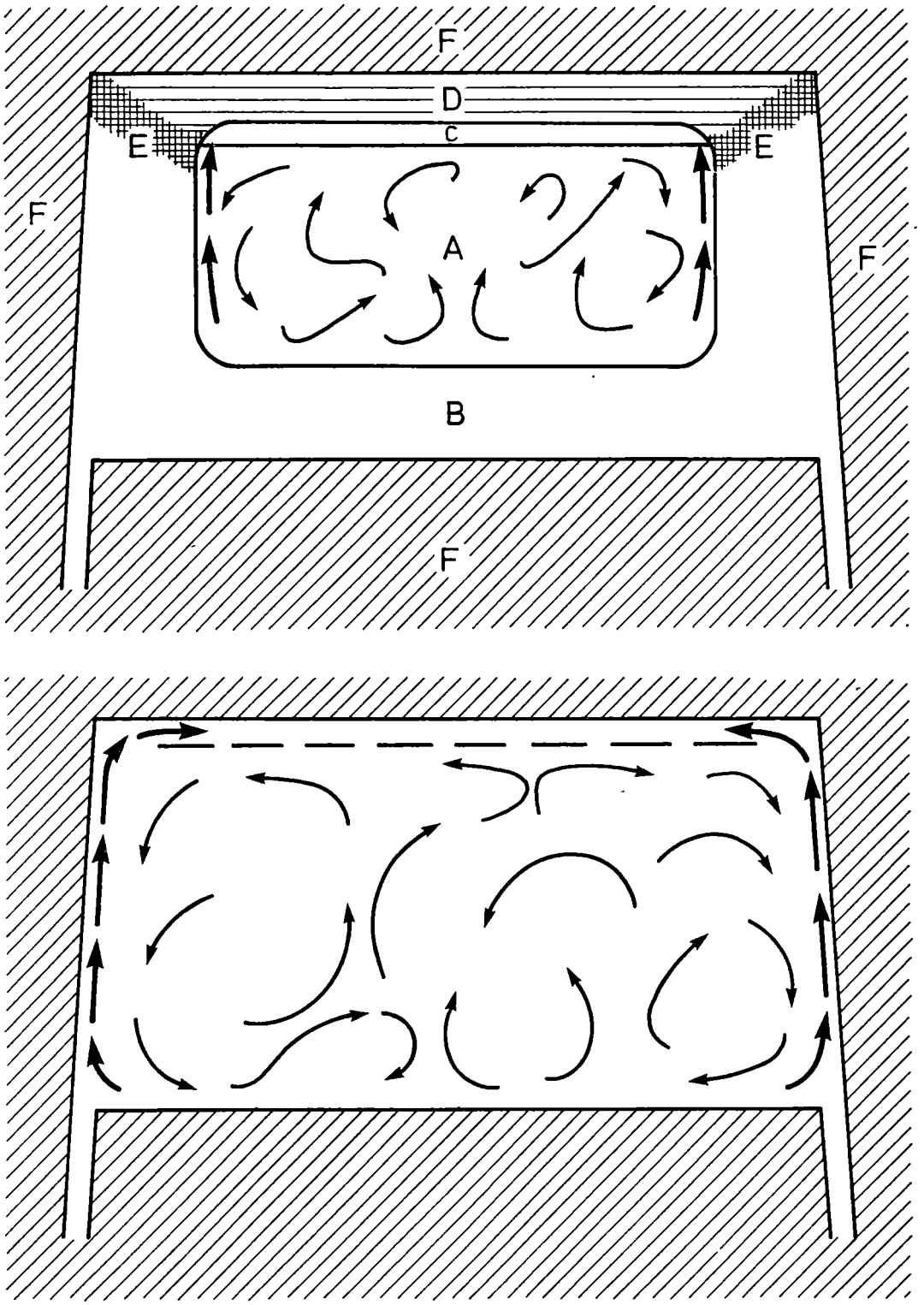

Stages of magma chamber evolution. A - crystal-rich lower magma; B - accreted residua from lower magma evolution yielding lower zone granites; C - liquid-rich upper magma; D - silicified upper magma:upper zone granites; E - transition zone between upper and lower zone granites; F - country rock.

← transient directions of convection currents

⬅ phyric-poor boundary layer transporting liquid-rich magma to upper chamber.

Experimental petrological studies might determine the exact equilibrium assemblages and phase compositions for each set of proposed $P_{\Sigma}P_{W}T$ conditions. Phase compositions which are the least well-known are proably those of biotite liquid and magmatic alkali feldspar.

The model should be isotopically testable, using the SmNd chronometer. SmNd isotopic studies undertaken on Babel Island Suite rocks indicate it to have higher $\varepsilon_{Nd}^{T=370\ my}$ values than have Boobyalla Suite rocks (Sun et al., 1986). The values are ~-3.4 and -5.5 respectively.

A difference between the time-corrected ε_{Nd} values for the rocks of these suites is inconsistent with their respective magmas being derived from the same isotopically homogeneous protolith. If however, the garnet in this protolith **retained** the isotopic characteristics of a pre-magmatic time of formation, then partial melting of the protolith could generate a magma in which garnet was out of isotopic as well as chemical equilibrium. Selective transfer of the Nd isotopic characteristics of the garnet to the buoyant boundary-layer melt-phase should occur during high-level magmatic evolution involving garnet-consuming peritectoid reaction. By this means, a difference between the ε_{Nd} values of rocks derived from the liquid-rich buoyant boundary magma (the Babel Island Suite) and those of rocks derived from the crystal-rich side-wall cumulate (the Boobyalla Suite) could be generated.

Samples of phyric and equigranular Boobyalla and Babel Island Suite rocks and whole-garnet separates from Boobyalla and Musselroe Suite mafic mineral segregations, are currently being isotopically analysed by Dr S.-S. Sun (Bureau of Mineral Resources, Canberra), in order to to test the petrogenetic model. The preliminary results (Appendix T) are ambiguous because

(a) the emplacement ages of the Furneaux Granite plutons are unknown, and
(b) only **whole-garnet** as distinct from **core-garnet** has been isotopically analysed.

12.6 IMPLICATIONS

12.6.1 The Nature of Multiphase Granitic Magmas

It is petrologenetically useful to consider multiphase granitic magmas as a set of three sub-assemblages of phases, based upon the phase-state and the degree of chemical equilibrium attained with the melt during magmatic evolution, as is discussed in Chapter 2. The three sub-assemblages are melt, restite and non-restite, as illustrated in Fig. 12.8.

Restite consists of the crystalline phases which retain their source-region chemical and isotopic compositions throughout magmatic evolution. Examples of phases which could qualify for this category are the cores of

alkali feldspar megacrysts, and the cores of garnet, plagioclase, and zircon crystals. Quartz cores are also included in view of the low rates of oxygen diffusion in this phase compared with the rates in feldspars (Freer, 1981). These rates in quartz are comparable to Fe- and Mg-diffusion rates in garnet at similar temperatures (op. cit., Cygan & Lasaga, 1985).

Non-restite consists of the crystalline phases which have compositions indicative of equilibrium or near-equilibrium with the melt, at magmatic PT conditions subsequent to the magma leaving the source region. Examples of non-restite phases in magmas which have been emplaced into low-pressure regions would be biotite, amphiboles, pyroxenes and cordierite together with the rims of the felsic phases garnet and zircon.

This magmatic phase classification cannot be absolute because crystalline material will exist which is neither of restitic composition nor in near-equilibrium with the melt phase (for instance, that where restitic core material is overgrown by or modified to compositions which are in equilibrium with the melt). However such crystalline material is probably only a small proportion of the total amount present in any magma. The classification should therefore be used to designate the nature of magmatic phases to first-order accuracy.

12.6.2 Trace Elements

The major differences between the whole-rock compositions of the Boobyalla and Babel Island Suites, are in the relative concentrations of certain trace elements (Chapter 5). Concentrations of Sc, Y, Nb and Ga are all higher in the Babel Island Suite. Mineral separate analyses indicate that garnet has high concentrations of Sc and Y and that biotite is high in Nb and Ga. The other major mineral phases have much lower concentrations of these elements (Chapter 6). Consumption of garnet and finally biotite by peritectoid reaction, as is implied from the assemblage sequences in Fig. 12.3 and in equilibria intersected by the cooling portion of the $P_{\Sigma}P_{W}T$ path in the analogue system (Fig. 11.6), is consistent with these trace-element data. Destruction of these two phases should lead to higher concentrations of these particular elements in the residual melt of the magma, because the bulk solid partition coefficients for these elements in the late-stage magmas are very low.

Babel Island Suite whole rocks should be relatively rich in these elements because they are thought to have been derived by solidification of magmas which were largely liquid. Felsic porphyritic Boobyalla Suite whole rocks should be poorer in these elements because their magmas consisted largely of the trace element-depleted bulk-solid.

FIGURE 12.9: Stages in peritectic fractionation process.

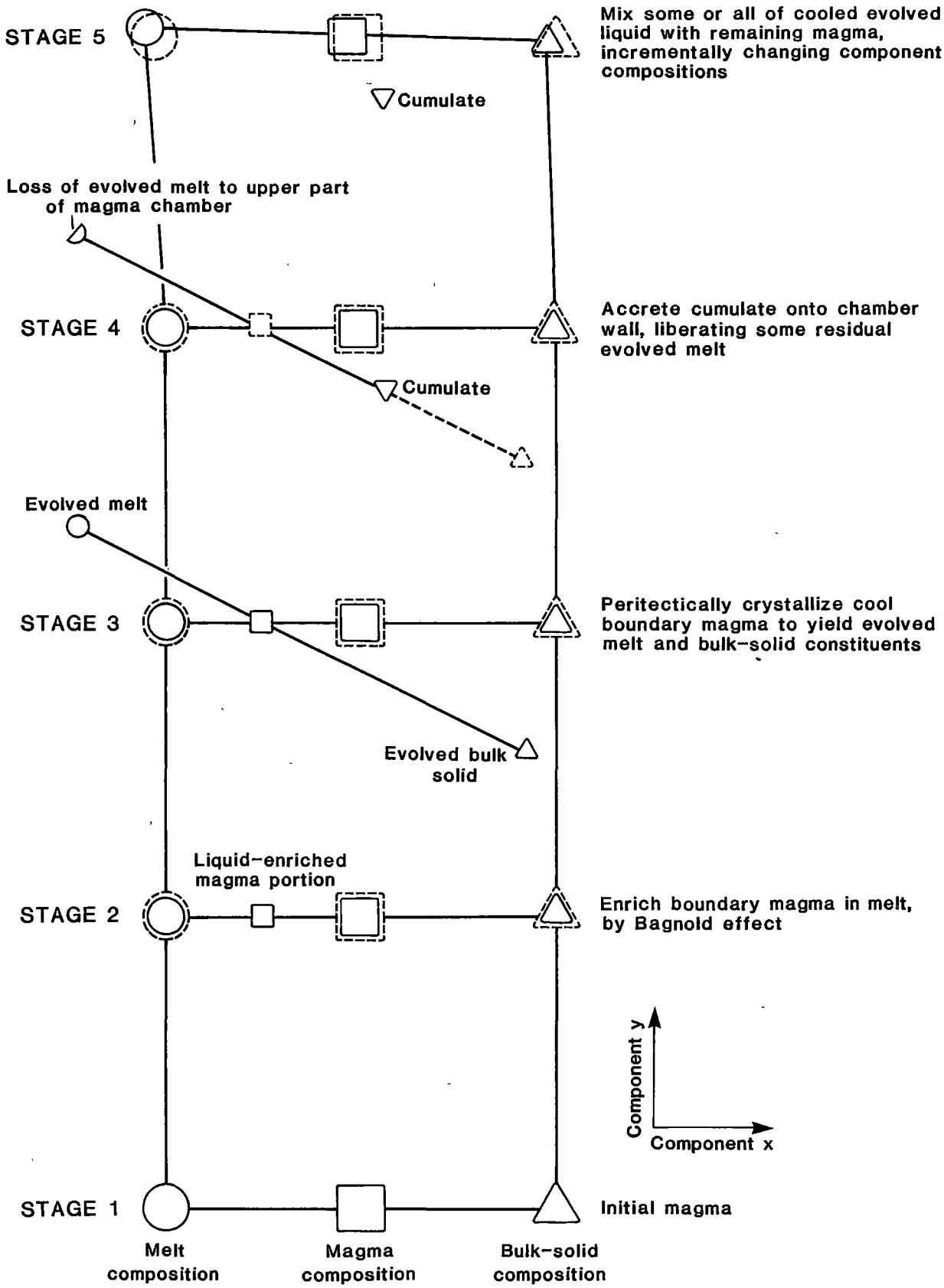

The role of accessory phases will complicate this explanation of whole rock and mineral trace-element data, because crystallizing trace phases such as xenotime and monazite should also partition Y and Sc. Ga may also be partitioned by crystallising andalusite. A detailed analysis of the trace element behaviour during petrogenesis of these rocks is beyond the scope of this work. It constitutes another test of the major-element model that has been presented

12.6.3 Magmatic Processes

Magmatic processes by which the model magmas have evolved must accommodate the following features:

(a) the derivation of all phyric rocks from crystal-rich magmas;

(b) mineral-melt reactions of peritectoid rather than of eutectoid type; and

(c) the occurrence of a major restite portion in the solid phase assemblage of early magmas but a major non-restite portion in the late magmas.

Magmatic processes which are therefore not indicated by the model, are pure restite-unmixing and pure fractional crystallization. The operation of each of these as the sole differentiation process is contrary to the features noted (cf. Chapter 1).

The magma constituent grids and whole-rock data of Fig. 12.6 show features which implicate the simultaneous operation of at least two differentiation processes. The two recognised are **restite-unmixing** and **peritectoid fractionation**. The former has been described in Chapter 1. The latter is a process proposed to occur during the evolution of phenocryst-rich magmas. It differs from the process of pure crystal fractionation (cf. Chapter 1). It consists of progressively changing the composition of an equilibrium phyric magma, by continual extraction of a liquid-poor cumulate. The proportion of crystals in the liquid-enriched magma can then be maintained by peritectoid crystallization as the temperature decreases. The boundary mechanisms by which this process could work, should be similar to those described for the evolution of aphyric magmas by McBirney et al. (1985) (Chapter 1). In phyric magmas, sidewall crystallization will involve reactions of peritectoid, rather than of eutectoid type. The operation of this process is schematically detailed in Fig. 12.9.

In contrast to the porphyritic Boobyalla Suite granites, the Babel Island and Boobyalla Suite equigranular granites could have evolved partly by fractional crystallization because they formed by solidification of crystal-poor magmas. However their major-element compositions are consistent with those of liquids which are in peritectic reaction

relationship with a solid-phase assemblage. The magmas of these rocks are therefore considered to have been derived largely by peritectoid fractionation.

Unlike the low-temperature magmas considered here, high-temperature granitic magmas, which are at or above their liquidi, should initially evolve by the eutectoid-reaction controlled differentiation process: fractional crystallization. Examples of such granites are the early phases of the St Marys Porphyrite (Turner et al., 1986; Higgins et al., 1985) and the Barrington Tops Granodiorite (Eggins & Hensen, 1987). However, as magmatic temperatures decrease and concentrations of suspended crystalline phases increase, the role of peritectoid fractionation is expected to become dominant.

12.6.4 Granite Classification

In this work, granitic suites have been designated ultimately on the basis of their geochemical coherence (Chapters 1 and 5). This procedure is the same as that taken for example by White & Chappell (1977), Hine et al. (1978) and Chappell et al. (in press). In previous studies such as these, each suite was regarded as having been derived from a different source, because the only magmatic differentiation process which was considered, was restite-unmixing (op. cit.).

It has been shown here however, that two different geochemical suites (the Boobyalla and Babel Island Suites) can be modelled as coming from a common source. The geochemical distinction is considered merely to reflect the compositional differences between crystal-rich and crystal-poor magmas, which are in turn due to the different compositional trends of the liquid and bulk-solid constituents of the magmas.

The A-type character of the Babel Island Suite granites (Chapter 2), is therefore thought to be a reflection of its magmas having been:

(a) liquid- rather than crystal-rich; and
(b) extracted from phenocryst-rich magmas in which low-pressure peritectoid fractionation was a major differentiation process.

It is suggested that the small class of A-type granites might be similarly derived. In terms of their protoliths, granites would then simply be of I- or S-type, in the sense of Chappell (1984). A-type character is seen as a consequence of evolution especially that at very low total pressures subsequent to the magma leaving the source region, . This is consistent with the ocurrence of transitional features between A- and I-type granites in the Bega Batholith (Collins et al., 1982) and the spatial association of A-type granites with those of other types (Whalen, in press; this work).

The petrogenesis described here is consistent with classic features of A-type granites, such as their aphyric textures, interstitial late-stage

biotite and high levels of fluorine and high field-strength transition elements (Collins et al., 1982; Clemens et al., 1986). Magmas which are emplaced at total pressures near to or below those at which the assemblages{hydrous phases+quartz±melt±vapour} were stable, should yield upon magmatic evolution, buoyant boundary melts which have trace-element concentrations reflecting the peritectoid reactions occurring at those ambient conditions. In these reactions, the hydrous phases which were stable at higher pressures are destroyed and low-pressure anhydrous phases such as olivine, pyroxenes, feldspars, etc. are formed in their place. The latter phases have low solid/liquid partition coefficients for the high field-strength transition elements which are so abundant in the hydrous phases (e.g. Jensen, 1973; Mahood & Hildreth, 1983; Nash & Crecraft, 1985). As a consequence, the melt is selectively enriched in these particular trace elements. For the same reasons these melts and the rocks derived from them, will contain high relative concentrations of halogens.

That A-type granites are uncommon in southeastern Australia (Collins et al., 1982; Chappell & White, 1984) is probably because:

(a) they were volumetrically subordinate to their phyric-rich compliments; and

(b) they represent the stratigraphic ceilings of plutons which will therefore be eroded first.

This proposal for the petrogenesis of A-type granites could be tested by drilling. A-type granites by the above arguments, should overlie granites of either I- or S-type, as occurs for plutons of the Babel Island and Boobyalla Suites in the NBTB (Chapter 3).

12.6.5 Provenance

Assessment of the features of Boobyalla and Babel Island Suite rocks indicates that they were derived from peraluminous magmas which were generated by partial melting at ~850°C and 0.6 GPa. The average geothermal gradient indicated is therefore ~1400 K GPa^{-1}. This value is somewhat higher than that for average continent (~900 K GPa^{-1}, Wyllie, 1971) as is expected in a terrane in which voluminous amnounts of granite have been generated.

The source-region magma probably contained assemblages such as {alkali feldspar, apatite, biotite, cordierite, garnet, ilmenite, melt, monazite, plagioclase, quartz, sillimanite and zircon}. The protolith bulk-chemical composition cannot be quantitatively modelled because the magmatic reactions and rheological processes which occurred during the **decompression stage** of magmatic evolution are insufficiently well known. For instance, early high-pressure melts in equilibrium with sillimanite, could have been more peraluminous than those used to model the start of the

low-pressure stage of magnatic evolution (Fig. 12.5). The source composition is probably roughly similar to that of the mafic end of the trend of porphyritic Boobyalla granites. This is a pelitic composition. These two suites are probably therefore derived from the partial melting of pelitic metasediments.

12.6.6 The Potential for Metallogenesis

Knowledge of the constitution, intensive variables and the evolutionary processes of granitic magmas will be of great benefit in predicting the potential for economic mineralization. Within the context of the petrogenetic model described, it is likely that granites derived from low-pressure liquid-rich magmas (alkali feldspar- or A-type granites) will be more prospective because their magmas will have contained higher concentrations of incompatible, potentially economic trace-elements such as tin, molybdenum, copper, etc.

In contrast to these, granites derived by cumulate processes should be relatively depleted in potentially economic trace elements.

For both magma types, incompatible trace-element concentrations will increase as magma evolution proceeds. Those in late-stage A-type magmas however, should always be greater than those of their related cumulate counterparts.

12.7 CONCLUSION

Geological, rheological, chemical and phase equilibrium evidence is consistent with the Boobyalla and Babel Island Suite granites being a complementary pair of source-related suites that were simultaneously derived in the same pluton, by the solidification of crystal-rich and crystal-poor magmas, respectively. How widespread this pattern is amongst southeast Australian granites, will require assessment of the phase-equilibria, -disequilibria and -compositions of the magmas which gave rise to them.

REFERENCES

Abbott, R.N. & Clarke, D.B., 1979: Hypothetical liquidus relationships in the subsystem Al_2O_3-FeO-MgO projected from quartz, alkali feldspar and plagioclase for $a(H_2O) \leq 1$. *Can. Mineral.* 17: 549-560.

Abs-Wurmbach, I., Langer, K. & Schreyer, W., 1983: The influence of Mn^{3+} on the stability relations of the Al_2SiO_5 polymorphs with special emphasis on manganian andalusites (viridines), $(Al_{1-x}Mn^{3+}_x)_2(O/SiO_4)$: an experimental investigation. *J. Petrol.* 24: 48-75.

Allegre, C.J. & Minster, J.F., 1978: Quantitative models of trace element behaviour in magmatic processes. *Earth Planet. Sci. Lett.* 38: 1-25.

Allegre, C.J. & Othman, D.B., 1980: Nd-Sr isotopic relationship in granitoid rocks and continental crust development: a chemical approach to orogenesis. *Nature* 286: 355-341.

Anderson, D.E., 1981: Diffusion in electrolyte mixtures. *In* A.C. Lasaga & R.J., Kirkpatrick (eds): *Kinetics of Geochemical Processes*. Reviews in Mineralogy, Vol.8. Mineralogical Society of America.

Arth, J.G., 1976: Behaviour of trace elements during magmatic processes - a summary of theoretical models and their applications. *J. Res. U.S. Geol. Surv.* 4(1): 41.

Arzi, A.A., 1978: Critical phenomena in the rheology of partially melted rocks. *Tectonophysics* 44: 173-184.

Bacon, C.R., MacDonald, R., Smith, R.L. & Baedecker, P.A., 1981. Pleistocene high-silica rhyolites of the Coso Volcanic Field, Inyo County, California. *J. Geophys. Res.* 86B: 10223-10241.

Bagby, W.C., Cameron, K.L. & Cameron, M., 1981: Contrasting evolution of calc-alkalic volcanic and plutonic rocks of western Chihuahua, Mexico. *J. Geophys. Res.* 86B: 10402-10410.

Bagnold, R.A., 1954: Experiments on a gravity-free dispersion of large solid spheres in a Newtonian fluid under shear. *Proc. R. Soc.* A225: 49-63.

Bailey, J.C., 1977: Petrochemistry of the Claret Creek Ring Complex, northeast Queensland. *J. Geol. Soc. Aust.* 24: 1-14.

Bailey, S.W., 1984: Crystal chemistry of the true micas. *In* S.W. Bailey (ed.): *Micas*. Reviews in Mineralogy, Vol.13. Mineralogical Society of America.

Baillie, P.W., 1985: A Palaeozoic suture in eastern Gondwanaland. *Tectonics* 4: 653-660.

Baillie, P.W., 1986: *Eddystone*. Geological Survey Explanatory Report, Sheet 25. Tasm. Dept Mines.

Baker, B.H. & McBirney, A.R., 1985: Liquid fractionation. Part III: Geochemistry of zoned magmas and the compositional effects of liquid fractionation. *J. Volcan. Geotherm. Res.* 24: 55-81.

Barker, F., 1961: Phase relations in cordierite-garnet-bearing Kinsman quartz monzonite and the enclosing schist, Lovewell Mountain quadrangle, New Hampshire. *Am. Mineral.* 46: 1166-1176.

Barriere, M., 1976: Flowage differentiation:: limitation of the 'Bagnold effect' to the narrow intrusions. *Cont. Mineral. Petrol.* 55: 139-145.

Barth, T.F.W., 1951: The feldspar geological thermometers. *Neues Jahrb. Mineral.* 82: 143-154.

Bateman, P.C. & Nokleberg, W.J., 1978: Solidification of the Mount Givens Granodiorite, Sierra Nevada, California. *J. Geol.* 86: 563-579.

Bateman, P.C. & Chappell, B.W., 1979: Crystallization, fractionation and solidification of the Tuolomne Intrusive Series, Yosemite National Park, California. *Bull. Geol. Soc. Am.* 90: 465-482.

Beane, R.E., 1974: Biotite stability in the porphyry copper environment. *Econ. Geol.* 69: 241-256.

Bhatia, M.R. & Taylor, S.R., 1981: Trace-element geochemistry and sedimentary provinces: a study from the Tasman Geosyncline, Australia. *Chem. Geol.* 33: 115-125.

Bickford, M.E., Sides, J.R. & Cullers, R.L., 1981: Chemical evolution of magmas in the Proterozoic terrane of the St Francoise Mountains, southeastern Missouri. 1. Field, petrographic and major element data. *J. Geophys. Res.* B86:: 10365-10386.

Bohlen, S.R., Boettcher, A.L., Wall, V.J. & Clemens, J.D., 1983: Stability of phlogopite-quartz and sanidine-quartz: a model for melting in the lower crust. *Contrib. Mineral. Petrol.* 83: 270-277.

Bohlen, S.R., Peacor, D.R. & Essene, E.J., 1980: Crystal chemistry of a metamorphic biotite and its significance in water barometry. *Am. Mineral.* 65: 55-62.

Bowen, N.L., 1928: *The Evolution of the Igneous Rocks.* Dover, New York.

Brady, J.B., 1975: Reference frames and diffusion coefficients. *Am. J. Sci.*, 275: 954-983.

Brady, J.B. & Yund, R.A., 1983: Interdiffusion of K and Na in alkali feldspars: homogenization experiments. *Am. Mineral.* 68: 106-111.

Broecker, W.S. & Oversby, V.M., 1971: *Chemical Equilibria in the Earth.* McGraw-Hill Book Co., New York.

Brooks, C., 1971: Letter to the Director, Tasmanian Department of Mines. From University of Montreal (Ref. No. 5052/71).

Brown, W.L. & Parsons, I., 1981:: Towards a more practical two-feldspar geothermometer. *Contrib. Mineral. Petrol.* 76: 369-277.

Burnham, W.C., 1967: Hydrothermal fluids at the magmatic stagge. *In* H.L. Barnes (ed.): *Geochemistry of Hydrothermal Ore Deposits*. Holt, Reinhard & Winston, Inc., New York.

Burnham, C.W., 1975: Water and magmas; a mixing model. *Geochim. Cosmochim. Acta* 39: 1077-1084.

Burnham, C.W., 1979: The importance of volatile constituents. *In* H.S. Yoder (ed.): *The Evolution of the Igneous Rocks: Fiftieth Anniversary Perspectives*. Princeton University Press.

Burnham, C.W., Holloway, J.R. & Davis, N.F., 1969: Thermodynamic properties of water to 1000°C and 10,000 bars. *Geol. Soc. Am. Spec. Pap.* 132.

Burnham, C.W. & Nekvasil, H., 1986: Equilibrium properties of granite pegmatite magmas. *Am. Mineral.* 71: 239-263.

Burrett, C.F. & Findlay, R.H., 1984: Cambrian and Ordovician conodonts from the Robertson Bay Group, Antarctica and their tectonic significance. *Nature* 307(5953): 723-725.

Buseck, P.R. & Veblen, D.R., 1978: Trace elements, crystal defects and high resolution electron microscopy. *Geochim. Cosmochim. Acta* 42: 669-678.

Cameron, W.E., 1976: Coexisting sillimanite and mullite. *Geol. Mag.* 113: 497-514.

Carmichael, I.S.E. & Nicolls, J., 1967: Iron-titanium oxides and oxygen fugacities in volcanic rocks. *J. Geophys. Res.* 72: 4665-4687.

Carmichael, I.S.E., Turner, F.J. & Verhoogen, J., 1974: *Igneous Petrology*. McGraw-Hill Book Co., Sydney.

Carpenter, M.A. & Ferry, J.M., 1984: Constraints on the thermodynamic mixing properties of plagioclase feldspars. *Contrib. Mineral. Petrol.* 87: 138-148.

Cawthorne, R.G. & O'Hara, M.J., 1976: Amphibole fractionation in calc-alkaline magma genesis. *Am. J. Sci.*, 276: 309-329.

Chappell, B.W., 1966: *Moonbi Granites*. Ph.D. thesis, A.N.U., Canberra.

Chappell, B.W., 1978: Granitoids from the Moonbi district, New England Batholith, eastern Australia. *J. Geol. Soc. Aust.* 25(5): 267-283.

Chappell, B.W., 1984: Source rocks of I- and S-type granites in the Lachlan Fold Belt, southeastern Australia. *Phil. Trans. R. Soc. London* A310: 693-707.

Chappell, B.W. & White, A.J.R., 1974: Two contrasting granite types. *Pac. Geol.* 8: 173-174.

Chappell, B.W. & White, A.J.R., 1984: I- and S-type granites in the Lachlan Fold Belt, southeastern Australia. *In* Geology of Granites and

Their Metallogenetic Relations, Proc. Int. Symposium, Nanjing, China, 1982.

Chappell, B.W., White, A.J.R. & Wyborn, D., 1987: The importance of residual source material (restite) in granite petrogenesis. *J. Petrol.*, in press.

Chatterjee, N.D. & Johannes, W., 1974: Thermal stability and standard thermodynamic properties of synthetic $2M_1$-muscovite, $KAl_2[AlSi_3O_{10}(OH)_2]$. *Contrib. Mineral. Petrol.* 48: 89-114.

Clarke, D.B., 1981: The mineralogy of peraluminous granites: a review. *Can. Mineral.* 19: 3-17.

Clarke, D.B. & Halliday, A.N., 1980: Strontium isotope geology of the South Mountain batholith, Nova Scotia. *Geochim. Cosmochim. Acta* 44: 1045-1058.

Clarke, D.B., McKenzie, C.B., Muecke, G.K. & Richardson, S.W., 1976: Magmatic andalusite from the South Mountain Batholith, Nova Scotia. *Contrib. Mineral. Petrol* 56: 279-287.

Clemens, J.D., Holloway, J.R. & White, A.J.R., 1986: Origin of an A-type granite: experimental constraints. *Am. Mineral.* 71: 317-324.

Clemens, J.D. & Wall, V.J., 1981: Origin and crystallization of some peraluminous (S-type) granitic magmas. *Can. Mineral.* 19: 111-131.

Clemens, J.D. & Wall, V.J., 1984: Origin and evolution of a peraluminous silicic ignimbrite suite: the Violet Town Volcanics. *Contrib. Mineral. Petrol.* 88:: 354-371.

Cocker, J.D., 1977: *Petrogenesis of the Tasmanian Granitoids*. Ph.D. thesis, University of Tasmania.

Cocker, J.D., 1982: Rb-Sr geochronology and Sr isotopic composition of Devonian granitoids, eastern Tasmania. *J. Geol.Soc. Aust.* 29: 139-158.

Collerson, K.D., Reid, E., Millar, D. & McCulloch, M.T., 1983: Lithological and Sr-Nd isotopic relationships in the Vestfold Block: implications for Archaean and Proterozoic crustal evolution in East Antarctica. *In* R.L. Oliver, P.R. Jones & J.B. Jago (eds): *Antarctic Earth Science*. Proc. 4th Int. Symp. on Antarctic Earth Sciences, Adelaide. Australian Academy of Science.

Collins, W.J., Beams, B.D. & White, A.J.R., 1982: Nature and origin of A-type granites with particular reference to southeastern Australia. *Contrib. Mineral. Petrol.* 80: 189-200.

Compston, W. & Chappell, B.W., 1979. Sr-isotope evolution of granitoid source rocks. *In* M.W. McElhinny (ed.): *The Earth*. Academic Press: 377-426.

Cortecci, G., Del Moro A., Leone, G. & Pardini, G.C., 1979: Correlation between strontium and oxygen isotopic compositions of rocks from the Adamello massif (northern Italy). *Contrin. Mineral. Petrol.* 68: 421-427.

Crecraft, H.R., Nash, W.P. & Evans, S.H., 1981: Late Cenozoic volcanism at Twin Peaks, Utah: geology and petrology. *J. Geophys. Res.* 86B: 10303-10320.

Cressy, D., 1981: Entropies and enthalpies of aluminosilicate garnets. *Contrib. Mineral. Petrol.* 76: 413-419.

Cressy, G., Schmid, R. & Wood, B.J., 1978: Thermodynamic properties of almandine-grossular garnet solid solutions. *Contrib. Mineral. Petrol.* 67: 397-404.

Cullers, R.L., Koch, R.L. & Bickford, M.E., 1981: Chemical evolution of magmas in the Proterozoic terrane of the St Francois Mountains, southeastern Missouri. 2. Trace element data. *J. Geophys. Res.* B86: 10388-10401.

Cygan, R.T. & Lasaga, A.C., 1985: Self-diffusion of magnesium in garnet at 750° to 900°C. *Am. J. Sci.* 285: 328-350.

Czamanske, G.K. & Wones, D.J., 1973: Oxidation during magmatic differentiation, Finnmarka Complex, Oslo area, Norway: Part 2, The mafic silicates. *J. Petrol.* 14: 349-380.

Deer, W.A., Howie, R.A. & Zussman, J., 1962: *The Rock Forming Minerals.* Vol. 3. *Sheet Silicates.* Longmans, England.

Deer, W.A., Howie, R.A. & Zussman, J., 1982: *The Rock Forming Minerals.* Vol. 1A. *Garnet Group.* Second edition. Longman Group Ltd. England.

De Michele, V., 1974: Qualche osservazione paragenetica sull' osumilite del Monte Arci (Caligari). *Natura. Soc. Ital. Sci. Nat. Milano* 65: 39-45.

De Paolo, D.J., 1981: Trace element and isotopic effects of combined wallrock assimilation and fractional crystallization. *Earth Planet. Sci. Lett.* 53: 189-202.

De Paolo, D.J., 1981: A neodymium and strontium isotopic study of the Mesozoic calc-alkaline granitic batholiths of the Sierra Nevada and Peninsula Ranges, California. *J. Geophys. Res.* B86: 10470-10488.

De Paolo, D.J. & Farmer, G.L., 1984: Isotopic data bearing on the origin of Mesozoic and Tertiary granitic rocks in the western United States. *Phil. Trans. R. Soc. Lond.* A310: 743-753.

Didier, J., 1963: Vue D'ensemble sur les enclaves des granites du massif centrale Francais. Extrail des Comptes-Rendus du 88 Congres National des Societies Savantes tenu a Clermont-ferrand II: 23-28.

Didier, J., 1973: *Granites and their Enclaves.* Elsevier, Amsterdam.

Didier, J., 1987: Contribution of enclave studies to the understanding of origin and evolution of granitic magmas. *Geol. Rund.* 76(1): 41-50.

Dowty, E., 1977: The importance of adsorption in igneous partitioning of trace elements. *Geochim. Cosmochim. Acta* 41: 1643-1646.

Dutch, S.I., 1979: The Creighton Pluton, Ontario: an unusual example of a forcefully emplaced intrusion. *Can. J. Earth Sci.* 16: 333-349.

Eggins, S. & Hensen, B.J., 1987: Evolution of mantle-derived, augite-hypersthene granodiorites by crystal-liquid fractionation: Barrington Tops Batholith, eastern Australia. *Lithos* 20: in press.

Ellis, D.J., 1984: Fe-loss to noble metal capsules - a possible solution. *In* V.J. Wall & I.A. Nicholls (eds): *Workshop on Experimental Geochemistry: Australia, Monash University.*

Ellis, D.J., 1986: Garnet-liquid Fe^{2+}-Mg equilibria and implications for the beginning of melting in the crust and subduction zones. *Am. J. Sci.* 286: 765-791.

Ellis, D.J., Sheraton, J.W., England, R.N. and Dallwitz, W.B., 1980: Osumilite-sapphirine-quartz granulites from Enderby Land, Antarctica - mineral assemblages and reactions. *Contrib. Mineral. Petrol.* 72: 123-143.

Ellis, D.J. & Thompson, A.B., 1986: Subsolidus and partial melting reactions in the quartz-excess CaO + MgO + Al_2O_3 + SiO_2 + H_2O system under water-excess and water-deficient conditions to 10 kb: some implications for the origin of peraluminous melts from mafic rocks. *J. Petrol.* 27(1): 91-121.

Emmerman, R., Daieva, L. & Schneider, J., 1975: Petrologic significance of rare earths distribution in granite. *Contrib. Mineral. Petrol.* 52: 267-283.

Essene, E.J., 1982: Geologic thermometry and barometry. *In* J.M. Ferry (ed.): *Characterization of Metamorphism Through Mineral Equilibria.* Reviews in Mineralogy, Vol.10.

ESSO Exploration, 1965: Aeromagnetic anomaly map of northeast Tasmania. Report #306, Map 2.

Etheridge, M.A., Branson, J.C., Falvey, D.A., Lockwood, K.L., Stuart-Smith, P.G., & Scherl, A.S., 1985: Basin-forming structures and their relevance to hydrocarbon exploration in Bass Basin, southeastern Australia. *BMR J. of Aust. Geol. & Geophys.* 9: 197-206.

Eugster, H.P. & Wones, D.R., 1962:: Stability relations of the ferruginous biotite, annite. *J. Petrol.* 3(1): 82-125.

Evans, N.H. & Speer, J.A., 1984: Low-pressure metamorphism and anatexis of Caroline Slate Belt phyllites in the contact aureole of the Lilesville Pluton, North Carolina, USA. *Contrib. Mineral. Petrol.* 87: 297-309.

Ewart, A., 1981: The mineralogy and chemistry of the anorogenic Tertiary silicic volcanics of S.E. Queensland and N.E. New South Wales, Australia. *J. Geophys. Res.* 86B: 10242-10256.

Ewart, A., 1985: Aspects of the mineralogy and chemistry of the intermediate-silicic Cainozoic volcanic rocks of eastern Australia. Part 2: mineralogy and petrogenesis. *Aust. J. Earth Sci.* 32: 383-413.

Ewart, A., Chappell, B.W. & Le Maitre, R.W., 1985: Aspects of the mineralogy and chemistry of the intermediate-silicic Cainozoic volcanic rocks of eastern Australia. Part 1: introduction and geochemistry. *Aust. J. Earth Sci.* 32: 359-382.

Ewart, A., Hildreth, W. & Carmichael, I.S.E., 1975: Quaternary acid magma in New Zealand. *Contrib. Mineral. Petrol.* 51: 1-27.

Ewart, A., Oversby, V.M. & Mateen, A., 1977: Petrology and isotope geochemistry of Tertiary lavas from the northern flank of the Tweed Volcano, southeastern Queensland. *J. Petrol.* 18: 73-113.

Fenn, P.M., 1977: The nucleation and growth of alkali feldspars from hydrous melts. *Can Mineral.* 15: 135-161.

Ferry, J.M. & Spear, F.S., 1978: Experimental calibration of the partitioning of Fe and Mg between biotite and garnet. *Contrib. Mineral. Petrol.* 66: 113-117.

Flood, R.H. & Vernon, R.H., 1978: The Cooma granodiorite, Australia: an example of in situ crustal anatexis? *Geology* 6: 81-84.

Flood, R.H., Vernon, R.H., Shaw, S.E. & Chappell, B.W., 1977: Origin of pyroxene-plagioclase aggregates in a rhyodacite. *Contrib. Mineral. Petrol.* 60: 299-309.

Folano, K.A., Henderson, C.M.B. & Gleason, J., 1985: Petrogenesis of the magmatic complex at Mount Ascutney, Vermont, USA. I. Assimilation of crust by mafic magmas based on Sr and O isotopic and major element relationships. *Contrib. Mineral. Petrol.* 90: 331-345.

Foley, S.F., Taylor, W. & Green, D.H., 1986: The effect of fluorine on phase relationships in the system $KAlSiO_4$-Mg_2SiO_4-SiO_2 at 28 kbar and the solution mechanism of fluorine in silicate melts. *Contrib. Mineral. Petrol.* 93: 46-55.

Fonarev, V.I. & Korolkov, G. Ja., 1980: The assemblage orthopyroxene + cummingtonite + quartz. The low-temperature stability limit. *Contrib. Mineral. Petrol.* 73: 413-420.

Forbes, W.C., 1977: Stability relations of grunerite, $Fe_7Si_8O_{22}(OH)_2$. *Am. J. Sci.* 277: 735-749.

Fraser, D.G., 1977: Thermodynamic properties of silicate melts. *In* D.G. Fraser (ed.): *Thermodynamics in Geology*. D. Reidel Pub. Co., Holland:: 301-325.

Freer, R., 1981: Diffusion in silicate minerals and glasses: a data digest and guide to the literature. *Contrib. Mineral. Petrol.* 76: 440-454.

Frost, C.D. & O'Nions, R.K., 1985: Caledonian magma genesis and crustal recycling. *J. Petrol.* 26(2): 515-544.

Furman, T. & Spera, F.J., 1985: Co-mingling of acid and basic magma with implications for the origin of mafic I-type xenoliths: field and petrochemical relations of an unusual dike complex at Eagle Lake, Sequoia National Park, California, U.S.A. *J. Volcan. Geotherm. Res.* 24: 151-178.

Ganguly, J. & Saxena, S.K., 1984: Mixing properties of aluminosilicate garnets: constraints from natural and experimental data, and applications to geothermo-barometry. *Am. Mineral.* 69: 88-97.

Gee, R.D. & Groves, D.I., 1971: Structural features and mode of emplacement of part of the Blue Tier batholith in northeast Tasmania. *J. Geol. Soc. Aust.* 18: 41-56.

Gerlach, D.C. & Grove, T.L., 1982: Petrology of Medicine Lake highland volcanics: characterization of endmembers of magma mixing. *Contrib. Mineral. Petrol.* 80: 147-159.

Ghent, E.D., 1976: Plagioclase-garnet-Al_2SiO_5-quartz: a potential geobarometer-geothermometer. *Am. Mineral.* 61: 710-714.

Ghent, E.D., Robbins, D.B. & Stout, M.Z., 1979: Geothermometry, geobarometry, and fluid compositions of metamorphosed calc-silicates and pelites, Mica Creek, British Columbia. *Am. Mineral.* 64: 874-885.

Ghiorso, M.S., 1984: Activity/composition relations in the ternary feldspars. *Contrib. Mineral. Petrol.* 87: 282-296.

Ghiorso, M.S., Carmichael, I.S.E., Rivers, M.L. & Sack, R.O., 1983: The Gibbs Free Energy of mixing of natural silicate liquids: an expanded regular solution approximation for the calculation of magmatic intensive variables. *Contrib. Mineral. Petrol.* 84: 107-145.

Gilbert, M.C. & Popp, R.K., 1982: End-member relations. *In* D.R. Veblen & P.H. Ribbe (eds): *Amphiboles: Petrology and Experimental Phase Relations*. Chapter 2. Experimental Studies of Amphibole Stability. Reviews in Mineralogy, Vol.9B. Mineralogical Society of America.

Goldman, D.S. & Albee, A.L., 1977: Correlation of Mg/Fe partitioning between garnet and biotite with $^{18}O/^{16}O$ partitioning between quartz and magnetite. *Am. J. Sci.* 277: 750-767.

Goldsmith, J.R., 1980: Melting and breakdown reactions of anorthite at high pressures and temperatures. *Am. Mineral.* 65: 272-284.

Grambling, J.A. & Williams, M.L., 1985: The effects of Fe^{3+} and Mn^{3+} on aluminium silicate phase relations in north-central New Mexico, USA. *J. Petrol.* 26(2): 324-354.

Grant, J.A., 1968: Partial melting of common rocks as a possible source of cordierite-anthophyllite bearing assemblages. *Am. J. Sci.* 266: 908-931.

Grant, J.A., 1973: Phase equilibria in high-grade metamorphism and partial melting of pelitic rocks. *Am. J. Sci.* 273: 289-317.

Grant, J.A., 1981: Orthoamphibole and orthopyroxene relations in high-grade metamorphism of pelitic rocks. *Am. J. Sci.* 281: 1127-1143.

Grant, J.A., 1985: Phase equilibria in low-pressure partial melting of pelitic rocks. *Am. J. Sci.* 285: 409-435.

Green, D.H. & Ringwood, A.E., 1967: The genesis of basaltic magmas. *Contrib. Mineral Petrol.* 15: 103-190.

Green, T.H., 1976a: Experimental generation of cordierite or garnet-bearing granitic liquids from a pelitic composition. *Geology* 4: 85-88.

Green, T.H., 1976b: Garnet in silicic liquids and its possible use as a P-T indicator. *Contrib. Mineral. Petrol.* 65: 59-67.

Grew, E.J., 1980: Sillimanite and ilmenite from high-grade metamorphic rocks of Antarctica and other areas. *J. Petrol.* 66: 702-722.

Griffin, T.J., White, A.J.R. & Chappell, B.W., 1978: The Moruya Batholith and geochemical contrasts between the Moruya and Jindabyne suites. *J. Geol. Soc. Aust.* 25(4): 235-247.

Grove, T.L., Baker, M.B. & Kinzler, R., 1984: Coupled CaAl-NaSi diffusion in plagioclase feldspar: experiments and applications to cooling rate speedometry. *Geochim. Cosmochim. Acta* 48: 2113-2121.

Groves, D.I., 1970: Notes on a reconnaissance of the granitic rocks of Flinders Island. *Tasm. Dept Mines Tech. Rept* 15.

Groves, D.I., 1972: The geochemical evolution of the tin-bearing granites in the Blue Tier Batholith, Tasmania. *Econ. Geol.* 67: 445-457.

Groves, D.I., Cocker, J.D. & Jennings, D.J., 1977: The Blue Tier batholith. *Geol. Surv. Tasm. Bull.* 55. Dept of Mines, Tasmania.

Groves, D.I. & McCarthy, T.S., 1978: Fractional crystallization and the origin of tin deposits in granitoids. *Mineral. Deposita* 13: 11-26.

Halliday, A.N., Aftalion M., Van Breemen, O. & Jocelyn, J., 1980: Petrogenetic significance of Rb-Sr and U-Pb isotopic systems in the 400 Ma old British Isles granitoids and their hosts. *J. Geol. Soc. London* : 653-661.

Hards, N.J., 1976: Distribution of elements between the fluid phase and silicate melt phase of granites and nepheline syenites. *Prog. Exp. Petr. NERC* 3: 88-90.

Hariya, Y. & Kennedy, G.C., 1968: Equilibrium study of anorthite under high pressure and temperature. *Am. J. Sci.* 266: 193-203.

Harley, S.L., 1984: The solubility of alumina in orthopyroxene coexisting with garnet in FeO-MgO-Al_2O_3-SiO_2 and CaO-FeO-MgO-Al_2O_3-SiO_2. *J. Petrol.* 25: 665-696.

Harris, K.L., Crawford, A.J. & Green, D.H., in prep. Phase relationships of an eclogite-derived tonalite from 0-30 kilobars.

Haselton, H.T., Hovis, G.L., Hemingway, B.S. & Robie, R.A., 1983: Calorimetric investigation of the excess entropy of mixing in analbite-sanidine solid solutions: lack of evidence for Na,K short range order and implications for two-feldspar thermometry. *Am. Mineral.* 68: 398-413.

Hays, J.F., 1967: Lime-alumina-silica. *Carnegie Inst. Wash Yrbk* 65: 234-239.

Helgeson, H.C., Delany, J.M., Nesbitt, H.W. & Bird, D.K., 1978: Summary and critique of the thermodynamic properties of rock-forming minerals. *Am. J. Sci.* 278A: .

Hellman, P.L. & Green, T.H., 1979: The role of sphene as an accesory phase in the high pressure partial melting of hydrous mafic compositions. *Earth Planet. Sci. Lett.* 42: 191-201.

Helz, R.T., 1979: Alkali exchange between hornblende and melt: a temperature-sensitive reaction. *Am. Mineral.* 64: 953-965.

Hensen, B.J., 1970: *Experimental Study of the Stability of Cordierite and Garnet*. Ph.D. thesis, Australian National University.

Hensen, B.J. & Green, D.H., 1971: Experimental study of the stability of cordierite and garnet in pelitic compositions at high pressures and temperatures. *Contrib. Mineral. Petrol* 33: 309-330.

Hensen, B.J. & Green, D.H., 1972: Experimental study of the stability of cordierite and garnet in pelitic compositions at high pressures and temperatures. *Contrib. Mineral. Petrol* 35: 331-354.

Hensen, B.J. & Green, D.H., 1973: Experimental study of the stability of cordierite and garnet in pelitic compositions at high pressures and temperatures. III: Synthesis of experimental data and geological applications. *Contrib. Mineral. Petrol.* 38: 151-166.

Hibbard, M.J., 1981: The magma mixing origin of mantled feldspars. *Contrib. Mineral. Petrol.* 76: 158-170.

Higgins, N.C., Solomon, M. & Varne, R., 1985: The genesis of the Blue Tier batholith, northeastern Tasmania, Australia. *Lithos* 18: 129-149.

Higgins, N.C., Turner, N.J. & Black, L.P., 1986: The petrogenesis of an I-type volcanic-plutonic suite: the St Marys porphyrite, Tasmania. *Contrib. Mineral. Petrol.* 92: 248-259.

Hildreth, W., 1979: The Bishop Tuff: evidence for the origin of compositional zonation in silicic magma chambers. *Geol. Soc. Am. Spec. Pub.* 180: 43-75.

Hildreth, W., 1981: Gradients in silicic magma chambers: implications for lithospheric magmatism. *J. Geophys. Res.* 86B: 10153-10192.

Hill, R.I., Silver, L.T., Chappell, B.W. & Taylor, H.P., 1985: Solidification and recharge of SiO_2-rich plutonic magma chambers. *Nature* 313(6004): 643-646.

Hine, R., Williams, I.S., Chappell, B.W., & White, A.J.R., 1978: Contrasts between I- and S-type granitoids of the Koscuisko Batholith. *J. Geol. Soc. Aust.* 25(4): 219-234.

Hoffer, E. & Grant, J.A., 1980: Experimental investigation of the formation of cordierite-orthopyroxene parageneses in pelitic rocks. *Contrib. Mineral. Petrol.* 73: 15-22.

Holdaway, M.J., 1971: Stability of andalusite and the aluminium silicate phase system. *Am. J. Sci.* 271: 97-131.

Holdaway, M.J. & Lee, S.M., 1977: Fe-Mg cordierite stability in high-grade pelitic rocks based on experimental, theoretical and natural observations. *Contrib. Mineral. Petrol.* 63: 175-198.

Holloway, J.R. & Burnham, W.C., 1972: Melting relations of basalt with equilibrium water pressure less than total pressure. *J. Petrol.* 13: 1-29.

Huang, W.L. & Wyllie, P.J., 1974: Melting relations of muscovite with quartz and sanidine in the K_2O-Al_2O_3-SiO_2-H_2O system to 30 kilobars and an outline of paragonite melting relations. *Am. J. Sci.* 274: 378-395.

Huang, W.L. & Wyllie, P.J., 1981: Phase relationships of S-type granite with H_2O to 35 kbar: muscovite granite from Harney Peak, South Dakota. *J. Geophys. Res.* B86: 10515-10529.

Huang, W.L. & Wyllie, P.J., 1986: Phase relationships of gabbro-tonalite-granite-water at 15 kbar with applications to differentiation and anatexis. *Am. Mineral.* 71: 301-316.

Huggins, F.E. Virgo, D. & Huckenholz, H.G., 1977; Titanium containing silicate garnets I. The distribution of Al, Fe^{3+} and Ti^{4+} between octahedral and tetrahedral sites. *Am. Mineral.* 62: 475-490.

Huppert, H.E. & Sparks, R.S.J., submitted. Cooling and contamination of mafic and ultramafic magmas during ascent through continental crust. *J. Petrol.*

Huppert, H.E. & Turner, J.S., 1981: Double-diffusive convection. *J. Fluid Mech.* 106: 299-330.

Hyndman, D.W., 1984: A petrographic and chemical section through the northern Idaho Batholith. *J. Geol.* 92: 83-102.

Indares, A. & Martignole, J., 1985: Biotite-garnet geothermometry in the granulite facies: the influence of Ti and Al in biotite. *Am. Mineral.* 70: 272-278.

Ishihara, S., 1977: The magnetite-series and ilmenite-series granitic rocks. *Mining Geol.* 27: 293-305.

Jambon, A. & Semet, M.P., 1978: Lithium diffusion in silicate glasses of albite, orthoclase and obsidian composition: an ion-microprobe determination. *Earth Planet. Sci. Lett.* 37: 445-450.

James, R.S. & Hamilton, D.L., 1969: Phase relations in the system $NaAlSi_3O_8$-$KAlSi_3O_8$-$CaAl_2Si_2O_8$-SiO_2 at 1 kilobar water vapour pressure. *Contrib. Mineral. Petrol.* 21: 111-141.

Jaques, A.L. & Green, D.H., 1980: Anhydrous melting of peridotite at 0-15 kb. pressure and the genesis of tholeiitic basalts. *Contrib. Mineral. Petrol.* 73: 287-310.

Jennings, D.J., 1980. Written communication.

Jensen, B.B., 1973; Patterns of trace element partitioning. *Geochim. Cosmochim. Acta* 37: 2227-2242.

Johannes, W., 1978: Melting of plagioclase in the system Ab-An-H_2O and Qz-Ab-An-H_2O at P_{H2O} = 5 kbars, an equilibrium problem. *Contrib. Mineral. Petrol* 66: 295-303.

Johannes, W., 1980: Metastable melting in the granite system Qz-Or-Ab-An-H_2O. *Contrib. Mineral. Petrol.* 72: 73-80.

Johannes, W., 1984: Beginning of melting in the granite system Qz-Or-Ab-An-H_2O. *Contrib. Mineral. Petrol.*, 86: 264-273.

Johannes, W., Bell, P.M., MaO, H.H., Boettcher, A.L., Chipman, D.W., Hays, D.W., Newton, R.C. & Seifert, F., 1971: An interlaboratory comparison of piston-cylinder pressure calibration using the albite breakdown reaction. *Contrib. Mineral. Petrol.* 32: 24-38.

Joplin, G.A., 1942: Petrological studies in the Ordovician of New South Wales. I. The Cooma complex. *Proc. Linn. Soc. N.S.W.* 67: 156-196.

Kershaw, R.C. & Sutherland, F.L., 1971: Quaternary geomorphology of Flinders Island. *Rec. Queen Victoria Museum* 43.

Kilinc, I.A. & Burnham, W.C., 1972: Partitioning of chloride between a silicate melt and coexisting aqueous phase from 2 to 8 kilobars. *Econ. Geol.* 67: 231-235.

Kirkpatrick, R.J., 1981: Kinetics of crystallization of igneous rocks. *In* A.C. Lasaga & R.J. Kirkpatrick (eds): *Kinetics of geochemical processes*. Reviews in Mineralogy, Vol.8. Mineralogical Society of America.

Kirkpatrick, R.J., 1983: Theory of nucleation in silicate melts. *Am. Mineral.* 68: 66-77.

Kistler, R.W., Chappell, B.W., Peck, D.L. & Bateman, P.C., 1986: Isotopic variation in the Tuolumne Intrusive Suite, central Sierra Nevada, California. *Contrib. Mineral. Petrol.* 94: 205-220.

Kistler, R.W. & Peterman, Z.E., 1973: Variations in Sr, Rb, K, Na and initial $^{87}Sr/^{86}Sr$ in granitic rocks and intruded wall rocks in central California. *Geol. Soc. Am. Bull.* 84: 3489-3512.

Kitto, P.A., 1982: *The Geology and Geochemistry of the Ansons Bay Batholith, Northeastern Tasmania.* B.Sc. Honours thesis, University of Tasmania.

Klusman, R.W., 1972: Calcium fractionation in zoned plagioclase from the Tobacco Root batholith, southwestern Montana. *Chem. Geol.* 9: 45-56.

Kobayashi, T., 1978: Osumilites from Rishiri Islands, Hokkaido and Hayato-cho, Kagoshima Prefecture. *Rept Fac. Sci. Kagoshima Univ. (Earth Sci. & Biol.)* 8: 61-69.

Komar, P.D., 1976: Phenocryst interactions and the velocity profile of magma flowing through dikes or sills. *Geol. Soc. Am. Bull.* 87: 1336-1342.

Korshinskii, D.S., 1959: *Physicochemical Basis of the Analysis of Paragenesis of Minerals.* [English translation.] Consultants Bureau Inc., New York.

Kretz, R., 1959: Chemical study of garnet, biotite and hornblende from gneisses of SW Quebec, with emphasis on distribution of elements in coexisting minerals. *J. Geol.* 67: 371-402.

Kretz, R., 1964: Analysis of equilibrium in garnet-biotite-sillimanite gneisses from Quebec. *J. Petrol.* 5: 1-20.

Kontak, D.J., Pichavant, M., & Clark, A.H., 1984: Petrology of the Pliocene peraluminous volcanics from Macusani, SE Peru. *EOS* 65: 299.

Lasaga, A.C., 1979: Multicomponent exchange and diffusion in silicates. *Geochim. Cosmochim. Acta* 43: 455-469.

Lasaga, A.C., 1983: Geospeedometry: an extension of geothermometry. *In* S.K. Sakena (ed.): *Kinetics and Equilibrium Mineral Reactions.* Advances in Physical geochemistry. Vol.3. Springer-Verlag, New York.

Leeman, W.P. & Phelps, D.W., 1981: Partitioning of rare earths and other trace elements between sanidine and coexisting volcanic glass. *J. Geophys. Res.* 86: 10193-10199.

Le Fort, P., 1981: Manaslu leucogranite: a collision signature of the Himalaya. A model for its genesis and emplacement. *Jour. Geophys. Res.* B86: 10545-10568.

Lindstrom, D.J., 1983: Kinetic effects on trace element partitioning. *Geochim. Cosmochim. Acta* 47: 617-622.

Lofgren, G., 1972: Temperature induced zoning in synthetic plagioclase feldspar. *In* W.S. McKenzie (ed.): *The Feldspars*. Univ. Manchester Press: 362-377.

Long, P.E., 1978: Experimental determination of partition coefficients for Rb, Sr and Ba between alkali feldspar and silicate liquid. *Geochim. Cosmochim. Acta* 42: 833-846.

Lonker, S.W., 1981: The P-T-X relations of the cordierite-garnet-sillimanite-quartz equilibrium. *Am. J. Sci.* 281: 1056-1090.

Loomis, T.P., 1982: Numerical simulation of disequilibrium growth processes of garnet in chlorite-bearing, aluminous pelitic rocks. *Can. Min.* 20: 411-423.

Loomis, T.P., 1983a: Compositional zoning of crystals: a record of growth and reaction history. *In* S.K. Sakena (ed.): *Kinetics and Equilibrium in Mineral Reaction. Advances in Physical Geochemistry*, 3: 1-60.

Loomis, T.P., 1983b: Numerical simulations of crystallization processes of plagioclase in complex melts: the origin of major and oscillatory zoning in plagioclase. *Contrib. Mineral. Petrol.* 81: 219-229.

Lorenzoni, S., Messina, A., Russo, S., Stagno, F. & Zanettin-Lorenzoni, E., 1979: The two-mica Al_2SiO_5-granites of Sila (Calabria). *N. Jb Miner. Mh.*, 421-436.

Ludington, S., 1981: The Redskin Granite: evidence for thermogravitational diffusion in a Precambrian granite batholith. *J. Geophys. Res.* B86: 10423-10430.

Luth, R.W. & Boettcher, A.L., 1986: Hydrogen and the melting of silicates. *Am. Mineral.* 71: 264-276.

Luth, W.C., 1967: Studies in the system $KAlSiO_4$-Mg_2SiO_4-SiO_2-H_2O: I, Inferred phase relations and petrologic applications. *J. Petrol.* 8(3): 372-416.

Luth, W.C., 1969: The systems $NaAlSi_3O_8$-SiO_2 and $KAlSi_3O_8$-SiO_2 to 20 kb and the relationship between H_2O content, P_{H2O} and T_{total} in granitic magmas. *Am. J. Sci.* 267A: 325-341.

Luth, W.C., 1976: Granitic rocks. *In* D.K. Bailey & R. McDonald (eds): *The Evolution of the Crystalline Rocks*. Academic Press: 335-417.

Luth, W.C., Jahns, R.H. & Tuttle, O.F., 1964: The granite system at pressures of 4 to 10 kilobars. *J. Geophys. Res.* 69: 759-771.

Lynch, G.V. & Pride, C., 1984: Evolution of a high-level, high-silica magma chamber: the Pattison pluton, Nisling Range alaskites, Yukon. *Can. J. Earth Sci.* 21: 407-414.

Macdonald, G.A. & Katsura, T., 1965: Eruption of Lassen Peak, Cascade Range, California in 1915: examples of mixed magmas. *Geol. Soc. Am. Bull.* 76: 475-482.

Mahood, G.A., 1981: A summary of the geology and petrology of the Sierra La Primavera, Jalisco, Mexico. *Jour. Geophys. Res.* 86B: 10137-10152.

Mahood, G.A. & Hildreth, W., 1983: Large partition coefficients for trace-elements in high-silica rhyolites. *Geochim. Cosmochim. Acta* 47: 11-30.

Manning, D.A.C., 1981: The effect of fluorine on liquidus phase relationships in the system Qz-Ab-Or with excess water at 1 kb. *Contrib. Mineral. Petrol.* 76: 206-215.

Marsh, B.O. & Maxey, M.R., 1985: On the distribution and separation of crystals in convecting magma. *In* B.H. Baker & A.R. McBirney (eds): Processes in Magma Chambers. *J. Volcanol. Geotherm. Res.* 24: 95-150.

Martin, H., 1979: Geochemical behaviour of major and trace elements during incongruent melting of biotite in the St Malo Massif migmatites. *N. Jb Miner. Mh.*: 509-524.

McBirney, A.R., 1980: Mixing and unmixing of magmas. *J. Volcanol. Geotherm. Res.* 7: 357-371.

McBirney, A.R., Baker, B.H. & Nilson, R.H., 1985: Liquid fractionation. Part I: Basic principles and experimental simulations. *J. Volcanol. Geotherm. Res.* 24: 1-24.

McCarthy, T.S. & Groves, D.I., 1979: The Blue Tier batholith, northeastern Tasmania. *Contrib. Mineral. Petrol.* 71: 193-209.

McCarthy, T.S. & Hasty, R.A., 1976: Trace element distribution patterns and their relationship to the crystallization of granitic melts. *Geochim. Cosmochim. Acta* 40: 1351-1358.

McClenaghan, M.P., in press. The Mid-Palaeozoic granites of Tasmania. *Geol. Soc. Aust. Bicentennial Volume.*

McClenaghan, M.P., Turner, N.J., Baillie, P.W., Brown, A.V., Williams, P.R & Moore, W.R., 1982: Geology of the Ringarooma-Boobyalla area. *Geol. Surv. Tasm. Bull.* 61.

McClenaghan, M.P. & Williams, P.R., 1982: Distribution and characterization of granitoid intrusions in the Blue Tier area. *Tasm. Dept Mines, Geol. Surv. Paper* 4: 1-32.

McCulloch, M.T. & Chappell, B.W., 1982: Nd isotopic characters of S- and I-type granites. *Earth Planet. Sci. Lett.* 58: 51-64.

McCulloch, M.T., Jaques, A.L., Nelson, D.R. & Lewis, J.D., 1983: Nd and Sr isotopes in kimberlites and lamproites from Western Australia: an enriched mantle origin. *Nature* 302: 400-403.

McDougall, I. & Leggo, P.J., 1965: Isotopic age determinations on granitic rocks from Tasmania. *J. Geol. Soc. Aust.* 12(2): 295-332.

McKenzie, D., 1985: The extraction of magma from the crust and mantle. *Earth Planet. Sci. Lett.* 44: 81-91.

Mehnert, K.R. & Busch, W., 1982: The initial stage of migmatite formation. *N. Jb Minerah. Abh.* 145: 211-238.

Menzies, M.A. & Murthy, V.R., 1980a: Nd and Sr isotope geochemistry of hydrous mantle nodules and their host alkali basalts: implications for local heterogeneities in metasomatically veined mantle. *Earth Planet. Sci. Lett.* 46: 323-334.

Menzies, M.A. & Murthy, V.L., 1980b: Enriched mantle: Nd and Sr isotopes in diopsides from kimberlite nodules. *Nature* 283: 634-636.

Michard-Vitrac, A., Albarede, F., Dupuis, C. & Taylor, H.P. Jr, 1980: The genesis of Variscan (Hercynian) plutonic rocks: inferences from Sr, Pb and O studies on the Maladeta Igneous Complex, central Pyrenees (Spain). *Contrib. Mineral. Petrol.* 72: 57-72.

Miller, C.F. & Mittlefehldt, D.W., 1984: Extreme fractionation in felsic magma chambers: a product of liquid-state diffusion or fractional crystallization? *Earth Planet. Sci. Lett.* 68: 151-158.

Miyachi, S. & Miyachi, M., 1978: New occurrence of a magnesian 'osumilate' from Iriki, Kagoshima Prefecture, Japan. *Rept Earth Sci. Dept Gen. Educ., Kyusha Univ.* 20: 1-8.

Miyashiro, A., 1956: Osumilite, a new silicate mineral and its crystal structure. *Am. Mineral.* 41: 104-116.

Miyashiro, A., 1975: *Metamorphism and Metamorphic Belts*. Allen & Unwin, London.

Miyashiro, A. & Shido, F., 1985: Tschermak substitution in low- and middle-grade pelitic schists. *J. Petrol.* 26(2): 449-487.

Montel, J.M., 1985: "Is monazite guilty?" Experimental determination of Ce-monazite solubility in Na_2O-K_2O-SiO_2-Al_2O_3 melts. *Terra Cognita* 5: 330.

Mysen, B.O. & Virgo, D., 1985: Iron-bearing silicate melts: relations between pressure and redox equilibria. *Phys. Chem. Minerals* 12: 191-200.

Nakada, S., 1983: Zoned magma chember of the Osuzuyama acid rocks, southwest Japan. *J. Petrol.* 24(4): 471-494.

Nance, W.B. & Taylor, S.R., 1977: Rare earth element patterns and crustal evolution II. Archean sedimentary rocks from Kalgoorlie, Australia. *Geochim. Cosmochim. Acta* 41: 225-231.

Naney, M.T., 1983: Phase equilibria of rock-forming ferromagnesian silicates in granitic systems. *Am. J. Sci.* 283: 993-1033.

Nash, W.P. & Crecraft, H.R., 1985: Partition coefficients for trace elements in silicic magmas. *Geochim. Cosmochim. Acta* 49: 2309-2322.

Nekvasil, H. & Burnham, W.C., 1987: The calculated individual effects of pressure and water content on phase equilibria in th granite system. *In* B.O. Mysen (ed.): *Magmatic Processes: Physicochemical Principles*. The Geochemical Society Special Publication 1.

Nesbitt, H.W., 1980: Genesis of the New Quebec and Adirondack granulites: evidence for their production by partial melting. *Contrib. Mineral. Petrol.* 72: 303-310.

Newton, R.C., 1972: An experimental determination of the high-pressure stability of magnesian cordierite under wet and dry conditions. *J. Geol.* 80: 398-420.

Newton, R.C. & Haselton, H.T., 1981: Thermodynamics of the garnet-plagioclase-Al_2SiO_5-quartz geobarometer. *In* R.C. Newton, A. Navrotsky & B.J. Wood (eds): *Thermodynamics of Minerals and Melts*. Springer-Verlag: 131-147.

Newton, R.C. & Perkins, A., 1982: Thermodynamic calibration of geothermometers based on the assemblages garnet-plagioclase-orthopyroxene (clinopyroxene)-quartz. *Am. Mineral.* 67: 203-222.

Newton, R.C. & Wood, B.J., 1979: Thermodynamics of water in cordierite and some petrologic consequences of cordierite as a hydrous phase. *Contrib. Mineral. Petrol.* 68: 391-405.

Nilson, R.H., McBirney, A.R. & Baker, B.H., 1985: Liquid fractionation. Part II: Fluid dynamics and quantitative implications for magmatic systems. *J. Volcan. Geotherm. Res.* 24: 25-54.

Noble, D.C., Vogel, T.A., Peterson, P.S., Landis, G.P., Grant, N.K., Jezek, P.A. & McKee, E.H., 1984: Rare-earth-enriched, S-type ash-flow tuffs containing phenocrysts of muscovite, andalusite, and sillimanite, southeastern Peru. *Geology* 12: 35-39.

Norrish, K. & Chappell, B.W., 1977: X-ray fluorescence spectrometry. *In* J. Zussman (ed.): *Physical Methods in Determinative Mineralogy*. 2nd ed. Academic Press, London: 254-272.

Norrish, K. & Hutton, J.T., 1969: An accurate X-ray spectrographic method for analysis of a wide range of geological samples. *Geochim. Cosmochim. Acta* 33: 431-453.

Oates, C.J. & Price, R.C., 1983: Geochemistry of the Jemba rhyolite, northeastern Victoria. *J. Geol. Soc. Aust.* 30: 41057.

Ohta, T., Takeda, H. & Takeuchi, Y., 1982: Mica polytypism: similarities in the crystal structures of coexisting 1M and $2M_1$, oxybiotite. *Am. Mineral.* 67: 298-310.

Olesch, M. & Seifert, F., 1981: The restricted stability of osumilite under hydrous conditions in the system K_2O-MgO-Al_2O_3-SiO_2-H_2O. *Contrib. Mineral. Petrol.* 76: 362-367.

O'Nions, R.K. & Powell, R., 1977: The thermodynamics of trace element distribution. *In* D.G. Fraser (ed.): *Thermodynamics in Geology*. D. Reidel Publ. Co., Holland: 349-363.

Orville, P.M., 1972: Plagioclase cation exchange equilibria with aqueous chloride solution: results at 700°C and 2000 bars in the presence of quartz. *Am. J. Sci.* 272: 234-272.

Oxtoby, S. & Hamilton, D.L., 1978: The discrete association of water with Na_2O and SiO_2 in NaAl silicate melts. *Contrib. Mineral. Petrol.* 66: 185-188.

Parkinson, W.D. & Hermanto, R., 1986: The Tamar conductivity anomaly. *Exploration Geophysics* 17: 33-35.

Pattison, D.R.M., Carmichael, D.M. & St Onge, M.R., 1982: Geothermometry and geobarometry applied to early Proterozoic "S-type" granitoid plutons, Wopmay Orogen, Northwest Territories, Canada. *Contrib. Mineral. Petrol.* 79: 394-404.

Pearce, J.A., Harris, N.B.W. & Tindale, A.G., 1984: Trace element discrimination diagrams for the tectonic interpretation of granitic rocks. *J. Petrol.* 25: 956-983.

Perchuk, L.L. & Lavrent'eva, I.V., 1983: Experimental investigation of exchange equilibria in the system cordierite-garnet-biotite. *In* S.K. Sakena (ed.): *Advances in Physical Geochemistry*. Vol.3. *Kinetics and Equilibrium Reactions.*

Perfit, M.R., Brueckner, H., Lawrence, J.R. & Kay, R.W., 1980: Trace element and isotopic variations in a zoned pluton and associated volcanic rocks, Unalaska, Alaska: A model for fractionation in the Aleutian calcalkaline suite. *Contrib. Mineral. Petrol.* 73: 69-87.

Peterson, R.C. & McMullan, R.K., 1986: Neutron diffraction studies of sillimanite. *Am. Mineral.* 74: 742-745.

Phillips, G.N., Wall, V.J. & Clemens, J.D., 1981: Petrology of the Strathbogie Batholith: a cordierite-bearing granite. *Can. Mineral.* 19: 47-63.

Pichavant, M., 1981: An experimental study of the effect of boron on a water saturated haplogranite at 1 kbar vapour pressure. *Contrib. Mineral. Petrol.* 76: 430-439.

Pichavant, M., Herrera, J.V., Boulmoers, S., Brique, L., Joron, J-L., Juteau, M., Marin, L., Michard, A., Sheppard, S.M.F., Treuil, M. & Vernet, M., 1987: The Macusani glasses, S.E. Peru: evidence of chemical fractionation in peraluminous magmas. *In* B.O. Mysen (ed.):

Magmatic Processes: Physicochemical Principles. The Geochemical Society Special Pub. 1.

Pitcher, W.S., 1974: The Mesozoic and Cenozoic batholiths of Peru. *Pacific Geol.* 8: 51-62.

Pitcher, W.S., 1978: Anatomy of a batholith. *J. Geol. Soc. London* 135: 157-182.

Pitcher, W.S., 1979: The nature, ascent and emplacement of granitic magmas. *J. Geol. Soc. London* 136: 627-662.

Pitcher, W.S., 1987: Granites and yet more granites forty years on. *Geol. Rund.* 76/1: 57-79.

Pitcher, W.S. & Berger, A.R., 1972: *The Geology of Donegal: A Study of Granite Emplacement and Unroofing*. Wiley-Interscience, New York.

Piwinski, A.J. & Wyllie, P.J., 1968: Experimental studies of igneous rock series: a zoned pluton in the Wallowa batholith, Oregon. *J. Geol.* 76: 205-234.

Powell, M. & Powell, R., 1977: Plagioclase-alkali feldspar geothermometry revisited. *Min. Mag.* 41: 253-256.

Powers, R.E. & Bohlen, S.R., 1985: The role of synmetamorphic igneous rocks in the metamorphism and partial melting of metasediments, northwest Adirondacks. *Contrib. Mineral. Petrol.* 90: 401-409.

Presnall, D.C. & Bateman, P.C., 1973: Fusion relations in the system $NaAlSi_3O_8$-$CaAl_2Si_2O_8$-$KAlSi_3O_8$-SiO_2-H_2O and generation of granite magmas in the Sierra Nevada Batholith. *Bull. Geol. Soc. Am.* 84: 3181-3202.

Price, J.G., 1985: Ideal mixing in solid solutions, with an application to two-feldspar geothermometry. *Am. Mineral.* 70: 696-701.

Price, R.C., 1983: Geochemistry of a peraluminous granitoid suite from north-eastern Victoria, south-eastern Australia. *Geochim. Cosmochim. Acta* 47: 31-42.

Pride, C. & Muecke, GG.K., 1980: Rare earth element geochemistry of the Scourian Complex, N.W. Scotland - evidence for the granite-granulite ink. *Contrib. Mineral. Petrol.* 73: 403-412.

Ragland, P.C. & Butler, J.R., 1972: Crystallization of the West Farrington Pluton, North Carolina, U.S.A. *J. Petrol.* 13(3): 381-404.

Rapela, C.W. & Shaw, D.M., 1979: Trace and major element models of granitoid genesis in the Pampean Ranges, Argentina. *Geochim. Cosmochim. Acta* 43: 1117-1129.

Reid, E.J., 1980: *The Geology and Geochemistry of the Murrumbucka Region*. M.Sc. thesis, A.N.U., Canberra.

Reid, E.J., in press: The Furneaux Granites. *Geol. Soc. Aust. Bicentennial Vol.*

Reid, J.B. Jr, Evans, O.C. & Fates, D.G., 1983: Magma mixing in granitic rocks of the central Sierra Nevada, California. *Earth Planet. Sci. Lett.* 66: 243-261.

Rice, A., 1986: Convective fractionation: a mechanism to provide cryptic zoning (macrosegregation), layering, crescumulates, banded tuffs and explosive volcanism in igneous processes. *Jour. Geophys. Res.* 86: 405-417.

Richardson, S.W., Gilbert, M.C. & Bell, P.M., 1969: An experimental determination of kyanite-andalusite and andalusite-sillimanite equilibria: the aluminium silicate triple point. *Am. J. Sci.* 267: 259-272.

Robie, R.A. & Hemingway, B.S., 1984: Entropies of kyanite, andalusite, and sillimanite: additional constraints on the pressure and temperature of the Al_2SiO_5 triple point. *Am. Mineral.* 69: 298-306.

Robie, R.A., Hemingway, B.S. & Fisher, J.R., 1978: Thermodynamic properties of minerals and related substances at 298.15K and 1 bar (10^5 pascals) pressure and at higher temperatures. *U.S. Geol. Surv. Bull.* 1452.

Robinson, P., 1982: Metamorphosed igneous rocks at high temperature: the breakdown of amphiboles. *In* D.R. Veblen & P.H. Ribbe (eds): *Amphiboles: Petrology and Experimental Phase Relations*. Reviews in Mineralogy, Vol.9B. Mineralogical Society of America.

Roddick, J.C. & Compston, W., 1976: Radiometric evidence for the age of emplacement and cooling of the Murrumbidgee Batholith. *J. Geol. Soc. Aust.* 23: 223-233.

Roddick, J.C. & Compston, W., 1977: Strontium isotopic equilibriation: a solution to a paradox. *Earth Planet. Sci. Lett.* 34: 238-246.

Roeder, P.L. & Emslie, R.F., 1970: Olivine-liquid equilibrium. *Contrib. Mineral. Petrol.* 29: 275-289.

Rose, A.W. & Burt, D.M., 1979: Hydrothermal alteration. *In* H.L. Barnes (ed.): *Geochemistry of Hydrothermal Ore Deposits*. 2nd ed. Wiley, New York: 173-35.

Ross, D.C., 1985: Mafic gneissic complex (batholithic root?) in the southernmost Sierra Nevada, California. *Geology* 13: 288-291.

Sack, R.O., 1980: Some constraints on the thermodynamic mixing properties of Fe-Mg orthopyroxenes and olivine. *Contrib. Mineral. Petrol.* 71: 237-246.

Salje, E., 1986: Heat capacities and entropies of andalusite and sillimanite: the influence of fibrolitization on the phase diagram of the Al_2SiO_5 polymorphs. *Am. Mineral.* 71: 1366-1371.

Scarfe, C.M., 1986: Viscosity and density of silicate melts. *In* C.M. Scarfe (ed.): *Short Course in Silicate Melts*. Mineralogical Assoc. of Canada.

Schairer, J.F. & Yagi, K., 1952: The system $FeO-Al_2O_3-SiO_2$. *Am. J. Sci.* (Bowen Volume): 471-512.

Schott, J., 1983: Thermal diffusion and magmatic differentiation: a new look at an old problem. *Bull. Mineral.* 106: 247-262.

Schreurs, J., 1985: Prograde metamorphism of metapelites, garnet-biotite thermometry and prograde changes of biotite chemistry in high-grade rocks of West Uuisimaa, southwest Finland. *Lithos* 18: 69-80.

Schwab, R.G. & Kustner, D., 1981: The equilibrium fugacities of important oxygen buffers in technology and petrology. *Neues Jb. Minerah. Abh.* 140: 111-142.

Schwerdtner, W.M., 1978: The Barnum Lake Pluton, Thunder Bay, Ontario: discussion. *Canadian. J. Earth Sci.* 15: 863-864.

Sederholm, J.J., 1891: Uber die finnlandischem Rapakivigesteine. *Tschermaks Mineral. Petrog. Mitt.* 12: 1-31.

Seifert, F., 1976: Stability of the assemblage cordierite + K feldspar + quartz. *Contrib. Mineral. Petrol.* 57: 179-185.

Seki, Y. & Kennedy, G.C., 1964: The breakdown of potassium feldspar, $KAlSi_3O_8$ at high temperatures and high pressures. *Am. Mineral.* 49: 1688-1706.

Shand, S.J., 1927: *The Eruptive Rocks*. Wiley, New York.

Shaw, H.R., 1963a: Obsidian-H_2O viscosities at 1000 and 2000 bars in the temperature range 700° to 900°C. *J. Geophys. Res.* 68: 6337-6343.

Shaw, H.R., 1963b: The four-phase curve sanidine-quartz-liquid-gas between 500 and 4000 bars. *Am. Mineral.* 48: 883-896.

Shaw, H.R., 1965: Comments on viscosity, crystal settling, and convection in granitic rocks. *Am. J. Sci.* 263: 120-152.

Shaw, H.R., 1972: Viscosities of magmatic silicate liquids: an empirical method of prediction. *Am. J. Sci.* 272: 870-893.

Sighinolfi, G.P. & Gorgoni, C., 1978: Chemical evolution of high-grade metamorphic rocks - anatexis and remotion of material from granulite terrains. *Chem. Geol.* 22: 157-176.

Sparks, R.S.J., Huppert, H.E. & Turner, J.S., 1984: The fluid dynamics of evolving magma chambers. *Phil. Trans. R. Soc. London* A310: 511-534.

Sparks, R.S.J., Sigurdsson, H. & Wilson, L., 19 : Magma mixing: a mechanism for triggering acid explosive eruptions. *Nature* 267: 315-318.

Speer, J.A., 1981: Petrology of cordierite- and almandine-bearing granitoid plutons of the Southern Appalachian Piedmont, U.S.A. *Can. Min.* 19: 35-46.

Spencer, K.J. & Lindsley, D.H., 1981: A solution model for coexisting iron-titanium oxides. *Am. Mineral.* 66: 1189-1201.

Spiering, B. & Siefert, F.A., 1985: Iron in silicate glasses of granitic composition: a Mossbauer spectroscopic study. *Contrib. Mineral. Petrol.* 90: 63-73.

Spulber, S.D. & Rutherford, M.J., 1983: The origin of rhyolite and plagiogranite in oceanic crust: an experimental study. *J. Petrol.* 24(1):: 1-25.

Stormer, J.C., 1975: A practical two-feldspar geothermometer. *Am. Mineral.* 60: 667-674.

Streckeisen, A.L., 1973: Plutonic rocks. Classification and nomenclature recommended by the IUGS Subcommission on the Systematics of Igneous Rocks. *Geotimes* 18: 26-30.

Sun, S.-S., Higgins, N.C. & McCulloch, M.T., 1986: Nd and Sr isotope study of granitoids of the Blue Tier and Eddystone Batholiths, NE Tasmania, and associated Sn-W mineralisation. *B.M.R. Record* 1986/10.

Swanson, S.E., 1977: Relation of nucleation and crystal growth rate to the development of granitic textures. *Am. Mineral.* 62: 966-978.

Swanson, S.E., 1979: The effect of CO_2 on the phase equilibria and crystal growth in the system $KAlSi_3O_8$-$NaAlSi_3O_8$-$CaAl_2Si_2O_8$-SiO_2-H_2O-CO_2 to 8000 bars. *Am. J. Sci.* 279: 703-720.

Sykes, M.L. & Holloway, J.R., 1987: Evolution of granitic magmas during ascent: a phase equilibrium model. *In* B.O. Mysen (ed.): *Magmatic Processes: Physicochemical Principles.* The Geochemical Society Special Publication 1.

Taylor, H.P. Jr, 1980: The effects of assimilation of country rocks by magmas on $^{18}O/^{16}O$ and $^{87}Sr/^{86}Sr$ systematics in igneous rocks. *Earth Planet. Sci. Lett.* 47.

Taylor, H.P. Jr & Silver, L.T., 1978: Oxygen isotope relationships in plutonic igneous rocks of the Peninsular Rangers batholith, southern and Baja California. *In* R.E. Zartmann (ed.): *Short Papers of the 4th Int. Conf., Geochronology, Cosmochronology, Isotope Geology.* U.S.G.S. Open File Rept 78-701: 423-426.

Taylor, M., Brown, G.E. & Fenn, P.M., 1979: Structure of mineral glasses - III. $NaAlSi_3O_8$ supercooled liquid at 805°C and the effects of thermal history. *Geochim. Cosmochim. Acta* 44: 109-117.

Taylor, S.R., Gorton, M.P., Muir, P., Nance, W.B., Rudowski, R. & Ware, N., 1973: Composition of the Descartes Region, Lunar Highlands. *Geochim. Cosmochim. Acta* 37: 2665-2683.

Thompson, A.B., 1976a: Mineral reactions in pelitic rocks: I. Prediction of P-T-X (Fe-Mg) phase relations. *Am. J. Sci.* 276: 401-424.

Thompson, A.B., 1976b: Mineral reactions in pelitic rocks: II. Calculation of some P-T-X (Fe-Mg) phase relations. *Am. J. Sci.* 276: 425-454.

Thompson, A.B., 1982: Dehydration melting of pelitic rocks and the generation of H_2O-undersaturated granitic liquids. *Am. J. Sci.* 282: 1567-1595.

Thompson, A.B. & Tracy, R.J., 1979: Model systems for anatexis of pelitic rocks II. Facies series melting and reactions in the system CaO-$KAlO_2$-$NaAlO_2$-Al_2O_3-SiO_2-H_2O. *Contrib. Mineral. Petrol.* 70: 429-438.

Thompson, J.B. Jr, 1982: Compositional space: an algebraic and geometric approach. *In* J.M. Ferry (ed.): *Characterization of the Metamorphism Through Mineral Equilibria.* Reviews in Mineralogy, Vol.10: 1-32.

Thompon, M.E. & McBirney, A.R., 1985: Redistribution of phenocrysts by convective flow in a viscous boundary layer. *J. Volcanol. Geotherm. Res.* 24: 83-94.

Torres-Roldan, R.L., 1983: Fractionated melting of metapelite and further crystal-melt equilibria. The example of the Blanca Unit migmatite complex, north of Estepona (southern Spain). *Tectonophysics* 96: 95-123.

Tsuchiyama, A., 1985: Partial melting kinetics of plagioclase-diopside pairs. *Contrib. Mineral. Petrol.* 91: 12-23.

Tsuchiyama, A. & Takahashi, E., 1983: Melting kinetics of a plagioclase feldspar. *Contrib. Mineral. Petrol.* 84: 345-354.

Turner, N.J., Baillie, P.W. & McClenaghan, M.P., 1983: Definition of the Eddystone Batholith. Tasm. Dept Mines Unpub. Rept 1983/57.

Turner, N.J., Black, L.P. & Higgins, N.C., 1986: The St Marys porphyrite - a Devonian ash-flow tuff and its feeder. *Aust. J. Earth Sci.* 33: 201-218.

Tuttle, O.F. & Bowen, N.L., 1958: Origin of granite in the light of experimental studies in the system $NaAlSi_3O_8$-$KAlSi_3O_8$-SiO_2-H_2O. *Mem. Geol. Soc. Am.* 74.

Van der Molen, I. & Paterson, M.S., 1979: Experimental deformation of partially-melted granite. *Contrib. Mineral Petrol.* 70: 299-318.

Verniers, J., Joron, J.L., Treuil, M., Coulon, C. & Dupuy, C., 1977: Coefficient de partage de quelques elements en trace entre plagioclase et verre dans les ignimbrites - implications petrogenetiques. *Chem. Geol.* 19: 309-325.

Vernon, R.H., 1983: Restite, xenoliths and microgranitoid enclaves in granites. *J. Roy. Soc. N.S.W.* 116: 77-103.

Vernon, R.H., 1984: Microgranitoid enclaves in granites - globules of hybrid magma quenched in a plutonic environment. *Nature* 309: 438-439.

Vernon, R.H., 1985: Possible role of superheated magma in the formation of orbicular granitoids. *Geology* 13: 843-845.

Vernon, R.H., Etheridge, M.A. & Wall, V.J., 1983: Magma mixing in the development of metaluminous granitoid suites of the Moruya Batholith around Tuross Head, N.S.W. *In* Lithosphere Dynamics and Evolution of Continental Crust. *Geol. Soc. Aust. Abstracts* 9: 185.

Visona, D., 1983: Cumulate-like textures and chemical relationships in the Bressanone (Brixen) Granodiorite (eastern Alps, Italy) - a new genetic approach. *Chem. Geol.* 40: 279-292.

Vogel, T.A. & Walker, B.M., 1975: The Tichka Massif, Morocco - an example of contemporaneous acidic and basic plutonism. *Lithos* 8: 29-38.

Vogel, T.A. & Wilband, J.T., 1978: Coexisting acidic and basic melts: geochemistry of a composite dike. *J. Geol.* 86: 353-371.

von Platen, H., 1965: Experimental anatexis and genesis of migmatites. *In* W.S. Picher & G.W. Flinn (eds): *Controls of Metamorphism*. Oliver & Boyd, Endinburgh & London.

Vrana, S., Rieder, M. & Podlaha, J., 1978: Kanonaite $(Mn^{3+}_{0.76}Al_{0.23}Fe^{3+}_{0.02})^{6}Al^{5}(O/SiO_4)$, a new mineral isotypic with andalusite. *Contrib. Mineral. Petrol.* 66: 325-332.

Ware, N.G., 1981: Computer programs and calibration with the PIBS technique for quantitative electron probe analysis using a lithium-drifted silicon detector. *Computers and Geosciences* 7: 167-184.

Walker, D. & De Long, S.E., 1982: Soret separation of mid-ocean ridge basalt magma. *Contrib. Mineral. Petrol. 79: 231-240.*

Watson, E.B., 1979: Zircon saturation in felsic liquids: experimental results and application to trace element geochemistry. *Contrib. Mineral. Petrol.* 70: 407-419.

Watson, E.B., 1980: Some experimentally determined zircon/liquid partition coefficients for the rare earth elements. *Geochim. Cosmochim. Acta* 44: 895-897.

Watson, E.B. & Green, T.H., 1981: Apatite/liquid partition coefficients for the rare earth elements and strontium. *Earth Planet. Sci. Lett.* 56: 405-421.

Watson, E.B. & Harrison, T.M., 1983: Zircon saturation revisited: temperature and composition effects in a variety of crustal magma types. *Earth Planet. Sci. Lett.* 64: 295-304.

Weber, C., Barbey, P., Cuney, M. & Martin, H., 1985: Trace element bahviour during migmatization. Evidence for a complex melt-residium-fluid interaction in the St Malo migmatitic dome (France). *Contrib. Mineral. Petrol.* 90: 52-62.

Weisbrod, A., 1972-3: Cordierite-garnet equilibrium in the system Fe-Mn-Al-Si-O-H. *Carnegie Inst. Geophys. Lab. Ann. Rept* 1972-3.

Wells, A.K. & Woolridge, S.W., 1931: The rocks groups of Jersey, with special reference to intrusive phenomena. *Proc. Geol. Assoc.* 42: 178-215.

Whalen, J.B., 1980: *Aspects of Granites and Related Mineralization.* Ph.D. thesis, A.N.U., Canberra.

Whalen, J.B., 1983: The Ackley City Batholith, southeastern Newfoundland: evidence for crystal versus liquid-state fractionation. *Geochim. Cosmochim. Acta* 47: 143-1457.

Whalen, J.B., 1985: The McGerrigle plutonic complex, Gaspe, Quebec: evidence of magma mixing and hybridization. *Geol. Surv. Canada Paper* 85-1A: 795-800.

Whalen, J.B. & Currie, K.L., 1984: The Topsails igneous terrane, western Newfoundland: evidence for magma mixing. *Contrib. Mineral. Petrol.* 87: 319-327.

Whalen, J.B., Currie, K.L. & Chappell, B.W., 1987: A-type granites: geochemical characteristics, discrimination and petrogenesis. *Contrib. Mineral. Petrol.* 95: 407-419.

White, A.J.R., 1986: Granites around Ballarat, Ararat and Stawell. *AMIRA Field Excursion Guide.*

White, A.J.R. & Chappell, B.W., 1977: Ultrametamorphism and granitoid genesis. *Tectonophysics* 43: 7-22.

White, A.J.R., Chappell, B.W. & Cleary, J.R., 1974: Geologic setting and emplacement of some Australian Palaeozoic batholiths and implications for intrusive mechanisms. *Pacific Geol.* 8: 159-171.

Whitney, J.A., 1975: The effects of pressure, temperature and X_{H2O} on phase assemblage in four synthetic rock compositions. *J. Geol.* 83: 1-31.

Wickham, S.M., 1987: Crustal anatexis and granite petrogenesis during low-pressure regional metamorphism: the Trois Seigneurs Massif, Pyrenees, France. *J. Petrol.* 28(1): 127-169.

Wiebe, R.A., 1973: Relations between coexisting basaltic and granitic magmas in a composite dyke. *Am. J. Sci.* 273: 130.

Williams, E., 1979: Tasman Fold Belt System in Tasmania. Explanatory notes for the 1:500,000 structural map of pre-Carboniferous rocks of Tasmania. Department of Mines, Tasmania.

Winkler, H.G.F., Das, B.K. & Breitbart, R., 1977: Further data of low-temperature melts existing on the quartz + plagioclase + liquid + valpour isobaric cotectic surface within the system Qz-Ab-Or-An-H_2O. *N. Jb. Miner. Mh.* 1977: 241-247.

Winter, J.K. & Ghose, S., 1979: Thermal expansion and high-temperature crystal chemistry of the Al_2SiO_5 polymorphs. *Am. Mineral.* 64: 573-586.

Wood, B.J. & Fraser, D.G., 1976: *Elementary Thermodynamics for Geologists.* Oxford University Press, Oxford.

Wones, D.R., 1981: Mafic silicates as indicators of intensive variables in granitic magmas. *Mining Geol.* 31: 191-212.

Wones, D.R. & Dodge, F.C.W., 1977: The stability of phlogopite in the presence of quartz and diopside. *In* D.G. Fraser (ed.): *Thermodynamics in Geology.* D. Reidel Publ. Co., Holland.

Wones, D.R. & Gilbert, M.C., 1982: Amphiboles in the igneous environment. *In* D.R. Veblin & P.H. Ribbe (eds): *Amphiboles: Petrology and Experimental Phase Relations.* Reviews in Mineralogy, Vol. 9B. Mineralogical Society of America.

Wood, B.J. & Fraser, D.G., 1977: *Elementary Thermodynamics for Geologists.* Oxford University Press.

Wyborn, D., 1983: *Fractionation Processes in the Boggy Plain Zoned Pluton.* Ph.D. thesis, A.N.U., Canberra.

Wyborn, D. & Chappell, B.W., 1986: The petrogenetic significance of chemically related plutonic and volcanic rock units. *Geol. Mag.* 123(6): 619-628.

Wyborn, D., Chappell, B.W. & Johnston, R.M., 1981: Three S-type volcanic suites from the Lachlan Fold Belt, southeast Australia. *Jour. Geophys. Res.* 86B: 10335-10348.

Wyborn, D., Turner, B.S. & Chappell, B.W., 1987: The Boggy Plain Supersuite - a distinctive belt of I-type igneous rocks of potential economic significance in the Lachlan Fold Belt. *Aust. J. Earth Sci.* 34: in press.

Wyllie, P.J., 1971: *The Dynamic Earth: A Textbook in Geosciences.* Wiley, New York.

Wyllie, P.J., 1977: Crustal anatexis: an experimental review. *Tectonophysics* 43: 41-71.

Yoder, H.J. Jr, 1973: Contemporaneous basaltic and rhyolitic magmas. *Am. Mineral.* 58: 153-171.

Yoder, H. & Kushiro, I., 1969: Melting of a hydrous phase: phlogopite. *Am. J. Sci.* 267A: 558-582.

Zen, E-An, 1966: Construction of pressure-temperature diagrams for multicomponent systems after the method of Schreinemakers - a geometrical approach. *U.S. Geol. Surv. Bull.* 1225.

Zen, E-An, 1985: An oxygen buffer for some peraluminous granites and metamorphic rocks. *Am. Mineral.* 70: 65-73.

Appendix A

CATALOGUE OF ROCK SAMPLES COLLECTED FROM THE NORTHERN PART OF THE BLUE TIER BATHOLITH

Abbreviations and symbols used in each category of this catalogue are defined below:

University of Tasmania Geology Department Catalogue Number (TU#):

* : collected by J.C. Cocker (1977)

F : collected by D. Jennings, Tasmanian Department of Mines, over the period 1975 to 1977 (Jennings, 1980).

The correlation between the University and the Department of Mines catalogue numbers is as follows:

TU#	Mines Dept #
62576	77/879
62577	77/880
68530	77/891
68531	77/886
68532	77/898
68533	77/900
68539	not catalogued
68544	not catalogued

Rock Type:

AF - alkali feldspar phenocryst-rich
AP - aplite
ap - aphyric
flysch
at - altered
BI - biotite phenocryst-rich
cg - coarse grained variety (relative scale)
fg - fine grained variety (relative scale)
GA - garnet phenocryst-rich
GR - granite (i.e. mean grainsize of matrix phases > 1 mm)
in - inclusion within granite
MB - metabasalt
MD - psammopelitic country-rock
MS - mineral segregation within granite
my - mylonitized
PF - porphyry (i.e. mean grainsize of matrix phases $\leq$ 1 mm)
pp - phyric-poor
pr - phyric-rich
PG - pegmatite
QZ - quartz phenocryst-rich

Suite:

b - basalt
BI - Babel Island
BO - Boobyalla
GA - Gardens
MU - Musselroe
LB - Lady Barron
PO - Poimena
WY - Wybalenna
/ - symbol indicating hybridized sample with minor constituent on the left hand side

Unit:

I - Island
Is - Islands
Pt - Point
R - River
int - intruding into

Grid Reference:

Use is made of the universal 1:100,000 scale grid system. The preceeding letters refer to the particular 100,000 metre square in which the point lies.

Sample Type:

AF - alkali feldspar phenocryst separate
BI - biotite phenocryst separate
C - coarse grained unit (relative scale)
CD - cordierite phenocryst separate
e - felsic
f - fine grained unit (relative scale)
GA - garnet phenocryst separate
h - porphyritic
i - portion taken more than 80 mm from contact with granite
l - mafic
MX - matrix separate
o - portion taken from within 80 mm of contact with granite
PL - plagioclase phenocryst separate
RD - separate of felsic rind to inclusion
s - pseudomorphic
t - tourmaline-rich portion of unit
WR - whole rock

Sample Representation:

A - chemical analysis
H - hand specimen
I - SmNd isotopic analysis
T - thin section (polished)

TU#	Rock Type	Suite	Unit	GR	Sample Type	Sample Representation
43083*	pp GR	PO	Modder R	ER962386	WR	A,H
62575	pr PF	BI	Babel I	FR138758	WR	A,H,T
62576F	pr fg GR	GA	Little Chalky I	ER755612	WR	A,H
62577F	pp GR	WY	Big Green I	ER834517	WR	A,H
62578	pr cg PF	BO	Loccota	ER886449	WR	A,H,T
62579	ap PF	BI	Babel I	FR138759	c WR	A,H,I,T
					f WR	A
					l f WR	A
62580	ap cg GR	BI	Babel I	FR138759	WR	A,H,T
62581	pr fg GR in	PO	Modder R	ER857300	WR	A,H,T
62582	pr cg GR	PO	Modder R	ER857300	WR	A,H,T
62583	pr fg GR in	BO	Rum I	ER932131	WR	A,H,I,T
62584	pr cg GR	BO	Rum I	ER932131	WR	A,H,T
62585	pp cg GR	BO	Rum I	ER932131	WR	A,H,T
62586	pp fg GR	MU	Clarke I	ER935136	WR	A,H,T
62587	pp fg GR	MU	Clarke I	ER937138	WR	A,H,T
62588	pr GR	MU	Clarke I	ER933135	WR	H
					RD	A,H,T
62589	pp PF	WY	Wybalenna	ER799674	WR	A,H,T
					MX	A
					PL	A
62590	pp cg PF	WY	Wybalenna	ER799674	WR	A,H
62591	pp cg GR	PO	Modder R	ER918339	WR	A,H,T
62592	pr cg GR	PO	Modder R	ER918339	WR	A,H,T

TU#	Rock Type	Suite	Unit	GR	Sample Type	Sample Representation
62593	pp PF in	WY	Wybalenna	ER733691	WR	A,H,T
					MX	A
					PL	A
62594	pr PF in	PO	Modder R	ER847296	WR	A,H,T
					MX	A
					PL	A
62595	pr cg PF	BO	Rum I	ER868239	WR	A,H,T
					MX	A
					AF	A
					PL	A
62596	pr cg PF	PO	Battery Hills	ER977333	WR	A,H,T
					MX	A
					AF	A
					PL	A
62597	pr cg PF	PO	Battery Hills	ER971329	WR	A,H,T
62598	pr cg PF	PO	Battery Hills	ER951337	WR	A,H,T
62599	ap GR	PO	Modder R	ER844291	WR	A,H,T
62600	pp GR	PO	Modder R	ER844292	WR	A,H,T
62601	pr PF in	PO/PO	Modder R	ER844292	WR	A,H,T
					PL	A
62602	pp PF in	WY	Modder R	ER844292	WR	A,H,T
					i MX	A
					o MX	A
					PL	A
62603	pp cg GR	BO	Cape Barren	FR245222	WR	A,H
62604	pr cg GR	BO	Cape Barren	FR245222	WR	A,H,T
62605	pp PF	BO	Cape Barren	FR245222	WR	A,H,T
					MX	A
62606	pr PF	BO	Cape Barren	FR245222	WR	A,H,T
					MX	A
62607	pp GR	WY	Chappell Is	ER837250	WR	A,H,T
62608	pp GR	WY	Chappell Is	ER842246	WR	A,H,T
62609	pp cg PF in	WY	Chappell Is	ER837250	WR	A,H
62610	pp PF in	WY	Chappell Is	ER837250	WR	A,H,T
					MX	A
					PL	A
62611	pp GR	PO	Lughrata	ER760816	WR	A,H,T
62612	pp cg PF	PO	Holts Pt	ER886449	WR	A,H,T
					MX	A
					PL	A
62613	QZ pr PF	BO	Loccota	ER886449	WR	A,H,T
62614	pr cg PF	BO/PO	Loccota/Holts Pt	ER886450	WR	A,H,T
					AF	A
					PL	A
62615	fg BI MS	BO	Loccota	ER886449	WR	A,H,T
62616	ap PF	BO	Loccota	ER886449	c WR	A,H
					f WR	A,H,T
62617	ap PF	BO	Loccota	ER886449	WR	A,H,T
62618	pp PF	BO	Loccota	ER886449	WR	A,H,T
					MX	A
62619	pr PF	BO	Loccota	ER886449	WR	A,H,T
					MX	A
					h BI	A
					s BI	A
					PL	A
62620	pr PF	BO	Loccota	ER886449	WR	A,H,T
62621	pp GR	BO	Loccota	ER886445	WR	A,H,T
62622	pr fg GR	BO	Loccota	ER886445	WR	A,H,T
					AF	A
					PL	A

TU#	Rock Type	Suite	Unit	GR	Sample Type	Sample Representation
62623	pr fg GR	BO	Loccota	ER925416	WR	A,H,T
62624	AP	BO	Strzelecki	ER925418	WR	A,H,T
62625	pp GR	BO	Strzelecki	ER932505	WR	A,H,T
62626	at pp PF	BO	Strzelecki	ER990431	WR	A,H,T
62627	pr PF	BO	Strzelecki	ER990429	WR	A,H,T
					MX	A
					AF	A
62628	pp fg GR	WY	Pats R	ER860637	WR	A,H,T
62629	pp PF in	WY	Pats R	ER860637	WR	
62630	pp PF in	WY	Pats R	ER860637	WR	
62631	pp GR	WY	Pats R	ER860637	WR	T
62632	pp PF in	WY	Pats R	ER850631	WR	
62633	pp GR	WY	Pats R	ER853629	WR	T
62634	GA MS	BO	Rum I	ER869240	WR	A,H,T
					AF	A
					BI	A
					GA	A,I
					PL	A
62635	pp GR	WY	Wybalenna	ER749692	WR	A,H,T
62636	pr GR in	?	Wybalenna	ER749692	WR	A,H,T
					RD	A,H
62637	pr GR	MU	Martins Rise	ER908552	WR	A,H,T
62638	pr GR	MU	Martins Rise	ER890584	WR	A,H,T
62639	pp GR	PO	The Patriarchs	ER970678	WR	A,H,T
62640	pp GR	LB	Lady Barron	FR067477	WR	A,H,T
62641	pp GR	LB	Lady Barron	FR078471	WR	A,H,T
62642	pp GR	LB	Puncheon Pt	FR110365	WR	A,H,T
67530	pp fg PF	PO/b	Long Toms Nose	FR101390	WR	A,H,T
					e MX	A
					m MX	A
67531	pp fg PF	PO/b	Long Toms Nose	FR101391	WR	A,H
67532	pr fg PF	PO	Long Toms Nose	FR112367	WR	A,H,T
67533	ap fg PF	PO	Long Toms Nose	FR112367	WR	A,H,T
					l WR	A
67534	my GR	WY	Chappell Is	ER836252	WR	A,H,T
67535	ap GR in	BO	Rum I	ER877236	WR	A,H,I,T
67536	pp GR in	BO	Strzelecki	ER904432	WR	A,H,T
67537	AP	PO	Modder R	ER850298	WR	A,H,T
					l WR	A
					t WR	A
67538	MB		int:Lady Barron	FR077472	WR	A,H,T
67539	GA MS	MS	Ansons Bay	FQ105583	WR	A,H,T
					BI	A
					CD	A
					GA	A
67540	MD in			ER886447	WR	A,H,T
67541	MD in			ER886447	WR	A,H,T
67542	MD in			ER886447	i WR	A,H
					o WR	A,H
67543	ap GR	BI		FR138782	WR	A,H,T
67544	pp PF	BI		FR143775	WR	A,H,T
67545	pp PF	LB	Castle Rock Pt	ER769741	WR	A,H,T
67546	ap PF	?	Emita	ER764719	WR	A,H,T
67547	pr GR	BO	Strzelecki	ER904434	WR	A,H,T
67548	pr GR	BO	Strzelecki	ER877460	WR	A,H,T
68523	GA MS	BO	Strzelecki	ER908429	WR	H,T
68524	GA MS	BO	Cape Barren	FR185170	WR	H,T
68525	GA MS	BO	Loccota	ER895440	WR	H,T
68526	pp cg PF	PO/BO	Holts Pt/Loccota	ER886449	WR	H,T
68527	pr GR	LB	Dover R	FR118318	WR	H
68528	pp GR	LB	Lady Barron	ER994540	WR	H

TU#	Rock Type	Suite	Unit	GR	Sample Type	Sample Representation
68529	GA MS	BO	Strzelecki	ER877460	WR	H,T
68530F	pp GR	?	Franklin Sound	FR073458	WR	H,I,T
68531F	pp fg GR	?	Prime Seal I	ER653647	WR	H,T
68532F	pr cg PF	PO	The Patriarchs	FR027775	WR	H,T
68533F	ap GR	PO	Lughrata	ER809748	WR	H,T
68534	fg Gr	?	Franklin Sound	FR088428	WR	H
68535	GR	?	Franklin Sound	FR088428	WR	H
68536	GR	PO	Lughrata	ER876681	WR	H,T
68537	cg PF	?	Franklin Sound	FR088401	WR	H
68538	fg GR	?	Franklin Sound	FR098418	WR	H
68539F	cg GR	BO	Rum I	FR013063	WR	H,T
68540	ap GR in	WY	Rum I	ER875243	WR	H
68541	pr PF GR	?	Franklin Sound	ER719927	WR	H
68542	pp cg PF	?	Franklin Sound	ER719925	WR	H
68543	GR	PO	Lughrata	ER879673	WR	H
68544F	cg GR	BO	Cape Barren	FR145165	WR	H
68545	PF	BO	Strzelecki	ER925416	WR	H,T
68546	cg GR/MD in	BO	Strzelecki	ER904434	WR	H
68547	PG	BO	Strzelecki	ER886449	WR	H,T
68548	PG	BO	Loccota	ER886449	WR	H,T
68549	pp PF	MU	Musselroe	EQ988795	WR	H
68550	GA MS	BI	Babel I	FR137758	WR	T
68551	PG	BI	Babel I	FR147758	WR	H,T

Appendix B

METHODS OF CALCULATING MESONORMATIVE QUARTZ, ALKALI FELDSPAR AND PLAGIOCLASE FROM GRANITIC CHEMICAL COMPOSITIONS

The method described below uses the chemical and CIPW normative compositions of a granitic rock to calculate the proportions of quartz, alkali feldspar and plagioclase present in a mesonormative composition containing the normative minerals biotite and aluminosilicate rather than hypersthene and corundum, respectively. The resulting mesonormative mineralogy is more appropriate than that of the CIPW norm for referencing most granitic compositions because of its greater resemblance to the modal mineralogy of most granites. The calculated proportions of the three felsic phases should then be similar to the modal proportions present in the rock, because the mesonormative and modal mineralogies are similar. Proportions of the mesonormative quartzofeldspathic phases are listed for the Furneaux granitic rocks and porphyry matrix separates in Appendix E and are depicted graphically in Fig. 2.1.

The CIPW normative phases used to generate the mesonormative minerals are quartz, albite, anorthite, hypersthene, ilmenite, magnetite and corundum. In the following description, they are referred to by the lower-case symbols: qz, or, ab, an, hy, il, mt and co, respectively. The weight proportions of these phases were themselves calculated according to the standard methods (Kelso, 1958?), from chemical compositions listed in Appendices A, E and O using a program for a desk-top Hewlett-Packard 9825 computer written by Dr B.W. Chappell (A.N.U., Canberra). A weight ratio of 0.25 was assumed for Fe_2O_3/FeO as the iron oxidation states of the samples were not determined.

The mesonormative minerals used in the calculation are: quartz, alkali feldspar, plagioclase, biotite and aluminosilicate. They are referred to by symbols starting with upper-case letters, viz: Qz, Af, Pl, Bi and As, respectively.

Mesonormative biotite is defined as being an oxyannite-oxyphlogopite solid-solution. On a molar basis therefore,

$$\begin{aligned}\text{Biotite} &= K(Fe,Mg)_3AlSi_3O_{12} \\ &= KALSi_3O_8 + 3(Fe,Mg)SiO_3 - 3SiO_2 \\ &= 1(\text{orthoclase})_{\text{in biotite}} + 3(\text{hypersthene})_{\text{in biotite}} \\ &\qquad - 3(\text{quartz})_{\text{in biotite}}.\end{aligned} \tag{B1}$$

Mesonormative aluminosilicate:

$$\begin{aligned} As &= Al_2SiO_5 \\ &= Al_2O_3 + SiO_2 \\ &= 1(\text{corundum})_{\text{in aluminosilicate}} + 1(\text{quartz})_{\text{in aluminosilicate}} \end{aligned} \quad (B2)$$

Alkali feldspar (Af) consists of CIPW-normative orthoclase + albite ± anorthite solid solution. It has up to two components, both of which are solid solutions of CIPW normative constituents. The major component has an assumed molar composition of $or_{75}ab_{25}$, i.e. similar in composition to the alkali feldspar phenocryst separate from sample #62595 (cf. Appendix F). This component is termed (α) below and consists of CIPW normative orthoclase (or) and albite (ab) less the quantity of (or) required to generate mesonormative biotite (Bi) according to equation B1. However sodic and calcium-poor samples contain another component: sodic feldspar: $ab_{95}an_5$, termed (β) below. Its molecular composition is that designated as the limiting calcic composition of the sodic component of alkali feldspar by Streckeisen (1973, 1976) in his classification of felsic plutonic rocks.

Plagioclase (Pl) consists of albite-anorthite solid-solution. Its composition is assumed to be $ab_{\leq 75}an_{\geq 25}$. This compositional limit is similar to the limiting sodic compositions of plagioclase crystal cores of many Furneaux granitic rocks (Chapter 7, Fig. 7.12).

Mesonormative quartz (Qz) consists of CIPW normative quartz together with the excess SiO_2 generated by conversion of hypersthene to biotite (equation B1) less the SiO_2 required to generate aluminosilicate from corundum (equation B2).

For alkali feldspar, the weight fraction of the $or_{75}ab_{25}$ component (α) will be:

$$\alpha = \left[WF_{or} - \left(\frac{WF_{hy}.MW_{or}}{3.MW_{hy}}\right)\right].\left[1 + \left(\frac{MW_{ab}}{3.MW_{or}}\right)\right] \quad (B3)$$

for WF = weight fraction, and MW = molecular weight.
and where MW_{hy} is assumed to be a linear combination of the molecular weights of the endmembers: orthogerrosilite and enstatite, i.e.

where $$MW_{hy} = 131.93 - 0.3154*(mg)_{hy} \quad (B4)$$

$$\text{for } (mg)_{hy} = \left[\frac{100 \text{ moles } (Mg)_{\text{sample}}}{\text{moles}[(FeO)_{\text{sample}} - (FeO)_{il} - FeO_{mt}] + \text{moles}(MgO)_{\text{sample}}}\right]$$

$$\text{i.e.} \quad (mg)_{hy} = \left| \frac{100(\%MgO_{sample}/MW_{MgO})}{\left(\frac{\%FeO^*_{sample} - 0.4735(il)}{MW_{FeO}}\right) + \left(\frac{\%MgO_{sample}}{MW_{MgO}}\right)} \right| \tag{B5}$$

When the molar ratio: [(an)/(an+remaining (ab))] < 0.25 then the (an) and remaining (ab) are divided into two portions, termed β and γ. Portion β has a molar composition of albite$_{95}$anorthite$_5$ as described above and is assigned to alkali feldspar.

$$\beta = \left| \frac{0.25 - \frac{(WF_{an}/MW_{an})}{(WF_{an}/MW_{an}) + (WF_{\text{remaining ab}}/MW_{ab})}}{(0.25 - 0.05)} \right| \cdot \left(\frac{(WF_{an} + WF_{\text{remaining ab}})}{MW_{[(an)+\text{remaining (ab)}]}} \right) \cdot MW_{ab_{95}an_5} \tag{B6}$$

Portion γ has a molar composition of $ab_{75}an_{25}$ and is assigned to plagioclase, as described above, and is given by the equation:

$$\gamma = \left| \frac{\left(\frac{(WF_{an}/MW_{an})}{(WF_{an}/MW_{an}) + (WF_{\text{remaining ab}}/MW_{ab})} \right) - 0.05}{0.25 - 0.05} \right| \cdot \left(\frac{(WF_{an} + WF_{\text{remaining ab}})}{MW_{[(an)+\text{remaining (ab)}]}} \right) \cdot MW_{ab_{75}an_{25}} \tag{B7}$$

So in the mesonorm:

$$WF_{Af} = \alpha + \beta \tag{B8}$$

and

$$WF_{Pl} = \gamma \tag{B9}$$

However, if the molar ratio of an/(an + remaining (ab)) < 0.25, then

$$WF_{Pl} = WF_{an} + WF_{ab} - \left[WF_{or} - \left(\frac{WF_{hy} \cdot MW_{or}}{3 \cdot MW_{hy}} \right) \right] \cdot \left(\frac{MW_{ab}}{3 \cdot MW_{or}} \right) \tag{B10}$$

In the mesonorm:

$$WF_{Qz} = WF_{qz} + \frac{WF_{hy} \cdot MW_{qz}}{MW_{hy}} - \frac{WF_{co} \cdot MW_{qz}}{MW_{co}} \tag{B11}$$

Proportions of mesonormative felsic phases listed in Appendix E were calculated using these equations.

Appendix C

THE METHOD USED TO ESTIMATE THE SAMPLE SIZE OF PORPHYRY MATRIX SEPARATES

The sample sizes of porphyry matrixes were determined using a relationship which was derived assuming that the square of the sampling error (SE) is proportional to the reciprocal of the number of grains (n), i.e.

$$\text{that } (SE)^2 \propto 1/n$$
$$\text{or } SE \propto n^{-1/2} \quad (1)$$

The number of grains can be independently estimated for a given mass using the mass-volume relationship, if the mean grain density and shape are known. By assuming that the grains are cubic, then the number of grains in a sample of mass (n) is

$$n = \frac{m}{a^3 \rho} \quad (2)$$

where a = average grain diameter and ρ is the mean grain density. Average grainsizes were measured using a binocular microscope. Most matrixes were separated in quantities sufficient for (n) to be ~250,000 for an assumed mean grain density of 2.7 gcm^{-3}. Sampling errors for matrix separates are therefore thought to be within a factor of 2 of each other, as indicated below.

Table C1

Sample Number	Mass of matrix separated (g)	Mean grainsize (mm)	Standard error (SE) relative to SE for 250,000 grains
62589	6	0.2	1.0
62593	30	0.25	0.6
62602i	20	0.25	0.7
62602o	18	0.25	0.8
62610	6	0.15	0.6
62594	8.5	0.25	1.1
62596	104	0.7	1.5
67537	8.9	0.25	1.1
62595	81	0.8	2.1
62605	81	0.4	0.7
62606	52	0.4	0.9
62616c	97	0.6	1.2
62616v	20	0.3	1.0
62618	49	0.4	0.9
62619	14.5	0.3	1.1
62627	35	0.5	1.6
62579bp	4.8	0.25	1.5
62579f	29	0.25	0.6
62579c	62	0.5	1.17
62612	154	0.45	0.6
67530	3.5	<0.01	~0
67530bl	4.5	<0.01	~0
67533	33	<0.01	~0

Appendix D

CHEMICAL ANALYTICAL METHODS

1. X-RAY FLUORESCENCE SPECTROMETRY (XRFS)

Whole rocks and separates of porphyry matrixes and phenocryst phases were analysed for major and selected trace elements by XRFS. Sample powders used were prepared in different ways for different sample types. Whole rock samples were trimmed of weathered portions, split (using hydraulic hardened steel apparatus) then crushed to <5 mm diameter fragments using a Sturtevant roll jaw crusher. The crushed sample was then quartered and a 250 g split taken.

Any abraded jaw-mill steel fragments were removed from the split using a hand magnet. This procedure was necessary because jaw-mill steel could contaminate felsic granitic rocks in Fe, Mn, Cr, V and Ni. (The procedure was validated because magnetite is absent from these rocks. Had it been present, it would have also been removed, thereby depleting the sample in trace elements such as V and Sc.) Steel fragments collected by this procedure were uncommon.

The 250 g split was then ground for 3 minutes in a tungsten carbide Siebtechnik swing mill, and bottled.

Matrix separate samples (cf. Chapter 5) which exceeded 35 g in weight were also crushed in the tungsten swing mill (for times proportional to their weights). Matrix separates of less than 35 g were crushed in a "Spex" tungsten carbide ball mill for times proportional to their weights (5-25 minutes). This procedure however, contaminated these powders in Nb.

Mineral samples, with or without "Spex" silica dilutant (cf. Appendix F) were each hand ground in an agate mortar under acetone for ~45 minutes, dried and bottled.

Major Element Analyses

Major element concentrations were determined by X-ray fluorescence spectroscopy (XRFS) on duplicate glass discs using an automated Phillips PW1410 spectrometer. Glass preparation and XRF analyses were undertaken using the method of Norrish & Hutton (1969). Spectrometric analytical conditions are given in Table D1. H_2O^- is the percentage loss in weight after heating ~0.8 g of sample for 4 hours at 110 C. H_2O^+ is the percentage change in weight of the same oven-dried sample after heating in air for 2 hours in a muffle furnace at ~1000°C. Loss on ignition (LOI) is the sum of H_2O^+ and H_2O^-. A composite internal granite standard: TASGRAN was used. Typical precision for major element compositions determined by XRFS are indicated for TASGRAN in Table D2.

Table D1

Analytical Conditions for X-ray Fluorescence Spectrometry

Chemical Component	Analytical Line	Elements corrected for	X-ray Tube	Analysing Crystal	Collimator	Detector	Counting Time (sec)
SiO_2	K_α	-	Rh	PE	c	F	100
TiO_2	K_α	-	Rh	LiF(200)	c	F	20
Al_2O_3	K_α	-	Rh	PE	c	F	100
Fe_2O_3	K_α	-	Rh	LiF(200)	f	F	20
MnO	K_α	-	Rh	LiF(200)	f	F	40
MgO	K_α	-	Rh	TIAP	c	F	100
CaO	K_α	-	Rh	LiF(200)	f	F	20
Na_2O	K_α	-	Rh	TIAP	c	F	2x100
K_2O	K_α	-	Rh	PE	c	F	20
P_2O_5	K_α	-	Rh	GE	C	f	40
Ba	$K_{\alpha 1}$	Ti	Cr	LiF(200)	f	F	100,100,100
Rb	K_α	-	Rh	LiF(200)	f	S	40,100,40
Sr	K_α	-	Rh	LiF(220)	f	S	40,100,40
Zr	K_α	Sr	Rh	LiF(220)	f	S	40,100,40
Nb	K_α	Y,U,Th	Rh	LiF(220)	f	S	100,100,100
Y	K_α	Rb	Rh	LiF(220)	f	S	40,100,40
Sc	K_α	Ca	Cr	LiF(200)	c	F	100,100,100
V	K_α	Ti	Au	LiF(220)	f	F	100,100,100
Mn	K_α	Cr	Au	LiF(200)	f	F	20,40,20
Ga	K_α	-	Mo	LiF(200)	f	F+S	20,40,20
Sn	K_α	-	Au	LiF(200)	f	S	2x200,200, 100

f = fine, c = coarse, F = flow counter, S = scintillation counter

Table D2

Typical Precision (2σ) for Major Element Analysis of Internal Granite Standard: TASGRAN

Oxide	SiO_2	TiO_2	Al_2O_3	Fe_2O_3*	MnO	MgO	CaO	Na_2O	K_2O	P_2O_5
%	72.60	0.29	13.65	2.29	0.035	0.59	1.87	2.82	4.61	0.12
2σ	0.17	0.01	0.08	0.03	0.003	0.04	0.02	0.10	0.04	0.02

Trace Element Analysis

Single to multiple analyses of 6 g pressed powder pellets were made using the XRFS methods of Norrish & Chappell (1977). Element concentrations were determined using mass absorptions for samples which were calculated from the major element analyses.

Pellets of the silica-diluted minerals and the most felsic rocks were structurally stabilized by adding a few drops of a dilute PVA solution binder obtained from Dr Norrish, University of Adelaide. Analytical conditions are given in Table D1. Standards used were G2, BHVO-1, ZGIGM, GH, T1 and TASGRAN. Detection limits for single determinations are listed in Table D3. For multiple determinations of the concentration of a trace element, the detection limit was assumed to have been lowered by an amount proportional to the reciprocal of the square root of the number of determinations.

Table D3

Detection Limits (2σ) for Trace Elements Determined by X-ray Fluorescence Spectroscopy

Element	Ba	Ga	Mn	Nb	Rb	Sc	Sr	Sn	V	Y	Zr
2σ (ppm)	2.3	0.7	1.1	0.6	0.9	0.5	1.1	0.7	1.7	1.1	0.7

Detection limits (2σ) for mineral phases which were diluted by "Spex" SiO_2 are assumed to be:

$$D_e = \left[D.n^{-1/2}.(1-x)^{-1} \right] \text{ ppm}$$

where D is the detection limit (2σ) for element (e) as listed in Table D3, (n) is the number of determinations made and (x) is the proportion of "Spex" SiO_2 in the sample mixture. Quartz-diluted samples were analysed many times in order to counteract the increase in (D_e) caused by dilution.

For lead, $L_{\beta 1}^{Pb}$ was measured by XRFS on pressed powder pellets of matrix and selected mineral separates (Appendices E and F), using the Siemens - spectrometer at the Geology Department of the Australian National University, by Dr B.W. Chappell. Trace concentrations of magnesium were also measured by XRFS on pressed powder pellets of the feldspars (or {feldspar+quartz} mixtures) using an end-windowed rhodium X-ray tube operating at 30 kV and 64 mA, a fine collimator, a TLAP crystal from 44.55 to 45.15° (2σ). X-rays were detected using an Ar/CH4 gas flow counter. An assymetric pulse height analyser window was used in order to reduce the contribution from the adjacent Ca-escape peak. G2 was used as the standard and a "Herasil" glass disc as the blank. A linear calibration was assumed.

2. ATOMIC ABSORPTION SPECTROPHOTOMETRY (AAS)

Powders of whole rocks and porphyry matrix separates which by XRFS indicated MgO contents of ≤1% MgO, were re-analysed by AAS because of the greater precision of this method for magnesium. Determinations were made on duplicate solutions containing less than 10 ppm of dissolved Mg. Samples were dissolved using HF and $HClO_4$ and an Al-, Fe-, Ca- and Sr-containing radiation-buffering solution was added in order to minimize element interference effects. Distilled water was used throughout. Absorption current measurement was made using a Varian-AA6 spectrophotometer. The absorption wavelength was 285.2 nm, the lamp current: 4 mA and the detection slit width: 0.17 nm. An air-C_2H_2 flame was used with a crossed burner.

MgO concentrations were obtained from absorption current measurements by calibration using radiation-buffered standard solutions of magnesium chloride made from calcined Analar-grade MgO and distilled hydrochloric acid. The MgO concentrations are those quoted to three decimal places in Appendix E.

Precision at the 2σ level derived from the duplicate analytical data is estimated to be:

$$2\sigma_{MgO}^{AAS} = \left[(0.125 \exp\{-2.36.(\text{apparent \% MgO})\}.(\text{apparent \% MgO}) \right] \%$$

3. ENERGY DISPERSIVE MICROPROBE ANALYSIS

All major element analyses tabulated in Appendix H were obtained using the JEOL JXA-50A microprobe in the Central Science Laboratory of the University of Tasmania. Specimens were prepared by carbon coating polished thin sections. Analytical conditions consisted of a 15 kV accelerating voltage, a beam current of 1 nA, an excited sample volume diameter of ~1 μm, a counting period of 60 seconds (real time) with an average count-rate of ~5000 cps. Up to 13 elements can be determined simultaneously. The programs utilized for data reduction are those of Ware (1981), modified by Dr R. Berry (Geology Department, University of Tasmania). For single analyses, the precision of each component concentration determined, is estimated to be ±3% relative error (2σ) with absolute minimum errors at the 2σ level being ±0.3% for Na_2O and ±0.2% for other oxides (including Cl_2O_{-1}).

The standards used were:

(a) San Carlos olivine for Mg, Fe and Si
(b) omphacite (USNM110607) for Na
(c) ilmenite (USNM96189) for Ti
(d) Durango apatite for P
(e) Lake County plagioclase for Al
(f) pure metal samples for Cr, Mn and Ni
(g) pure NaCl for Cl
(h) wollastonite for Ca, and
(i) sanidine for K.

Appendix E

Chemical and Normative Compositions of Whole Rocks and Porphyry Matrix Separates from Furneaux Islands, northern Blue Tier Batholith

Suite	WYBALENNA							WYBALENNA						
Rock	Granite							Porphyry						
#	62577	62607	62608	62628	62631	62633	62635	62589	62590	62593	62602	62609	62610	62629
SiO_2	68.52	70.62	71.30	69.25	68.93	68.94	70.56	64.29	66.68	63.55	62.75	66.36	62.44	59.19
TiO_2	0.55	0.45	0.37	0.43	0.50	0.52	0.40	0.77	0.71	0.61	1.19	0.76	0.84	0.46
Al_2O_3	14.56	14.42	14.43	14.44	14.41	14.42	14.42	16.15	15.85	16.92	16.16	15.44	16.80	14.28
FeO*	4.87	3.36	2.97	4.03	4.41	4.50	3.04	5.50	4.81	5.31	6.22	5.52	5.50	8.16
MnO	0.11	0.07	0.07	0.09	0.10	0.10	0.08	0.12	0.11	0.12	0.12	0.12	0.14	0.28
MgO	2.04	1.35	1.14	1.88	1.91	1.85	1.52	3.25	1.85	2.16	3.06	2.19	2.88	5.37
CaO	4.5	3.01	2.77	4.21	4.37	4.37	3.01	4.80	4.15	5.41	5.27	4.33	5.79	8.13
Na_2O	1.88	2.58	2.68	2.47	2.22	2.16	2.67	2.26	3.05	3.16	2.53	2.62	3.07	2.84
K_2O	2.63	3.86	4.02	3.00	2.93	2.93	4.02	2.54	2.46	2.27	2.23	2.39	2.21	1.11
P_2O_5	0.10	0.13	0.10	0.08	0.09	0.09	0.13	0.16	0.19	0.33	0.30	0.15	0.18	0.06
H_2O-	0.21	0.14	0.14	0.19	0.17	0.14	0.14	0.21	0.17	0.19	0.19	0.28	0.25	0.22
LOI	1.39	0.57	0.48	0.67	0.92	0.62	0.72	1.21	0.73	0.71	1.27	0.83	0.68	1.03
Σ	100.26	99.65	99.93	100.35	99.91	99.81	100.07	99.78	99.82	100.13	100.04	99.81	100.13	99.75
Ba	438	565	490	365	420	413	491	357	296	279	357	175	377	78
Rb	114	169	188	138	136	132	229	200	181	171	191	217	154	67
Sr	156	173	151	162	149	145	189	204	144	323	266	157	249	162
Zr	153	144	135	117	149	140	139	168	179	225	201	170	154	91
Nb	8.6	10.1	9.6	6.6	8.6	7.6	11.1	9.7	12.2	14.7	14.8	12.7	10.6	5.6
Y	28	27	37	24	30	26	42	35	42	34	33	25	33	47
Sc	21.4	13.2	12.6	17.1	18.3	20.3	12.6	19.9	16.2	17.2	18.9	21.4	20.3	33.3
V	97	60	56	83	86	87	61	130	105	106	117	31	124	210
Mn	810	552	565	678	740	733	589	918	847	889	906	888	1087	2136
Ga	16.1	16.0	15.7	15.3	15.8	16.0	16.0	16.3	18.3	19.2	19.6	19.5	18.2	15.8
Sn	3.1	3.0	3.0	3.0	1.0	3.0	5.0	<0.7	6.1	3.0	3.6	3.1	2.5	4.6
Pb														
mg'	42.1	41.1	40.1	44.8	43.0	41.8	46.4	50.7	40.1	41.4	46.2	40.9	47.6	53.1
al	4.0	9.1	10.7	-3.1	-1.3	-0.2	6.0	7.7	8.5	1.7	4.0	7.2	-5.0	-32.2
qz	31.55	30.99	31.34	31.35	31.46	31.37	29.86	24.80	26.10	20.05	22.19	27.30	20.98	
co	0.45	0.77	0.81				0.47	1.30	1.05	0.17	0.65	1.02		
or	15.51	22.81	23.73	17.70	17.34	17.30	23.75	15.03	14.51	13.40	13.20	14.14	13.05	
ab	15.93	21.86	27.70	20.91	18.82	18.26	22.56	19.10	25.84	26.71	21.40	22.14	25.96	
an	22.29	14.23	13.25	19.47	20.66	21.01	14.23	22.88	19.43	24.84	24.38	20.55	25.54	
hy	10.21	7.07	6.23	8.25	9.59	9.42	7.03	13.29	9.72	11.20	13.25	13.30	10.70	
di				0.83	0.45	0.16							1.80	
il	1.04	0.85	0.71	0.82	0.95	0.98	0.77	1.45	1.35	1.15	2.27	1.45	1.60	
ap	0.24	0.31	0.23	0.19	0.21	0.21	0.30	0.38	0.45	0.78	0.69	0.36		
mt	1.57	1.08	0.96	1.30	1.42	1.45	0.98	1.77	1.55	1.71	2.00	1.78	1.77	
Qz	36.6	34.3	34.2	35.6	36.4	36.2	33.3	31.3	30.7	25.7	28.8	33.7	26.5	
Af	9.8	22.7	24.8	14.6	12.8	13.0	23.8	5.6	9.0	6.0	3.4	4.8	5.9	
Pl	35.9	30.7	30.0	36.9	36.4	36.2	31.1	40.6	43.1	50.1	45.0	41.5	50.1	

Suite	WYBALENNA		WYBALENNA					GARDENS	POIMENA					
Rock	Porphyry		Porphyry matrix					Granite	Granite					
#	62630	62636	62589	62593	62602i	62602o	62610	62576	62581	62582	62591	62592	62599	62600
SiO_2	61.20	60.81	65.41	63.30	62.60	62.53	60.99	68.35	71.90	69.29	72.46	73.83	71.32	70.97
TiO_2	0.49	0.61	0.81	0.62	1.26	1.27	0.95	0.49	0.49	0.79	0.41	0.29	0.60	0.61
Al_2O_3	14.93	16.24	15.66	16.89	16.22	16.18	16.93	14.53	14.11	14.72	14.19	13.99	14.08	14.18
FeO*	7.35	7.25	5.39	5.45	6.32	6.33	6.24	3.99	2.78	3.80	2.44	1.73	3.24	3.34
MnO	0.23	0.16	0.11	0.11	0.12	0.12	0.16	0.09	0.06	0.07	0.07	0.04	0.10	0.07
MgO	4.25	3.41	3.20	2.22	3.00	3.06	3.08	2.39	0.836	1.173	0.664	0.466	0.955	0.977
CaO	7.17	6.89	4.31	5.45	5.41	5.43	5.87	3.85	2.28	2.83	1.68	1.70	2.41	2.40
Na_2O	2.39	2.19	2.16	3.05	2.24	2.28	2.94	2.34	2.77	2.98	2.93	3.06	2.87	3.05
K_2O	1.81	2.23	2.61	2.40	2.35	2.33	2.40	3.60	4.41	3.93	4.84	4.64	4.05	4.02
P_2O_5	0.07	0.08	0.17	0.36	0.31	0.30	0.29	0.18	0.21	0.26	0.18	0.12	0.22	0.23
H_2O-	0.20	0.18	0.28	0.21	0.22	0.20	0.10	0.16	0.13	0.12	0.16	0.14	0.15	0.17
LOI	1.10	1.19	1.35	0.81	2.08	1.09	0.68	0.69	0.59	0.53	0.56	0.62	0.54	0.64
Σ	99.94	100.12	99.67	99.98	100.37	99.93	100.08	100.23	100.07	99.80	100.03	100.06	99.66	99.59
Ba	169	300	381	284	424	375	381	619	510	372	363	480	453	461
Rb	113	114	196	174	187	196	164	185	211	242	288	235	219	222
Sr	172	165	192	321	265	268	229	270	162	162	111	121	151	149
Zr	68	109	183	241	210	198	171	157	167	202	139	105	204	199
Nb	8.2	4.6		15.7				11.6	12.6	9.7	15.1	9.6	14.7	14.2
Y	59	26	25	39	36	36	40	32	29	37	45	28	36	29
Sc	40.3	30.1	17.4	17.3	19.5	20.4	23.8	16.6	8.1	10.1	6.6	5.5	9.1	8.6
V	191	174	126	97	124	122	138	87	38	47	35	18	41	41
Mn	1747	1221	875	856	935	913	1243	698	444	517	512	299	470	511
Ga	16.7	17.5	16.9	19.3	17.4	18.3	16.2	16.3	17.5	19.6	17.9	16.3	18.2	18.9
Sn	6.1	6.6	1.0	4.6	2.3	3.3	3.0	6.6	7.1	6.6	14.1	9.6	9.6	9.1
Pb			12.1	15.5	14.8	9.0	15.5							
mg'	50.8	45.0	50.9	41.6	45.4	45.8	46.2	51.1	34.4	35.1	32.1	31.9	33.8	33.8
al	-21.5	-12.4	10.5	1.7	5.1	4.2	-2.9	1.7	15.6	10.8	22.3	23.3	13.6	12.0
qz			27.45	19.79	23.07	22.64	18.00		31.81	27.92	31.34	33.13	31.38	30.08
co			1.80	0.17	0.83	0.68			1.08	0.98	1.46	1.07	1.07	0.95
or			15.44	14.15	13.87	13.79	14.18		26.04	23.25	28.59	27.40	23.92	23.75
ab			18.29	25.77	18.91	19.32	24.84		23.46	25.25	24.82	25.93	24.32	25.84
an			20.40	24.88	25.01	25.18	25.92		10.08	12.46	7.28	7.79	10.62	10.54
hy			12.95	11.49	13.19	13.28	12.58		5.15	6.79	4.47	3.23	5.94	6.04
di							1.20							
il			1.54	1.18	2.39	2.42	1.81		0.94	1.50	0.78	0.55	1.13	1.16
ap			0.40	0.83	0.72	0.69	0.68		0.49	0.61	0.42	0.28	0.52	0.54
mt			1.74	1.76	2.04	2.04	2.01		0.90	1.23	0.79	0.56	1.04	1.08
Qz			33.6	25.6	29.6	29.3	24.5		34.0	31.0	33.0	34.3	34.0	32.8
Af			6.5	6.7	4.4	4.1	5.4		29.0	23.6	33.0	32.7	25.4	25.1
Pl			37.1	49.0	42.9	43.5	49.5		26.6	32.1	24.2	25.9	28.9	30.4

Suite	POIMENA			POIMENA						POIMENA				
Rock	Granite			Porphyry						Porphyry matrix				
#	62611	62639	43083	62594	62596	62597	62598	62612	67532	62594	62596	62612	67533b	67533c
SiO_2	72.10	76.43	71.32	68.22	76.25	75.80	76.73	69.36	72.51	69.25	76.53	68.43	76,53	77.07
TiO_2	0.37	0.09	0.63	1.06	0.08	0.09	0.05	0.54	0.38	0.98	0.06	0.60	0.02	0.04
Al_2O_3	14.24	13.01	14.08	14.72	13.20	13.38	12.95	15.51	13.99	14.17	13.20	15.70	13.17	12.98
FeO*	2.65	1.13	3.35	5.15	1.05	1.09	0.90	3.75	2.64	4.91	0.78	4.28	0.87	0.90
MnO	0.07	0.04	0.06	0.09	0.04	0.06	0.04	0.07	0.04	0.09	0.03	0.09	0.02	0.03
MgO	1.020	0.137	1.071	1.90	0.124	0.124	0.049	1.045	0.484	1.79	0.085	1.166	0.047	0.037
CaO	2.28	0.55	2.41	3.39	0.75	0.81	0.68	3.49	1.71	3.31	0.60	3.65	0.60	0.60
Na_2O	2.67	3.59	2.84	2.97	3.56	3.66	3.71	3.30	3.32	2.98	3.58	3.18	3.59	3.51
K_2O	4.31	4.89	3.89	2.11	4.82	4.88	4.79	2.61	4.64	2.12	5.03	2.56	5.07	4.77
P_2O_5	0.14	0.03	0.21	0.25	0.03	0.02	0.01	0.16	0.14	0.27	0.02	0.19		
H_2O-	0.20	0.19	0.21	0.21	0.25	0.25	0.30	0.23	0.20	0.27	0.18	0.26	0.23	0.05
LOI	0.62	0.59	0.38	0.65	0.97	0.59	0.51	1.35	0.92	0.53	0.54	1.54	0.42	0.41
Σ	100.01	99.77	99.74	99.90	99.84	99.92	99.56	100.01	99.89	99.80	99.71	99.85	99.92	99.71
Ba	487	299	453	243	101	117	36	369	515	269	67	344	60	44
Rb	241	265	198	270	368	391	415	212	232	259	382	217	348	329
Sr	138	63	160	133	42	47	22	256	116	118	30	247	51	49
Zr	135	89	221	229	94	96	82	213	194	237	80	231	90	88
Nb	12.6	10.6	15.2	16.2	15.1	15.1	16.2	14.8	12.7		12.6	15.9	15.1	
Y	28	52	35	37	68	62	66	26	33	37	59	31	69	66
Sc	9.6	5.0	9.6	14.7	4.5	4.0	2.0	9.2	7.1	15.7	2.8	8.7	5.0	5.0
V	46	8	47	77	9	6	7	52	26	80	5	59	7	5
Mn	550	316	455	674	337	444	346	557	341	667	246	690	186	218
Ga	16.6	15.7	18.4	19.1	17.7	17.1	18.2	18.3	18.2	17.7	16.2	19.4	17.1	16.1
Sn	5.1	4.0	6.1	6.6	14.1	23.1	18.7	11.2	<0.7	5.1	11.4	12.9	7.6	7.6
Pb										14.1	37.2	6.1	36.2	32.1
mg'	40.1	17.2	35.9	39.2	16.8	16.2	8.4	32.8	24.4	38.9	15.8	32.2	8.6	6.7
al	17.5	30.7	15.0	14.1	31.3	25.1	26.1	13.9	12.8	12.2	38.1	14.2	33.1	40.8
qz	32.59	34.63	32.02	31.25	34.61	33.12	34.62	24.49	29.78	32.61	34.49	28.73	34.21	36.39
co	1.31	0.86	1.28	1.97	0.84	0.64	0.45	1.24	0.68	1.58	0.83	1.46	0.67	0.96
or	25.49	28.87	22.99	12.46	28.47	28.81	28.31	15.41	27.44	12.53	29.73	15.12	29.94	28.17
ab	22.57	30.41	24.03	25.14	30.08	30.96	31.37	27.92	28.05	25.23	30.26	26.93	30.34	29.68
an	10.55	2.59	10.69	15.23	3.54	3.95	3.32	16.42	7.71	14.70	2.85	17.00	3.03	2.98
hy	5.55	1.96	6.20	9.70	1.84	1.89	1.47	6.87	4.38	9.26	1.47	7.78	1.42	1.41
di														
il	0.71	0.17	1.19	2.00	0.15	0.17	0.10	1.03	0.71	1.87	0.12	1.15	0.04	0.08
ap	0.33	0.07	0.49	0.59	0.07	0.05	0.02	0.38	0.33	0.64	0.05	0.45	-	-
mt	0.85	0.36	1.08	1.66	0.34	0.35	0.29	1.21	0.85	1.58	0.25	1.38	0.28	0.29
Qz	34.9	35.2	34.7	35.5	35.2	33.8	35.1	32.5	31.7	36.7	34 8	32.1	34.6	36.7
Af	27.8	54.2	23.9	6.3	50.1	50.1	52.6	13.3	31.7	6.9	54.3	12.0	53.9	51.6
Pl	26.5	6.2	29.0	38.9	10.6	12.3	9.3	41.2	28.2	38.3	7.6	41.1	8.4	8.2

Suite	POIMENA	LADY BARRON				MUSSELROE				BOOBYALLA				
Rock	Porph.m.	Granite			Porphyry	Granite				Granite				
#	67537fr	62640	62641	62642	67545	62586	62587	62637	62638	62578	62583	62584	62585	62603
SiO_2	76.58	72.92	72.16	71.18	72.99	72.36	73.82	74.72	74.58	75.85	74.77	74.71	77.45	76.50
TiO_2	0.05	0.22	0.30	0.37	0.18	0.51	0.48	0.29	0.31	0.18	0.32	0.29	0.15	0.15
Al_2O_3	13.17	14.98	15.10	14.45	14.89	14.13	13.40	13.54	13.49	13.07	13.29	13.46	12.34	12.73
FeO*	0.24	1.55	1.95	2.15	1.49	3.05	3.02	1.97	2.06	1.65	2.47	2.16	1.50	1.74
MnO	0.01	0.04	0.04	0.04	0.04	0.05	0.06	0.04	0.04	0.02	0.04	0.03	0.03	0.04
MgO	0.046	0.592	0.716	0.814	0.478	0.702	0.842	0.438	0.453	0.189	0.315	0.278	0.148	0.200
CaO	0.37	1.63	1.88	2.39	1.06	1.81	1.54	1.39	1.48	0.93	1.17	1.33	0.56	0.78
Na_2O	3.48	3.58	3.58	3.40	2.71	2.70	2.37	2.79	2.78	2.61	2.64	2.65	2.42	2.91
K_2O	5.96	4.16	3.94	3.86	5.85	4.28	4.12	4.51	4.50	5.24	4.71	4.81	5.21	4.75
P_2O_5		0.20	0.22	0.22	0.18	0.24	0.20	0.17	0.17	0.15	0.13	0.14	0.10	0.09
H_2O-	0.14	0.17	0.15	0.16	0.18	0.20	0.18	0.19	0.20	0.13	0.19	0.21	0.17	0.16
LOI	0.31	0.85	0.80	0.85	0.76	0.54	0.56	0.60	0.65	0.58	0.43	0.49	0.52	0.68
Σ	99.32	99.72	99.82	99.60	99.62	99.86	100.04	99.83	99.73	99.81	100.00	99.56	99.56	99.71
Ba	12	270	241	392	538	546	404	455	467	313	476	551	111	300
Rb	448	237	220	199	230	259	220	233	226	339	348	304	345	265
Sr	7	151	156	210	117	124	111	114	117	55	72	89	43	59
Zr	38	69	86	101	111	217	197	145	131	132	209	192	110	131
Nb		9.6	12.7	12.2	8.1	15.2	12.6	11.6	11.7	11.6	18.6	17.2	11.1	12.7
Y	21	15	16	17	45	34	33	21	20	23	44	52	44	45
Sc	2.0	5.1	6.1	6.6	5.1	8.1	7.6	5.1	5.1	2.9	4.5	6.1	3.5	4.1
V	5	24.4	28.4	31.4	17.2	31.3	38.3	19.2	19.2	10	9	13	9	9
Mn	82	320	337	290	313	395	498	311	275	165	289	263	242	299
Ga	14.1	17.3	18.0	18.7	13.1	19.2	17.2	17.4	17.7	20.2	19.6	22.3	19.2	19.2
Sn	19.7	10.7	8.6	5.6	3.0	4.0	3.0	9.1	7.1	8.1	9.1	6.6	10.1	5.6
Pb	48.7													
mg'	24.5	39.8	39.7	39.8	35.8	28.7	32.8	27.9	27.8	16.8	18.3	18.4	14.7	16.7
al	42.8	35.8	30.9	26.5	43.6	27.5	29.5	32.8	30.0	38.7	31.9	32.5	43.3	34.6
qz	32.53	31.33	30.65	29.69	31.32	34.22	38.57	36.76	36.48	37.62	37.17	36.62	41.23	38.44
co	0.35	2.06	2.04	1.81	2.55	2.29	2.68	1.90	1.71	1.75	2.00	1.78	1.93	1.58
or	35.23	24.60	23.30	22.81	34.58	25.33	24.32	26.67	26.62	30.97	27.81	28.38	30.80	28.07
ap	29.45	30.32	30.28	28.90	22.91	22.84	20.06	23.63	23.52	22.04	22.33	22.38	20.47	24.60
an	1.72	6.88	7.94	10.53	4.22	7.54	6.46	5.88	6.36	3.70	5.06	5.80	2.14	3.35
hy	0.50	3.37	4.04	4.41	3.10	5.22	5.52	3.49	3.60	2.62	3.85	3.38	2.38	2.85
di														
il	0.09	0.42	0.58	0.70	0.35	0.96	0.92	0.56	0.60	0.35	0.61	0.56	0.29	0.29
ap	0.04	0.47	0.52	0.52	0.42	0.56	0.47	0.40	0.40	0.35	0.30	0.33	0.23	0.21
mt	0.08	0.50	0.63	0.69	0.48	0.98	0.97	0.64	0.66	0.53	0.80	0.70	0.48	0.56
Qz	32.6	32.3	31.9	31.3	31.8	35.9	40.3	37.8	37.6	38.2	38.3	37.6	41.6	39.2
Af	62.9	33.8	28.3	25.4	43.6	28.1	26.4	31.6	31.4	41.2	33.0	34.0	44.8	42.9
Pl	3.1	25.3	30.0	33.4	15.9	23.7	20.2	22.0	22.4	13.5	19.3	20.1	6.8	11.1

Suite	BOOBYALLA									BOOBYALLA				
Rock	Granite									Porphyry				
#	62604	62621	62622	62623	62625	67535	67536	67547	67548	62595	62605	62606	62613	62618
SiO_2	75.02	76.03	74.37	76.67	76.09	76.27	75.43	77.28	75.74	75.53	76.44	78.08	80.21	77.20
TiO_2	0.15	0.08	0.08	0.07	0.10	0.09	0.09	0.10	0.21	0.23	0.05	0.08	0.12	0.13
Al_2O_3	13.57	13.60	14.56	13.22	13.53	13.27	13.85	12.49	13.06	12.76	13.13	12.19	10.82	12.32
FeO*	1.59	1.28	1.12	1.33	1.41	1.40	1.24	1.19	1.70	2.28	1.02	1.26	1.33	1.77
MnO	0.03	0.03	0.02	0.02	0.04	0.02	0.03	0.02	0.03	0.03	0.02	0.02	0.02	0.03
MgO	0.192	0.102	0.098	0.110	0.116	0.084	0.134	0.155	0.224	0.229	0.076	0.096	0.130	0.150
CaO	0.85	0.51	0.71	0.65	0.59	0.52	0.59	0.63	1.22	0.90	0.49	0.53	0.49	0.45
Na_2O	3.20	2.98	2.90	2.87	3.20	3.14	2.57	2.59	2.38	2.43	3.08	2.72	1.88	2.13
K_2O	5.17	5.14	5.86	4.78	4.66	4.98	5.84	5.37	5.16	5.37	5.54	4.89	4.81	5.59
P_2O_5	0.08	0.17	0.17	0.18	0.16	0.13	0.19	0.10	0.15	0.10	0.08	0.07	0.12	0.15
H_2O-	0.16	0.22	0.20	0.19	0.19	0.14	0.14	0.11	0.11	0.26	0.26	0.23	0.21	0.20
LOI	0.73	0.68	0.61	0.83	0.76	0.54	0.74	0.39	0.41	0.65	0.45	0.40	0.45	0.58
Σ	99.92	99.90	100.04	99.94	99.67	99.69	99.58	100.00	99.58	99.58	100.00	99.50	99.64	99.98
Ba	471	51	298	57	67	81	107	125	372	339	50	71	30	37
Rb	270	469	445	493	522	471	361	327	300	294	276	256	319	383
Sr	76	18	46	22	33	18	28	36	68	70	25	28	19	17
Zr	131	65	66	79	77	72	61	81	138	193	73	96	100	90
Nb	12.6	12.1	9.1	12.6	16.2	14.6	9.6	7.0	11.5	12.7	8.6	9.6	11.6	12.1
Y	42	26	19	19	28	22	15	23	20	86	38	44	23	26
Sc	3.0	2.0	1.5	2.0	3.0	2.5	3.5	2.5	3.0	4.1	3.0	3.5	2.0	2.3
V	9	7	8	7	7	5	7	7	12	11	6	7	7	6
Mn	267	199	175	162	340	172	223	163	204	267	138	162	167	209
Ga	19.4	21.2	20.2	21.2	24.1	25.1	20.3	18.1	19.8	20.3	17.3	16.2	15.2	18.2
Sn	5.1	14.1	12.6	25.8	23.3	7.1	13.2	6.0	3.5	6.6	6.5	6.6	8.6	7.6
Pb														
mg'	17.4	12.2	13.3	12.7	12.5	9.5	15.9	17.6	18.8	15.0	11.6	11.8	14.7	13.0
al	32.7	55.6	58.0	54.1	51.8	48.2	56.3	41.9	36.0	28.7	44.9	44.2	46.3	44.1
qz	33.53	37.36	33.03	39.62	37.59	37.04	36.38	39.45	38.40	37.81	35.57	41.52	49.02	41.39
co	1.31	2.64	2.55	2.57	2.53	2.07	2.74	1.49	1.66	1.52	1.35	1.62	1.93	2.30
or	30.58	30.28	34.60	28.27	27.55	29.44	34.51	31.73	30.51	31.72	32.75	28.89	28.40	33.01
ab	27.10	25.22	24.56	24.31	27.09	26.59	21.70	21.95	20.17	20.52	26.09	28.04	15.92	18.03
an	3.80	1.40	2.46	2.04	1.88	1.72	1.54	2.52	5.17	3.91	1.94	2.17	1.63	1.28
hy	2.61	2.06	1.82	2.15	2.28	2.16	2.08	2.01	2.73	3.54	1.66	2.00	2.13	2.78
di														
il	0.29	0.15	0.15	0.13	0.19	0.17	0.17	0.19	0.40	0.44	0.09	0.15	0.23	0.25
ap	0.19	0.40	0.40	0.42	0.38	0.30	0.45	0.23	0.35	0.23	0.19	0.17	0.28	0.35
mt	0.51	0.41	0.36	0.43	0.45	0.45	0.40	0.38	0.55	0.74	0.33	0.40	0.43	0.57
Qz	34.3	37.3	32.9	39.7	37.7	37.3	36.4	39.9	39.1	38.9	35.8	41.9	49.3	41.8
Af	46.9	53.1	52.7	47.8	51.1	52.9	52.1	46.4	37.4	38.7	54.9	46.4	38.9	46.6
Pl	12.7	2.3	7.6	5.2	3.7	3.3	4.1	8.3	16.4	14.9	4.7	6.2	5.5	3.7

Suite	BOOBYALLA			BOOBYALLA									
Rock	Porphyry			Porphyry matrix									
#	62619	62620	62627	62595	62605	62606	62616c	62616v	62617	62618	62619	62624	62627
SiO_2	74.83	76.20	75.99	74.42	76.18	76.24	75.44	75.56	75.54	75.94	75.62	74.23	75.30
TiO_2	0.28	0.19	0.10	0.17	0.05	0.07	0.08	0.03	0.15	0.10	0.07	0.10	0.04
Al_2O_3	13.18	12.89	13.55	13.41	13.26	13.03	13.52	12.52	12.84	13.05	13.20	15.23	13.62
FeO*	2.61	1.76	1.50	1.91	0.84	1.12	1.34	0.97	2.13	1.57	1.10	0.76	1.32
MnO	0.03	0.03	0.03	0.02	0.01	0.02	0.02	0.02	0.02	0.02	0.01	0.05	0.02
MgO	0.242	0.175	0.113	0.194	0.065	0.089	0.130	0.095	0.189	0.139	0.111	0.012	0.088
CaO	0.97	1.02	0.60	0.60	0.51	0.53	0.53	0.59	0.47	0.39	0.40	0.34	0.54
Na_2O	2.64	2.31	2.89	2.54	3.06	3.15	2.80	3.39	2.40	2.57	2.70	4.87	3.30
K_2O	4.95	5.14	4.96	6.52	5.89	5.61	5.93	5.66	6.03	6.01	6.58	4.00	5.53
P_2O_5	0.17	0.17	0.16	0.09	0.08	0.07	0.14	0.12	0.14	0.13	0.13	0.36	0.14
H_2O-	0.20	0.22	0.18	0.17	0.15	0.21	0.15	0.20	0.19	0.23	0.24	0.09	0.21
LOI	0.55	0.47	0.97	0.60	0.46	0.50	0.52	0.53	0.73	0.58	0.60	0.44	0.83
Σ	99.83	99.65	99.78	99.72	99.65	99.81	99.77	99.81	100.16	100.17	99.73	99.84	99.83
Ba	45	338	106	266	40	67	16	17	30	22	38	6	60
Rb	413	325	519	321	276	271	328	309	388	402	433	1042	549
Sr	32	60	25	60	22	26	16	18	16	14	20	9	21
Zr	157	145	95	154	66	74	48	41	105	78	48	21	73
Nb	18.2	13.7	13.2	10.1	7.6	9.6			15.6	9.6		23.7	11.1
Y	28	25	26	88	36	43	24	29	48	30	17	8	25
Sc	2.8	3.0	2.0	4.1	2.2	3.0	1.8	1.2	3.5	2.1	1.4	1.5	1.1
V	13	10	8	9	5	6	5	5	6	6	7	6	5
Mn	242	191	202	179	74	128	176	135	269	162	82	412	160
Ga	22.2	18.2	20.3	18.7	16.2	16.2	19.2	19.2	19.2	20.1	17.2	34.2	20.3
Sn	9.6	7.1	26.4	6.4	7.6	6.1	8.1	7.1	6.6	8.6	7.8	67.4	26.3
Pb				38.5			29.0	26.9	29.8	29.1	30.5		23.2
mg'	14.0	14.9	11.7	15.2	12.0	12.2	14.7	14.8	13.5	13.5	15.1	2.6	10.5
al	32.8	41.3	52.6	28.8	45.2	35.0	39.2	40.0	34.2	42.2	39.9	72.7	42.6
qz	38.86	39.93	38.08	32.02	34.23	34.52	34.56	32.41	36.12	36.15	33.27	30.70	33.05
co	2.12	2.06	2.72	1.28	1.12	0.98	1.88	1.06	1.83	1.90	1.23	3.13	1.56
or	29.22	30.36	29.32	38.55	34.80	33.17	35.03	33.42	35.61	35.54	38.86	23.61	32.67
ab	22.33	19.50	24.46	21.48	25.89	26.65	23.68	28.63	20.33	21.74	22.86	41.22	27.93
an	3.71	4.03	1.96	2.44	1.99	2.16	1.69	2.13	1.44	1.10	1.11	-0.66	1.76
hy	3.94	2.73	2.36	3.75	1.37	1.81	2.22	1.68	3.34	2.52	1.83	1.22	2.13
di													
il	0.54	0.36	0.19	0.33	0.09	0.13	0.15	0.06	0.29	0.19	0.13	0.02	0.08
ap	0.40	0.40	0.38	0.21	0.19	0.17	0.33	0.28	0.33	0.30	0.31	0.84	0.33
mt	0.84	0.57	0.48	0.62	0.27	0.36	0.43	0.31	0.69	0.51	0.36	0.24	0.42
Qz	37.9	40.5	38.2	33.3	34.5	35.0	34.9	32.8	37.0	36.6	33.7		33.5
Af	39.1	37.3	49.2	51.2	56.5	55.1	54.4	58.0	50.9	54.4	59.3		57.4
Pl	13.3	14.6	4.8	8.5	5.2	5.6	4.3	5.0	4.0	2.2	2.2		3.4

Suite	BABEL ISLAND							MATHINNA BEDS			
Rock	Granite		Porphyry		Porphyry matrix			Pelite	Psammopelite		
#	62580	67543	62575	67544	62579c	62579f	62579bp	62541	62540	62542i	62542o
SiO_2	77.90	77.54	76.05	76.35	76.16	76.62	77.04	68.67	70.97	69.52	69.07
TiO_2	0.10	0.09	0.05	0.03	0.08	0.08	0.08	0.24	0.81	0.88	0.79
Al_2O_3	12.16	12.51	13.37	13.26	12.88	12.62	12.67	18.09	14.95	15.85	14.33
FeO*	1.24	1.37	1.03	1.41	1.34	1.31	0.85	4.02	5.11	5.22	5.48
MnO	0.02	0.03	0.02	0.02	0.03	0.02	0.02	0.14	0.08	0.09	0.07
MgO	0.074	0.065	0.044	0.041	0.060	0.058	0.039	2.59	2.47	2.62	2.65
CaO	0.49	0.41	0.43	0.34	0.34	0.40	0.42	0.48	0.48	0.48	0.45
Na_2O	3.00	2.99	3.67	3.31	3.17	3.35	3.00	1.28	1.26	1.11	1.54
K_2O	4.85	4.83	5.19	5.06	5.89	5.61	5.33	4.00	3.52	3.87	5.29
P_2O_5	0.06	0.09	0.06	0.10	0.05	0.05	0.05	0.32	0.17	0.19	0.14
H_2O-	0.16	0.20	0.26	0.18	0.20	0.25	0.06	0.24	0.25	0.59	0.22
LOI	0.63	0.49	0.72	0.51	0.54	0.58	0.44	2.98	1.35	2.56	1.29
Σ	100.02	99.54	99.52	99.54	99.79	99.65	99.61	99.79	99.52	99.72	99.59
Ba	288	182	150	8	16	14	14	297	517	472	479
Rb	270	299	360	341	331	323	291	253	270	257	440
Sr	26	17	14	5	7	7	7	46	70	68	66
Zr	95	48	75	43	50	64	54	657	229	295	236
Nb	15.6	17.2	18.3	18.7	21.2	20.8		7.3	17.4	25.0	24.6
Y	65	47	53	22	44	49	37	43.6	37.9	38.5	36.9
Sc	7.1	6.1	7.6	6.1	8.7	8.2	5.6	4.7	14.9	14.0	15.4
V	6	5	3	5	4	3	3	28	106	106	107
Mn	150	216	146	187	203	188	142	1084	614	707	541
Ga	20.8	21.7	21.3	23.9	21.2	20.3	17.2	19.7	18.5	18.7	18.4
Sn	8.6	5.6	8.6	6.1	9.1	8.6	8.1	5.2	5.1	10.9	10.8
Pb					26.1	24.1					
mg'	9.5	7.7	7.0	4.9	7.2	7.2	6.8	52.6	45.9	46.8	46.0
al	38.1	46.4	40.4	47.8	30.4	26.5	33.5	48.1	38.7	39.9	27.7
qz	39.94	39.97	33.23	36.14	33.96	34.97	35.62				
co	1.19	1.84	1.07	1.95	0.91	0.73	0.73				
or	28.66	28.54	30.65	29.91	34.81	33.15	31.50				
ab	25.42	25.27	31.09	28.02	26.16	26.82	28.36				
an	2.13	1.46	1.75	1.05	1.38	1.63	1.78				
hy	1.88	2.07	1.58	2.15	2.03	1.97	1.39				
di											
il	0.19	0.17	0.10	0.06	0.15	0.15	0.15				
ap	0.14	0.21	0.14	0.23	0.12	0.12	0.12				
mt	0.40	0.44	0.33	0.45	0.43	0.42	0.30				
Qz	40.4	40.2	33.6	36.4	34.6	35.6	36.0				
Af	49.4	51.4	59.9	57.5	58.6	57.1	57.3				
Pl	5.4	2.4	2.4	0	2.3	3.1	3.3				

Suite	WYBALENNA		POIMENA				POIMENA BASALT			
Rock	Mylonite	Inclusion rind	Bleached aplite	Tour. aplite	Hybrid porph.	Hybrid porph.mat.	Hybrid porph.	Hybrid porph.	Hybrid Felsic	Hybrid matrix Mafic
#	67534	62636	67537	67537	62601	62601	67530	67531	67530	67530
SiO_2	56.65	79.26	77.05	76.12	69.26	67.54	74.68	75.66	73.03	55.48
TiO_2	0.60	0.01	0.01	0.21	0.80	0.97	0.44	0.34	0.46	1.76
Al_2O_3	21.66	12.52	13.25	14.23	14.58	14.92	11.88	12.05	12.75	15.13
FeO*	4.46	0.12	0.05	3.35	4.38	5.22	3.45	2.88	3.57	10.11
MnO	0.11	0.01		0.09	0.08	0.09	0.10	0.05	0.07	0.24
MgO	1.73	0.067	0.011	0.476	1.36	1.58	0.455	0.234	0.547	3.84
CaO	4.78	2.95	0.78	0.41	3.26	3.36	1.88	1.63	1.72	6.91
Na_2O	4.76	3.26	4.41	2.75	3.84	3.86	2.68	2.61	2.64	3.81
K_2O	4.87	1.70	4.37	2.30	2.09	2.13	4.04	4.16	4.82	2.23
P_2O_5	0.17	0.03	0.02	0.01	0.23	0.23	0.08	0.07	0.06	0.32
H_2O-	0.32	0.15	0.21	0.18	0.21	0	0.19	0.17	0.09	0.24
LOI	1.54	0.50	0.25	0.83	0.55	0.44	0.51	0.57	0.52	0.66
Σ	100.09	99.46	99.49	97.97	100.39	99.94	100.06	99.62	100.22	100.06
Ba	741	267	20	29	167	117	1669	1800	1992	305
Rb	235	67	291	170	209	239	152	157	152	203
Sr	211	185	11	10	129	85	161	150	157	206
Zr	203	28	32	39	214	155	407	383	274	256
Nb	14.3	<0.6	4.0		20.7		20.6	21.2		
Y	50	9.1	22.2	21.7	39.3	39.4	66	68	70	55
Sc	19.4	1.0	<0.5	17.1	11.1	11.1	17.6	15.2	18.6	34.1
V	99	7	5	8	57	68	32	18	39	238
Mn	866	50	36	721	636	715	755	406	510	1831
Ga	23.5	11.1	15.1	29	19.1	22.2	15.1	17.2	16.1	24.4
Sn	5.6	<0.7	6.1	35.2	9.6	10.2	1.0	1.0	1.0	5.5
Pb			34.1	14.6		18.3				
mg'	40.3	47.9	28.0	19.8	35.2	34.6	18.6	12.4	21.1	39.8
al	2.5	6.7	~0.0	51.6	6.0	5.7	-2.1	8.9	3.1	-28.1
qz										
co										
or										
ab										
an										
hy										
di										
il										
ap										
mt										
Qz										
Af										
Pl										

Suite	MUSSELROE	MUSSELROE	BOOBYALLA	BOOBYALLA	BOOBYALLA & POIMENA		UNDIFF.	UNDIFF.	POIMENA
Rock	Garnet-rich seg.	Inclusion rind	Ga-rich seg.	Bi-rich seg.	Hybrid porphyry	Hybrid por.mat.	Granite	Porphyry	Metabasalt
#	67539	62588	62634	62615	62614	62614	62636	67546	67538
SiO_2	58.63	73.66	65.70	64.40	73.57	71.90	73.73	73.12	49.26
TiO_2	0.97	0.01	0.80	0.97	0.27	0.38	0.19	0.19	1.42
Al_2O_3	14.84	14.66	14.32	14.36	14.22	14.89	13.78	15.12	17.59
FeO*	17.36	0.14	9.81	11.05	2.23	3.16	1.44	1.02	9.20
MnO	0.73		0.21	0.10	0.04	0.06	0.04	0.03	0.23
MgO	2.27	0.04	0.88	1.05	0.47	0.67	0.64	0.42	8.47
CaO	1.15	0.24	1.80	0.50	1.75	2.06	1.72	0.75	11.07
Na_2O	0.79	2.16	2.14	1.17	3.23	3.97	2.32	2.99	2,22
K_2O	2.65	8.90	3.80	6.08	3.89	2.60	5.86	5.96	0.17
P_2O_5	0.35	0.05	0.32	0.20	0.19	0.20	0.09	0.26	0.25
H_2O-	0.28	0.18	0.19	0.17	0.21	0.28	0.20	0.13	0.31
LOI	-0.23	0.33	0.54	0.59	0.73	1.38	0.53	0.89	2.39
Σ	100.15	99.70	99.61	99.92	100.07	99.98	100.07	99.69	100.10
Ba	157	612	157	20	333	145	897	545	52
Rb	246	344	363	692	311	304	222	286	15
Sr	24	102	75	10	137	152	192	116	345
Zr	573	8	550	115	144	169	114	92	114
Nb	28.5	<0.6	43		14.6		4.5	10.6	4.7
Y	739	7.0	347	82.6	22	23	19	30	27
Sc	64	0.8	22.0	16.4	5.0	6.6	4.0	1.0	25.9
V	83	5	37	12	24	34	27	16	228
Mn	5659	24	1653	734	300	462	290	242	1764
Ga	22.4	11.1	30.6	42.8	20.2	23.4	11.9	16.2	16.6
Sn	3.6	7.0	7.7	10.7	10.1	13.8	0.7	6.6	<0.7
Pb									
mg'	18.3	32.0	13.6	14.4	27.0	26.9	43.6	41.4	61.6
al	23.1	79.8	20.3	22.7	30.9	26.8	16.0	54.1	-19.8
qz					34.53	32.07			
co					1.94	2.26			
or					22.98	15.35			
ab					27.35	33.63			
an					7.52	8.95			
hy					3.95	5.51			
di									
il					0.52	0.72			
ap					0.45	0.47			
mt					0.72	1.02			
Qz					35.7	33.9			
Af					26.3	20.7			
Pl					28.6	33.0			

Appendix F

MINERAL SEPARATE CHEMICAL COMPOSITIONS

Alkali Feldspar Cores

Sample	62595 af+q	62595 af	62596	62614	62622	62627	62634
SiO_2	87.28	66.81	66.14	65.61	65.97	65.46	66.07
TiO_2					0.01		
Al_2O_3	6.90	18.31	18.55	19.06	18.97	18.78	19.09
Fe_2O_3*	0.04	0.17	0.18	0.08	0.16	0.26	0.14
MnO							
MgO	0.02	0.036**	0.036**	0.018**	0.014**	0.016**	0.016**
CaO	0.13	0.34	0.28	0.37	0.32	0.49	0.55
Na_2O	0.97	2.59	2.46	2.91	3.52	3.32	3.08
K_2O	4.22	11.99	11.59	11.22	10.39	10.7	10.58
P_2O_5	0.02	0.06		0.13	0.1	0.11	0.07
LOI	0.31		0.31	0.33	0.39	0.5	0.37
Σ	99.89	99.51	99.55	99.73	99.84	99.68	99.97
% Spex SiO_2	62.22						
Ba	1270	3360	1170	1110	1960	1040	655
Rb	157	417	568	534	528	737	420
Sr	62.8	166	169	123	153	102	110
Pb	28	74	52	56	60	55	68
Zr	15.9	42	16.5	15	46	27	14
Nb	<0.4	<0.4	<0.4	<0.4	<0.4	<0.4	<0.7
Y	3	9	11	5	3	8	4
Sc	0.3	0.9	1.2	0.5	0.4	<0.2	0.7
V	2	6	3	4	3	3	4
Mn	4.3	11	44	20	<0.9	46	36
Ga	7.3	19.2	15.3	19	17.4	19.1	20.6
Sn	3.5	9.3	2.5	4.5	3.5	10.3	2.2

Biotite

Sample	62619 ph+q	62619 adj	62619 ps+q	62619 adj	62634 av s	62634 adj	67539 av s	67539 adj
SiO_2	75.11	34.0	74.15	34.0	39.79	34.1	35.98	34.5
TiO_2	1.22	3.3	1.42	3.7	2.33	2.7	2.73	2.8
Al_2O_3	7.44	20.2	7.56	19.9	17.47	20.0	18.95	19.7
Fe_2O_3	10.88	2.9	11.25	1.0	26.22	2.4	27.15	1.9
FeO		24.0		25.7		24.9		23.6
MnO	0.12	0.3	0.12	0.3	0.28	0.3	0.24	0.2
MgO	0:97	2.6	0.98	2.6	2.57	2.9	4.88	5.1
CaO	0.14		0.25		0.85	0.2	0.29	
Na_2O	0.06	0.2	0.07	0.2	0.18	0.2	0.13	0.1
K_2O	3.22	8.8	3.33	8.8	7.46	8.6	7.96	8.3
P_2O_5	0.11		0.18		0.45		0.19	
LOI	0.61		0.65		1.41		1.29	
Σ	99.88	96.3	99.96	96.2	99.01	96.3	99.79	96.2
% Spex SiO_2	61.42		58.63					
Ba	124	350	54	150	216	255	428	460
Rb	629	1780	667	1820	1010	1200	775	840
Sr	1.7	5	1.9	5	5.7	6	3.2	3
Pb	6.1	17	8.8	23	10	12	6.5	7
Zr	139	390	192	520	707	840	513	553
Nb	66	180	76	200	127	150	85	92
Y	18.7	52	27.4	74	215	255	252	272
Sc	15.3	42	15.4	40	55	65	95.2	102
V	57	160	72	190	116	138	218	235
Mn	864	2440	1080	2950	1995	2370	1688	1820
Ga	33.5	95	33.6	91	63.2	75	48.7	53
Sn	19.9**	61	20.1**	60	18.6	22	11.4	12

Appendix F cont.

	Cordierite	Garnet						
Sample	67539	62634	67539	62589 pl+q	62589 pl	62593	62594 pl+q	62594 pl
SiO_2	46.56	37.04	37.29	92.41	54.04	56.00	91.73	61.46
TiO_2	0.01	0.12	0.30	0.01	0.06	0.01		
Al_2O_3	32.05	21.03	21.09	4.43	28.14	26.95	5.00	23.89
Fe_2O_3*	15.11	39.12	37.14	0.09	0.76	0.26	0.04	0.27
MnO	0.52	2.32	2.88					
MgO	4.62	1.73	2.35	0.05	0.28	0.045**	0.023**	0.11
CaO	0.02	1.38	1.45	1.72	10.89	9.52	1.48	7.09
Na_2O	0.31			0.74	4.67	5.89	1.36	6.48
K_2O	0.27	0.05	0.08	0.17	1.05	0.57	0.10	0.47
P_2O_5		0.05	0.08			0.03	0.01	0.07
LOI	1.82	-3.65	-3.28	0.36		0.58	0.22	
Σ	101.29	99.19	99.38	99.98	99.89	99.89	99.96	99.84
% Spex SiO_2				84.08			79.04	
Ba	12	28	39	35	220	125	30.5	146
Rb	27	11	12.4	10	66	17	8	8
Sr	3.7	3.4	2.8	77	487	514	92	441
Pb	2	1	2	5	31	24	6.5	31
Zr	<0.7	46	117	17	109	99	30	145
Nb	<0.4	<0.7	2	<0.4	<0.4	<0.4	<0.4	<0.4
Y	2.5	1780	1860	2	11	7.7	2.5	12
Sc	<0.2	125	174	0.6	3.7	1.8	0.3	1.6
V	<2.5	56	87	5	29	6	4	18
Mn	3670	13200	16500	18	110	67	18	87
Ga	51.5	15.5	11.3	4.4	27.7	27.0	6.0	28.8
Sn	<0.5	<0.5	<0.5			0.7	2.3	13.5

Appendix F cont.

Plagioclase

Sample	62595	62596	62601	62602 pl+q	62602 pl	62610 pl+q	62610 pl
SiO_2	58.71	61.23	58.4	92.43	58.46	69.16	56.77
TiO_2		0.03	0.01	0.01	0.05	0.01	0.02
Al_2O_3	25.7	23.52	25.6	4.55	25.55	19.08	27.00
Fe_2O_3	0.02	0.50	0.14	0.06	0.39	0.20	0.32
MnO	0.01	0.01	0.01				
MgO	0.035**	0.104**	0.037**	0.027**	0.15	0.049**	0.069
CaO	7.30	5.33	7.57	1.53	8.61	6.56	9.29
Na_2O	5.91	6.95	6.83	1.07	6.02	3.98	5.64
K_2O	1.04	0.83	0.75	0.11	0.62	0.50	0.71
P_2O_5	0.03	0.04	0.07	0.01	0.06	0.03	0.05
LOI	0.95	1.44	0.32	0.25		0.40	
Σ	99.89	99.98	99.74	100.05	99.91	99.97	99.87
% Spex SiO_2				82.2		29.11	
Ba	282	140	140	42	236	162	229
Rb	59	87	23	4.6	26	11.3	16
Sr	410	394	430	94	527	338	479
Pb	26	25	29	5	28	18	25
Zr	39	65	90	30	167	78	110
Nb	<0.4	2.2	0.6	<0.4	<0.4	<0.4	<0.4
Y	15	55	7.3	2	9	6	8
Sc	1.0	4.4	1.3	0.6	3.2	1.7	2.4
V	3	6	4	4	26	6	9
Mn	66	127	60	8	47	50	70
Ga	35.9	29	29.2	4.4	24.9	18.5	26.1
Sn	2.9	4.3	1.9	2.9	20.0	0.4	0.8

Plagioclase

Sample	62612 pl+q	62612 pl	62614	62619	62622	62634
SiO_2	79.72	58.93	60.19	60.74	60.89	59.23
TiO_2					0.01	
Al_2O_3	12.24	25.3	24.43	24.16	23.85	25.39
Fe_2O_3	0.13	0.31	0.13	0.17	0.27	0.18
MnO				0.01	0.02	0.01
MgO	0.023**	0.047	0.027**	0.04**	0.035**	0.043**
CaO	3.68	7.62	6.11	6.27	5.31	7.43
Na_2O	3.26	6.73	6.83	6.63	6.88	6.3
K_2O	0.39	0.80	1.71	0.75	1.07	0.81
P_2O_5	0.03	0.07	0.13	0.09	0.10	0.05
LOI	0.49		0.74	0.74	1.18	0.64
Σ	99.96	99.81	100.3	99.60	99.61	100.08
% Spex SiO_2	51.33					
Ba	82	169	200	130	107	238
Rb	19	39	82	57	107	36
Sr	211	436	258	251	220	382
Pb	12	25	30	27	25	29
Zr	33	68	82	42	68	26
Nb	0.7	1.5	<0.4	0.7	0.7	0.7
Y	5	10	11	7	9	10
Sc	1.1	2.2	1.6	1.5	0.9	1.4
V	4	9	5	4	5	4
Mn	43	90	63	73	79	86
Ga	16	33	32.3	32.1	32.5	36.5
Sn	2	4.4	2.1	1.5	2.5	1.7

* Total Fe as Fe_2O_3

** MgO determined by XRFS by Dr B.W. Chappell, A.N.U., Canberra (cf. Appendix D).

adj - adjusted; af - alkali feldspar; av s - average separate; ph - phenocrysts; pl - plagioclase; ps - pseudomorphs; q - quartz

Appendix G

IRON OXIDATION STATE IN NATURAL MINERAL SEPARATES AND SYNTHETIC SIMPLE SYSTEM GLASSES

The following partial analyses by semi-microvoltametric titration were made by E. Kiss of the R.S.E.S., Australian National University, Canberra.

Mineral Separates (duplicate analyses)

Mineral or Mineral Mixture	Sample	% FeO	% Fe_2O_3	FeII/FeIII
Biotite (phenocrystic)+ "Spex" SiO_2	62619	9.24±0.03	1.13	9.09
Biotite (pseudomorphic)+ "Spex" SiO_2	62619	10.24±0.03	0.41	28.09
Biotite	62634	23.06±0.09	2.18	11.78
Biotite	67539	23.83±0.02	1.95	13.60
Cordierite	67539	13.72±0.04	<0.01	>1520
Garnet	62634	36.80±0.01	0.06	68.01
Garnet	67539	35.67±0.04	<0.01	>584

KFMASHO-System Glasses (single analyses)

Run Number	Wt (mg)	Mix	P (GPa)	T (C)	% FeO	% Fe_2O_3	FeII/FeIII
T1541	0.81	1	0.9±0.05	1000±15	9.94	3.30	3.35
T1576	3.78	1	0.9±0.05	1000±15	11.33	1.65	7.61

Appendix H

MICROPROBE ANALYSES OF MINERAL PHASES AND PHASE-PSEUDOMORPHING ASSEMBLAGES FROM BLUE TIER BATHOLITH GRANITIC ROCKS

Eight hundred and ninety-five single and composite analyses obtained using the JEOL JXA50A electron microprobe analyser at the University of Tasmania, are presented in this appendix. They are listed in order of granitic suite, sample number and mineral or assemblage type. Each original compositional total is presented together with that for the normalized analysis. The spot mode of analysis was used for anhydrous phases where compositional zoning was being determined. The scanning mode was used for other analyses. The following symbols and abbreviations have been used.

Mineral Names:

AC	actinolite	GU	grunerite
AD	andalusite	HB	hornblende
AF	alkali feldspar	IL	ilmenite
AP	apatite	MS	muscovite
BI	biotite	QZ	quartz
CD	cordierite	PL	plagioclase
CL	chlorite	SI	sillimanite
CM	cummingtonite	SP	sphene
GA	garnet	TM	tourmaline

Assemblage Names:

MYR	myrmekite
PMA	porphyry matrix assemblage
SHA	sheet silicate assemblage

Abbreviations Used in Textural Descriptions:

co	core	mx	matrix
in	inclusion within	ph	phenocryst
ma	"mantle around" or "mantle of"	ps	pseudomorphic after
		rm	rim

Analysis Name Codes:

Real numbers refer to distances in millimeters along phenocryst traverses from a datum analysis at the edge of the crystal.

In number/letter combinations the first number refers to that of the garnet compositional map of Fig. 7.8. The remaining letter and number are the analysis name. Their positions are indicated in Appendix I.

Biotite/garnet compositional pairs used for thermometry, are also indicated here as "pair 1", "pair 2" etc.

Chemical Indexes:

mg′ = [MgO/(MgO+MnO+FeO*)] mol.% except where FeO can be determined by stoichiometry, when mg′ = [MgO/(MgO+MnO+FeO)] mol.%.

al = $[A'/(A'+F'+M)] = [Al_2O_3-(CaO+Na_2O+K_2O)]/\left[[Al_2O_3-(CaO+Na_2O+K_2O)]+FeO+MnO+MgO\right]$ mol.%

an = [Ca/(Ca+Na)] mol.%

Compositions are presented and cation proportions calculated assuming that:

(a) amphiboles, apatite, cordierite, sphene, micas and chlorite contain 2%, 2%, 2%, 2%, 4% and 12% of $\Sigma(H_2O + F_2O_{-1})$, respectively.

(b) tourmalines contain 13% of $\Sigma(B_2O_3 + H_2O$ and $F_2O_{-1})$.

(c) the number of oxygen equivalents in the formulae of the minerals or mineral assemblages analysed are:

5: aluminosilicates
6: orthopyroxene and ilmenite
8: feldspars
10: myrmekite and matrix assemblages
12: garnet
18: cordierite and sphene
22: micas and sheet silicate assemblages
23: amphiboles
28: chlorite
49: tourmaline

(d) Fe_2O_3 and FeO have been calculated on the basis of stoichiometry for the phases: actinolite, cummingtonite, garnet, ilmenite and orthopyroxene.

Suite	Babel Island																Babel Island												Babel Island			
Sample #	62579																67543												67544			
Mineral	Bt	Bt	Bt	Bt	CL	SHA	SHA	SHA	SHA	SHA	SHA	SHA	SHA	SHA	SHA	SHA	AD	Bt	GA	GA	GA	GA	GA	PL	SHA	SHA	SHA	SHA	SHA	AF	Bt	Bt	MYR
Type	mx	mx	mx	ps,CD	ps,CD	ps,CD	ps,CD	ps,CD	ps,CD	ps,CD	ps,CD	ps,CD	ps,CD	ps,CD	ps,CD	ps,CD	in,PL	mx	ph	ph	ph	ph,co	ph,rim	ph,co	ps,CD	ps,CD	ps,CD	ps,CD	ps,CD	M,ph	mx	ph	
Grain #	1	2	3	4	1	1	1	1	1	1	1	1	1	2	2	2	1	1	1	1	1	1	1	1	1	1	1	1	1	1	1	1	1
# analyses	2	2	2	5	2	1	1	1	1	1	1	1	1	1	1	1	1	3	1	1	1	2	1	1	1	1	1	1	1	2	2	8	2
Anal name																																	
SiO2	33 53	33 45	33 76	35 36	22 72	47 92	48 02	34 59	47 78	38 56	44 33	25 99	32 12	34 21	45 70	45 09	38 56	34 60	36,17	36 70	35 79	36 75	35 68	61 80	44 10	41 96	41 50	41 27	42 47	67 40	33 56	34 48	76 15
TiO2	2 02	2 27	1 74															2 12													0 92	1 48	
Al2O3	19 40	19 80	20 04	21 95	20 91	31 37	31 19	27 94	31 52	20 83	19 16	23 09	27 33	21 90	30 45	30 95	61 44	21 04	20 90	21 54	21 40	21 30	21 01	23 81	29 15	28 41	28 53	28 44	29 28	17 79	21 73	21 37	13 78
Fe2O3																			0 24			0 19	0 92										
FeO																			36 34			36 35	35 63										
FeO*	29 44	29 37	29 55	27 35	42 01	5 17	5 16	28 97	5 08	30 07	28 18	43 20	32 74	28 21	8 55	8 91		27 72		35 10	37 03				12 55	14 87	15 06	15 71	13 45		29 32	28 52	0 51
MnO	1 24	0 99	0 39	0 98	0 41			0 52		0 49		0 99	0 56	0 82				0 30	5 28	5 57	1 95	2 16	6 04								0 77	0 26	
MgO	1 39	1 15	1 44	1 34	1 94	0 70	0 84	1 53	0 87	1 05	0 90	2 30	1 52	1 79	0 88	0 94		1 14	0 38	0 57	2 12	2 52			1 17	1 28	1 20	1 45	1 37		0 62	0 69	
CaO																			0 69	0 52	0 71	0 73	0 72	5 73						0 08			0 34
Na2O											1 19													7 42	0 26					0 83			3 21
K2O	8 98	8 96	9 08	9 01		10 84	10 80	2 45	10 76	5 00	2 24	0 42	1 72	9 07	10 41	10 11		9 08						1 24	8 76	9 49	9 72	8 79	9 43	13 89	9 08	9 21	6 01
Total	96	96	96	96	88	96	96	96	96	96	96	96	96	96	96	96	100	96	100	100	100	100	100	100	96	96	96	96	96	100	96	96	100
Orig total	95 56	98 84	93 85	97 23	91 24	98 23	95 95	89 74	96 35	95 34	95 10	87 09	91 30	93 72	95 64	95 64	87 52	92 68	98 16	101 55	99 67	99 26	97 24	99 05	91 51	94 09	94 23	94 55	94 63	99 41	93 05	97 43	99 08
Si	5 351	5 326	5 360	5 517	5 267	6 444	6 456	5 173	6 421	5 879	6 500	4 284	4 915	5 380	6 270	6 192	1 038	5 417	2 978	2 996	2 984	2 977	2 948	2 749	6 147	5 974	5 927	5 894	5 988	3 063	5 319	5 420	4 129
Ti	0 242	0 272	0 207														0 250														0 109	0 174	
Al	3 648	3 716	3 750	4 037	5 713	4 972	4 942	4 926	4 992	3 744	3 311	4 486	4 928	4 059	4 924	5 009	1 949	3 882	2 028	2 072	2 045	2 033	2 046	1 248	4 789	4 766	4 803	4 786	4 866	0 953	4 053	3 960	0 880
FeIII																			0 015			0 011	0 057										
FeII	3 929	3 911	3 924	3 570	8 144	0 581	0 580	3 623	0 571	3 834	3 456	5 954	4 189	3 710	0 981	1 023		3 629	2 502	2 396	2 511	2 462	2 461		1 462	1 769	1 798	1 875	1 586		3 886	3 749	0 023
Fe																																	
Mn	0 167	0 133	0 052	0 129	0 081			0 066		0 063		0 138	0 072	0 109				0 039	0 385	0 385	0 133	0 147	0 422								0 103	0 034	
Mg	0 329	0 272	0 341	0 312	0 669	0 141	0 168	0 341	0 173	0 238	0 196	0 566	0 347	0 420	0 180	0 193		0 265	0 046	0 069	0 255	0 304			0 244	0 270	0 256	0 309	0 287		0 146	0 161	
Ca																			0 061	0 045	0 061	0 062	0 063	0 273						0 003			0 019
Na											0 338													0 640	0 070			0 092		0 073			0 337
K	1 828	1 821	1 840	1 794		1 859	1 851	0 467	1 845	0 973	0 419	0 088	0 336	1 818	1 821	1 77		1 814						0 070	1 557	1 732	1 771	1 601	1 697	0 805	1 835	1 847	0 415
mg	7 7	6 5	8 0	8 0	7 6	19 5	22 5	8 6	23 3	5 8	5 4	8 7	7 7	10 2	15 5	15 9		6 8	1 8	2 8	9 2	11 0			14 3	13 3	12 5	14,1	15 4		3 6	4,1	
al	17 1	18 0	18 1	21 8	24 3	68 3	67 4	35 6	67 9	25 1	25 9	24 8	33 2	20 9	57 2	57 1		20 8	24 8	25 8	24 9	24 8	25 5		48 1	42 7	42 5	41 4	45 8		21 2	21 1	
an																								29 9						5 0			

Suite	Babel Island										Babel Island																					
Sample #	67544 cont.										68550																					
Mineral	MYR	SHA	SHA	SHA	SHA	SHA	SHA	SHA	SHA	SHA	AP	Bt	Bt	Bt	Bt	GA	GA	GA	GA	SHA	SHA	SHA	SHA	SHA	SHA	Bt	MS	SHA	SHA	SHA	SHA	SHA
Type		ps,CD	ps,CD	ps,CD	ps,CD	ps,CD	ps,CD	ps,CD	ps,CD	ps,CD	in Bt	in Qz	ph	ps,GA	ps,GA	ph	ph	ph	ph,co	ps,CD	ps,CD	ps,CD	ps,CD	ps,CD	ps,CD	ph	ps,AD	ps,CD	ps,CD	ps,CD	ps,CD	ps,CD
Grain #	2	1	1	1	1	1	1	1	1	1	1	1	2	3	3	1	1	1	1	1	1	1	1	1	1	1	1	1	1	1	1	1
# analyses	7	1	1	1	1	1	1	1	1	1	1	1	3	1	1	1	1	1	1	1	1	1	1	1	1	3	4	1	1	1	1	2
Anal name																																
SiO2	76 30	45 88	35 83	44 27	35 85	45 76	47 31	35 76	43 54	43 35		36 22	34 51	34 53	34 63	36 74	36 02	36 00	36 43	41 81	47 78	41 41	35 18	40 92	42 98	33 67	47 31	39,73	47 22	47 26	37 22	43 90
TiO2												2 60	3 50	2 31	2 77											3 24						
Al2O3	13 78	32 97	24 14	29 72	22 20	31 01	31 19	24 58	28 96	29 39		19 54	18 92	20 50	20 03	21 31	21 25	20 92	21 23	28 74	34 26	28 53	22 04	27 01	28 25	19 59	35 02	27 28	31 47	31 44	24 77	29 70
Fe2O3																0 32	1 16	0 77	0 57													
FeO																36 68	37 17	35 10	35 08													
FeO*		6 41	25 10	11 32	26 51	8 50	6 97	25 64	13 33	12 68	1 24	22 69	26 99	26 77	26 69					13 76	2 70	12 00	26 11	16 40	13 16	29 21	2 87	20 33	5 77	5 64	26 28	12 00
MnO			1 00	0 26	0 98			0 90		0 25	2 02	0 08	0 37	0 17		1 35	2 06	5 88	1 34	0 26		0 28	0 69	0 33	0 30	0 08						
MgO		0 25	0 71	0 46	0 90	0 44	0 40	0 82	0 47	0 42	0 20	5 24	2 70	2 50	2 68	2 54	1 60	0 57	3 06	1 47	0 71	1 47	2 68	1 85	1 70	1 29	0 11	2 10	1 08	1 21	2 51	1 55
CaO	0 16										52 16					1 06	0 75	0 76	1 29													
Na2O	2 01	0 26																		0 53	0 54	0 38	0 09	0 28	0 37		0 56					
K2O	7 75	10 23	9 22	9 88	9 55	10 29	10 14	8 30	9 71	9 90	*42 38*	9 62	9 03	9 23	9 20					9 42	10 02	8 93	9 20	9 22	9 25	8 92	10 13	6 57	10 46	10 42	5 21	8 84
Total	100	96	96	96	96	96	96	96	96	96	98	96	96	96	96	100	100	100	100	96	96	96	96	96	96	96	96	96	96	96	96	96
Orig total	99 95	98 62	97 72	97 01	97 58	97 56	96 84	97 61	96 71	98 54	95 16	95 99	94 34	94 47	92 42	102 17	102 56	101 43	100 35	95 56	94 30	93 82	94 05	92 56	93 92	94 54	96 20	93 86	94 46	95 50	91 75	93 90
Si	4 146	6 209	5 507	6 172	5 578	6 265	6 399	5 475	6 128	6 097		5 538	5 407	5 391	5 402	2 979	2 941	2 961	2 941	5 939	6 318	6 192	5,462	5 903	6 063	5 331	6 266	5 750	6 365	6 366	5 559	6 101
Ti												0 299	0 412	0 270	0 325											0 385						
Al	0 882	5 259	4 373	4 882	4 072	5 004	4 972	4 435	4 803	4 872		3 521	3 494	3 771	3 682	2 033	2 045	2 029	2 021	4 812	5 340	4 688	4 032	4 592	4 697	3 655	5 466	4 653	5 001	4 993	4 360	4 864
FeIII																0 019	0 071	0 047	0 095													
FeII		0 725	3 227	1 319	3 450	0 973	0 788	3 283	1 569	1 491		2,901	3 537	3 494	3 481	2 482	2 538	2 414	2 369	1 635	0 298	1 399	3 390	1 978	1 552	3 868	0 318	2 461	0 650	0 638	3 283	1 395
Fe*											0 174																					
Mn			0 130	0 030	0 129				0 117		0 030	0 288	0 010	0 048	0 022		0 095	0 142	0 409	0 091	0 031			0 032	0 091	0 040	0 035	0 010					
Mg		0 051	0 162	0 094	0 207	0 090	0 080	0 186	0 097	0 087	0 050	1 194	0 629	0 581	0 623	0 306	0 154	0 070	0 368	0 310	0 140	0 306	0 621	0 397	0 356	0 304	0 021	0 452	0 216	0 242	0 559	0 321
Ca	0 009										9 400					0 091	0 065	0 066	0,111													
Na	0 211	0 069																		0 146	0 138	0 102	0 027	0 078	0 100		0 143					
K	0 537	1 766	1,809	1,773	1 896	1 797	1 750	1 621	1,743	1 725	*6 035*	1 876	1 804	1 837	1 831					1 707	1 690	1,588	1 821	1 697	1 664	1 800	1 711	1 212	1 798	1 791	0 994	1 567
mg		6 6	4 8	6 7	5 7	8 5	9 2	5 4	5 9	5 6		29 1	15 1	14 3	15 2	11 0	7 1	2 8	13 5	16 0	32 0	18 0	15 5	16 7	18 7	7 3	6 4	15 5	25 0	27 5	14 6	18 7
al		68 8	26 7	51 8	22 3	60 1	65 0	28 2	47 0	49 0		16 7	16 7	19 1	18 4	24 5	25 7	25 1	25 1	42 8	80 0	46 3	21 0	36 8	43 0	18 1	84 2	37,1	64 9	64 5	30 5	49 0
an																																

Suite	Babel Island		Boobyalla																			Boobyalla									
Sample #	68551 cont		43151																			43156									
Mineral	SHA	TM	Bt	Bt	Bt	Bt	Bt	Bt	Bt	Bt	Bt	Bt	Bt	Bt	GA	GA	GA	GA	GA	IL	IL	Bt	Bt	Bt	Bt	Bt	Bt	Bt	GA	GA	GA	GA
Type	ps,CD	ph	in IL	in IL	in IL	in IL,co	ph	ph	ph	ph	ph	ph,co	ph,rm	ph	ph,rm	ph	ph	ph	ph,co	In,Bt	In,Bt	In,GA	ps,GA	in,IL	in,IL	in,IL	in,IL	ph,rm	ph	ph	ph	ph
Grain #	1	1	1	1	1	1	2	3	3	3	3	3	3			1	1	1	1	1	2	1	2	3	3	3	3	4	1	1	1	1
# analyses	1	5	1	1	1	1	1	1	1	1	1	1	1	2	1	1	1	1	1	2	4	2	2	1	1	1	1	1	1	1	1	1
Anal name													par 1	pair1																	
SiO2	43 29	35 08	35 88	34 73	35 73	35 04	35 94	35 16	35 81	35 61	35 26	35 86	35 09	34 17	36 43	36 95	36 45	36 76	36 83			35 70	34 18	35 69	35 87	35 50	35 65	35 52	37 01	37 29	37 33	36 52
TiO2		0 10	2 91	2 44	3 04	2 15	2 98	0 75	2 28	2 69	1 11	2 91		4 06						53 76	54 85	3 93	0 43	2 72	3 21	3 87	3 46	2 46				
Al2O3	29 92	34 37	20 46	20 97	20 03	21 03	20 21	21 92	20 73	20 14	21 45	20 35	22 52	19 46	21 56	21 08	21 23	21 26	21 37			19 71	21 15	20 30	19 44	19 33	19 62	19 76	21 39	21 63	21 32	21 21
Fe2O3																													0 02			0 72
FeO															33 21	37 20	37 07	37 37	38 98										35 41	34 91	34 71	34 35
FeO*	12 85	15 12	25 56	26 57	25 78	26 79	25 42	26 81	25 86	26 06	26 40	25 68	27 04	26 11						41 04	38 45	25 56	28 80	26 23	26 80	26 99	26 52	26 94				
MnO				0 34	0 29		0 31	0 26		0 22	0 33			0 59	7 03	1 60	3 06	2 08	1 53	5 20	6 70	0 32	0 46	0 28	0 33		0 24	0 24	1 82	2 09	1 92	3 48
MgO	1 54	0 52	1 99	1 94	2 02	1 85	1 98	2 10	2 07	1 94	2 19	1 88	2 12	2 04	0 62	1 89	0 93	1 29	2 04			1 56	2 01	1 64	1 36	1 14	1 37	1 91	2 86	2 52	3 17	2 09
CaO															1 16	1 28	1 27	1 25	1 24										1 49	1 56	1 55	1 62
Na2O		1 81												0 17								0 20										
K2O	8 41		9 21	9 01	9 10	9 14	9 16	8 99	9 25	9 34	9 25	9 32	9 33	9 41								9 01	8 97	9 15	8 98	9 23	9 14	9 19				
Total	96	87	96	96	96	96	96	96	96	96	96	96	96	96	100	100	100	100	100	100	100	96	96	96	96	96	96	96	100	100	100	100
Orig total	93 54	87 40	94 24	95 94	95 80	93 35	96 25	94 20	92 15	91 61	93 27	91 96	94 16	97 82	101 98	100 00	100 01	100 01	99 99	99 62	99 86	100 12	96 59	96 09	95 86	93 00	95 39	96 02	99 99	100 00	100 00	9999
Si	6 032	11 753	5 538	5 405	5 533	5 448	5 551	5 458	5 535	5 528	5 476	5 544	5 450	5 355	2 976	2 999	2 980	2 993	2 985			5 527	5 387	5 536	5 581	5 534	5 544	5 538	2 983	2 999	2 998	2 963
Ti		0 025	0 338	0 285	0 353	0 251	0 348	0 088	0 265	0 314	0 129	0 338		0 478			2 045			2 028	2 056	0 457	0 050	0 317	0 376	0 453	0 404	0 287				
Al	4 913	13 572	3 721	3 847	3 655	3 854	3 679	4 010	3 777	3 685	3 926	3 707	4 122	3 594	2 076	2 017	2 534	2 040	2 041			3 597	3 928	3 712	3 564	3 553	3 597	3 631	2 032	2 050	2 018	2 028
FeIII																													0 001			0 044
FeII	1 497	4 237	3 299	3 457	3 338	3 483	3 284	3 481	3 342	3 383	3 429	3 320	3 511			2 525	0 211	2 544	2 507	1 721	1 603	3 310	3 796	3 402	3 487	3 511	3 449	3 512	2 386	2 347	2 331	2 331
Fe*														3 422	2 269		0 113															
Mn				0 044	0 038		0 040	0 034		0 028	0 043			0 078	0 486	0 110	0 111	0 143	0 105	0 221	0 283	0 041	0 061	0 036	0 043		0 031	0 031	0 124	0 142	0 130	0 239
Mg	0 319	0 260	0 457	0 450	0 467	0 429	0 457	0 485	0 477	0 448	0 507	0 433	0 490	0 477	0 076	0 228		0 156	0 245			0 360	0 471	0 378	0 315	0 263	0 317	0 443	0 343	0 302	0 379	0 252
Ca															0 102	0 111		0 109	0 107										0 128	0 134	0,133	0 140
Na		1 176												0 052								0 060										
K	1 494		1 813	1 787	1 797	1 813	1 804	1 780	1 824	1 849	1 833	1 818	1 827	1 881								1 780	1 804	1 811	1 783	1 835	1 813	1 828				
mg'	17,6	5 7	12 2	11 5	12 3	11 0	12 2	12 2	12 5	11,7	12 9	11 6	12 3	12 0	2 7	8 3	4 3	5 8	9 0			9 8	11 0	10 0	8 3	7 0	8 4	11 2	12 6	11 4	14 0	9 8
al	48 5	58 0	20 3	20 7	19 5	20 7	19 9	21 8	20 4	19 2	20 8	19 9	22 3	17,3	24 9	23 9	24 3	24 3	24 2			19,1	19 7	19 9	18 8	18 5	19 0	18 4	23 7	24 2	23 6	24,1
an																																

Suite	Boobyalla			Boobyalla											Boobyalla		Boobyalla															
Sample #	43156 cont			43199											43202		43204															
Mineral	GA	GA	IL	Bt	Bt	Bt	Bt	Bt	Bt	Bt	Bt	Bt	GA	GA	Bt	GA	Bt	Bt	Bt	Bt	Bt	Bt	Bt	Bt	Bt	Bt	Bt	Bt	Bt	GA	GA	GA
Type	ph,co	ph,rm		In,GA	In,GA	In,GA	ma,IL	ma,IL	ma,IL	ph	ph,co	ph,rm	ph	ph,co	ps,GA	ph,rm	ma	mx	mx	ph	mx	mx co	mx rm	ma IL	ma IL	ma IL	ma IL	in ga	ma IL	ph	ph	ph co
Grain #	1	1	1	1	1	1	2	2	2	3	3	3	1	1	1	1	1	2	3	4	5	5	5	6	6	6	6	7	8	1	1	1
# analyses	1	1	2	1	1	1	1	1	1	1	1	1	1	1	par 1	par 1	2	3	4	3	1	1	1	1	1	1	1	2	4	1	1	1
Anal name																																
SiO2	37 49	36 51		34 42	34 19	34 32	34 13	34 34	34 21	34 28	34 78	34 21	36 78	36 94	32 82	34 96	35 55	35 83	35 76	35 13	35 73	35 98	36 05	35 24	35 84	35 41	35 93	35 31	35 73	37 05	36 22	36 96
TiO2			53 34	1 60	2 35	0 80	2 84	3 27	2 67	2 24	2 36	1 23			2 24		3 67	3 20	3 21	3 71	3 45	3 60	3 14	3 78	2 96	3 93	2 71	4 10	3 78				
Al2O3	21 57	21 14		20 34	19 62	21 01	19 13	19 01	19 57	20 11	19 61	20 82	21 26	21 16	19 44	21 20	17 24	17 43	17 56	17 45	17 32	17 11	17 56	17 35	17 47	17 08	17 63	16 76	16 68	21 02	21 18	21 14
Fe2O3																															0 66	
FeO	33 61	34 67											37 15	37 00		38 70														36 39	34 89	37 03
FeO*			42 47	27 70	27 75	27 89	28 34	27 75	28 11	27 93	27 74	28 43		1 64	29 64		25 28	25 52	25 47	25 79	25 52	25 18	24 96	25 61	25 47	25 54	24 91	24 09	25 51				
MnO	1 88	5 11	4 19										1 78	1 92		4 13													0 05	2 65	4 56	1 94
MgO	3 78	1 06		3 01	3 12	3 28	2 44	2 64	2 51	2 54	2 57	2 14	1 68	1 33	2 78	0 58	5 03	4 95	4 92	4 78	4 92	4 95	5 07	5 03	5 28	4 84	5 80	7 10	5 19	1 59	1 20	1 81
CaO	1 66	1 50											1 34			0 42														1 31	1 30	1 13
Na2O																												0 34				
K2O				8 94	8 96	8 71	9 11	9 00	8 86	8 90	8 94	9 18			9 08		9 23	9 08	9 08	9 14	9 05	9 19	9 21	8 98	8 98	9 20	9 02	8 39	9 07				
Total	100	100	100	96	96	96	96	96	96	96	96	96	100	100	96	100	96	96	96	96	96	96	96	96	96	96	96	96	96	100	100	100
Orig total	99 99	99 99	99 89	94 21	95 86	93 95	92 81	96 15	94 79	95 24	95 57	92 56	99 99	99 99	95 78	103 69	96 45	94 92	95 03	93 85	96 93	96 12	99 22	98 44	96 02	96 43	98 85	94 49	95 52	100 01	100 00	100 01
Si	2 994	2 982		5 588	5 365	5 365	5 382	5 392	5 374	5 375	5 445	5 379	2 989	2 997	5 229	2 902	5 522	5,560	5 547	5 472	5 546	5 577	5 578	5 479	5 556	5 510	5 554	5 443	5 554	3 009	2 959	3 000
Ti			2 017	0 188	0 277	0 093	0 337	0 386	0 315	0 263	0 278	0 146			0 268		0 429	0 372	0 374	0 435	0 402	0 419	0 365	0 442	0 345	0 460	0 315	0 475	0 441				
Al	2 030	2 035		3 752	3 628	3 870	3 554	3 519	3 623	3 716	3 618	3 858	2 036	2 023	3 649	2 074	3 156	3 186	3 210	3 204	3 169	3 126	3 202	3 179	3 191	3 133	3 211	3 048	3 056	2 012	2 039	2 022
FeIII																															0 040	
FeII	2 245	2 368	1 786	3 625	3,642	3,645	3 737	3 644	3 693	3,662	3 633	3 739	2,524	2 510			3 284	3 311	3,304	3 360	3 313	3 264	3 230	3 329	3 302	3 323	3 220	3 106	3 316	2 472	2 384	2 514
Fe*															3 948	2 686																
Mn	0 127	0 353	0 178										0 122	0 112		0 290													0 006	0 182	0 315	0 133
Mg	0 450	0 129		0 701	0 730	0 764	0 573	0 617	0 602	0 593	0 600	0 500			0 660	0 072	1 163	1 143	1 137	1 109	1 138	1 144	1 169	1 166	1 219	1 122	1 335	1 611	1 201	0 192	0 146	0 219
Ca	0 142	0 131														0 038														0 114	0 113	0 098
Na																												0 100				
K				1,784	1,794	1,735	1 833	1 802	1,776	1,780	1 785	1 841			1 845		1 828	1,797	1,797	1 817	1,792	1,817	1,818	1 781	1 775	1 826	1,778	1 650	1 797				
mg'	16 7	5 2		16 2	16 7	17 3	13 3	14 5	14 0	13 9	14 2	11 8	7,5	8 5	14 3	2 4	26 2	25 7	25 6	24 8	25 6	26 0	26,6	25 9	27 0	25 2	29 3	34 2	26 6	7 2	5,8	8 0
al	23 6	23 7		18 5	17 3	19 5	16 6	16 8	17,7	18 5	17 8	19 2	24 0	23 9	16 4	24 7	13 0	13 5	13 7	13 4	13 4	12 9	13 6	13 5	13 5	12 8	13 6	12 1	12 2	23 9	24 6	24 2
an																																

Suite	Boobyalla		Boobyalla																	Boobyalla											
Sample #	43204 cont		43242																	43248											
Mineral	GA	IL	Bt	Bt	Bt	Bt	Bt	Bt	Bt	Bt	Bt	Bt	GA	GA	GA	GA	GA	GA	IL	Bt	Bt	Bt	Bt	Bt	Bt	Bt	Bt	Bt	Bt	Bt	Bt
Type	ph rm		in GA	ph rm	mx co	mx rm	in IL	in IL	in IL	in IL	in IL	ph co	ph	ph	ph	ph	ph co	ph rm	Bt,IL	in AF	ps GA	in AF	in AF	in GA	in AF	in AF	in AF	in AF	in GA	mx	mx	mx
Grain #	1	1	1	2	3	3	4	4	4	4	4	5	1	1	1	1	1	1	1	1	2	3	3	3	3	3	3	4	4	5	5	5
# analyses	1	3	1	1	3	3	1	1	1	1	1	1	1	1	1	1	1	1	3	1	1	1	1	1	1	1	1	1	1	1	1	1
Anal. name																																
SiO2	36.96		35.26	36.07	35.42	35.33	35.01	35.18	35.24	35.22	34.59	35.42	37.08	37.17	37.03	37.47	37.49	37.07		35.54	34.39	35.99	35.46	35.77	35.76	35.48	35.60	34.59	35.61	36.26	35.93	36.09
TiO2		54.42	4.25	1.59	2.88	2.54	1.86	2.41	2.17	2.53	2.07	4.45							53.78	4.58		3.38	3.99	4.38	4.15	4.38	5.38	2.09	2.70	1.82	2.06	2.13
Al2O3	21.21		16.71	18.44	20.34	20.77	20.98	21.23	21.20	20.81	21.33	17.32	21.31	21.41	21.34	21.06	21.26	21.17	39.45	17.54	20.65	19.37	18.70	18.61	18.71	18.56	16.94	19.85	19.52	21.27	21.15	21.11
Fe2O3																																
FeO	36.53												36.01	35.94	36.66	35.88	35.71	34.76														
FeO*		42.88	26.18	25.58	25.28	25.61	25.79	25.14	25.21	25.32	26.02	26.32								25.70	29.20	23.74	24.60	24.02	24.07	24.24	25.09	27.79	26.24	24.53	24.98	24.64
MnO	2.16	2.70					0.20						1.66	1.92	1.61	2.82		4.42	8.77		0.22											
MgO	1.82		4.95	5.27	2.91	2.78	3.06	2.88	2.97	2.78	2.93	3.52	2.42	2.05	1.95	1.35	1.53	1.20		3.82	3.01	4.29	4.19	4.28	4.33	4.23	4.01	2.78	2.89	3.03	2.73	2.82
CaO	1.31												1.52	1.52	1.41	1.42	2.45	1.38														
Na2O																	1.56															
K2O			8.65	9.04	9.16	8.98	9.11	9.17	9.22	9.33	9.06	8.98								8.81	8.54	9.23	9.06	8.93	8.99	9.11	8.98	8.89	9.04	9.10	9.15	9.22
Total	100	100	96	96	96	96	96	96	96	96	96	96	100	100	100	100	100	100	100	96	96	96	96	96	96	96	96	96	96	96	96	96
Orig. total	99.99	99.45	95.03	95.25	94.92	93.91	96.61	95.14	94.84	93.79	96.13	95.86	100.00	100.01	100.00	100.00	100.00	99.30	99.99	96.74	97.09	95.50	95.73	97.03	96.48	94.54	95.83	94.45	94.61	96.72	95.55	96.78
Si	2.998		5.491	5.582	5.469	5.455	5.423	5.424	5.436	5.444	5.362	5.522	2.794	3.002	2.997	3.036	3.018	3.012	2.028	5.513	5.411	5.519	5.471	5.494	5.496	5.468	5.518	5.416	5.523	5.551	5.521	5.537
Ti		2.046	0.498	0.185	0.334	0.294	0.216	0.279	0.251	0.293	0.241	0.521								0.534		0.389	0.469	0.506	0.479	0.507	0.527	0.246	0.314	0.209	0.238	0.246
Al	2.028		3.067	3.364	3.702	3.780	3.230	3.858	3.854	3.791	3.897	3.181	2.028	2.088	2.036	2.011	2.017	2.027		3.208	3.829	3.501	3.401	3.369	3.388	3.371	3.094	3.664	3.569	3.838	3.831	3.817
FeIII																			1.655													
FeII	2.478	1.792	3.410	3.310	3.265	3.306	3.341	3.241	3.253	3.273	3.374	3.431	2.432	2.427	2.482	2.431	2.404	2.362		3.335	3.842	3.045	3.174	3.086	3.093	3.124	3.253	3.639	3.404	3.140	3.210	3.161
Fe'																			0.287													
Mn	0.148	0.114					0.026						0.113	0.131	0.110	0.193	0.104	0.304			0.029											
Mg	0.220		1.149	1.215	0.670	0.639	0.706	0.662	0.682	0.641	0.676	0.816	0.291	0.246	0.235	0.163	0.294	0.145		0.883	0.705	0.981	0.964	0.981	0.991	0.972	0.925	0.650	0.668	0.690	0.626	0.644
Ca	0.113												0.131	0.131	0.122	0.123	0.194	0.120														
Na																																
K			1.718	1.784	1.805	1.767	1.800	1.804	1.814	1.840	1.791	1.786								1.774	1.714	1.605	1.782	1.750	1.761	1.790	1.774	1.776	1.789	1.777	1.794	1.803
mg'	8.2		25.2	26.9	17.0	16.2	17.5	16.9	17.3	16.4	16.7	19.2	10.7	9.2	2.7	6.3	10.9	5.8		20.9	15.5	24.4	23.3	24.1	24.3	23.7	22.2	15.2	16.4	18.0	16.3	16.9
al	24.0		12.9	14.9	19.4	20.3	19.9	20.8	20.6	19.9	20.6	14.1	23.7	24.0	24.1	24.0	23.8	24.1		14.8	18.8	17.4	16.4	16.6	16.6	16.2	13.6	18.0	17.9	21.2	21.0	20.9
an																																

Suite	Boobyalla													Boobyalla		Boobyalla								Boobyalla			Boobyalla			
Sample #	43248 cont													43252		62584											62585			62595		
Mineral	Bt	Bt	Bt	Bt	Bt	Bt	Bt	GA	GA	GA	GA	GA	IL	IL	Bt	GA	Bt	Bt	GA	GA	GA	GA	GA	GA	GA	GA	AD	Bt	Bt	MS	AP	Bt	Bt	GA
Type	mx rm	mx co	mx rm	mx rm	ph	ph rm	ph co	ph	ph	ph	ph co	ph rm	Bt,IL	in GA	in GA	ph,rm	mx	ph	ph	ph	ph	ph	ph,co	ph,co	ph,rm	ps SI?	ph	ps,OP	ps,CD	in mx Bt	mx	ps,GA	mx,rm
Grain #	5	6	6	6	7	7	7	1	1	1	1	1	1	1			1	2	1	1	1	1	1	1	1	1	1	2	1	1	1		
# analyses	1	1	1	1	1	1	1	1	1	1	1	1	2	1	1	1	6	4	1	1	1	1	1	1	1	5	2	9	4	1	4	3	1
Anal. name															par 1	par 1																par 1	par 1
SiO2	35.30	34.95	35.39	35.39	34.69	35.14	35.23	36.98	36.75	37.11	37.23	36.60			33.96	35.10	34.29	34.33	35.86	36.14	35.63	36.49	36.10	36.15	37.17	34.53	34.52	46.98		34.10	33.23	36.18
TiO2	1.43	2.06	1.49	1.44	1.86	0.82	2.51						53.24	52.71	2.00		2.43	3.53								2.76	2.60			2.36	2.53	
Al2O3	21.78	20.64	20.94	21.10	20.61	21.59	19.81	21.27	21.28	21.41	21.19	21.81			20.04	20.57	20.31	19.49	20.99	21.21	21.23	21.35	21.02	21.19	62.70	20.31	20.10	35.07		19.87	19.69	21.48
Fe2O3																			1.63	1.60	2.74	0.75	2.05	0.48	0.13							
FeO								36.20	36.62	35.76	35.62	35.70				38.16			35.52	35.27	35.81	35.79	34.82	35.69								36.17
FeO*	25.99	26.28	26.52	26.20	27.02	26.49	26.76						44.33	46.92	27.34		26.11	25.76								25.47	26.04	2.30	1.31	27.42	27.89	
MnO		0.28		0.22				1.47	2.08	1.62	1.79	2.64	2.43	0.37	0.42	4.99	0.04		3.35	2.03	2.30	1.67	1.92	4.52		0.45	0.48		0.83	0.06	0.36	4.61
MgO	2.53	2.73	2.56	2.62	2.72	2.92	2.66	2.51	1.78	2.45	2.60	1.62			2.77	0.50	3.52	3.59	1.14	2.13	1.75	2.16	2.33	0.87		2.99	2.85	0.89		2.86	2.81	0.63
CaO								1.58	1.49	1.66	1.58	1.64				0.68			1.51	1.63	1.05	1.79	1.75	1.10		0.10	0.15	0.13	53.69			0.94
Na2O				0.27											0.32											0.06	0.04	0.54				
K2O	8.97	9.07	9.10	9.04	9.09	8.78	9.02								9.15		9.30	9.30								9.34	9.22	10.08	*42.17*	9.33	9.48	
Total	96	96	96	96	96	96	96	100	100	100	100	100	100	100	96	100	96	96	100	100	100	100	100	100	100	96	96	96	98	96	96	100
Orig. total	93.75	96.86	95.49	96.01	97.38	97.39	96.92	100.01	100.00	100.01	100.01	100.82	99.98	100.00	97.32	99.87	93.75	95.98	103.98	103.50	101.49	104.34	101.80	102.13	101.39	96.84	95.87	95.87	100.65	100.00	97.73	104.34
Si	5.450	5.432	5.488	5.462	5.409	5.443	5.483	2.988	2.984	2.993	3.002	2.967			5.342	2.921	5.343	5.346	2.936	2.935	2.909	2.957	2.931	2.962	1.002	5.373	5.385	6.215		5.355	5.262	2.965
Ti	0.166	0.241	0.173	0.167	0.218	0.095	0.292						2.015	2.001	0.236		0.284	0.413									0.322	0.305			0.301	
Al	3.963	3.780	3.828	3.852	3.788	3.941	3.633	2.025	2.037	2.035	2.014	2.084			3.716	2.018	3.729	3.578	2.025	2.031	2.043	2.039	2.011	2.046		1.993	3.725	3.696		5.467	3.675	2.075
FeIII																			0.100	0.097	0.137	0.046	0.125	0.029		0.002						
FeII	3.355	3.416	3.440	3.394	3.524	3.430	3.483	2.446	2.487	2.412	2.402	2.420	1.866	1.981			3.402	3.354	2.432	2.396	2.445	2.426	2.364	2.445			3.314	3.397		0.254		
Fe'													0.103	0.015	3.596	2.656													0.184		3.693	2.479
Mn		0.036		0.028				0.100	0.143	0.110	0.122	0.181			0.057	0.352	0.005		0.232	0.139	0.159	0.114	0.132	0.313			0.058	0.063	0.118		0.048	0.320
Mg	0.582	0.631	0.592	0.605	0.632	0.673	0.618	0.302	0.215	0.294	0.312	0.195			0.650	0.062	0.818	0.833	0.139	0.258	0.213	0.261	0.282	0.103			0.694	0.663		0.175	0.663	0.077
Ca								0.136	0.129	0.143	0.195	0.142				0.080			0.132	0.141	0.092	0.155	0.152	0.090			0.016	0.025	9.680	0.018		0.083
Na						0.079									0.097												0.017	0.012		0.138			
K	1.766	1.798	1.800	1.786	1.808	1.785	1.791								1.836		1.848	1.848									1.853	1.835	*6.007*	1.701	1.915	
mg	14.8	15.6	14.7	15.1	15.2	16.4	15.1	11.0	8.0	10.9	11.5	7.5			15.1	2.0	19.4	19.9	5.4	9.7	8.0	9.7	10.7	4.2		17.3	16.3	40.8		15.7	15.1	2.7
al	21.8	19.5	20.1	20.4	19.2	20.6	18.3	23.5	23.8	23.7	23.5	24.3			17.2	23.6	18.2	17.1	24.9	24.8	26.2	24.0	24.8	24.7		18.3	17.9	80.7		17.5	16.7	24.9
an																																

Suite	Boobyalla				Boobyalla																		Boobyalla								
Sample #	62595 cont				62605																		62616								
Mineral	GA	GA	MS	SHA	Bt	MS	SHA	SHA	SHA	SHA	SHA	SHA	SHA	SHA	SHA	SHA	SHA	SHA	SHA	SHA	SHA	SHA	AD	AD	AD	AD	AD	AD	Bt	SHA	SHA	SHA
Type	mx,co	mx	ps CD	ps CD	mx	ps CD	ps CD	ps CD	ps CD	ps CD	ps CD	ps CD	ps CD	ps CD	ps CD	ps CD	ps CD	ps CD	ps CD	ps CD	ps CD	ps CD	ph	ph	f ph	ph	ph co	ph frm	ph	ps CD	ps CD	ps CD
Grain #	1	1	1	1	1	1	1	1	1	1	1	1	1	1	1	1	1	1	1	1	1	1	1	1	1	1	1	1	1	1	1	1
# analyses	2	2	2	3	4	2	1	1	1	1	1	1	1	2	1	1	1	1	1	1	1	1	3	1	2	1	1	2	3	1	1	1
Anal. name																																
SiO2	35 91	36 05	47 32	40 63	33 30	46 61	33 34	43 72	43 06	45 87	35 14	46 35	33 26	35 39	33 43	32 89	44 71	35 76	46 38	46 29	36 49	36 63	37 39	37 49	37 25	36 93	37 37	37 54	34 31	49 60	38 37	50 59
TiO2			0 26		2 03																								2 11			
Al2O3	21 06	21 10	35 09	27 47	20 70	35 58	21 05	32 81	30 42	34 48	21 77	35 56	20 81	23 04	20 86	20 63	34 88	23 86	36 56	36 25	20 78	25 19	61 03	61 00	62 11	61 40	60 93	62 46	30 79	29 25	33 11	29 76
Fe2O3	1 44	0 82																														
FeO	35 83	35 60																														
FeO*			1 75	15 40	28 08	2 59	28 89	8 50	10 85	4 07	26 17	2 97	29 19	25 09	28 91	30 29	5 72	23 95	1 80	1 97	26 84	23 28	1 58	1 51	0 55	1 67	1 70		27 26	7 73	15 44	5 57
MnO	3 41	4 41		0 18	0 34		0 91				0 67		0 92	0 58	0 93	0 86		0 32			0 58	0 38										
MgO	1 28	0 89	0 68	2 03	2 30	0 56	2 92	1 01	1 39	0 76	3 10	0 55	2 65	2 60	2 63	2 72	0 82	2 44	0 37	0 41	3 19	2 42							2 44	1 55	0 79	2 00
CaO	1 08	1 14							0.15																					0 25		0 27
Na2O			0 45		0 15	0 50		0 43		0 25		0 58					0 56		0 65	0 43											0 53	
K2O			10 46	10 29	9 11	10 15	8 79	9 54	10 13	10 58	9 15	9 98	9 17	9 30	9 24	8 61	9 31	9 66	10 25	10 63	8 11	8 10							9 09	7 62	7 76	7 81
Total	100	100	96	96	96	96	96	96	96	96	96	96	96	96	96	96	96	96	96	96	96	96	100	100	100	100	100	100	96	96	96	96
Orig. total	100 19	101 83	94 85	98 55	91 45	93 79	93 38	93 61	93 80	93 72	97 34	94 26	92 31	93 93	92 34	91 21	92 57	95 42	93 58	90 91	95 64	93 20	96 47	95 38	97 01	96 47	95 14	96 70	92 01	92 07	87 67	
Si	2 939	2 955	6 246	5 863	5 255	6 174	5 281	5 990	6 008	6 145	5 456	6 149	5 290	5 453	5 310	5 439	6 013	5 469	6 124	9 130	5 629	5 505	1 013	1 015	1 008	1 002	1 013	1 011	5 361	6 620	5 452	
Ti	0 278				0 240																								0 247			
Al	3 678	2 032	2 038	4 672	3 850	5 554	3 931	5 298	5 002	5 444	3 983	5 561	3 901	4 183	3 904	3 880	5 529	4 302	5 690	5 657	3 778	4 463	1 949	1 948	1 977	1 963	1 947	1 984	3 830	4 601	5 545	
FeIII		0 088	0 050																				0 032	0 030	0 011	0 034	0 034					
FeII	3 601	2 453	2 440		3 706	0 286	3 839	0 974	1 266	0 455	3 399	0 330	3 883	3 233	3 840	4 042	0 643	3 064	0 198	0 218	3 463	2 926							3 563	0 862	1 834	
Fe*				1 859																												
Mn	0 007	0 236	0 305	0 022	0 044		0 122				0 088		0 123	0 076	0 124	0 116		0 041			0 077	0 048										
Mg	0 669	0 155	0 109	0 437	0 540	0 111	0 689	0 205	0 269	0 151	0 716	0 108	0 628	0 596	0 622	0 645	0 164	0 557	0 072	0 081	0 734	0 542							0 568	0 309	0 167	
Ca		0 094	0 100						0 023																					0 035		
Na					0 045	0 128		0 114		0 063		0 149					0 146		0 165	0 111			0 000	0 000	0 000	0 000	0 000	0 000			0 144	
K	1 869			1 894	1 854	1 715	1 776	1 667	1 803	1 808	1 813	1 689	1 861	1 927	1 872	1 752	1 597	1 884	1 726	1 796	1 596	1 552							1 811	1 297	1 407	
mg'	6 0	4 3	40 8	18 8	12 7	27 9	15 2	17 4	18 6	24 9	17 4	24 8	13 9	15 6	14 0	13 8	20 3	15 4	26 8	27 1	17 5	15 6							13 8	26 4	8 3	
al	25 3	24 9	84 6	37 5	18 7	82 3	18 8	59 9	50 3	74 6	20 5	80 9	18 0	23 2	18 1	18 1	70 1	24 8	87 5	86 2	20 3	29 3							19 6	58 0	49 9	
an																																

Suite	Boobyalla		Boobyalla															Boobyalla													
Sample #	62616 cont		62617															62618													
Mineral	SHA	SHA	AD	Bt	Bt	CL	MS	MS	MS	SHA	SHA	SHA	SHA	SHA	SHA	SHA	SHS	Bt	Bt	Bt	Bt	CL	MS	SHA	SHA	SHA	SHA	SHA	SHA	SHA	SHA
Type	ps,CD	ps,CD	mx	mx	mx	ps,CD	ps,AD	ps,AD	ps,AD	ps,CD	ps,CD	ps,CD	ps,CD	ps,CD	ps,CD	ps,CD	ps,CD	mx	mx	ph	ps,CD	ps,CD	ps,CD	ps,CD	ps,CD	ps,CD	ps,CD	ps,CD	ps,CD	ps,CD	ps,CD	ps,CD
Grain #	1	1	1	1	2	1	1	1	1	1	1	1	1	1	1	1	1	1	2	3	4	1	1	1	1	1	1	1	1	1	1	1
# analyses	1	1	1	3	2	1	1	1	1	1	1	1	1	1	1	1	1	5	3	2	1	1	1	1	1	1	1	1	1	1	1	1
Anal. name																																
SiO2	50 31	49 54	37 33	33 93	34 03	25 00	47 45	47 80	47 79	30 36	43 36	36 36	36 63	37 81	46 67	34 55		33 93	34 26	34 15	33 96	23 56	47 34	42 10	47 35	47 62	33 53	45 19	40 75	40 61	43 67
TiO2				2 37	2 19			0 32										2 34	1 54	1 95											
Al2O3	28 36	31 08	61 81	20 29	20 66	20 63	35 39	34 37	36 20	25 40	30 69	27 67	28 01	21 79	33 77	21 40		20 11	21 08	20 45	21 38	21 39	34 91	28 79	34 95	34 51	21 53	32 93	28 72	28 49	29 25
Fe2O3			0 86																												
FeO																															
FeO*	7 66	5 36		27 52	27 75	38 08	1 82	2 24	1 22	34 69	11 90	24 71	23 67	22 58	4 54	28 71		27 70	27 06	27 62	28 29	38 21	2 18	14 79	2 48	2 30	28 91	6 46	16 22	15 27	11 57
MnO						0 32				0 28								0 18		0 17	0 68	0 70			0 31		0 82		0 28	0 29	0 56
MgO	1 47	2 25		2 52	2 43	3 61	0 47	0 60	0 24	3 22	1 64	2 38	2 24	2 37	0 84	3 13		2 51	2 69	2 41	2 78	4 01	0 60	1 70	0 52	0 58	3 01	1 05	1 84	1 46	1 62
CaO	0 34	0 24																													
Na2O							0 33	0.31					0 27									0 50		0 37	0 37		0 24		0 24		
K2O	7 87	7 53		9 37	8 94	0 37	10 53	10 35	10 56	2 04	8 47	4 88	5 19	8 44	10 18	8 20		9 21	9 38	9 26	8 92	0 12	10 47	8 31	10 33	10 62	8 20	10 12	8 19	9 65	9 40
Total	96	96	100	96	96	88	96	96	96	96	96	96	96	96	96	96		96	96	96	96	88	96	96	96	96	96	96	96	96	96
Orig. total	93 49	87 54	103 59	98 78	98 79	91 03	98 16	98 02	93 85	92 32	98 21	94 18	93 93	95 56	98 63	96 16		93 56	93 65	94 66	93 01	86 18	92 17	90 77	92 94	93 27	91 58	90 32	91 90	92 84	91 51
Si	6 118	6 529	1 009	5 330	5 332	5 636	6 261	6 315	6 270	4 737	6 004	5 369	5 391	5 649	6 238	5 396		5 336	5 356	5 361	5 345	5 339	6 263	5 954	6 284	6 305	5 280	6 127	5 820	5 833	6 092
Ti				0 260				0 032										0 276	0 180	0 229											
Al	4 464	4 828	1 970	3 756	3 815	5 481	5 504	5 351	5 598	4 672	5 016	4 817	4 858	4 365	5 321	3 940		3 727	3 884	3 783	3 965	5 714	5 444	4 798	5 450	5 385	3 996	5 262	4 834	4 823	4 816
FeIII			0 017																												
FeII	0 855	0 591		3 615	3 636	7 179	0 200	0 247	0 133	4 526	1 379	3 051	2 912	2 821	0 507	3 750		3 643	3 538	3 626	3 724	7 242	0 240	1 748	0 274	0 254	3 807	0 732	1 937	1 834	1 351
Fe*																															
Mn						0 060				0 037								0 024		0 022	0 090	0 135		0 036			0 109		0 034	0 035	0 065
Mg	0 292	0 441		0 589	0 567	1 211	0 092	0 117	0 046	0 749	0 339	0 522	0 490	0 527	0 166	0 729		0 589	0 625	0 564	0 651	1 355	0 119	0 358	0 101	0 113	0 706	0 212	0 391	0 312	0 336
Ca	0 048	0 034																													
Na							0 085	0 080					0 075										0 128		0 095	0 095		0 064		0 066		
K	1 340	1 266		1 677	1 786	0 105	1 772	1 744	1 766	0 405	1 497	0 919	0 974	1 608	1 736	1 633		1 848	1 870	1 854	1 790	0 035	1 766	1 499	1 743	1 793	1 646	1 750	1 492	1 767	1 675
mg	25 5			14 0	13 5	14 4	31 5	32 2	25 6	14 2	19 7	14 6	14 4	15 8	24 8	16 3		13 9	15 0	13 5	14 9	15 8	33 1	17 9	27 1	30 9	15 6	22 5	16 8	14 5	19 9
al	56 9			16 3	19 4	24 1	86 2	82 8	91 4	28 6	50 6	35 3	35 9	29 2	72 7	20 5		18 1	19 5	18 6	19 6	24 5	83 1	43 5	82 8	82 6	20 3	64 6	41 4	40 6	47 2
an																															

Suite	Boobyalla									Boobyalla																					
Sample #	62618 cont									62619																					
Mineral	SHA	SHA	SHA	SHA	SHA	SHA	SHA	SHA	SHA	AD	Bt	Bt	AP	AP	Bt	Bt	CL	MS	MS	MS	MS	PL	PL	PL	PL	PL	PL	PL	PL	PL	PL
Type	ps,CD	ps,CD	ps,CD	ps,CD	ps,CD	ps,CD	ps,CD	ps,CD	ps,CD	ph	in,QZ	rim	in Bt	in Bt	ph	ps,OP	ps,CD	ps,AD	ps,AD	ps,AD	ps,AD	ph,co	ph,rim	ph	ph	ph	ph	ph	ph	ph	ph
Grain #	1	1	1	1	1	1	1	1	1	1	1	2	1	2	3	4	1	1	1	1	1	1	1	2	2	2	2	2	2	2	2
# analyses	1	1	1	1	1	1	1	1	1	2	1	3	1	1	2	2	3	1	1	1	1	1	1	1	1	1	1	1	1	1	1
Anal. name																								0 00	0 01	0 05	0 10	0 20	0 40	0 60	0 80	1 00
SiO2	33 49	33 64	42 31	31 27	47 57	33 06	47 76	47 53	45 81	37 55	33 91	34 02			33 73	34 14	23 61	48 10	47 09	47 08	47 78	58 21	58 63	67 69	65 96	66 06	65 19	62 52	58 86	58 98	58 63	58 57
TiO2											2 81	2 83			2 84	2 63																
Al2O3	22 18	21 39	28 15	22 04	34 94	21 81	34 26	34 43	34 15	62 12	19 89	20 09			19 95	19 70	20 20	34 94	36 98	37 94	35 69	27 06	20 39	20 70	21 86	21 80	22 45	24 22	26 52	26 74	26 73	26 78
Fe2O3										0 32																						
FeO																																
FeO*	29 16	29 16	15 67	33 45	1 97	22 61	2 53	2 83	5 28		27 18	27 24	0 92	0 33	27 37	27 79	40 06	1 74	0 92	0 54	1 67											
MnO	0 73	0 73	0 24	0 91		0 70						0 08	0 86	0 29			0 46															
MgO	3 19	3 12	1 81	3 35	0 50	3 04	0 67	0 54	0 78		2 88	2 57	0 18		2 75	2 53	3 67	0 38			0 25											
CaO													53 66	54 86								8 51	0 47	0 92	2 27	2 33	2 76	5 36	8 29	8 03	8 42	8 52
Na2O																		0 31	0 35			6 04	10 26	10 54	9 72	9 58	9 41	7 72	6 18	6 32	6 02	5 88
K2O	7 26	7 96	7 52	4 98	10 76	7 78	10 78	10 66	9 62		9 34	9 17	42 40	42 52	9 36	9 21		10 53	10 66	10 44	10 61	0 17	0 25	0 14	0 19	0 23	0 20	0 19	0 15	0 19	0 21	0 25
Total	96	96	96	96	96	96	96	96	96	100	96	96	98	98	98	98	88	96	96	96	96	100	100	100	100	100	100	100	100	100	100	100
Orig. total	91 27	92 27	89 75	88 46	93 59	89 70	91 96	92 00	93 01	101 64	95 82	96 63	99 91	99 11	90 38	86 40	85 62	93 96	94 59	92 79	94 18	98 84	97 25	103 93	101 53	101 96	102 17	99 45	98 78	99 58	100 36	99 20
Si	5 241	5 292	6 017	4 969	6 289	5 212	6 326	6 302	6 142	1 013	5 322	5 332			5 302	5 367	5 405	6 336	6 186	6 153	6 286	2 596	2 985	2 955	2 891	2 895	2 861	2 864	2 622	2 627	2 613	2 611
Ti											0 331	0 333			0 335	0 310																
Al	4 091	3 966	4 685	4 129	5 443	4 053	5 349	5 381	5 398	1 975	3 678	3 711			3 696	3 650	5 450	5 425	5 726	5 843	5 534	1 422	1 045	1 065	1 129	1 126	1 161	1 307	1 393	1 390	1 404	1 407
FeIII										0 006																						
FeII	3 816	3 837	1 850	4 445	0 217	3 904	0 279	0 313	0 592		3 567	3 571			3 597	3 653	7 671	0 191	0 101	0 058	0 184		2 985									
Fe*													0 129	0 046																		
Mn	0 096	0 097	0 028	0 122		0 092						0 010	0 122	0 041			0 089						1 045									
Mg	0 743	0 732	0 380	0 794	0 099	0 714	0 131	0 107	0 156		0 672	0 601	0 045		0 644	0 591	1 252	0 074			0 500											
Ca													9 647	9 843								0 406	0 022	0 043	0 107	0 109	0 130	0 263	0 396	0 383	0 402	0 407
Na					0 065				0 091									0 078	0 087			0 522	0 865	0 892	0 826	0 814	0 800	0 686	0 534	0 546	0 520	0 520
K	1 448	1 597	1 354	1 010	1 814	1 565	1 822	1 803	1 645		1 869	1 833	6 023	6 029	1 876	1 846		1 770	1 785	1 740	1 781	0 009	0 013	0 008	0 011	0 013	0 011	0 011	0 009	0 011	0 012	0 012
mg'	16 3	16 0	17 1	15 2	31 3	15 5	32 0	25 5	20 9		15 9	14 4			15 2	13 9	14 0	27 9	0 2	0 3	21 4											
al	22 1	20 2	42 4	22 5	84 9	20 9	81 1	81 0	71 0		17 6	18 3			17 7	17 5	23 2	87 1	95 0	97 2	88 9											
an																						43 8	2 5	4 6	11 5	11 9	14 0	27 7	42 6	41 3	43 6	43 6

Suite	Boobyalla																								Boobyalla							
Sample #	62619 cont																								62625							
Mineral	PL	PL	PL	PL	PL	PL	PL	PL	PL	PL	PL	PL	PL	PL	PL	PL	PL	PL	SHA	SHA	SHA	SHA	SHA	SHA	Bt	Bt	Bt	Bt	MS	PL	PL	PL
Type	ph	ph	ph	ph	ph	ph	ph	ph	ph	ph	ph	ph	ph	ph	ph	ph	ph	ph	ps CD	ps CD	ps CD	ps CD	ps CD	ps CD	in,QZ	in,QZ	in,QZ	ph		ph	ph	ph
Grain #	2	2	2	2	2	2	2	2	2	2	2	2	2	2	2	2	2	2	1	1	1	1	1	1	1	2	3	4	1	1	1	1
# analyses	1	1	1	1	1	1	1	1	1	1	1	1	1	1	1	1	1	1	1	1	1	1	1	1	2	2	2	7	7	1	1	1
Anal. name	1 40	1 80	2 00	2 20	2 60	2 80	3 20	3 60	4 00	4 40	4 80	5 00	5 10	5 15	5 20	5 30	5 36													0 00	0 22	0 72
SiO2	58 57	56 95	57 36	57 92	58 36	59 29	58 87	57 26	57 35	58 54	60 36	60 84	62 54	62 63	63 50	63 64	65 13	46 20	37 72	46 63	45 91	45 53	46 88	35 23	36 30	34 04	34 91	47 68	66 72	64 78	62 86
TiO2																								1 36	1 69	2 87	2 80	0 17				
Al2O3	26 69	27 55	27 63	26 98	26 84	26 49	26 41	26 62	27 70	26 80	25 43	25 36	24 23	24 23	23 40	23 28	22 87	33 19	27 95	35 12	22 02	31 31	34 27	20 52	20 18	18 83	19 65	32 50	21 26	22 43	23 85
Fe2O3																																
FeO																																
FeO*																		4 57	21 44	2 75	21 68	7 90	3 05	27 27	25 29	27 56	27 04	4 28				
MnO																								0 52	0 56	0 32	0 53					
MgO																		1 08	2 46	0 67	1 85	1 22	0 86	1 85	2 76	3 26	2 00	0 76				
CaO	8 43	10 28	8 94	9 14	8 80	7 31	8 44	7 93	8 26	8 16	6 82	6 28	4 92	4 59	4 04	3 99	1 68												1 44	3 16	4 52
Na2O	6 09	4 97	5 97	5 75	5 73	6 58	5 99	5 86	6 41	6 26	7 08	7 30	8 02	8 30	8 81	8 83	8 99	0 69	0 65	0 34	0 34	0 35	0 34					0 32	10 02	9 22	8 45
K2O	0 21	0 25	0 10	0 21	0 28	0 33	0 28	0 33	0 28	0 24	0 32	0 22	0 28	0 24	0 25	0 25	1 32	10 27	5 78	10 49	4 19	9 70	10 58	9 24	9 23	9 12	9 07	10 29	0 56	0 40	0 31
Total	100	100	100	100	100	100	100	100	100	100	100	100	100	100	100	100	100	96	96	96	96	96	96	96	96	96	96	96	100	100	100
Orig. total	100 38	94 88	106 17	99 71	100 22	95 44	99 85	99 87	104 80	98 19	97 65	100 42	100 72	102 07	100 06	101 40	100 64	91 58	89 20	92 54	90 64	93 13	94 62	96 27	94 95	94 75	95 34	96 62	97 10	99 35	99 53
Si	2 612		2 564	2 588	2 604	2 638	2 624	2 552	2 564	2 610	2 682	2 697	2 762	2 765	2 801	2 806	2 862	6 207	5 504	6 192	6 531	6 208	6 240	5 509	5 606	5 361	5 462	6 370	2 922	2 851	2 777
Ti		2 551																						0 159	0 196	0 339	0 329	0 017				
Al	1 403	1 455	1 455	1 421	1 411	1 389	1 388	1 503	1 460	1 408	1 332	1 325	1 261	1 260	1 216	1 210	1 185	5 256	4 806	5 496	3 691	5 031	5 376	3 782	3 674	3 494	3 623	5 118	1 098	1 163	1 242
FeIII																																
FeII																		0 513	2 616	0 305	2 579	0 900	0 339	3 566	3 266	3 630	3 538	0 478				
Fe*																																
Mn																								0 068	0 072	0 043	0 070					
Mg																		0 216	0 536	0 133	0 393	0 247	0 171	0 432	0 635	0 765	4 670	0 150				
Ca	0 403	0 493	0 428	0 438	0 421	0 348	0 403	0 379	0 396	0 390	0 325	0 298	0 233	0 217	0 191	0 189	0 079												0 068	0 149	0 214
Na	0 527	0 432	0 517	0 498	0 495	0 568	0 518	0 506	0,556	0 541	0,610	0 628	0 687	0 711	0,754	0 755	0 766	0 180	0 120	0 088	0 093	0 092	0 089					0 082	0 851	0 787	0 724
K	0 012	0 014	0 008	0 012	0 016	0 019	0 016	0 019	0 016	0 014	0 018	0 012	0 016	0 014	0,014	0 014	0 074	1,760	1,075	1 776	1,761	1,687	1,796	1 843	1,818	1 832	1,810	1 754	0 031	0,022	0 017
mg'																		29 6	17 0	30 4	13 2	21 5	33 5	10 8	16 3	17 4	11 7	23 9				
al																		69 4	36 0	80 5	32 3	58 6	77 4	19 2	18 9	15 8	18 2	72 3				
an	43 3	53 3	45 3	46 8	45 9	38 1	43 7	42 8	41 6	41 9	34 8	32 2	25 3	23 4	20 2	20 0	9 4												7 3	16 0	22 8

Suite	Boobyalla										Boobyalla																			
Sample #	62625 cont										62634																			
Mineral	PL	PL	PL	PL	PL	PL	PL	PL	PL	PL	Bt	Bt	CD	GA	GA	GA	GA	GA	IL	MS	SHA	SHA	SHA	SHA	SHA	SHA	SHA	SHA	SHA	SHA
Type	ph	ph	ph	ph	ph	ph	ph	ph	ph	ph	ps,OP	ps,CD	ph	ph	ph	ph	ph,co	ph,rim	ps,OP	ps,CD	ps,CD	ps,CD	ps,CD	ps,CD	ps,CD	ps,CD	ps,CD	ps,CD	ps,CD	ps,CD
Grain #	1	1	1	1	1	1	1	1	1	1	1	2	1	1	1	1	1	1	1	1	1	1	1	1	1	1	2	2	2	2
# analyses	1	1	1	1	1	1	1	1	1	1	8	2	8	1	1	1	1	1	3	3	1	1	1	1	1	1	1	1	1	1
Anal name	0 92	1 24	1 48	2 01	2 50	2 96	3 16	3 36	3 60	3 92																				
SiO2	63 97	59 79	58 33	58 60	59 96	59 70	62 99	64 47	63 54	63 78	34 12	32 92	45 75	36 27	36,72	369 78	37,01	36,17		46,44	42 71	42,97	42,52	41,32	33 74	39,20	43 76	37 11	33 51	34 68	33,43	46 72
TiO2											3 08								53 08											
Al2O3	23 05	25 94	26 66	26 87	25 75	25 78	23 69	22 77	23 44	23 28	19 34	20 78	32 42	21,71	21 69	21 81	21 80	21 53		36 67	30 51	30 43	29 93	29 81	21 90	28 05	31 21	21 54	21 99	22 82	21 58	38 01
Fe2O3														0 21				0 23												
FeO														37 00	37 13	36 60	36 11	36 75	44 81											
FeO*											26 90	29 71	15 74							1 54	10 76	10,66	11 40	13 44	27 95	16 15	8 90	24 03	27 61	25 57	27 65	1 67
MnO											0 23	0 42	0 80	2 22	1 56	1 46	1 29	3 09	2 11				0 19		0 35	0 34		0 71	0 59	0 60	0 69	
MgO											2 99	3 04	2 16	1 62	1 96	2 05	2 51	0 99		0 62	1 75	1,78	1 68	1 85	3 15	2 14	1 56	2 94	3 45	3 43	3 51	0 46
CaO	3 66	7 27	8 73	8 48	6 98	7 36	4 66	3 41	4 19	3 87	0 24			0 97	0 94	1 30	1 28	1 31			0 11		0 12			0 13	0 12	0 13			0 58	
Na2O	8 98	6 79	6 07	6 06	6 99	6 89	8 26	9 04	8 58	8 84	0 07		1 04							0 84	0 15	0 28	0 35	0 16		0 35	0 21	1 88				1 88
K2O	0 34	0 20	0 22		0 32	0 29	0 38	0 32	0 26	0 22	9 02	9 13	0 08							9 89	10 02	9 88	9 82	9 42	8 93	9 63	10 25	7 65	8 85	8 91	8 57	7 26
Total	100	100	100	100	100	100	100	100	100	100	96	96	98	100	100	100	100	100	100	96	96	96	96	96	96	96	96	96	96	96	96
Orig total	99 83	99 08	99 66	98 98	98 94	99 95	99 71	99 10	100 09	99 78	95 43	93 23	99 62	101 96	102 68	102 93	101 55	101 03	95 76	97 61	97 90	98 79	98 39	96 55	95 33	96 36	97 82	97 86	95 44	94 73	94 94	95 50
Si	2 819	2 658	2 604	2 610	2 666	2 658	2 782	2 837	2 801	2 810	5 350	5 243	4 932	2 952	2 975	2 974	2 981	2 955		6 116	5 962	5 988	5 963	5 846	5 292	5 688	6 042	5 660	5 255	5 358	5 252	6 076
Ti											0 363								2,011												
Al	1 197	1 359	1 403	1 410	1 350	1 352	1 233	1 181	1 218	1 209	3 575	3 900	4 120	2 082	2 071	2 078	2 070	2 074		5 691	5 019	4 997	4 947	4 970	4 049	4 798	5 079	3 872	4 064	4 156	3 995	5 825
FeIII														0 013				0 014													
FeII											3 527	3 956	1 419	2 518	2 516	2 474	2 432	2,511	1 887	0 170	1 255	1 242	1 336	1 590	3 666	1 959	1 027	3 065	3 621	3 304	3 632	0 181
Fe*																																
Mn											0 030	0 057	0 072	0 152	0 107	0 099	0 088	0 209	0 090				0 022					0 091				
Mg											0 698	0 721	0 347	0 196	0 236	0 247	0 301	0 120		0 121	0 363	0 369	0 350	0 390	0 797	0 463	0 321	0 669	0 806	0 788	0 821	0 089
Ca	0 173	0 348	0 418	0 405	0 333	0 351	0 220	0 161	0 198	0 183	0 040			0 084	0 082	0 112	0 110	0 114			0 016		0 017			0 020	0 017	0 020			0 097	
Na	0 767	0 585	0 525	0 523	0 603	0 595	0 709	0 771	0 733	0 755	0 021		0 218							0 213	0 039	0 076	0 095	0 043		0 098	0 055	0 557				0 474
K	0 019	0 012	0 013		0 018	0 016	0 022	0 018	0 015	0 013	1 805	1 855	0 010							1 662	1 782	1 756	1 755	1 699	1 787	1 783	1 804	1 448	1 771	1 755	1 718	1 204
mg											16 5	15 4	19 7	7 2	8 6	9 1	11 0	4 6		41 6	22 4	22 9	20 8	19 7	16 2	19 1	23 8	17 9	18 2	19 3	18 4	33 0
al											16 4	17 8	51 4	25 1	25 0	24 7	24,7	24,7		86 8	49 4	49 5	47 2	44 9	20 3	36 9	54 1	18 9	20 3	22 3	18 6	88 5
an	18 4	37 1	44 3	43 6	35 6	37 1	23 7	17 2	21 2	19 5																						

Suite	Boobyalla																Boobyalla															
Sample #	67536																68523															
Mineral	Bt	Bt	GA	GA	GA	MS	PL	SHA	SHA	SHA	SHA	SHA	SHA	SHA	SHA	SHA	AD	Bt	Bt	Bt	Bt	Bt	Bt	Bt	Bt	Bt	Bt	Bt	Bt	Bt	Bt	B
Type	ph	ps CD	ps Bt	ps Bt co	ps Bt rim	ps CD	co	ps,CD	ps,CD	ps,CD	ps,CD	ps,CD	ps,CD	ps,CD	ps,CD	ps,CD	ph	in,AF	ps OP,co	ln AFI	ln Af,co	ln AF,rim	ph	ph	ph	ph	ph,rim	ph	ph	ph	ph	ph
Grain #	1	2	1	1	1	1	1	1	1	1	1	1	1	1	1	1	1	1	2	3	3	3	4	4	4	4	4	4	5	5	5	5
# analyses	5	1	1	1	1	1	1	1	1	1	1	1	1	1	1	1	2	1	1	1	1	1	1	1	1	1	1	1	1	1	1	1
Anal name																																
SiO2	34 50	34 14	36 59	35 97	36 32	47 01	60 52	46 92	33 74	33 38	42 68	45 31	46 93	39 35	40 20	36 90	35 69	35 99	35 58	35 21	35 95	34 80	34 74	34 61	35 02	34 86	34 58	34 80	34 99	34 64	34 70
TiO2	2 19																3 00	3 60	3 05	3 04	3 09	2 47	2 13	2 00	2 19	2 04	1 54	3 34	3 28	3 37	3 18
Al2O3	19 96	21 53	21 13	21 14	21 17	35 08	25 42	35 39	21 65	21 66	31 45	28 34	35 54	28 18	28 70	62 73	19 68	18 48	19 56	19 51	19 25	19 70	20 14	20 21	19 77	20 09	20 40	19 43	19 32	19 32	19 48
Fe2O3				1 54	0 18												0 36														
FeO			37 04	36 40	35 92																										
FeO*	26 92	26 84				2 47		2 17	27 08	27 44	10 02	10 72	2 13	15 88	14 91		24 06	25 39	24 43	24 93	24 12	27 38	27 06	27 54	27 09	26 88	27 20	26 37	26 32	26 78	26 72
MnO	0 06	0 72	3 17	2 46	4 69				0 82	0 89				0 40	0 35								0 22				0 25				
MgO	3 09	3 47	1 44	1 87	1 11	0 77		0 65	3 50	3 35	1 37	1 51	0 58	2 22	1 91		4 49	3 63	4 27	4 11	4 53	2 98	3 14	3 05	3 19	3 11	3 17	2 98	2 98	2 84	2 94
CaO			0 63	0 62	0 61		6 31																								
Na2O	0 01					0 54	7 55	0 55			0 64	1 30	0 52	0 38	0 43												0 23		0 21			
K2O	9 21	9 30				10 13	0 19	10 31	9 21	9 28	9 85	8 42	10 30	9 57	9 51		9 08	8 92	9 11	9 20	9 07	8 67	8 57	8 60	8 73	8 79	8 87	8 87	9 09	9 05	8 98
Total	96	96	100	100	100	96	100	96	96	96	96	96	96	96	96	100	96	96	96	96	96	96	96	96	96	96	96	96	96	96	96
Orig total	94 49	94 05	100 91	101 70	103 23	94 87	98 51	94 56	92 87	92 98	94 03	93 80	93 35	95 07	94 43	99 34	99 20	95 50	95 98	93 74	95 46	94 63	96 93	94 93	94 54	96 08	93 09	97 20	96 18	96 91	97 58
Si	5 395	5 346	2 986	2 936	2 973	6 221	2 687	6 207	5 295	5 258	5 932	6 269	6 204	5 697	5 771	0 996	5 479	5 560	5 476	5 442	5 520	5 429	5 411	5 399	5 453	5 429	5 400	5 417	5 446	5 408	5 411
Ti	0 258																0 346	0 418	0 353	0 353	0 356	0 289	0 249	0 234	0 256	0 238	0 180	0 390	0 384	0 395	0 372
Al	3 679	3 972	2 032	2 033	2 042	5 472	1 330	5 517	4 003	4 021	5 152	4 621	5 538	4 809	4 856	1 997	3 562	3 364	3 549	3 554	3 483	3 622	3 697	3 715	3 628	3 688	3 754	3 564	3 544	3 554	3 580
FeIII				0 094	0 011											0 007															
FeII	3 520	3 514	2 528	2 484	2 458	0 273		0 240	3 554	3 615	1 164	1 240	0 235	1 923	1 790		3 089	3 281	3 144	3 223	3 096	3 572	3 524	3 593	3 528	3 500	3 553	3 432	3 426	3 496	3 484
Fe*																															
Mn	0 008	0 096	0 219	0 170	0 325				0 108	0 118				0 049	0 042								0 028				0 032				
Mg	0 719	0 810	0 174	0 226	0 135	0 151		0 128	0 819	0 785	0 283	0 312	0 113	0 479	0 409		1 027	0 835	0 979	0 946	1 035	0 693	0 728	0 710	0 740	0 721	0 737	0 692	0 692	0 661	0 683
Ca			0 055	0 054	0 053		0 300					0 059																			
Na	0 015					0 137	0 650	0 140			0 173	0 348	0 134	0,107	0 118											0,069		0 062			
K	1,838	1 857				1 710	0 010	1 740	1 843	1,865	1 747	1,486	1,737	1 768	1 741		1 777	1 757	1 789	1 813	1,776	1,726	1 702	1,710	1 734	1,747	1,766	1 761	1 805	1 803	1 786
mg	17 0	18 7	6 5	8 4	5 2	35 7		34,8	18 7	17 8	19 6	20 1	32 5	20 0	18 6		25 0	20 3	23 8	22 7	25 1	16 3	17 1	16 5	17 3	17 1	17 0	16 8	16 8	15 9	16 4
al	17 7	19 3	24 7	26 0	25 0	81 0		83 2	19 4	19 3	52 7	46 2	84 0	37 4	40 1		17 8	16 3	17 6	17 3	17 1	18 2	18 9	18 9	18 2	12 1	18 7	17 4	17 4	17 4	17 7
an							31 6																								

Suite	Boobyalla							Boobyalla							Boobyalla							Boobyalla											
Sample #	68523 cont							68524							68525							68529											
Mineral	SHA	SHA	SHA	SHA	SHA	SHA	SHA	Bt	GA	GU	GU	GU	GU	GU	Bt	Bt	GA	GA	PL	AP	AP	Bt	Bt	Bt	Bt	GA	GA	GA	GA	PL	PL
Type	ps,CD	ps,CD	ps,CD	ps,CD	ps,CD	ps,CD	ps,CD	ph	ph	in GA	in GA	in GA	in GA	in GA	in GA	ph	ph	ph,rm	ph,co	co,in Bt	rm,in Bt	ph	ph	ps,OP,co	ps,OP,rm	ph	ph,co	ph,rm	ph	ph,co	ph,co	ph,co
Grain #	2	2	2	2	2	2	2	1	1	1	1	1	1	1	1	3	1	1	1	1	1	1	1	2	2	1	1	1	2	1	2
# analyses	1	1	1	1	1	1	1	2	4	2	1	1	1	1	1	1	1	1	1	1	1	1	1	1	1	1	1	1	1	2	2
Anal name															pair 1	pair 2	pair 1	pair 2													
SiO2	49 63	33 13	49 18	49 07	50 42	33 71	48 89	34 10	36 45	49 97	49 87	49 29	49 35	49 21	35 23	34 95	35 50	34 41	57,77			35 37	35 73	38 55	35,65	36 65	36,73	36 49	37 05	57 64	58 11
TiO2								2 55							2 14	3 92						1 64	3,73	1,11	2,17						
Al2O3	32 34	20 98	32 09	32 22	31 44	21,84	25 98	18 64	21 26	0 65	0 73		2 16	0 41	18 46	18 39	21 19	20 22	27 11			17 56	16 02	14 20	15,77	21 33	21 68	21 18	21 36	27 02	26,78
Fe2O3									0 47		1 34			1 08												1 54	1 42	1 55				
FeO									36 07		39 92			41 57			35 41	36 51								34 21	33 98	34 89	35 21			
FeO*	3 88	30 20	4 37	4 64	5 38	28 57	10 91	29 44		40 87		45 45	41 63		24 44	23 80					0 32	24 74	24 35	20 07	24 49							
MnO		0 27							1 53	0 46	0 56	0 81	0 51	0 47		0 19	5 64	6 73								1 13	1 27	1 46	1 27			
MgO	1 12	4 45	1 14	0 94	0 70	3 78	1 59	2 39	2 40	6 05	6 27	2 44	4 19	5 24	5 83	5 14	0 88	0 57				7 76	7 36	13 09	8,10	3 78	3 96	3 16	3 84			
CaO			0 17				0 80		1 31				0 16				1 37	1 52	8,06	55 45	55 36					1 35	1 25	1 27	1 28	8 73	8 18	
Na2O							1 51				0 31				0 44	0 10			6,58											6 18	6 70	
K2O	9 03	6 98	9 04	9 12	8 06	8 10	6 32	8 87							8 46	9 51			0,19	42 55	42 32	8 92	8 81	8 99	8,81					0 39	0 24	
Total	96	96	96	96	96	96	96	96	100	98	98	98	98	98	96	96	100	100	100	98	98	96	96	96	96	100	100	100	100	100	100	
Orig total	97 35	91 66	93 54	86 61	83 97	92 80	84 37	97 43	102 64	99 00	98 69	98 69	92 91	96 95	98 36	97 89	102 93	97 56	101 39	99 57	99 10	100 79	100 40	101 61	101,67	106 49	107 98	107 27	105 90	99 07	98 83	
Si	6 534	5 209	6 502	6 495	6 637	5 270	6 658	5 403	2 954	7 943	7 898	8 044	7 872	7,895	5 462	5 407	2 925	2 882	2 583			5 472	5 522	5 813	5 518	2 943	2 942	2 945	2 974	2 581	2 597	
Ti								0 304							0 249	0 456						0 190	0 433	0 125	0 369						
Al	5 017	3 888	5 000	5 626	4 878	4 023	4 169	3 481	2 031	0 122	0 137		0 406	0 078	3 373	3 353	2 058	1 996	1 428			3 202	2 917	2 524	2 876	2 019	2 047	2 015	2 021	1 426	1 411
FeIII									0 059		0 159			0 131												0 093	0 067	0 094	2 364			
FeII	0 426	3 970	0 483	0 514	0 592	3 735	1 242	3 901	2 445	5 434	5 155	6 203	5 553	5 577															0 460			
Fe*															3 169	3 079	2 440	2 557			0 045											
Mn		0 036							0 102	0 061	0 074	0 112	0 068	0 064		0 025	0 394	0 478								0 077	0 086	0 099	0 110	0 419		
Mg	0 220	1 043	0 224	0 185	0 136	0 879	0 323	0 565	0 290	1 433	1 479	0 594	0 995	1 253	1 347	1 186	0 108	0 071				1 789	1 696	2 941	1 869	0 452	0 472	0 380		0 537		
Ca			0 024				0 116		0 114				0 027				0 121	0 136	0 400	9 937	9 942					0 116	0 107	0 109		0 022	0 392	
Na							0 399				0 094				0 132	0 030			0 570												0 581	
K	1 517	1 399	1 524	1 540	1 353	1 615	1 097	1 792							1 871	1 877			0 011	6 025	6 005	1 761	1,736	1 730	1 739						0 014	
mg	34 1	20 8	31 7	26 6	18 8	19 1	20 3	12 7	10 6	20 9	22 3	8 7	15 2	18 3	29 8	27 6	3 7	2 3				35 9	35,0	53 8	37 1	16,4	17 2	13 9	16 5			
al	73 0	19 8	70 8	71 3	70 7	20 7	43 8	15 9	24 7	0 9	1 5		2 6	1 5	13 2	14 4	23 6	21 7				12 6	10,9	6 8	10 1	25 0	25 1	25 0	24 4			
an																			41 3											43 8	40 3	

Suite	Boobyalla																																
Sample #	68523 cont																																
Mineral	Bt	Bt	Bt	Bt	Bt	Bt	Bt	Bt	Bt	Bt	Bt	Bt	Bt	Bt	Bt	GA	GA	GA	GA	GA	GA	GA	GA	GA	GA	GA	GA	GA	GA	SHA	SHA	SHA	SHA
Type	ph,rm	ph,co	ph	ph	ph,rm	ph,co	ph,co	ph,rm	ps,GA	ps,GA	ps,OP	ps,OP	ps,OP	ps,rm,OP	ph	ph	ph	ph	ph	ph	ph,co	ph	ph	ph	ph	ph	ph,rm	ph,co	ps,CD	ps,CD	ps,CD	ps,CD
Grain #	5	5	6	6	6	7	7	7	8	8	9	9	9	9	1	1	1	1	1	1	1	2	2	2	2	2	2	3	3	1	1	2	2
# analyses	1	1	1	1	1	1	1	1	1	1	1	1	1	1	1	1	1	1	1	1	1	1	1	1	1	1	1	1	1	2	5	1	1
Anal name																																	
SiO2	34 37	35 03	34 84	34 71	34 60	34 93	35 26	34 97	35 30	35 98	36 19	36 04	36 11	35 16	36 78	36 99	36 75	37 08	36 62	37 01	36 78	36 35	36 70	36 94	36 84	36 82	36 37	36 22	47 50	49 21	49 61	34 47
TiO2	2 98	3 16	3 19	2 99	2 88	2 32	2 28	1 90	1 09	1 44	2 54	3 78	3 10	2 32																			
Al2O3	19 22	19 61	19 80	19 38	19 36	20 01	20 43	19 87	20 55	20 20	19 70	18 18	18 59	20 07	21 40	21 50	21 28	21 46	21 43	21 42	21 62	21 37	21 70	21 54	21 57	21 57	21 49	21 58	35 14	32 95	32 35	21 46
Fe2O3																0 26				0 19	0 74	0 51	0 40	0 33		0 66		0 23				
FeO															37 27	35 74	37 10	36 36	36 19	35 98	35 17	36 58	36 07	35 62	36 49	35 29	36 75	36,81				
FeO*	27 53	25 88	26 33	26 90	27 24	26 86	26 59	27 33	26 79	25 92	24 78	25 35	25 62	25 96															2 17	4 89	4 18	27 18
MnO									0 23						1 25	0 99	1 85	0 95	3 94	1 01	0 96	2 28	1 07	0 96	1 33	0 99	3 51	2 70				0 24
MgO	2 84	3 14	2 88	2 94	3 00	2 87	2 68	3 05	3 28	3 30	3 81	3 64	3 71	3 67	2 20	3 40	1 86	3 09	0 84	3 25	3 53	1 68	3 06	3 36	2 51	3 49	0 63	1 26	0 75	0 88	1 00	4 17
CaO															1 10	1 11	1 16	1 05	0 97	1 13	1 20	1 23	0 99	1 25	1 27	1 18	1 24	1 14		0 20		
Na2O		0 26				0 24																							0 82			
K2O	9 05	8 93	8 95	9 08	8 91	8 78	8 76	8 89	8 76	9 15	8 98	9 02	8 87	8 82															9 62	7 87	8 86	8 48
Total	96	96	96	96	96	96	96	96	96	96	96	96	96	96	100	100	100	100	100	100	100	100	100	100	100	100	100	100	96	96	96	96
Orig total	94 26	93 16	98 66	94 96	95 25	96 81	100 63	97 10	92 81	89 99	94 53	94 80	93 79	96 44	99 73	99 70	99 53	99 66	99 56	99 57	99 53	99 38	99 60	100 01	99 40	99 73	99 65	99 70	90 49	91 70	92 17	95 19
Si	5 392	5 436	5 416	5 421	5 409	5 438	5 467	5 456	5 483	5 563	5 562	5 573	5 580	5 443	2 980	2 973	2 985	2 985	2 988	2 978	2 954	2 959	2 957	2 969	2 976	2 958	2 975	2 955	6 257	6 471	6 533	5 361
Ti	0 352	0 368	0 313	0 351	0 338	0 271	0 265	0 222	0 126	0 167	0 293	0 439	0 360	0 270																		
Al	3 553	3 558	3 628	3 567	3 568	3 672	3 734	3 654	3 762	3 682	3 568	3 313	3 385	3 662	2 043	2 036	2 037	2 036	2 061	2 031	2 047	2 050	2 060	2 040	2 053	2 043	2 071	2 075	5 456	5 103	5 021	3 934
FeIII																0 015				0 011	0 044	0 031	0 024	0 020		0 040		0 014				
FeII	3 611	3 359	3 423	3 514	3 562	3 498	3 447	3 566	3 479	3 352	3 184	3 277	3 311	3 361	2 526	2 402	2 520	2 448	2 470	2 421	2 362	2 490	2 430	2 394	2 465	2 371	2 513	2 515	0 239	0 537	0 460	3 535
Fe*																																
Mn									0 029						0 086	0 067	0 127	0 065	0 272	0 069	0 065	0 157	0 073	0 065	0 090	0 067	0 243	0 186				0 031
Mg	0 664	0 725	0 667	0 684	0 700	0 665	0 619	0 708	0 759	0 759	0 872	0 837	0 853	0 847	0 265	0 407	0 225	0 370	0 102	0 390	0 422	0 203	0 367	0 402	0 301	0 417	0 077	0 153	0 147	0 172	0 198	0 965
Ca															0 095	0 095	0 100	0 090	0 085	0 097	0 102	0,107	0 085	0 107	0 109	0 101	0 109	0 100		0 028			
Na		0 078				0 071																							0 208			
K	1 811	1 767	1 775	1 808	1,777	1 743	1 732	1 769	1 735	1 805	1 759	1 779	1 749	1,741															1 617	1 320	1 489	1 682
mg'	15 5	17 8	16 3	16,3	16 4	16 0	15 2	16 6	17 9	18 5	21 5	20 4	20,5	20 1	9 5	14 5	8 2	13 2	4 0	13 9	15 2	7 6	13 1	14 4	10 9	15 0	3 0	5 8	38 2	24 3	29 9	21 5
al	16 9	17 6	18 5	17 3	17 4	18 2	19 8	18 1	19 2	18 6	18 2	15 7	16,4	18,6	24 4	24 4	24 2	24 3	24 9	24 3	24 9	24 7	25 0	24 4	24 3	24 8	24 6	24 9	82 4	72 4	72 9	19 9
an																																

H.9

Suite	Boobyalla	Boobyalla						Boobyalla			Boobyalla/Pormena Hybrid				Gardens						Lady Barron	Lady Barron									
Sample #	68529 cont	68546						68548			62614				62578						62638		62640								
Mineral	TM	Bt	Bt	SHS	SHS	SHS	SHS	Bt	CD	MS	Bt	Bt	Bt	CD	HB	PL	PL	PL	PL	Bt	GA	PL	PL	PL	PL	PL	PL	PL	PL	PL	PL
Type	ps,OP	matrix	ph	ps,CD	ps,CD	ps,CD	ps,CD	ph	ph	ps,AD	in OZ	matrix	MYRM	ph	ph	ph,co	ph,rm	ph,rm	ph,co	ps,GA	ph	ph	ph	ph	ph	ph	ph	ph	ph	ph	ph
Grain #	1	1	2	1	1	1	1	1	1	1	1	2	3	1	1	1	1	2	2		1	0	1	1	1	1	1	1	1	1	1
# analyses	3	4	3	1	1	1	1	3	4	4	2	2	2	3	3	2	1	1	1	1	1	0	1	1	1	1	1	1	1	1	1
Anal. name																						0 00	0 23	0 43	0 53	0 73	0 83	0 93	1 03	1 23	1 33
SiO2	36 43	35 59	34 33	35 56	34 21	47 11	46 68	33 58	45 55	46 95	34 57	34 95	35 65	46 16	46 43	53 01	61 03	57 40	48 80	34 04	35 74	67 28	64 86	61 92	62 24	60 52	57 59	56 43	59 74	53 56	55 87
TiO2	0 65	2 05	2 79					2 06			2 75	3 16	2 60		1 57					3 00											
Al2O3	30 15	20 49	20 69	21 75	21 99	35 09	35 59	20 43	31 56	34 92	19 83	19 59	19 43	32 70	7 60	29 43	24 96	26 87	32 27	19 36	20 65	20 81	22 50	24 44	24 21	25 48	27 41	28 04	25 89	29 94	28 42
Fe2O3																															
FeO																					35 51										
FeO*	11 21	22 03	24 40	24 38	25 64	2 04	2 13	28 59	18 02	3 15	23 71	22 67	22 71	15 18						24 60											
MnO		0 30	0 33	0 29	0 86				0 33		0 38	0 46	0 41	0 37						0 45	4 05										
MgO	5 67	6 01	4 21	4 44	3 82	1 09	0 91	2 41	1 95	0 18	5 48	5 72	5 63	2 37						5 19	2 73										
CaO	0 71				0 12							0 11	0 10		11 40	12 61	8 12	9 97	16 13		1 31	1 32	3 34	5 41	5 27	6 71	8 93	9 78	7 34	12 30	10 46
Na2O	2 18	0 23	0 11	0 16	0 17	0 31	0 43	0 13	0 53	0 50				1 20	1 19	3 17	7 22	5 77	2 06			10 39	9 18	8 03	8 33	7 06	5 96	5 58	6 93	4 05	5 09
K2O		9 30	9 14	9 42	9 19	10 36	10 27	8 79	0 05	10 29	9 27	9 34	9 46	0 04	0 78	1 76	0 68	0 24	0 73	9 36		0 19	0 12	0 19	0 25	0 23	0 10	0 17	0 10	0 16	0 17
Total	87	96	96	96	96	96	96	96	98	96	96	96	96	98	98	100	100	100	100	96	100	100	100	100	100	100	100	100	100	100	100
Orig. total	91 58	95 57	96 39	95 43	96 40	96 06	94 28	90 73	97 38	93 82	95 64	96 26	94 91	95 65	98 35	99 16	100 38	100 56	100 35	99 72	101 46	101 98	100 07	101 40	100 55	100 14	100 98	100 50	100 57	101 05	102 05
Si	12 074	5 426		5 471	5 325	6 225	6 172	5 291	4 947	6 237	5 334	5 367	5 468	4 948	6 909	2 412	2 709	2 575	2 238	5 293	2 926	2 942	2 850	2 741	2 753	2 686	2 573	2 530	2 657	2 417	
Ti	0 161	0 235						0 244			0 319	0 365	0 299							0 351							1 444				2 508
Al	11 778	3 682		3 944	4 034	5 464	5 546	3 794	4 040	5 468	3 607	3 546	3 512	4 134	1 333	1 578	1 306	1 410	1 744	3 548	1,992	1 072	1 166	1 276	1 262	1,333		1 482	1 327	1 593	
FeIII																															1 504
FeII	3 107	2 809		3 137	3 338	0 225	0 235	3 767	1 637	0 350	3 059	2 911	2 912	1,632																	
Fe*																				3 199	2 431										
Mn		0 038		0 038	0 112				0 030		0 049	0 059	0 053	0 033						0 059	0 281										
Mg	2 801	1 365		1 017	0 887	0 214	0 178	0 566	0 316	0 036	1 260	1 310	1 287	0 378						1 203	0 333										
Ca	0 253				0 019							0 018	0 016		1 817	0 616	0 291	0 477	0 792		0 115	0 062	0 157	0 257	0 250	0 319	0 427	0 470	0 350	0 595	0 503
Na	1 398	0 068		0 048	0 051	0 079	0 109	0 036	0 112	0 127				0,249	0 342	0 279	0 621	0 501	0 183			0 881	0 783	0 689	0 688	0 608	0 517	0 485	0 597	0 354	0 443
K		1 809		1 848	1,825	1 746	1 733	1 767	0 007	1 744	1 825	1 831	1 850	0 005	0 147	0 102	0 038	0 013	0 042	1 857		0 011	0 007	0 011	0 014	0 013	0 006	0 010	0 006	0 009	0 010
mg'	47 4	32 7		24 5	21 0	48 8	43 1	13 1	16 2	9 4	29 2	31 0	30 7	21 7						27 0	10 9										
al	45 5	17 6		19 6	19 6	80 5	81 7	18 7	49 7	82 3	16 9	16 4	16 1	52 2						15 9	22 4										
an																68 8		48 7	81 2			6 6	16 7	27 2	26 7	34 4	45 2	49 2	37 0	62 7	53 2

Suite	Lady Barron											Gardens																				
Sample #	62640											62641																				
Mineral	PL	PL	PL	PL	PL	PL	PL	PL	PL	PL	PL	Bt	Bt	Bt	Bt	Bt	CL	MS	SHA	SHA	SHA	SHA	SHA	SHA	SHA	SHA	SHA	SHA	SHA	SHA	SHA	SHA
Type	ph	ph	ph	ph	ph	ph	ph	ph	ph	ph	ph	in OZ	matrix	ph	ph	ps,CD	ps,CD	ps,CD	ps,CD	ps,CD	ps,CD	ps,CD	ps,CD	ps,CD	ps,CD	ps,CD	ps,CD	ps,CD	ps,CD	ps,CD	ps,CD	ps,CD
Grain #	1	1	1	1	1	1	1	1	1	1	1	1	2	3	4	1	2	1	1	1	1	1	1	1	1	1	1	1	1	1	1	2
# analyses	1	1	1	1	1	1	1	1	1	1	1	2	6	2	6	1	3	1	1	1	1	1	1	1	1	1	1	1	1	1	1	1
Anal. name	1 43	1 53	1 63	1 73	1 83	1 93	2 13	2 23	2 33	2 43	2 53																					
SiO2	55 87	55 65	55 86	55 82	55 57	58 57	56 41	55 66	61 60	63 68	66 28	35 36	35 30	35 03	36 51	36 11	25 14	45 92	34 39	43 68	38 62	43 24	42 48	27 79	46 21	35 43	45 69	43 57	47 27	44 04	42 83
TiO2												3 16	3 27	3 17	3 69																	
Al2O3	28 45	28 50	28 49	28 48	28 62	26 76	28 07	29 58	24 47	23 72	21 64	18 88	19 22	18 71	16 38	21 41	21 78	33 49	21 34	30 20	29 81	29 71	29 69	24 55	33 92	21 25	31 70	33 22	34 34	31 72	31 99
Fe2O3																															
FeO																															
FeO*												21 39	21 24	21 31	19 30	17 60	26 84	3 39	20 28	6 84	13 88	7 58	8 89	28 46	3 65	18 86	4 66	6 66	2 37	6 69	8 88
MnO												0 13	0 12	0 39		0 51	0 54		0 39		0 23			0 53		0 38					
MgO												7 67	7 45	8 01	10 64	11 25	13 69	2 64	11 64	5 00	7 45	5 23	5 50	14 23	2 38	11 43	3 45	3 79	2 04	4 26	4 40
CaO	10 49	10 61	10 47	10 40	10 33	8 17	10 12	8 55	5 86	3 92	2 08																	0 37			
Na2O	5 05	5 05	5 03	5 06	5 29	6 36	5 29	6 05	7 83	8 47	9 79														0 36						
K2O	0 15	0 19	0 14	0 24	0 19	0 14	0 12	0 16	0 23	0 22	0 21	9 41	9 41	9 38	9 48	9 39		10 57	7 96	10 29	6 00	10 23	9 44	0 42	9 47	8 64	10 51	8 39	9 99	9 29	7 90
Total	100	100	100	100	100	100	100	100	100	100	100	96	96	96	96	96	88	96	96	96	96	96	96	96	96	96	96	96	96	96	96
Orig. total	100 45	100 30	100 37	101 58	102 52	105 06	102 14	105 32	100 72	99 09	99 74	95 40	95 82	93 45	87 71	94 68	87 23	94 31	93 12	94 34	89 13	94 55	92 92	88 18	95 10	94 91	94 64	94 35	95 73	91 65	93 89
Si	2 507	2 500	2 507	2 506	2 497	2 611	2 528	2 491	2 730	2 802	2 903	5 391	5 375	5 352	5 517	5 385	5 328	6 139	5 174	5 987	5 422	5 958	5 874	4 224	6 147	5 299	6 160	5 888	6 241	5 979	5 844
Ti												0 362	0 374	0 364	0 419																	
Al	1 505	1 509	1 507	1 507	1 516	1 406	1 483	1 560	1 278	1 230	1 117	3 392	3 449	3 369	2 918	3 716	5 441	5 277	3 784	4 880	4 933	4 824	4 839	4 396	5 317	3 746	5 038	5 291	5 343	5 076	5 145
FeIII																															
FeII												2 726	2 705	2 722	2 438	2 195	4 758	0 379	2 551	0 784	1 630	0 873	1 027	3 617	0 406	2 359	0 525	0 753	0 261	0 760	1 012
Fe*																															
Mn												0 016	0 015	0 050		0 064	0 097		0 049		0 026			0 068		0 048					
Mg												1 742	1 692	1 824	2 396	2 502	4 325	0 525	2 610	1 021	1 559	1 073	1 132	3 226	0 472	2 548	0 693	0 762	0 400	0 862	0 894
Ca	0 505	0 511	0 507	0 500	0 497	0 390	0 486	0 410	0 279	0 185	0 098																				
Na	0 439	0 440	0 438	0 440	0 461	0 550	0 460	0 525	0 673	0 723	0 831														0 093			0 096			
K	0 008	0 011	0 008	0 014	0 011	0 008	0 007	0 009	0 013	0 012	0 012	1 830	1 827	1 828	1 827	1 786		1 802	1 527	1 799	1 074	1 798	1 665	0 082	1 606	1 648	1 807	1,447	1 682	1 609	1 375
mg												39 0	38 5	40 1	49 6	53 3	47 6	58 1	50 6	56 6	48 9	55 1	52 4	47 1	53 7	51 9	56 9	50 3	60 5	53 2	46 9
al												14 8	15 5	14 4	10,1	16 9	22 9	65 8	17,8	46 0	37 5	43 7	42 3	23 8	67 3	17 5	57 0	55 3	73 4	51 6	49 7
an	53 5	53 7	53 5	53 2	51 9	41 5	51 4	43 9	29 3	20 4	10 5																				

Suite	Lady Barron	Lady Barron									Musselroe												Musselroe							
Sample #	62641 cont	62642									43271												43276							
Mineral	SHA	SHA	Bt	MS	SHA	SHA	SHA	SHA	SHA	SHA	SHA	Bt	Bt	Bt	Bt	Bt	Bt	GA	GA	GA	GA	GA	GA	Bt	Bt	Bt	Bt	Bt	GA	GA	GA	GA
Type	ps,CD	ps,CD	ps,CD	ps,CD	ps,CD	ps,CD	ps,CD	ps,CD	ps,CD	ps,CD	ps,CD	in QZ	mx	ph,co	ph,rm	ph,rm	ph,rm	ph	ph	ph	ph	ph,co	ph,rm	ms,co	ms,rm	ma,ll	ma,ll,rm	rm	ph	ph	ph	ph,co
Grain #	2	2	1	1	1	1	1	1	1	1	1	1	2	3	3	4	4	1	1	1	1	1	1	1	1	2	2	2	1	1	1	1
# analyses	1	1	1	1	1	1	1	1	1	1	2	9	3	1	1	1	1	1	1	1	1	1	1	1	1	1	1	1	1	1	1	1
Anal name																																
SiO2	44 93	46 99	36 46	46 52	45 27	44 64	46 01	43 07	43 02	38 70	44 33	35 42	35 56	35 21	35 41	35 17	35 13	36 93	36 60	36 67	37 10	37 36	36 38	35 52	35 37	35 13	35 40	36 39	37 29	37 82	37 72	37 18
TiO2												3 68	3 35	3 56	3 15	3 06	3 86							2 94	2 41	3 27	3 48	2 71				
Al2O3	34 53	36 05	21 05	36 58	33 05	32 23	36 80	30 32	30 65	24 63	31 74	18 36	19 01	18 87	18 90	19 28	19 07	21 17	21 00	21 09	21 13	21 23	20 88	18 55	18 97	18 73	18 62	18 58	21 62	21 47	21 49	21 09
Fe2O3																		0 14	0 40	0 55			0 62						0 80			1 78
FeO																		34 35	32 21	33 82	33 57	34 58	30 89						32 06	32 97	32 87	31 74
FeO*	4 76	1 22	17 98	0 91	4 82	5 57	1 15	7 11	7 24	14 70	5 71	24 15	23 49	23 63	23 78	24 05	23 44							24 25	24 06	24 29	23 78	22 68				
MnO														0 26	0 35			3 62	6 59	4 20	5 09	2 56	8 62	0 34	0 37		0 21	0 26	1 94	1 79	1 86	1 73
MgO	2 39	0 92	10 83	0 89	2 80	3 66	0 70	4 67	4 50	8 73	3 70	5 43	5 46	5 36	5 35	5 43	5 31	2 59	1 55	2 13	1 79	2 93	1 11	5 31	5 63	5 35	5 36	6 29	5 00	4 73	4 86	5 30
CaO																		1 20	1 65	1 55	1 31	1 33	1 49						1 30	1 22	1 21	1 19
Na2O	0 35	0 51		0 25			0 26	0 25			0 14																					
K2O	9 06	10 31	9 69	10 26	10 07	9 90	11 07	10 58	10 59	9 24	10 37	8 97	9 14	9 08	9 05	9 03	9 19							9 09	9 20	9 24	9 14	9 09				
Total	96	96	96	96	96	96	96	96	96	96	96	96	96	96	96	96	96	100	100	100	100	100	100	96	96	96	96	96	100	100	100	100
Orig_total	94 45	94 99	94 35	90 97	90 49	93 97	89 92	95 02	94 41	95 26	94 69	95 82	96 42	95 98	97 37	95 82	95 42	100 00	100 00	100 00	99 99	99 99	100 01	95 79	96 17	91 41	95 99	97 17	100 00	100 00	100 01	100 20
Si	6 006	6 184	5 438	6 129	6 088	6 037	6 033	5 935	5 925	5 596	6 027	5 455	5 457	5 418	5 451	5 411	5 398	2 986	2 979	2 975	3 007	3 006	2 974	5 482	5 457	5 425	5 452	5 556	2 963	3 004	2 996	2 958
Ti												0 425	0 386	0 412	0 365	0 353	0 446							0 340	0 279	0 379	0 403	0 310				
Al	5 441	5 591	3 701	5 681	5 233	5 137	5 734	4 924	4 974	4 194	5 086	3 333	3 437	3 423	3 429	3 496	3 453	2 017	2 015	2 016	2 019	2 013	2 012	3 374	3 449	3 408	3 380	3 344	2 025	2 010	2 012	1 977
FeIII																		0 080	0 024	0 033			0 038						0 047			0 106
FeII	0 531	0 134	2 242	0 100	0 541	0 629	0 127	0 819	0 833	1 778	0 648	3 110	3 014	3 042	3 061	3 049	3 012	2 322	2 194	2 294	2 276	2 327	2 111	3 130	3 104	3 137	3 063	2 896	2 130	2 190	2 184	2 111
Fe*																																
Mn														0 033	0 045			0 247	0 454	0 288	0 349	0 174	0 597	0 044	0 048		0 027	0 033	0 130	0 120	0 125	0 116
Mg	0 476	0 180	2 407	0 174	0 561	0 737	0 138	0 958	1 924	1 881	0 749	1 246	1 247	1 234	1 228	1 235	1 216	0 312	0 188	0 257	0 216	0 351	0 135	1 222	1 294	1 230	1 230	1 432	0 591	0 560	0 575	0 628
Ca																		0 104	0 143	0 134	0 119	0 114	0 130						0 110	0 103	0 103	0 101
Na	0 089	0 128		0 064			0 065	0 067			0 037																					
K	1 544	1 730	1 843	1 825	1 727	1 707	1 867	1 859	1 859	1 704	1 798	1 761	1 789	1 783	1 777	1 772	1 802							1 789	1 811	1 820	1 795	1 770				
mg	47 2	57 3	51 8	63 5	50 9	53 9	52 1	53 9	52 6	51 4	53 6	28 6	29 3	28 9	28 6	28 7	28 8	11 8	7 9	10 1	8 7	13 1	6 0	28 1	29 4	28 2	28 7	33 1	27 7	20 4	20 9	22 9
al	65 4	85 6	16 7	87 4	61 4	55 6	87 7	45 7	47 0	25 4	53 7	15 3	16 2	16 0	16 0	16 6	16 3	24 0	23 6	23 9	24 0	23 8	23 9	15 3	15 5	15 4	15 5	15 3	24 5	23 9	23 8	24 8
an																																

Suite	Musselroe	Musselroe																											Musselroe			
Sample #	43276 cont	62586																											62638			
Mineral	GA	MS	Bt	CD	GA	PL	PL	PL	PL	PL	PL	PL	PL	PL	PL	PL	PL	PL	PL	PL	PL	PL	SHS	SHS	SHS	Bt	Bt	GA	GA	TM	TM	Bt	GA
Type	ph,rm	ps,CD	mx	mx	mx	ph	ph	ph	ph	ph	ph	ph	ph	ph	ph	ph	ph	ph	ph	ph	ph	ph	ps,CD	ps,CD	ps,CD	ms	ph	ph	ph,co	co	rm	ps,CD	ph,co
Grain #	1	1	1	1	1	1	1	1	1	1	1	1	1	1	1	1	1	1	1	1	1	1	1	1	1	1	2	1	1	1	1	1	1
# analyses	1	1	2	2	2	1	1	1	1	1	1	1	1	1	1	1	1	1	1	1	1	1	1	1	1	4	2	1	1	3	2	1	3
Anal_name						0	0 47	0 95	1 2	1 7	2 2	2 7	3 1	3 55	4 1	4 6	5 1	5 2	5 3	5 6	6 02													
SiO2	37 59	46 97	34 49	47 95	36 25	63 26	60 15	60 04	59 79	62 95	60 18	55 24	54 48	54 39	58 68	58 06	55 27	55 97	60 29	59 59	61 74	43 60	43 96	36 38	34 61	34 22	36 30	36 37	37 13	35 71	35 50	37 31
TiO2			3 67																						3 31	3 64			0 26	0 87			
Al2O3	21 39	35 41	19 27	32 24	20 84	23 46	25 72	25 59	25 46	23 77	25 56	29 04	29 26	29 35	26 58	26 17	28 69	28 44	25 59	25 83	24 64	31 09	35 17	19 81	19 15	18 94	21 08	21 27	35 09	34 10	20 93	22 34
Fe2O3				0 22	1 71																						1 00	1 07					
FeO	33 40			11 16	31 35																						34 26	34 18					32 67
FeO*		2 32	23 27																			8 02	2 03	20 06	23 85	24 31			9 53	9 67	22 19		
MnO	2 03			0 57	6 12																			0 69	0 11	0 15	4 32	3 55			0 41	2 54	
MgO	4 27	0 70	6 00	5 36	2 02																	3 28	1 09	9 31	5 56	5 18	1 72	2 29	3 48	4 30	7 98	3 94	
CaO	1 32				1 71	4 56	7 18	7 27	6 81	5 06	6 80	10 56	11 66	11 45	8 15	9 05	10 78	10 22	6 92	7 47	5 60						1 32	1 28	0 23	0 81	0 12	1 20	
Na2O				0 40		8 56	6 77	6 90	7 58	8 04	7 15	4 85	4 48	4 64	6 37	6 55	5 10	5 16	7 00	6 88	7 64							1 28	1 54				
K2O		10 60	9 30			0 15	0 18	0 20	0 36	0 18	0 32	0 33	0 12	0 17	0 23	0 17	0 16	0 21	0 19	0 23	0 38	10 01	10 75	9 76	9 40	9 55					8 87		
Total	100	96	96	98	100	100	100	100	100	100	100	100	100	100	100	100	100	100	100	100	100	96	96	96	96	96	100	100	87	87	96	100	
Orig_total	100 02	88 79	96 79	100 64	100 55	99 07	95 29	97 54	101 74	101 57	101 86	97 07	101 43	101 80	101 63	99 18	97 68	100 30	100 75	99 76	99 61	92 80	98 13	97 62	96 01	95 95	99 14	101 41	91 04	90 69	96 35	100 77	
Si	2 998	6 214	5 309	5 031	2 948	2 792	2 671	2 669	2 666	2 778	2 675	2 482	2 454	2 451	2 617	2 602	2 486	2 511	2 678	2 653	2 734	5 990	6 213	5 510	5 346	5 313	2 957	2 950	12 022	11 675	5 401	2 970	
Ti			0 424																						0 384	0 425			0 063	0 214			
Al	2 010	5 521	3 497	4 000	1 998	1 220	1 346	1 341	1 338	1 237	1 339	1 538	1 553	1 559	1 397	1 382	1 521	1 504	1 339	1 356	1 286	5 033	5 484	3 536	3 487	3 466	2 024	2 033	13 391	13 140	3 754	2 095	
FeIII			0 017	0 104																							0 061	0 065					
FeII	2 228	0 257	2 995	0 979	2 132																												
Fe*																						0 921	0 225	2 541	3 081	3 157	2 334	2 319	2 581	2 644	2 823	2 174	
Mn	0 137		0 051	0 421																				0 088	0 014	0 019	0 298	0 240			0 052	0 171	
Mg	0 507	0 138	1 377	0 839	0 245																												
Ca	0 112				0 148	0 216	0 342	0 347	0 325	0 239	0 324	0 508	0 563	0 553	0 389	0 434	0 520	0 491	0 329	0 357	0 266	0 671	0 214	2 102	1 284	1 199	0 209	0 276	1 680	2 096	1 810	0 467	
Na				0 081		0 732	0 583	0 595	0 651	0 688	0 616	0 423	0 392	0 406	0 551	0 569	0 445	0 449	0 603	0 594	0 656						0 115	0 111	0 080	0 284	0 019	0 102	
K		1 788	1 827			0 009	0 010	0 011	0 020	0 010	0 018	0 019	0 007	0 010	0 013	0 010	0 009	0 012	0 011	0 013	0 021	1 754	1 814	1 885	1 852	1 892			0 804	0 976			
																															1 721		
mg	18 6	35 0	31 5	46 1	10 3																	42 2	43 7	45 3	29 4	27 5	8 2	10 6	39 4	44 2	39 1	17 7	
al	23 7	82 5	16 0	51 3	24 4																	50 7	80 7	14 9	15 7	15 2	24 6	24 8	59 3	55 0	17 5	25 2	
an						22 8	37 0	36 8	33 3	25 8	34 5	54 6	59 0	57 7	41 4	43 3	53 9	52 2	35 3	37 5	28 9												

Suite	Musselroe													Musselroe																		
Sample #	62638 cont													67539																		
Mineral	GA	MS	MS	SHS	SHS	SHS	SHS	SHS	SHS	SHS	SHS	SHS	SHS	BI	BI	BI	BI	BI	BI	BI	BI	BI	CD	CD	CD	CD	CD	CD	CD	CD	CD	CD
Type	ph,vn		ps,CD	ps,CD	ps,CD	ps,CD	ps,CD	ps,CD	ps,CD	ps,CD	ps,CD	ps,CD	ps,CD	in GA	in GA	in GA	in GA	in GA	in GA	in GA	in GA	in GA	in GA	in GA	in GA	in GA	in GA	in GA	in GA	in GA	in GA	in GA
Grain #	1	1	1	1	1	1	1	1	1	1	1	1	1	1	2	3	4	5	6	6	7	8	9	1	1	1	1	1	1	1	1	2	2
# analyses	1	2	1	1	1	1	1	1	1	1	2	1	1	3	3	1	1	1	1	1	1	1	1	1	1	1	1	1	1	1	1	1	1
Anal name																1A1	1B1	1C1	1D1	1E1	1F1	1G1	2A1	1H1	1J1	*J1	1K1	1L1	1M1	1N1	1O1	1P1	1Q1
SiO2	36 78	45 80	46 05	41 68	34 87	44 55	42 60	43 09	42 80	46 14	46 56	40 36	46 46	34 61	34 24	36 24	35 24	36 48	36 74	36 46	35 20	34 95	35 37	48 13	47 97	48 80	48 00	48 11	48 02	48 10	47 99	47 85	47 65
TiO2		1 05												1 25	1 76	1 33	5,41	1 34	2 06	1 98	3,51	3,13											
Al2O3	22 21	36 19	36 53	29 31	20 88	33 20	30 32	30 94	30 69	36 44	36 47	29 74	36 40	21 13	20 05	20 27	18 92	19 70	19 22	19 42	19 38	20,48	20 43	32 79	32 95	34 36	33 05	33 01	32 76	32 86	32 89	32 96	33 03
Fe2O3	0 30																																
FeO	33 00																																
FeO*		1 16	1 15	10 44	23 02	5 13	9 27	8 32	8 58	1 49	1 31	12 76	1 25	21 45	25 30	18 03	17 52	17 99	16 21	16 69	19 22	16 32	22 02	8 89	8 84	7 11	9 83	9 50	9 37	8 99	10 15	9 61	9 89
MnO	2 83				0 34																							0 21					
MgO	3 70	0 71	0 98	4 13	8 36	2 29	3 55	3 27	3 46	1 09	0 84	4 39	1 05	8 27	5 83	11 46	9 64	11 47	12 31	11 95	10 16	11 58	9 18	7 91	7 93	6 82	7 12	7 17	7 59	7 82	6 97	7 30	7 15
CaO	1 18		0 12	0 10	0 09	0 15		0 09	0 12	0 16			0 08																				
Na2O		0 35	0 35	0 22		0 19		0 16	0 14	0 57	0 41	0 19	0 50	0 20			0 41	0 31	0 37	0 26				0 27	0 32	0 48			0 25	0 23		0 28	0 29
K2O		10 74	10 82	10 12	8 45	10 50	10 26	10 12	10 20	10 11	10 42	8 55	10 27	9 09	8 83	8 68	8 86	8 71	9 10	9 24	8 53	9 54	9 00			0 44							
Total	100	96	96	96	96	96	96	96	96	98	96	96	96	96	96	96	96	96	96	96	96	96	96	98	98	98	98	98	98	98	98	98	98
Orig total	100 16	96 75	96 45	95 08	97 05	95 32	94 34	95 68	95 52	97 51	98 25	95 02	97 88	97 02	96 16	94 60	96 64	94 59	93 81	91 47	91 87	96 89	98 53	100 11	97 80	100 68	96 92	97 07	98 19	98 51	97 58	96 84	95 15
Si		6 056	6 086	5 846	5 322	6 030	5 916	5 946	5 923	6 088	6 134	5 686	6 120	5 262	5 303	5 397	5 266	5 429	5 438	5 414	5 281	5 201	5 377	4 987	4 970	5 013	4 936	4 994	4 985	4 984	4 992	4 973	4 960
Ti	2 943	0 104												0 142	0 204	0 148	0 608	0 150	0 229	0 221	0 396	0 350											
Al		5 639	5 689	4 845	3 576	5 296	4 964	5 032	5 006	5 666	5 662	4 938	5 651	3 785	3 659	3 550	3 335	3 456	3 353	3 398	3 428	3 592	3 661	4 004	4 024	4 161	4 047	4 039	4 011	4 013	4 033	4 038	4 053
FeIII	2 094																																
FeII	0 017	0 128	0 127	1 224	2 938	0 580	1 076	0 959	0 993	0 164	0,144	1 503	0 137	2 727	3 276	2 241	2 191	2 240	2 006	2 072	2 412	2 031	2 799	0 770	0 765	0 610	0 853	0 824	0 813	0 779	0 883	0 835	0 860
Fe*	2 208																																
Mn				0 043																								0 018					
Mg	0 192	0 140	0 192	0 863	1 901	0 461	0 735	0 672	0 713	0 214	0 154	0 922	0 206	1 974	1 945	2 538	2 147	2 544	2 716	2 645	2 272	2 569	2 080	1 221	1 224	1 045	1 102	1 109	1 173	1 207	1 080	1 130	1 109
Ca	0 441		0 016	0 015	0 014	0 021		0 013	0 017	0 022			0 011																				
Na	0 101	0 089	0 089	0 060		0 050		0 043	0 037	0 146	0 104	0 052	0 127	0 358			0 118	0 090	0 105	0 075					0 055	0 064	0 095		0 000	0 050	0 046		0 057	0 058
K		1 810	1 823	1 810	1 644	1 813	1 817	1 782	1 800	1 701	1 750	1 536	1 725	1 763	1 743	1 645	1 690	1 653	1 718	1 749	1 632	1 811	1 746			0 057					0 000		
mg	16 7	52 3	60 1	41 3	39 3	44 3	40 6	41 2	41 8	56 7	53 3	38 0	60 0	40 7	29 1	53 1	49 5	53 2	57 5	56 1	48 5	55 9	42 6	61 3	61 5	63 1	56 3	57 4	59 1	60 8	55 0	57 5	56 3
al	25 2	87 4	85 4	41 4	17 6	61 9	46 5	49 3	47 9	83 3	86 0	40 8	84 6	17 6	17 2	16 6	15 0	15 2	13 9	14 3	16 1	16 2	16 4	49 8	49 9	54 8	50 8	50 8	49 9	50 0	50 7	50 3	50 3
an																																	

Suite	Musselroe																																
Sample #	67539 cont																																
Mineral	CD	CL	GA	GA	GA	GA	GA	GA	GA	GA	GA	GA	GA	GA	GA	GA	GA	GA	GA	GA	GA	GA	GA	GA	GA	GA	GA	GA	GA	GA	GA	GA	GA
Type	in GA	ps,CD	ph	ph	ph	ph	ph	ph	ph	ph	ph	ph	ph	ph	ph	ph	ph	pt	ph	ph	ph	ph	ph	ph	ph	ph	ph	ph	ph	ph	ph	ph	ph
Grain #	2	1	1	1	1	1	1	1	1	1	1	1	1	1	1	1	1	1	1	1	1	1	1	1	1	1	1	1	1	1	1	1	1
# analyses	1	1	4	4	1	1	1	1	1	1	1	1	1	1	1	1	1	1	1	1	1	1	1	1	1	1	1	1	1	1	1	1	1
Anal name	1R1				1S1	1T1	1U1	1V1	1W1	1X1	1Y1	1Z1	1A2	1B2	1C2	1D2	1E2	1F2	1G2	1H2	1J2	1K2	1L2	*M2	1N2	1O2	1P2	1Q2	1R2	1S2				
SiO2	48 31	26 09	36 07	36 82	36 37	36 53	36 69	36 98	36 40	36 40	35 77	36 28	36 34	36 35	36 33	36 81	36 73	36 81	36 76	37 08	36 48	36 50	36 75	36 63	36 82	36 67	36 65	36 58	36 56	36 80	36 87		
TiO2																				3 00													
Al2O3	33 90	22 55	21 25	21 54	21 61	21 30	21 53	21 40	21 32	21 49	21 27	21 52	21 77	21 43	21 45	21 31	21 35	21 60	21 59	21 82	21 56	21 34	21 39	21 53	21 68	21 67	21 60	21 35	21 57	21 82	21 31		
Fe2O3			0 76	0 80	1 04	0 59	0 09	0 03	1 41	1 38	0 39	1 48	0 84	1 34	0 91	0 57	0 97	1 03			1 31	1 23	1 14	1 01		1 11	1 35	0 94	0 76	0 69	0 64		
FeO		34 97	34 07	33 41	34 38	34 63	34 08	33 64	32 92	34 01	32 89	34 57	33 99	33 97	34 40	34 35	32 08	34 50	34 71	32 91	33 52	32 44	33 22	33 76	32 47	32 12	34 24	33 54	32 65	33 94			
FeO*	9 73	29 85																															
MnO			4 70	2 00	3 76	3 89	3 67	3 50	3 20	3 62	3 94	3 78	2 81	2 88	4 02	2 80	2 72	3 35	3 88	2 80	3 34	3 33	3 49	3 17	3 59	3 24	3 22	2 86	3 58	3 18	2 81		
MgO	5 84	9 40	1 07	3 62	2 78	2 25	2 37	2 90	2 94	3 13	2 64	2 93	2 66	2 91	2 29	3 01	3 10	3 96	2 22	2 52	3 38	3 02	3 68	3 35	3 10	3 77	3 94	2 88	2 87	3 80	3 24		
CaO			1 17	1 15	1 03	1 05	1 02	1 11	1 10	1 07	0 97	1 12	1,01	1 08	1 02	1 11	1 07	1 16	1 11	1 07	0 99	1 07	1 10	1 09	1 05	1 08	1 11	1 14	1 12	1 07	1 18		
Na2O	0 23																																
K2O		0 11																															
Total	98	88	99	100	100	100	100	100	100	100	100	100	100	100	100	100	100	100	100	100	100	100	100	100	100	100	100	100	100	100	100		
Orig total	84 13	90 42	102 68	102 24	100 93	96 70	97 37	98 24	100 85	101 23	98 64	99 41	98 41	100 69	99 75	100 44	99 77	101 05	99 33	103 40	100 44	99 61	102 35	100 12	100 48	100 20	102 80	101 49	100 23	101 62	100 47		
Si	5 008	5 573	2 951	2 956	2 939	2 963	2 970	2 982	2 941	2 936	2 974	2 930	2 937	2 937	2 946	2 969	2 961	2 949	2 911	2 985	2 937	2 947	2 952	2 948	2 965	2 941	2 938	2 032	2 950	2 948	2 969		
Ti																												0 057					
Al	4 142	5 676	2 049	2 038	2 058	2 036	2 054	2 033	2 030	2 043	2,028	2 048	2 074	2 044	2 051	2 026	2 029	2 039	2 060	2 070	2,045	2 030	2 025	2 042	2 057	2 049	2 041	2 312	2 052	2 060	2 022		
FeIII			0 045	0 048	0 063	0 035	0 005	0 002	0 085	0 083	0 024	0 090	0 051	0 081	0 055	0 034	0 046	0 062			0 079	0 074	0 068	0 061		0 067	0 081		0 046	0 041	0 038		
FeII	0 843	5 331	2 993	2 288	2 257	2 332	2 344	2 298	2 273	2 221	2 300	2 221	2 337	2 296	2 301	2 320	2 309	2 149	2 336	2 337	2 218	2 263	2 179	2 235	2 273	2 178	2 153	0 196	2 264	2 187	2 286		
Fe*																												0 347					
Mn			0 325	0 136	0 257	0 267	0 251	0 239	0 218	0 247	0 270	0 258	0 192	0 196	0 275	0 191	0 186	0 227	0 265	0 190	0 227	0 227	0 237	0 216	0 245	0 220	0 218	0 098	0 244	0 215	0 192		
Mg	0 901	2 993	0 130	0 432	0 335	0 272	0 286	0 348	0 354	0 376	0 318	0 353	0 320	0 350	0 277	0 361	0 373	0 473	0 268	0 302	0 405	0 363	0 440	0 402	0 371	0 450	0 471		0 345	0 453	0 389		
Ca			0 102	0 099	0 089	0 091	0 088	0 095	0 095	0 092	0 084	0 097	0 087	0 093	0 088	0 096	0 092	0 099	0 096	0 092	0 085	0 092	0 094	0 093	0 091	0 092	0 095		0 096	0 092	0 102		
Na	0 046																																
K		0 029																															
mg	51 7	36 0	5 2	15 9	12 9	10 5	10 9	13 2	13 5	14,5	12 2	13 7	12 1	13 2	10 7	13 5	13 9	18 0	10 3	11 5	15 5	13 8	16 8	15,2	14 0	17 1	18 0	13 1	13 2	17 2	14 5		
al	54 0	25 3	24 9	24 8	25 4	24,7	24 6	24 2	25 3	25,5	24 6	25,5	25 5	25 4	25,2	24 5	24 8	25 0	24 6	25 0	25 5	25 2	25 0	25 1	24 5	25 3	25 4	24 9	25 0	25 1	24 5		
an																																	

Suite	Musselroe																												
Sample #	67539 cont																												
Mineral	GA	GA	GA	GA	GA	GA	GA	GA	GA	GA	GA	GA	GA	GA	GA	GA	GA	GA	GA	GA	GA	GA	GA	GA	GA	GA	GA	GA	GA
Type	ph	ph	ph	ph	ph	ph	ph	ph	ph	ph	ph	ph	ph	ph	ph	ph	ph	ph	ph	ph	ph	ph	ph	ph	ph	ph	ph	ph	ph
Grain #	1	1	1	1	1	1	1	1	1	1	1	1	1	1	1	1	1	1	1	1	1	1	1	1	1	1	1	1	1
# analyses	1	1	1	1	1	1	1	1	1	1	1	1	1	1	1	1	1	1	1	1	1	1	1	1	1	1	1	1	1
Anal name	1T2	1U2	1V2	1W2	1X2	1Y2	1Z2	1A3	1B3	1C3	1D3	1E3	1F3	1G3	1H3	1I3	1J3	1K3	1L3	1M3	1N3	1O3	1P3	1Q3	1R3	1S3	1T3	1U3	1V3	1W3	1X3
SiO2	36 55	36 86	36 70	36 88	37 31	37 06	36 59	36 80	36 39	36 65	36 40	36 42	36 63	36 26	36 62	36 05	36 62	36 53	36 49	36 38	36 60	36 28	36 45	36 95	36 80	36 77	36 69	36 58	36 70	36 72	36 31
TiO2																															
Al2O3	21,53	21 51	21 30	21 59	21,90	21 75	21,64	21,57	22 12	21,38	21 46	21,52	21,75	21 55	21,46	21,66	21,46	21,35	21 33	21 62	21 33	21,30	21,46	21 53	21 26	22,71	21 67	21,69	21 41	21 57	21 41
Fe2O3	1 16	0 58	0 69	0 86			0,84	0,37		0 36	1 33	1 34		1 54	0 35	1 40	0 46	0 87	1 88	1 25	0 39	0 91	1 47	1 04	0 73	0 03	0 17	0 65	1 06	1 17	1 37
FeO	33 93	33 19	33 53	32 44	33 81	34 17	33 88	33 55	34 71	34 36	32 81	33 14	34 60	32 89	34 21	33 38	33 98	33 62	31 89	33 80	34 34	34 43	32,76	31 69	34 17	32 93	34 54	33 42	32 69	32 14	34 14
FeO*																															
MnO	2 46	3 33	3 41	3 22	2 66	2 82	2 78	3 59	3 71	3 81	3 90	3 33	3 76	3 69	3 93	4 06	3 83	3 87	3 53	2 78	4 05	4 11	3 40	3 40	2 81	2 45	3 23	3 65	3 63	3 41	2 90
MgO	3 37	3 40	3 11	3 98	3 31	3 10	3 18	3 08	2 21	2 40	3 02	3 17	2 28	3 02	2 41	2 37	2 51	2 67	3 82	3 09	2 20	1 97	3 37	4 27	3 13	3 98	2 66	2 96	3 46	3 87	2 76
CaO	1 00	1 13	1 03	1 01	1 00	1 11	1 09	1 03	0 86	1 04	1 08	1 07	0 97	1 06	1 02	1 08	1 13	1 08	1 06	1 07	1 09	1 00	1 09	1 11	1 09	1 14	1 04	1 05	1 04	1 11	1 10
Na2O																															
K2O																															
Total	100	100	100	100	100	100	100	100	100	100	100	100	100	100	100	100	100	100	100	100	100	100	100	100	100	100	100	100	100	100	100
Orig total	99 25	102 46	101 63	99 80	104 50	101 74	101 85	97 85	95 44	101 10	100 33	99 49	99 39	100 18	100 32	100 99	100 45	100 84	101 43	99 55	99 42	100 41	102 03	102 13	100 50	100 14	101 25	99 88	100 64	102 51	99 45
Si	2 943	2 963	2 957	2 954	2 987	2 977	2 947	2 964	2 945	2 968	2 938	2 936	2 964	2 927	2 965	2 922	2 962	2 955	2 932	2 934	2 968	2 950	2 936	2 954	2 967	2 932	2 963	2 949	2 952	2 945	2 937
Ti																															
Al	2 043	2 038	2 042	2 038	2 067	2 060	2 054	2 048	2 109	2 040	2 042	2 045	2 074	2 050	2 048	2 069	2 046	2 036	2 021	2 056	2 038	2 042	2 037	2 028	2 020	2 134	2 062	2 061	2 030	2 039	2 041
FeIII	0 070	0 034	0 042	0 052			0 051	0 022	0 000	0 022	0 080	0 081		0 093	0 021	0 085	0 028	0 053	0 113	0 075	0 024	0 055	0 089	0 062	0 044	0 001	0 010	0 039	0 064	0 070	0 083
FeII	2 285	2 231	2 259	2 173	2 263	2 296	2 282	2 260	2 349	2 327	2 215	2 234	2 341	2 220	2 316	2 263	2 299	2 274	2 143	2 280	2 329	2 342	2 206	2 119	2 304	2 195	2 333	2 253	2 199	2 155	2 310
Fe*																															
Mn	0 167	0 226	0 232	0 218	0 180	0 192	0 189	0 244	0 254	0 261	0 266	0 227	0 257	0 252	0 269	0 279	0 262	0 265	0 240	0 189	0 279	0 283	0 231	0 230	0 192	0 165	0 220	0 249	0 247	0 231	0 198
Mg	0 404	0 407	0 373	0 475	0 395	0 370	0 381	0 370	0 266	0 290	0 362	0 381	0 275	0 363	0 291	0 286	0 302	0 321	0 457	0 371	0 266	0 238	0 404	0 509	0 376	0 473	0 319	0 355	0 415	0 462	0 333
Ca	0 086	0 097	0 091	0 086	0 086	0 095	0 094	0 089	0 074	0 090	0 093	0 092	0 083	0 091	0 088	0 093	0 098	0 093	0 091	0 092	0 094	0 086	0 093	0 095	0 094	0 097	0 089	0 090	0 089	0 095	0 095
Na																															
K																															
mg	15 0	15 5	14 2	18 0	14 9	13 9	14 3	14 1	10 2	11 1	14 1	14 6	10 5	14 1	11 2	11 2	11 6	12 4	17 6	14 0	10 3	9 3	15 5	19 4	14 0	17 7	12 1	13 6	15 9	17 7	12 6
al	25 4	24 7	24 9	25 1	25 0	24 6	25 2	24 8	25 5	24 6	25 4	25 4	24 9	25 7	24 8	25 8	24 7	24 9	25 6	25 5	24 6	25 2	25 4	24 9	24 6	25 5	24,8	25 1	25 1	25 2	25 4
an																															

Suite	Musselroe																														
Sample #	67539 cont																														
Mineral	GA	GA	GA	GA	GA	GA	GA	GA	GA	GA	GA	GA	GA	GA	GA	GA	GA	GA	GA	GA	GA	GA	GA	GA	GA	GA	GA	GA	GA	IL	PL
Type	ph	ph	ph	ph	ph	ph	ph	ph	ph	ph	ph	ph	ph	ph	ph	ph	ph	ph	ph	ph	ph	ph	ph	ph	ph	ph	ph	ph	ph	in GA	ph
Grain #	1	1	1	1	1	1	1	1	1	1	1	1	1	1	1	1	1	1	1	1	1	1	1	1	1	1	1	1	1	1	1
# analyses	1	1	1	1	1	1	1	1	1	1	1	1	1	1	1	1	1	1	1	1	1	1	1	1	1	1	1	1	1	1	1
Anal name	2M1	2N1	2O1	2P1	2Q1	2R1	2S1	2T1	2U1	2V1	2W1	2X1	2Y1	2Z1	2A2	2B2	2C2	2D2	2E2	2F2	2G2	2H2	2I2	2J2	2K2	2L2	2M2	2N2	1O4	0 00	
SiO2	36 06	36 00	35 47	36 66	36 46	36 72	36 31	36 25	36 53	36 54	35 19	36 64	36 49	36 72	36 66	36 62	36 58	37 04	36 62	36 43	36 62	36 82	36 60	36 79	36 50	36 85	36 80	36 81			59 99
TiO2																														51 51	
Al2O3	21 00	21 50	20 97	21 35	21 31	21 62	21 06	21 13	21 44	21 40	20 86	21 27	21 51	21 24	21 31	21 40	21 15	21 43	21 42	21 09	21 38	21 53	22 40	21 72	21 64	21 58	21 67	21 72			25 79
Fe2O3	1 46	1 18	2 56	0 34	0 57	0 88	0 92	1 11	1 06	0 63	3 21	0 32	0 36	0 70	0 65	0 74		0 41	0 56	0 63	0 49	0 45		0 74	0 60		0 40		2 18		
FeO	34 81	34 90	34 22	35 20	34 66	33 47	35 47	34 94	33 83	34 80	34 04	35 35	35 28	34 39	34 27	34 97	35 75	33 97	35 08	35 13	34 95	34 79	33 75	33 60	34 49	35 17	34 83	35 00	45 53		
FeO*																															
MnO	3 88	3 62	4 28	2 88	3 90	2 63	3 46	3 56	3 01	2 99	4 33	3 22	3 10	2 95	3 27	2 32	4 13	2 45	2 56	3 91	2 94	2 86	2 71	2 34	3 11	2 82	1 93	3 02	0 78		
MgO	1 62	1 77	1 30	2 30	2 02	3 56	1 77	1 87	3 03	2 39	1 23	2 18	2 07	2 97	2 67	2 81	1 33	2 57	2 57	1 74	2 43	2 66	2 46	3 73	2 61	2 40	3 24	2 41			
CaO	1 16	1 03	1 21	1 26	1 08	1 12	1 01	1 14	1 09	1 24	1 14	1 02	1 19	1 22	1 18	1 14	1 08	1 08	1 19	1 07	1 18	1 07	1 08	1 08	1 05	1 19	1 12	1 03			6 38
Na2O																															7 18
K2O																															0 66
Total	100	100	100	100	100	100	100	100	100	100	100	100	100	100	100	100	100	100	100	100	100	100	100	90	100	100	100	100	100	100	
Orig total	105 08	100 50	99 13	100 23	104 30	102 92	100 23	101 39	103 48	101 18	99 04	100 22	101 52	105 74	101 97	101 40	101 52	101 42	102 55	102 07	102 28	101 97	104 55	101 90	102 88	102 70	102 29	102 49	95 85	97 30	
Si	2 944	2 931	2 917	2 970	2 962	2 950	2 960	2 951	2 947	2 959	2 890	2 973	2 960	2 967	2 964	2 958	2 985	2 973	2 961	2 968	2 964	2 959	3 005	2 951	2 950	2 977	2 960	2 973			2 870
Ti							0 056																						1 958		
Al	2 021	2 063	2 026	2 039	2 040	2 046	2 417	2 028	2 039	2 043	2 020	2 034	2 056	2 023	2 030	2 038	2 033	2 027	2 042	2 025	2 040	2 053	2 110	2 053	2 062	2 055	2 055	2 067			1 352
FeIII	0 089	0 072	0 158	0 020	0 034	0 053		0 068	0 064	0 038	0 198	0 019	0 022	0 042	0 039	0 044		0 024	0 034	0 038	0 029	0 027		0 044	0 036		0 023		0 023		
FeII	2 377	2 377	2 346	2 385	2 354	2 248	0 236	2 379	2 283	2 357	2 339	2 399	2 394	2 323	2 317	2 362	2 439	2 280	2 372	2 393	2 366	2 351	2 256	2 253	2 332	2 377	2 343	2 364	1 925		
Fe*							0 215																								
Mn	0 268	0 249	0 297	0 197	0 268	0 179	0 087	0 245	0 205	0 205	0 301	0 221	0 213	0 201	0 224	0 158	0 285	0 166	0 175	0 269	0 201	0 195	0 183	0 159	0 212	0 193	0 131	0 206	0 033		
Mg	0 197	0 214	0 158	0 278	0 244	0 426		0 227	0 365	0 288	0 150	0 264	0 250	0 335	0 321	0 338	0 161	0 432	0 310	0 211	0 293	0 320	0 292	0 445	0 314	0 288	0 389	0 290			
Ca	0 101	0 090	0 106	0 109	0 094	0 096		0 099	0 094	0 108	0 100	0 088	0 103	0 105	0 101	0 099	0 093	0 093	0 103	0 093	0 102	0 092	0 092	0 092	0 090	0 102	0 096	0 089			0 304
Na																															0 619
K																															0 037
mg	7 7	8 3	8 3	10 4	9 4	15 9	8 2	8 7	13 8	10 9	6 0	9 9	9 5	12 6	12 2	12 5	6 2	16 0	11 6	8 1	11,0	12 0	11 5	16 5	11,9	10 8	14 2	10 9			
al	25 1	25,6	26,0	24 3	24 8	25 1	24 9	25,0	25,1	24 7	26 6	24,5	24 7	24,5	24 6	24,8	24 2	24 5	24,7	24 6	24 6	24 8	26 1	25 1	25 1	24 4	24 8	24 8	2 1		
an																															33 0

Suite	Musselroe																													
Samrple #	67539 cont.																													
Mineral	PL	PL	PL	PL	PL	PL	PL	PL	PL	PL	PL	PL	PL	PL	PL	PL	PL	PL	PL	SHA	SHA	SHA	SHA	SHA	SHA	SHA	SHA	SHA	SHA	SHA
Type	ph	ph	ph	ph	ph	ph	ph	ph	ph	ph	ph	ph	ph	ph	ph	ph	ph	ph	ph	ps,CD	ps,CD	ps,CD	ps,CD	ps,CD	ps,CD	ps,CD	ps,CD	ps,CD	ps,CD	ps,CD
Grain #	1	1	1	1	1	1	1	1	1	1	1	1	1	1	1	1	1	1	1	1	2	2	3	3	4	5	6	6	6	7	8
# analyses	1	1	1	1	1	1	1	1	1	1	1	1	1	1	1	1	1	1	1	1	1	1	1	1	1	1	1	1	1	4	1
Anal name	0 13	0 27	0 33	0 53	0 58	0 62	0 72	0 82	0 92	1 22	1 32	1 42	1 62	1 72	1 82	2 02	2 22	2 32	2 52	1R4	1S4	1T4	2O2	2P2	2O2	2R2					
SiO2	57 31	58 03	59 05	58 96	57 76	57 97	57 89	57 20	57 76	58 28	58 99	57 77	56 96	57 76	59 60	60 06	60 33	60 54	67 64	49 11	47 49	44 88	49 71	50 13	48 37	51 78	44 90	45 56	34 60	46 35	50 79	43 98
TiO2																																
Al2O3	27 54	26 75	26 12	26 17	26 73	26 60	26 86	26 86	27 03	26 58	26 17	26 95	27 37	27 02	25 76	25 35	25 14	25 01	20 44	32 35	38 31	40 98	29 26	29 70	29 74	29 07	30 34	31 09	21 30	30 03	31 06	30 05
Fe2O3																																
FeO																																
FeO*																				5 99	5 89	5 56	10 50	9 19	9 82	8 70	9 53	8 26	24 23	8 10	6 61	9 13
MnO																																
MgO																				3 21	2 18	2 56	3 44	3 80	4 28	2 48	6 73	6 24	7 17	5 97	4 31	3 52
CaO	8 17	8 33	7 70	7 76	8 56	8 44	8 29	8 97	8 58	8 18	7 74	8 72	9 29	8 62	7 10	6 63	6 57	6 34	0 89	0 16	0 73	0 19	0 56	0 58	0 52	0 55	0 93	0 93		0 35	0 77	
Na2O	6 65	6 60	6 81	6 66	6 46	6 47	6 45	6 52	6 25	6 51	6 62	6 18	6 17	6 28	7 18	7 32	7 27	7 37	10 45		0 39	0 32			0 38						0 25	
K2O	0 33	0 28	0 32	0 56	0 49	0 53	0 51	0 45	0 38	0 45	0 48	0 38	0 21	0 32	0 37	0 65	0 69	0 74	0 18	5 17	1 00	1 50	2 53	2 60	2 89	2 42	4 17	4 51	8 70	5 19	2 21	9 31
Total	100	100	100	100	100	100	100	100	100	100	100	100	100	100	100	100	100	100	100	96	96	96	96	96	96	96	96	96	96	96	96	96
Orig_total	91 71	97 77	97 58	102 24	96 28	96 02	96 11	97 23	97 21	98 68	96 36	94 40	96 21	94 69	95 04	97 04	97 83	95 24	95 28	90 48	78 66	80 10	77 07	79 38	83 26	77 88	90 02	89 69	95 51	89 44	87 46	97 33
Si	2 565	2 598	2 634	2 632	2 588	2 596	2 591	2 569	2 585	2 606	2 633	2 585	2 555	2 584	2 656	2 676	2 687	2 695	2 957	6 405	6 049	5 735	6 538	6 549	6 384	6 719	6 006	6 055	5 309	6 173	6 537	6 050
Ti																																
Al	1 453	1 410	1 373	1 377	1 412	1 404	1 417	1 422	1 425	1 401	1 377	1 421	1 447	1 425	1 353	1 331	1 320	1 312	1 053	4 972	5 752	6 171	4 535	4 573	4 626	4 445	4 784	4 870	3 852	4 715	4 712	4 879
Felli																																
Fetl																				0 653	0 628	0 594	1 155	1 004	1 084	0 944	1 066	0 918	3 110	0 902	0 711	1 050
Fe*																																
Mn																																
Mg																				0 624	0 414	0 488	0 674	0 739	0 841	0 672	1 341	1 236	1 639	1 184	0 827	0 722
Ca	0 392	0 399	0 368	0 366	0 411	0 405	0 398	0 432	0 411	0 392	0 379	0 418	0 446	0 413	0 339	0 316	0 313	0 302	0 042	0 022	0 100	0 026	0 079	0 081	0 079	0 077	0 047	0 047		0 050	0 106	
Na	0 577	0 572	0 589	0 576	0 561	0 562	0 560	0 568	0 542	0 565	0 572	0 537	0 577	0 545	0 620	0 632	0 626	0 636	0 919		0 096	0 080			0 097						0 063	
K	0 019	0 016	0 018	0 032	0 028	0 030	0 029	0 026	0 022	0 026	0 028	0 022	0 012	0 018	0 021	0 037	0 039	0 042	0 010	0 859	0 162	0 244	0 424	0 433	0 487	0 399	0 711	0 763	1 704	0 882	0 362	1 634
mg																				48 9	39 8	45 1	36 9	42 4	43 7	41 6	55 7	57 4	34 5	56 8	53 8	40 7
al																				61 4	71.7	72 8	51 9	53 9	50 3	54 6	45 2	48 2	18 4	47 2	57 0	47.7
an	40 4	41 1	38 4	38 9	42 2	42 0	41 5	43 2	43 1	41 0	39 2	43 8	45 4	43 1	35 3	33 4	33 3	32 2	4 3													

Suite	Musselroe												Musselroe						Poimena													
Sample #	67539 cont.												68549						62594													
Mineral	SHA	SHA	SHA	SHA	SHA	SHA	SHA	SHA	SHA	SI	SI	SI	TM	MS	SHA	SHA	SHA	SHA	BI	BI	PL	PL	PL	PL	PL	PL	PL	PL	PL	PL	PL	PL
Type	ps,CD	ps,CD	ps,CD	ps,CD	ps,CD	ps,CD	ps,CD	ps,CD	ps,CD	in GA	in GA	in GA	ps,GA	ps,CD	ps,CD	ps,CD	ps,CD	ps,CD	mx	ph	ph,co	ph,rm	ph	ph	ph	ph	ph	ph	ph	ph	ph	ph	ph
Grain #	8	8	9	9	9	9	9	9	9	1	2	3	1	1	1	1	1	1	1	2	1	2	3	3	3	3	3	3	3	3	3	3
# analyses	1	1	1	1	1	1	1	1	1	1	1	1	1	1	1	1	1	1	2	2	3	2	1	1	1	1	1	1	1	1	1	1
Anal name										1U4	1V4	1W4											0 00	0 20	0 40	0 60	1 10	1 50	2 01	2 50	3	3 5
SiO2	46 83	47 00	40 63	39 39	42 41	28 18	50 94	48 63	46 57	37 24	37 42	37 13	36 63	46 43	40 54	33 77	46 41	42 88	35 65	35 53	56 60	59 69	58 06	60 30	60 40	59 59	60 26	60 58	60 18	60 08	60 34	60 54
TiO2																			3 19	3 73												
Al2O3	29 82	30 44	37 42	23 40	29 22	24 30	27 53	27 04	26 20	61 92	62 31	62 23	33 25	35 83	30 16	23 26	36 27	30 99	17 77	17 24	28 35	25 88	27 01	25 56	25 31	25 50	25 45	25 14	25 53	25 62	25 64	25 26
Fe2O3										0 84	0 27	0 64																				
FeO																																
FeO*	10 24	9 51	10 04	18 19	11 29	35 74	7 87	14 79	14 55				9 28	1 68	12 03	22 99	1 53	8 07	21 35	21 66												
MnO															0 14	0 45		0 11	0 24	0 12												
MgO	3 60	3 49	3 97	5 49	3 47	6 45	3 57	6 13	5 31				5 39	1 03	5 29	9 54	0 91	3 94	3 77	8 58												
CaO	0 39	0 32	0 81				1 36	0 81	0 69				0 77	0 16	0 23	0 37		0 14			9 63	7 45	9 03	6 56	6 93	7 27	7 10	6 96	7 21	7 28	7 00	7 01
Na2O			0 45				1 54	0 56	0 90				1 67	0 39			0 57	0 34			5 16	6.61	5 91	6 40	6 87	6 42	6 76	7 00	6 84	6 81	6 82	6 90
K2O	5 11	5 24	2 89	9 53	9 61	1 34	3 19	2 84	1 79				10 48	7 60	5 62	10 31	9 53	9 02	9 13		0 26	0 37		1 18	0 50	0 42	0 41	0 33	0 24	0 20	0 20	0 29
Total	96	96	96	96	96	96	96	96	96	100	100	100	87	96	96	96	96	96	96	96	100	100	100	100	100	100	100	100	100	100	100	100
Orig_total	92 59	93 81	74 52	94 07	95 50	89 88	87 82	91 16	83 59	98 97	99 52	102 92	85 34	97 22	89 91	87 34	96 42	97 52	96 52	95 32	99 29	100 79	48 18	99 08	99 35	92 25	97 86	96 70	94 62	93 84	98 64	100 03
Si	6 282	6 279	5 428	5 792	5 934	4 438	6 693	6 019	6 313	1 007	1 009	1 003	11 942	6 139	5 660	5 071	6 124	5 902	5 430	5 429	2 532	2 656	2 591	2 683	2 686	2 665	2 680	2 692	2 675	2 670	2 676	2 689
Ti																			0 365	0 428												
Al	4 714	4 794	5 893	4 055	4 819	4 511	4 262	4 377	4 185	1 973	1 981	1 982	12 778	5 584	4 963	4 117	5 642	5 027	3 191	3 105	1 495	1 357	1 421	1 340	1 328	1 356	1 333	1,316	1 337	1 342	1 341	1 322
Felli										0 017	0 005	0 013																				
Fetl	1 149	1 602	1 121	2 236	1 321	4 707	0 864	1 698	1 649				2 529	0 185	1 405	2 888	0 169	0 929	2 720	2 768												
Fe*																																
Mn															0 016	0 057		0 012	0 030	0 015												
Mg	0 719	0 694	0 790	1 203	0 723	1 514	0 700	1 254	1 072	0 000	0 000	0 000	2 620	1 202	1 099	2 136	0 178	0 807	1 992	1 954												
Ca	0 056	0 045	0 086				0 190	0 119	0 100				0 269	0 022	0 035	0 060		0 020			0 461	0 355	0 432	0 313	0 330	0 346	0 338	0 331	0 343	0 347	0 333	0 334
Na			0 116				0 392	0 148	0 235				1 056	0 101				0 092			0 447	0 570	0 511	0 552	0 592	0 553	0 582	0 603	0 589	0 587	0 587	0 594
K	0 874	0 893	0 491	1 787	1 715	0 268	0 595	0 498	0 309					1 767	1 354	1 076	1 736	1 673	1,753	0 780				0 067	0 028	0 024	0 023	0 019	0 014	0 011	0 012	0 016
mg	38 5	39 5	41 3	35 0	35 4	24 3	44 7	42 5	39 4				50 9	52 2	43 9	42 5	51 3	46 5	42 3	41 4												
al	49 9	39 5	57 2	24 8	43 2	25 4	48 5	37 2	38 7				52 0	82 6	41 2	22 3	84 4	47 9	13 2	12 3												
an																					50 8	38 4	45 8	36 2	35 8	38 5	36 7	35 5	36 8	37 1	36 2	36 0

Suite	Wybalenna																		
Sample #	67530	62589																	
Mineral	PMA	HB	PL	PL	PL	PL	PL	PL	PL	PL	PL	PL	PL	PL	PL	PL	PL	PL	PL
Type		mx	ph	ph	ph	ph	ph	ph	ph	ph	ph	ph	ph	ph	ph	ph	ph	ph	ph
Grain #		1	1	1	1	1	1	1	1	1	1	1	1	1	1	1	1	1	1
# analyses	10	3	1	1	1	1	1	1	1	1	1	1	1	1	1	1	1	1	1
Anal name			0 00	0 12	0 37	0 40	0 47	0 54	0 63	0 65	0 80	1 20	1 58	2 13	2 49	3 00	3 50	4 02	4 70
SiO2	75 43	50 59	57 06	56 70	56 91	55 84	50 36	50 28	48 55	56 52	57 24	56 69	56 67	56 75	55 79	56 30	56 68	56 70	56 87
TiO2	0 33	0 30																	
Al2O3	12 69	4 34	27 48	27 92	27 74	28 38	32 71	32 21	32 99	28 01	27 55	28 27	27 89	27 77	28 50	27 85	27 81	27 69	27 68
Fe2O3																			
FeO																			
FeO*	2 42	15 62																	
MnO		0 72																	
MgO	0 27	13 67																	
CaO	1 66	12 15	9 77	9 79	9 69	10 55	14 62	14 98	16 31	10 07	9 71	9 28	9 63	9 73	10 60	10 20	9 90	9 93	9 82
Na2O	2 77	0 41	5 58	5 41	5 52	5 10	2 18	2 53	2 15	5 13	5 30	5 49	5 65	5 55	4 98	5 43	5 48	5 45	5 50
K2O	4 49	0 20	0 11	0 18	0 14	0 12	0 13			0 27	0 20	0 27	0 17	0 21	0 13	0 22	0 13	0 17	0 13
Total	100	98	100	100	100	100	100	100	100	100	100	100	100	100	100	100	100	100	100
Orig total	99 07	98 74	99 59	100 10	100 05	100 49	96 83	100 79	100 96	98 34	99 89	99 89	100 57	100 66	100 23	100 32	99 75	100 34	100 11
Si	4 112	7 416	2 555	2 540	2 548	2 507	2 284	2 285	2 220	2 533	2 560	2 537	2 539	2 543	2 504	2 528	2 540	2 542	2 547
Ti	0 013	0 033																	
Al	0 811	0 750	1 450	1 474	1 464	1 502	1 748	1 725	1 778	1 480	1 452	1 491	1 473	1 467	1 508	1,474	1 469	1 463	1 461
FeIII																			
FeII																			
Fe*	0 110	1 915																	
Mn		0 089																	
Mg	0 022	2 987																	
Ca	0 096	1 908	0 469	0 470	0 465	0 508	0 710	0 730	0 800	0 484	0 465	0 445	0 462	0 467	0 510	0 491	0 475	0 479	0 471
Na	0 292	0 117	0 485	0 470	0 480	0 444	0 192	0 223	0 190	0 446	0 460	0 476	0 491	0 482	0 434	0 473	0 476	0 474	0 478
K	0 312	0 037	0 006	0 010	0 008	0 007	0 008			0 015	0 011	0 016	0 010	0 012	0 008	0 013	0 008	0 010	0 007
mg	16 6	59 8																	
al	4 5	-47 6																	
an	24 9		49 1	49 9	49 2	53 4	78 7	76 6	80 8	52 0	50 3	48 3	48 5	49 2	54 0	50 9	49 9	50 3	49 6

Suite	Poimenia							Poimena			Poimena				Poimena		Poimena							Poimena/basalt hybrid						
Sample #	62594 cont.							62601			62612				67532		67533							67530						
Mineral	PL	PL	PL	PL	PL	PL	PL	Bi	Bi	PL	AF	Bi	MS	PL	Bi	SP	AF	Bi	Bi	Bi	IL	PL	PL	PL	Bi	Bi	Bi	HB	HB	PL	PL	PL
Type	ph	ph	ph	ph	ph	ph	ph	mx	ph	ph,co	mx	mx	mx	ph,co	mx	ph		in OZ	mx	mx		ph,co	ph,co	ph	mx	mx	mx	mx	in AF	ph	ph	pn
Grain #	3	3	3	3	3	3	3	1	2	1	1	1	1	1	1	1	1	1	2	3	1	1	2	3	1	2	3	1	2	1	1	2
# analyses	1	1	1	1	1	1	1	5	3	1	1	3	1	1	1	5	1	3	3	4	2	1	1	1	4	1	4	5	2	1	9	1
Anal name	4 00	4 50	5 00	5 40	5 45	5 50	5 57																									
SiO2	60 40	60 25	60 29	60 44	58 77	59 46	58 53	35 82	35 73	55 68	65 07	36 48	47 82	53 06	35 39	32 03	65 40	34 98	35 47	34 36		46 03	50 02	68 15	35 78	36 10	35 69	44 22	44 76	59 46	59 89	56 53
TiO2								4 05	3 98			3 26				23 84		1 63	1 73	1 60	51 83				3 02	2 50	2 79	0 36	0 72		0 01	
Al2O3	25 24	25 34	25 24	25 35	26 48	25 91	26 81	15 52	15 67	28 59	18 75	17 07	33 62	30 14	18 45	10 60	18 55	19 46	15 50	17 04		25 48	23 79	20 22	14 82	14 61	15 00	8 65	7 96	21 43	25 69	25 34
Fe2O3																0 94					1 63											
FeO																					40 73											
FeO*								23 45	20 54			22 06	2 08		26 21			27 66	27 95	28 04					28 87	28 83	27 94	27 09	25 65	1 02		0 36
MnO								0 27	0 18			0 41						0 37	0 18		5 80				0 27	0 23	0 30	0 70	0 73			
MgO								7 70	7 70		0 12	7 30	1 39	0 13	7 10			2 95	6 24	5 97					4 50	4 28	5 30	4 06	4 80			
CaO	6 89	7 06	7 09	7 08	8 22	7 84	8 47			10 84	0 19	0 13	0 13	12 34	0 17	30 59						28 49	22 96	0 42		0 58	0 19	10 83	11 42	10 60	7 03	11 06
Na2O	6 83	6 87	6 96	6 87	6 39	6 58	6 09			4 71	0 99			4 21										10 76	0 31			1 17	0 99	6 13	6 97	5 06
K2O	0 66	0 48	0 42	0 27	0 15	0 20	0 10	9 20	9 20	0 15	14 87	9 29	10 97	0 12	8 68		16 05	8 95	8 94	8 98			3 23	0 44	8 75	8 87	8 78	0 92	0 96	1 34	0 40	1 65
Total	100	100	100	100	100	100	100	96	96	100	100	98	96	100	96	98	100	98	96	96	100	100	100	100	96	96	96	98	98	100	100	100
Orig total	100 41	101 07	98 54	97 10	100 11	99 59	103 63	94 69	96 11	99 09	100 04	94 71	94 78	98 64	103 31	97 92	101 13	95 59	96 63	97 08	99 83	96 92	98 53	101 41	95 30	87 60	98 94	98 63	101 59	92 86	99 44	97 50
Si	2 687	2 680	2 683	2 685	2 620	2 648	2 609	5 536	5 522	2 499	2 989	5 581	6 337	2 398	5 498	3 990	3 009	5 482	5 595	5 425		2 196	2 371	2 975	5 662	5 723	5 631	6 922	6 969	2 704	2 665	2 570
Ti								0 470	0 462			0 375				2 223		0 191	0 205	0 190	1 969				0 359	0 297	0 331	0 042	0 084			
Al	1 323	1 329	1 323	1 327	1 392	1 360	1 408	2 827	2 855	1 512	1 015	3 078	5 250	1 605	3 377	1 556	1 006	3 595	2 881	3 170		1 433	1 329	1 040	2 765	2 730	2 789	1 597	1 460	1 150	1 347	1 358
FeIII																0 088					0 062											
FeII								3 031	3 043			2 822	0,230		3 405	0 000		3 625	3 686	3 703	1 720											
Fe*																									3 823	3 823	3 687	3 546	3 339	0 038		0 013
Mn								0 035	0 023			0 052						0 049	0 023		0 048				0 036	0 030	0 040	0 092	0 096			
Mg								1 772	1 774		0 008	1 664	2 740	0 008	1 643	0 000	0 000	0 689	1 467	1 405					1 062	1 012	1 246	0 948	1 114			
Ca	0 328	0 337	0 338	0 337	0 393	0 374	0 405			0 521	0 009	0 021	0 018	0 597	0 027	4 084	0 942					1 456	1 166	0 019		0 098	0 032	1 816	1 905	0 516	0 335	0 538
Na	0 589	0 592	0 600	0 591	0 552	0 568	0 526			0 412	0 088			0 368		0 000						0 000	0 000	0 910				0 355	0 299	0 540	0 601	0 445
K	0 037	0 027	0 024	0,015	0 008	0 012	0 006	1 813	1 813	0,008	0 871	1 814	1 854	0 007				1 789	1,799	1 808			0 195	0 024	1 768	1 793	1 767	0 184	0 189	0 077	0 022	0 095
mg								36 9	36 8			37 1	54 4		32 6			16 0	28 5	27 5					21 8	20 9	25 3	21 1	25 0			
al								9 5	9 7			11 9	76 9		13 7	0 0		17 11	9 5	11 8	1 6				9 2	7 1	8 8	39 0	45 3			
an	35 8	36 2	36 0	36 3	41 6	39 7	43 5			55 8	9 5			61 8									0 0	2 1						48 9	35 8	54 7

Suite	Wybalenna													Wybalenna		Wybalenna								Wybalenna	Wybalenna					
Sample #	62589													62593		62602								62610	62628					
Mineral	PL	PL	PL	PL	PL	PL	PL	PL	PL	PL	PL	PL	PL	HB	HB	Bt	Bt	HB	HB	HB	HB	PL	PL	PL	HB	AC	AC	Bt	Bt	CM	CM
Type	ph	ph	ph	ph	ph	ph	ph	ph	ph	ph	ph	ph	ph	ph,co	ph,rm	in QZ	in PL	mg	in PL	in PL	in PL	ph,co	ph,co	ph,rm	rra	rra CM	rra CM	ma HB	ph	ma OP	ma OP
Grain #	1	1		1	1	1	1	1	1	1	1	1	2	1	1	1	2	1	2	3	4	1	2	3	1	1	1	1	2	1	1
# analyses	1	1	1	1	1	1	1	1	1	1	1	1	2	4	1	2	2	3	1	1	1	1	1	1	3	1	1	1	2	1	1
Anal. name	5 2	5 7	6 25	6 55	6 65	6 75	6 9	7 45	8 00	8 48	8 54	8 58																			
SiO2	56 79	56 80	55 65	55 86	47 85	50 09	58 17	57 35	56 01	56 54	56 47	57 10	56 14	50 99	43 60	36 72	36 33	50 74	50 34	51 08	52 04	55 89	56 49	59 99	47 54	52 47	50 18	36 58	35 96	52 07	52 73
TiO2														0 27	0 85	3 43	3 11	0 31	0 27	0 42					0 82			2 13	3 79		
Al2O3	27 73	27 81	28 60	28 39	34 50	31 94	26 82	27 41	28 40	27 97	27 62	28 59	28 31	3 07	8 70	14 72	14 74	4 20	4 54	3 46	1 70	27 59	28 04	25 36	5 72	0 62	3 00	14 90	14 51	1 15	0 54
Fe2O3														0 14*											0 15*	2 10	4 41			2 23	1 63
FeO														16 25	21 20										18 54	26 07	21 88			25 72	26 35
FeO*																21 24	22 23	16 89	18 24	19 27	16 70							22 24	22 77		
MnO														0 75	0 77			0 53	0 42	0 58	0 57				0 90	1 04	0 52		0 32	1 01	0 95
MgO														13 57	9 07	10 82	10 57	12 91	11 36	11 34	11 41				11 15	14 95	12 30	10 71	9 57	14 46	14 95
CaO	9 76	9 98	10 84	10 41	16 27	14 96	8 71	9 48	9 94	9 83	9 59	8 11	9 60	12 40	11 68			11 82	11 52	11 45	15 48	11 16	10 08	7 87	12 15	0 75	5 51			1 36	0 83
Na2O	5 58	5 27	4 90	5 24	1 24	2 92	6 16	5 76	5 33	5 55	6 12	5 93	4 76	0 37	1 14			0 31	0 27	0 26		4 88	5 29	6 66	0 46						
K2O	0 14	0 14		0 10	0 15	0 09	0 14		0 32	0 11	0 19	0 28	1 19	0 19	0 95	9 07	9 02	0 29	0 23	0 13	0 10	0 48	0 11	0 12	0 57		0 21	9 45	9 08		
Total	100	100	100	100	100	100	100	100	100	100	100	100	100	98	98	96	96	98	98	98	98	100	100	100	98	98	98	96	95	98	98
Orig. total	100 16	99 80	99 51	100 43	97 96	101 08	99 24	99 55	95 56	101 30	100 35	93 11	99 40	97 83	101 06	96 44	92 72	95 61	96 75	96 52	96 74	99 93	101 30	98 84	96 33	97 84	90 18	95 11	96 98	97 02	97 44
Si	2 544	2 543	2 498	2 508	2 182	2 282	2 598	2 565	2 514	2 534	2 537	2 547	2 523	7 508	6 688	5 597	5 570	7 464	7 515	7 578	7 712	2 518	2 531	2 669	7 132	7 827	7 507	5 616	5 546	7 773	7 860
Ti														0 030	0 098	0 393	0 358	0 034	0 030	0 046					0 093			0 245	0 439		
Al	1 464	1 468	1 513	1 502	1 854	1 715	1 412	1 444	1 502	1 477	1 462	1 503	1 500	0 533	1 572	2 645	2 664	0 728	0 806	0 605	0 297	1 465	1 480	1 330	1 011	0 109	0 528	2 696	2 637	0 202	0 095
FeIII														0 016											0 017	0 235	0 496			0 250	0 183
FeII																										3 251	2 737	2 855	2 936	3 210	3 285
Fe*														2 001	2 718	2 708	2 850	2 078	2 250	2 391	2 070				2 326						
Mn														0 094	0 100			0 066	0 051	0 072	0 071				0 114	0 131	0 065		0 041	0 127	0 120
Mg														2 979	2 073	2 459	2 415	2 832	2 499	2 507	2 519				2 494	3 324	2 742	2 450	2 200	3 217	3 321
Ca	0 469	0 479	0 521	0 501	0 795	0 730	0 417	0 454	0 478	0 472	0 462	0 388	0 452	1 956	1 918			1 862	1 836	1 820	2 457	0 538	0 483	0 375	1 953	0 119	0 882			0 217	0 133
Na	0 485	0 457	0 427	0 456	0 110	0 258	0 533	0 500	0 464	0 482	0 533	0 513	0 415	0 106	0 339			0 087	0 078	0 075		0 426	0 459	0 574	0 134						
K	0 008	0 008		0 006	0 009	0 005	0 008		0 018	0 006	0 011	0 016	0 068	0 036	0 186	1 763	1 763	0 053	0 043	0 025	0 019	0 027	0 006	0 006	0 109		0 039	1 850	1 785		
mg														58 7	42 4	47 6	45 9	57 7	52 6	51 2	54 9				50 5						
al														53 1	-39 9	7 9	7 9	-46 0	-45 0	-46 0	-87 0				-46 6						
an	49 2	51 2	55 0	52 4	87 8	73 9	43 9	47 6	50 7	49 5	46 4	43 1	52 7									55 8	51 3	39 5							

Suite	Wybalenna														
Sample #	62628 cont														
Mineral	CM	CM	HB	HB	HB	HB	HB	HB	tl	OP	OP	OP	OP	PL	PL
Type	rra OP,co	rra OP,rm	rra CM	rra CM,co	rra CM,rm	ph	ph,co	ph,rm	in Bt	ph	ph	ph,co	ph,rm	ph,co	ph,rm
Grain #	1	1	1	1	1	2	2	2	1	1	2	2	2	1	1
# analyses	1	1	1	1	1	1	1	1	2	4	1	1	1	1	2
Anal. name															
SiO2	52 73	51 84	48 92	50 17	47 10	47 94	47 09	49 91		49 70	49 36	50 10	50 13	55 60	56 14
TiO2			0 42	0 21	0 30	1 01	1 41	0 23	51 74						
Al2O3	0 54	1 43	5 06	3 59	6 94	6 08	6 85	4 97	0 12	0 59	0 64	0 52	1 06	28 49	28 31
Fe2O3	1 63	1 69							1 66	2 10	2 71	1 47	0 79		
FeO	26 35	26 53							43 65	31 01	30,74	31 40	31 27		
FeO*			19 74	22 61	20 77	18 94	18 64	18 30							
MnO	0 95	1 07	0 51	0 72	0 35	0 53	0 23	0 45	2 83	0 93	1 00	0 76	0 85		
MgO	14 95	13 20	11 98	12 26	10 34	11 12	11 17	12 60		14 76	14 68	15 09	14 84		
CaO	0 83	2 24	10 43	8 25	10 85	11 00	11 00	10 69		0 92	0 87	0 65	1 06	10 62	9 60
Na2O			0 60		0 85	0 86	0 96	0 46						4 77	4 76
K2O			0 35	0 19	0 49	0 53	0 65	0 40						0 51	1 19
Total	98	98	98	98	98	98	98	98	100	100	100	100	100	100	100
Orig. total	97 44	97 87	98 63	97 92	96 95	98 29	97 77	96 62	99 03	102 10	100 75	100 95	101 54	99 71	99 49
Si	7 860	7 778	7 297	7 504	7 091	7 161	7 034	7 379		1 955	1 944	1 966	1,963	2 500	2 523
Ti			0 046	0 023	0 034	0 113	0 158	0 025	1 964						
Al	0 095	0 252	0 889	0 633	1 232	1 070	1 205	0 866	0 007	0 027	0 029	0 024	0 049	1 510	1 500
FeIII	0 183	0 190							0 062	0 062	0 080	0 043	0 023		
FeII	3 285	3 329	2 463	2 828	2 615	2 366	2 329	2 262	1 843	1 020	1 012	1 030	1 024		
Fe*															
Mn	0 120	0 135	0 064	0 091	0 045	0 066	0 029	0 055	0 121	0 030	0 033	0 025	0 028		
Mg	3 321	2 953	2 664	2 733	2 320	2 475	2 486	2 776		0 865	0 862	0 882	0 866		
Ca	0 133	0 360	1 667	1 321	1 749	1 760	1 759	1 693		0 038	0 036	0 027	0 044	0 511	0 462
Na			0 172		0 247	0 248	0 278	0 130						0 416	0 415
K			0 066	0 036	0 093	0 100	0 124	0 074						0 029	0 068
mg'															
al															
an														55 1	52 7

APPENDIX I

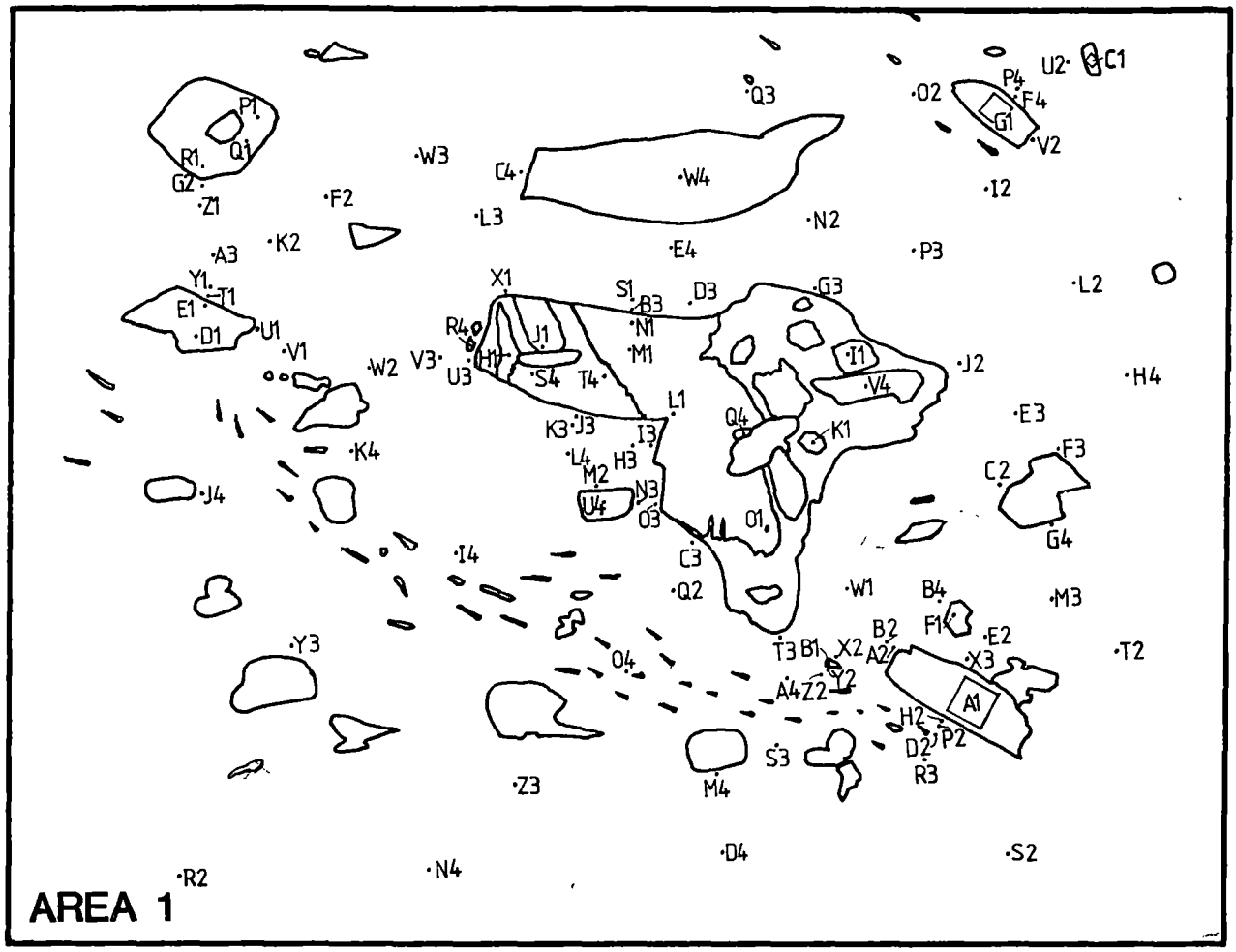

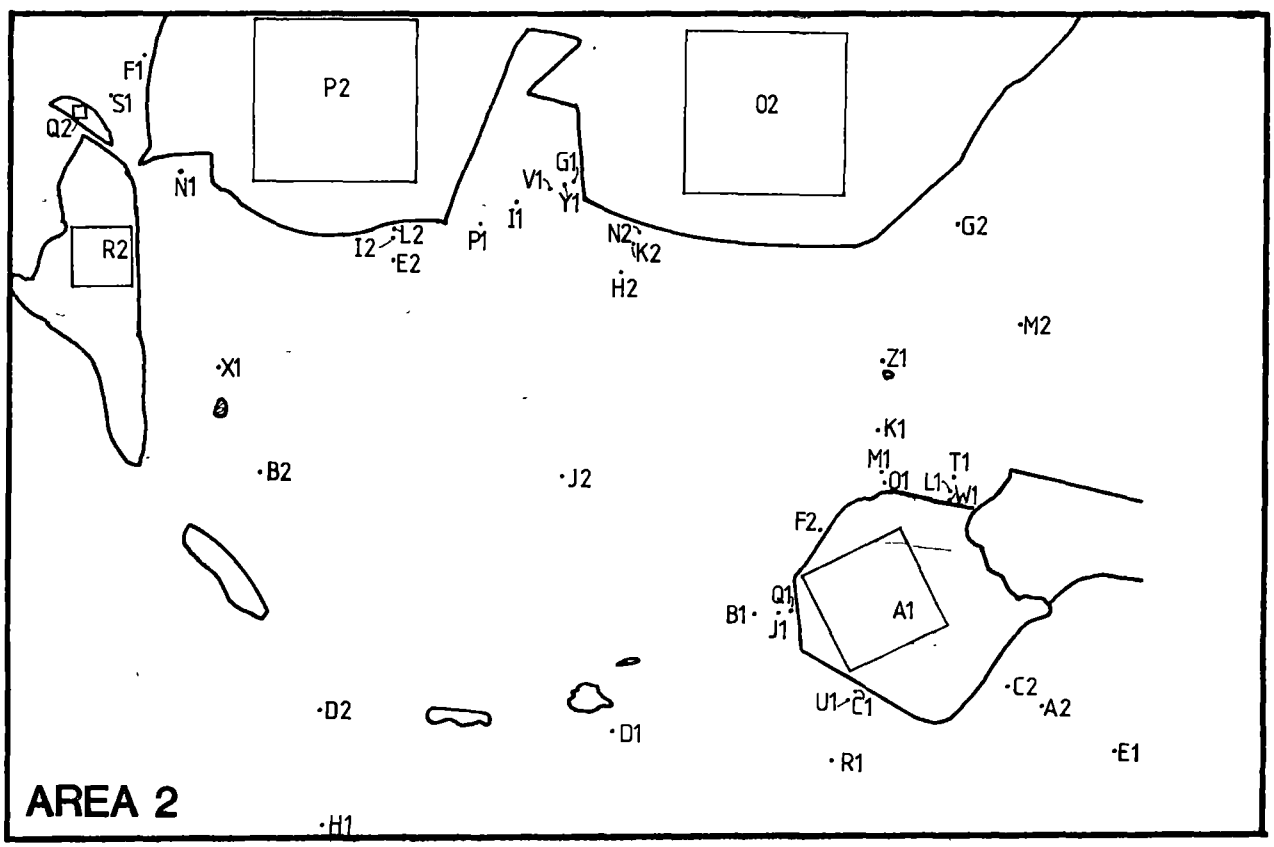

This appendix consists of maps of the analysis locations used to construct Fig. 7.8. The analyses for each labelled location (either point or area-scan) given, are listed in Appendix H. Other contoured diagrams can be constructed using these maps and the data of Appendix H.

Appendix J

PREPARATIVE METHODS FOR EXPERIMENTAL STARTING PHASES

Synthetic starting phases were made with Analar Grade chemicals using the methods discussed below.

Almandine

Synthetic fayalite, quartz and $Al(OH)_3$ were ground under acetone in agate mortar to dryness three times (~1 hour). After drying at 110°C, the mixture was heated at 900°C and 2.0 GPa in an $Ag_{50}Pd_{50}$ capsule for 24 hours, to generate almandine plus water. The pink-coloured product consisted of icosohedra averaging ~5 μm in diameter.

Biotite

Dry K_2CO_3 and quartz were ground then heated in a Pt crucible at 800°C overnight, to produce a clear glass with the composition $K_2Si_3O_7$. This was quenched, quickly dry-ground and stored in the oven at 110°C. It was then ground with synthetic fayalite and $Al(OH)_3$ to produce a mixture with a bulk composition of stoichiometric annite plus excess water. This mixture was then dry-mixed with 0.2682 times its weight of the mixture used to prepare phlogopite (* below). This mixture was then heated to 750°C at 0.5 GPa with 5% of its weight of excess water, in an $Ag_{50}Pd_{50}$ capsule for 142 hours. The product was fine-grained and consisted of green hexagonal platey crystals. No phase other than mica was observed petrographically or indicated in the XRD pattern. Microprobing of the product yielded the composition indicated in Table B1.

Table B1

	SiO_2	Al_2O_3	FeO*	MgO	K_2O	Σ
$\bar{x}$	35.90	10.22	33.41	7.13	9.34	96.00
2σ	1.8	0.55	2.59	1.35	0.39	
Cations per 11 ox	2.940	0.985	2.285	0.870	0.975	8.055
2σ	0.145	0.055	0.175	0.165	0.040	

This composition yields a magnesian number [mg = 100Mg/(Mg+Fe*)] of 27.6 and a peraluminous index [200(Al-K)/(2Al-2K+Mg+Fe*)] or (al) value of 0.2.

These values are within error of the values 26.0 and 0.0 chosen for the mica, on the basis of the materials used to produce it.

Cordierite

$Al(OH)_3$, quartz and calcined MgO were mixed in proportions to give 10 wt% excess SiO_2. A silica-saturated mixture was prepared so as to suppress the formation of spinel. The mixture was heated to 850°C at 0.8 GPa for 24 hours in an Au capsule. These conditions are within the stability field of hydrous cordierite determined experimentally by Newton (1972). The product was fine-ground, then heated to 1200°C for 15 hours in air (to dehydrate it within the stability field of cordierite (op. cit.), cooled and finally reground. Petrographic observations indicate that rare tiny spinel crystals occur in this product. However, its XRD pattern indicates only the presence of cordierite and quartz.

Fayalite

Fayalite was prepared by heating a stoichiometric mixture of quartz, "Spex" iron powder and "Spex" iron III oxide in an evacuated silica tube at 1000°C for 24 hours at atmospheric pressure. The product consisted of clear green crystals.

Ilmenite

The ilmenite used was that made by the (now defunct) American company: TemPress. Any impurities present are below the detection limits of the microprobe at the University of Tasmania. These limits are given in Appendix D.

Magnetite

This phase was produced from "Spex" iron powder and "Spex" iron III oxide which were mixed in the stoichiometric proportions and then pelletized. Pellets were sealed into an evacuated silica tube and heated at atmospheric pressure to 1000°C for 24 hours.

Phlogopite

Dry K_2CO_3, Al_2O_3, quartz and MgO in proportions such that upon sintering at 900°C for 15 hours, a product of bulk composition: $K_2Mg_6Al_{0.26}Si_6O_{19.4}$ is obtained. This was dry-crushed, then ground with sufficient $Al(OH)_3$ to produce a mixture with a composition of stoichiometric phlogopite and excess water. This mixture* was heated at 900°C at 0.4 GPa for 66 hours in an $Ag_{50}Pd_{50}$ capsule. The product consisted of tiny colourless platey crystals. Only phlogopite could be detected either optically or by XRD spectroscopy.

Quartz

$Si(OH)_4$ was dehydrated by heating at 950°C and at atmospheric pressure for 8 hours.

Sanidine

Al_2O_3 was obtained by calcining $Al(OH)_3$ as for quartz above. This was mixed in with dry K_2CO_3 and SiO_2 in the appropriate proportions and the mixture dry-ground. The mixture was then heated for 3 hours at 800°C, then 1 day at 900°C and finally for 2 days at 950°C. After quenching the resulting glass was fine-ground then heated to 1100°C at 2.5 GPa for 23 hours in a graphite capsule. These conditions are within the stability field of sanidine as determined experimentally by Seki & Kennedy (1964). After crushing, the resulting powder was ignited at 900°C for 48 hours in air to burn off excess carbon. This product only contained birefringent material. Its XRD pattern was that of high sanidine, with no leucite in evidence.

Sillimanite

Small pieces of natural sillimanite amounting to 1.3 g were hand-picked from a large prismatic crystal from Broken Hill, New South Wales (#19545). These were crushed to #60 grade in an agate mortar and shaken with distilled 2N hydrochloric acid. The acid was decanted and its suspended fines, containing some clay minerals, were discarded. The coarse powder was rinsed six times with distilled water, discarding fines each time. It was then dried at 200°C, and ground under acetone for 2 hours. The resulting powder had a grainsize comparable with that of the prepared quartz.

Appendix K

THE CHEMICAL COMPOSITIONS OF EXPERIMENTALLY-DERIVED PHASES

Mix	2				2			2			
Run	T1542				T1486			T1489			
T	800°C				850°C			900°C			
P	0.9 GPa				0.9 GPa			0.9 GPa			
Time	670 hours				238 hours			166 hours			
	Gl	Bi	Ga	Co	Gl	Bi	Ga	Gl	Bi	Ga	Hc
SiO_2	72.89 (1.78)	35.50 (0.3)	37.91 (1.79)		70.38 (0.76)	36.05 (0.77)	37.83 (2.93)	66.71 (0.24)	34.90 (0.37)	37.80 (0.67)	
TiO_2		0.09 (0.24)				0.25 (0.09)			0.46 (0.16)		
Al_2O_3	15.67 (0.57)	22.27 (0.12)	21.77 (2.43)	99.19	16.24 (0.24)	21.29 (0.73)	21.80 (2.02)	16.9 (0.3)	20.23 (0.41)	21.81 (0.59)	58.44 (0.53)
Cr_2O_3											0.06 (0.24)
Fe_2O_3				0.81							3.41 (0.14)
FeO											32.15 (1.04)
FeO*	3.27 (0.51)	19.08 (0.4)	34.57 (1.12)		4.72 (0.36)	20.27 (0.79)	33.19 (0.41)	7.41 (0.1)	20.63 (0.51)	32.91 (0.52)	
MgO	0.63 (0.16)	9.60 (0.22)	5.75 (0.16)		0.81 (0.24)	9.72 (0.89)	6.40 (0.38)	1.27 (0.12)	10.29 (0.19)	7.47 (0.08)	5.94 (0.4)
K_2O	7.53 (0.97)	9.46 (0.12)			7.85 (0.48)	9.43 (0.21)		7.71 (0.24)	9.50 (0.13)		
Σ	100	96	100	100	100	96	100	100	96	100	100
n	6	5	7	1	12	5	5	4	4	5	4
mg	25.6	47.3	22.9	0	23.4	46.1	25.6	23.4	47.1	28.8	24.8
al	54.7	19.0	25.5	100	46.9	17.2	25.6	38.4	15.2	24.9	50
Si	4.006	2.660	2.997		3.918	2.687	2.996	3.784	2.649	2.968	
Ti		0.005				0.014			0.026		
Al	1.015	1.967	2.028	3.979	1.066	1.870	2.035	1.130	1.810	2.019	1.927
FeIII				0.021							0.072
FeII											0.752
Fe*	0.150	1.196	2.286		0.220	1.264	2.199	0.351	1.310	2.161	
Mg	0.052	1.072	0.678		0.067	1.080	0.756	0.107	1.164	0.874	0.248
K	0.528	0.904			0.558	0.897		0.558	0.920		
Cr											0.001

Mix	2			1		1	1			
Run	T1502			T1541		T1576	T1470			
T	950°C			1000°C		1000°C	850°C			
P	0.9 GPa			0.9 GPa		0.9GPa	0.5 GPa			
Time	74 hours			24.4 hours		29.3 h	192 hours			
	Gl	Bi	Hc	Gl	Hc	Gl	Gl	Bi	Ga	Hc
SiO_2	60.57 (0.48)	35.11 (0.38)		58.75 (1.76)		58.55 (0.79)	70.09 (0.38)	35.24 (0.66)	38.13 (1.51)	
TiO_2		0.08 (0.24)						0.21 (0.22)		
Al_2O_3	16.99 (0.22)	18.71 (0.32)	52.84 (0.97)	18.35 (0.92)	55.28 (1.64)	18.54 (0.52)	15.32 (0.30)	19.45 (0.24)	21.84 (1.74)	56.14 (1.17)
Cr_2O_3			0.06 (0.22)		0.74 (1.44)					
Fe_2O_3			9.75 (0.39)		6.71 (0.14)					5.77 (0.18)
FeO			31.84 (1.22)		30.78 (0.57)					32.91 (0.91)
FeO*	14.74 (0.48)	21.69 (0.46)		14.47 (0.94)		14.29 (0.26)	6.33 (0.32)	22.03 (0.42)	33.04 (0.6)	
MgO	2.41 (0.2)	10.98 (0.38)	5.51 (0.6)	2.66 (0.18)	6.48 (0.51)	2.60 (0.08)	0.90 (0.08)	9.79 (0.24)	6.99 (0.16)	5.18 (0.35)
K_2O	5.29 (0.38)	9.43 (0.12)		5.77 (0.22)		6.12 (0.11)	7.36 (0.16)	9.28 (0.04)		
Σ	100	96	100	100	100	100	100	96	100	100
n	10	6	4	6	7	3	10	7	7	3
mg	22.6	47.4	23.6	24.7	27.3	24.5	20.2	44.2	27.4	21.9
al	29.4	12.7	50	30.8	50	30.7	39.5	14.4	25.3	50
Si	3.553	2.683		3.462		3.452	3.925	2.690	2.992	
Ti		0.005						0.012		
Al	1.175	1.685	1.788	1.275	1.841	1.288	1.011	1.750	2.020	1.877
FeIII			0.211		0.143					0.123
FeII			0.764		0.727					0.781
Fe*	0.723	1.386		0.713		0.715	0.296	1.406	2.168	
Mg	0.211	1.252	0.236	0.234	0.273	0.229	0.075	1.114	0.818	0.219
K	0.396	0.919		0.434		0.460	0.526	0.904		
Cr			0.001		0.017					

Mix	2	2	2
Run	T1492	T1558	T1573
T	850°C	850°C	950°C
P	1.2 GPa	1.5 GPa	0.9 GPa ($a_W^m < 1$)
Time	242 hours	324 hours	189 hours

	Gl	Bi	Ga	Co	Gl	Ga	Co	Gl	Bi	Ga	Hc
SiO_2	72.91 (0.52)	36.40 (0.98)	37.32 (2.08)		71.73 (0.65)	37.05 (0.56)		66.42 (1.72)	35.4 (0.84)	38.14 (0.75)	
TiO_2		0.09 (0.22)					0.18 (0.36)		0.19 (0.22)		
Al_2O_3	15.35 (0.34)	21.71 (0.48)	21.87 (0.62)	99.46 (0.24)	15.5 (0.25)	21.61 (0.38)	98.98 (0.43)	16.92 (0.87)	18.99 (0.37)	21.92 (0.81)	58.05 (0.31)
Cr_2O_3											0.37 (0.16)
Fe_2O_3				0.54 (0.24)			0.86 (0.18)				3.58 (0.15)
FeO											32.01 (0.40)
FeO*	2.7 (0.31)	18.14 (0.66)	33.79 (1.58)		2.64 (0.29)	36.35 (0.75)		7.83 (1.01)	21.31 (0.37)	33.02 (0.59)	
MgO	0.50 (0.12)	9.96 (0.72)	7.02 (0.4)		0.34 (0.1)	4.94 (0.15)		1.02 (0.18)	10.70 (0.37)	6.92 (0.31)	5.99 (0.25)
K_2O	8.55 (0.44)	9.70 (0.22)			9.80 (0.54)			7.81 (0.22)	9.40 (0.22)		
Σ	100	96	100	100	100	100	100	100	96	100	100
n	13	9	6	2	6	9	3	10	5	6	6
mg	24.8	49.5	27.0	0	18.7	19.5	0	18.8	47.2	27.2	23.3
al	54.5	18.0	25.0	100	51.5	25.2	100	38.2	13.3	25.4	50
Si	4.019	2.714	2.946		3.989	2.963		3.778	2.696	2.992	
Ti		0.005					0.005		0.011		
Al	0.997	1.908	2.035	3.986	1.016	2.037	3.972	1.134	1.705	2.027	1.916
FeIII				0.014			0.022				0.075
FeII											0.750
Fe*	0.124	1.131	2.231		0.123	2.431		0.372	1.357	2.166	
Mg	0.041	1.107	0.826		0.028	0.589		0.086	1.215	0.809	0.250
K	0.601	0.923			0.695			0.567	0.913		
Cr											0.008

Mix 3
Run T1491
T 850°C
P 0.5 GPa
Time 245 hours

	Gl	Bi	Cd	Hc	Il	Us
SiO_2	75.33 (0.32)	34.48 (1.74)	47.69 (4.75)			
TiO_2	0.05 (0.18)	4.48 (0.52)		0.77 (0.54)	46.01 (1.68)	11.47 (0.61)
Al_2O_3	13.46 (0.22)	17.82 (0.42)	31.50 (3.28)	49.47 (3.65)	1.43 (2.09)	11.04 (1.5)
Cr_2O_3						
Fe_2O_3				11.31 (1.14)	12.51 (0.20)	34.54 (0.72)
FeO				34.89 (3.19)	38.40 (0.57)	41.77 (0.79)
FeO*	3.16 (0.2)	23.15 (2.48)	11.37 (1.6)			
MgO	0.35 (0.12)	6.95 (1.96)	6.88 (0.93)	3.56 (1.15)	1.65 (0.75)	1.18 (0.56)
K_2O	7.65 (0.14)	9.12 (0.22)	0.57 (0.29)			
Σ	100	96	98	100	100	100
n	9	5	6	3	4	10
mg	16.5	34.9	51.9	15.4	7.1	4.8
al	49.1	13.6	47.8	50	13.8	34.7
Si	4.126	2.657	5.014			
Ti	0.002	0.260		0.017	1.724	0.307
Al	0.869	1.619	3.904	1.717	0.084	0.463
FeIII				0.251	0.469	0.925
FeII				0.859	1.600	1.243
Fe*	0.145	1.492	1.000			
Mg	0.029	0.798	1.078	0.156	0.123	0.063
K	0.535	0.897	0.075			
Cr						

Mix	3			4		4		4	
Run	T1490			T1485		T1573		T1576	
T	850°C			850°C		950°C		1000°C	
P	0.9 GPa			0.7 GPa		0.9 GPa		0.9 GPa	
Time	258 hours			168 hours		189 hours		29.3 hours	
	Gl	Bi	Ga	Il	Il	Us	Il	Us	Il	Us
SiO_2	73.05 (0.87)	34.86 (1.7)	37.16 (3.93)							
TiO_2	0.44 (0.33)	5.12 (1.22)	0.90 (2.71)	49.26 (1.89)	49.98 (0.57)	26.33 (0.37)	49.44 (0.24)	26.35 (0.79)	49.25 (1.03)	25.90 (1.31)
Al_2O_3	14.84 (0.42)	19.26 (0.74)	21.78 (1.49)	1.17 (3.47)		0.45 (0.14)		0.38 (0.09)	0.44 (0.11)	2.77 (0.77)
Cr_2O_3										
Fe_2O_3				6.95 (0.49)	5.09 (0.08)	17.68 (0.08)	6.18 (0.04)	17.68 (0.22)	6.73 (0.14)	16.07 (0.37)
FeO				40.57 (2.62)	44.93 (0.57)	55.54 (0.23)	44.38 (0.21)	55.59 (0.63)	42.70 (0.82)	54.59 (1.16)
FeO*	3.51 (0.46)	18.84 (1.2)	33.41 (2.18)						0.88 (0.22)	0.66 (0.14)
MgO	0.64 (0.1)	8.60 (0.3)	6.73 (0.39)	2.04 (0.73)						
K_2O	7.52 (0.22)	9.36 (0.34)								
Σ	100	96	100	100	100	100	100	100	100	100
n	8	8	8	6	9	8	7	6	6	7
mg	24.5	44.8	26.4	8.2	0	0	0	0	3.6	2.1
al	50.4	15.8	25.3	8.2	4.8	13.0	5.9	12.9	7.0	14.1
Si	4.021	2.626	2.931							
Ti	0.018	0.290	0.053	1.838	1.903	0.742	1.884	0.742	1.860	0.717
Al	0.963	1.710	2.025	0.068		0.020		0.017	0.026	0.120
FeIII				0.259	0.194	0.498	0.236	0.499	0.254	0.445
FeII				1.684	1.903	1.740	1.880	1.742	1.793	1.681
Fe*	0.162	1.187	2.204							
Mg	0.053	0.966	0.791	0.151						0.036
K	0.528	0.900								
Cr										

Bi - biotite; Cd - cordierite; Co - alumina; Ga - garnet rim; Gl - glass; Hc - hercynite; Il - ilmenite; Us - ulvospinel

Appendix L

THE METHODS OF APPLICATION OF THE ALUMINOSILICATE+GARNET+PLAGIOCLASE+QUARTZ (THE AGPQ) BAROMETER

The net-transfer reaction which relates the endmembers of these phases is:

grossular + aluminosilicate + quartz --> anorthite

i.e.

$$Ca_3Al_2Si_3O_{12} + 2Al_2SiO_5 + SiO_2 \rightarrow 3CaAl_2Si_2O_8 \qquad (1)$$

In the general chemical system, the reaction coefficient is:

$$K = (a_{pl}^{an})^3 \ (a_{as}^{Al_2SiO_5})^{-2} \ (a_{qz}^{SiO_2})^{-1} \ (a_{ga}^{gr})^{-1}$$

for pl = plagioclase, as = aluminosilicate, qz = quartz, ga = garnet, an = anorthite and gr = grossular.

The activities of Al_2SiO_5 in aluminosilicate and of SiO_2 in quartz are assumed to be 1 because both phases are nearly pure (cf. Chapter 7). K is therefore given by:

$$K = (a_{pl}^{an})^3 (a_{ga}^{gr})^{-1} = [(X_{pl}^{an})^3/(X_{ga}^{gr})^3] \bullet [(\gamma_{pl}^{an})^3/(\gamma_{ga}^{gr})^3]$$

so $$K = K_X \bullet K_\gamma \qquad (2)$$

for the molar proportions, X, of the Ca-endmember present in the garnet and plagioclase solid solutions, and γ, the corresponding activity coefficients.

Version A

The calibration of Ghent (1976) for the kyanite-bearing endmember reaction was made using the experimental data for the reaction obtained by Hays (1967) and Hariya & Kennedy (1968). The free-energy equation describing this equilibrium was thermodynamically converted to that for the reaction involving sillimanite instead of kyanite (Ghent, 1976):

$$\Delta G_{sill}^{P,T} = 0 = \frac{2551.4}{T(K)} + 7.1711 - \frac{0.2842\ P\ (bar)}{T(K)} - \log_{10}K \qquad (3)$$

Ghent et al. (1979) presented an empirical value of +0.4 for the activity coefficient function $\log_{10}K_\gamma$ which yields:

$$K_\gamma = 2.512 \qquad (4)$$

This value was obtained by back-calculation using PTX data of those samples containing co-existing equilibrium kyanite and sillimanite which indicates that the equilibrium conditions of their respective assemblages are constrained to lie close to the kyanite/sillimanite boundary of Holdaway

(1971). For these samples, equilibrium temperatures were independently estimated, therefore enabling their equilibrium pressures also to be estimated.

Substitution of equations 4 and 2 into equation 3 and re-arrangement, yields the barometric expression:

$$P(GPa) = T(K) \bullet [0.0023825 - 0.00045844 \ln(X_{pl}^{an}/X_{ga}^{gr})] - 0.89774 \quad (5)$$

Equation 5 is version A of the AGPQ barometer. Ghent et al. (1979) estimate the 2σ error for pressures estimated by this formulation to be ± 0.16 GPa.

Version B

From the Second Law Equation for equilibria in the general chemical system:

$$\text{pressure, } P = \left(\frac{\Delta S_R}{\Delta S_R} - \frac{R \ln K}{\Delta V_R}\right) \bullet T - \frac{\Delta H_R}{\Delta V_R} \quad (6)$$

where ΔS_R, ΔH_R and ΔV_R are the molar entropy, enthalpy and volume charge of the reaction, R is the gas constant (equal to 8.31435 J $mol^{-1}K^{-1}$), T is temperature and K is the equilibrium coefficient defined by equation 2.

The barometric expression for the sillimanite-bearing endmember AGPG reaction given by E. Froese **in** Ganguly & Saxena (1984) is:

$$P(kbar) = -1.17 + 0.0238\ T(C)$$

$$\text{i.e.} \quad P\ (GPa) = -0.76722 + 0.00238\ T(K) \quad (7)$$

It is based upon the experimental results of the kyanite-bearing endmember reaction determined by Goldsmith (1980). Equating the coefficients of equations 6 and 7 for the endmember reaction yields:

$$\Delta S_R/\Delta V_R = 0.00238 \quad \text{and} \quad \Delta H_R/\Delta V_R \quad (8)$$

In complex chemical systems however, strong non-ideality is indicated for the partial molar volume of grossular in garnet and for the activities of both grossular in garnet and anorthite in plagioclase.

Molar Volume Model

Experimental studies by Cressy et al. (1978) reveal the partial molar volume of grossular in both CaFe and CaMg binary garnet solid-solutions to be nearly linear functions of the grossular mole fractions in the respective solid solutions, where $X_{ga}^{gr} < 0.14$. The partial molar volumes of grossular in these solid solutions are:

$$\left.\begin{aligned} V_{gr\text{-}py}^{o,gr} &= 119900 + 72140\ X_{gr\text{-}py}^{gr}\ J\ GPa^{-1} \\ \text{and} \quad V_{gr\text{-}al}^{o,gr} &= 121180 + 63000\ X_{gr\text{-}al}^{gr}\ J\ GPa^{-1} \end{aligned}\right\} \quad (9)$$

where gr = grossular, py = pyrope and al = almandine.

If it is assumed that $V^{o,gr}_{gr\text{-}sp} = V^{o,gr}_{gr\text{-}al}$, where sp = spessartine, then in quaternary garnet,

$$V^{o,gr}_{ga} = \left(\frac{X^{py}_{ga}}{X^{sp}_{ga}+X^{al}_{ga}+X^{py}_{ga}}\right) \bullet V^{o,gr}_{gr\text{-}py} + \left(\frac{X^{sp}_{ga}+X^{al}_{ga}}{X^{sp}_{ga}+X^{al}_{ga}+X^{py}_{ga}}\right) \bullet V^{o,gr}_{gr\text{-}al}$$

But because $X^{gr}_{ga} + X^{py}_{ga} + X^{al}_{ga} + X^{sp}_{ga} = 1$, then, using equations 9,

$$V^{o,gr}_{ga} = [119900X^{py}_{ga}+(1+0.602X^{gr}_{ga})+121180X^{sp+al}_{ga}+(1+0.52X^{gr}_{ga})]/(1-X^{gr}_{ga}) \text{ J GPa}^{-1} \quad (10)$$

In the complex chemical system therefore:

$$\Delta V_R = 3V^{o}_{anorthite} - 2V^{o}_{sillimanite} - V^{o}_{quartz} - V^{o,gr}_{ga}$$

i.e.

$$\Delta V_R = 180282 - V^{o,gr}_{ga} \quad (11)$$

for the endmember molar volumes given in Table L1.

Table L1

Molar Volumes of Pure AGPQ Reaction Phases

Phase	V^o (J GPa^{-1})	Source
Sillimanite	49910	Obtained from the average of the unit cell volumes determined on sillimanite single crystals (Cameron, 1976; Winter & Ghose, 1979; Peterson & McMullan, 1986)
Grossular	125230	Newton & Perkins (1982)
Anorthite	100930	Newton & Perkins (1982)
Quartz	22688	Helgeson et al. (1978)

Activity and Activity Coefficient Models

The symmetric ternary solution model gives the activity coefficient expression:

$$RT \ln \gamma^1 = X_2^2 W_{12} + X_3^2 W_{13} + X_2 X_3 (W_{12}+W_{13}-W_{23}) \qquad (12)$$

for Cations 1, 2 and 3 and interaction parameters W_{12}, W_{13} and W_{23}. If 1 is assigned to Ca, 2 to (Fe+Mn) and 3 to Mg in garnet, then

$$\ln \gamma_{ga}^{gr} = \left(\frac{1661}{T(K)} - 0.755\right)\left(X_{ga}^{sp+al} \bullet X_{ga}^{py}\right)\left(1+X_{ga}^{py}\right) \qquad (13)$$

when $W_{CaFe} = W_{CaMn} = 0$

and $W_{CaMg} = 13807 - 6.276\ T(K)\ J\ mol^{-1}$ (Newton & Haselton, 1981).

A thermochemically-derived model of the activity of anorthite in plagioclase, (a_{pl}^{an}), was proposed by Newton & Haselton (1981), based upon the results of cation exchange equilibria in plagioclase which were experimentally determined by Orville (1972). From this model,

$$\left.\begin{aligned} a_{pl}^{an} &= \left[\frac{X_{pl}^{an}(1+X_{pl}^{an})}{4}\right] \bullet \gamma_{pl}^{an} \\ \text{for} \quad \gamma_{pl}^{an} &= \frac{(X_{pl}^{an})^2}{T}\left[1032 + 4726 X_{pl}^{an}\right] \end{aligned}\right\} \qquad (14)$$

The barometric expression which results from substituting equations 2, 8, 10, 11, 13 and 14 into equation 6 is:

$$\begin{aligned} P(GPa) = T(K) \bullet \Bigg\{ & 0.00238 - 24.943 \Bigg[\ln\left(\frac{X_{pl}^{an}(1+X_{pl}^{an})^2}{4}\right) + \frac{(1-X_{pl}^{an})}{T(K)} \\ & \bullet (1032+4726X_{pl}^{an}) - \ln X_{ga}^{gr} - (1+X_{ga}^{py})(X_{ga}^{sp+al} \bullet X_{ga}^{py}) \\ & \bullet \left(\frac{1661}{T(K)} - 0.755\right) \Bigg] \Big/ \Big[180282 - \{119900 X_{ga}^{py}(1+0.602X_{ga}^{gr}) \\ & + 121180 X_{ga}^{sp+al}(1+0.52X_{ga}^{gr})\}/(1-X_{ga}^{gr}) \Big] \Bigg\} - 0.76722 \end{aligned} \qquad (15)$$

Equation 15 is Version B of the AGPQ barometer. Pressures estimated using this formulation should have a 2σ relative error which is similar to that for the AGPQ barometer of Newton and Haselton (1981), namely 0.11 GPa.

Version C

This version differs from the last only in the model for the activity of anorthite in plagioclase. From the data of Carpenter & Ferry (1984):

$$a_{pl}^{an} = X_{pl}^{an} \bullet \gamma_{pl}^{an} \qquad (16)$$

where the possible range in γ_{pl}^{an} as a function of temperature is given in Table L2 below.

Table L2

Estimates of γ_{pl}^{an} as a Function of Temperature

Temperature	Probable Range in γ_{pl}^{an}
900	1.7 - 2.4
800	1.9 - 2.9
700	2.2 - 3.5
600	2.7 - 4.6

This version of the barometer gives pressures to ±>0.09 GPa. The error estimate is only a minimum, because the errors in terms other than in the activity coefficient of anorthite in plagioclase, have not been incorporated.

Appendix M

THE BAROMETRIC METHOD FOR VAPOUR-CONTAINING ASSEMBLAGES

1. INTRODUCTION

The ACGQV, ABCKQV and the ABCGKQV reactions have been used as barometers for natural systems in Chapter 9. In all of these reactions, the vapour phase of the assemblage plays a considerable role in determining the volume change for the reaction and therefore the pressure estimate. The barometric expression used at constant temperature is derived from the Second Law Equation. It is described and used by both Thompson (1976b) and Holdaway & Lee (1977), viz.

$$P_{C,T} = \frac{RT}{\Delta V_R}. \ln K_T + P_{S,T}$$

or

$$\Delta P.\Delta V_{R,T} = RT \ln K_T \qquad (1)$$

where $P_{C,T}$ is the equilibrium pressure of an assemblage at temperature T, which is chemically complex compared with the simple system assemblage at the same temperature, for which the equilibrium pressure: $P_{S,T}$ is independently known. The reaction volume $\Delta V_{R,T}$ is the average reaction volue over the pressure range from $P_{S,T}$ to $P_{C,T}$. K_T is the equilibrium coefficient for the reaction, at temperature T.

2. ABCKQV BAROMETRY

The reaction: Fe-biotite + andalusite + quartz --> Fe-cordierite + orthoclase + vapour was experimentally studied by Holdaway & Lee (1977). Biotites in equilibrium with aluminosilicate and cordierite at ~500-600°C contain a substantial tschermak component in solid solution (op. cit.; Thompson, 1976; Holdaway et al., 1980). Under these conditions, the Fe-endmember reaction is approximated by the equation:

$$K_{0.84}Fe_{2.52}Al_{1.72}Si_{2.74}O_{10}(OH)_2 + 2.08Al_2SiO_5 + 4SiO_2 \text{ ---> } 1.26Fe_2Al_4Si_5O_{18}.nH_2O + 0.84KAlSi_3O_8 + (1-1.26n)H_2O \qquad (2)$$

Equation (1) may be applied to give:

$$P_{C,T} = P_{S,T} - \frac{RT}{\Delta V_{R,T}} \ln \left\{ \frac{(a_{cd}^{Fe\text{-}cd})^{1.26} . (a_{af}^{or})^{0.84} . (a_{v}^{w})^{(1-1.26n)}}{(a_{bi}^{Fe\text{-}Al\text{-}bi}) . (a_{as}^{Al2SiO5})^{2.08} . (a_{qz}^{SiO2})^{4}} \right\} \qquad (3)$$

where af = alkali feldspar, as = aluminosilicate, bi = biotite, cd = cordierite, n = moles of water per mole of anhydrous endmember cordierite, or = orthoclase, qz = quartz and v = vapour.

Activity Models

Without evidence to the contrary, cordierite and biotite are assumed to be ideal Fe-Mg solid solutions (Lonker, 1981; Newton, 1983). In biotite 7 mol.% of the iron is assumed to be FeIII, therefore $a_{bi}^{Fe\text{-}Al\text{-}bi} = 0.93 X_{bi}^{FeAlbi}$.

Alkali feldspar is also assumed to behave ideally, because $\gamma_{Af}^{Or} = 1$ at the PT conditions concerned of 700-850°C and 0.2-0.6 GPa (Brown & Parsons, 1981). Water is chosen to be represented in the reaction volume term rather than as a fugacity in the ln K term. The a_{v}^{w} is therefore unity because there is no other component in the vapour phase. The a_{qz}^{SiO2} is also assumed to be unity. The $a^{Al2SiO5}$ in the aluminosilicates is assumed to equal $X^{Al2SiO5}$. Substitution of these values into equation 3 yields:

$$P_{C,T} = P_{S,T} - \frac{RT}{\Delta V_{R,T}} \left[2.52 \ln \left(\frac{X_{Cd}^{FeCd}}{X_{bi}^{FeAlbi}} \right) + 0.1829 - 0.84 \ln X_{af}^{or} + 2.08 \ln X_{as}^{Al2SiO5} \right] \qquad (4)$$

Molar Volume

The reaction volume has two components: one for the solid phases and one for the vapour phase:

$$\Delta V_{R,T} = \Delta V_{S,T} + \Delta V_{V,T} \qquad (5)$$

The value of $\Delta V_{S,T}$ may be approximated using the molar volume terms for the endmember phases listed in Table M1, assuming that the feldspar, biotite and cordierite solid solutions behave ideally and that $\Delta V_{S,T} = \Delta_{V,20c}$.

Table M1

Molar Volumes of Endmember Phases

Phase	V^o (J GPa^{-1})	Source
Fe-Al-biotite	152880	Holdaway & Lee (1977)
Mg-Al-biotite	148620	"
Fe cordierite	237090	"
Mg cordierite	233230	"
Orthoclase or_{100}	108870	Helgeson et al. (1978)
Plagioclase $(ab_{94}an_6)$	100270	Calculated from Newton & Perkins (1982)
Andalusite	51540	Averages of single crystal determinations by Burnham (1963), in Robie & Hemingway (1984) and that of Winter & Ghose (1979)
Sillimanite	49910	cf. Appendix L
Quartz	22688	cf. Appendix L

These data give

$$\Delta V_{S,T} = \Delta V_S^o = 1.26\left[(1-X_{Cd}^{Mg-Cd}).V_{Fe-Cd}^o + X_{Cd}^{Mg-Cd}.V_{Mg-Cd}^o\right]$$
$$+ 0.84\left[X_{af}^{or}.V_{or}^o + (1-X_{af}^{or})V_{ab_{94}an_6}^o\right]$$
$$- \left[(1-X_{bi}^{Mg-Al-bi})\ V_{Fe-Al-bi}^o + X_{bi}^{Mg-Al-bi}.V_{Mg-Al-bi}^o\right] - 4V_{qz}^o$$
$$- 2.08V_{ad}^o \quad \text{or} \quad - 2.08V_{si}^o$$

for ab = albite, ad = andalusite, an = anorthite, and si = sillimanite.

This equation yields:

$$\left.\begin{aligned} \Delta V_S^{ad} &= 37326 - 4864\ X_{Cd}^{Mg-Cd} + 4260\ X_{bi}^{Mg-Al-bi} \\ \text{and}\quad \Delta V_S^{Si} &= 40716 - 4864\ X_{Cd}^{Mg-Cd} + 4260\ X_{bi}^{Mg-Al-bi} \end{aligned}\right\} \quad (6)$$

The molar volume term $\Delta V_{V,T}$ is evaluated using:

(i) the equation of Sen & Bhatticharya (1985) to determine the mole fraction of water in cordierites (n) as a function of $P, G_W^{O,T}$, f_W and T, viz:

$$n = \left\{ \frac{f_w^{P,T}}{\exp\left[7.02+4.529P(GPa)-\frac{2587.6}{T(K)}\left(P(GPa)+12.597\right)-\frac{G_w^{O,T}(J)}{RT(K)}\right] + f_w^{P,T}} \right\} \qquad (7)$$

for $f_W^{P,T}$ = fugacity of water at P,T (GPa)
and $G_W^{O,T}$ = the free energy of water at 0.0001 GPa and temperature T(K) (J)
and **(ii)** the partial molar volume of water: $\bar{V}_w^{P,T}$ (Burnham et al., 1972), to give

$$\Delta V_{V,T} = (1-1.26\ n)\ \bar{V}_w^{P,T} \qquad (8)$$

Substitution of equations 6, 7 and 8 into equation 4 leads to the barometric expression:

$$\begin{aligned} P_{C,T}(GPa) = P_{S,T}(GPa) &- 8.3143T\left[2.52\ln\left(\frac{X_{cd}^{Fe-cd}}{X_{bi}^{FeAlbi}}\right) + 0.1829\right. \\ &\left. - 0.84\ \ln X_{af}^{Or} + 2.08\ \ln X_{as}^{Al2SiO5}\right] \left[4260X_{bi}^{MgAlbi}\right. \\ &- 4864\ X_{cd}^{Mg-cd} + \bar{V}_W^{P,T}(J\ GPa^{-1})\left[1 - 1.26f_W^{P,T}(GPa)\right. \\ &\left.\left\{f_W^{P,T}(GPa) + \exp[7.02+4.529P(GPa)-\frac{2587.6}{T(K)}\left(P(GPa)+12.597\right)\right.\right. \\ &\left.\left. - \frac{G_W^{O,T}(J)}{8.3143T(K)}]\right\}\right] + \alpha\ \Bigg] \end{aligned} \qquad (9)$$

where α = 37326 for andalusite-bearing assemblages and 40716 for sillimanite-bearing assemblages

Estimation of Pressure in Divariant Chemical Systems

Using equation 9, pressure is estimated given the temperature and the composition of one of the ferromagnesian phases (biotite or cordierite) by:

(i) determining $P_{S,T}$ at the temperature concerned using the experimentally derived curve for the iron endmember reaction;

(ii) choosing appropriate values for X_{af}^{Or} and $X_{as}^{Al2SiO5}$ (usually 0.72 and 1.0, respectively);

(iii) deducing the equilibrium composition of the other ferrogmagnesian phase, using the biotite-garnet and cordierite-garnet Fe-Mg exchange thermometers of Holdaway & Lee (1977);;

(iv) determining $f_W^{P,T}$ and $\bar{V}_W^{P,T}$ using data of Burnham et al. (1972);

(v) evaluating equation 9 to determine an approximate value for the pressure (P_1) for the equilibrium assemblage in the complex chemical system;

(vi) repeating stages (iii) to (v) for the pressure: P_1, to obtain a second pressure estimate: P_2;

(vii) averaging P_1 and P_2 to yield $P_{C,T}$; and

(viii) repeating stage (iii) using the pressure: $P_{C,T}$ to obtain the final estimate of the composition of the second ferromagnesian phase.

The divariant PT grids of Figs 9.3 and 9.4 were constructed using this method at several different temperatures.

3. ACGQV BAROMETRY

The equation appropriate to this assemblage is:

Fe-cordierite ---> aluminosilicate + almandine + quartz + vapour

i.e.

$$3Fe_2Al_4Si_5O_{18}.nH_2O \text{ --> } 4Al_2SiO_5 + 2Fe_3Al_2Si_3O_{12} + 9SiO_2 + nH_2O \qquad (10)$$

Giving:

$$K = \left\{ \frac{(a_{qa}^{al})^2}{(a_{cd}^{Fe\text{-}cd})^3} \right\} \qquad (11)$$

Using the symmetric ternary solution and partial molar volume models for garnet described in Appendix L, the Fe endmember reaction volume derived using data of Tables L1 and M1 and the activity model for cordierite described for the previous barometer, then the barometric expression for the sillimanite-bearing assemblage becomes

$$P_{C,T} = P_{S,T} - 49.886T\left[\ln\left(\frac{X_{ga}^{al}}{X_{cd}^{Fe\text{-}cd}}\right) + X_{ga}^{gr}\, X_{ga}^{py}(0.755 - 1660/T)\right]$$

$$\left[833130\, X_{ga}^{gr} - 88964 + 11580\, X_{cd}^{Mg\text{-}cd} + (22250\, X_{ga}^{gr} - 227585)X_{ga}^{py}\right.$$

$$+ V_W^{P,T}(J\ GPa^{-1})\left[f_W^{P,T}(GPa)\ \left[f_W^{P,T}(GPa) + \exp\left\{7.02+4.529P(GPa)\right.\right.\right.$$

$$\left.\left.\left. - \frac{2587.6}{T(K)}\left(P(GPa) + 12.597\right) - \frac{G_W^{O,T}(j)}{8.3143T(K)}\right\}\right]\right] \qquad (12)$$

Application of equation 12 is similar to that described above for equation 9. However for equilibria in which $P_W < P_T$, as depicted on Fig. 9.4, $P_{C,T}$ increases as $(f_W^{P,T})$ decreases at constant P_{total}.

4. <u>ABCGKQV BAROMETRY</u>

The univariant line in PT space which describes the occurrence of this assemblage was determined graphically. It occurs at the intersection of the divariant grids for the ABCKQV and ACGQV assemblages.

Appendix N

{BIOTITE+VAPOUR} OXYGEN FUGACIMETER

The net transfer reaction:

annite + oxygen --> proton-deficient oxy-annite + water

i.e.

$$KFeII_3AlSi_3O_{10}(OH)_2 + 3/4\ O_2 \rightarrow KFeIII_3AlSi_3O_{10}O_2H_{-1} + 3/2\ H_2O \qquad (1)$$

relates components present in the phases of the assemblage: {biotite+water}. Biotite can therefore be used as an internal fO_2 sensor.

Application of the Second Law equation to this reaction at equilibrium leads to the expression:

$$-\log_{10}\left(\frac{fO_2}{fO_2^o}\right) = \frac{4}{3\ \ln\ 10}\left[\frac{1}{R}\left\{\left(\frac{\Delta H_T^R + P\Delta V_T^R}{T}\right) - \Delta S_T^R\right\} + \frac{3}{2}\ln fH_2O + \ln\left(\frac{a_{PDO}}{a_{ANN}}\right)\right] \qquad (2)$$

$$\left.\begin{array}{l}\text{where } a_{PDO} = X_{PDO}\cdot\gamma_{PDO} \\ \text{and } a_{ANN} = X_{ANN}\cdot\gamma_{ANN}\end{array}\right\} \qquad (3)$$

for a: activities, X: mole fractions and γ: activity coefficients of the biotite endmember components: proton deficient oxyannite (PDO) and annite (ANN) respectively.

Activity coefficient values estimated by Beane (1974) are:

$$\gamma_{PDO} = 10^{(-27.6X_{ANN}^2 - 6.7X_{PHL}^2 - 34.4X_{ANN}X_{PHL})} \quad \text{and}$$
$$\gamma_{ANN} = 10^{(0.1X_{PHL}^2 - 27.6X_{PDO}^2 - 20.8X_{PDO}X_{PHL})} \qquad (4)$$

In his model, Beane (1974) represented biotite by a symmetric ternary solution of annite, proton-deficient oxyannite and phlogopite (PHL).

The partial molar volume for the reaction:

$$\Delta V_T^R \approx V_{PDO} - V_{ANN} = 11{,}120\ JGPa^{-1}\ \text{(Helgeson et al., 1978)}.$$

Values for the reaction entropy and enthalpy calculated from the thermodynamic data of Beane (1974) for the mica endmembers and oxygen, and for water vapour of Robie et al. (1978) at four temperatures are:

T(K)	700	800	900	1000
ΔS_T^R ($Jmol^{-1}K^{-1}$)	-29.37	-29.95	-29.28	-27.73
ΔH_T^R ($kJmol^{-1}$)	-151.58	-157.70	-163.02	-167.63

Exponential regression of these data against temperature and substitution of the expressions for the activities of annite and proton deficient oxyannite (equations 3 and 4) into equation 2 yields

$$\log_{10}(fO_2/fO_2^o) = 25.495 \exp(-0.0009695T) - \frac{775P}{T} + 0.8686 \ln (f_W/f_W^o)$$

$$- 27.73X_{PHL}(1.654X_{ANN}+0.3077X_{PHL}-X_{PDO})$$
$$- 36.8(X_{ANN}^2-X_{PDO}^2) - 0.5791 \ln (X_{ANN}/X_{PDO})$$

for fO_2, fO_2^o, f_W, f_W^o and P (GPa) and for T (K).

Evaluation of equation (5) is possible if f_W and biotite composition are known. The oxidation state of iron in four biotite separates was determined by semi-micro-analytical titration by E. Kiss (Australian National University; Appendix G) and compositions of these biotites are given in Appendix F. The cation proportions which lead to estimates of the mole fractions of the three relevant biotite endmembers are listed in Table N1, below.

Table N1

Mole Fractions of Some Endmember Molecules in Four Biotite Separates

Sample	62619ph	62619ps	62634	67539
Endmember:				
X_{ANN}	0.518	0.558	0.539	0.506
X_{PHL}	0.100	0.101	0.112	0.195
X_{PDO}	0.0564	0.0196	0.0468	0.0367

where mole fraction X, equals the relevant octahedral cation proportion (on the basis of 22 oxygens) divided by six. Estimates of f_W may be made from the estimates of total pressure by assuming that $P_W = P_\Sigma$. Temperatures have been estimated using the garnet-biotite exchange thermometer of Holdaway & Lee (1977).

The T-$\log_{10}fO_2$ fields derived for the four {biotite-vapour} assemblages are shown in Fig. 9.9.

Appendix O

CHEMICAL AND NORMATIVE COMPOSITIONS OF REFERENCE WHOLE ROCKS FROM THE BLUE TIER BATHOLITH

Suite	Poimena							Musselroe		
Type	Granite							Granite		
Sa #	TB25	TB26	TB27	TB28	TB29	TB30	TB38	TB46	43128	43129
SiO_2	73.34	72.97	72.58	72.38	73.39	72.46	71.56	73.92	74.23	74.57
TiO_2	0.29	0.38	0.37	0.33	0.3	0.39	0.39	0.31	0.52	0.49
Al_2O_3	14.04	13.87	14.14	14.4	13.91	14.07	14.42	14.28	13.14	12.82
FeO^*	1.9	2.47	2.34	2.17	1.96	2.4	2.98	1.97	2.91	2.72
MnO	0.05	0.06	0.06	0.05	0.05	0.06	0.07	0.04	0.05	0.05
MgO	0.59	0.66	0.73	0.68	0.6	0.76	1.18	0.51	0.73	0.70
CaO	1.66	1.7	2.16	2.04	1.78	2.04	2.82	1.43	1.49	1.49
Na_2O	3.1	3.15	3.29	3.22	3.19	3.28	2.51	3.02	2.34	2.66
K_2O	4.9	4.59	4.17	4.6	4.69	4.39	3.97	4.38	4.23	4.16
P_2O_5	0.13	0.15	0.14	0.13	0.12	0.14	0.11	0.13	0.18	0.18
Ba	409	411	360	430	350	381	475	833	815	688
Rb	271	253	235	247	260	251	223	163	199	223
Sr	128	123	144	147	122	143	144	140	116	106
Zr	138	153	155	144	125	158	206	170	268	259
Nb	12.5	13.0	12.5	11.5	11.5	13	13.5	9.5	18.7	12.6
Y	32	33	32	27	30	34	34	22	33	33
Sc	11	14	14	12	11	14	17	9	10.1	9.1
V	21	26	29	27	24	31	35	14	40	31
Mn	358	450	451	420	426	483	500	320	358	353
Ga	17.6	18.0	17.8	17.4	16.8	17.8	18.2	17.2	18.2	16.1
Sn									3.5	4.5
mg'	35.0	31.7	35.1	35.3	34.7	35.5	40.8	31.1	30.6	30.9
al	17.9	15.8	10.6	13.0	12.7	9.2	13.4	35.5	28.8	22.7
qz									38.98	37.88
co									2.37	1.60
or									25.01	24.57
ab									19.79	22.49
an									6.39	6.38
hy									5.05	4.76
di										
il									0.98	0.94
ap									0.42	0.42
mt									0.94	0.88
Qz									19.5	22.3
Af									27.8	27.5
Pl									19.5	22.3
Source	1	1	1	1	1	1	1	1	6	7

Suite	MUSSELROE									
Type	Granite									
Sa #	43128	43129	43131	43134	43138	63064	63065	63051	63054	63057
SiO_2	74.23	74.57	74.05	74.09	75.07	75.09	72.67	75.16	73.65	75.26
TiO_2	0.52	0.49	0.49	0.50	0.51	0.17	0.29	0.58	0.56	0.54
Al_2O_3	13.14	12.82	13.13	13.22	12.94	13.62	14.54	120.3	13.18	12.30
FeO^*	2.91	2.72	2.86	2.88	2.93	1.74	2.32	3.56	3.39	3.27
MnO	0.05	0.05	0.05	0.04	0.04	0.04	0.03	0.05	0.04	0.05
MgO	0.73	0.70	0.82	0.64	0.63	0.31	0.45	0.83	0.76	0.77
CaO	1.49	1.49	1.61	1.48	1.39	1.14	1.79	1.67	1.53	1.55
Na_2O	2.34	2.66	2.47	2.26	1.74	3.20	3.28	2.11	2.07	1.93
K_2O	4.23	4.16	4.25	4.51	4.44	4.63	4.51	3.87	4.66	4.18
P_2O_5	0.18	0.18	0.13	0.20	0.14	0.06	0.13	0.15	0.16	0.15
Ba	815	688	627	760	738	298	640	843	862	689
Rb	199	223	223	226	219	290	191	180	223	206
Sr	116	106	102	109	96	95	146	123	114	121
Zr	268	259	234	273	247	103	170	272	256	264
Nb	18.7	12.6	11.6	12.2	10.1	12	12	16	16	14
Y	33	33	34	34	31	62	67	45	37	47
Sc	10.1	9.1	8.1	7.6	7.1	4.6	5.4	11.8	8.8	3.7
V	40	31	32	31	30					
Mn	358	353	349	309	323					
Ga	18.2	16.1	20.2	19.2	18.2					
Sn	3.5	4.5	3.5	3.0	5.1	10	<3	<3	<3	<3
mg'	30.6	30.9	33.4	28.1	27.4	23.7	25.4	29.1	28.3	29.2
al	28.8	22.7	23.2	29.6	34.8	30.0	22.8	19.1	25.7	24.4
qz	38.98	37.88	37.51	38.43	42.70					
co	2.37	1.60	1.81	2.35	3.03					
or	25.01	24.57	25.13	26.64	26.22					
ab	19.79	22.49	20.86	19.12	14.74					
an	6.39	6.38	7.27	6.20	6.13					
hy	5.05	4.76	5.21	4.84	4.88					
di										
il	0.98	0.94	0.92	0.94	0.96					
ap	0.42	0.42	0.30	0.47	0.33					
mt	0.94	0.88	0.92	0.93	0.94					
Qz	40.6	37.7	39.4	39.9	44.0					
Af	27.8	27.5	27.7	30.2	29.6					
Pl	19.5	22.3	21.5	18.1	13.8					
Source	6	7	5	6	4	4	4	4	4	4

Suite	MUSSELROE				BOOBYALLA					
Type	Porphyry				Granite					
Sa #	63256	63257	63083	63084	63101	63132	63136	63139	63201	63241
SiO_2	73.16	73.85	74.17	72.71	75.38	75.49	75.89	77.04	76.50	76.57
TiO_2	0.35	0.31	0.28	0.34	0.27	0.37	0.27	0.24	0.23	0.19
Al_2O_3	14.23	14.18	14.29	14.59	12.90	12.31	12.94	12.49	12.34	12.40
FeO*	2.17	1.98	1.94	2.17	2.16	2.68	1.92	1.95	1.91	1.83
MnO	0.04	0.04	0.04	0.04	0.03	0.03	0.03	0.03	0.03	0.03
MgO	0.71	0.52	0.37	0.62	0.36	0.42	0.29	0.17	0.24	0.15
CaO	1.98	1.22	1.10	1.93	1.08	1.66	0.96	1.28	1.09	0.93
Na_2O	3.69	3.42	3.07	3.79	2.51	2.41	2.34	2.06	2.35	2.73
K_2O	3.35	4.12	4.62	3.71	5.02	4.27	5.07	4.52	5.05	4.91
P_2O_5	0.17	0.18	0.11	0.11	0.15	0.18	0.16	0.09	0.11	0.10
Ba	511	808	962	761	562	668	391	460	374	599
Rb	118	150	162	158	264	208	300	249	273	222
Sr	168	148	133	166	86	116	68	80	70	79
Zr					171	247	180	176	168	155
Nb			12.3	10.3	22.4	12.1	13.1	11.2	22.0	26.2
Y			25	26	32	37	36	33	28	38.2
Sc	8.6	7.0	6.1	7.6	5.6	7.1	4.0	4.6	7.1	7.0
V	20	26			14	17	12	13	8.1	3
Mn	215	206			220	248	202	204	197	211
Ga	17.2	16.1			19.3	18.2	20.2	21.3	18.6	18.5
Sn	2.0	2.0	<3	4	5.6	3.5	6.1	4.6	4.5	5.5
mg'	36.4	31.4	25.0	33.3	22.5	21.8	21.1	13.5	18.2	12.7
al	21.5	35.6	40.0	18.9	30.3	19.0	39.1	39.4	27.7	27.7
qz					37.69	39.72	39.59	43.68		
co					1.69	1.09	2.21	2.06		
or					29.67	25.23	29.94	26.72		
ab					21.25	20.41	19.77	17.41		
an					4.49	7.19	3.81	5.86		
hy					3.57	4.29	3.11	2.90		
di										
il					0.52	0.71	0.52	0.46		
ap					0.35	0.42	0.38	0.21		
mt					0.69	0.86	0.62	0.63		
Qz					38.8	41.4	40.3	44.3		
Af					35.6	28.9	36.7	32.3		
Pl					17.2	20.7	14.5	15.5		
Source	2	2	4	4	1	6	7	6	1	1

Suite	BOOBYALLA									
Type	Granite								Porphyry	
Sa #	63216	63066	63068	63069	63070	63071	63072	TB44	63203	63204
SiO_2	73.30	74.34	76.35	75.47	76.03	75.37	76.12	73.83	73.04	72.84
TiO_2	0.28	0.33	0.26	0.24	0.28	0.21	0.22	0.28	0.53	0.59
Al_2O_3	13.99	13.20	12.62	12.78	12.73	13.19	12.76	13.18	13.05	12.92
FeO^*	2.29	2.60	2.07	2.24	2.37	2.17	2.18	2.02	3.17	3.56
MnO	0.04	0.03	0.02	0.02	0.03	0.02	0.03	0.03	0.05	0.05
MgO	0.36	0.39	0.28	0.22	0.32	0.21	0.23	0.29	0.56	0.79
CaO	1.24	1.56	1.29	1.04	1.15	1.13	1.06	1.44	1.50	1.74
Na_2O	2.67	2.29	2.04	2.55	2.03	2.44	2.47	2.40	2.56	2.43
K_2O	5.46	5.13	4.95	5.32	4.94	5.15	4.80	5.38	5.11	4.66
P_2O_5	0.19	0.13	0.12	0.12	0.12	0.11	0.13	0.14	0.23	0.25
Ba	735	886	529	558	373	446	378	610	860	525
Rb	298	230	240	299	277	332	319	245	239	284
Sr	105	123	89	79	82	71	71	100	102	91
Zr		215	178	180	175	162	159	189		
Nb		15	12	18	16	15	13	11.5		
Y		41	30	33	37	36	27	36		
Sc	6.1	7.3	3.5	3.5	3.9	3.2	3.6	7	8.6	11.1
V	17							9	26	42
Mn	347							225	378	400
Ga	19.7							19.6	18.7	19.6
Sn	5.1	<3	4	7	5	8	8		4.6	7.5
mg'	21.7	20.9	19.3	14.8	19.2	14.6	15.6	20.1	23.6	27.9
al	31.0	22.8	33.5	24.5	34.7	33.2	33.6	23.6	16.0	15.5
qz										
co										
or										
ab										
an										
hy										
di										
il										
ap										
mt										
Qz										
Af										
Pl										
Source	1	4	4	4	4	4	4	1	2	2

Suite	BOOBYALLA								
Type	Porphyry								
Sa #	63205	63154	63156	63219	63227	63242	63251	63254	63217
SiO_2	75.59	77.25	76.78	76.51	74.13	76.61	73.87	75.73	76.14
TiO_2	0.32	0.08	0.08	0.11	0.15	0.17	0.31	0.22	0.24
Al_2O_3	12.34	12.73	12.99	12.79	13.73	12.40	13.84	12.89	12.71
FeO^*	2.30	1.15	1.12	1.51	1.66	1.65	2.38	1.90	1.88
MnO	0.04	0.03	0.03	0.02	0.02	0.03	0.04	0.04	0.03
MgO	0.37	0.12	0.15	0.15	0.19	0.26	0.36	0.27	0.25
CaO	1.12	0.30	0.46	0.49	0.61	0.76	1.38	0.83	0.77
Na_2O	2.57	3.56	3.38	2.91	2.94	3.08	3.57	2.89	2.51
K_2O	5.01	4.56	4.82	5.24	6.20	4.67	3.94	4.91	5.12
P_2O_5	0.20	0.15	0.15	0.17	0.20	0.22	0.19	0.18	0.20
Ba	376	97	108	66	687	247	160	489	509
Rb	302	382	380	379	385	273	244	285	301
Sr	71	20	18	24	62	59	73	71	82
Zr									
Nb									
Y									
Sc	6.0	3.5	3.0	3.0	3.5	4.5	7.1	5.6	4.0
V	18	7	7	7	8	13	16	13	11
Mn	272	213	234	134	171	267	331	282	206
Ga	19.1	21.2	21.3	20.1	21.1	17.6	20.3	19.2	20.2
Sn	6.5	23.7	17.8	7.5	9.5	6.5	7.6	9.1	7.6
mg'	22.1	15.4	19.1	15.0	16.8	21.6	20.7	20.1	19.1
al	20.9	47.0	46.3	42.1	35.0	31.8	27.7	33.8	39.0
qz									
co									
or									
ab									
an									
hy									
di									
il									
ap									
mt									
Qz									
Af									
Pl									
Source	2	2	2	2	2	2	2	2	2

Suite	BABEL ISLAND					MATHINNA BEDS				
Type	Granite					Psammopelite				
Sa #	63708	63709	63722	63723	63725	63105	63107	63108	63109	63110
SiO_2	76.30	76.55	77.64	77.33	77.93	78.23	69.92	78.84	74.72	73.83
TiO_2	0.02	0.03	0.02	-	0.01	0.51	0.65	0.62	0.70	0.49
Al_2O_3	13.34	13.48	12.95	13.39	13.23	11.51	16.69	10.72	12.21	14.28
FeO^{*3}	1.01	0.88	1.0	0.72	0.89	3.41	5.09	4.23	4.58	3.55
MnO	0.03	0.03	0.02	0.02	0.03	0.04	0.07	0.05	0.05	0.05
MgO	0.07	-	-	0.02	-	1.24	2.01	1.76	1.75	1.29
CaO	0.42	0.38	0.32	0.33	0.36	0.43	0.36	1.41	0.36	0.45
Na_2O	4.32	4.07	3.85	3.93	3.50	0.71	-	0.76	0.79	0.58
K_2O	4.40	4.50	4.14	4.19	3.97	3.81	5.09	1.50	4.73	5.37
P_2O_5	-	-	-			0.10	0.13	0.11	0.11	0.11
Ba	31	26	32	6	26	466	847	214	716	718
Rb	367	354	333	357	358	178	253	114	229	226
Sr	7	7	8	3	6	72	90	79	78	87
Zr	68	58	55	56	60	256	169	222	265	144
Nb	17.1	17.1	16.3	26.3	18.4	14	15	16	15	12
Y	65	63	28	63	45	22	22	27	24	26
Sc	15.5	14.6	14.2	10.6	13.8	9.3	13.7	13.2	11	9.6
V	6	6	6	6	22					
Mn	242	208	178	149	232					
Ga	23.1	23.1	25.4	23.3	23.6					
Sn	15	<4	8	11	16					
mg'	10.7	-	-	4.6	-	39.0	41.0	42.3	40.2	39.0
al	29.6	48.5	51.1	62.1	65.8	41.4	46.6	34.5	32.9	45.4
qz	32.48	34.17	37.97	37.15	40.91					
co	0.69	1.21	1.56	1.79	2.51					
or	26.02	26.57	24.45	23.75	23.48					
ab	36.58	34.47	32.60	33.21	29.63					
an	2.10	1.90	1.57	1.66	1.78					
hy	1.71	1.28	1.44	1.15	1.33					
di										
il	0.04	0.06	0.04		0.02					
ap										
mt	0.33	0.28	0.32	0.23	0.29					
Qz	33.0	34.3	38.0	37.0	40.6					
Af	61.0	60.1	56.9	57.8	51.6					
Pl	2.2	1.9	0.7	1.0	2.4					
Source	3	5	5	5	5	4	4	4	4	4

* Total iron as FeO.

Sources

1 Dr B.W. Chappell, A.N.U. (unpublished data).

2 Cocker (1977) for ME's, Rb and Sr. Other TE's: this work.

3 Higgins et al. (1985) for ME's, Ba, Rb, Sr, Zr, Nb, Y, Sn, Ga. For Sc, V, Mn and Sn where quoted to one decimal place: this work.

4 Kitto (1982).

5 Dr N.C. Higgins, B.M.R. (unpublished), elements as for 3 above.

6 Averaged analyses of Cocker (1977) and Dr N.C. Higgins, B.M.R. (unpublished) for ME's, Rb and Sr; Dr N.C. Higgins, B.M.R. (unpublished) for Ba, Zr, Nb, Y, Sn, Ga; this work for Sc, V, Mn and Sn where quoted to one decimal place.

7 Averaged analyses of Cocker (1977) and Higgins et al. (1985) and this work as for 6.

Appendix P

WHOLE-ROCK AND MATRIX SEPARATE DENSITIES

Densities of most of the Furneaux Granite whole rocks and matrix separates were obtained using the Archimedian relationship that the weight of a submerged object is decreased by an amount equal to the weight of the displaced water. This relationship yields the equation:

$$\rho_R = [f_D/(f_D-f_S)].\rho_W \qquad (R1)$$

where ρ_R and ρ_W are the densities of the rocks and of water and f_D and f_S are the dry and submerged weights of the sample. Duplicate rock-density determinations were made of kilogram quantities of whole-rock samples and of the gram quantities of whole-matrix separates. The procedure involved the use of a top-loading balance, a retort stand, distilled water, low breaking-strain fishing line and a thermometer for temperature correction of the density of water. Duplicate density determinations were always in agreement at the second and often at the third decimal place.

Sample #	Density (gcm^{-3})
62675	2.600
62576	2.716
62577	2.728
62578	2.625
62579c	2.615
62579f	2.626
62580	2.614
62581	2.660
62582	2.692
62583	2.650
62584	2.634
62585	2.623
62586	2.671
62587	2.665
62591	2.657
62592	2.640
62593	2.749
62593MX	2.762
62594MX	2.729
62594	2.790
62595	2.632
62595m	2.624
62596	2.609
62596MX	2.606
62597	2.606
62598	2.597
62599	2.680
62600	2.682
62601	2.706
62602	2.773
62602iMX	2.773
62602oMX	2.796
62603	2.633
62604	2.624
62605	2.624
62605MX	2.605
62606	2.621
62606MX	2.616
62607	2.688
62608	2.676
60610	2.771
62610MX	2.856
62612	2.692
62612MX	2.716
62613	2.627
62614	2.648
62614MX	2.716
62615	2.739
62616c	2.625
62616f	2.622
62617	2.633
62618	2.632
62618MX	2.634
62619	2.649
62619MX	2.635
62620	2.634
62621	2.627
62622	2.622
62623	2.631

Sample #	Density (gcm^{-3})
62624	2.653
62625	2.627
62626	2.588
62627	2.627
62627m	2.633
62628	2.715
62631	2.725
62632	2.804
62633	2.719
62635	2.686
62636	2.631
62637	2.648
62638	2.651
62639	2.605
62640	2.635
62641	2.645
62642	2.666
67530	2.674
67530eMX	2.717
67530mMX	2.966
62532	2.644
62533	2.624
67534	2.702
67535	2.628
67536	2.622
67537	2.630
675371	2.592
675371	2.747

Appendix Q

MODAL PROPORTIONS OF PHENOCRYST PHASES IN SELECTED FURNEAUX ISLAND PORPHYRIES

In each of the following samples, in excess of 2000 points were petrographically assessed under the binocular microscope using a half-centimetre grid on slabs stained with trisodium heaxanitritocobaltate III:

Suite	Sample number	Number of points counted	% phenocrysts (versus matrix)
Wybalenna	62593	2121	12
	62602	2513	9
	62610	2036	13
Poimena	62594	2231	21
	62596	2032	20
	67532	2038	44
Boobyalla	62595	2380	24
	62605	2069	5
	62606	2031	21
	62618	2121	15
	62619	2093	33
	62627	2012	23
Boobyalla/ Poimena hybrid	62614	2153	31

Appendix R

CHEMICAL COMPOSITIONS OF MAGMA CONSTITUENTS USED IN MAJOR ELEMENT OF THE BOOBYALLA SUITE PORPHYRITIC GRANITE WHOLE-ROCK TREND

Model A Magma Constituent	Bulk magma			Melt		
Dependent Variable	FeO*			FeO*		
Regressional Parameter	$\hat{y}$	m	r^2	$\hat{y}$	m	r^2
SiO_2	77.442	-0.8986	0.17	76.598	-0.6790	0.32
TiO_2	-0.126	0.1799	0.89	-0.056	0.0979	0.82
Al_2O_3	13.753	-0.3591	0.08	13.558	-0.2145	0.13
FeO*[3]	0	1	1	0	1	1
MnO	0.023	0.0033	0.04	0.006	0.0084	0.56
MgO	-0.115	0.1845	0.80	-0.029	0.0757	0.89
CaO	-0.105	0.6015	0.73	0.514	-0.0070	0
Na_2O	3.161	-0.3302	0.22	3.785	-0.6286	0.62
K_2O	5.823	-0.3767	0.22	5.505	0.3259	0.15
P_2O_5	0.147	-0.0045	0	0.087	0.0209	0.11
Source Compositions	Appendix E - whole rocks: 62578,62583, 62604,62620,62622, 62623,62625,67536, 67547,67548. Appendix O: 43201, 43216,43101,43132, 43136,43139,T1344, 68066,68068,68069, 68070,68071,68072.			Appendix E - matrixes: 62605,62606,62616c, 62616v,62617,62618, 62619,62627,62595 NB: Compositions are transposed in FeMg, as described in text of Chapter 12.)		

FeO* - total iron as FeO

Appendix R - cont.

Magma Constituent	Melt: Model B			Biotite	
Dependent Variable	FeO*			MgO	
Regressional Parameter	$\hat{y}$	m	r^2	$\hat{y}$	m
SiO_2	77.720	-0.5082	0.03	37.187	-0.0357
TiO_2	-0.120	0.1555	0.87	3.808	0.2086
Al_2O_3	14.631	-1.5405	0.65	21.084	-0.4700
FeO*[3]	0	1	1	28.514	-0.7214
MnO	0.024	0.0012	0	0.117	-0.0040
MgO	-0.074	0.1038	0.56	0	1
CaO	0.278	0.0969	0.18	0	0
Na_2O	5.409	-1.7142	0.63	0	0
K_2O	2.249	2.2717	0.66	9.296	0.0214
P_2O_5	-0.117	0.1339	0.80	0	0
Source Compositions	Appendix E - porphyry matrixes: 62579c, 62579f. Whole rocks: 62580,62543. Appendix O: 707708, 707709,707722,707723, 707725.			Average for high-Ti phenocrystic biotites from #43156 and average for high-Ti biotite inclusions in megacrystic alkali feldspar crystal from #43248.	

Magma Constituent	Cordierite		Orthopyroxene	
Dependent Variable	MgO		MgO	
Regressional Paramater	$\hat{y}$	m	$\hat{y}$	m
SiO_2	46.134	0.3614	44.851	0.3544
TiO_2	0	0	0	0
Al_2O_3	31.315	0.2457	1.82	0
FeO*[3]	21.910	-1.5986	52.329	-1.3544
MnO	0.147	-0.0114	0	0
MgO	0	1	0	1
CaO	0	0	1	0
Na_2O	0.3	0	0	0
K_2O	0.2	0	0	0
P_2O_5	0	0	0	0

Appendix S

MAJOR ELEMENT COMPOSITIONS AND PROPORTIONS OF PHASES IN BOOBYALLA SUITE MODEL MAGMAS

KEY:				
	Af	alkali feldspar	Pl	plagioclase
	As	aluminosilicates	Qz	quartz
	Ap	apatite	Lq	melt
	Bi	biotite	M	magma = whole rocks
	Cd	cordierite	S	bulk crystalline phases
	Ga	garnet	an	anorthite
	Il	ilmenite	ab	albite
	op	orthopyroxene		

$mg' = [Mg/(Mg+Fe^*+Mn)]$ mol%,

$$al = [A'/(A'+F'+M)] \text{ mol\%} = \left(\frac{Al_2O_3-(K_2O+Na_2O+CaO)}{Al_2O_3-(K_2O+Na_2O+CaO)+Fe^*O+MnO+MgO} \right) \text{ mol\%}$$

Fe* - total iron as FeII
FeO* - total iron as FeO

Appendix S

MAJOR ELEMENT COMPOSITIONS AND PROPORTIONS OF PHASES IN BOOBYALLA SUITE MODEL MAGMAS

KEY:				
	Af	alkali feldspar	Pl	plagioclase
	As	aluminosilicates	Qz	quartz
	Ap	apatite	Lq	melt
	Bi	biotite	M	magma = whole rocks
	Cd	cordierite	S	bulk crystalline phases
	Ga	garnet	an	anorthite
	Il	ilmenite	ab	albite.
	op	orthopyroxene		

$mg' = [Mg/(Mg+Fe^*+Mn)]$ mol%,

$$al = [A'/(A'+F'+M)] \text{ mol\%} = \left(\frac{Al_2O_3-(K_2O+Na_2O+CaO)}{Al_2O_3-(K_2O+Na_2O+CaO)+Fe^*O+MnO+MgO} \right) \text{ mol\%}$$

Fe* - total iron as FeII
FeO* - total iron as FeO

Model A; temperature 700°C

Phase	Af	As	Ap	Bi	Cd	Ga	Il	Pl	Qz	Lq	M	S
Comp.												
SiO_2	65.65	37.05		37.12	47.07	37.04		60.94	99.99	76.19	76.45	76.86
TiO_2				4.24			52.66				0.07	0.18
Al_2O_3	19.06	62.62		20.10	31.95			24.58		13.46	13.36	13.22
FeO*		0.33		27.00	17.76		46.33			0.6	1.10	1.88
MnO				0.11	0.12		1.00			0.01	0.03	0.02
MgO				2.1	2.60					0.02	0.09	0.19
CaO	0.40		56.84					6.06		0.51	0.56	0.65
Na_2O	3.92				0.30			7.91		3.41	2.80	1.86
K_2O	10.97			9.34	0.20			0.51		5.70	5.41	4.96
P_2O_5			43.16							0.10	0.14	0.18
mg'				12.2	20.6	14.5				4.5	12.2	14.9
al				18.5	49.4	23.7				52.3	54.9	56.0
wt% in												
magma	16.28	1.6	0.16	1.28	1.15	0.47	0.03	1.48	16.86	60.69		
2σ	6.93	1.36	0.06	2.70	3.90	2.16	0.24	0.63	2.46	9.48		

$\Sigma(r^2)$ = 0.0004 $[an/(an+ab)]^{Pl}_{mol}$ = 0.31

Model A; temperature 721°C

Phase	Af	As	Ap	Bi	Cd	Ga	Il	Pl	Qz	Lq	M	S
Comp.												
SiO_2	65.49	37.01		37.07	47.46	37.34		59.30	99.99	76.05	76.18	76.37
TiO_2				4.47			52.66			0.02	0.13	0.31
Al_2O_3	19.01	62.33		19.58	32.21	21.12		25.68		13.42	13.25	12.99
FeO*		0.66		26.21	16.08	35.54	46.33			0.80	1.40	2.37
MnO				0.10	0.11	1.32	1.00			0.01	0.03	0.03
MgO				3.20	3.65	3.52				0.03	0.14	0.31
CaO	0.40		56.84			1.16		7.35		0.51	0.74	1.12
Na_2O	3.44				0.30			7.15		3.28	2.70	1.76
K_2O	11.65			9.36	0.20			0.51		5.77	5.30	4.54
P_2O_5			43.16							0.10	0.14	0.20
mg'				17.8	28.7	14.5				5.5	15.1	18.8
al		100		17.2	49.4	23.7				47.2	46.3	46.4
wt% in												
magma	12.96	1.23	0.18	1.90	1.03	0.58	0.06	3.48	16.78	61.80		
2σ	2.11	0.54	0.06	0.78	1.32	0.64	0.08	0.57	1.08	3.56		

$\Sigma(r^2)$ = 0.0002 $[an/(an+ab)]^{Pl}_{mol}$ = 0.376

Model A; temperature 742°C

Phase	Af	As	Ap	Bi	Cd	Ga	Il	Pl	Qz	Lq	M	S
Comp.												
SiO_2	65.41	36.94		37.05	47.63	37.34		58.46	99.99	75.92	75.91	75.92
TiO_2				4.58			52.66			0.04	0.18	0.38
Al_2O_3	18.99	61.74		19.34	32.34	21.12		26.25		13.37	13.14	12.82
FeO*		1.32		25.85	15.28	35.54	46.33			1.00	1.70	2.68
MnO				0.10	0.10	1.32	1.0			0.01	0.03	0.03
MgO				3.70	4.15	3.52				0.05	0.20	0.41
CaO	0.40		56.84			1.16		8.25		0.51	0.92	1.49
Na_2O	3.20				0.30			6.76		3.16	2.60	1.82
K_2O	12.01			9.37	0.20			0.51		5.83	5.18	4.27
P_2O_5			43.16							0.11	0.14	0.18
mg'				20.3	32.5	14.5				7.6	17.0	21.0
al				16.6	49.5	23.7				43.4	39.3	37.5
wt% in												
magma	12.68	0.65	0.17	2.19	1.49	0.75	0.11	5.60	18.13	58.23		
2σ	0.93	0.34	0.04	0.44	0.76	0.36	0.06	0.41	0.68	1.92		

$\Sigma(r)^2$ = 0.0001 $[an/(an+ab)]^{Pl}_{mol}$ = 0.41

Model A; temperature 763°C

Phase	Af	As	Ap	Bi	Cd	Ga	Il	Pl	Qz	Lq	M	S
Comp.												
SiO_2	65.36			37.04	47.76	37.34		57.97	99.99	75.78	75.64	75.47
TiO_2				4.66			52.66			0.06	0.23	0.43
Al_2O_3	18.97			19.15	32.42	21.12		26.58		13.33	13.03	12.67
FeO*				25.56	14.72	35.54	46.33			1.20	2.00	2.95
MnO	-			0.10	0.10	1.32	1.00			0.02	0.03	0.04
MgO				4.10	4.50	3.52				0.06	0.26	0.50
CaO	0.40		56.84			1.16		8.41		0.51	1.10	1.81
Na_2O	3.05				0.30			6.53		3.03	2.50	1.87
K_2O	12.21			9.38	0.20			0.51		5.90	5.07	4.08
P_2O_5			43.16							0.11	0.14	0.18
mg				22.2	35.1	14.5				8.3	18.2	23
al				16.1	49.5	23.7				40.8	33.3	29.6
wt% in												
magma	12.78		0.19	2.50	2.06	0.94	0.15	7.53	19.54	54.31		
2σ	0.08		<0.01	0.04	0.02	0.04	<0.01	0.04	0.06	0.18		

$\Sigma(r)^2$ = <0.00005 $[an/(an+ab)]^{Pl}_{mol}$ = 0.43

Model A; temperature 783°C

Phase	Af	Ap	Bi	Cd	Ga	Il	Op	Pl	Qz	Lq	M	S
Comp.												
SiO_2	65.34		37.03	47.85	37.34		46.62	57.77	99.99	75.65	75.36	75.11
TiO_2			4.72			52.66				0.08	0.29	0.49
Al_2O_3	18.97		19.02	32.48	21.12		1.82	26.72		13.29	12.93	12.59
FeO^{*3}			25.34	14.32	35.54	46.34	45.58			1.40	2.30	3.14
MnO			0.10	0.10	1.32	1.00				0.02	0.03	0.34
MgO			4.4	4.75	3.52		4.98			0.08	0.31	0.52
CaO	0.40	56.84			1.16		1.00	8.56		0.50	1.28	2.10
Na_2O	3.00			0.30				6.44		2.90	2.4	1.93
K_2O	12.29		9.39	0.20				0.51		5.96	4.96	4.02
P_2O_5		43.16								0.12	0.14	0.16
mg'			23.6	37.0	14.5		16.3			8.8	19.1	22.7
al			15.8	49.4	23.7		0.0			39.6	28.3	23.5
wt% in magma	13.42	0.19	3.64	1.38	0.85	0.15	0.28	9.74	21.93	48.42		
2σ	0.16	0.02	0.14	0.16	0.24	0.02	0.16	0.12	0.20	0.46		

$\Sigma(r)^2$ = <0.00005 $[an/(an+ab)]^{Pl}_{mol}$ = 0.438

Model A; temperature 804°C

Phase	Af	Ap	Bi	Cd	Ga	Il	Op	Pl	Qz	Lq	M	S
Comp.												
SiO_2	65.33		37.01	47.93	37.34		46.78	57.72	99.99	75.51	75.11	74.83
TiO_2			4.83			52.66				0.10	0.34	0.50
Al_2O_3	18.97		18.78	32.53	21.12		1.82	26.75		13.24	12.82	12.54
FeO^{*3}			24.98	14.00	35.54	46.33	44.98			1.60	2.6	3.25
MnO			0.10	0.09	1.32	1.00				0.02	0.03	0.03
MgO			4.90	4.95	3.52		5.43			0.09	0.37	0.55
CaO	0.40	56.84			1.16		1.00	8.60		0.50	1.46	2.08
Na_2O	2.98			0.30				6.42		2.78	2.30	1.99
K_2O	12.32		9.40	0.20				0.51		6.03	4.84	4.07
P_2O_5		43.16								0.12	0.14	0.16
mg'			25.0	38.5	14.5		17.7			9.2	19.8	23.0
al			15.5	49.5	23.7		0.0			37.5	24.0	19.5
wt% in Magma	16.11	0.22	4.20	1.06	0.99	0.19	0.75	11.94	25.36	39.18		
2σ	0.13	0.02	0.12	0.12	0.18	0.02	0.14	0.09	0.18	0.38		

$\Sigma(r)^2$ = <0.00005 $[an/(an+ab)]^{Pl}_{mol}$ = 0.44

Model A; temperature 825°C

Phase	Af	Ap	Bi	Cd	Ga	Il	Op	Pl	Qz	Lq	M	S
Comp.												
SiO_2	65.33		37.01	47.98	37.34		46.91	57.72	99.99	75.39	74.84	74.64
TiO_2			4.85			52.66				0.12	0.40	0.51
Al_2O_3	18.97		18.73	32.57	21.12		1.82	26.75		13.20	12.71	12.51
FeO^{*3}			24.91	13.78	35.54	46.34	44.46			1.80	2.9	3.34
MnO			0.10	0.09	1.32	1.00				0.02	0.03	0.03
MgO			5.00	5.10	3.52		5.81			0.11	0.42	0.54
CaO	0.40	56.84			1.16		1.00	8.60		0.50	1.64	2.09
Na_2O	2.98			0.30				6.42		2.65	2.20	2.02
K_2O	12.32		9.40	0.20				0.51		6.09	4.73	4.19
P_2O_5		43.16								0.12	0.13	0.13
mg'			26.3	39.6	14.5		18.9			9.5	20.4	22.3
al			15.1	49.5	23.7		0.0			36.3	20.1	15.9
wt% in magma	19.63	0.22	4.89	0.58	1.20	0.24	1.24	14.25	29.27	28.48		
2σ	0.05	<0.01	0.04	0.04	0.04	<0.01	0.04	0.03	0.06	0.12		

$\Sigma(r)^2$ = <0.00005 $[an/(an+ab)]^{Pl}_{mol}$ = 0.44

Model B; temperature 700°C

Phase	Af	As	Ap	Bi	Cd	Ga	Il	Pl	Qz	Lq	M	S
Comp.												
SiO_2	65.65	37.05		37.13	46.91	37.34		60.94	99.99	77.26	76.45	76.01
TiO_2				4.16			52.66			0.02	0.07	0.10
Al_2O_3	19.06	62.62		20.29	31.84	21.12		24.58		13.24	13.36	13.42
FeO*[3]		0.33		27.29	18.48	35.54	46.34			0.90	1.10	1.21
MnO				0.11	0.12	1.32	1.00			0.03	0.03	0.01
MgO				1.70	2.15	3.52				0.02	0.09	0.12
CaO	0.40		56.84			1.16		6.06		0.37	0.56	0.68
Na_2O	3.92				0.30			7.91		3.87	2.80	2.24
K_2O	10.97			9.33	0.20			0.51		4.29	5.41	5.99
P_2O_5			43.16								0.14	0.20
mg′				10.0	17.1	14.5				3.5	12.2	15.1
al				19.1	49.4	23.7				53.4	54.9	54.9
wt% in												
magma	34.82	0.98	0.30	0.30	3.03	0.29	0.10	1.99	23.94	34.25		
2σ	4.43	1.88	0.06	3.02	5.56	2.56	0.26	0.25	1.16	5.24		

$\Sigma(r)^2 = 0.0003$ $\quad [an/(an+an)]^{Pl}_{mol} = 0.31$

Model B; temperature 721°C

Phase	Af	As	Ap	Bi	Cd	Ga	Il	Pl	Qz	Lq	M	S
Comp.												
SiO_2	65.49	37.01		37.09	47.22	37.34		59.3	99.99	77.20	76.18	75.48
TiO_2				4.33			52.66			0.04	0.13	0.19
Al_2O_3	19.01	62.33		19.91	32.05	21.12		25.68		13.06	13.25	13.38
FeO*[3]		0.66		26.71	17.12	35.54	46.34			1.02	1.40	1.66
MnO				0.11	0.11	1.32	1.00			0.03	0.03	0.02
MgO				2.50	3.00	3.52				0.03	0.14	0.21
CaO	0.40		56.84			1.16		7.35		0.38	0.74	1.00
Na_2O	3.44				0.30			7.15		3.67	2.70	2.03
K_2O	11.65			9.35	0.20			0.51		4.56	5.30	5.81
P_2O_5			43.16							0.02	0.14	0.22
mg′				14.2	23.7	14.5				5.2	15.1	18.5
al				18.1	49.4	23.7				48.1	46.3	45.7
wt % in												
magma	27.86	0.64	0.30	1.14	2.78	0.40	0.12	3.91	21.96	40.89		
2σ	1.61	0.48	0.04	1.12	1.26	0.74	0.10	0.23	0.52	2.02		

$\Sigma(r)^2 = 0.0001$ $\quad [an/(an+ab)]^{Pl}_{mol} = 0.376$

Model B; temperature 742°C

Phase	Af	As	Ap	Bi	Cd	Ga	Il	Pl	Qz	Lq	M	S
Comp.												
SiO_2	65.41	36.94		37.08	47.44	37.34		58.46	99.99	77.14	75.91	75.00
TiO_2				4.45			52.66			0.06	0.18	0.27
Al_2O_3	18.99	61.74		19.62	32.20	21.12		26.25		12.89	13.14	13.32
FeO*[3]		1.32		26.28	16.16	35.54	46.34			1.13	1.70	2.13
MnO				0.10	0.11	1.32	1.0			0.03	0.03	0.02
MgO				3.10	3.60	3.52				0.04	0.20	0.32
CaO	0.40		56.84			1.16		8.02		0.39	0.92	1.31
Na_2O	3.20				0.30			6.76		3.47	2.60	1.96
K_2O	12.01			9.36	0.20			0.51		4.82	5.18	5.45
P_2O_5			43.16							0.03	0.14	0.22
mg′				17.2	28.3	14.5				6.3	17.0	20.8
al				17.3	49.4	23.7				43.1	39.3	37.8
wt% in												
magma	23.86	0.24	0.29	1.92	2.91	0.51	0.13	5.86	21.71	42.57		
2 σ	0.61	0.20	0.02	0.38	0.48	0.26	0.04	0.15	0.26	0.90		

$\Sigma(r)^2 = <0.00005$ $\quad [an/(an+ab)]^{Pl}_{mol} = 0.41$

Model B; temperature 763°C

Phase	Af	As	Ap	Bi	Cd	Ga	Il	Pl	Qz	Lq	M	S
Comp.												
SiO_2	65.36			37.06	47.60	37.34		57.97	99.99	77.08	75.64	74.60
TiO_2				4.56			52.66			0.07	0.23	0.34
Al_2O_3	18.97			19.39	32.31	21.12		26.58		12.71	13.03	13.27
FeO*[3]				25.92	15.44	35.54	46.34			1.25	2.00	2.55
MnO				0.10	0.10	1.32	1.00			0.03	0.03	0.03
MgO				3.60	4.15	3.52				0.06	0.26	0.41
CaO	0.40		56.84			1.16		8.41		0.40	1.10	1.61
Na_2O	3.05				0.30			6.53		3.27	2.50	1.94
K_2O	12.21			9.37	0.20			0.51		5.09	5.07	5.05
P_2O_5			43.16							0.05	0.14	0.20
mg′				19.8	31.7	14.5				7.2	18.2	22.2
al				16.7	49.4	23.7				38.3	33.3	31.5
wt% in												
magma	21.01		0.27	2.74	2.66	0.80	0.14	7.83	22.17	42.38		
2σ	0.17		<0.01	0.10	0.06	0.08	0.02	0.07	0.14	0.36		

$\Sigma(r)^2 = <0.00005$ $\quad [an/(an+ab)]^{Pl}_{mol} = 0.43$

Model B; temperature 783°C

Phase	Af	Ap	Bi	Cd	Ga	Il	Op	Pl	Qz	Lq	M	S
Comp.												
SiO_2	65.34		37.04	47.73	37.34		46.46	57.77	99.99	77.03	75.36	74.28
TiO_2			4.66			52.66				0.09	0.29	0.42
Al_2O_3	18.97		19.15	32.40	21.12		1.82	26.72		12.53	12.93	13.19
FeO^{*3}			25.56	14.88	35.54	46.34	46.19			1.37	2.30	2.9
MnO			0.10	0.10	1.32	1.00				0.03	0.03	0.03
MgO			4.10	4.4	3.52		4.54			0.07	0.31	0.47
CaO	0.40	56.84			1.16		1.00	8.56		0.41	1.28	1.84
Na_2O	3.00			0.30				6.44		3.07	2.40	1.97
K_2O	12.29		9.38	0.20				0.51		5.35	4.96	4.71
P_2O_5		43.16								0.07	0.14	0.19
mg′			22.1	34.4	14.5		14.9			8.0	19.1	22.1
al			16.1	49.5	23.7		0.0			34.1	28.3	26.9
wt% in magmas	19.99	0.26	3.20	2.31	0.84	0.20	0.45	9.90	23.54	39.31		
2σ		0.04	<0.01	0.02	0.04	0.06	<0.01	0.04	0.02	0.04	0.10	

$\Sigma(r)^2$ = <0.00005 $[an/(an+ab)]^{Pl}_{mol}$ = 0.438

Model B; temperature 804°C

Phase	Af	Ap	Bi	Cd	Ga	Il	Op	Pl	Qz	Lq	M	S
Comp.												
SiO_2	65.33		37.03	47.83	37.34		46.66	57.72	99.99	76.97	75.11	74.15
TiO_2			4.72			52.66				0.11	0.34	0.46
Al_2O_3	18.97		19.02	32.47	21.12		1.82	26.75		12.35	12.82	13.06
FeO^{*3}			25.34	14.40	35.54	46.34	45.41			1.48	2.60	3.18
MnO			0.10	0.10	1.32	1.0				0.03	0.03	0.03
MgO			4.40	4.70	3.52		5.11			0.08	0.36	0.51
CaO	0.40	56.84			1.16		1.0	8.60		0.42	1.46	1.99
Na_2O	2.98			0.30				6.42		2.87	2.30	2.01
K_2O	12.32		9.38	0.20				0.51		5.62	4.84	4.44
P_2O_5		43.16								0.08	0.14	0.17
mg′			23.6	36.6	14.5		16.7			8.6	19.8	21.9
al			15.8	49.5	23.7		0.0			29.3	24.0	22.9
wt% in magma	20.34	0.26	3.42	2.06	0.99	0.27	1.02	11.99	25.80	33.85		
2 σ	0.10	<0.01	0.08	0.08	0.12	<0.01	0.10	0.06	0.12	0.28		

$\Sigma(r)^2$ = <0.00005 $[an/(an+ab)]^{Pl}_{mol}$ = 0.44

Model B; temperature 825°C

Phase	Af	Ap	Bi	Cd	Ga	Il	Op	Pl	Qz	Lq	M	S
Comp.												
SiO_2	65.33		37.02	47.94	37.34		46.85	57.72	100.0	76.91	74.84	74.19
TiO_2			4.81			52.66				0.13	0.40	0.48
Al_2O_3	18.97		18.83	32.54	21.12		1.82	26.75		12.17	12.71	12.88
FeO^{*3}			25.05	13.92	35.54	46.34	44.72			1.60	2.90	3.31
MnO			0.10	0.09	1.32	1.00				0.03	0.03	0.03
MgO			4.80	5.00	3.52		5.62			0.09	0.42	0.53
CaO	0.40	56.84			1.16		1.00	8.6		0.43	1.64	2.03
Na_2O	2.98			0.30				6.42		2.67	2.20	2.05
K_2O	12.32		9.40	0.20				0.51		5.88	4.73	4.36
P_2O_5		43.16								0.10	0.13	0.14
mg′			25.4	38.9	14.5		18.3			9.2	20.4	21.9
al			15.3	49.5	23.7		0.0			25.5	20.1	19.1
wt% in magma	23.22	0.25	3.39	1.85	1.11	0.39	1.86	14.28	29.47	24.18		
2σ	0.06	<0.01	0.06	0.04	0.06	<0.01	0.06	0.04	0.08	0.18		

$\Sigma(r)^2$ = <0.00005 $[an/(an+ab)]^{Pl}_{mol}$ = 0.44

Appendix T

SmNd ISOTOPIC DATA FOR WHOLE ROCKS AND A GARNET SEPARATE FROM SELECTED GRANITIC ROCKS OF THE BLUE TIER BATHOLITH

Four SmNd analyses of Furneaux Island sanples were made by Dr S.-S. Sun (Bureau of Mineral Resources, Canberra). They form part of his isotopic study of the granitic rocks of the Blue Tier Batholith.

TU#	Suite	Nd (ppm)	Sm (ppm)	$\frac{^{143}Nd}{^{144}Nd}$	$\frac{^{147}Sm}{^{144}Nd}$	$\varepsilon_{Nd}^{t=0}$	$\varepsilon_{Nd}^{t=370Ma}$
62579c	Babel Is	13.53	4.77	0.511702±22	0.21321	-2.62±0.44	-3.41±0.44
62583	Boobyalla	51.11	11.07	0.511409±14	0.13106	-8.35±0.26	-5.25±0.26
67535	Boobyalla	14.93	4.97	0.511511±22	0.18493	-6.35±0.42	-5.79±0.42
62634 (garnet separate)	Boobyalla	14.85	9.70	0.512078±16	0.39521	+4.72±0.32	-4.68±0.32

Data from sample TU62579c may be compared with that of the Babel Island Suite sample #702708 (Tasmanian Department of Mines) from the Mt William Pluton, NE Tasmania.

702708	Babel Is	15.28	6.04	0.511766±12	0.23945	-1.36±0.24	-3.40±0.24

All errors are quoted to 2σ (Dr S.-S. Sun, pers. comm.).

At 370 Ma, ε_{Nd}^{t} values for Babel Island Suite whole rocks are ~2 ε-units higher than those of Boobyalla Suite whole rocks. That of the whole-garnet separate is intermediate in value.